INVESTIGATIONS OF OPEN - FRAMEWORK METAL PHOSPHATES AND MESOPOROUS SOLIDS

A Thesis

Submitted for the Degree of

Doctor of Philosophy

By

S. NEERAJ

TO

MANIPAL ACADEMY OF HIGHER EDUCATION

THROUGH

JAWAHARLAL NEHRU CENTRE FOR ADVANCED SCIENTIFIC RESEARCH,

BANGALORE - 560 064, INDIA

AUGUST 2000

for my parents

DECLARATION

I hereby declare that the matter embodied in this thesis entitled **"Investigations of open-framework metal phosphates and mesoporous solids"** is the result of investigations carried out by me in the Chemistry and Physics of materials unit, Jawaharlal Nehru Centre for Advanced Scientific Research, Jakkur, Bangalore, India, under the supervision of Professor C.N.R. Rao and Dr. S. Natarajan.

In keeping with the general practice of reporting scientific observations, due acknowledgement has been made whenever the work described has been based on the findings of the other investigators. Any omission which might have been occurred by oversight or error of misjudgement is regretted.

S. Neeraj.

S. NEERAJ

ACKNOWLEDGEMENTS

I wish to express my sincere gratitude to Prof. C.N.R. Rao, FRS for suggesting the problems, invaluable guidance during the course of the research work and moral support. He has not just been a research supervisor, but a real father figure. He has groomed me from an excited boy to a more composed scientist. The foremost character of Prof. Rao, which has affected me most, is his passion and commitment to science. I have learnt various facets of science from him, and how to maintain levelheaded approach when problems do not work. I hope that the training, which he has imparted, will take me a long way into my research career.

I would like to acknowledge my regards and thanks to Dr. Srinivasan Natarajan who has jointly guided me on the investigations of open-framework metal phosphates. He has taught me crystallography and was helpful on a day to day basis whenever I have sought help during experimental work.

I am thankful to all the faculty members of both JNCASR and IISc who have offered courses and have been extremely generous. In particular, I would like to thank Profs. S. Chandrasekharan, S. Ramasesha, and J. Chandrsekhar, Drs. G. U. Kulkarni, A. R. Raju, K. S. Narayan, and S. Narasimhan who have been generous with their knowledge and invaluable advice at all times. I would also like to thank Dr. Madhusudan who has been very helpful as coordinator and academic counselor. I would also like to thank Dr. Bala for maintaining a pleasant computing environment.

I could not have asked for better labmates and collaborators, than Drs. Eswaramoorthy, Ulagappan, and Ayyappan, Amitava Choudhury, Vaidhyanathan, Gautam, Charusheela and Jayaraman. I am deeply indebted to them as they have been mere scientific collaborators but have helped me in many ways.

Apart from the labmates I would like to acknowledge all the students of JNC, specially, Dr. Govindraj, Gopalan, Anupama, Manashi, Sudhee, Sarathy, Sachin, Vanitha, Gargi, and John who have been helpful at various times during the course of my research work. I want to specially thank shivshankar for helping we with thesis work.

I would like to acknowledge the sincere efforts by all the technical staff of JNCASR, especially Anil, Vasu, Srinivas, Srinath, Rengan and BVN who have carried out numerous measurements for me which form the part of this work. In IISc I would like to acknowledge the help from Mr. Jarali (SSCU) and Mr. Wilson (SIF) who have helped me with FT-IR and NMR measurements. Mr Samuel (IPC) and Zaheer (MRC) have helped me with the glass blowing and fabrication of autoclaves. Vinayak and Rajesh have ensured the functioning of

computers in computation and our lab, failing which many things would have come to a stand still.

I thank the office staff of JNCASR and CSIR-COE. They have made my stay in the center convenient and saved my time from usual official chores. I am obliged to Jawaharlal Nehru Center for financial assistance to carry out this venture.

My friends Gopalan, Sujay, Akash, Amitava, Manashi, Swarna, Smita, GP, Dwairath and Suhrit have made my stay both in IISc and JNC a plesant memory. They have shared with me both excitements and depression. I really owe them for backing me up in times when I have been down.

Finally, I would like to express my deepest regards for my parents and family who have given me unquestioned support, despite all odds. I lack appropriate words to thank them for their love, immense patience and faith. I dedicate this thesis to my parents.

CONTENTS

PART 2

INVESTIGATIONS OF MESOPOROUS SOLIDS

PREFACE

Porous solids with varying pore sizes form an important class of solids. Considerable effort has been devoted to the study of various aspects of these materials in the past few decades. This thesis consists of two parts. Part 1 deals with the results of investigations of open-framework metal phosphates with channel diameters less than 1nm, and Part 2 deals with a study of mesoporous solids with pore diameter larger than 2nm.

In **Part 1,** results of detailed investigations on the various aspects of open-framework metal phosphates are described. Several new open-framework zinc phosphates have been synthesized under hydrothermal conditions in the presence of organic amines, and characterized by single crystal x-ray crystallography and other techniques. These metal phosphates exhibit different dimensionalities such as one-dimensional linear chains and ladders, two-dimensional layers, and three-dimensional architectures with channels. Unusual zinc phosphates wherein the amine, in addition to being present in the channels, also acts as a ligand to the metal center have been isolated. Open-framework chlorophosphates have been synthesized for the first time. An important contribution to this area is the discovery of amine phosphates as possible intermediates in the formation of open-framework phosphates. Reactions of the amine phosphates with various metal ions under relatively mild conditions are found to yield open-framework structures. Another significant finding is the isolation of a zero-dimensional monomeric zinc phosphate, which transforms to an open-framework structure on heating in water at room temperature. This last observation throws light on the mechanism of formation of the plethora of phosphate-based architectures of varying degrees of complexity.

In **Part 2,** the focus is on mesoporous solids. Mesoporous ZrO_2, Al_2O_3, silicophosphates, RuO_2 and metal chalcogenides have been synthesized by employing self-organized assemblies of ionic as well as neutral surfactants. The mechanism of lamellar-hexagonal-cubic phase transformations of mesoporous zirconia has been examined. Transition metal complexes, such as the Cu-acetate dimer and $[Mn(bipy)_2]^{2+}$ encapsulated in the pores of cubic mesoporous silica are shown to exhibit extraordinarily high oxygen activation in the oxidation of phenol to catechol and for the oxidation of

styrene to styrene oxide via singlet oxygen. Liquid-crystalline templating with short-chain amine has been employed to synthesize silica and aluminophosphate with an intermediate pore size of ~1.4nm.

PART 1

INVESTIGATIONS OF OPEN-FRAMEWORK METAL PHOSPHATES*

SUMMARY

Synthesis of complex inorganic materials with novel pore structures possessing open architectures is an area of great interest in materials chemistry. At the bottom of the synthesis of such structures lies the idea of rational design, involving the assemblage of small atomic or molecular units to obtain the desired solid. Traditionally known porous materials include zeolites and other related materials with pore sizes in the range 3-14Å. Zeolites are aluminosilicates and are synthesized using hydrated alkali or alkaline earth cations as templates. The pore structure in these materials is well defined and forms the back-bone of heterogeneous catalysis. Employing the chemical knowledge gained from zeolites, open-framework aluminophosphates ($AlPO_4$) were synthesized in 1982. Since then, various other framework materials have been synthesized first by substituting the metal ions in the aluminum site and later on open-framework metal phosphates have also been prepared. Prominent among the open-framework phosphates are those of magnesium, gallium, indium, molybdenum, iron, cobalt, zinc and tin. Unlike, zeolites the phosphate-based frameworks are synthesized under acidic conditions. The synthesis is carried out hydrothermally in a pressure container, in the presence of organic amines or alkali / alkaline earth cations. In spite of the large number of materials synthesized, the nature of formulations required to make these materials remains obscure. The synthesis of these solids, by and large, is accomplished by the trial and error. It therefore, becomes necessary to synthesize a large variety of open-framework phosphates by employing different amines and metal ions, so as to eventually develop structure-property-function relations. In order to address this problem, a systematic investigation of open-framework zinc phosphates has been carried out.

Several open-framework zinc phosphates have been synthesized in the presence of organic amines such as 1,3-diamino-2-hydroxypropane, 1,3-diaminopropane,

diethylenetriamine, 1,3-diaminoguanidine hydrochloride and cyclohexylamine under hydrothermal conditions. Two-dimensional layered structures as well as three-dimensional zinc phosphates have been prepared by this means. The layered structure, obtained with 1,3-diamino-2-hydroxypropane contains layers with bifurcated 12-membered channels. Chiral three-dimensional zinc phosphates are produced with 1,3-diaminopropane and diethylenetriamine. The structures obtained with 1,3-diaminopropane possess 8-membered channels, one of them built up of double crankshaft chains and the other built of building units similar to that of the naturally occurring aluminosilicate mineral, thomsonite. The chiral solid obtained with diethylenetriamine has intersecting helical channels. The reaction of a zinc *tris*(DAP) complex with phosphoric acid in the presence of oxalic acid gave a layered zinc phosphate, with layers containing tubular structures. Diethylenetriamine also gives a layered zinc phosphate with ladder-like corrugations, in as well as one-dimensional Zn – O – Zn chains. The unusual presence of chains exclusively formed by 3-membered rings bordering those containing 4- or 3- and 4-membered rings is a unique feature in this material. Another three-dimensional zinc phosphate, obtained with diethylentriamine shows Zn_4O_4 tetrameric clusters, observed for the first time, in open-framework zinc phosphates. The most interesting three-dimensional structures are obtained with diethylenetriamine and 1,3-diaminoguanidine, which in addition to being present in the channel also act as a ligand to the metal centre. With cyclohexylamine a layered zinc chlorophosphate, has been obtained, wherein the chlorines protrude in a direction perpendicular to the plane of the layer.

Despite the synthesis of a large number of open-framework phosphates, it is difficult to rationalize their formation. The role of the amine in these syntheses is unclear. There are some suggestions in the literature with regard to the role of the amine as a structure-directing agent, and/or as a space filler. The amines are usually protonated during acidic synthetic conditions they maintain charge-neutrality of the anionic framework and stabilize the structure through hydrogen-bonding and other interactions. Another aspect, which requires understanding, is the relationship between the metal phosphates of different dimensionalities. The variety of structures obtained in a given metal phosphate system, often with the same amine, may arise because of the small

energy differences amongst them or due to kinetic control of the reactions. We have tried to probe the role of amine in some detail. During the hydrothermal synthesis of open-framework metal phosphates, we isolated several amine phosphates as additional products. Normally the amine phosphates are not isolated due to their high solubility in water. Their isolation from the synthesis mixtures points towards them being, possible reaction intermediate, which can lead to the open-framework phosphates. Our studies have shown that the amine phosphates react with metal ions under hydrothermal conditions in absence of additional phosphoric acid to give open-framework metal phosphates. We have also studied the reactions using in situ ^{31}P NMR and ex situ x-ray diffraction. Not only have we shown the amine phosphates to be reaction intermediates we have also developed this as a methodology to synthesize new open-framework phosphates by reaction of various amine phosphates with Zn^{II}, Co^{II}, Al^{III}, Ga^{III} and Sn^{II} ions yielding both known and new structures at temperatures much below the hydrothermal conditions, (in some cases at as low a temperature as 30°C) This demonstrates the seminal role of amine phosphates in the formation of open architectures.

We have employed the amine phosphate route to synthesize a large number of open-framework zinc, cobalt phosphates with different dimensionalities. The cobalt phosphates have been difficult to prepare via regular hydrothermal synthesis. We have also synthesized open-framework tin phosphates by this method.

In our pursuit of understanding the formation of the complex phosphate structures, we have isolated a metal phosphate with a structure simpler than the linear chain, a monomeric 4-membered ring zinc phosphate. This monomeric phosphate on heating in water transforms to an open-framework layered zinc phosphate.

---

* Papers based on the above studies have appeared in Chem Commun.(1998) J. Solid State Chem (1999), New J. Chem. (1999), Chem. Mater. (1999), Angew. Chem. Int. Ed. Engl. (1999), , Int. J. Inorg. Mater. (1999), J. Mater. Chem (1999) J. Solid state Chem . (2000), Inorg. Chem. (2000), J. Am. Chem. Soc. (2000), Solid State Sci (2000).

1. OPEN-FRAMEWORK MATERIALS: AN OVERVIEW

1.1 Introduction

Present day materials embrace systems ranging widely in size and complexity and include infinite solid arrays. Framework solids, which are generally prepared under harsh synthetic conditions, are gradually coming under the delicate regime of self-assembly where they can be synthesized under mild conditions. The design of inorganic and organic framework solids with novel structures and properties has been of great fascination to materials chemists. These materials are attractive not only because of their chemical and structural diversity and aesthetic appeal because of the possible control in their construction. An important class of open-framework materials, are porous solids of which, zeolites constitute the prime example. Then there are the whole variety of metal phosphates and carboxylates. We shall briefly examine the salient features of these materials in this section.

1.2 Zeolites – the first molecular sieves

First discovered in the mid-1700s (Cronsted, 1756), zeolites are hydrated, crystalline aluminosilicates that organize into stable discrete frameworks.[1-3] Basic structures of these employ tetrahedral atoms, silicon or aluminum AlO_4, and SiO_4 tetrahedra are primary building units, where each oxygen is shared between two metalloid tetrahedra to produce open-frameworks with the chemical formula $[Al_xSi_{1-x}O_2]^{x-}$. The resulting covalent lattices can either be neutral or negatively charged (as a result of bridging oxides and substitution). The negative charge is balanced by extra-framework positive ions (M^{n+}) which reside inside the channels and cages of the zeolite. In natural, zeolites this role is played by alkali or alkaline earth metal ions where as in synthetic zeolites the charge can be balanced by inorganic, organic, or combinations of inorganic and organic cations. Silica-polymorphs (framework formula SiO_2) which are electronically neutral can also be prepared. As a consequence of this ordered structure, zeolites both benefit from and are limited by their highly geometrical nature: their rigid

structures are inherently robust, yet they are difficult to process. Even so, these underlying impediments, have not prevented a large score of researchers from constructing a myriad of architectures, based on zeolite host lattices.[4] Leaving aside the strengths and weaknesses of these porous zeolites/ zeolite-like materials, they demonstrate a major objective of materials chemistry: the ability to manifest macroscopic physical properties based on embedded microscopic structure. The strong motivation towards the study of these porous materials is their role in ion-exchange, adsorption and heterogeneous catalysis.[5] Zeolites are generally synthesized hydrothermally from a mixture of silicon and aluminum compounds, alkali metal cations, organic molecules and water in an alkaline supersaturated solution. The process of forming complex microporous crystalline aluminosilicate is called *zeolitization*. Common sources of silicon are colloidal silica, water glass, pyrogenic silica or silicon alkoxides such as tetramethyl or tetraethyl orthosilicate. Aluminum can be introduced as compounds such as gibbsite, pseudo-boehmite, aluminate salts or the metal powder. Cationic and neutral organic species are added as solvents or as structure-directing agents. When the reactants are mixed, they rapidly form an aluminosilicate hydrogel or precipitate. After the gel point this hydrogel is aged at room temperature or at a slightly increased temperature, remaining below that applied during the crystallization. After ageing, the hydrogel is heated to the appropriate crystallization temperature, which is in the range from 333K to 473K.

Isomorphous replacements in the anionic framework of the zeolites by elements such as aluminium, gallium, germanium, beryllium, boron, iron, chromium, phosphorous, magnesium was proposed by Barrer.[2,6] During such replacements, which are achieved during the synthesis process, the number of occupiable sites becomes an important parameter. In many zeolites the number of sites available for occupation is more than the number of cations required for balancing the framework charge. This allows isomorphous substitution to be done in ways that allows the total number of cations to vary, which permits one to play around with the Si / Al ratio during the synthesis. However, a restriction

or limitation is imposed on the Si/Al ratio in the framework, defined by *Lowenstein's Rule*[7], which states that linking of two AlO_4 tetrahedra is energetically unfavorable, since two $[AlO_2]^-$ units next to each other will result in undesirable repulsive interactions, i.e. Al-O-Al + Si-O-Si is less stable than 2 [Si-O-Al]. This limits the Si/Al ratio to ≥ 1. Structures obeying this rule should have strictly alternating AlO_4 and SiO_4 tetrahedra. Till today a handful of structures with Al-O-Al links have been reported, which constitute all non-zeolitic (condensed) forms of the sodalite framework (SOD) such as $Ca_4(Al_6O_{12})$[8] and bicchulite $Ca_4(Si_2Al_4O_{12})(OH)_4$.[9] The variation in Si/Al ratio has serious implications on the acidic properties of the zeolites and hence becomes a parameter of reckoning.

1.3 Secondary Building Units

Meier[10] proposed several fundamental building blocks, called secondary building units or SBUs (the primary building units being single TO_4 tetrahedra). These consist of four to sixteen TO_4 tetrahedra which, when assembled, form the known zeolite structure types. These are shown schematically in Fig. 1.1, and have been derived assuming that each framework can be assembled from just one type of SBU. The zeolites ZSM-5, as well as ferrierite can be described by their 5-1 building units (Fig. 1.2). Offretite, zeolite-L, cancrinite, and erionite are generated using only 6-member ring. In a few systems, combinations of SBUs are found, for example, lovdarite (formed from spiro-5 and 4), and melanophlogite (formed from 5 and three5-1's).[2] Some other zeolites like sodalite framework can be built from either the single 6-member ring or the single 4-member ring. Framework density is an important parameter and is a measure of the available pore volume in a zeolite structure. It is defined as the number of tetrahedral atoms per 1000Å^3. Most condensed silicate structures, such as α-quartz, cristoballite and tridymite, have values around 20, whereas most zeolites range from 12-19. Cloverite, a gallophosphate, which has one of the largest 20-member ring systems, has a value of 11.1 (Fig. 1.3a).[11] Figure 1.1b

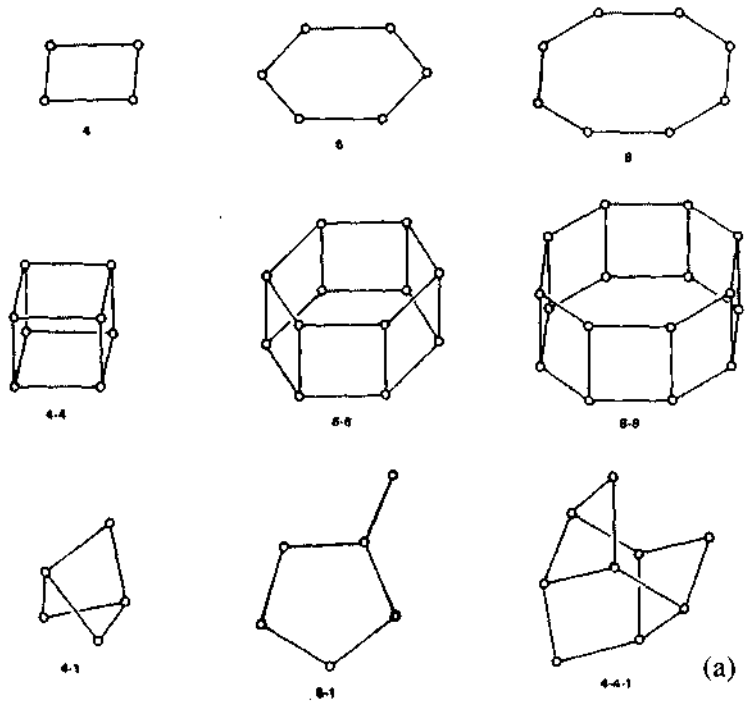

(a)

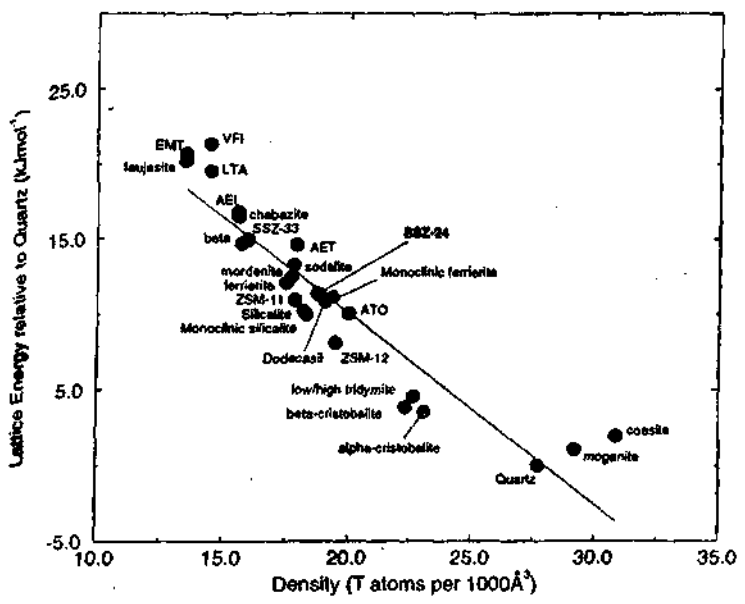

(b)

Fig. 1.1. (a)Secondary building units (SBU's) found in zeolite structures. (b) Variation of calculated lattice energy with framework density of silica structures.

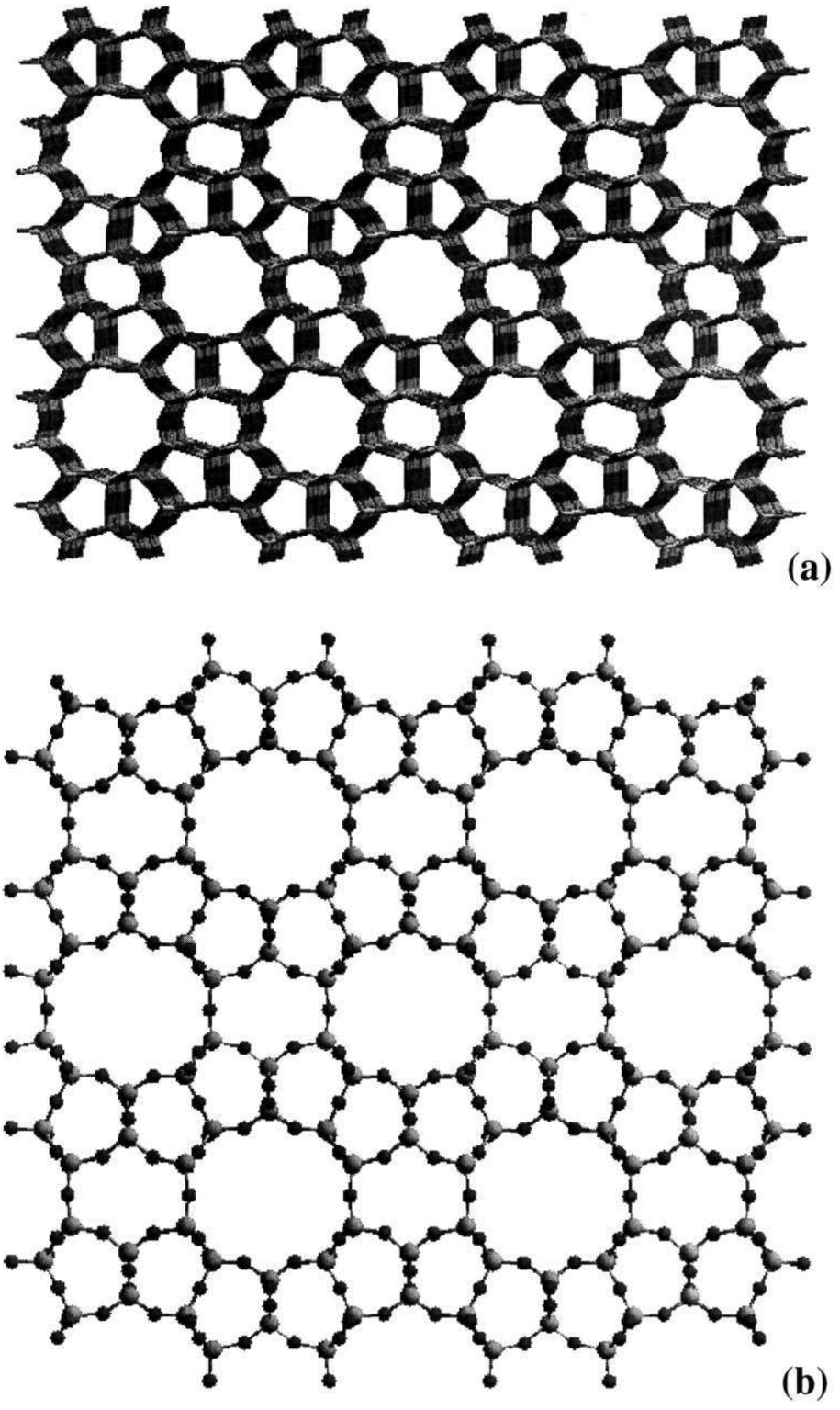

Fig. 1.2 (a) Channel structure of ZSM–5. (b) Ball and stick representation of Ferrierite showing10–membered channels. Note the 5–1 building units in these structures.

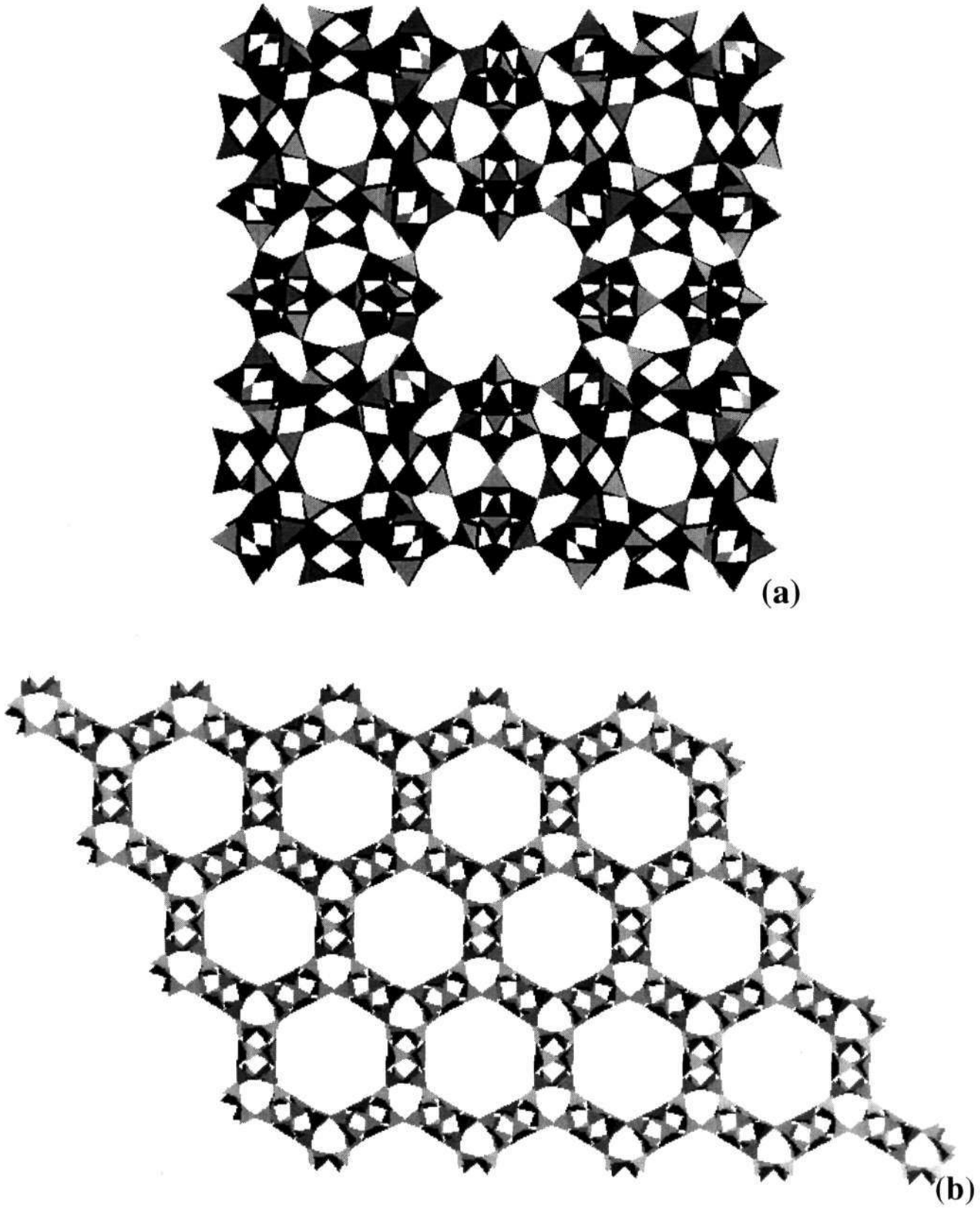

Fig. 1.3 (a) 20–membered channel structure of gallophosphate 'cloverite'. (b) 18–membered channels present in aluminophosphate 'VPI–5'.

gives the calculated lattice energies for various silica structures with varying framework density.[12-14] Quartz lies at the energy minimum, and most of the open-framework structures are predicted to be around 8-20kJ mol^{-1} less stable than quartz.

1.4 From zeolites to the other porous solids

Taking lessons from the principles of zeolite synthesis one can conceive various other framework structures. In the past 15 years or so, materials with different chemical compositions but with similar structural characteristics have been prepared. The most numerous of these are the aluminophosphates ($AlPO_4$) discovered by Flanigen and co-workers in 1982 at Union Carbide.[15] The $AlPO_4$ family, as it is known, shows an even greater diversity of structure, at least in terms of pore size and architecture, than the zeolites. These microporous phosphates are synthesized by hydrothermal methods in the temperature range of 100°- 250°C, and using amines or quartenary ammonium salts as templates (all designated R) under mild acidic conditions in contrast to the alkaline conditions employed for zeolites. In contrast to the zeolites, majorities of the aluminophosphates exhibit frameworks with Al and P occupying alternating tetrahedral sites. This limits the possible building rings to be even-numbered. Hence although the aluminophosphate analogues of some of the zeolites such as erionite (ERI) or sodalite (SOD) are known ($AlPO_4$-17 and $AlPO_4$-20 respectively),[16] no $AlPO_4$ exists with the MFI structure, which contains 5 ring units. The $AlPO_4$-11, like many silicates, is made up of 10-membered rings or 12-membered puckered rings. During the last decade microporous-aluminophosphate based materials have witnessed many novel topologies, some of them possessing extra-large pores delimited by more than 12T atoms (aluminosilicates 14 ring UTD-1 is the largest pore material). The quest for large-pore molecular sieves initiated with synthesis of VPI-5 (VFI) by Davis and co-workers.[17] This molecular sieve contains one-dimensional circular channels with an 18-membered ring aperture and possesses a free-diameter of 12-13Å

(Fig. 1.3b) The VFI network, can be viewed as the insertion of two adjacent 4-ring units between the 6-ring units of $AlPO_4$-tridymite. The structure of $AlPO_4$-8 (AET),[18] which, contains 14-ring channels, is a close relative of the VPI-5 network. Contrary to zeolites where silicon always exhibits tetrahedral fourfold coordination Al in aluminophosphates exhibits both fivefold (trigonal bipyramidal), or six-fold coordination (octahedral). In these cases terminal water molecules or hydroxide groups complete the coordination sphere of aluminum, which leads to connectivities observed in mineral aluminum phosphates[19] in which $[AlO_n]$ polyhedra may share corners or edges through Al-O-Al linkages. It also results in the formation of odd-membered rings, as in case of $AlPO_4$-14A[20] and $AlPO_4$-21.[21] The appearance of higher coordinations for Al seems to limit the channel sizes in these cases.

The other elements in the Group 13 B, Ga and In also form phosphate based framework solids. The early reports on gallophosphates appeared from Parise[22-24], which were structurally related to $AlPO_4$-n family. Gallium occurs in 4- 5- and 6-fold coordinations in these phosphate frameworks but prefers higher coordinations when compared to aluminum. The speedy progress in the synthesis of gallophosphates came with introduction of fluoride ion as mineralizer in the synthesis medium. Kessler and co-workers started the use of fluoride ions in synthesis of phosphates.[25,26] They found that fluoride acts both as a mineralizer and a source of fluorine, and sometimes gets incorporated in the $AlPO_4$ and $GaPO_4$ frameworks. The first interesting fluorophosphate was cloverite,[11] a gallophosphate with extra-large pore openings comprising of 20T atoms and a three dimensional channel system similar to that of faujasite type zeolites.[16] The effective pore size of 13.2Å gets limited by the terminal hydroxyl groups which protrude into the channel. The basic building unit is a double four-ring D4R cage with an occluded fluoride ion (Fig 1.4a). The Ga-F distance is 2.3-2.6Å and fluorine is weakly linked to Ga. Alternatively, fluorine can also participate directly in the coordination sphere and increase the coordination to six. Ferey and coworkers have successfully synthesized a series of oxy-fluorinated gallium

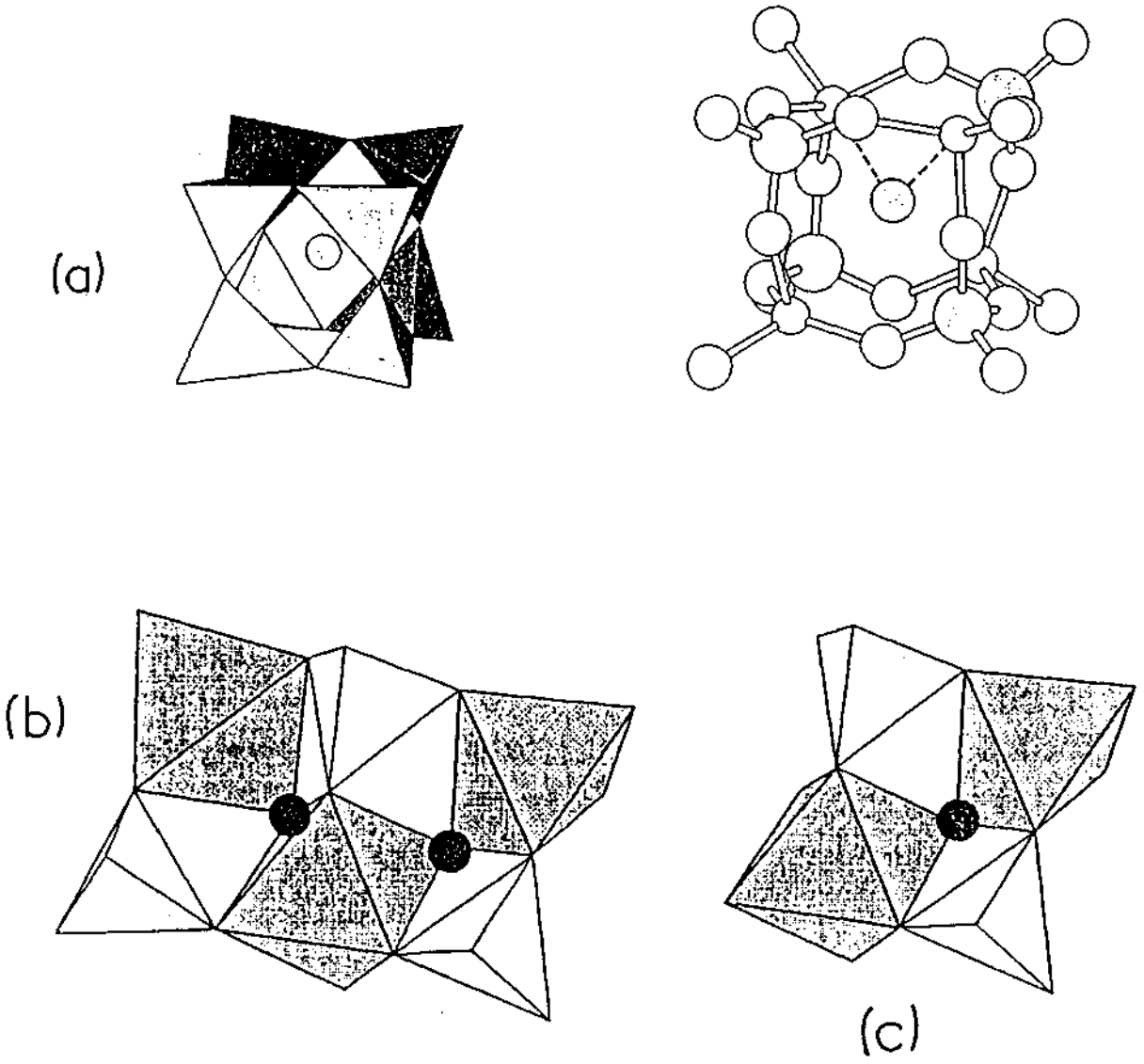

Fig. 1.4. (a) D4R cage with an encapsulated fluoride anion; (b) $[M_3P_3]$ hexameric unit; (c) $[M_2P_2]$ tetrameric unit in gallium fluorophosphates.

phosphates ULM-n.[27,28] In this family the basic building units are either tetramers commonly found in many phosphates,[29] or hexamers (Fig. 1.4b and c). For the tetramers connection of the metal atoms is by means of corner- or edge-sharing fluorine atoms. The hexameric unit is quite common in fluorinated materials. It is composed of centrally coordinated Al or Ga linked by two Al or Ga atom with the trigonal-bipyramidal coordination, through flourine. The trimer is capped by three phosphate groups. The connection of these hexamers generates different structures such as ULM-3 or ULM-4 where channels are delimited by 10-ring windows. The hexameric unit can be found with other building units, such as D4R rings in ULM-5[27] (Fig. 1.4a) or the double crankshaft chain in ULM-16. Both these materials possess extra-large 16-membered channels. Another example of a material built only with hexameric units is TREN-GaPO.[31]

Indium, in comparison to smaller sized Al and Ga, which favour 4-, 5- and 6-fold coordinations, prefers to be octahedral. The first report of indium phosphate came from Haushalter,[32] which was templated with ethylenediamine molecules. Several other indium phosphates have followed this work with various amine molecules,[33-35] including a pillared layer structure obtained with imidazole.[33] Other structures, analogous to known minerals have been isolated.[36,37] There are also fluorinated indium phosphates. One of the three-dimensional fluorinated indium phosphate $[In_9(PO_4)_6(HPO_4)_2F_{16}]$, is characterized by presence of high-fluorine content and possesses large 14-ring channels adjacent to 8-ring channels.[38]

Interest in the incorporation of metal ions came up primarily due the implications these solids may have as catalysts. AlPOs can tolerate a higher degree of elemental substitution into the tetrahedral cation sites, giving rise to MeAPOs[39] (Me = Li, Be, Mg,[40,41] Zn, B, Ga, V, Cr, Mn, Fe, Co,[39] Ni, Ti,[42] Ge, and As). It is also possible to introduce silicon into a number of $AlPO_4$ materials to produce SAPO.[39] Substitution of metal in SAPO leads to (metalsilicoaluminophosphates (MAPSO-n).[43] The role of the element substituted

in structure direction can be judged from the fact that SAPO-37 and SAPO-40 have been prepared only in the silicon-containing system. MeAPO-36, on the other hand, has no known $AlPO_4$ or SAPO equivalent (Fig. 1.5). MeAPSO-46 synthesis requires the presence of both the metal (Co, Fe, Mg, Mn or Zn) and silicon to form the structure. Unlike SAPO molecular sieves in MAPOs the metal ions substitute exclusively for aluminum rather than for Phosphorus. The net result of such a substitution is a neutral framework (when M^{3+} is substituted for Al^{3+}), or an anionic framework structure (where M^{2+} substitutes for Al^{3+}). Such materials exhibit ion exchange, and acid-type catalytic properties.[44] The thermal and hydrothermal stability of these materials is lower than that of parent $AlPO_4$ and SAPO molecular sieves. To date there are no structurally new synthetic metallosilicates prepared, but the same does not hold true in case of MAPO systems. A lot of reports exist on the synthesis of cobalt substituted aluminum and gallium phosphates.[45-48] Many of these substitutions result in the formation of zeolitic frameworks and some of them are hitherto unknown.[49,50] The work has also been extended to other divalent metal ions. Another noteworthy feature is that apart from tetrahedral geometry metal ions also sometimes, occupy octahedral geometry as in $NH_4[CoGa_2(PO_4)_3(H_2O)_2]$[51] and the cobalt-aluminum phosphate $CoAl(PO_4)_2.en$.[52] In the manganese-gallium phosphate, the manganese ion is in square-pyramidal geometry.[53] On a whole the ability of the transition metals to appear in variable coordinations leaves a lot of room to explore the synthesis of the pure-transition metal based molecular sieves.

1.5 Transition metal phosphates

Transition metal ions with d-electrons display a wide variety of electronic and magnetic properties. With a view to exploit these properties, considerable effort has been diverted in past few years, towards the synthesis of transition metal phosphate frameworks. Some of the prominent transition metal phosphate-based frameworks are discussed below.

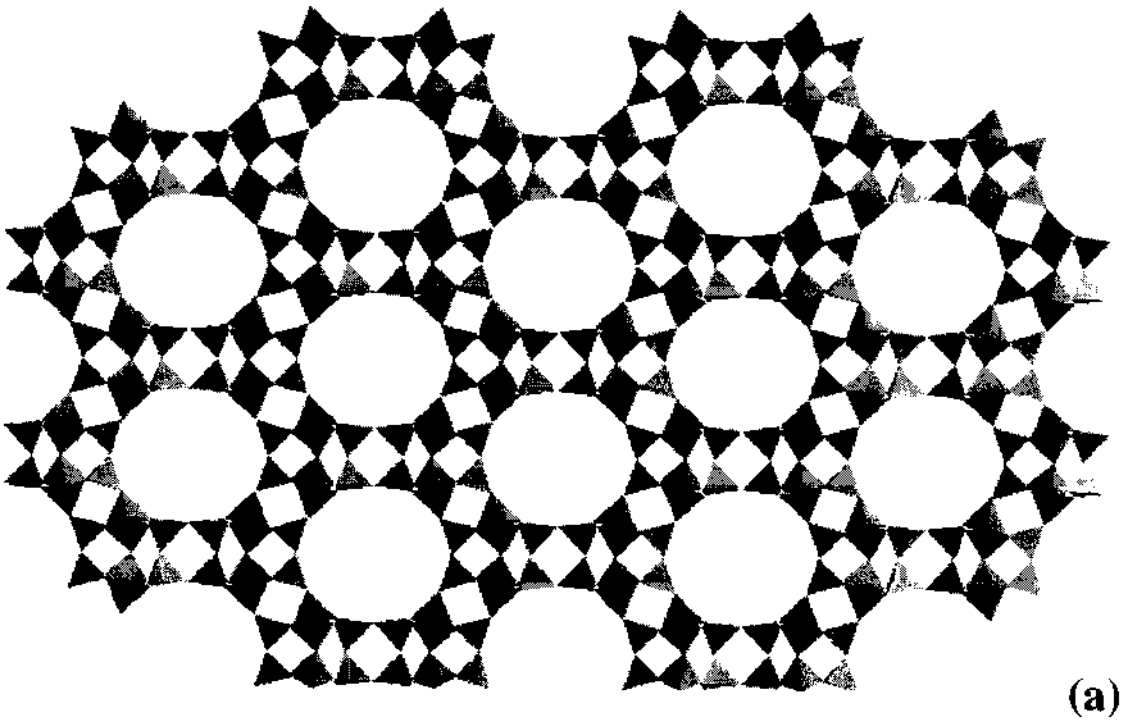

(a)

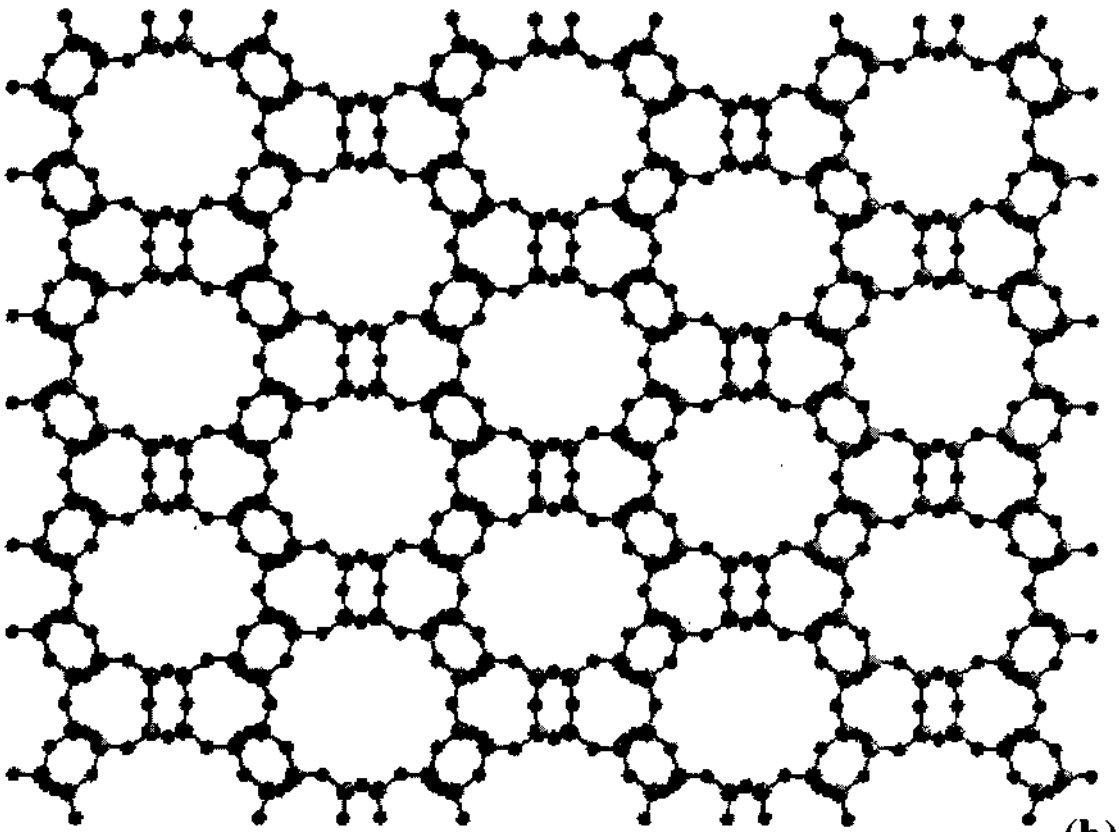

(b)

Fig. 1.5 (a) Polyhedral structure of SAPO–40 molecular sieve. (b) Ball and stick representation of MAPO–36.

Molybdenum Phosphates : The first reduced molybdenum phosphates were studied by Haushalter and Raveau groups.[54,55] The first few phosphates were synthesized by conventional solid state methods. In the series of high temperature materials inorganic cations are accommodated in the condensed frameworks with various architectures. These solids were classified on the basis of molybdenum polyhedra.[54] Class I involves structures in which the MoO_6 are isolated from each other, and octahedra have long (≈2.5 Å) and short (≈ 1.65Å) Mo-O distances. Five of the oxygens are shared with PO_4 tetrahedra whereas one is terminal. Class II is characterized by infinite $[MoO_{6/2}]_\infty$ octahedral chains in which long and short bonds alternate. All the four apices are shared with PO_4 tetrahedra. All these high temperature MoPOs show very poor ion-exchange properties. Later Haushalter et.al. prepared some of the molybdenum phosphates with open-frameworks via hydrothermal methods at temperatures of 200-400°C.[55] Several other solids were also synthesized later in the same way by changing the template, they contain a third form of octameric unit described in leucophosphite[56] and spheniscidite,[57] in which central tetramer is composed of two edge-sharing octahedra on the edge of which are grafted two other octahedra over shared corners. Finally, another open-framework topology was obtained when mixture of inorganic and organic cations is used in the synthesis medium. The oxygen linking the layers, is replaced by a phosphate group in this solid.[58]

Vanadium phosphates: Another interesting candidate is vanadium, which is important in many catalytic materials, and the phosphates of it were synthesized using both high temperature and hydrothermal means. The association of V oxidation states (V, VI, and III) with various polyhedra (tetrahedra, square pyramids, distorted and regular octahedra) leads to a large diversity in the resulting structures. A comprehensive list of references of the work done by various workers can be looked into ref. [59]. The successful hydrothermal methods for the synthesis of these solids in presence of organic templates were applied by Haushalter[60] and Ferey.[61] Two noteworthy compounds appeared from these studies. a) The first inorganic double helix in $[(CH_3)_2NH_2]$

$K_4[V_{10}O_{10}(H_2O)_2(OH)_4(PO_4)_7].4H_2O$,[60] b) the existence of giant voids in the two square-pyramidal-tetrahedral framework vanadium phosphates $Cs_3[V_5O_9(PO_4)_2].xH_2O$ and $[NH(CH_2\text{-}CH_2)_3NH]$ $K_{1.35}\text{-}V_5O_9(PO_4)_2].xH_2O$.[62] Besides these compounds a mixed valence material synthesized needs special mention, $(H_2en)_3[V^{III}(H_2O)_2(V^{VI}O)_8(OH)_4(HPO_4)_4(PO_4)_4(H_2O)_2].2H_2O$.[63] Ferey et.al., have employed the fluoride route in the synthesis of vanado(V)flurophosphate.[64]

Iron Phosphates: The mineral Cacoxenite is a naturally occurring framework Iron phosphate, which contains cylindrical tunnels occupied by water molecules, with a free diameter of 14.2Å.[65] Ferey[28] and coworkers extended the fluoride route to iron phosphates and first iron oxyfluorides were synthesized in 1996.[66] The oxide homologues of iron phosphates were synthesized by group of Lii.[67] The building units encountered in iron phosphates are Fe_4P_4 octamers. In case of fluorinated iron phosphates fluorine resides in the center of the octamer whereas in oxidic iron phosphates a Fe_4P_4 cube with surrounding a central μ_4-oxygen is with bridging oxygens approximately on each edge of the cube is found. This topology is also known in cloverite,[11] octadecasil[68] and ULM-5.[31,69] Many of these are either pure Fe^{III} or mixed valence Fe^{II}/Fe^{III} solids. These solids display interesting structural features analogous to that of gallium compounds. In the hexamer, two of the three iron ions are octahedrally coordinated, including a water molecule in the coordination, while in the dimer, a square pyramidal coordination of Fe is observed with just one aqua ligand. The corner-sharing assembly of these oligomers defines the 8-ring channels in which DABCO ions are housed. The main interest in these ferroflurophosphates concerns their magnetic properties. Despite the existence of isolated clusters linked by phosphate groups, three-dimensional magnetic ordering takes place in the range of 15-40K, with either antiferro- or ferri-magnetic properties.

Cobalt (II) phosphates: Cobalt (II) can exhibit tetrahedral, octahedral and five-fold coordination with equal fervor. Moreover, magnetic coupling can give rise to interesting magnetic properties, similar to those described for Iron phosphates.

Also Co^{2+} doping enhances the catalytic performance of certain zeolites and related compounds. This property has led to many reports of Co^{2+} doped alumino-, gallo-, and zincophosphates.[70,49] The first success[71] in synthesis of pure cobalt phosphate concerned the pseudo tetragonal three-dimensional material $CoPO_4.0.5C_2H_{10}N_2$. The framework consists of three systems of channels with 8-ring windows limited by Co and P tetrahedra in strict alternation. The channel size is around 3.9 x 4.7Å and it becomes anti-ferromagnetic at 2K. With higher diamines (1,3diaminopropane 1,4diaminobutane), the solids become two-dimensional.[72] One of the major contributions came from Stucky's group who focussed on the idea that structural similarities existed between cobalt phosphates and aluminosilicates, which had been recognized earlier in case of AlPOs. This led them to synthesize chiral cobalt phosphates of type $MCoPO_4$ where M= Na, K, Rb and NH_4^+.[73] These either exhibit zeolite Li-ABW structure type[13] with NH_4^+ and Rb^+, or a hexagonal structure, intermediate between the ABW and tridymite structures, with Na^+, K^+ and NH_4^+ cations. Despite the usually anti-ferromagnetic behavior of these $CoPO_4$ materials, the sodium compound is ferromagnetic at 2K.

Manganese phosphates with open framework are scarce, and the first compound has appeared recently from the group of Rojo.[74] Similarly, Nickel phosphates are still in infancy stage, and not many compounds are known except VSB-1, which shows interesting sorption, and magnetic properties.[75] The fluoride route has also led to the synthesis of zirconium and Titanium phosphates.[76-78] Titanium fluorophosphates are mixed valence with 7-ring channels.[78]

Zinc Phosphates: Zinc phosphates for the reason of their chemical similarity with Al^{3+} became the obvious case for study. Zinc adopts tetrahedral coordination and its oxide is amphoteric which is true also for aluminum compounds. In much of the work this strategy has been put to use. At the beginning of 1990s, the group of Stucky described the synthesis of zincophosphates and arsenates.[80] Most of these compounds were prepared under hydrothermal conditions, although some

of them were obtained under milder conditions –20 - 70°C. Their structures consist of vertex-sharing networks of MO_4 (M = Zn) and XO_4 (X = P, As) *tetrahedra, corresponding to anionic frameworks* $[MXO_4^-]$, *that are equivalent to* those encountered in aluminosilicates of composition $[AlSiO_4^-]$. By the use of alkaline cations several zeolite analogues have been synthesized, for example ZnPO, ZnAsO sodalites,[80,81] ZnPO faujasites,[82] ZnPO, ZnAsO ABW (Fig. 1.6a).[79,83] New topologies like chiral framework, $NaZnPO_4.H_2O$ (CZP),[84] and $A_3Zn_4O(XO_4)_3.nH_2O$ (A = alkaline, X= P, As) series[85] in which both Zn – O –P and Zn – O – Zn occur have been found (Fig. 1.6b). Certain of the zinc phosphates contain tetrahedral units with terminal hydroxyl groups (HPO_4^{2-} or/and $H_2PO_4^-$), thereby limiting the connection of these units to other MO_4 tetrahedra. Consequently, several three-dimensional topologies with interrupted networks have been prepared.[86-92] With the exception of few compounds like $H[Zn_4(PO_4)_3].H_2O$ and $(NH(CH_3)_3)[Zn_4(H_2O)(PO_4)_3]$,[92] the Zn/P ratio in these compounds is less than 1. A higher zinc content implies some Zn – O – Zn linkages; the bridging oxygen is in trigonal coordination with a link to a phosphorus atom. Such kind of M – O – M linkages with metal atom in tetrahedral environment are not observed in aluminosilicates or AlPOs unless the coordination exceeds to five or six. More recently, Harrison and Philips[93,94] have synthesized a series of zinc phosphates templated with guanidinium cations, which possess large 12-[93] and 18-membered[94] cavities. Although the Zn/P ratio is greater than 1 there is no Zn – O – Zn linkage present in these structures, only terminal Zn - OH_2 bonds occur, as was also observed in case of the zincophosphates templated by DABCO molecule.[87] In $N(CH_3)_4[ZnH_3(PO_4)_3]$[95] the three-dimensional network is characterized by one of the lowest framework densities so far for a microporous compound (10.1T atoms /1000Å^3).

1.6 Progressing from Silicates and Phosphates

The vastness of molecular sieves *per se* is not confined to zeolites and phosphate based materials, but comprise of a big family of porous octahedral manganese oxides,[96] all - carbon molecular sieves , pillared clays, aluminum

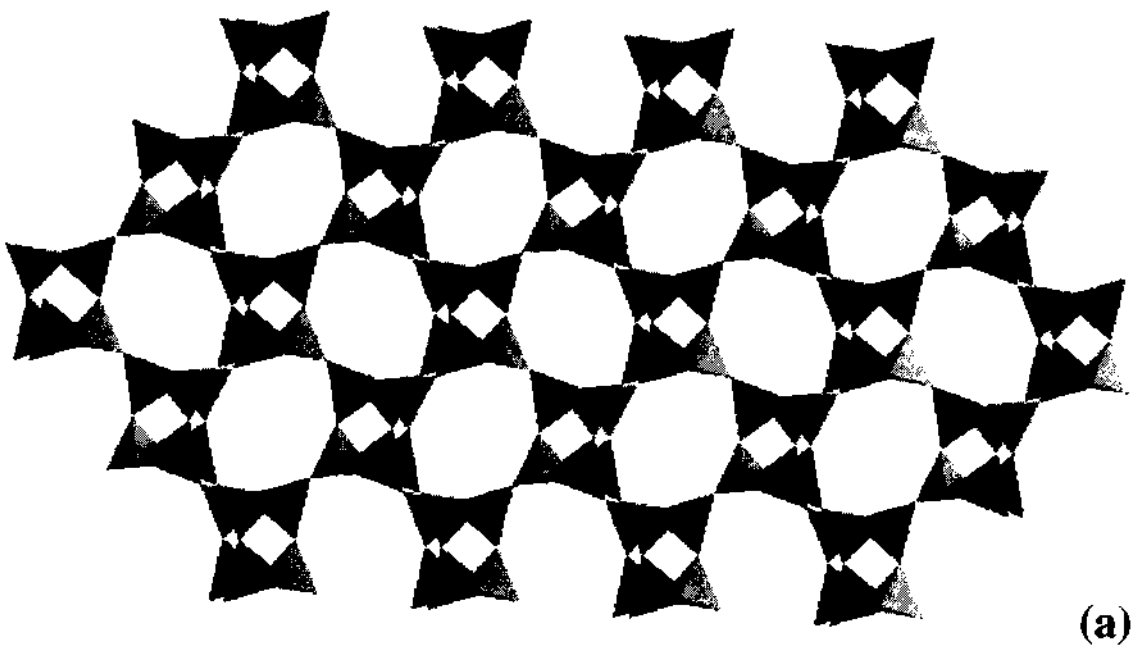

Fig. 1.6 (a) Zinc phosphate with ABW structure. (b) Zinc phosphates $A_3Zn_4O(XO_4)_3.nH_2O$ (A = alkaline, X = P, As) showing the Zn_4O clusters.

methyl phosphonates,[97] metal carboxylates,[98-101] hybrid systems like metal oxalate-phosphates,[102-105] chalcogenides,[106,107] halides[108] and nitrides[109] to name but a few. The range of the building blocks in these materials is not limited to just tetrahedra but includes other polyhedra, octahedra XO_6, pentacoordinated XO_5, or pyramidal XO_4 or XO_3. With the inclusion of lanthanides and heavier transition metals the scenario is going to be even more complicated with appearance of even higher-coordinated polyhedra.

1.7 Synthesis of Framework solids

Molecular sieves are almost exclusively synthesized under hydrothermal conditions at temperatures of between 100 and 250°C under autogenous pressure, under either strongly basic conditions (for zeolites), or weakly acidic or neutral conditions (for metal phosphates or derivatives). The versatility of the hydrothermal technique derives from the extremely effective solvating ability of water under these conditions. This allows the dissolution and mixing of the solid reagents to form an inhomogeneous gel in the initial stages of the reaction. At later times the nucleation centers are formed which subsequently grow as the reaction proceeds to form the final crystalline product. The hydrothermal reaction has a number of reaction variables which include time, temperature, pressure, reactant source and type, pH, the inorganic or organic cation used, aging time of the gel, reaction cell fill volume, and so on.[6] Since, in general, variation in one of these parameters can have an effect on several others, it makes it difficult to evaluate the effect of a parameter independent of others. A greater understanding of the processes occurring during the course of a hydrothermal reaction is highly desired as this may lead to a more rational approach to the synthesis of these solids. Nevertheless, despite these difficulties, certain guidelines for the effect of various reaction variables on the course of reaction can be laid down.

It has been observed that with the rise in temperature, solids with low intra-crystalline voids and lower water content are formed. This is due to

exponential increase in vapor pressure of water with rising temperature. With even higher temperatures sometimes the formation of thermodynamically stable condensed phase results. Changing the composition changes the concentration of the both the solid and the solution phases, thereby affecting the nature of the final phase formed.

Molecular sieves are thermodynamically metastable phases, which are unstable with respect to dense oxide phases. It is therefore clear that formation of these solids must involve strong kinetic influence. Hence, with the passage of time the kinetic phases formed give way to the thermodynamically stable phases. For example zeolite A converts to more stable sodalite after long reaction times and if left further forms condensed aluminosilicate.

The nature of the cation (organic or inorganic) has also a great effect on the chemical composition of these materials. Like use of alkali metal cation results in synthesis of aluminum rich zeolites, but use of organic cations results in solids with higher silicon content. This makes sense, because for large size organic cations where charge per unit surface area is small and it can support less negative charge on the framework, hence less aluminum substitution thereby leading to silicon rich framework.

The synthesis of phosphate based-molecular sieves and other derivatives follow the same principles as for zeolites, with the important difference that phosphate based molecular sieves are always synthesized under either acidic, neutral or mildly basic conditions as opposed to the strongly alkaline conditions used in the synthesis of zeolites.[15,110,111] The synthesis pH lies in the range 4.0 – 6.5 and temperatures are in the range 130-200°C. Phosphate based molecular sieves are mostly synthesized in the presence of organic amines or alkylammonium ions. The exception to this is VPI-5,[17] which can be synthesized under certain conditions in the absence of any structure-directing agent.[112]

1.8 Organic templates and their role

The concept of templating emerged because of the close correlation between the size and shape of the template and the shape of the cavities formed. For example in the synthesis of high silica ZSM-5 using the tetrapropylammonium cation as the organic species, the cation is located at the intersection of the two intersecting channel systems with, four long alkyl chains lying along the four individual channels.[113] This strengthened the notion of templating where oxide tetrahedra condensed around the organic molecule to form the solid of particular geometry.[114,115] This situation however, is not as simple at it appears because, ZSM-5 can be synthesized in the absence of any organic molecule,[116] not only that it can also be synthesized with atleast 22 different organic molecules. Furthermore, the correlation between the template shape and pore shape is often weak. In case of AlPOs too the same structure $AlPO_4$-5 can be synthesized using 20 different templates. Interestingly very large-pore based molecular sieves (e.g. VPI-5,[17] JDF-20,[117] $AlPO_4$-8,[118] cloverite,[11] ULM-5[30] and ULM-16[119]) have all been synthesized using relatively small organic molecules. This leads us to conclude that the effect is not a true templating. A more clear perspective was put forth by Davis and Lobo[4] in their review where they suggested that organic molecule can act in three-distinct ways: *as space filling species, as structure directing agent and true templates.* Space filling refers to situation where organic excludes water from the voids in the zeolitic framework to avoid unfavorable energetic interactions between solvent and growing molecular sieve. In ZSM-5 and $AlPO_4$-5 the organic molecule just acts as a space-filler.

Structure-direction is implied when a particular organic molecule results in a unique structure, which cannot be synthesized by other templates. Gies and Marler did a detailed study on the effect of organic templates on crystallization of porosils.[120] They concluded that, since no ionic interactions are present between the guest molecules and the framework, hence the closeness of the geometrical fit, must be due to an optimized arrangement of the inorganic around

the organic to maximize the van der Waals interaction. These results were supported by solid state NMR measurements of Burkett and Davis which suggested the presence on non-covalent interactions between the organic molecule and silicate species.[121] Since $AlPO_4$ frameworks are neutral this must also hold true for them. For other phosphate based molecular sieves there is a finite possibility of role of ionic interactions too.

Examples of true-templating in strict sense are very rare and one such notable example is the formation of zeolite ZSM-18. This was first synthesized using the triquaternary amine $[C_{18}H_{30}N_3^{3+}]$.[122] The extremely close registry between the shape of the organic molecule and the shape of the pore system in ZSM-18 suggested true templating, which was confirmed by Energy minimization calculations performed by Davis and Lobo,[4] wherein the template is held in a cage that has the same three-fold symmetry as that of the organic template and the organic molecule is not able to rotate inside the cage. It is obvious that the role of organic is still not entirely understood and it is still a matter of debate and discussion.

1.9 Mechanism of formation of molecular sieves

Although the mechanism of zeolite synthesis is not available, there is a reasonable proposal explaining the formation. The reaction involves organization of silicate anions around the additive (organic template) to form solution complexes that form the basis of nucleation centers from which the zeolite crystallites form. Van der Waals' interactions between the framework species (the silicate anions) and the templates provide the enthalpic driving force for the reaction, while the release of ordered solvent back into the bulk provide the entropic driving force.

There are two extremes by which this reaction can take place, from a clear solution where all the starting materials are fully dissolved (the solution mediated transport mechanism), or from the dissolution and recrystallization of

an amorphous gel which is in contact with the liquid phase (solid phase transformation mechanism). Examples of both types of processes are known, and some zeolites have shown to form from either mechanism depending on reaction conditions.

A lot of work has been done in probing the mechanism of formation of zeolitic solids by employing various spectroscopic techniques. One of the experiments performed by Burkett and Davis investigated the mechanism of formation of Si-ZSM-5. By employing ^{1}H-^{29}Si CP MASNMR between the protons of the NPr_4^+ and the silicon atoms of the zeolite precursors they were able to study the interactions between inorganic and organic components.[121] They found the presence of short-range molecular interactions in the synthesis gel prior to the evolution of long range order in crystalline solid. Furthermore, they also showed that the conformation adopted by NPr^{4+} to be similar to that present in the final product. Burkett and Davis provided the first direct evidence of preorganised organic-inorganic composite structures during the synthesis of Si-ZSM-5. Further work on the same system allowed them to refine their proposed mechanism.[123-125] As shown in Fig. 1.7, they suggested that formation of the organic-inorganic composite is initiated by overlap of the hydrophobic hydration spheres around the NPr^{4+} cation[126] and hydrophobically hydrated domains of soluble silicate species. (Hydrophobic hydration is the reorientation of the water molecules in the vicinity of a hydrophobic solute species in order to accommodate them whilst still maintaining a fully hydrogen-bonded network.)[127] This allows the establishment of favorable van der Waals contacts between the alkyl chains of the NPr^{4+} and the hydrophobic silica species, whilst at the same time allowing the release of the water molecules from the ordered hydration spheres around the NPr^{4+} and silica species. This process provides both and enthalpic and entropic driving force for the formation of organic-inorganic species, which provide the precursor units for the formation of the final crystalline product. The crystal growth is presumed to occur via diffusion of these composite species to the growing crystalline surface in a layer-by-layer

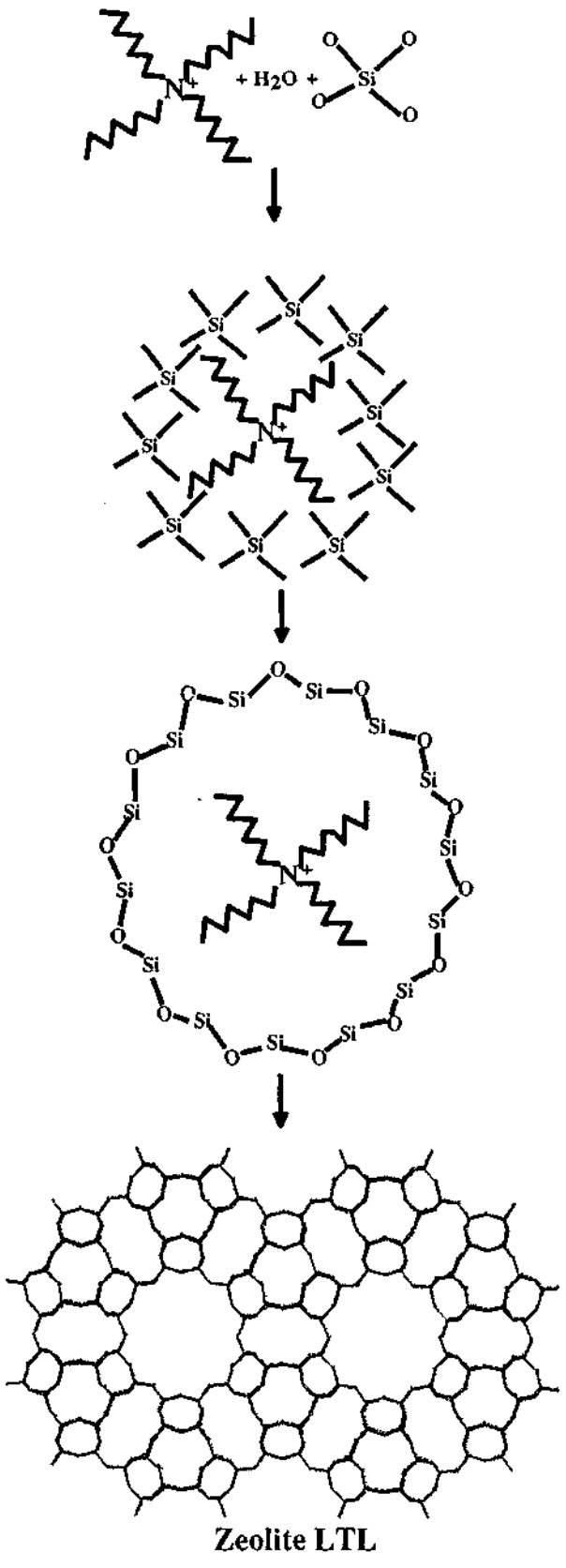

Fig. 1.7. Schematic representation of a model zeolite. Adapted from the work of Davis and Lobo [4].

growth fashion which is consistent with known layered intergrowth structures such as ZSM-5/11[128] and SSZ-26/33/CIT-1[129,130]. In the formation of Si-ZSM-5 and Si-ZSM-48 using 1,6-diaminohexane as the organic SDA, at lower temperatures, (120°C) ZSM-5 is formed. Organic and inorganic component interactions are observed during the synthesis suggesting the formation of inorganic-organic composites prior to the formation of long range ordered material. At higher temperature ZSM-48 is formed and no interactions are seen between inorganic and organic components. This can be interpreted as the formation of hydrophobic hydration spheres is feasible at lower temperatures but higher temperatures can disrupt them. The question which, remains unanswered, is whether the ability to form a hydrophobic hydration spheres is a prerequisite for a particular organic molecule to serve as a SDA. The mechanism of formation of aluminophosphates and related class of solids has not been studied thoroughly. Its considered that in case of aluminophosphates first the reaction of aluminum source (usually pseudo-boehmite or aluminum alkoxide) occurs with phosphoric acid to form an amorphous aluminum phosphate layer.[131,132] The next stage, which is still unclear may involve either a solid-state transformation or a complete dissolution of the aluminophosphate layer occurs to produce small solution phase building units, which subsequently recondense to form the final product.[28] There is some evidence for the existence of aluminophosphate entities in solution, but there is little evidence that these species are the direct precursors of the final crystalline product. More recently, Ozin and coworkers[133] have proposed a model for the formation of aluminophosphates in which two and three-dimensional structures are formed via hydrolysis and condensation of an initial chain structure, which forms first in solution (Fig. 1.8). Whilst there is compelling evidence for the transformation of chain structures to layered structures in some systems studied,[134] it is far from clear at this time as to what pathway is in the formation of framework phosphates and related materials.

An alternative approach, has been to use computational techniques and molecular modeling as tools, to probe the relationship between the template

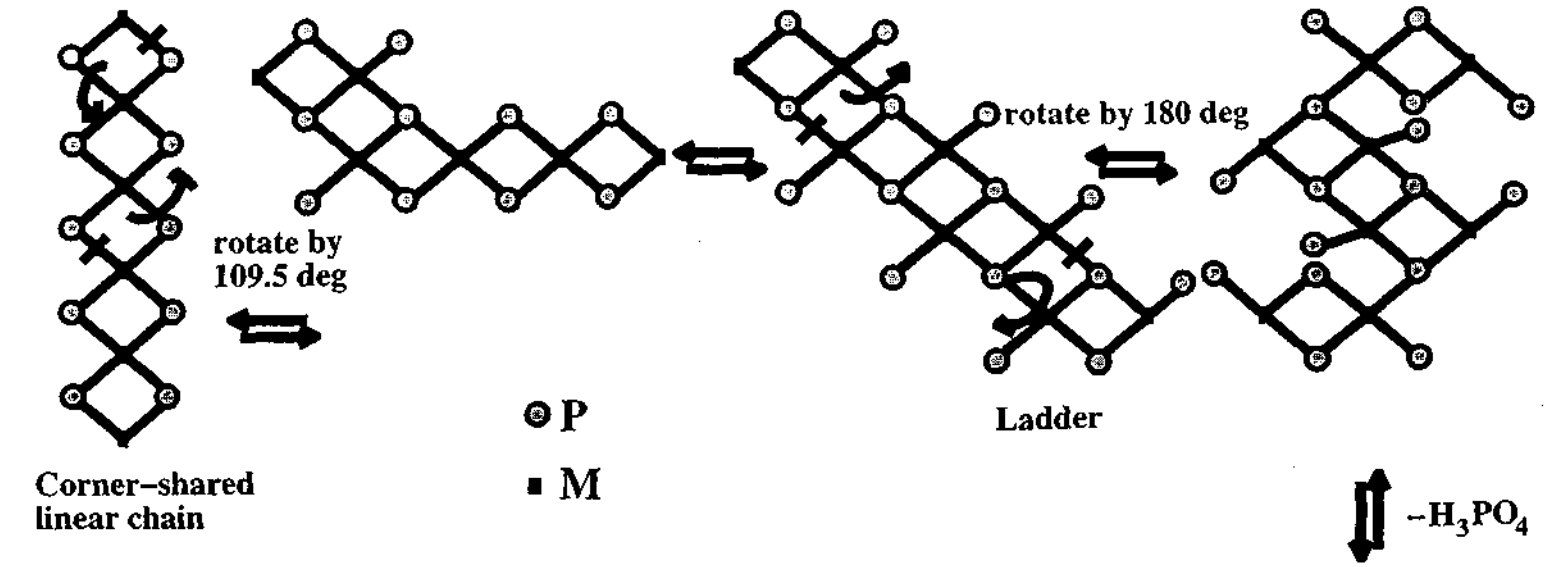

Fig. 1.8. A Possible scheme for the transformation of a linear–chain into a layer architecture via a ladder structure and from there on to a 3D structure.

molecules and the inorganic framework.[135] Molecular mechanics studies have yielded some information on how a particular organic molecule can act as a template for a given host structure, and therefore be used as a guide for selecting an effective template for a given target framework structure.[136-141] Recent work of Lewis and co-workers[142,143] has made the 'rational' design of a target microporous material a much more realizable goal. They have developed 'de novo' molecular design methodology in which potential template molecules are 'grown' from an initial seed molecule. The potential templates thus grown are ranked according to their binding energy within a given pore system, which gives a good guide to the likely effectiveness of a particular organic molecule as a template for that molecular sieve structure. A good example of this was provided by Lewis et.al.[144] when they successfully synthesized DAF-5 (a CoAPO with chabazite structure) using a computationally designed template 4-piperidinopiperidine. Whilst the experimental studies have shed light on the processes occurring during the hydrothermal syntheses, and revealed details of mechanisms of crystal nucleation and growth in numerous specific cases but an overall mechanism of formation is still unavailable. Given the range of applications the molecular sieves offer a more complete mechanistic understanding of their formation leading to a more rational approach to their synthesis is still a highly sought after goal in materials science. The lack of universal crystallization mechanism for molecular sieve material, forces one to employ a range of techniques to study them which are often unambiguous. The trend of today is to employ non-invasive 'in situ' studies to probe the course of crystallizations, which are capable of delivering more and accurate information. Cheetham and Mellot[145] have recently reviewed the application of in situ techniques to the study of a wide-variety of materials synthesized from sol-gel precursors.

1.10 Characterization of framework solids

Characterization is one of the essential steps in the science of framework solids. While *single crystal x-ray crystallography* employing single crystals has

contributed immensely to our understanding of these complex structures, many other techniques have also been employed to great benefit. The first and foremost of the techniques employed is X-ray powder diffraction.

X-ray diffraction: Powder X-ray diffraction indicates uniqueness in the structure, as the powder diffraction pattern is a fingerprint of a crystalline solid. The most important information about the solid obtained from the powder diffraction patterns is as follows:

(1) successful (or unsuccessful) formation of a crystalline material,

(2) presence of a single phase or mixture of phases,

(3) In the absence of single crystals with the presence of sufficient peaks, the identification of the structure type or structure types comprising the mixture is possible.

(4) With proper techniques from a good powder data structure solution is also possible (employing Reitveld refinement).

The x-ray powder diffraction pattern is usually recorded for these materials between 5° and 40° 2θ, at higher angles than 40° 2θ, the peaks have very low intensities depending on the degree of crystallinity. Many a times it is possible to pick up the different phases present in diffraction pattern in case the pure powder patterns of the individual phases are known. Changes in peak intensities occur:

(1) upon removal of an organic additive from the pores or changing the cations within the pores of the higher-silica containing materials,

(2) upon changing the counter-ions,

(3) when large crystals have a preferred orientation in the X-ray sample holder, and

(4) when other ions are substituted into the framework structure.

In many cases where structure elucidation becomes unfeasible because of the lack of single crystals, twinning within the crystals, faulting, pseudo-symmetry, disorder, and impurity problems structure determination from powder

methods is the sole method. Structure-solution form powder data is a nontrivial task and has lot of difficulties involved. Non-resolved or overlapping peaks result in poor data, impeding the attainment of reliable structure information. The usual process involves model building, testing of the model for the observed symmetry and crystallographic unit-cell dimensions. Later on the geometry-optimized model is used to calculate the powder-diffraction pattern. The pattern can be compared with the experimentally observed one. These simulated structures can be obtained using Distance Least Squares (DLS) programme.[146,147] The production of a reasonable model is not the structure solution, it is only a creation of a feasible structure proposal. A powder pattern comparison of the model and the observed solid can only tell the correctness of the chosen model. The successful refinement of the model with the measured diffraction data is necessary for structure solution. Since many a times the materials are polycrystalline the preferred method is Reitveld refinement[148] (whole pattern refinement). Since framework models are generated in the highest possible space group, refinement is also necessary to establish the correct symmetry. The most informative way of judging the goodness of fit of a Reitveld refinement is a visual inspection of a plot of the intensity versus 2θ of the entire observed, calculated and difference patterns. Inconsistencies in fit can be rapidly detected in if they are confined to certain regions such as low 2θ, or if certain peaks show intensities that may be poorly matched by an imperfect peak shape function, for example. In cases where the framework topology is known, further information can be obtained about the locations of cations, water, and sorbate molecules that occupy extra-framework positions by Fourier method, where the phases of the structure factors, calculated with the framework atoms only, are assigned to observe structure factors, a technique referred to as the "heavy atom" method. From the resulting electron density map, the extra-framework atoms that fully occupy specific sites can be determined, and with further calculations the "not-fully-occupied" ones can also be determined.

Solid State MASNMR: The unique and important structural information that cannot be derived from any other techniques such as x-ray diffraction (XRD), may be obtained from solid state NMR measurements. MASNMR can provide information on distinct local orderings in solids whereas XRD measurements yield only their averages. It is not just useful in studying the structure but it can also give information on the dynamic processes.[149] Figure 1.9a illustrates the types of information which, may be derived from NMR signals.

Site Identification: Nuclear spins (of specific isotopes) at atomic sites in a molecule, in a crystalline lattice, in a glassy material, or on a surface can be associated with NMR spectral lines at characteristic frequencies that depend on the atomic environments of the spins. Among the interactions that determine the NMR frequencies are influenced by interactions between the nuclear spins and electrons in the surrounding localized orbitals (chemical shifts) or metallic conduction bands (Knight shifts). In addition the NMR frequencies are influenced by the interactions between the nuclear spins and the spins at other atomic sites (electron mediated or dipole-dipole couplings) and those between the electric-quadrupole moments of the nuclei and electric field gradients arising from the surrounding atomic charge distributions (quadrupole shifts and couplings). Chemical and Knight shifts can be used to distinguish different Si and Al sites in zeolites.

Intersite correlations: Beyond the site occupancies it is possible to investigate interatomic correlations in chemical systems by observing spin-spin couplings and by exploiting the transfer of spin polarization and coherence between sites. Such coherence are often discernible in multidimensional spectra.

Dynamics and Reactions: The effect of motion on NMR signals can be observed both directly in the spectra and indirectly through spin relaxation. The range of time scales accessible by NMR is enormous, from molecular reorientational correlation times of picoseconds to solid impurity diffusion of hours. Over short-time scales, it is the rapidly fluctuating local fields at the sites of nuclear spins,

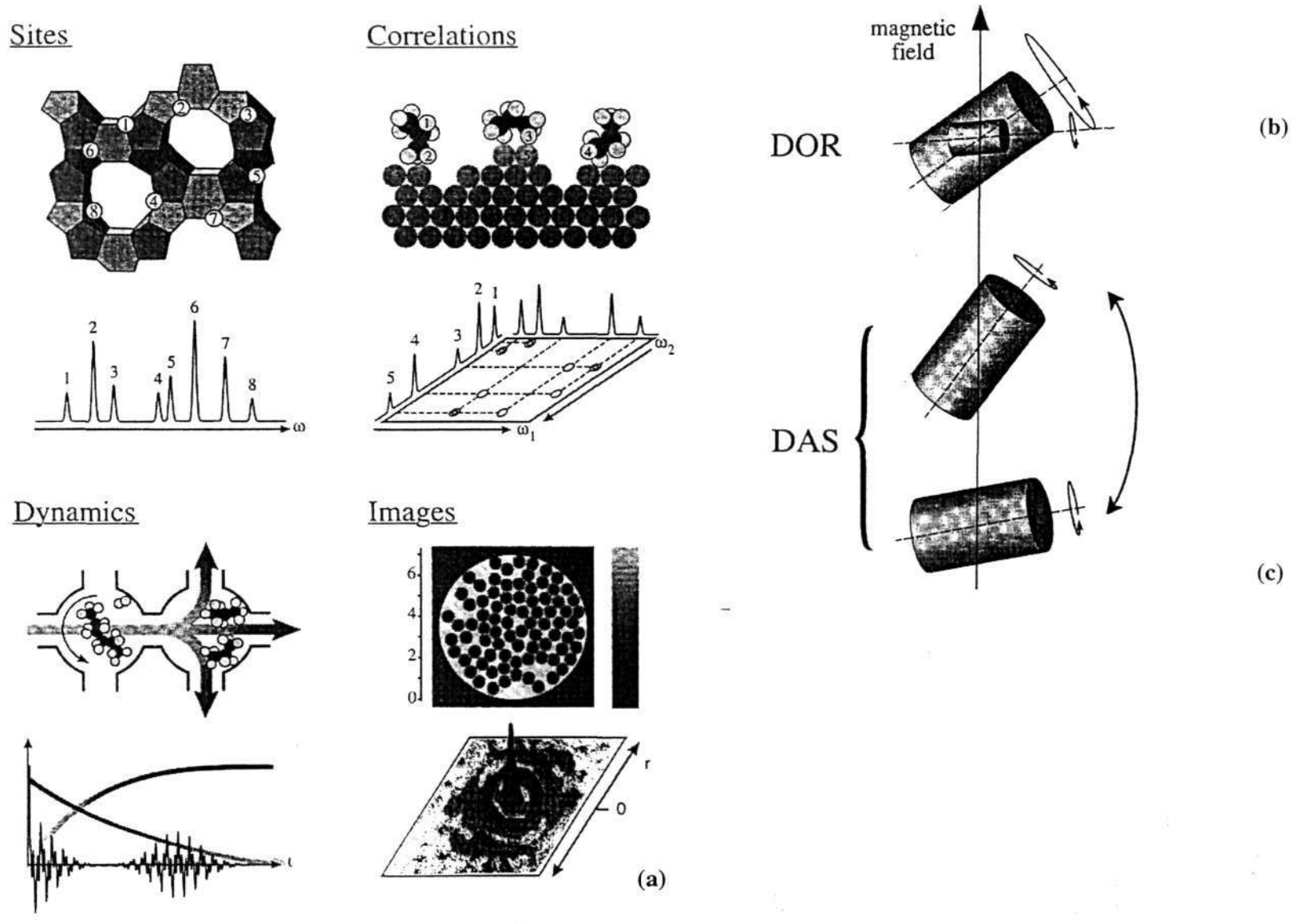

Fig 1.9 (a) Various types of information derived from NMR spectroscopy. Schematic representation of the two averaging second–order interaction: (b) double rotation and (c) dynamic–angle spinning.

due primarily to molecular motions and paramagnetic centers, that are responsible for spin-lattice relaxation and spin-spin relaxation. Over intermediate to slow time scales, the effect of motion arising from the reorientation of molecules or from chemical exchange or reactions can be observed by multidimensional NMR spectra through the appearance and time-dependence of off-diagonal peaks. It is also possible to follow atomic and molecular translational diffusion both within a particle and between the particles by observing attenuation and phase shifts of spin echoes using pulsed magnetic field gradients.

Imaging and Microscopy: NMR in presence of magnetic field gradients makes it possible to obtain images of spin density inside intact samples.

All the atoms making up the zeolite lattice have NMR active isotopes ^{29}Si (4.7%), ^{27}Al(100%) and ^{17}O (0.04%). Because of low natural abundance of ^{17}O isotopic enrichment is usually necessary. The 100% abundant nucleus is present in phosphate based framework solids. In addition ^{1}H (100%) may be present in any of the framework structures in OH groups at defect sites. ^{29}Si and ^{31}P are spin ½ nuclei and MAS yields particularly simple spectra with complete averaging of the chemical shift tensor components. The average "isotopic" shift values are field independent and correspond to solution chemical shifts. ^{27}Al and ^{17}O are quadrupolar nuclei with non-integral spins greater than 1, and their solid-state spectra are often quite complex. Various complicated spinning techniques have been introduced to average the anisotropies in the spectra of quadrupolar systems, which help in elucidation of local microstructure. ^{1}H MASNMR yields information about the proton sites present in the material, which is of great interest in studying the acidic nature of the proton. ^{17}O MASNMR spectra are important from the point of view of the lattice structures. The static spectra here are more informative as the quadrupolar effect is dominant. That is, "resolution" should be considered here as the relative separation of spectroscopic features and not width of the resonances.

A more promising development relevant to quadrupolar nuclei has been the introduction of experiments in which the spinner axis undergoes a time dependent trajectory with respect to the magnetic field axis namely double rotation (DOR) and dynamic angle spinning (DAS). In DOR the axis of the rotor is moved continuously in a cone by placing the sample in a spinner within another spinner (Fig. 1.9b). By correct choice of angles for the two spinner axes, second order effects are averaged.[150] Under DAS, the sample is contained with in a single spinner but the orientation axis of the spinner is switched between two discrete angles relative to the external magnetic field as shown in Fig. 1.9c. Sets of complementary angles are available, but different times must be spent by the sample at each of the orientations depending on the particular pair of angle chosen.[151]

Infrared Spectroscopy: Infrared (IR) spectroscopy can yield information concerning the structural details of the material. In addition, it can be used to confirm the acid characteristics and isomorphous substitution, as well as aid in relating different materials by their common structural features. The mid-infrared region of the framework contains fundamental framework vibrations of the $Si(Al)O_4$ groupings. These vibrations include asymmetric and symmetric stretch, double ring vibrations, T-O bending modes, and possibly pore opening modes. The infrared spectrum can be classified into two groups of vibrations: (1) internal vibrations of the framework TO_4, which are insensitive to the structural variation: and (2) vibrations related to the external linkage of the TO_4 units in the structure. The latter are sensitive to structural variation. A shift in the asymmetric and symmetric vibrations has been observed in the mid-IR region with successful incorporation of P, Ga, Fe, B and Ti into the silicate structure. Boron substitution results in lighter mass of the Si – O – B oscillator compared to that of Si – O – Si(Al) and hence appear at higher wavenumber.[152] The bands characteristic of the hydroxyl functions in the region of the infrared spectrum around 3000 cm^{-1} have been associated with the acidity and related acid

activities of the molecular sieves.[153] Presence of excessive amounts of water, can suppress the desired hydroxyl features.

High Resolution Electron Microscopy: The techniques discussed so far do not give direct information on localized structural features contained within the crystals. Whereas X-ray diffraction and other techniques provide spatially averaged information, electron microscopy can provide finer, and more detailed information on the subtle aspects of the framework structure. HREM can give information on the defects, pore arrangement, nature and extent of twinning in crystals etc.

Adsorption Properties: A property that has been utilized extensively in characterizing molecular sieve materials is the ability to adsorb selected molecules. From examination of adsorption properties, substantial information can be discerned about the molecular sieve material. The most fundamental characteristic is the pore volume of the individual molecular sieve. Several probe molecules have been routinely used to determine the pore volume, including oxygen, n-hexane, and H_2O. Other adsorbates that have been used include CO_2, Ar, N_2 and n-butane. Typically several different probe molecules are utilized to provide a more meaningful determination of the pore volume. The adsorption measurements are usually made on the thermally dehydrated samples. In case of samples where organic material is present prior treatment to remove the organic from the pores is necessary. Generally, the adsorption of probe molecules within the molecular sieves results in a type I adsorption isotherm; thus the void volume can be calculated using Gurvitsch rule.[154] The crystalline quality of a material can also be assessed from the adsorption measurements by comparison with materials which are defined to be 100% crystalline. Adsorption properties of the material have also been utilized to follow the course of crystallization, for example N_2 adsorption in mordenite.[155] To get the reliable information on pore openings of the pores and cages, the adsorption of various-size molecules is studied. The selectivity of the material for different-size molecules can help one

to rapidly determine if the pore system contains 6-, 8-, 10-, or 12-member rings. For example, the difference between the selectivity in adsorption for the *ortho-* and *para-* forms of ethyltoluene in silicalite. In large pore structures both the isomers are similarly adsorbed whereas in 10-ring ZSM-5, the *para-* isomer is adsorbed, while the larger *ortho-* is precluded from the interior of the crystal. Water adsorption in various solids can give information about the hydrophilicity / hydrophobicity of the interior surface. Pure silica base molecular sieves, graphitized carbon etc are hydrophobic where as zeolites and other phosphate based frameworks have hydrophilic interiors. Temperature programmed desorption (TPD) of ammonia is commonly used to measure both the acid site concentration and strength. In case of the phosphate based frameworks $AlPO_4$ molecular sieves display adsorption capacities for different-size molecules.[156] They exhibit intra-crystalline pore volume from 0.04 to 0.35cm^3/g and adsorption pore size from 0.3-0.8nm spanning entire range of pore volume and sizes known in zeolites and silica molecular sieves. These AlPOs show excellent molecular recognition properties. For example $AlPO_4$-20 admits only water but not methanol, $AlPO_4$-14 and $ALPO_4$-33 adsorb Xe (0.40nm) selectively over n-butane (0.43nm), while $AlPO_4$-17 and $AlPO_4$-18 adsorb parrafins (0.46nm) and excludes isoparaffins. $AlPO_4$-11 adsorbs cyclohexane (0.6nm) and rejects 2,2-dimethyl propane (0.62nm). In case of other phosphate based frameworks where template molecules (usually protonated amine molecules) help in maintaining electroneutrality of the framework, removal of them leads to collapse of the framework, There are however, cases wherein the water of crystallization occluded with in the channels can be dehydrated and rehydrated reversibly. In addition to this in some cases small organic molecules have been successfully adsorbed in place of water molecules. The inaccessibility of complete pore-space forbids adsorption methods to yield much significant information on the interior surface and pore characteristics in great detail, but the methods are still indispensable in obtaining the much sought information on the chemical nature of pores and surfaces of zeolites and other porous solids where it is accessible.

Thermal Analysis: Thermogravimetric analysis (TGA) is a readily available source of important information on the total free volume of a porous material, and possible template trapping sites, and therefore of possible structural sub-units. The temperatures at which templates are released serve as pointers to the interaction of the template with the framework, possible window size etc.

Other Methods: Apart from the above routinely practiced methods there are another whole gamut of characterization techniques which have been developed to yield highly specific and relevant information.[157] Some of these methods like X-ray absorption fine structure (EXAFS) and to a lesser degree X-ray absorption near-edge structure (XANES), yield information about local chemical environment and crystallinity of a material is not a prerequisite in these techniques. X-ray induced-photoelectron emission (XPS-ESCA) has been of comparatively little value in clarifying the structure of zeolites but has been quite important in establishing the chemical identity (oxidation state) of transition metal phosphate based systems. It has also yielded approximate elemental ratios in many cases. Some of the greatest opportunities have been conferred by Synchrotron radiation and these lie in the domain of X-ray diffraction.[158] Two approaches are possible. First advantage can be taken of the intense flux of X-rays and of smoothly adjustable wavelength for microcrystal diffraction. This method now is in routine use for structure determination from microcrystalline samples. Second prospect lies in undertaking an *ab-initio* determination of a hitherto unknown structure.[159] Recent developments show that *ab-initio* crystal-structure determination can in principle be carried out from the high resolution diffractometric data that synchrotron sources are now capable of yielding.[160] Unlike X-rays, which are scattered by the electrons of the atoms, neutrons are scattered by the nucleus. Consequently, the interference effects that cause X-ray scattering to diminish with ($Sin\theta/\lambda$) are absent with neutrons, and the scattering intensity shows no angular dependence. Scattering power is a nuclear property, hence it shows only a weak dependence upon atomic number and unlike X-ray scattering amplitude, it may vary dramatically from one

element to the next.[161] The neutron also has a magnetic moment, and magnetic scattering is observed from paramagnetic ions, in addition to nuclear scattering. These properties lead to the possibility applications of neutron diffraction in location of light atoms, especially hydrogen atoms, in the presence of heavy elements, the differentiation between adjacent elements in the periodic table, and the determination of the spin arrangements in magnetically ordered materials (e.g. antiferromagnets). Since flux of the neutron beam is relatively low compared with that of X-ray source, rather large samples (at least $1mm^3$) are required for single-crystal neutron diffraction experiments. Such crystals are certainly difficult to prepare; thus powder neutron diffraction techniques have been developed to a point where they can now be used to refine complex, low symmetry structures. A conventional refinement with structure factors obtained from single, integrated powder intensities is quite feasible for high-symmetry structures, but is clearly impracticable for low-symmetry materials because of overlap between adjacent Bragg reflections. Last but not the least Electron diffraction, which can always be recorded, is a very good method of narrowing down, if not unequivocally determining the space group for a high-symmetry structure. This is also invariably accompanied by the unit-cell dimensions, which are also readily retrievable from the diffraction patterns. To ensure the correctness many different zone axes are selected and diffraction patterns are recorded as a function of specimen tilt about one or more axes. Caution needs to be exercised concerning the occurrence of multiple scattering, which can lead the unguarded to arrive at the wrong space group. Local elemental analysis for $Z>10$ is achieved from the X-ray emission spectra which, with the aid of energy dispersive crystal detector can, under optimized conditions, yield quantitative results at a spatial resolution of some 50 x 50 x $100Å^3$. With the rapid developments in electron-energy loss spectroscopy (EELS) now underway, there are good prospects of being able to analyze elemental composition of all the elements heavier than lithium by electron microscopy. EELS also shows very considerable promise in being able to distinguish the coordination numbers of light elements such as Li, Be, B, I, Al and Si.

1.11 Applications of molecular sieves

The question of foremost important is why there is a need to synthesize such large number of open-framework solids. These microporous materials contain uniformly sized pores of few angstroms size, and can thus display molecular recognition, discriminating and organizational properties with atomic resolution (~1Å). It is this property which manifests itself in the various applications these materials perform.

The many advantages of zeolites as catalysts over other amorphous materials, are numerous, the more important being:

A high density of catalytic sites: Zeolites have very high density of catalytic sites in the intracrystalline surfaces.

Well defined active sites: Contrary to amorphous materials which display surface heterogeneity and a range of ill-characterized catalytic sites with varying activity and differing environment, zeolites being crystalline have regular structures with well defined sites. The locations of balancing cations in zeolites are often well identified.[162]

Molecular sieving properties: The space inside the zeolites is similar to the size of reactant and product molecules. This leads to shape 'selective catalysis'. Three varieties of shape selective catalysis are possible; (i) reactant selective catalysis in which reactants having dimension less than critical can have access to the pores, (ii) product selective catalysis, in which products below the critical size have ability to transport themselves out, (iii) transition state selective catalysis in which the reaction products may be governed by the inability of the transition state, for one of the several reaction pathways, to be accommodated in the available space. Shape selectivity may also occur as a result of mass discrimination. The bulkier molecules may have high diffusion times and the residence times in the channel space may be high leading to preferential exit of lighter molecules.

Controllable electrostatic fields: If multivalent cations eg. Ce^{3+} are used to replace the original singly charged Na^+ ions in a zeolite they will position themselves closer to three AlO_4^- tetrahedra. These tetrahedra may not be close to each other, particularly in case of high silica zeolites, and the resultant separation of charges causes high electric field gradients. Such fields will be sufficiently large to ionize, or atleast activate, adsorbed molecules and may well contribute to catalytic activity of zeolites. Rabo[163] has gone as far as proposing zeolites as solid ionizing solvents.

Sites for occluded and grafted species: Zeolites may be used as well-defined backbones onto which organometallic or other entities with highly specific catalytic properties may be grafted, thus heterogenizing homogeneous catalysts. In some cases[164] zeolites have been shown to be capable of stabilizing occluded complexes which have no homogeneous equivalent but are highly active for reactions of considerable commercial significance. For example, $[Ru(NH_3)_x(OH)_y(CO)_z]^{n+}$ in zeolite X or Y exceeds the activity of conventional copper-based catalysts for the low temperature water-gas shift reaction.

Their large internal surface areas renders them high sorption capacities for molecules which are small enough to pass through the entrance ports, slightly larger molecules being limited to the exterior of the crystallites. Zeolites thus constitute extremely selective adsorbents with a marked 'sieving' ability. They are used for separation of pure oxygen and nitrogen from air, to the production of p-xylene from a mixed xylene stream. The channel sizes can be modified, and the adsorption capacities can be altered, by incorporating appropriate cations in the cages leaving more space. The nature of the surface can be altered to adsorb different molecules. Highly siliceous zeolites are inherently hydrophobic in character, whereas materials with a preponderance of surface hydroxyl groups tend to be hydrophilic. Hydrophobic zeolites have been used to remove organic molecules from aqueous solutions.

While the unique ion exchange and sorptive properties of zeolites have been recognized and utilized the large-scale use of zeolites as catalysts is a rather

recent development. In 1950s and 1960s it became fully apparent that zeolite-based catalysts, especially those containing rare-earth ions and protons, possessed activity for *cracking of hydrocarbons* that is of several orders of magnitudes greater than that of conventional silica-alumina catalysts. Compared with an amorphous aluminosilicate, a lanthanum ion-exchanged faujasite (zeolite Y) possesses a first-order kinetic rate coefficient for the cracking of n-Hexane that is more than 10^4 times as large.[165] The H^+ form of mordenite exhibits similar performance. Cracking catalysts based on Zeolite Y were first introduced commercially in 1962 by the Mobil Oil Company. Such catalysts yielded less coke and more gasoline. The key role of the catalyst is to function as a rich source of protons, thereby facilitating the formation of carbocations. These is turn greatly accelerate the processes of polymerization, isomerization, alkylation and cracking. Recent work has shown that higher octanes can be obtained by adding small amounts of ZSM-5, either as a separate catalyst, or admixed with REY or high silica Y.[166] *Hydrocracking*, the second largest application of zeolite catalysis, involves cracking under high partial pressures of hydrogen in the presence of supported metal and acid functions. Zeolites were an improvement over other acidic catalysts in this process because they proved to be more resistant to nitrogen and sulfur poisoning. The large-pore zeolites Y, X, and mordenite are the most widely used zeolites for hydrocracking. Mordenite is satisfactory for hydrocracking naphtha. However, for heavier feeds, the faujasite-type zeolites are in either rare-earth exchanged or high silica forms are preferred. Hydrocracking occurs by a combination of metal-catalyzed and acid-catalyzed reactions. The hydrogenation-dehydrogenation function is provided by Pt or Pd, or by a combination of base metal sulfides, such as Ni or Co promoted with either W or Mo.

The *selectoforming* (selective cracking) properties of zeolites have been used to good effect in cracking n-alkanes to mainly propane.[167] n-alkanes generally have low octane numbers which causes knocking, their concentrations in motor gasoline is undesirable. Besides selective cracking it leaves the higher

octane branched alkanes almost untouched, and LPG is produced as a valuable byproduct. *Dewaxing*[168]a process, in which those components of heavy oil responsible for its poor flow properties at low temperatures are removed, has made it possible to provide high-grade lubricating oils at relatively low costs. The scenario of the zeolite catalysis changed when it was shown that, by addition of appropriate cations to synthesis mixtures, completely novel structures could be obtained. One of the most significant developments was the synthesis of ZSM-5 by Mobil.[169] This material which has 10-ring windows with diameters of the order of 5.5Å, allows the entry and exit of aromatic molecules with *p*-alkyl substituents more easily than *o*- and *m*-isomers. This coupled with the high stability and the inherent strongly acidic sites, makes ZSM-5 a catalyst with unprecedented ability to isomerise a mixed xylene feed form which the *p*-isomer is required. Para-xylene is of course, used in the manufacture of terephthalic acid, a monomer used in the production of Terylene. The chemical properties and size constraints imposed by its structure limit the maximum size of the hydrocarbons, which are ideal for high octane fuel. The reaction products are mainly branched chain and aromatic hydrocarbons, which are ideal for high octane fuel. Since the reaction sequence involves ethers and alkenes as intermediates,[170] and methanol being easily available from carbon monoxide and hydrogen, a direct synthetic route from *methanol to gasoline* (MTG) is possible. Methanol is by no means the only oxygen containing molecule which can be converted to gasoline components but molecules with almost any functional group containing oxygen can be converted into aromatic molecules. Apart from production of alkylbenzenes zeolites are still limited in synthesis of other intermediates. In the synthesis of intermediates only oxidation of phenol to catechol and hydroquinone with aqueous hydrogen peroxide over Titanium containing MFI zeolite (TS-1), the production of terbutylamine from ammonia and isobutene over zeolite MFI,[171] the selective conversion of methanol and ammonia to mono- and dimethylamine over modified mordenites[172] or zeolite Rho[173] and the hydration of cyclohexene to cyclohexanol are currently performed. The encapsulation of chiral transition metal complexes within the

cavities of zeolites has been shown to give rise to enantiomeric excesses in the products.[174] A measure of the growing importance of microporous catalysts may be gleaned from Table 1.1. There are many excellent reviews on the subject dealing with the present state of heterogeneous catalysis using these porous-framework materials.[175-177] Molecular sieves are obvious candidates for preparing inorganic membranes because of their uniform pore sizes and thermal stability. This area seems to have rich rewards in separations of gases and liquids when problems of processing thin films of these are overcome.[178] Researchers are also looking at zeolites as hosts for charge and separation processes, where zeolite-encased molecular ions have longer-lived charge-separated states than other similar systems- a property that may be used to improve the efficiency of energy storage devices.[179]

MAPOs[180,181] and SAPOs[39] are some of the good catalysts based on phosphate based frameworks. The other phosphate based solids as of yet display either ion-exchange and sorption properties to a small extent. The frameworks based on metal-aluminum phosphates are very interesting and some of them which, have zeolitic structures, may be of potential interest. Some other phosphates like those of tin have shown potential to catalyze the base-catalyzed reactions.[182] Other phosphates like those of gallium, zinc and cobalt may show interesting shape-selective catalysis and adsorption properties. Unfortunately, the thermal and hydrothermal stability of these phosphate-based frameworks limits their use, although they show promise for reactions such as acid-catalyzed production of alkenes from methanol.[183] Transition metal phosphates like those of Iron, Cobalt, Cr, and Mn are interesting from the point of view of the magnetic properties which they may offer. Systems like those of Zr, V and Zn have been explored for their interesting intercalation,[184] ionic conduction,[185] and charge-storage properties.[186] The organics used in the synthesis medium under acidic conditions are protonated and participates in the charge-neutrality of the framework and hence is occluded with in the channels and hence the space is unavailable for catalytic explorations. The challenge lies in establishing a

Table 1.1 Several innovations in applied catalysis since 1980 which utilize crystalline molecular sieves.

Process	Catalyst
1980-1989	
Conversion of ethene and benzene to ethyl benzene	H^+-ZSM-5
Methanol to gasoline (petrol)	H^+-ZSM-5
Hydrotreating of hydrocarbons	Pt/zeolite, Ni/zeolite, H^+-ferrierite
Dehydrocyclization ('Cyclar') of alkanes	Ga-ZSM-5
Conversion of light alkanes to aromatics	Ga-ZSM-5
1990-1993	
Conversion of phenol to hydroquinone and catechol	Ti-silicalite
Isomerization of but-1-ene to 2-methylpropene	H^+-ferrierite, H^+-Theta-1 (acidic zeolites)
Isomerization of oxime of cyclohexanone to ε-caprolactam	Silicoaluminophosphate molecular sieve (SAPO-11)
Ammoxidation of cyclohemanone to its oxime using H_2O_2	Ti-silicalite
Oxidation of benzene to phenol via cyclohexene	Zeolites
Methanol to light alkenes	Silicoaluminophosphate molecular sieve
Alkene oligomerization ("Shell" polygasoline and kerosene process)	Zeolite
Production of 2,6-diisopropylnapthalene using propene as alkylating agent	Acidic zeolite (mordenite)

successful methodology to remove the occluded template inside the channels, keeping the framework intact.

1.12 Creating space with in frameworks

The key issue, which comes to light when we think of the applications of framework solids, is to remove the template present inside and make accessible the space inside. In case of zeolites contacting a given zeolite with a dilute solution of the soluble salt of the desired exchange cation will usually result in a major exchange of cations.[187] The process being:

Na(zeolite) + Ca(solution) → Na(solution) + Ca(zeolite)

Most exchange reactions take place rapidly (5 to 30 min) at moderate temperatures (20 -80°C). In cases where there is a steric hindrance (a molecular sieve effect) such that a hydrated cation is too large to enter the zeolite structure, other solvents may be used which do not solvate the cation. Alternatively zeolite may be mixed with a low melting salt, heated to the salt melting temperature where exchange takes place, and then washed with water to remove the unwanted exchanged counterion. In some cases only partial exchange occurs, as in the case of lanthanum exchange of faujasite in the preparation of cracking catalysts. This process is illustrated in Fig. 1.10 and comprises steps of exchange, calcination, fabrication, and further exchange. In this case La exchanges with Na cation in the accessible large cage of the zeolite (sites 2 and 3) and then is heated above 300°C. At this temperature the shell water is stripped off the La ion, allowing it to move to smaller cage, where it exchanges with Na in sites 1 and 1'. After cooling, the cycle is repeated. Total removal of Na from this zeolite may take four such cycles of exchange and calcination. Some zeolites are unstable at low pH because of the hydrolysis of the framework Al, and so alternative methods need to be used to exchange transition metals or other cations that readily precipitate in basic solutions. One approach to exchanging transition metals is to first form ammonia complexes by dissolving them in dilute aqueous ammonium

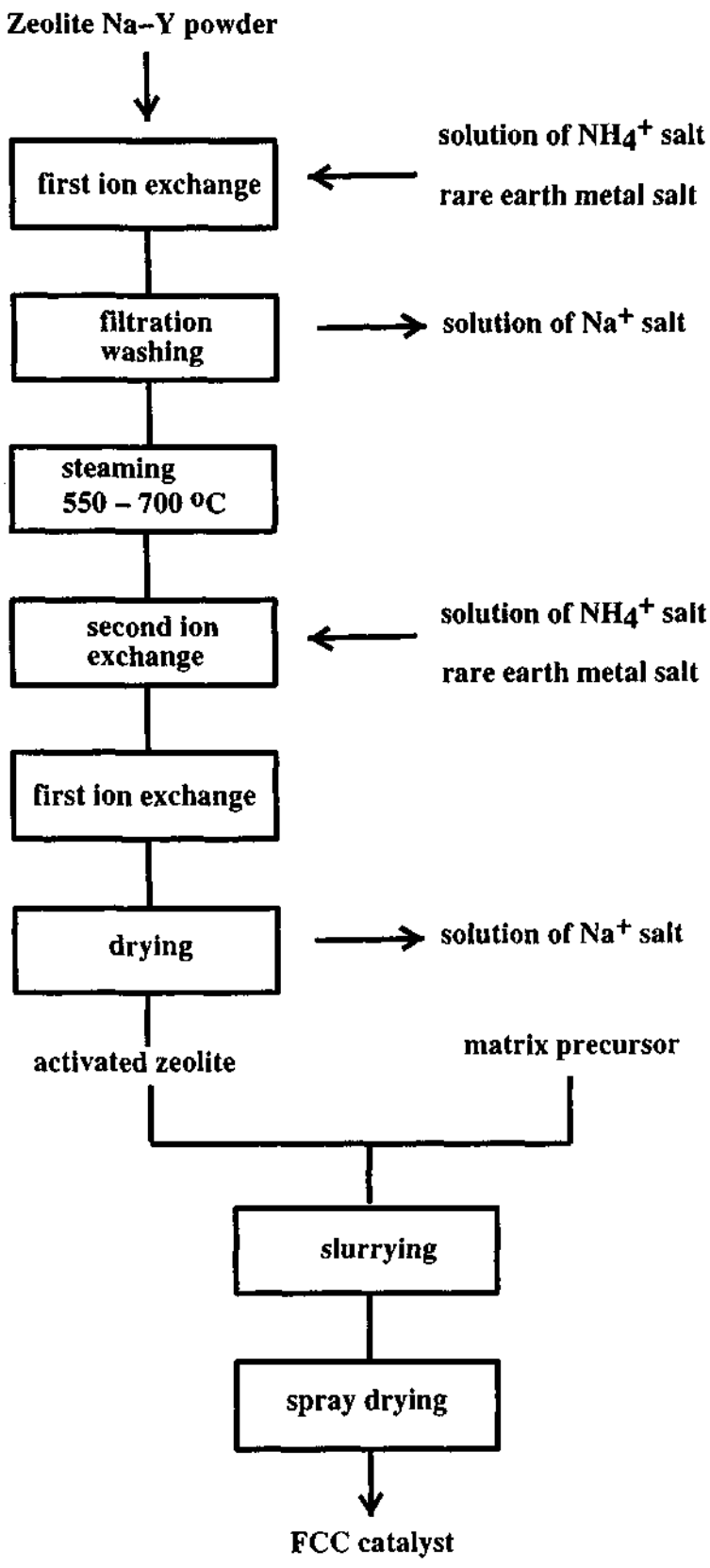

Fig. 1.10. Flow chart for the industrial synthesis of US-Y zeolite.

hydroxide and then carrying out the ion-exchange at high pH. When the zeolite is made with an organic template it needs to be calcined prior to exchange. The other method is to exchange the organic ammonium ions with ammonium ions and then deammoniate the ammonium form by burning it in air. Deammoniation of zeolite ZSM-5 is typically accomplished at temperatures around 500°C.

In case of phosphate-based frameworks template removal from AlPOs is not much difficult and the method of choice is calcination in air. In other phosphate based frameworks where the framework is not neutral unlike $AlPO_4$ the template participates in charge balancing and the removal of it usually leads to collapse of the framework architecture. The simplest way is to exchange the organic ammonium ion with alkali metal ions. This can create the desired space inside. If exchanged with NH_4^+ ions then ammonia can be removed by heating but the proton residing inside can cause the immediate collapse of the highly sensitive metal phosphate frameworks by dissolution of the metal ions. The best way is to use to deammoniate them in vacuum and use them as catalysts in inert medium. There is still a lack of an elegant method to remove the trapped template molecules from these cavities to create much needed space for use.

1.13 Key Issues in Framework Solids

Despite the great strides made in the synthesis of open-framework materials there remain a large number of issues which are yet unresolved. To unravel these long-standing mysteries one needs to employ a multi-pronged approach. Some of the prominent issues are the following:

1. A clear understanding of the synthetic mechanism of zeolites and phosphate-based molecular sieves has eluded us. What controls which specific framework structure? What are the interactions between the various components in the system? What are the species formed in the solid and in the solution as the reaction proceeds? What is the mechanism of structure direction? or, how is the geometry and electronic structure of the template transmitted to the silicate/phosphate species in solution in such a way as to

translate in to the structure of the final product?; How does nucleation occur? And, what is the first species formed in the hydrothermal reaction? To understand these processes one needs to track these reactions by employing panoply of techniques. This would require determination of structures of solution species under the conditions of reactions, therefore in situ techniques should be deployed.[157, 188,189] The crux of the problem is that the hydrothermal reaction bomb is really a black box.

2. *Rational design of open architectures:* The laborious methods of trial and error which have served so well for so long should give way to more streamlined methods. One can do a reterosynthetic analysis to come up with the smaller fragments, or the entities required to design a solid.[190] Excellent reviews have been devoted to design of framework solids of various kinds starting from various building units.[191-193] To synthesize the new microporous crystalline solids two interrelated approaches may be pursued: 1) design by experiment, based on intuition and accumulated chemical experience, and 2) design by computer modeling. Chemical combinatorial synthesis methods allows the rapid preparation an processing or large libraries of solid-state materials.[194,195] The use of these methods, together with the appropriate screening techniques, has recently led to the discovery of materials with promising superconducting,[196] magnetoresistive,[197] luminescent,[198,199]and dielectric properties.[200] Framework solids and other microporous materials which may have important applications in various chemical industries represent another class of material amenable to combinatorial synthesis. Recently this method has been applied to synthesize aluminophosphate frameworks.[201]
3. The other issues relate to exploitation of these cavities, which have been inaccessible so far. The stability of many of these solids poses another question.

1.14 Advent of Large-pore Molecular sieves: The Mesoporous materials

Although zeolites are of great importance in more than one way, they suffer from a severe limitation, i.e., in terms of their channel size. The largest pore openings of ≈ 7.4Å present in zeolitic (aluminosilicate) solids such as FAU, LTL, and DFO, pose a strict restriction on the size of molecules that can be subjected to shape-selective catalytic conversions. The recent advent of mesoporous siliceous solids, however, radically transformed the prospects in this regard. With the so-called MCM-41 large-pore mesoporous structures reported by Kresge et.al.,[202] and Beck et.al.[203] all this has changed. The dimensions of the pores vary from 20Å to 100Å in regular fashion. The findings in silica systems have led to further explorations of other mesoporous materials based on transition metal oxides, chalcogenides etc. All this has translated into numerous potential applications of these solids such as protein separation, selective adsorption of large organic molecules from waste water, chromatographic separation, catalysis of large molecules as well as electronic (quantum confinement of guest molecules in the cavities, electron transfer reactions), optical (nonlinear optics) and other applications.[204]

1.15 Porous Organic Solids – Expanding the regime

The field of porous solids is not a sole domain of inorganic materials. More recently, the interest in designing architectures that lead to organic host solids akin to their inorganic counterparts (zeolites and other framework solids) have resulted in the generation of many unique systems.[205-210] The promise of these materials stems from the diversity of organic molecules and the ability to organize them by harnessing the power of supramolecular chemistry. Traditional chemical synthesis involves the stepwise generation of covalent bonds via reaction to produce novel molecules. In comparison, supramolecular synthesis involves equilibrium, of noncovalent interactions (van der Waals forces, hydrogen bonds, and electrostatic forces) between the surfaces of molecular objects to produce novel supermolecules. The "reactions" of supramolecular chemistry are self-organization and self-assembly. These two terms are used to

refer to non-atom specific (i.e., van der Waals forces) and atom-specific (i.e., hydrogen-bonding) interactions, respectively. The design of solids in recent times has been way of *aufbau* (building up) principles.[211,212]

1.16 Concluding Remarks

Drawing inspiration from biology, chemists have been turning their attention to the deliberate design of self-assembling aggregates of molecular building blocks with some specific structural or functional purpose in mind. The present day solids embrace not only the conventional inorganic solids, but also organic and metal-organic systems with varying dimensionality and complexity. Deliberate control of structure, and hence the properties and function, still continues to be an important objective. Clearly, the area of framework solids has still a tremendous future, because of potential applications and the vast possible diversity.

2. SCOPE OF THE PRESENT INVESTIGATIONS

2.1 Hydrothermal synthesis of Open-framework zinc phosphates

Open-framework aluminosilicates (zeolites) and aluminophosphates of varying dimensionalities are of great interest for their chemical and physical properties and applications.[3,5,213] Amongst the non-zeolitic solids, the phosphate based open-framework materials display considerable structural diversity[214]. Of these, the bivalent metal phosphates, especially those of zinc, have been studied in considerable detail owing to their vast structural variety. The synthesis of these phosphate-based materials is accomplished under hydrothermal conditions in the presence of an organic amine. One of the persistent problems in the synthesis of these materials is the lack of control in directing a reaction toward a desired framework configuration. This difficulty arises because of our poor understanding of the mechanisms of kinetically controlled reactions. It has been

suggested recently that the shape of the amine and its pKa are of significance.[215] Davis and Lobo[4], on the other hand, propose that the amine acts as a space-filling agent if the open-framework structure is flexible, and acts as a structure-directing agent when the shape of the amine and framework are related. In spite of such formulations, the synthesis of open-framework materials is by and large, accomplished by the *trial and error*. It therefore becomes necessary to synthesize a large variety of open-framework solids by employing different amines and metal ions, so as to develop eventually structure-property-function relations in these materials.

Several open-framework zinc phosphates have been characterized in recent years,[79-95] their structures depending partly on the organic amine employed. Some of the features of the zinc phosphates are the presence of infinite Zn – O – Zn chains and 3-membered rings besides the variety of structures arising from the arrangement of 4-, 6-, 8- and higher membered rings. The relation between the structure and the amine template or the mechanism of formation of the different ring structures is, however, not clear. Thus, tetramethylammonium and guanidinium cations give rise to large-pore zinc phosphate framework structures,[94,95] but there are instances where the same amine gives two different ZnPO structures, as exemplified by the recent study with 1,3-diaminopropane.[216] It appears that the origin of formation of a rich variety of structures lies partly in the relative ease of convertibility of the rings and points to possible relations amongst the structures.

Since the bivalent metal phosphates (+2 and +5) are associated with the same total charge as the aluminosilicate zeolites (+3 and +4), active research is being pursued in this aspect. A large number of such zeolitic analogues have been isolated and characterized.[79,217] The framework structures of zeolites are generally built from tetrahedra sharing vertices (usually Si and/or Al). This type of tetrahedral connectivity can be regarded, mathematically as 4-connected 3D nets, constructed from 3-connected 2D sheets.[218] 4-connected 3D nets and 3-connected 2D sheets are common among the open-framework structures. Bu *et*

al[219] have recently observed the layers that are constructed only by 4-connected 2D sheets in a lamellar zinc arsenate. Interruptions can occur within the layers and disrupt the 4-connected sheets,[72] with all the tetrahedral groups not making four bonding connections to their neighbors. There are extensive reviews on theoretical nets designed from simple rules of crystal chemistry, but whether such nets are feasible in materials is still unresolved, the understanding of this issue may be a crucial step towards rational design of these solids.

Apart from the fundamental understanding, the real driving force to study the open-framework metal phosphates is due to their potential applications in heterogenous catalysis, for example, materials required for enantioselective separation and synthesis have become increasingly important in past few years,[220] and it is known that chiral rhodium complexes supported on a zeolite matrix give rise to asymmetric hydrogenation of N-acyldehydrophenylalanine derivatives with a enantioselectivity of greater than 95%.[215] In this context, it is desirable to have materials, which are chiral or possess helical channels. There have been some efforts to make chiral solids, which could also be shape-selective. Zeolite-β (polymorph A) is chiral with a 4-fold screw axis but it has not been able to synthesize this material in pure form.[222] Chiral open-framework phosphates have been prepared in the presence of chiral metal complexes and structure-directing agents.[223,224] Recently, a chiral tin(II) phosphate has been prepared using an achiral template and both the enantiometers of this material have been isolated and characterized.[225] A helical metal borophosphate with the helix running along the 6_1 screw axis has also been reported.[226] Very recently, Gier et al[227] have reported chiral zinc and beryllium arsenates with three-dimensional helical structure containing two independent crosslinked helical channels. The goal to synthesize chiral frameworks with channels capable of displaying enantioselectivity remains a hot pursuit.

Recently, there has been some interest in the use of coordination complexes and organometallic species as structure-directing agents in the synthesis of zeolitic materials, notably for UTD-1.[228] Such synthetic strategies

have also been employed for the preparation of open-framework phosphates resulting in the isolation of chiral solids.[223,229,230] The main advantage of such methods lies in the variety of shapes and charges offered by the complexes, as well as the possibility of introducing a transition metal directly inside the pores. Innovative modification on this theme is to employ the coordination complexes as a starting source material, for the metals. This approach has resulted in the formation of new types of solids.[231-233] It is possible that coordination complexes control the pH of the synthesis mixture by slowly releasing the amine molecule, needed for the formation of the structure. The exact mechanism, however, is still unclear. In order to probe the formation of framework solids from coordination complexes, we have taken up the system involving the complexes of zinc.

The synthesis of some of the open-framework metal phosphates such as those of gallium, iron, vanadium and niobium has been carried out in the presence of F^- ions but the role of F^- is not entirely understood.[11,28] In many cases F^- ions acts as a mineralizer.[234] However, there are some cases where F^- ion is also part of the structure and acts as a bridge between the metal centers. Chloride ions are also known to act as a mineralizer in the synthesis of open-framework metal phosphates. However there is no chlorophosphate reported in the literature wherein the Cl^- ion is part of the network. It would be interesting to look into the possibility of open-framework chlorophosphates. In addition the role of solvent, additives like oxalic acid, acetic acid, etc. added during the synthesis is again not well understood. On needs to explore in depth these various issues to arrive at a complete understanding of phosphate-based framework materials.

In addressing these various issues and to evolve a better understanding of phosphate based open-framework architectures, we have carried out the synthesis of several open-framework zinc phosphates in the presence of organic amines such as 1,3-diamino-2-hydroxypropane (DAHP), 1,3-diaminopropane (DAP), diethylenetriamine (DETA), 1,3-diaminoguanidine hydrochloride (DAG) and cyclohexylamine (CHA) under hydrothermal conditions. We have obtained both

two-dimensional layers and three-dimensional zinc phosphates architectures by this means. We list below the compositions and salient structural features of the open-framework zinc phosphates obtained by us. The layered structure obtained with DAHP, $[NH_3CH_2CH(OH)CH_2NH_3][Zn_2(HPO_4)_3]$, **I** contains layers with bifurcated 12-rings. We have also obtained two chiral 3-dimensional open-framework zinc phosphates $[NH_3(CH_2)_3NH_3]_2[Zn_4(PO_4)_4]$, **II** and $[NH_3(CH_2)_3NH_3][Zn_5(H_2O)(PO_4)_4(HPO_4)]$, **III** with DAP, and both of them possess 8-membered channels. **II** is built of double crankshaft chains whereas **III** possesses similar building units as that of the naturally occurring aluminosilicate mineral, thomsonite, but interruptions in the connectivity between the building units creates marginal differences. The reaction of a zinc *tris*(DAP) complex with phosphoric acid and oxalic acid as an additive gave a layered zinc phosphate, $[NH_3(CH_2)_3NH_3]$ $2[Zn_2PO_4(HPO_4)]$, **IV** with channels and possessed double four-ring units. The two-dimensional zinc phosphate obtained with DETA, $[NH_3(CH_2)_2NH(CH_2)_2NH_3]^{2+}2[Zn_2PO_4(HPO_4)]^-$, **V**, contains layers with ladder-like corrugations, as well as one-dimensional Zn – O – Zn chains. The unusual presence of chains exclusively formed by 3-membered rings bordering those containing 4- or 3- and 4-membered rings is a unique feature in this material. In connection with the synthesis of chiral framework structures we have been successful in isolating another three-dimensional structure with DETA $[NH_3(CH_2)_2NH_2$ $(CH_2)_2NH_3][Zn_4(PO_4)_3(HPO_4)].H_2O$, **VI**, which forms under hydrothermal conditions in the presence of achiral amine. **VI** possesses intersecting helical channels. Another three-dimensional zinc phosphate, $[NH_3(CH_2)_2NH(CH_2)_2NH_3][Zn_5(PO_4)_4]$, **VII**, has been synthesized in presence of DETA and oxalic acid as an additive, with Zn_4O_4 tetrameric clusters, found for the first time, in an open-framework zinc phosphate. The cluster in turn forms basket-shaped building units, which in combination with PO_4 tetrahedra give rise to one-dimensional channels. In the three-dimensional zinc phosphates obtained with DETA $[NH_3(CH_2)_2NH(CH_2)_2NH_3]^{2+}[Zn_5(PO_4)_4]^{2-}$, **VIII** and DAG, $[CN_5H_6]^+$ $[Zn_2(PO_4)(HPO_4)]^-$, **IX** the amine acts as a ligand to the metal centre, in addition to being present in the channel. **VIII**, forms a 10-membered one-dimensional

channel, akin to that in aluminosilicates, while **IX** has 8-membered channels. With CHA, a layered zinc chlorophosphate, $[C_6NH_{14}][ZnCl(HPO_4)]$, **X**, with 4- and 8-membered rings has been obtained, the Cl- ions protrude in a direction perpendicular to the plane of the layer. The positioning of the Cl^- ions is reminiscent of lone-pairs of Sn(II) in open-framework layered Sn(II) phosphates.[235,236]

2.2. Amine Phosphates as Possible Intermediates in the Formation of Open-Framework Structures

In spite of the successful synthesis of a large number of open-framework phosphates in the presence of organic amines, one is still unable to rationalize the formation of such a large variety of open-framework phosphate structures. The role of the amine has not been understood hitherto. There have been some suggestions with regard to the role of amine in the formation of these structures.[4] The amine could act as a structure-directing agent, or merely fill the available voids and stabilize the structure through hydrogen-bonding and other interactions. Since the amine generally gets protonated in the reaction, it also helps in charge compensation with respect to the framework. Another aspect not clear to date is the relation between the metal phosphates of different dimensionalities. In the case of aluminophosphates, it is proposed that linear chains of corner-sharing metal phosphate units are progressively transformed into ladder, layer, and three-dimensional structures.[133] In tin phosphates, four-rings of the metal phosphate are believed to transform to into larger rings and give rise to layer and other complex structures.[235] While the variety of structures generated in a given metal phosphate system, often with the same amine, may arise because of the small energy differences amongst them or due to kinetic control of the reactions, the exact role of the amines is not fully understood, in spite of several hypotheses.[215] We considered it of great importance to understand how the initial chain or layer structures of metal phosphates are formed, and therefore investigated whether a stable reaction intermediate, formed

during hydrothermal synthesis, plays a key role, and if so, whether this intermediate can be directly used to generate novel metal phosphates.

In the hydrothermal synthesis of open-framework metal phosphates, we isolated several amine phosphates as additional products. Although, amine phosphates are known to occur as by-products in the synthesis of metal phosphates,[237] they are normally not encountered because of their high solubility in water and the usual preoccupation with less soluble crystalline products. The fact that they are isolated from the synthesis mixtures gave us a clue that they possibly could be the elusive reaction intermediate, which can lead to the open-framework phosphates. Initial experiments showed that the amine phosphates react with metal ions under hydrothermal conditions in absence of additional phosphoric acid to give open-framework metal phosphates. This suggested that amine phosphates could indeed act as intermediates in the formation of open-framework structures. An extensive and systematic study would be necessary to validate the initial results, and we have sought to probe this in a detailed manner. The Reactions of various amine phosphates with Zn^{II}, Co^{II}, Al^{III}, Ga^{III} and Sn^{II} ions yielding both known and new open-framework metal phosphates at temperatures much below the hydrothermal conditions, (in some cases as low as room temperature) demonstrates that amine phosphates could act as possible intermediates in the formation of these architectures. This finding is supported by in situ ^{31}P NMR and ex situ x-ray diffraction study, of the reaction of amine phosphates with Zn^{II} ions.

We have not only probed amine phosphates as intermediates but also employed the amine phosphate route to synthesize new open-framework phosphates. The isolation of a variety of open-framework architectures obtained by the reaction between an amine phosphate (PIPP) with different metal ions, demonstrates the efficacy of the amine phosphate route to the synthesis of the open architectures and underscores the role of amine phosphates in the formation of these compounds. A large number of zinc phosphates **XI - XVI**, $[C_4N_2H_{12}][Zn(HPO_4)_2(H_2O)]$ **XI**, $[C_4N_2H_{12}][Zn_{3.5}(PO_4)_3(H_2O)]$ **XII**,

$[C_4N_2H_{12}][Zn_2(HPO_4)_2(H_2PO_4)_2]$ **XIII**, $[C_4N_2H_{12}][Zn(H_2O)Zn(HPO_4)(PO_4)]_2$ **XIV**, $[C_4N_2H_{12}][Zn_2(PO_4)(H_2PO_4)_2]_2$ **XV**, $[C_3N_2H_6][Zn_4(OH)(PO_4)_3]$ **XVI**, have been obtained. **XI-XV** with PIPP where as **XVI** forms with Imidazole phosphate. A large number of pure cobalt phosphates **XVII - XXI** with varying dimensionalities have been obtained. $[C_4N_2H_{12}]_{1.5}[Co_2(HPO_4)_2(PO_4)H_2O]$ **XVII**, has one-dimensional strip like architecture, $[C_4N_2H_{12}]_{1.5}[Co_2(HPO_4)_2(PO_4)H_2O]$ **XVIII** and $[C_{10}N_4H_{28}]_{0.5}[Co(PO_4)Cl]$ **XIX** have two-dimensional layered architecture and $[C_4N_3H_{16}]_3[Co_6(PO_4)_5(HPO_4)_3]H_2O$ **XX**, and $[C_6N_2H_{14}][Co_2(HPO_4)_2]$ **XXI** have three-dimensional framework with channels. **XVII** and **XVIII** are formed with PIPP, **XIX** and **XX** with APPIPP and DETAP whereas **XXI** was obtained with DABCOP. We have also synthesized a layer tin phosphate $[C_4N_2H_{12}]_{0.5}[Sn(PO_4)]$ **XXII**, with PIPP possessing elliptical 8-membered channels.

2.3. Isolation of a monomeric zinc phosphate formed by a 4-membered ring

If the amine phosphate plays a crucial role in the formation of open-framework metal phosphates, it should be possible to obtain a metal phosphate with a structure even simpler than the linear chain such as the monomeric 4-membered ring metal phosphate. We have been able to obtain such a monomeric zinc phosphate by the reaction of N,N,N',N'-tetramethylethylenediamine phosphate (TMED-P) with Zn(II) ions $[C_6N_2H_{18}]^{2+}[Zn(H_2PO_4)_2(HPO_4)]^{2-}$, **XXIII**. **XXIII** on heating in water transformed to a layered structure $[C_6N_2H_{18}]^{2+}[Zn_3(H_2O)_4(HPO_4)_4]^{2-}$ **XXIV.** Although we do not have an exact control on the structure of the products obtained because of the comparable energies of the various structures, the amine phosphate route gives us the hope that, rational synthesis of the open-framework metal phosphates may indeed become possible in the not too distant a future.

3. EXPERIMENTAL

3.1 Synthesis of open-framework zinc phosphates

The various compounds (**I - X**) were synthesized by the hydrothermal method. In a typical synthesis, the zinc source (ZnO or $Zn(CH_3COO)_2$ ($Zn(ac)_2$), Zn *tris*(DAP) was taken in appropriate solvent (generally, water except in one case where butanol-water mixture was used as a solvent) and dissolved in 35% HCl (hydrochloric acid). Additives such as oxalic acid or acetic acid were added in some of the syntheses as shown in the table, followed by the addition of an appropriate quantity of 85 % H_3PO_4 to the reaction mixture. Finally the organic amine (DAHP for **I**, DAP in the case of **II, III** and **IV**), DETA in the case of **V, VI, VII** and **VIII**, DAG for **IX**, CHA for **X**) was added to form a colorless gel. The gel was stirred for approx. 30 min. for homogenizing and it was transferred to a teflon-lined stainless steel Parr autoclave and heated at the mentioned temperature for the required duration. At the end of the experiment, the resulting mixture contained crystals, which were filtered, washed with a minimum amount of water and dried at ambient conditions. All the products were stable under atmospheric conditions. The starting compositions and synthetic conditions for all these compounds are listed in Table 1.2.

3.2 Synthesis of Amine Phosphates

Piperazine phosphate (PIPP): To a PTFE container containing 50mmol of water was added 12mmol of 85% H_3PO_4. To the resulting solution 10mmol of piperazine (anhydrous) was added slowly under stirring. The gel, thus formed, was heated in a 23 ml sealed Parr (Moline, USA) acid-digestion bomb at 110 °C for 12 hours. The contents of the bomb were filtered, washed with water and dried at ambient conditions. The product was characterized by single crystal X-ray diffraction. This compound has already been reported in the literature.[238] PIPP, like other amine phosphates, is stable under hydrothermal conditions.

Table 1.2 Compositions employed for the synthesis of the zinc phosphates *via* regular hydrothermal route.

Cmpd. No.	Gel Composition	T (K)	t (h)	Composition of the product
I	ZnO : 4.9 H_3PO_4 : 1.35 DAHP 4.5 H_2O.	433	48	$[NH_3CH_2CH(OH)CH_2NH_3][Zn_2(HPO_4)_3]$
II	$Zn(ac)_2.2H_2O$: 1.6H_3PO_4 : HCl : 2DAP : 100H_2O	438	24	$[NH_3(CH_2)_3NH_3]_2[Zn_4(PO_4)_4]$
III	$Zn(ac)_2.2H_2O$: 5H_3PO_4 : HCl : 6DAP : 100H_2O	438	24	$[NH_3(CH_2)_3NH_3][Zn_5(H_2O)(PO_4)_4(HPO_4)]$
IV	Zn *tris*(DAP): 2$H_2C_2O_4$: H_3PO_4 :100H_2O.	443	24	$[NH_3(CH_2)_3NH_3]$ 2$[Zn_2PO_4(HPO_4)]$
V	ZnO : DETA : 2H_3PO_4 : 2HCl : 125H_2O	453	128	$[NH_3(CH_2)_2NH(CH_2)_2NH_3]^{2+}2[Zn_2PO_4(HPO_4)]^-$
VI	ZnO : 2CH_3COOH : 2HCl : DETA : 2H_3PO_4 : 100H_2O	453	80	$[NH_3(CH_2)_2NH(CH_2)_2NH_3]^{3+}[Zn_4(PO_4)_3(HPO_4)]^{3-}.H_2O$
VII	ZnO : $H_2C_2O_4$: 2HCl : DETA : 2H_3PO_4 : 100 H_2O	453	56	$[NH_3(CH_2)_2NH(CH_2)_2NH_3]^{2+}$ $[Zn_5(PO_4)_4]$
VIII	ZnO : 2 H_3PO_4 : 2 HCl : DETA : 100 H_2O.	453	216	$[NH_3(CH_2)_2NH(CH_2)_2NH_3]^{2+}$ $[Zn_5(PO_4)_4]$
IX	ZnO : 2.3 H_3PO_4 : 4.8 DAG : 55 H_2O.	383	96	$[CN_5H_6]^+[Zn_2(PO_4)(HPO_4)]^-$
X	ZnO : 2HCl : 2H_3PO_4 : CHA : 100(H_2O+C_4H_9OH)	443	115	$[C_6NH_{14}][ZnCl(HPO_4)]$

Various other amine phosphates such as N-methylpiperazine phosphate (MPIPP), Diethylenetriamine phosphate (DETAP), 1,4-diazabicylco[2.2.2]octane phosphate (DABCOP), 1,2-diaminopropane phosphate (1,2-DAPP), Ethylenediamine phosphate (ENP), 1,6-diaminohexane phosphate (DAHP), 1,4-*bis*(3-aminopropyl)piperazine phosphate (APPIPP), 1,3-diaminopropane phosphate (DAPP) and N,N,N',N'-Tetramethyl-ethylenediamine phosphate (TMEDP) were synthesized following a similar procedure as in the case of PIPP, and their gel compositions are listed in Table 1.3 along with the final compositions of the products. The syntheses of APPIPP and TMEDP were carried out in methanol instead of water.

3.3. Reaction of amine phosphates with metal ions

In a typical reaction, 0.5mmol of ZnO was stirred in 100mmol of water, to which 1mmol of HCl (35%) was added. After stirring the mixture for a few minutes, 2.7mmol of amine phosphate (e.g. DAPP) was added, and the mixture was stirred for 30 min. The homogenized mixture was sealed in a 23-ml teflon-lined Parr autoclave and heated at the given temperature and for the given duration (Table 1.4).

Zn^{II}: A known amount of ZnO was taken in deionized water and dissolved in an appropriate quantity of 35 % HCl. In one of the synthesis, a 80:20 mixture of butan-2-ol and water was employed instead of water (see Table 1.5). To the resulting solution PIPP was added and the mixture was stirred for 30 min. The homogenized gel was heated in a 23 ml sealed Parr (Moline, USA) acid-digestion bomb at 180°C for the required duration. The reaction yielded products **XI – XV** (Table 1.4). We list the conditions of synthesis, gel compositions and the compositions of final products in Table 1.5. Of the five products, **XIV** and **XV** have been prepared earlier by the conventional hydrothermal method.[239] **XI – XIII**, however, could be obtained only through the amine-phosphate route. Our efforts to synthesize **XI – XIII** employing normal hydrothermal methods starting from individual constituents were not successful. It is noticed that, **XIV** and **XV**

Table 1.3. Conditions employed for the synthesis of amine phosphates.

Code	Gel composition	T, K	t, h	Product composition
PIPP	$1.0C_4N_2H_{10} : 1.2H_3PO_4 : 5.5H_2O$	383	10	$(C_4N_2H_{12})(HPO_4).H_2O$
MPIP-P[*,1]	$1.0C_5N_2H_{12} : 1.2H_3PO_4 : 5.5H_2O$	383	10	$(C_5N_2H_{14})_2(HPO_4)_2.3H_2O$
DETAP	$1.0C_4N_3H_{13} : 1.2H_3PO_4 : 5.5H_2O$	383	10	$(C_4N_3H_{15})(HPO_4)_2(H_2O)$
DABCO-P[*,1]	$1.0C_6N_2H_{12} : 1.2H_3PO_4 : 5.5H_2O$	383	10	$(C_6N_2H_{14})(HPO_4).H_2O$
1,2-DAPP[*]	$1.0C_3N_2H_{10} : 1.2H_3PO_4 : 5.5H_2O$	383	10	$(C_3N_2H_{12})(HPO_4)$
ENP	$1.0C_2N_2H_8 : 1.2H_3PO_4 : 5.5H_2O$	383	10	$(C_2N_2H_{10})(HPO_4)$
DAHP[*]	$1.0C_6N_2H_{16} : 1.2H_3PO_4 : 5.5H_2O$	383	10	$(C_6N_2H_{18})_3(HPO_4)_3.4H_2O$
APPIP-P[*,1]	$1.0C_{10}N_4H_{24} : 1.2H_3PO_4 : 50MeOH$	353	2	$(C_{10}N_4H_{26})(HPO_4).2H_2O$
DAPP	$1.0C_3N_2H_{10} : 1.2H_3PO_4 : 5.5H_2O$	383	10	$(C_3N_2H_{12})(HPO_4).H_2O$
TMED-P[*,1]	$1.0C_6N_2H_{16} : 1.2H_3PO_4 : 50MeOH$	353	2	$(C_6N_2H_{18})(HPO_4).2H_2O$

[*] New amine phosphates; [1] Described in the present study

PIPP – piperazinium hydrogen phosphate; **MPIP-P** - N-methylpiperazinium hydrogen phosphate; **DETAP** diethylenetriammonium hydrogen phosphate; **DABCO-P** 1,4diazabicyclo[2.2.2]octane hydrogen phosphate **1,2-DAPP** - 1,2propanediammonium hydrogen phosphate; **ENP** – ethylenediammonium hydrogen phosphate; **DAHP-** 1,6hexanediammonium hydrogen phosphate; **APPIP-P-** 1,4bis(aminopropyl)piperazine hydrogen phosphate; **DAPP** – 1,3propanediammonium hydrogen phosphate; **TMED-P** – N,N,N',N' tetramethylethylenediammonium hydrogen phosphate

Table 1.4 Open-framework zinc phosphates obtained through the reaction of amine phosphates with metal ions.

Composition	Temp °C(Time h)	a, b, c (Å)	α, β, γ (°)	Sp.gp	R(F)[a]	Framework
DAPP : $[DAPH_2][HPO_4].H_2O$ [b]		7.009(9),16.775(8),7.845(9)	90.00,113.78,90.00	$P2_1/c$	7.8	(Fig 1a)
$[Zn(HPO_4)_2][DAPH_2]$	150(40), 95(40), 50(48), 30(96)	5.222(0),12.756(1),15.674(1)	90.00,90.00,90.00	$P2_12_12_1$	2.2	Chain(9) (Fig1b)
$[Zn_2(HPO_4)_3][DAPH_2]$	150(40), 85(96)	8.614(5),9.618(7),17.037(8)	90.00,93.57,90.00	$P2_1/c$	4.5	Layer* (Fig 1c)
$[SnPO_4]_2[dapH_2]$	180(24), 85(48), 50(96)	18.096(7),7.888(6),9.150(7)	90.00,111.84,90.00	C2/c	2.6	Layer (Fig 4)
$[Al_5Co_2(OH)(HPO_4)_4(PO_4)][DAPH_2]$	180(96), 110(300)[d]	9.177(4),9.250(5),13.175(4)	93.07,92.31,112.06	P(-1)	13.0	3-D*
PIPP : $[PIPH_2][HPO_4].H_2O$[b]		6.425(6),12.296(8),11.220(8)	90.00,97.14,90.00	$P2_1/n$	6.4	Fig 2a
$[Zn(HPO_4)(H_2O)][PIPH_2]$	180(36)	8.930(6),14.025(4),9.310(7)	90.00,95.41,90.00	$P2_1/n$	4.0	Chain* (Fig 2b)
$[Zn_4(PO_4)_3(OH)][PIPH_2]$	180(36)[e]	16.104(8),8.256(4),22.997(9)	90.00,104.00,90.00	C2/c	2.0	3-D* (Fig 2c)
$[Zn(H_2O)Zn(HPO_4)(PO_4)]_2$ $[PIPH_2]$	180(36), 85(300)	12.075(5),14.888(7),11.835(8)	90.00,97.72,90.00	C2/c	3.0	3-D(10)
$[Zn_2(PO_4)(H_2PO_4)_2][PIPH_2]$	180(36), 85(300)	13.388(3),12.838(6),8.224(6)	90.00,94.77,90.00	C2/c	---	3-D(10)
DABCOP: $[DABCOH_2][HPO_4].H_2O$[b]		6.906(2),9.018(4),9.271(2)	92.21,104.51,111.76	P(-1)	3.9	--------
$[Zn_2(HPO_4)_3][DABCOH_2]$	150(20), 95(20)	9.528(4),9.948(3),9.996(4)	107.65,98.04,114.86	P(-1)	5.5	3-D(11)
$[Zn_4(PO_4)_2(HPO_4)_2][dabcoH_2].3H_2O$	150(20), 95(20), 50(48), 30(60)	9.475(1),9.524(9),12.312(4)	93.73,91.044,98.70	P(-1)	6.1	3-D(11)
ENP : $[ENH_2][HPO_4]$[b]		7.507(1),11.816(4),8.055(4)	90.00,110.13,90.00	$P2_1/c$	3.0	--------
$[Zn(HPO_4)_2][ENH_2]$	150(36)	5.161(1),15.842(2),12.027(2)	90.00,92.36,90.00	$P2_1/c$	6.0	Ladder
$[Zn_2(HPO_4)_2(H_2PO_4)_2][ENH_2]$	150(36), 50(40)	16.420(2),7.826(1),14.640(1)	90.00,116.47,90.00	$P2_1/c$	5.0	Layer
$[Zn_6(PO_4)_4(HPO_4)][ENH_2]$	150(36)	19.182(0),5.036(0),21.202(4)	90.00,103.29,90.00	C2/c	3.6	3-D

[a] Here $R(F) = \Sigma \| F_0 | - | F_C \| / \Sigma | F_0 |$ with $F_0 > 4.0\sigma(F)$. [b] The amine phosphates were recovered first during the hydrothermal synthesis and later synthesized using the composition : Amine : 1.2 H_3PO_4 : 5H_2O at 110 °C for 12h. [c]New structure found in this study; [d] Synthesis was carried out in ethylene glycol. [e] Different composition of the starting gel.

Table 1.5. Syntheses conditions and product compositions for compounds **XI – XXII** obtained by the reaction of amine phosphates with metal ions.

Code	Gel composition	T, K	Time, h	pH	Product composition
PIP	$C_4N_2H_{10}$:1.2H_3PO_4 : 50H_2O	383	12		$[C_4N_2H_{12}][HPO_4].H_2O$
XI	ZnO : 4HCl : 2PIPP : 50H_2O	453	36	2	$[C_4N_2H_{12}][Zn(HPO_4)_2(H_2O)]$
XII	ZnO : 4HCl : 1.75PIPP : 100H_2O	453	24	2	$[C_4N_2H_{12}][Zn_{3.5}(PO_4)_3(H_2O)]$
XIII	ZnO : 6HCl : 2.5PIPP : 80 2-BuOH : 20H_2O	443	24	2	$[C_4N_2H_{12}]\{Zn_2(HPO_4)_2(H_2PO_4)_2\}$
XIV	ZnO : 4HCl : PIPP : 50H_2O	453	36	2	$[C_4N_2H_{12}][Zn(H_2O)Zn(HPO_4)(PO_4)]_2$
XV	ZnO : 4HCl : PIPP : 50H_2O	453	36	2	$[C_4N_2H_{12}][Zn_2(PO_4)(H_2PO_4)_2]_2$
XVI	ZnO : 2HCl : 1.5ImidazoleP : 50 2-BuOH	443	64	2	$[C_3N_2H_6][Zn_4(OH)(PO_4)_3]$
XVII	$CoCl_2.6H_2O$: 2PIPP : 50 2-BuOH	453	36	7-8	$[C_4N_2H_{12}]_{1.5}[Co_2(HPO_4)_2(PO_4)H_2O]$
XVIII	$CoCl_2.6H_2O$: 2PIPP : 50 2-BuOH	453	36	7-8	$[C_4N_2H_{12}]_{1.5}[Co_2(HPO_4)_2(PO_4)H_2O]$
XIX	$CoCl_2.6H_2O$: APPIP-P : 50 2-BuOH	433	90	7-8	$[C_{10}N_4H_{28}]_{0.5}[Co(PO_4)Cl]$
XX	$CoCl_2.6H_2O$: 1.4DETAP : 50 2-BuOH	453	40	7-8	$[C_4N_3H_{16}]_3[Co_6(PO_4)_5(HPO_4)_3]H_2O$
XI	$CoCl_2.6H_2O$: 1.84DABCO-P : 50 2-BuOH	453	36	7-8	$[C_6N_2H_{14}][Co_2(HPO_4)_2]$
XXII	SnC_2O_4 : 3HCl : 2PIP : 80 2-BuOH : 20H_2O	443	72	5-6	$[C_4N_2H_{12}]_{0.5}[Sn(PO_4)]$

always form together and our efforts to synthesize them as a single phase compounds were not successful. The open-framework structures **XI – XV** could also be prepared by carrying out the reaction of PIPP with Zn^{II} ions at 85°C for a period of 4 weeks. Similar synthetic procedure was employed to synthesize the zinc phosphate, **XVI,** with imidazole phosphate. The synthetic conditions are listed in Table 1.5.

Co^{II}: A known amount of $CoCl_2.6H_2O$ was dissolved in 2-butanol. To the resulting deep blue solution PIPP was added and stirred until the gel was homogenous. The pH was adjusted to ~ 7-8 by adding 25 % aqueous ammonia. The gel was heated in a 23 ml sealed Parr (Moline, USA) acid-digestion bomb at 180°C for 36h. The reaction yielded products **XVII** and **XVIII**. The synthesis of the cobalt (II) phosphates, **XIX - XXI,** were facilitated by employing amine phosphate, APPIPP, DETAP,[240] and DABCOP, as the starting source of phosphorus and amine. In a typical preparation, 1mmol of cobalt chloride was dispersed in 50mmol of butan-2-ol and 1.36mmol of DETAP was added to the above mixture and stirred. The resulting pH was adjusted to ~7-8 by the addition of 25% aq. ammonia solution. The mixtures were stirred until homogeneous, sealed in a 23 ml PTFE-lined stainless-steel pressure vessels (Parr, Moline, USA) and heated at desired temperature for required duration. The resulting product contained large quantities of deep blue-colored crystals, was filtered and washed with plenty of water and dried at ambient temperature. The starting compositions and synthetic conditions for compounds **XVII – XXI** are mentioned in Table 1.5 which were also prepared in an analogous manner to that of **XVII**.

Sn^{II}: A known quantity of SnC_2O_4 was stirred in (80:20) 2-butanol-water mixture, 35 % HCl was added to the mixture followed by addition of PIPP. The gel was homogenized under constant stirring and heated in a 23 ml sealed Parr (Moline, USA) acid-digestion bomb at 170 °C for 72h. Plate like crystals of compound **XXII** were obtained. The gel composition, synthetic conditions and product composition is listed in Table1.5

3.4. Monomeric zinc phosphate and a study of its transformation

The monomeric zinc phosphate of the composition $[C_6N_2H_{18}]$ $[Zn(H_2PO_4)_2(HPO_4)]$, **XXIII** was synthesized by two different methods. In the first method, the direct reaction involving the amine, phosphoric acid and the zinc salt was employed and in the other the reaction between the Zn^{2+} ions and the amine phosphate (TMED-P) was used; both the reactions occurring at room temperature. In a typical synthesis of **XXIII**, 10mM of $ZnSO_4.7H_2O$ was added to a mixture of 40mM of water and 20mM of 85% H_3PO_4 in a polypropylene bottle. 10mM of TMED was added to the above under continuous stirring. The homogenized mixture was allowed to crystallize at room temperature. After several months, crystals of **XXIII** were found in the bottle, which were filtered and dried. The product consisted entirely of **XXIII**. In order to synthesize **XXIII** in the laboratory time scale, the reaction of the amine phosphate (TMEDP) and Zn^{2+} ions was carried out at room temperature. A mixture of 1mM of $ZnSO_4.7H_2O$ dissolved in 10mM of H_2O and 2mM of TMEDP was stirred to obtain a homogeneous gel. The gel was left to crystallize at room temperature. Colorless crystals of **XXIII** were obtained within a week (yield ~60%). The transformation of **XXIII** was carried out, by heating 25mM of the dried crystals of **XXIII** in 10mM of water at 50°C for 2 days, in a PTFE-lined stainless steel autoclave. The transformed material consisted of thick plate-like single crystals of **XXIV**, was filtered, washed with water and dried at room temperature.

Time-dependent powder XRD studies on the evolution of different phases with the progress of reaction was carried out using a Rich-Siefert 3000-TT model. The reaction was followed by an ex-situ study in which the reaction gel was quenched after different duration, and the powder pattern recorded. The low-angle reflections were analyzed to check for various phases present at given time in the reaction gel. The course of the reaction was also pursued by carrying out ^{31}P in situ NMR studies, in which, the reaction gel was sealed in a thin cell and heated at 85°C. NMR spectrum was recorded at various time-intervals and analyzed for the various phases present.

3.5. Characterization

Structure Determination by Single Crystal X-ray Crystallography: All the metal phosphates (Zn^{II}, Co^{II} and Sn^{II}) obtained were initially characterized using Single crystal X-ray diffraction. For this purpose, a suitable single crystal of each compound was carefully selected under a polarizing microscope and glued to a thin glass fiber with cyanoacrylate (superglue) adhesive. Single crystal structure determination by X-ray diffraction was performed on a Siemens Smart-CCD diffractometer equipped with a normal focus, 2.4 kW sealed tube x-ray source (Mo-K_α radiation, λ = 0.71073 Å) operating at 50 kV and 40Ma (T = 298K). A hemisphere of intensity data was collected at room temperature in 1321 frames with ω scans (width of 0.30° and exposure time of 10-30s per frame). The crystal structures were determined by direct methods using SHELXS-86[241] and difference Fourier syntheses. An empirical absorption correction based on symmetry equivalent reflections was applied using SADABS[242] program. All the hydrogen positions were initially located in the difference map, for the final refinement the hydrogen atoms were placed geometrically and held in the riding mode. The last cycles of refinement included atomic positions for all nonhydrogen atoms and the isotropic thermal parameters for all the hydrogen atoms. Full-matrix least-squares refinement against $|F^2|$ was carried out using SHELXTL-PLUS[243] suite of programs. Pertinent crystallographic details for the open-framework zinc phosphates, **I – X** are listed in Table 1.6, for amine phosphates in Table 1.7, for the various metal phosphates, **XI-XVI** in Table 1.8, for **XVII – XXII** in Table 1.9 and for **XXIII –XXIV** in Table 1.10.

Powder XRD: The metal phosphates were also characterized by powder x-ray diffraction (XRD) (Rich-Siefert, Model:XRD-3000-TT, CuKα, Ni filter, 40kV x 30mA) to ensure the phase purity. The powder XRD pattern indicated that the patterns were entirely consistent with the structures determined using the single-crystal X-ray diffraction. Least-squares refinement was carried out over the powder x-ray data in case of **II**, **III**, **X** and **XXIII**. A least-squares fit of the

Table 1.6. Crystal Data and Structural Refinement Parameters for Compounds I – X

	I	II	III	IV	V	VI	VII	VIII	IX	X
a (Å)	8.615(1)	10.200(1)	9.299(4)	17.279(1)	25.075(5)	10.021(4)	15.934(6)	27.071(2)	8.089(1)	13.653(1)
b (Å)	9.648(1)	9.998(1)	9.751(1)	5.193(1)	5.127(1)	8.286(3)	7.403(9)	5.215(1)	12.771(1)	9.718(1)
c (Å)	17.209(1)	10.447(1)	14.334(1)	20.115(1)	17.726(4)	11.856(7)	16.209(2)	17.920(1)	10.067(1)	8.691(1)
α (°)	90.0	90.0	90.0	90.0	90.0	90.0	90.0	90.0	90.0	90.0
β (°)	93.02(1)	92.24(2)	90.97(4)	92.6(1)	125.4(1)	103.1(3)	111..9(1)	130.3(1)	105.3(1)	94.9(1)
γ (°)	90.0	90.0	90.0	90.0	90.0	90.0	90.0	90.0	90.0	90.0
Volume ($Å^3$)	1428.4(2)	1064.62	1299.67(9)	1803.12(1)	1857.6(6)	958.7(7)	1774.52(11)	1930.8(3)	1003.2(2)	1148.9(1)
Z	4	2	2	8	8	2	4	4	4	4
Formula mass	510.8(1)	793.6	973.02	719.28	748.28	766.1	812.93	811.01	409.80	297.9
$\rho_{calc}(gcm^{-3})$	1.785	2.476	2.486	2.054	2.06	2.593	3.043	2.789	2.713	1.723
$\mu(mm^{-1})$	2.83	4.840	4.955	5.62	4.16	5.36	7.117	6.543	5.151	2.499
R $(F_0^2)[I>2\alpha(I)]$	2.98	3.8	2.8	3.7	3.2	5.4	4.5	3.89	4.22	4.0
wR_F^2	10.01	9.9	6.3	9.3	8.0	14.0	9.4	9.01	9.93	11.0
GOF	1.23	1.069	1.051	1.11	1.08	1.13	1.061	1.14	1.08	1.08

Table 1.7. Crystallographic parameters for the amine phosphates.

Code	Cell Parameters						Sp. Grp	Ref
	a (Å)	b (Å)	c (Å)	α (°)	β (°)	γ (°)		
PIPP	6.426	12.297	11.221	90.0	97.1	90.0	$P2_1/n$	232
MPIP-P	12.163	6.776	25.740	90.0	103.3	90.0	$P2_1/n$	*
DETAP	6.116	10.667	17.061	90.0	90.0	90.0	$P2_12_12_1$	234
DABCO-P	6.906	9.018	9.271	92.2	104.5	111.8	P(-1)	*
1,2-DAPP	10.869	6.278	11.389	90.0	104.5	90.0	$P2_1/n$	*
ENP	7.507	11.816	8.055	90.0	110.1	90.0	$P2_1/c$	255
DAHP	10.307	13.456	15.109	66.6	77.5	68.3	P(-1)	*
APPIP-P	6.608	8.571	10.130	112.4	96.6	102.6	P(-1)	*
DAPP	7.001	16.776	7.846	90.0	113.8	90.0	$P2_1/c$	255
TMED-P	8.209	8.412	8.618	114.3	94.9	118.1	P(-1)	*

* This work

Table 1.8. Crystal data and structure refinement parameters for compounds X1 – XVI

	XI	XII	XIII	XVI
Habit	Thin needle	Chunky, rod like	Chunky rod	Plate-like
Color	Clear transparent	Clear transparent	Clear transparent	Transparent
Size (μm^3)	40 x 60 x 120	140 x 160 x 260	120 x 120 x 200	60 x 120 x 120
a (Å)	8.931(2)	16.104(8)	13.414(3)	5.235(2)
b (Å)	14.025(6)	8.256(4)	12.871(2)	15.437(2)
c (Å)	9.311(2)	22.997(9)	8.225(1)	17.975(2)
α (°)	90.0	90.0	90.0	90.0
β (°)	95.4(1)	104.0(1)	94.8(1)	91.8(1)
γ (°)	90.0	90.0	90.0	90.0
V ($Å^3$)	1161.0(6)	2967.2(1)	1415.2(2)	1452.0(3)
Z, $2\theta_{max}$ (deg)	4, 46.64	4, 46.52	4, 46.52	4, 46.84
Space group	$P2_1/n$	C2/c	C2/c	$P2_1/n$
No. of reflections	4788	5956	2908	6034
Unique data	1668	2121	1018	2089
Data with $I > 2\sigma(I)$	1338	1982	918	1390
No of parameters	171	288	106	205
R_1[a]	0.04	0.02	0.03	0.07
WR_2[b]	0.08	0.05	0.07	0.17
GOF	1.139	1.093	1.053	1.17

Table 1.9. Crystal data and structure refinement parameters for compounds **XVII - XXII**

	XVII	**XVIII**	**XIX**	**XX**	**XXI**	**XXII**
Habit	Needle like	Thick plate	Thick plate	Thick plate	Chunky	Thick plate
Color	Blue	Blue	Blue	Blue	Blue	Clear translucent
Size (μm^3)	80 x 12 x 200	60 x 120 x 160	120 x 160 x 80	200 x 240 x120	80 x 80 x 160	200 x 200 x 80
a (Å)	8.387(7)	8.169(4)	11.484(1)	31.950(1)	9.552(1)	9.063(9)
b (Å)	8.575(8)	26.340(0)	8.723(9)	8.360(1)	9.980(1)	7.810(7)
c (Å)	23.898(9)	8.385(1)	11.011(7)	15.920(1)	10.001(1)	10.067(2)
α (°)	90.0	90.0	90.00	90.0	107.68(1)	90.0
β (°)	93.9(1)	110.9(1)	111.37(5)	96.6(1)	97.93(1)	115.3(1)
γ (°)	90.0	90.0	90.00	90.0	114.91(2)	90.0
V ($Å^3$)	1714.9(2)	1685.3(9)	1027.3(3)	4223.4(2)	783.8(1)	644.5(8)
Z, $2\theta_{max}$ (deg)	4, 46.56	4, 46.42	4, 46.42	4, 46.46	2, 46.58	4, 46.48
Space group	$P2_1/c$	$P2_1/c$	$P2_1/c$	$P2_1/c$	P(-1)	$P2_1/c$
No. of reflections	6858	7015	4153	16643	3315	2595
Unique data	2464	2404	1459	5932	2213	919
Data with $I > 2\sigma(I)$	2282	2144	1340	4946	2162	849
No of parameters	253	253	127	608	226	83
R_1[a]	0.04	0.03	0.03	0.05	0.04	0.03
WR_2[b]	0.10	0.09	0.08	0.12	0.11	0.09
GOF	1.125	1.228	1.053	1.076	1.11	1.164

Table 1.10. Crystal data and structure refinement parameters for the zinc phosphate monomer, **XXIII** and the layer phosphate, **XXIV**.

	XXIII	**XXIV**
Habit	Thick chunk	Thick plate
Color	Clear transparent	Clear transparent
Size (μm^3)	120 x 80 x 200	140 x 160 x 260
a (Å)	8.627(2)	8.953(9)
b (Å)	8.894(9)	9.712(9)
c (Å)	12.674(2)	13.533(7)
α (°)	88.9(4)	90.0
β (°)	75.1(7)	95.9(8)
γ (°)	63.0(6)	90.0
V ($Å^3$)	832.8(2)	1170.5(9)
Z, $2\theta_{max}$ (deg)	2, 46.48	4, 46.52
Space group	P(-1)	$P2_1/c$
No. of reflections	3555	4801
Unique data	2369	1679
Data with I >2σ(I)	2346	1343
No of parameters	218	177
R_1[a]	0.048	0.033
WR_2[b]	0.131	0.087
GOF	1.084	1.098

powder XRD (CuKα) lines, using the *hkl* indices generated from single crystal X-ray data, gave the following cell for **II**: a = 10.149(4), b = 9.951(5), c = 10.399(6) Å, β = 92.2(2)° and for **III**: a = 9.279(3), b = 9.724(3), c = 14.297(3) Å, β = 90.9(1)°, which is in good agreement with that determined using the single-crystal XRD. The powder x-ray data for **II**, and **III** is given in Table 1.11 and 1.12. A least squares fit of the powder XRD for **X** lines, using the *hkl* indices garnered from single crystal X-ray data, gave the following cell: a = 13.653(2), b = 9.718(5), c = 8.692(2) Å, β = 94.97(3)°, which is in good agreement with that determined by single crystal XRD. Powder XRD pattern of **XXIII** is entirely consistent with the structure determined by single crystals X-ray diffraction and is given in Table 1.13.

EDAX: Energy dispersive analysis of X-rays (EDAX) was carried out using a scanning electron microscope Leica S440i fitted with a link ISIS spectrometer. This analysis gave the metal-phosphorus ratios in the various compounds studied here.

MASNMR: Magic angle spinning nuclear magnetic resonance (MASNMR) spectra were recorded on a Bruker DX-300 (300 MHz) spectrometer.

TGA: The thermogravimetric analysis (TGA) of the samples was carried out using a Mettler-Toledo TG850 instrument. Apart from compound **XI, XII, XIV** and **XV** where mixed phases were obtained, and the pure phases could not be isolated despite the modifications in synthetic conditions, most of the compounds have been obtained in pure phase, and characterized using thermogravimetric analyses.

Table 1.11 X-ray powder data for **II**, $[C_3N_2H_{12}]_2[Zn_4(PO_4)_4]$

h	k	l	$2\theta_{obs}$	$\Delta(2\theta)^a$	d_{calc}	$\Delta(d)^b$	$I_{rel}{}^c$
0	1	1	12.419	-0.104	7.187	-0.060	98.1
1	1	0	12.461	0.001	7.103	0.001	99.6
1	1	-1	14.934	-0.015	5.938	-0.006	7.9
1	1	1	15.396	-0.099	5.792	-0.037	6.5
0	0	2	17.114	-0.048	5.196	-0.015	14.8
2	1	0	19.653	-0.004	4.518	-0.001	15.8
1	1	-2	20.896	0.016	4.248	0.003	18.4
2	1	-1	21.204	-0.028	4.196	-0.006	17.1
1	2	-1	21.558	-0.037	4.129	-0.007	22.6
1	2	1	21.815	-0.027	4.079	-0.005	32.8
2	0	2	25.105	-0.105	3.562	-0.015	18.8
2	2	-1	26.131	0.170	3.388	0.022	22.0
2	2	1	26.828	-0.085	3.333	-0.010	16.8
0	1	3	27.220	0.040	3.271	0.005	100.0
3	1	0	27.871	0.002	3.201	0.000	74.4
1	3	0	28.304	0.003	3.153	0.001	25.3
1	1	-3	28.377	-0.013	3.147	-0.001	8.1
1	3	-1	29.558	-0.047	3.027	-0.005	7.1
2	1	-3	32.002	0.018	2.795	0.002	4.6
1	2	-3	32.502	-0.060	2.760	-0.005	29.9
3	2	-1	32.928	-0.020	2.722	-0.002	25.5
3	2	1	33.476	-0.029	2.679	-0.002	5.7
0	0	4	34.533	-0.008	2.598	-0.001	4.7
4	0	0	35.468	-0.065	2.535	-0.004	9.7
2	2	-3	35.697	0.025	2.513	0.002	5.0
0	4	0	36.149	-0.045	2.488	-0.003	6.7
4	0	1	36.751	0.057	2.442	0.004	3.1
4	1	-1	37.244	0.051	2.411	0.003	5.1
0	3	3	37.488	0.054	2.396	0.003	3.4
3	2	3	42.210	-0.042	2.143	-0.002	6.9
2	4	2	44.376	0.042	2.040	0.002	3.1
4	3	0	45.055	-0.052	2.014	-0.002	5.1
3	3	-3	45.824	0.018	1.979	0.001	3.6
4	3	1	46.080	0.082	1.966	0.003	2.9
5	1	1	46.876	-0.016	1.939	-0.001	2.9
2	5	0	49.142	0.037	1.853	0.001	8.6

[a] $2\theta_{obs} - 2\theta_{calc}$;

[b] $d_{obs} - d_{calc}$;

[c] $100 \times I/I_{max}$

Table 1.12. X-ray powder data for **III**, $[C_3N_2H_{12}]_2[Zn_5(H_2O)(PO_4)_4(HPO_4)]$

h	k	l	$2\theta_{obs}$	$\Delta(2\theta)^a$	d_{calc}	$\Delta(d)^b$	$I_{rel}{}^c$
1	0	0	9.576	-0.043	9.278	-0.042	15.4
0	0	2	12.407	-0.024	7.148	-0.014	100.0
1	1	0	13.204	-0.015	6.713	-0.008	88.7
0	2	0	18.269	-0.023	4.862	-0.006	21.8
2	0	1	20.230	-0.008	4.391	-0.002	5.7
1	0	-3	20.818	-0.002	4.267	-0.001	3.1
2	1	1	22.197	0.015	4.002	0.003	11.5
2	0	-2	22.717	-0.037	3.921	-0.006	16.4
2	0	2	23.042	-0.016	3.862	-0.003	14.0
1	2	-2	24.045	-0.001	3.701	-0.000	11.6
0	0	4	24.936	-0.023	3.574	-0.003	4.9
2	2	0	26.568	-0.011	3.356	-0.001	8.6
2	2	-1	27.203	0.017	3.276	0.002	8.1
1	1	-4	28.128	0.019	3.170	0.002	33.7
1	3	0	29.175	0.008	3.060	0.001	14.9
3	0	1	29.657	-0.003	3.012	-0.000	19.2
1	3	1	29.886	0.008	2.989	0.001	23.2
0	2	4	31.046	0.010	2.880	0.001	12.1
2	0	-4	31.317	0.028	2.854	0.002	11.4
2	0	4	31.843	0.015	2.809	0.001	6.5
0	1	5	32.668	-0.022	2.743	-0.002	6.1
1	0	5	32.897	0.034	2.720	0.003	4.8
3	0	3	34.840	0.001	2.575	0.000	2.6
2	2	4	36.956	0.002	2.432	0.000	5.0
4	2	0	43.211	0.005	2.093	0.000	5.0
1	2	6	43.574	-0.024	2.078	-0.001	1.7
0	0	7	44.353	0.003	2.042	0.000	1.0

[a] $2\theta_{obs} - 2\theta_{calc}$;

[b] $d_{obs} - d_{calc}$;

[c] $100 \times I/I_{max}$

Table 1.13 Powder X-ray diffraction pattern of **XXIII**, $[C_6N_2H_{18}]^{2+}[Zn(H_2PO_4)_2(HPO_4)]^{2-}$

h	k	l	d_{obs}	d_{calc}	Δd	I_{rel}
0	0	1	12.181	12.187	-0.006	36.5
0	1	0	7.880	7.883	-0.003	94.6
1	0	0	7.391	7.392	-0.001	22.9
1	0	1	7.285	7.279	0.006	28.6
0	1	-1	6.991	6.990	0.001	7.7
1	1	1	6.838	6.839	-0.001	100.0
0	1	1	6.299	6.301	-0.002	10.1
0	0	2	6.088	6.093	-0.005	14.7
1	1	-1	5.872	5.873	-0.001	21.0
1	0	2	5.511	5.512	-0.001	10.1
1	-1	0	4.458	4.457	0.001	17.8
1	2	0	4.441	4.438	0.003	38.9
1	1	-2	4.341	4.344	-0.003	21.7
2	1	1	4.294	4.296	-0.002	9.3
1	2	1	4.221	4.223	-0.002	8.7
2	1	0	4.174	4.174	-0.000	9.4
1	0	-2	4.169	4.168	0.001	10.4
1	-1	-1	3.902	3.905	-0.003	8.1
0	2	-1	3.878	3.881	-0.003	43.6
1	1	3	3.845	3.845	0.000	70.6
0	1	-3	3.790	3.790	0.000	54.6
2	2	1	3.697	3.703	-0.006	40.9
2	0	0	3.697	3.696	0.001	46.3
2	2	0	3.678	3.681	-0.003	8.1
1	2	2	3.655	3.656	-0.001	17.1
2	0	2	3.637	3.639	-0.002	24.3
0	2	1	3.633	3.632	0.001	14.3
0	1	3	3.461	3.455	0.006	34.1
2	2	2	3.419	3.420	-0.001	9.2
1	1	-3	3.328	3.325	0.003	8.4
2	0	-1	3.305	3.292	0.013	15.4
0	2	-3	3.003	3.004	-0.001	24.6
2	-1	1	2.979	2.972	0.007	7.6
1	3	0	2.945	2.945	0.000	9.8

2	-1	0	2.873	2.872	0.001	8.8
3	1	1	2.845	2.845	0.000	14.3
2	3	1	2.842	2.842	0.000	9.5
1	-1	4	2.840	2.840	0.000	7.1
2	0	-2	2.830	2.831	-0.001	9.1
3	2	2	2.746	2.744	0.002	21.8
0	3	-1	2.632	2.631	0.001	7.5
2	1	-3	2.600	2.600	0.000	8.0
1	0	-4	2.580	2.576	0.004	7.4
0	2	-4	2.555	2.555	0.000	7.5
1	0	5	2.534	2.533	0.001	7.1
1	3	-3	2.404	2.403	0.001	8.5
2	4	-1	2.165	2.168	-0.003	8.0
0	4	0	1.971	1.971	0.000	9.8

Refined lattice parameters (CuKα): a = 8.634(2), b = 8.904(1), c = 12.687(3) Å, α = 88.95(1), β = 75.19(1), γ = 63.01(2)°.

4. RESULTS AND DISCUSSION

4.1. Open-framework Zinc phosphates

$[NH_3CH_2CH(OH)CH_2NH_3.Zn_2(HPO_4)_3]$, I : The asymmetric unit of **I** (Fig. 1.11) contains 23 non-hydrogen atoms. The atomic coordinates for the non-hydrogen atoms are listed in Table 1.14. The structure consists of a network on ZnO_4 and HPO_4 moieties which are vertex linked forming a two-dimensional layer like arrangement and are held by strong hydrogen bonded interaction with the diprotonated 1,3-diammmonium –2-hydroxy propane. There are two crystallographically distinct Zn atoms and three crystallographically distinct P atoms in the asymmetric unit. Each Zn atom is four-coordinated with oxygens and the Zn-O distances are in the range 1.916 – 1.961Å [$(Zn(1) - O)_{ave.}$ = 1.939Å and $(Zn(2) - O)_{ave.}$ = 1.948Å] which are typical of tetrahedral Zn. All the Zn atoms are linked to P via Zn-O-P bonding. The P – O distances are in the range 1.510 – 1.595Å [$(P(1) - O)_{ave.}$ = 1.534Å; $(P(2) - O)_{ave.}$ = 1.534Å and $(P(3) - O)_{ave.}$ = 1.537Å). Of the four oxygens that are linked to P(1) and P(2), three are, respectively, bonded to Zn via the Zn-O-P linkage and the last one is a terminal P – O vertex. In the case of P(3), two oxygen atoms are linked to Zn and the remaining two are terminal P-O vertex. There are, therefore, four terminal P-O vertexes. Bond valence sum calculations[244] performed on the framework indicate that three of the terminal oxygen atoms are protonated. The P-O bond length considerations indicate that P – O distances of P(1) – O(9) = 1.568Å, P(2) – O(10) = 1.582Å and P(3) – O(12) = 1.593Å are protonated. Similar lengthening of P – OH distances have been found in several phosphate based open-framework materials. Thus, it is found that all the phosphate groups in **I** are protonated forming hydrogen phosphate (HPO_4) groups giving the molecular formula as $[(NH_3CH_2CH(OH)CH_2NH_3).Zn_2(HPO_4)_3]$. The O-Zn-O and O-P-O bond angles are as expected for atoms in a tetrahedral environment [$(O - Zn(1) - O)_{ave.}$ = 109.5°; $(O - Zn(2) - O)_{ave.}$ = 110.2°; $(O - P(1) - O)_{ave.}$ = 109.4°; $(O - P(2) - O)_{ave.}$ = 109.6° and $(O - P(3) - O)_{ave.}$ = 109.4°). The N-C and C-C and C-O bond

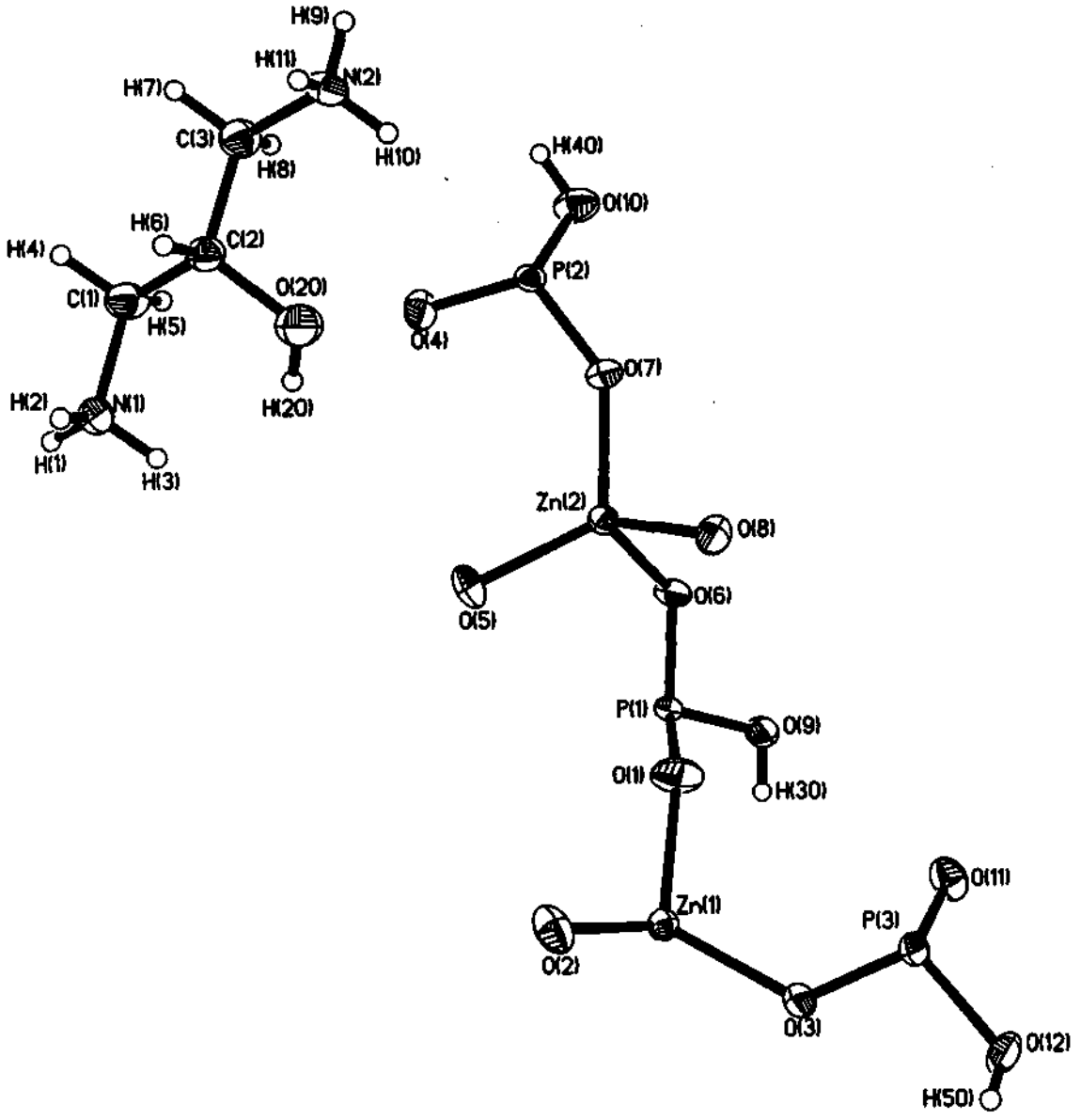

Fig. 1.11. Asymmetric unit of **I**, $[NH_3CH_2CH(OH)CH_2NH_3.Zn_2(HPO_4)_3]$. The thermal ellipsoids are given at 50% probability.

Table 1.14. Atomic coordinates and isotropic thermal parameters for the non-hydrogen atoms in **I**, $[NH_3CH_2CH(OH)CH_2NH_3.Zn_2(HPO_4)_3]$

Atom	x	y	z	U_{eq}/U_{iso}
Zn(1)	0.1724(1)	0.1334(1)	0.0210(1)	0.015
Zn(2)	-0.2600(1)	0.4831(1)	0.0223(1)	0.015
P(1)	0.0524(1)	0.4081(1)	0.1089(1)	0.014
P(2)	-0.4911(1)	0.7441(1)	0.0117(1)	0.014
P(3)	0.0463(1)	-0.1030(1)	0.1268(1)	0.015
O(1)	0.0448(4)	0.2739(4)	0.0637(2)	0.030
O(2)	0.1150(4)	0.1227(4)	-0.0891(2)	0.027
O(3)	0.1625(4)	-0.0494(3)	0.0698(2)	0.021
O(4)	-0.3919(4)	0.8263(4)	-0.0424(2)	0.025
O(5)	-0.1699(4)	0.4891(3)	-0.0785(2)	0.023
O(6)	-0.1080(4)	0.4752(3)	0.1112(2)	0.019
O(7)	-0.3980(4)	0.6301(3)	0.0533(2)	0.021
O(8)	-0.3641(4)	0.3057(3)	0.0339(2)	0.021
O(9)	0.1023(4)	0.3751(4)	0.1959(2)	0.025
O(10)	-0.5417(4)	0.8409(4)	0.0801(2)	0.028
O(11)	0.0387(4)	-0.0126(3)	0.1983(2)	0.024
O(12)	0.1109(4)	-0.2475(3)	0.1598(2)	0.025
O(20)	-0.4705(4)	0.7142(4)	-0.1914(2)	0.033
N(1)	-0.2599(5)	0.8356(4)	-0.2907(2)	0.022
N(2)	-0.7720(5)	0.8235(4)	-0.1773(3)	0.027
C(1)	-0.3854(6)	0.9192(5)	-0.2582(3)	0.026
C(2)	-0.5183(5)	0.8273(5)	-0.2380(3)	0.021
C(3)	-0.6425(6)	0.9131(5)	-0.2017(3)	0.025

distances and angles are in good agreement with the literature value. The important bond distances and angles are given in Table 1.15.

The connectivity between ZnO_4 and HPO_4 moieties result in a layered topology based on a two-dimensional network of 'bifurcated' 12-membered rings similar to that seen in zinc phosphate obtained with 1,6Hexanediamine (DAH). The 12-membered rings consist of 12-T atoms (T = tetrahedral centre: Zn or P) formed by 6 zinc and 6 phosphorus atoms which strictly alternate. Unlike the other solid, in this case there is only one type of layer that is formed (Fig. 1.12) along the *ab* plane. The 'bifurcated' 12-membered ring opening within the layer is arranged in an ordered fashion rather than in the zigzag fashion as in the other zinc phosphate with DAH. Alternatively, the layers can be considered as formed from a chain of 4-membered rings constructed from two Zn and P atoms ($Zn_2P_2O_4$ units) that are connected to each other via two PO_4 units, creating bifurcation within the layer (Fig. 1.12). The 1,3-diammonium-2-hydroxy propane cation occupies space between the layers, and interacts with the layers through N-H...O hydrogen bonds and C-O-H...O hydrogen bonds (Fig. 1.13). All the six N-H protons and the –O-H moiety of the amine molecule participate in extensive hydrogen bonding to the acceptor oxygen species. The different hydrogen bonded distances in **I** are given in Table 1.16.

$[N_2C_3H_{12}]_2[Zn_4(PO_4)_4]$, II : The asymmetric unit of II contains 34 non-hydrogen atoms as shown in Fig.1.14, of which 24 atoms belong to the 'framework' and 10 atoms to the 'guest' species The atomic coordinates are presented in Table 1.17. There are four crystallographically distinct Zn and P atoms. The zinc atoms are tetrahedrally coordinated by their O atom neighbors with Zn – O bond lengths in the range 1.910 – 2.005 Å (av. Zn(1) – O = 1.934, Zn(2) – O = 1.945, Zn(3) – O = 1.946, Zn(4) – O = 1.949 Å). The O – Zn – O angles are in the range 97.3 – 120.2° (av. O – Zn(1) – O = 109.6, O – Zn(2) – O = 109.6, O – Zn(3) – O = 109.4, O – Zn(4) – O = 109.2°). The four zinc atoms make four Zn – O – P bonds to four distinct P atom neighbors with a fairly wide spread of angles and an average Zn – O – P bond angle of 136.6°. The phosphorus atoms also make four P – O – Zn linkages. The P – O distances are in

Table 1.15. Selected bond lengths [Å] and angles [°] in **I**, $[NH_3CH_2CH(OH)CH_2NH_3.Zn_2(HPO_4)_3]$

Moiety	Distance, Å	Moiety	Angle (°)
Zn(1) – O(1)	1.916(3)	O(2) – Zn(1) – O(3)	110.9(2)
Zn(1) – O(2)	1.937(3)	O(1) – Zn(1) – O(3)	115.7(2)
Zn(1) – O(3)	1.957(3)	O(5) – Zn(2) – O(6)	114.61(14)
Zn(1) – O(4)$^{\#1}$	1.947(3)	O(5) – Zn(2) – O(7)	120.21(14)
Zn(2) – O(5)	1.938(3)	O(5) – Zn(2) – O(8)	109.02(14)
Zn(2) – O(6)	1.961(3)	O(7)– Zn(2) – O(6)	101.98(14)
Zn(2) – O(7)	1.944(3)	O(7) – Zn(2) – O(8)	108.76(13)
Zn(2) – O(8)	1.947(3)	O(8) – Zn(2) – O(6)	100.31(14)
P(1) – O(1)	1.510(4)	O(1) – P(1) – O(5)$^{\#1}$	113.0(2)
P(1) – O(5)$^{\#1}$	1.530(3)	O(1) – P(1) – O(6)	111.2(2)
P(1) – O(6)	1.528(3)	O(1) – P(1) – O(9)	108.7(2)
P(1) – O(9)	1.568(3)	O(5)$^{\#1}$ – P(1) – O(9)	107.8(2)
P(2) – O(4)	1.519(3)	O(6) – P(1) – O(5)$^{\#1}$	110.4(2)
P(2) – O(7)	1.518(3)	O(6) – P(1) – O(9)	105.4(2)
P(2) – O(8)$^{\#2}$	1.516(3)	O(4) – P(2) – O(10)	109.5(2)
P(2) – O(10)	1.582(4)	O(7) – P(2) – O(4)	111.5(2)
P(3) – O(2)$^{\#3}$	1.514(4)	O(7) – P(2) – O(10)	103.7(2)
P(3) – O(3)	1.527(3)	O(8)$^{\#2}$ – P(2) – O(4)	109.4(4)
P(3) – O(11)	1.513(4)	O(8)$^{\#2}$ – P(2) – O(7)	114.5(2)
P(3) – O(12)	1.595(3)	O(8)$^{\#2}$ – P(2) – O(10)	108.7(2)
Moiety	Angle (°)	O(2)$^{\#3}$ – P(3) – O(3)	112.7(2)
O(1) – Zn(1) – O(2)	106.9(2)	O(2)$^{\#3}$ – P(3) – O(12)	109.7(2)
O(1) – Zn(1) – O(4)$^{\#1}$	111.0(2)	O(3) – P(3) – O(12)	107.2(2)
O(2) – Zn(1) – O(4)$^{\#1}$	113.01(14)	O(11) – P(3) – O(2)$^{\#3}$	110.0(2)
O(4)$^{\#1}$ – Zn(1) – O(3)	99.38(14)	O(11) – P(3) – O(3)	112.7(2)
		O(11) – P(3) – O(12)	104.1(2)

Organic Moiety

Moiety	Distance, Å	Moiety	Angle (°)
N(1) – C(1)	1.482(6)	N(1) – C(1) – C(2)	110.2(4)
N(2) – C(3)	1.489(6)	C(1) – C(2) – C(3)	109.6(4)
C(1) – C(2)	1.504(7)	N(2) – C(3) – C(2)	110.8(4)
C(2) – C(3)	1.514(7)		

symmetry transformations used to generate equivalent atoms:

#1 –x, -y+1, -z #2 -x-1, -y+1, -z #3 -x, -y, -z

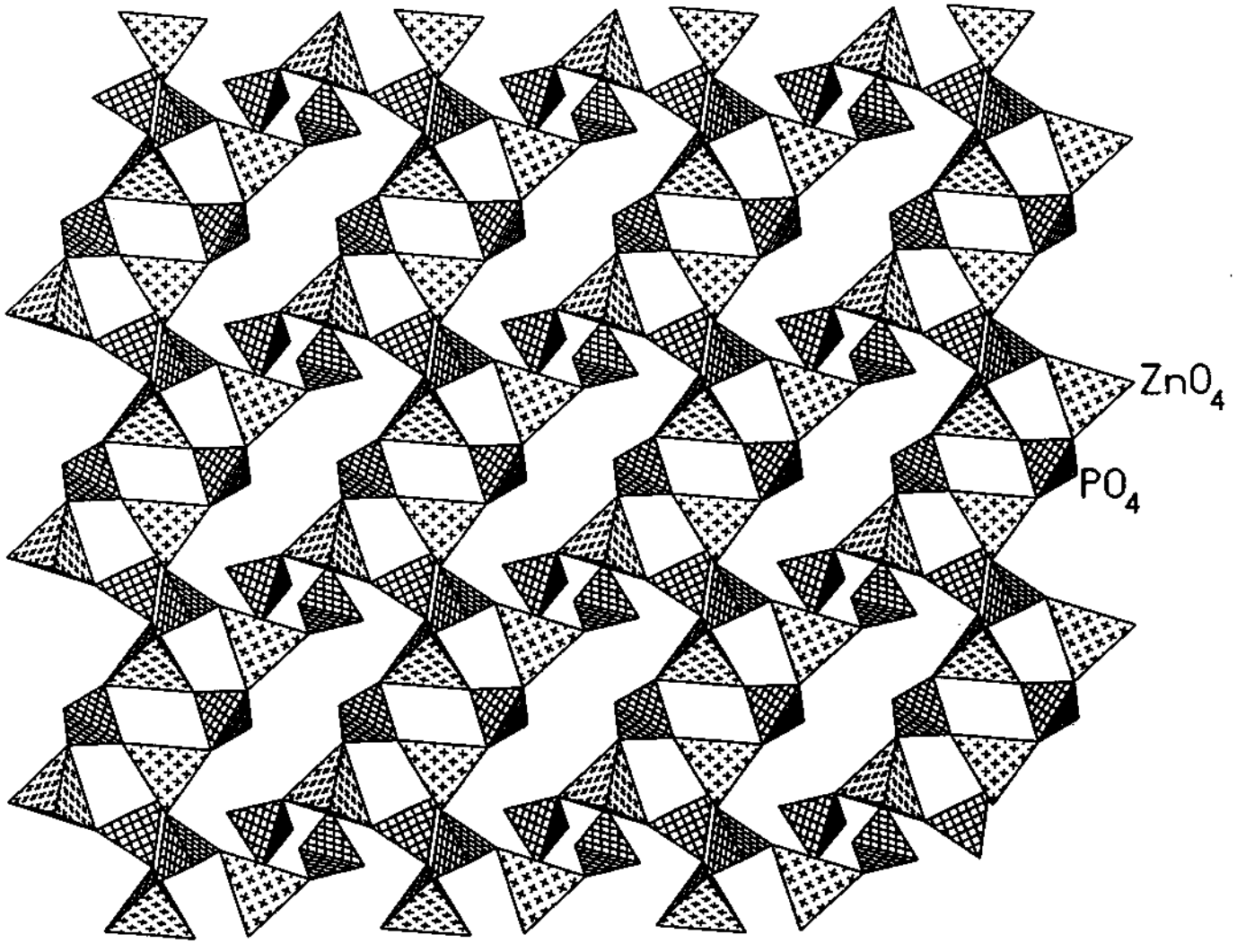

Fig 1.12 Polyhedral view of **I** , $[NH_3CH_2CH(OH)CH_2NH_3.Zn_2(HPO_4)_3]$ along the *ab* plane. Note that the 12–membered pore openings are more regular and ordered.

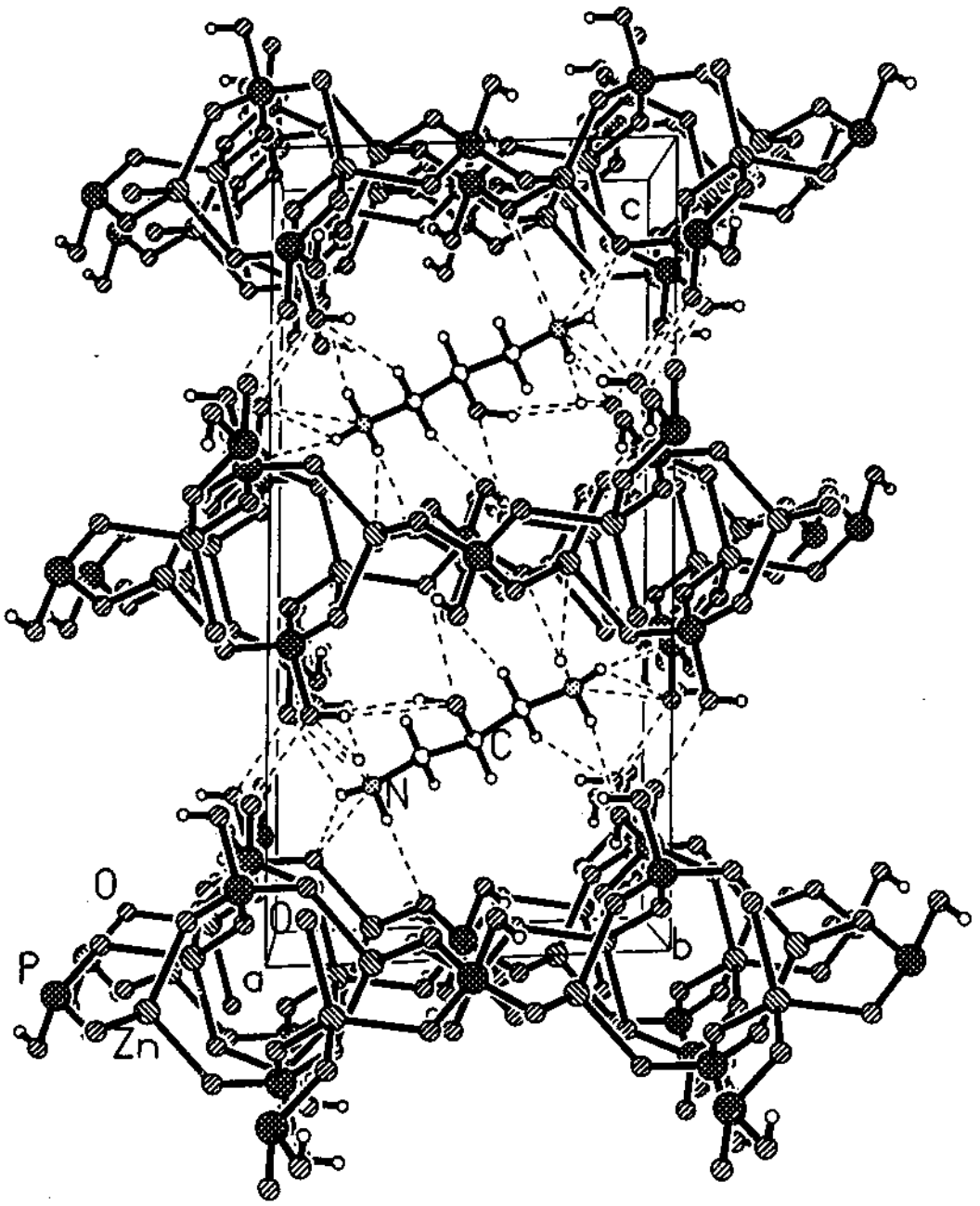

Fig 1.13 Structure of **I** , $[NH_3CH_2CH(OH)CH_2NH_3.Zn_2(HPO_4)_3]$ showing the layer arrangement and the amine molecules. Dotted lines represent hydrogen bonding in the solid.

Table 1.16. Important hydrogen bond distances and angles in compound I.

Compound I			
Moiety	Distance (Å)	Moiety	Distance (Å)
O(6) – H(1)	2.094(1)	O(6) – H(1) – N(1)	142.4(4)
O(9) – H(3)	2.031(1)	O(9) – H(3) – N(1)	164.6(2)
O(8) – H(10)	2.119(1)	O(8) – H(10) – N(2)	155.6(3)
O(12) – H(11)	2.179(1)	O(12) – H(11) – N(2)	157.4(4)
O(9) – H(20)	2.542(1)	O(9) – H(20) – O(20)	152.6(3)
O(20) – H(30)	2.495(1)	O(20) – H(30) – O(9)	164.5(3)
O(9) – H(7)	2.528(1)	O(9) – H(7) – C(3)	153.2(5)
O(10) – H(8)	2.573(1)	O(10) – H(8) – C(3)	157.6(4)
O(4) – H(40)$^{\&}$	2.594(1)	O(4) – H(40) – O(10)$^{\&}$	148.2(4)
O(5) – H(50)$^{\&}$	2.023(1)	O(5) – H(50) – O(12)$^{\&}$	153.2(4)

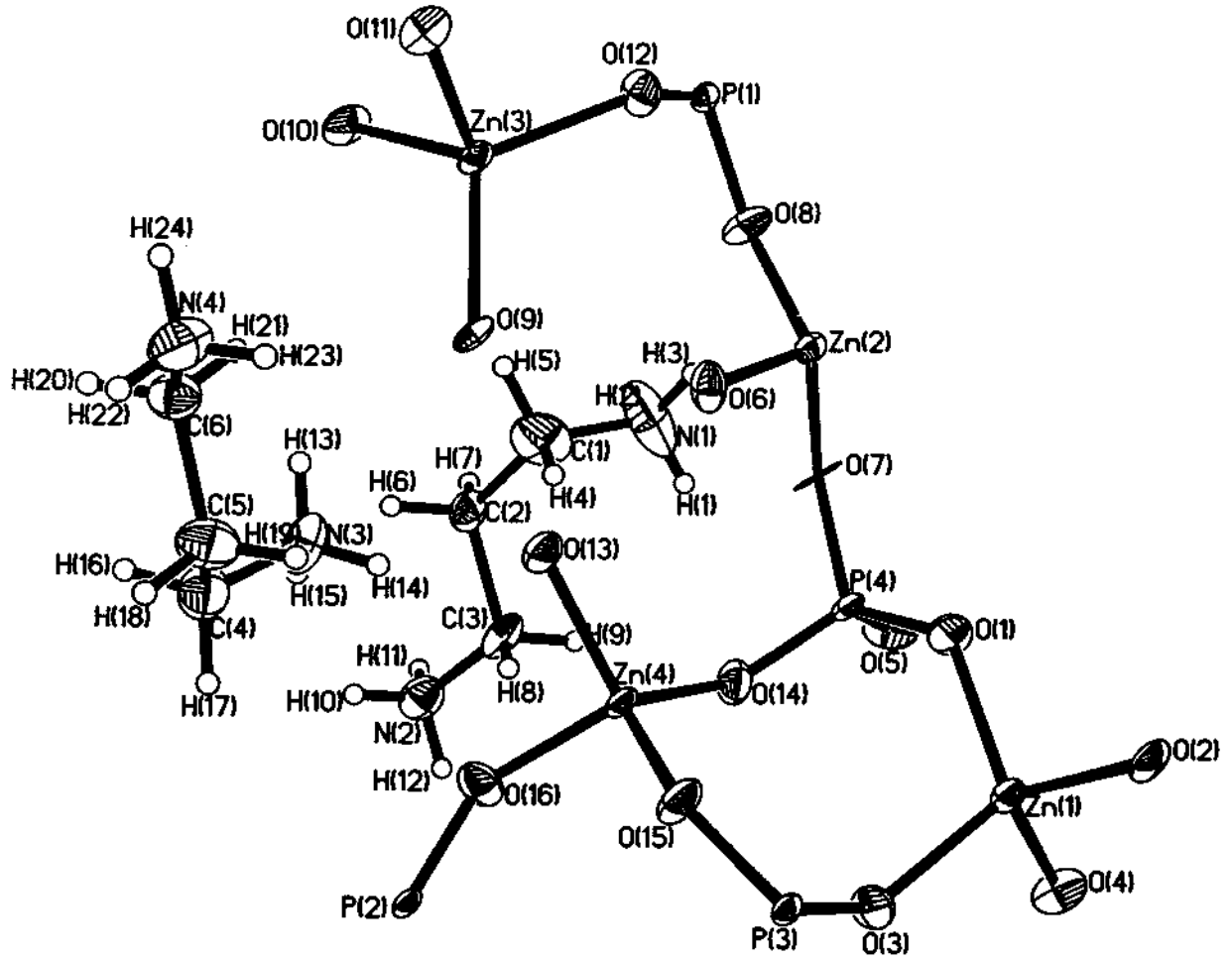

Fig 1.14 ORTEP plot of **II** , $[C_3N_2H_{12}]_2\,[Zn_4(PO_4)_4]$. Thermal ellipsoids are given at 50% probability.

Table 1.17. Atomic coordinates [x 10^4] and equivalent isotropic displacement parameters [$Å^2$ x 10^3] for **II**, $[C_3N_2H_{12}]_2[Zn_4(PO_4)_4]$.

Atom	x	y	z	U_{eq}[a]
Zn(1)	1372(1)	4235(1)	8927(1)	14(1)
Zn(2)	6276(1)	5989(1)	8789(1)	14(1)
Zn(3)	9170(1)	6501(1)	6012(1)	14(1)
Zn(4)	4208(1)	3143(1)	6250(1)	14(1)
P(1)	9282(2)	6173(2)	9058(2)	12(1)
P(2)	3841(2)	637(2)	4313(2)	11(1)
P(3)	1144(2)	3968(2)	5878(2)	12(1)
P(4)	4327(2)	3546(2)	9293(2)	13(1)
O(1)	3194(5)	4568(7)	9309(6)	28(2)
O(2)	591(5)	5973(7)	9170(5)	24(1)
O(3)	1009(5)	3448(7)	7242(5)	24(1)
O(4)	618(5)	2867(7)	9989(5)	27(2)
O(5)	4297(6)	2620(7)	10459(5)	27(1)
O(6)	5916(5)	6302(7)	6978(5)	21(1)
O(7)	5631(5)	4294(7)	9384(5)	23(1)
O(8)	8155(5)	5742(7)	9376(5)	24(1)
O(9)	7633(4)	5553(8)	5434(5)	27(2)
O(10)	10706(5)	5397(7)	5766(6)	26(1)
O(11)	9673(5)	8089(7)	5033(5)	24(1)
O(12)	9040(5)	7297(7)	7719(5)	22(1)
O(13)	5655(5)	4200(7)	5655(5)	23(1)
O(14)	4236(5)	2694(6)	8057(5)	23(1)
O(15)	2610(5)	3953(7)	5527(5)	24(1)
O(16)	4548(5)	1437(7)	5372(5)	24(1)
N(4)	7967(8)	5956(9)	2040(8)	37(2)
N(3)	7430(7)	2452(9)	4440(7)	32(2)
C(6)	8249(8)	4627(10)	2571(8)	27(2)
C(5)	6955(9)	3795(11)	2522(9)	36(2)
C(4)	7167(9)	2427(12)	3057(9)	35(2)
N(2)	6918(7)	-1049(8)	7082(7)	29(2)
N(1)	7790(9)	2679(12)	9283(8)	61(3)
C(3)	6751(8)	306(11)	7563(8)	27(2)
C(2)	8080(8)	1077(10)	7568(8)	23(2)
C(1)	7985(10)	2478(13)	7930(9)	43(3)

[a] U(eq) is defined as one third of the trace of the orthogonalized U_{ij} tensor.

the range 1.500 – 1.554 Å (av. P(1) – O = 1.533, P(2) – O = 1.531, P(3) – O = 1.526, P(4) – O = 1.537 Å) and the O – P – O bond angles are in the range 106-1 – 111.6° (av. 109.5°) (Table 1.18 and 1.19). Assuming the usual valence of Zn, P and O to be +2, +5 and –2 respectively, the framework stoichiometry of $Zn_4(PO_4)_4$ creates a net framework charge of –4. There presence of two molecules of $[NH_3(CH_2)_3NH_3]$ would account for +4 arising from the complete protonation of the amine. Bond valence sum calculations[244] on the framework agree with the above results.

The framework structure of **II**, is built from strictly alternating ZnO_4 and PO_4 tetrahedra that are linked through their vertices giving rise to three-dimensional architecture possessing channels. The connectivity between ZnO_4 and PO_4 tetrahedra result in 4-membered rings, which are connected to each other via oxygens. The connectivity between the 4-membered rings is such that they are arranged around the 2-fold screw axis forming a chain as shown in Fig. 1.15. The chains are further connected together within and out of the plane forming 8-membered helical channels along *c* axis (Fig. 1.16a). The width of this channel is 9.1 x 5.6 Å. Along the *a* axis, the connectivity between the tetrahedra gives rise to another 8-membered channels of width 6.7 x 6.5 Å as shown in Fig.1.16b. The diprotonated amine (DAP) molecule, sits in the middle of these channels and interact with the framework through hydrogen bonds (Fig. 1.17).

$[C_3N_2H_{12}]_2[Zn_5(H_2O)(PO_4)_4(HPO_4)]$, III : The asymmetric unit contains 41 non-hydrogen atoms as shown in Fig. 1.18 with five Zn and P atoms being crystallographically distinct. The atomic coordinates are presented in Table 1.20. The structure consists of strictly alternating ZnO_4, PO_4 and HPO_4 tetrahedra connected through Zn – O – P bonds, giving rise to the three-dimensional architecture. The Zn atoms are all tetrahedrally coordinated to four oxygen atoms with the Zn – O bond length in the range 1.886 – 1.978 Å (av. 1.939 Å). The O – Zn – O bond angles are in the range 98.3 – 123.9° (av. 109.5°). Of the

Table 1.18. Selected bond distances for **II**, $[C_3N_2H_{12}]_2[Zn_4(PO_4)_4]$.

Moiety	Distance (Å)	Moiety	Distance (Å)
Zn(1) - O(1)	1.916(5)	P(1) – O(4)$^{\#1}$	1.525(6)
Zn(1) - O(2)	1.932(7)	P(1) – O(12)	1.527(5)
Zn(1) - O(4)	1.939(6)	P(1) – O(2)$^{\#2}$	1.528(6)
Zn(1) - O(3)	1.950(5)	P(1) – O(8)	1.550(6)
Zn(2) - O(5)$^{\#1}$	1.911(6)	P(2) – O(16)	1.524(6)
Zn(2) - O(7)	1.929(7)	P(2) – O(13)$^{\#3}$	1.526(7)
Zn(2) - O(6)	1.938(5)	P(2) – O(6)$^{\#3}$	1.533(5)
Zn(2) - O(8)	2.005(5)	P(2) – O(9)$^{\#3}$	1.539(5)
Zn(3) - O(9)	1.910(6)	P(3) – O(10)$^{\#4}$	1.500(7)
Zn(3) - O(10)	1.942(6)	P(3) – O(11)$^{\#3}$	1.520(6)
Zn(3) - O(12)	1.962(5)	P(3) – O(3)	1.528(6)
Zn(3) - O(11)	1.968(6)	P(3) – O(15)	1.554(5)
Zn(4) - O(13)	1.937(6)	P(4) – O(7)	1.526(6)
Zn(4) - O(14)	1.940(5)	P(4) – O(5)	1.531(6)
Zn(4) - O(15)	1.946(5)	P(4) – O(1)	1.543(6)
Zn(4) - O(16)	1.973(6)	P(4) – O(14)	1.546(6)
		Organic Moiety	
N(1) – C(1)	1.448(13)	N(3) – C(4)	1.459(12)
C(1) – C(2)	1.46(2)	C(4) – C(5)	1.49(2)
C(2) – C(3)	1.559(12)	C(5) – C(6)	1.559(13)
C(3) – N(2)	1.457(14)	C(6) – N(4)	1.464(13)

Symmetry transformations used to generate equivalent atoms:

#1 -x+1, y+1/2, -z+2; #2 x+1, y, z; #3 -x+1, y-1/2, -z+1; #4 x-1, y, z

Table 1.19. Selected bond angles for II, $[C_3N_2H_{12}]_2[Zn_4(PO_4)_4]$.

Moiety	Angle (°)	Moiety	Angle (°)
O(1) – Zn(1) – O(2)	102.6(3)	$O(4)^{\#1}$ – P(1) – O(12)	108.2(4)
O(1) – Zn(1) – O(4)	114.0(3)	$O(4)^{\#1}$ – P(1) – $O(2)^{\#2}$	106.3(3)
O(2) – Zn(1) – O(4)	112.6(3)	O(12) – P(1) – $O(2)^{\#2}$	111.4(3)
O(1) – Zn(1) – O(3)	114.0(2)	$O(4)^{\#1}$ – P(1) – O(8)	111.4(3)
O(2) – Zn(1) – O(3)	114.7(3)	O(12) – P(1) – O(8)	110.0(3)
O(4) – Zn(1) – O(3)	99.6(3)	$O(2)^{\#2}$ – P(1) – O(8)	109.5(4)
$O(5)^{\#1}$ – Zn(2) – O(7)	120.2(2)	O(16) – P(2) – $O(13)^{\#3}$	109.2(3)
$O(5)^{\#1}$ – Zn(2) – O(6)	102.4(3)	O(16) – P(2) – $O(6)^{\#3}$	108.8(3)
O(7) – Zn(2) – O(6)	97.3(2)	$O(13)^{\#3}$ – P(2) – $O(6)^{\#3}$	111.2(3)
$O(5)^{\#1}$ – Zn(2) – O(8)	106.5(3)	O(16) – P(2) – $O(9)^{\#3}$	110.0(3)
O(7) – Zn(2) – O(8)	97.3(2)	$O(13)^{\#3}$ – P(2) – $O(9)^{\#3}$	106.0(4)
O(6) – Zn(2) – O(8)	117.4(2)	$O(6)^{\#3}$ – P(2) – $O(9)^{\#3}$	111.6(3)
O(9) – Zn(3) – O(10)	109.5(3)	$O(10)^{\#4}$ – P(3) – $O(11)^{\#3}$	110.4(3)
O(9) – Zn(3) – O(12)	113.9(2)	$O(10)^{\#4}$ – P(3) – O(3)	111.0(4)
O(10) – Zn(3) – O(12)	115.8(2)	$O(11)^{\#3}$ – P(3) – O(3)	108.7(3)
O(9) – Zn(3) – O(11)	117.6(3)	$O(10)^{\#4}$ – P(3) – O(15)	106.1(3)
O(10) – Zn(3) – O(11)	99.3(2)	$O(11)^{\#3}$ – P(3) – O(15)	110.9(3)
O(12) – Zn(3) – O(11)	100.0(3)	O(3) – P(3) – O(15)	109.8(3)
O(13) – Zn(4) – O(14)	117.1(2)	O(7) – P(4) – O(5)	106.9(3)
O(13) – Zn(4) – O(15)	106.6(3)	O(7) – P(4) – O(1)	109.0(4)
O(14) – Zn(4) – O(15)	117.0(2)	O(5) – P(4) – O(1)	110.7(3)
O(13) – Zn(4) – O(16)	100.0(2)	O(7) – P(4) – O(14)	110.2(3)
O(14) – Zn(4) – O(16)	104.9(3)	O(5) – P(4) – O(14)	109.2(4)
O(15) – Zn(4) – O(16)	109.8(3)	O(1) – P(4) – O(14)	110.7(3)
P(4) – O(1) – Zn(1)	127.1(4)	$P(2)^{\#6}$ – O(9) – Zn(3)	135.6(4)
$P(1)^{\#4}$ – O(2) – Zn(1)	142.1(4)	$P(3)^{\#2}$ – O(10) – Zn(3)	140.4(4)
P(3) – O(3) – Zn(1)	133.2(4)	$P(3)^{\#6}$ – O(11) – Zn(3)	130.1(3)
$P(1)^{\#5}$ – O(4) – Zn(1)	152.8(4)	P(1) – O(12) – Zn(3)	131.5(4)
P(4) – O(5) – $Zn(2)^{\#5}$	149.1(4)	$P(2)^{\#6}$ – O(13) – Zn(4)	140.1(3)
$P(2)^{\#6}$ – O(6) – Zn(2)	139.3(4)	P(4) – O(14) – Zn(4)	133.1(4)
P(4) – O(7) – Zn(2)	135.9(4)	P(3) – O(15) – Zn(4)	135.4(3)
P(1) – O(8) – Zn(2)	124.4(4)	P(2) – O(16) – Zn(4)	134.8(4)
Organic moiety			
N(1) – C(1) – C(2)	113.6(10)	N(3) – C(4) – C(5)	111.9(9)
C(1) – C(2) – C(3)	114.2(8)	C(4) – C(5) – C(6)	111.5(8)
C(2) – C(3) – N(2)	110.3(7)	C(5) – C(6) – N(4)	108.6(8)

Symmetry transformations used to generate equivalent atoms:

#1 -x+1, y+1/2, -z+2; #2 x+1, y, z; #3 –x+1, y-1/2, -z+1; #4 x-1, y, z; #5 -x+1, y-1/2, -z+2;

#6 -x+1, y+1/2, -z+1

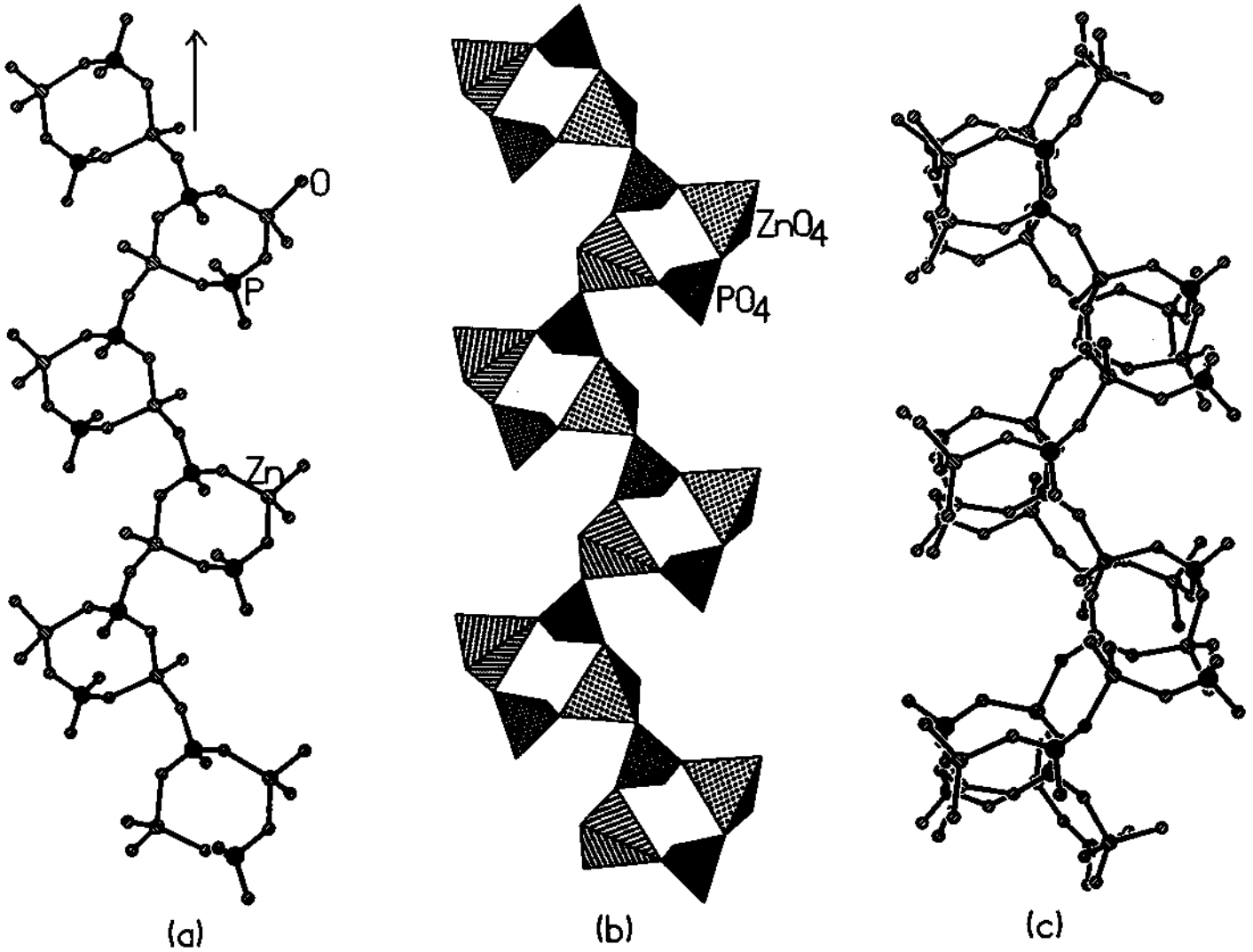

Fig 1.15 The chain–like structureformed by the connectivity between the 4–membered rings, in **II** , Arrow indicates the 2–fold screw axis formed along the *c*–axis. (b) Polyhedral representation showing the linkages between the 4–membered rings. (c) connectivity between two such chains along the *c*–axis.

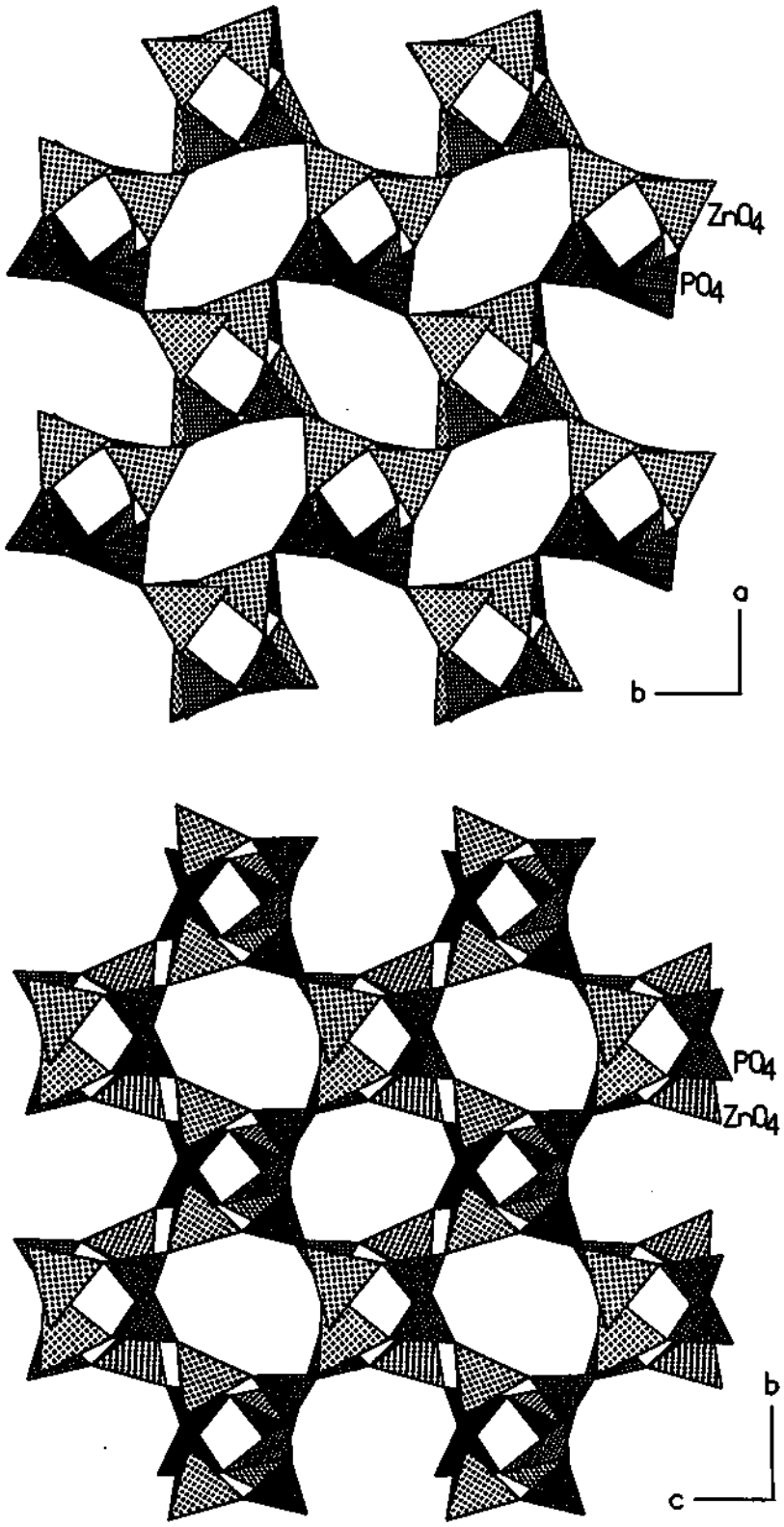

Fig. 1.16. Polyhedral view of **II** along *[001]* axis. Note that the connectivity creates a 8-membred channels. The amine molecule occupies these channels (not shown). (b) Polyhedral view of **II** along the [*100*] axis showing the 8-membred channels.

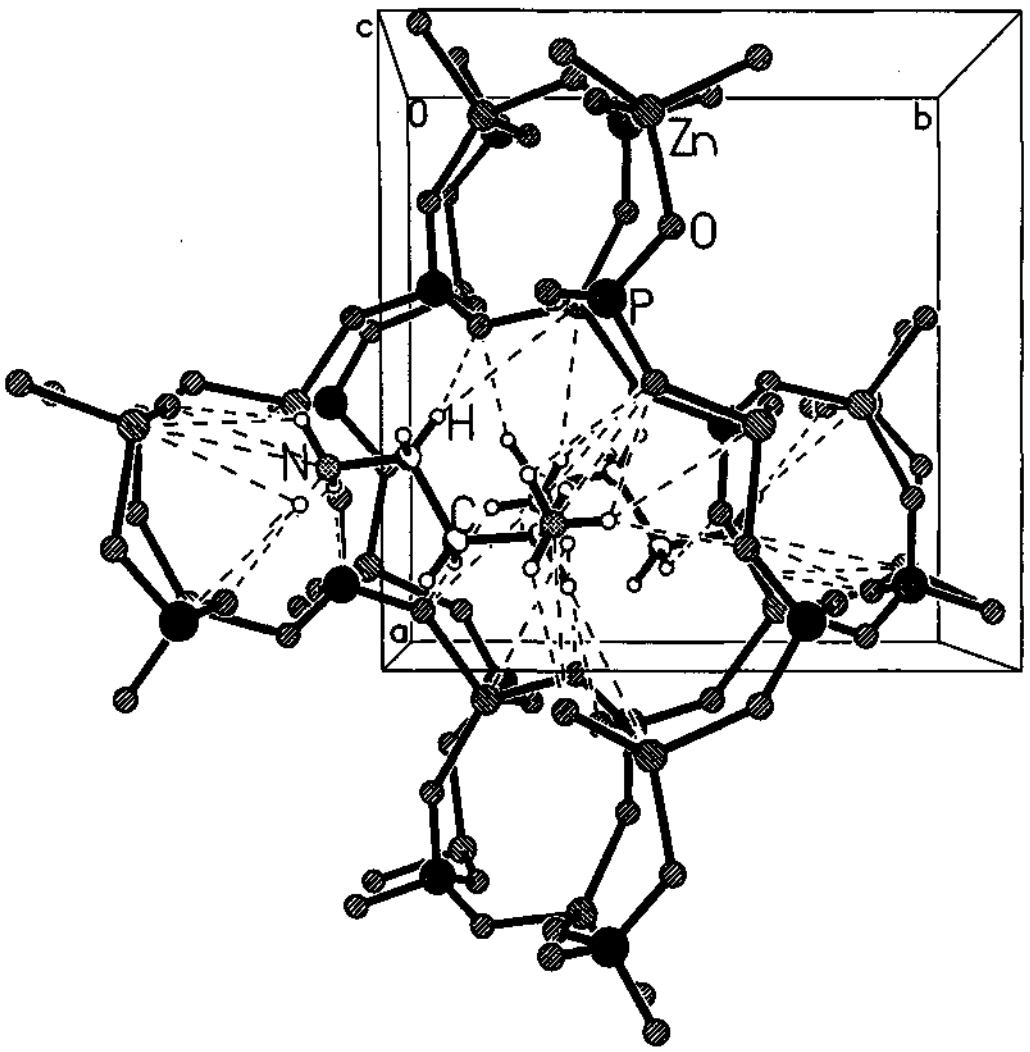

Fig. 1.17. Structure of **II** showing a single 8-memebred channel along with the amine. Dotted lines represent the various hydrogen bond interactions.

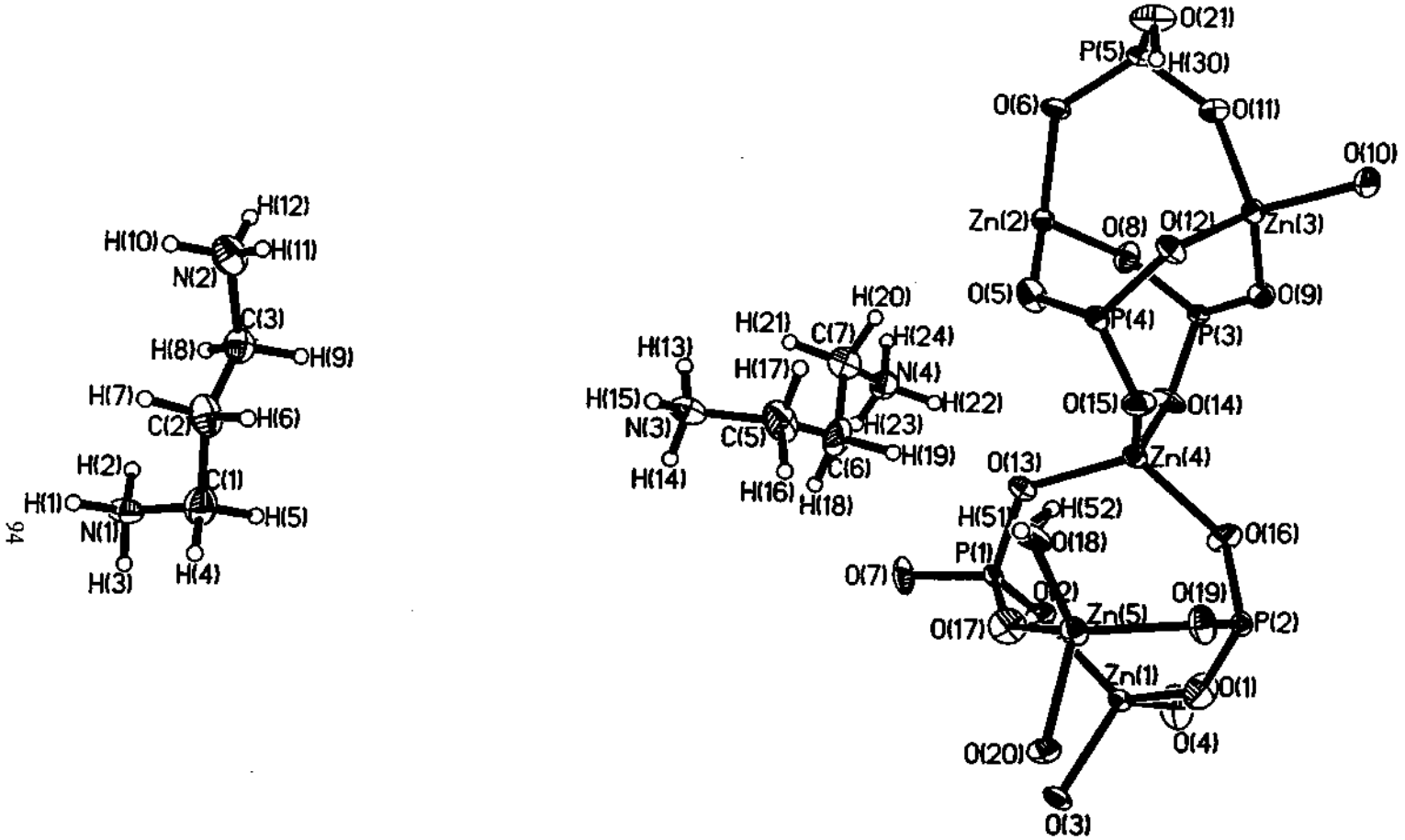

Fig 1.18 ORTEP plot of **III**, $[C_3N_2H_{12}]_2$ $[Zn_5(H_2O)(PO_4)_4(HPO_4)]$. The thermal ellipsoids are given at 50% probability.

Table 1.20. Final atomic coordinates [x 10^4] and equivalent isotropic displacement parameters [$Å^2$ x 10^3] for **III**, $[C_3N_2H_{12}]_2[Zn_5(H_2O)(PO_4)_4(HPO_4)]$.

Atom	x	y	z	U_{eq}[a]
Zn(1)	-4677(1)	8853(1)	2673(1)	14(1)
Zn(2)	2284(1)	13769(1)	3755(1)	14(1)
Zn(3)	2437(1)	14040(1)	1300(1)	15(1)
Zn(4)	-706(1)	11135(1)	2456(1)	15(1)
Zn(5)	-770(1)	7396(1)	2270(1)	18(1)
P(1)	-2046(2)	9262(2)	3935(1)	13(1)
P(2)	-2438(2)	9165(2)	986(1)	14(1)
P(3)	-444(2)	14289(2)	2378(1)	11(1)
P(4)	2646(2)	11220(2)	2423(1)	13(1)
P(5)	4444(2)	15628(2)	2725(1)	12(1)
O(1)	-3718(5)	8606(6)	1506(3)	36(1)
O(2)	-3611(5)	9699(4)	3709(3)	19(1)
O(3)	-5245(5)	7045(4)	3087(3)	20(1)
O(4)	-6355(6)	10012(5)	2483(4)	37(1)
O(5)	2416(6)	11857(5)	3378(3)	26(1)
O(6)	4123(4)	14629(4)	3518(3)	19(1)
O(7)	-1834(5)	8883(6)	4955(3)	29(1)
O(8)	582(4)	14608(5)	3193(3)	23(1)
O(9)	377(4)	14074(5)	1467(3)	21(1)
O(10)	2863(5)	14401(5)	26(3)	23(1)
O(11)	3242(5)	15618(4)	1994(3)	19(1)
O(12)	3238(5)	12292(5)	1740(3)	20(1)
O(13)	-1010(5)	10443(5)	3700(3)	24(1)
O(14)	-1369(5)	13025(4)	2579(3)	20(1)
O(15)	1196(5)	10699(5)	2030(3)	22(1)
O(16)	-1940(5)	10540(5)	1425(3)	24(1)
O(17)	-1687(5)	7987(5)	3363(4)	28(1)
O(18)	1325(7)	7620(8)	2482(5)	32(2)
O(19)	-1178(5)	8135(5)	1043(3)	25(1)
O(20)	-1471(5)	5511(4)	2250(3)	19(1)
O(21)	5820(5)	15024(5)	2219(4)	27(1)
N(1)	6030(6)	2529(6)	11083(4)	23(1)
N(2)	8921(7)	5632(6)	9971(4)	31(2)
C(3)	7481(8)	4995(7)	10064(5)	24(2)
C(2)	7501(8)	3487(8)	9837(5)	29(2)
C(1)	6125(8)	2742(9)	10073(5)	31(2)
N(3)	3783(6)	7535(6)	6152(4)	25(1)
N(4)	981(6)	10844(6)	5232(4)	25(1)
C(7)	2336(8)	10094(8)	5269(6)	31(2)
C(6)	2144(8)	8623(8)	4968(5)	34(2)
C(5)	3464(9)	7751(9)	5144(5)	36(2)

[a] U(eq) is defined as one third of the trace of the orthogonalized U_{ij} tensor.

five independent Zn atoms, one zinc [Zn(5)] atom makes three Zn – O – P linkages and possess a terminal Zn – O bond and the remaining Zn atoms make four Zn – O – P linkages, resulting in an average bond angle of 128.4° for such a connectivity. Similarly, P(5) makes only three P – O – Zn linkages with one terminal P – O bond, and the remaining P atoms make four P – O – Zn bonds. The P – O bond distances are in the range 1.501 – 1.595 Å (av. 1.532 Å) and the O – P – O angles are in the range 105.6 – 112.3° (av. 109.5°) (Table 1.21 and 1.22). These geometrical parameters are in good agreement with those reported for similar compounds in the literature.[79-95] The framework structure of $Zn_5O(PO_4)_5$ would result in a net framework charge of –7. The presence of two molecules of $[NH_3(CH_2)_3NH_3]$ would account for +4 charge arising from the di-protonation of the amine. The excess negative charge of –3 is then need to be balanced. Bond valence sum calculations[244] indicate that P(5) – O(21) with a distance of 1.595 Å is formally a –OH group and Zn(5) – O(18) with a distance of 1.978 Å is a water molecule, which also corresponds well with the proton positions located in the difference Fourier maps. Formation of terminal water molecules linked to Zn centers have been known to occur in open-framework zinc phosphates.[92]

The ZnO_4, PO_4 and HPO_4 tetrahedra in **III** are linked to each other forming 4-membered rings, which are connected variably forming the secondary building unit (SBU) as shown in Fig. 1.19. Similar SBU has been observed for the aluminosilicate, thomsonite. The SBUs are connected so as to form a dimeric unit, which are linked together forming the structure. The presence of a terminal water molecule and a –OH group creates interruptions in the connectivity of the SBUs in **III**, that the total structure is marginally different than that of thomsonite. The SBU's are connected and arranged around the 2-fold screw axis (Fig. 1.19). The SBU's are connected to each other leading to the formation of channels along the *a*-axis as shown in Figs. 1.20 and 1.21. The channels are bound by 8-T atoms (T = Zn, P), and have width 6.7 x 5.9 Å along the *a*-axis. The position of the amine molecules with in the channels, along the *a*-axis, is

Table 1.21. Selected bond distances for **III**, $[C_3N_2H_{12}]_2[Zn_5(H_2O)(PO_4)_4(HPO_4)]$.

Moiety	Distance (Å)	Moiety	Distance (Å)
Zn(1)-O(1)	1.924(4)	P(1)-O(7)	1.517(5)
Zn(1)-O(2)	1.954(5)	P(1)-O(17)	1.529(5)
Zn(1)-O(3)	1.936(4)	P(1)-O(13)	1.542(5)
Zn(1)-O(4)	1.942(5)	P(1)-O(2)	1.545(5)
Zn(2)-O(5)	1.946(5)	P(2)-O(10)$^{\#2}$	1.515(5)
Zn(2)-O(6)	1.940(4)	P(2)-O(1)	1.516(5)
Zn(2)-O(7)$^{\#1}$	1.907(4)	P(2)-O(19)	1.544(4)
Zn(2)-O(8)	1.944(4)	P(2)-O(16)	1.548(5)
Zn(3)-O(9)	1.934(4)	P(3)-O(8)	1.527(5)
Zn(3)-O(10)	1.908(4)	P(3)-O(14)	1.533(4)
Zn(3)-O(11)	1.974(4)	P(3)-O(20)$^{\#3}$	1.536(5)
Zn(3)-O(12)	1.960(5)	P(3)-O(9)	1.539(4)
Zn(4)-O(13)	1.933(5)	P(4)-O(4)$^{\#4}$	1.501(5)
Zn(4)-O(14)	1.952(4)	P(4)-O(5)	1.522(5)
Zn(4)-O(15)	1.928(4)	P(4)-O(15)	1.539(5)
Zn(4)-O(16)	1.945(5)	P(4)-O(12)	1.540(5)
Zn(5)-O(17)	1.886(5)	P(5)-O(3)$^{\#5}$	1.502(5)
Zn(5)-O(18)	1.978(7)	P(5)-O(11)	1.520(5)
Zn(5)-O(19)	1.933(5)	P(5)-O(6)	1.530(5)
Zn(5)-O(20)	1.951(4)	P(5)-O(21)	1.595(4)
		Organic Moiety	
N(1)-C(1)	1.467(9)	N(3)-C(4)	1.484(9)
C(1)-C(2)	1.515(10)	C(4)-C(5)	1.511(11)
C(2)-C(3)	1.506(10)	C(5)-C(6)	1.508(11)
C(3)-N(2)	1.484(9)	C(6)-N(4)	1.457(9)

Symmetry transformations used to generated equivalent atoms:

#1 -x, y+1/2, -z+1; #2 -x, y-1/2, -z; #3 x, y+1, z; #4 x+1, y, z; #5 x+1, y+1, z

Table 1.22. Selected bond angles for **III**, $[C_3N_2H_{12}]_2[Zn_5(H_2O)(PO_4)_4(HPO_4)]$.

Moiety	Angle (°)	Moiety	Angle (°)
O(1)-Zn(1)-O(3)	106.6(2)	O(7)-P(1)-O(17)	107.0(3)
O(1)-Zn(1)-O(4)	109.5(2)	O(7)-P(1)-O(13)	108.7(3)
O(3)-Zn(1)-O(4)	110.5(2)	O(17)-P(1)-O(13)	110.3(3)
O(1)-Zn(1)-O(2)	118.5(2)	O(7)-P(1)-O(2)	112.1(3)
O(3)-Zn(1)-O(2)	106.8(2)	O(17)-P(1)-O(2)	109.0(3)
O(4)-Zn(1)-O(2)	104.9(2)	O(13)-P(1)-O(2)	109.8(3)
$O(7)^{\#1}$-Zn(2)-O(6)	110.7(2)	$O(10)^{\#2}$-P(2)-O(1)	109.3(3)
$O(7)^{\#1}$-Zn(2)-O(8)	100.8(2)	$O(10)^{\#2}$-P(2)-O(19)	109.5(3)
O(6)-Zn(2)-O(8)	117.4(2)	O(1)-P(2)-O(19)	110.0(3)
$O(7)^{\#1}$-Zn(2)-O(5)	109.9(2)	$O(10)^{\#2}$-P(2)-O(16)	109.2(3)
O(6)-Zn(2)-O(5)	107.8(2)	O(1)-P(2)-O(16)	110.1(3)
O(8)-Zn(2)-O(5)	110.1(2)	O(19)-P(2)-O(16)	108.7(3)
O(10)-Zn(3)-O(9)	109.7(2)	O(8)-P(3)-O(14)	111.4(3)
O(10)-Zn(3)-O(12)	112.6(2)	$O(8)$-P(3)-$O(20)^{\#3}$	108.2(3)
O(9)-Zn(3)-O(12)	110.3(2)	$O(14)$-P(3)-$O(20)^{\#3}$	107.2(2)
O(10)-Zn(3)-O(11)	104.8(2)	O(8)-P(3)-O(9)	111.3(2)
O(9)-Zn(3)-O(11)	107.0(2)	O(14)-P(3)-O(9)	109.7(3)
O(12)-Zn(3)-O(11)	112.1(2)	$O(20)^{\#3}$-P(3)-O(9)	108.7(3)
O(15)-Zn(4)-O(13)	111.4(2)	$O(4)^{\#4}$-P(4)-O(5)	111.4(3)
O(15)-Zn(4)-O(13)	111.4(2)	$O(4)^{\#4}$-P(4)-O(15)	107.4(3)
O(15)-Zn(4)-O(16)	103.1(2)	O(5)-P(4)-O(15)	109.2(3)
O(15)-Zn(4)-O(16)	103.1(2)	$O(4)^{\#4}$-P(4)-O(12)	110.0(3)
O(13)-Zn(4)-O(14)	101.3(2)	O(5)-P(4)-O(12)	110.6(3)
O(16)-Zn(4)-O(14)	99.6(2)	O(15)-P(4)-O(12)	108.2(3)
O(17)-Zn(5)-O(19)	123.9(2)	$O(3)^{\#5}$-P(5)-O(11)	112.3(3)
O(17)-Zn(5)-O(20)	98.3(2)	$O(3)^{\#5}$-P(5)-O(6)	111.6(3)
O(19)-Zn(5)-O(20)	106.1(2)	O(11)-P(5)-O(6)	111.0(2)
O(17)-Zn(5)-O(18)	107.3(3)	$O(3)^{\#5}$-P(5)-O(21)	110.2(3)
O(19)-Zn(5)-O(18)	106.1(3)	O(11)-P(5)-O(21)	105.6(3)
O(20)-Zn(5)-O(18)	115.7(3)	O(6)-P(5)-O(21)	105.7(3)
P(2)-O(1)-Zn(1)	139.6(3)	P(5)-O(11)-Zn(3)	128.4(3)
P(1)-O(2)-Zn(1)	120.5(3)	P(4)-O(12)-Zn(3)	131.1(3)
$P(5)^{\#6}$-O(3)-Zn(1)	141.6(3)	P(1)-O(13)-Zn(4)	124.3(3)
$P(4)^{\#7}$-O(4)-Zn(1)	163.6(4)	P(3)-O(14)-Zn(4)	124.2(2)
P(4)-O(5)-Zn(2)	130.7(3)	P(4)-O(15)-Zn(4)	127.9(3)
P(5)-O(6)-Zn(2)	126.0(3)	P(2)-O(16)-Zn(4)	137.3(3)
$P(1)$-O(7)-$Zn(2)^{\#8}$	157.2(3)	P(1)-O(17)-Zn(5)	143.1(3)
P(3)-O(8)-Zn(2)	136.5(3)	P(2)-O(19)-Zn(5)	115.3(3)
P(3)-O(9)-Zn(3)	127.9(3)	$P(3)^{\#10}$-O(20)-Zn(5)	121.5(3)
$P(2)^{\#9}$-O(10)-Zn(3)	146.5(3)		
	Organic Moiety		
N(1)-C(1)-C(2)	110.7(6)	N(3)-C(4)-C(5)	113.0(6)
C(1)-C(2)-C(3)	114.0(6)	C(4)-C(5)-C(6)	113.3(7)
C(2)-C(3)-N(2)	112.0(6)	C(5)-C(6)-N(4)	111.6(6)

Symmetry transformations used to generated equivalent atoms:

#1 -x, y+1/2, -z+1; #2 -x, y-1/2, -z; #3 x, y+1, z; #4 x+1, y, z; #5 x+1, y+1, z; #6 x-1, y-1, z; #7 x-1, y,z; #8 -x, y-1/2, -z+1; #9 -x, y+1/2, -z; #10 x, y-1, z

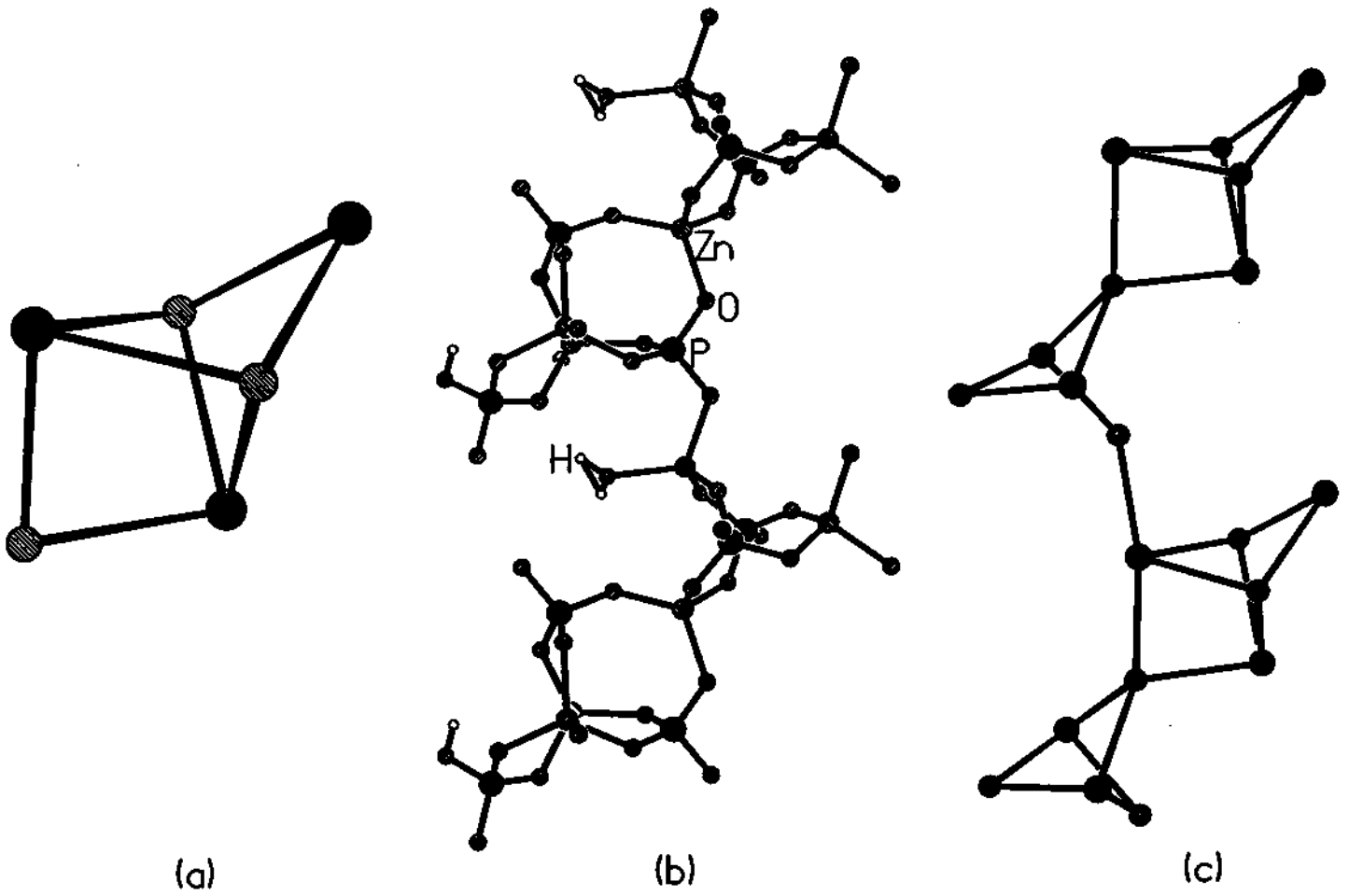

Fig 1.19 (a) The secondary building unit present in **III**. Only the T atom (T = Zn, P) connectivity is given. Similar SBU has been observed for thomsonite (see text). (b) The connectivity between the SBU's that forms a chain like arrangement around the 2–fold screw axis. (c) The T atom connectivity showing the same.

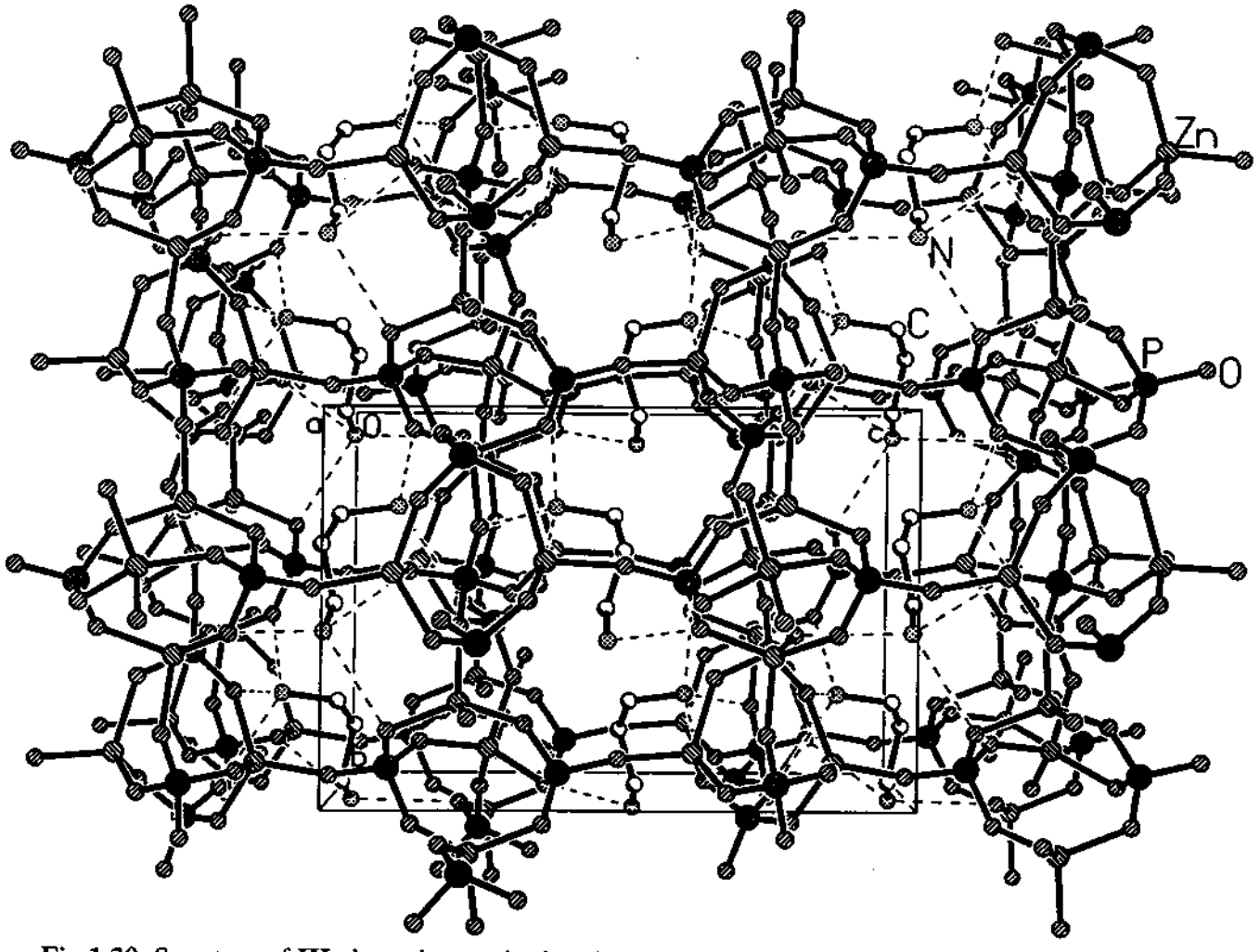

Fig 1.20 Structure of **III** along the *a* axis showing the 8–membered channels. and the position of the amine. Note the amine is arranged so as to replicate the screw axis. Dotted lines represents the various hydrogen bond interactions. Hydrogens are not shown for clarity.

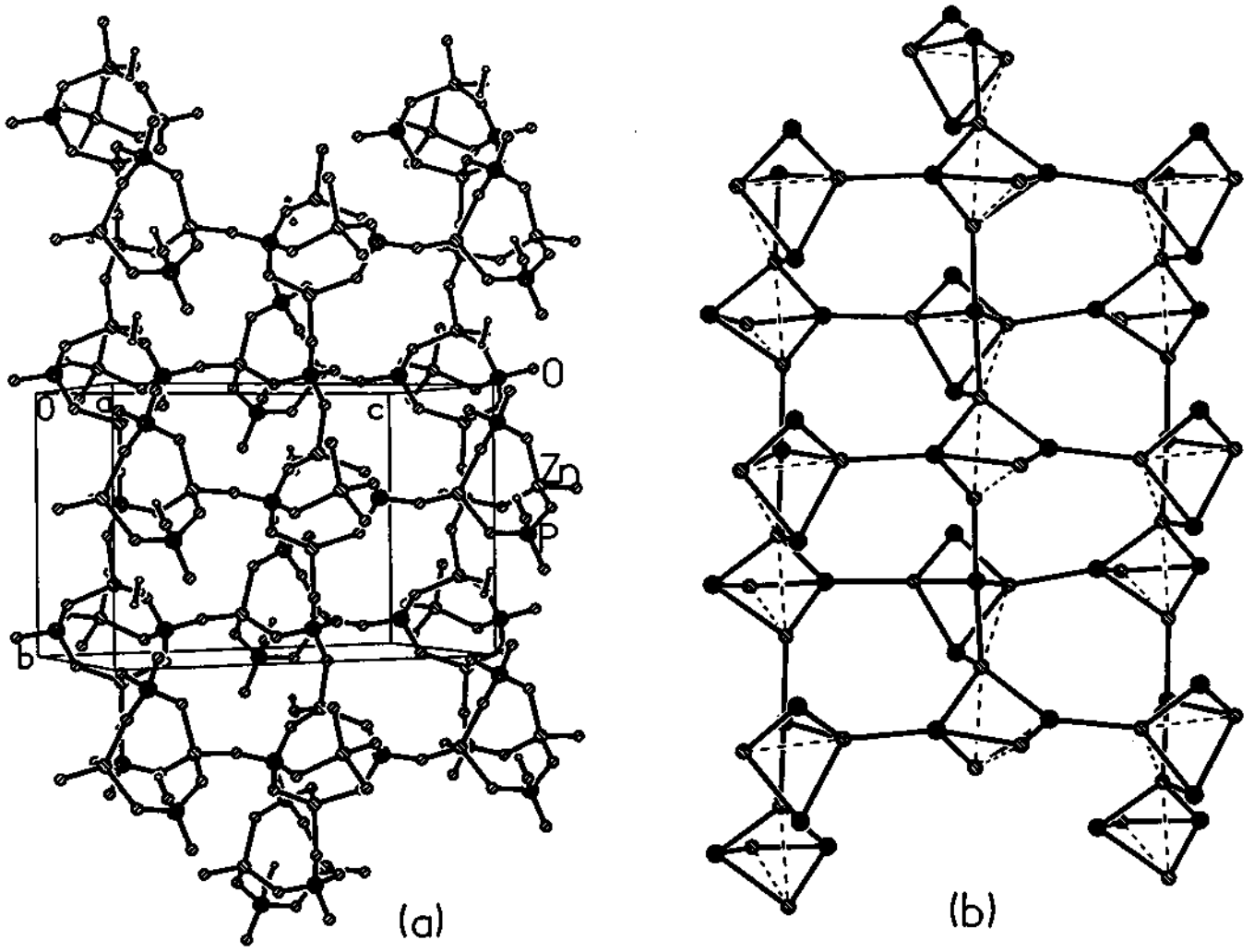

Fig 1.21 (a) Ball and stick view of the structure of **III** along the c axis showing the connectivity between the one–dimensional chains that form the channels. The amine molecules are not shown. (b) The T atom connectivity showing the channels. Note the interrupted connectivity between the SBU's (see text).

such as to replicate the 2-fold screw axis as shown in Fig. 1.20. Thermogravimetric analysis (TGA) of compounds **II** and **III** was carried out in nitrogen atmosphere in the range between 25° and 700° (Fig. 1.22). TGA study indicates that the weight loss occurs in two steps for **II** and in three steps for **III**. The total mass loss of 21.34% in case of **II** corresponds well with the loss of amine and condensation of the phosphate (calc. 20.95%), and a mass loss of 20.3% in case of **III** corresponds with the loss of bound water, amine and condensation of the phosphate (calc. 20.8%). In both the cases, the loss of the amine molecule resulted in collapse of the framework structure, leading to the formation of largely amorphous weakly diffracting materials (XRD) that corresponds to dense zinc phosphates phases [$Zn_2P_2O_7$, JCPDS: 34-623], consistent with the structures.

Though the structures of both **II** and **III** are formed from the expected tetrahedral building blocks of ZnO_4 and PO_4 units, sharing vertices, distinct differences exist between them. The syntheses of both the compounds were effected by minor variations in the synthesis mixture. The unpredictable nature of the kinetically controlled solvent-mediated reactions is well illustrated by the formation of two different phases by the small variation in the reaction mixture. As is typical of such reactions, there is no correlation between the starting composition and the majority solid-phase product.

Both compounds **II** and **III** consist of three-dimensional networks with Zn – O – P bonds strongly favored over possible Zn – O – Zn or P – O – P linkages. This may be largely due to the Zn:P ratio of 1:1, which is rather unusual as most of the zinc phosphates have Zn : P ratio > 1.0. The difficulty in obtaining a zinc phosphate structure with Zn : P ratio of 1 : 1, with Zn and P atoms fully ordered, as in the present case, is in packing enough bulky organic cations into the extra-framework pores to achieve the charge balance. It is to be noted that, in spite of the Zn : P ratio of 1 : 1 in **II** and **III**, there are no terminal P-OH linkages in the compounds (except in **III**, which possess a single P – OH bond). The formation of framework protons or P – OH type linkages arise in these materials essentially

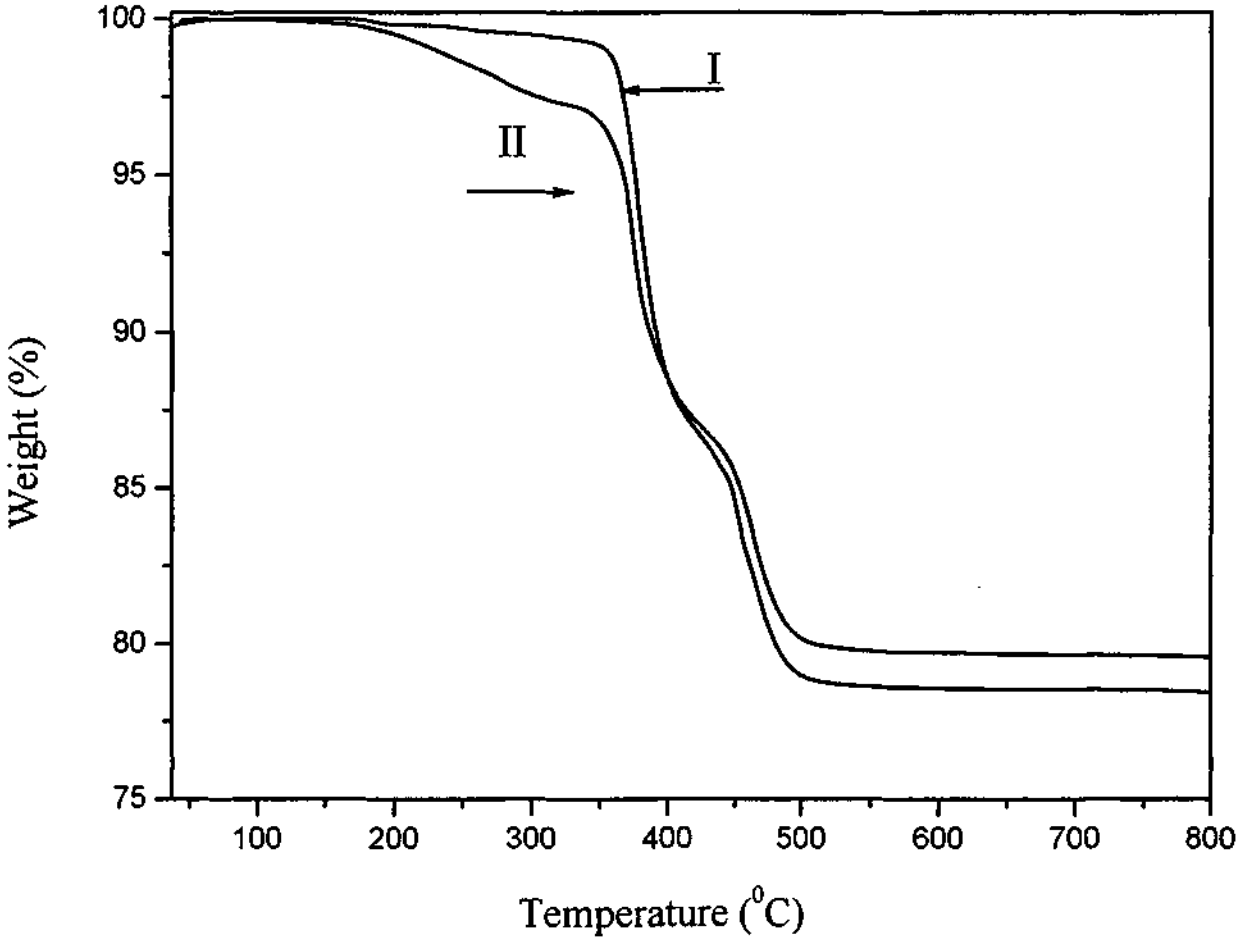

Fig. 1.22. TGA curves for **II**, $[C_3N_2H_{12}]_2[Zn_4(PO_4)_4]$, and **III**, $[C_3N_2H_{12}]_2[Zn_5(H_2O)(PO_4)_4(HPO_4)]$ showing the weight loss.

to obtain charge neutrality. In the present materials, the fact that the framework is built-up from 1 : 1 tetrahedral arrangement of Zn and P atoms, suggest indirectly that the organic cations, which is linear, are arranged in such a way that they charge-balance the framework. Such zinc phosphate structures without terminal P-OH bonds have been known in the literature, and are usually templated by alkali metals.[245]

II and **III**, prepared employing similar synthesis conditions, have dissimilar structures, in spite of having an identical Zn/P ratio of 1.0. It is in order to examine the possible cause of this. Structures of both **II** and **III** are formed by TO_4 tetrahedra (T = Zn, P), and the individual tetrahedra are more or less regular (Tables 1.18 and 1.21). But the average T – O – T bond angles are quite different in the both cases (Tables 1.19 and 1.22); while the Zn – O – P bond angle is 136.6° in **II**, it is 128.4° in **III**. Such differences in the bond angles may be responsible for the variations in the two structures observed in the present study. In the case of aluminosilicates, where the structures are made from AlO_4 and SiO_4 tetrahedra, the individual tetrahedra are close to being regular (109.5°), but the T – O – T bond angles can accommodate values ranging from ≈125° to 180°. The variations in the bond angles have been hypothesized as one of the reasons for the occurrence of many zeolitic structures, in spite of having similar Si/Al ratios.[16]

In addition to the above, unlike in many of the aluminosilicates, where the framework charges are generally matched with that of the templates by variations in the Si : Al ratio, with only a minor change in the framework topology, the zinc phosphates seem to have precisely defined Zn : P ratio for a particular topology. The resulting charge imbalance caused by the fixed Zn : P ratio, is usually compensated by the presence of phosphate units that are variably protonated. This limits our ability to change the framework charge distribution to match that of the template without significantly altering the framework structure. In the case of **III**, however, the presence of a terminal water molecule and a monohydrogen phosphate (HPO_4) group helps in maintaining the charge

neutrality and in the process giving rise to a completely different structure than that of **III**.

The 'openness' of a structure is defined in terms of the tetrahedral atom density[16] (framework density, FD), defined as the number of tetrahedral (T) atoms per 1000 Å^3. In the present materials, the number of T atoms per 1000 Å^3 (here T = Zn and P) is 15 for **II** and 15.4 for **III**. These values are in the middle of the range of FD values observed in aluminosilicate zeolites, where the presence of channels is common. The FD value of 15.4 observed for **III** is between 17.7 and 14.4 T/1000Å^3, which is the value for the normal thomsonite and the expanded one.

The multipoint hydrogen bond interactions are necessary in the formation and stability of open architectures. In the present case also, we find strong hydrogen bond interactions involving the hydrogens attached to the nitrogen of the amine and the framework oxygen atoms. The terminal water molecule and –OH group, in the case of **III**, in addition to the hydrogens attached to the carbon atoms also participate in hydrogen bonds. The majority of the interactions are quite strong as indicated by the short hydrogen acceptor distances (~2.2Å) and a donor-hydrogen-acceptor angle of ~150°. The important hydrogen bond interactions for **II** and **III** are presented in Table 1.23.

It is useful to compare the various zinc phosphates that have been prepared using the same amine, DAP. Harrison et al[216] reported zinc phosphates with ladder and layer architectures by the use of DAP. Recent, studies in this laboratory have shown that, the use of DAP results in the formation of a three-dimensional structure, wherein the amine molecule performs a dual role –that of a structure-directing agent and a ligand.[246] In the present case, we have obtained two different three-dimensional structures possessing channels, one of them (**III**) is closely related to the mineral, thomsonite. One of the reasons for the observed three-dimensional structure might be the choice of reagents used in the synthesis.

Table 1.23. Selected hydrogen bond interactions in **II** and **III**.

Moiety	Distance (Å)	Moiety	Angle (°)
		Compound II	
O(2) – H(2)	1.997(1)	O92) – H92) – N(1)	156.5(3)
O(8) – H(3)	2.233(1)	O(8) – H(3) – N(1)	160.4(1)
O(15) – H(10)	1.912(2)	O(15) – H(10) – N(2)	166.8(2)
O(12) – H(11)	1.988(1)	O(12) – H(11) – N(2)	148.3(2)
O(11) – H(13)	2.244(2)	O(11) – H913) – N(3)	150.8(2)
O(13) – H(14)	1.999(2)	O(13) – H(14) – N(3)	159.4(1)
O(8) – H(22)	2.027(2)	O(8) – H(22) – N(4)	145.4(2)
O(3) – H(5)	2.396(2)	O(3) – H(5) – C(1)	163.9(2)
O(16) – H(8)	2.395(2)	O(16) – H(8) – C(3)	165.5(3)
O(1) – H(9)	2.483(3)	O(1) – H99) – C(3)	148.5(2)
O(6) – H(17)	2.439(2)	O(6) – H(17) – C(4)	154.1(2)
O(7) – H(18)	2.593(2)	O(7) – H(18) – C(5)	163.0(1)
		Compound III	
O(16) – H(1)	1.971(2)	O(16) – H(1) – N(1)	160.2(2)
O(21) – H(2)	2.037(2)	O(21) – H(2) – N(1)	169.1(2)
O(12) – H(3)	1.996(2)	O(12) – H(3) – N(1)	144.3(2)
O(9) – H(10)	2.064(2)	O(9) – H(10) – N(2)	161.2(2)
O(15) – H(11)	2.050(1)	O(15) – H(11) – N(2)	149.1(2)
O(19) – H(12)	2.049(3)	O(19) – H(12) – N(2)	152.4(2)
O(13) – H(22)	2.046(2)	O(13) – H(22) – N(4)	156.8(3)
O(8) – H(23)	2.086(3)	O(8) – H(23) – N(4)	161.6(2)
O(7) – H(24)	2.268(4)	O(7) – H(24) – N(4)	148.4(2)
O(17) – H(24)	2.193(2)	O(17) – H(24) – N(4)	142.7(3)
N(1) – H(30)	2.170(2)	O(21) – H(30) – O(21)	151.4(4)
O(11) – H(51)[1]	1.924(4)	O(11) – H(51) – O(18)[1]	160.6(2)
O(15) – H(52)[1]	2.593(2)	O(15) – H(52) – O(18)[1]	151.7(2)
O(1) – H(5)	2.432(2)	O(1) – H(5) – C(1)	141.8(3)
O(10) – H(5)	2.521(2)	O910) – H(5) – C(1)	154.0(1)
O(21) – H(8)	2.509(3)	O(21) – H(8) – C(3)	165.5(2)

[1] intra-layer

The synthesis of **II** and **III** has been effected by the addition of acetic acid in the medium, in addition to hydrochloric acid. It is likely that the Cl^- ions might just be acting as a mineralizer similar to the F^- ions in some of the synthesis of the phosphates of Al and Ga.[234] The role of acetic acid in the formation of **II** and **III** is not clear. It is likely that the acetate ions, present in the mixture during the synthesis, might act as a base and favor the deprotonation of H_3PO_4. The fact that both **II** and **III** are essentially formed by the PO_4 units (completely deprotonated H_3PO_4), lends credence to this argument. In this connection it is to be noted that, a three-dimensional zinc phosphate has been prepared with DAP, by using oxalic acid as an additive.[246] It is possible that the oxalate ions performs a role similar to the acetate ions in the present synthesis – that of deprotonation of the phosphoric acid. The ladder and layer structures formed by DAP,[216] possess HPO_4 and H_2PO_4 moieties. In order to validate such an assumption, we sought to prepare **II** and **III** using zinc acetate instead of ZnO. As expected, pure phases of **II** and **III** were obtained in the preparations. In addition, we have employed several organic mono- and di- acids as additives in the synthesis of zinc phosphates, which invariably resulted in the formation of zinc phosphates possessing completely deprotonated PO_4 units. It therefore appears that by deprotonating the phosphoric acid, mono- and dicarboxylic acids help in maintaining the pH of the reaction mixture, which is crucial in the synthesis of open-framework phosphate materials.

$[NH_3(CH_2)_3NH_3]$ $2[Zn_2PO_4(HPO_4)]$, IV : The asymmetric unit of the zinc phosphate, $[NH_3(CH_2)_3NH_3]^{2+}$ $2[Zn_2PO_4(HPO_4)]^-$ contains 15 non-hydrogen atoms of which 12 belong to the 'framework' (2 Zn, 2 P and 8 O atoms) and three to the guest (1 N and 2 C atoms) (Fig. 1.23). The atomic coordinates are presented in Table 1.24. There are two crystallographically distinct Zn and P atoms in the asymmetric unit. Of the eight oxygens in the asymmetric unit, one oxygen connects two Zn and a P atom by a three-coordinated bond, one is a terminal oxygen and the remaining are normal Zn – O – P links. The three-

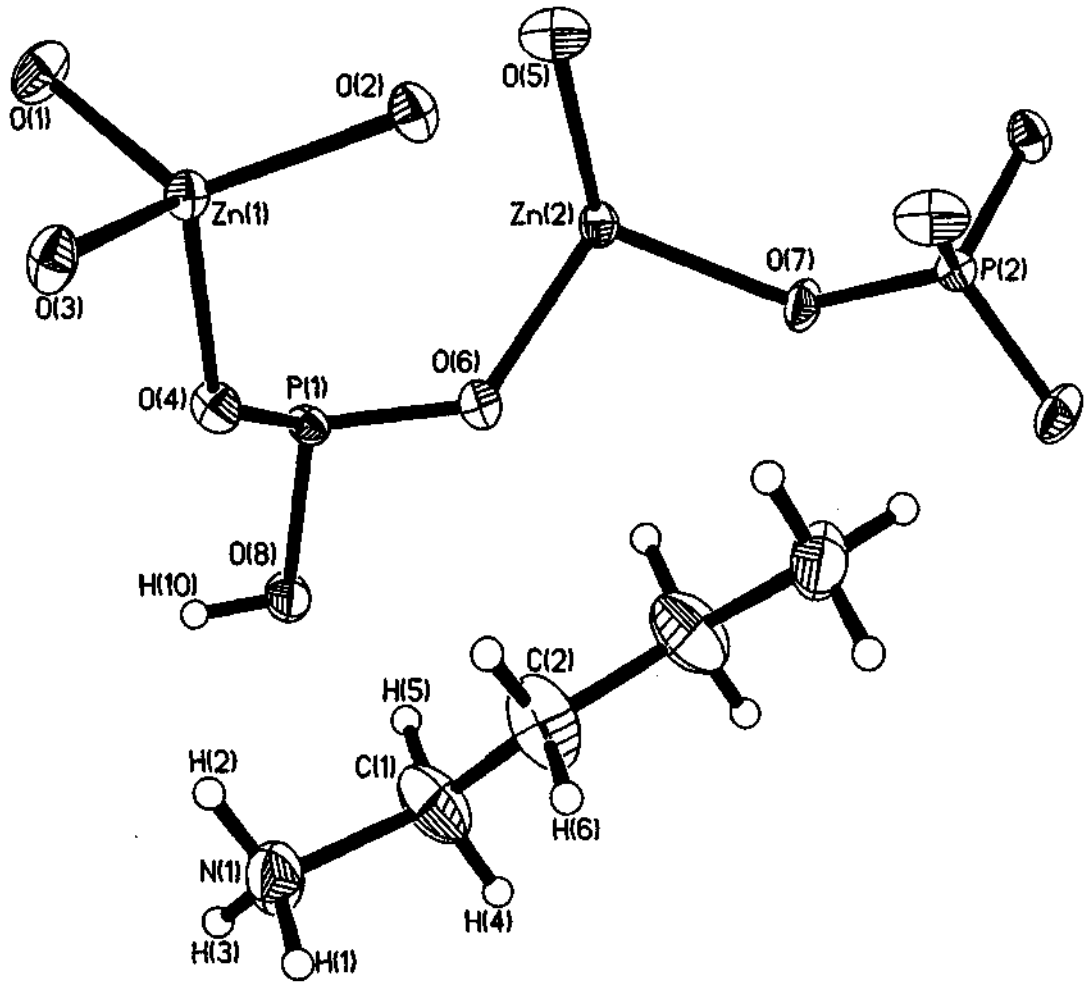

Fig. 1.23. ORTEP plot of IV, $[NH_3(CH_2)_3NH_3]^{2+}2[Zn_2PO_4(HPO_4)]^-$. Asymmetric unit is labeled. Thermal ellipsoids are given at 50% probability.

Table 1.24. Atomic coordinates [x 10^4] and equivalent isotropic displacement parameters [A^2 x 10^3] for **IV**, $[NH_3(CH_2)_3NH_3]^{2+}$ $2[Zn_2PO_4(HPO_4)]^-$.

Atom	X	y	z	U(eq)[1]
Zn(1)	2762(1)	11617(1)	8997(1)	14(1)
Zn(2)	4308(1)	17962(1)	9486(1)	14(1)
P(1)	3209(1)	16687(3)	8256(1)	13(1)
P(2)	6137(1)	17271(3)	9748(1)	12(1)
O(1)	1803(3)	12815(9)	9304(2)	22(1)
O(2)	3711(2)	11331(8)	9567(2)	17(1)
O(3)	2585(2)	8247(8)	8592(2)	19(1)
O(4)	2969(2)	13827(8)	8223(2)	16(1)
O(5)	3979(3)	15601(9)	10146(2)	23(1)
O(6)	4011(2)	17051(9)	8570(2)	20(1)
O(7)	5407(2)	18585(9)	9430(2)	19(1)
O(8)	3264(3)	17647(9)	7511(2)	21(1)
N(1)	3995(3)	11573(12)	6589(3)	32(2)
C(2)	5000	11581(24)	7500	39(3)
C(1)	4527(5)	13155(15)	7015(4)	36(2)

[1]U(eq) is defined as one third of the trace of the orthogonalized U_{ij} tensor.

coordinated oxygen atom is involved in the formation of 3-membered rings. The various bond distances and angles are presented in Table 1.25.

The framework structure is made from the tetrahedral linkage of ZnO_4, and PO_4 moieties sharing the vertices. The connectivity between these units form layers, which are anionic. The structure directing agent, DAP is doubly protonated and occupies spaces in between the layers. The entire structure is built up of alternating anionic (inorganic) and cationic (organic) layers. Within each inorganic layer, the connectivity between the ZnO_4 and PO_4 results in the formation of two types of distinct chains as shown in Fig.1.24a. One of the chains is the edge-shared 4-membered ring chain, which is commonly observed in many of the layered phosphate based open-framework materials[216] and the other is an alternating 3- and 4-membered ring chain, which was observed recently for the first time in a layered zinc phosphate. These chains are connected to each other via an out of plane 6-membered ring shown in Fig. 1.24b completing the layer (Fig. 1.24c). Because of the out of plane connectivity, the 6-membered ring, in fact, appears to be capped by a 3-membered ring on either side. This arrangement leads to the formation of another 4-membered ring, which connects two such 6-membered rings (Fig. 1.24b). This type of connectivity, to our knowledge, has been observed for the first time in a layered open-framework material and resulted in having layers that are more three-dimensional like rather than two-dimensional. The 6-membered rings along with the chains shown in Fig. 1.24a results in a channel type arrangement within the layer (Fig. 1.25). The terminal –OH (hydroxyl) of the HPO_4 group protrude into this channel.

The presence of 3-coordinated oxygen atom leads to the formation of short Zn – O – Zn chains. Such a trigonal coordination of the oxygen atom in the Zn – O – Zn bridge is an electrostatic valence requirement of the bridging oxygen atom. There are other examples of such electrostatic valence requirements of oxygens known in the literature.[92,247-249] In the present material, Zn(1), Zn(2) and P(2) are 4-connected via oxygens, whereas P(1) is 3-connected

Table 1.25. Selected bond lengths (Å) and angles (°) for, **IV**, $[NH_3(CH_2)_3NH_3]^{2+}$ $2[Zn_2PO_4(HPO_4)]^-$.

Moiety	Distance, (Å)	Moiety	Distance (Å)
Zn(1) - O(1)	1.899(5)	P(1) – O(6)	1.509(4)
Zn(1) - O(2)	1.963(4)	P(1) – O(3)$^{\#1}$	1.530(5)
Zn(1) - O(3)	1.948(4)	P(1) – O(4)	1.542(5)
Zn(1) - O(4)	1.980(4)	P(1) – O(8)	1.586(5)
Zn(2) - O(5)	1.913(4)	P(2) – O(1)$^{\#2}$	1.515(5)
Zn(2) - O(6)	1.950(4)	P(2) – O(5)$^{\#3}$	1.521(5)
Zn(2) - O(7)	1.934(4)	P(2) – O(7)	1.548(4)
Zn(2) - O(2)$^{\#1}$	2.041(4)	P(2) – O(2)$^{\#3}$	1.570(4)
Moiety	**Angle (°)**	**Moiety**	**Angle (°)**
O(1) - Zn(1) - O(3)	107.9(2)	O(4) – P(1) - O(8)	106.8(3)
O(1) - Zn(1) - O(2)	123.6(2)	O(1)$^{\#2}$ - P(2) - O(5)$^{\#3}$	111.9(3)
O(3) - Zn(1) - O(2)	106.7(2)	O(1)$^{\#2}$ - P(2) - O(7)	107.5(3)
O(1) - Zn(1) - O(4)	104.9(2)	O(5)$^{\#3}$ - P(2) - O(7)	112.4(3)
O(3) - Zn(1) - O(4)	102.9(2)	O(1)$^{\#2}$ - P(2) - O(2)$^{\#3}$	109.3(3)
O(2) - Zn(1) - O(4)	109.1(2)	O(5)$^{\#3}$ - P(2) - O(2)$^{\#3}$	110.4(3)
O(5) - Zn(2) - O(7)	118.2(2)	O(7) – P(2) - O(2)$^{\#3}$	105.1(2)
O(5) - Zn(2) - O(6)	115.2(2)	P(2)$^{\#4}$ - O(1) - Zn(1)	145.8(3)
O(7) – Zn(2) - O(6)	101.7(2)	P(2)$^{\#3}$ - O(2) - Zn(1)	125.4(3)
O(5) – Zn(2) -O(2)$^{\#1}$	109.1(2)	P(2)$^{\#3}$ - O(2) - Zn(2)$^{\#5}$	113.6(2)
O(7) – Zn(2) -O(2)$^{\#1}$	111.3(2)	P(1)$^{\#5}$ - O(3) - Zn(1)	124.1(3)
O(6) – Zn(2) -O(2)$^{\#1}$	99.8(2)	P(1) – O(4) - Zn(1)	125.6(3)
O(6) - P(1) – O(3)$^{\#1}$	113.6(3)	P(2)$^{\#3}$ - O(5) - Zn(2)	140.4(3)
O(6) - P(1) – O(4)	112.2(3)	P(1) – O(6) - Zn(2)	128.6(3)
O(3)$^{\#1}$ – P(1) - O(4)	109.6(3)	P(2) – O(7) - Zn(2)	133.3(3)
O(6) - P(1) – O(8)	105.2(3)	Zn(1) – O - Zn(2)$^{\#5}$	115.5(2)
O(3)$^{\#1}$ – P(1) - O(8)	109.0(3)	P(1) – O(8) - H(10)	109.5(2)

Organic Moiety

Moiety	Distance (Å)	Moiety	Angle (°)
N(1) - C(1)	1.477(9)	C(1) - C(2) - C(1)$^{\#6}$	113.4(10)
C(2) - C(1)	1.489(10)	N(1) - C(1) - C(2)	112.6(7)
C(2) - C(1)$^{\#6}$	1.489(10)		

#1 x, y+1, z; #2 x+1/2, y+1/2, z; #3 -x+1, -y+3, -z+2; #4 x-1/2, y-1/2, z; #5 x, y-1, z; #6 -x+1, y, -z+3/2

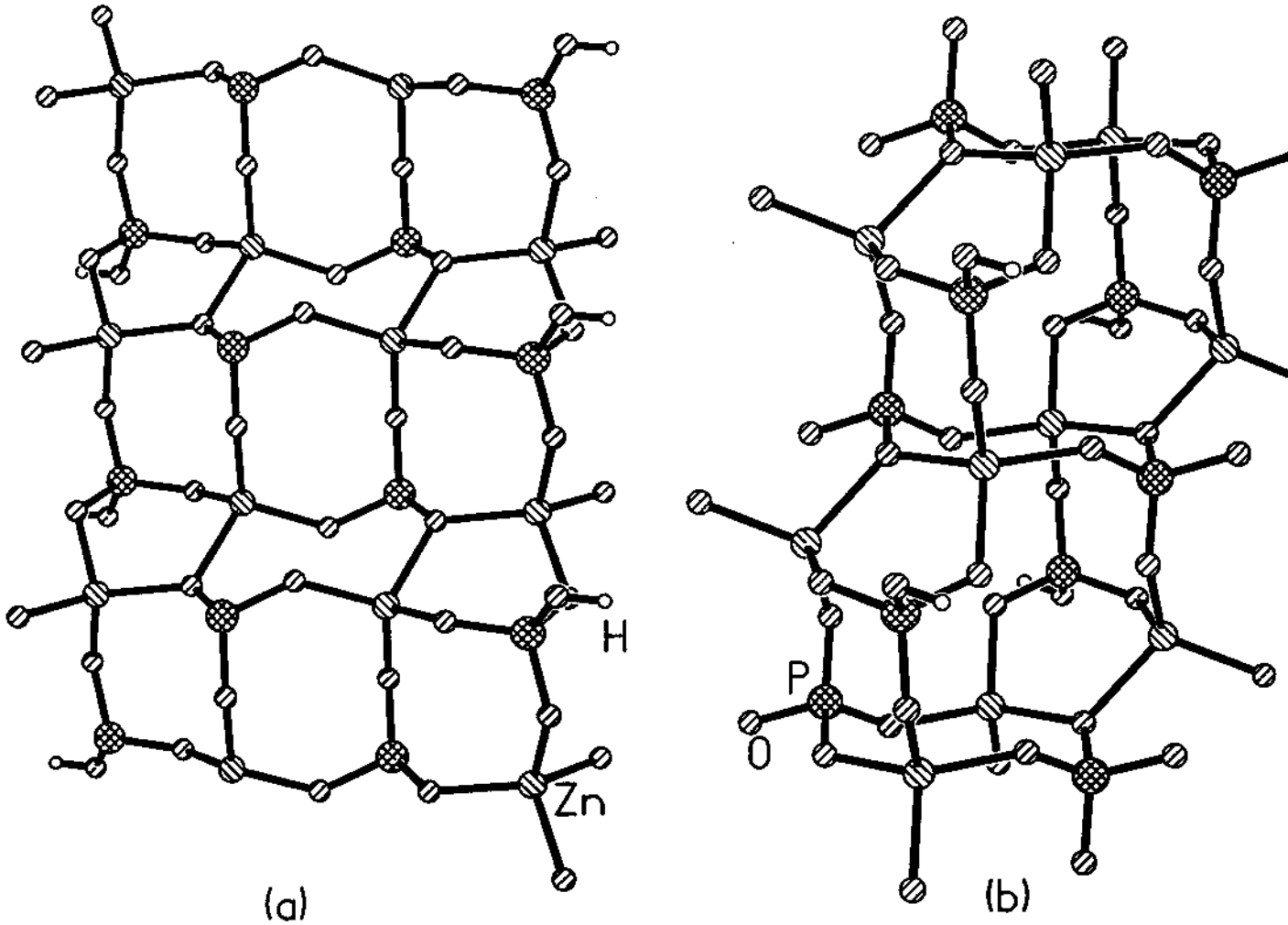

Fig. 1.24. (a) Structure showing the different type of chains within the layer. Note that there are two distinct chains. (b) The 6–membered ring that connects the chains with in the layers.

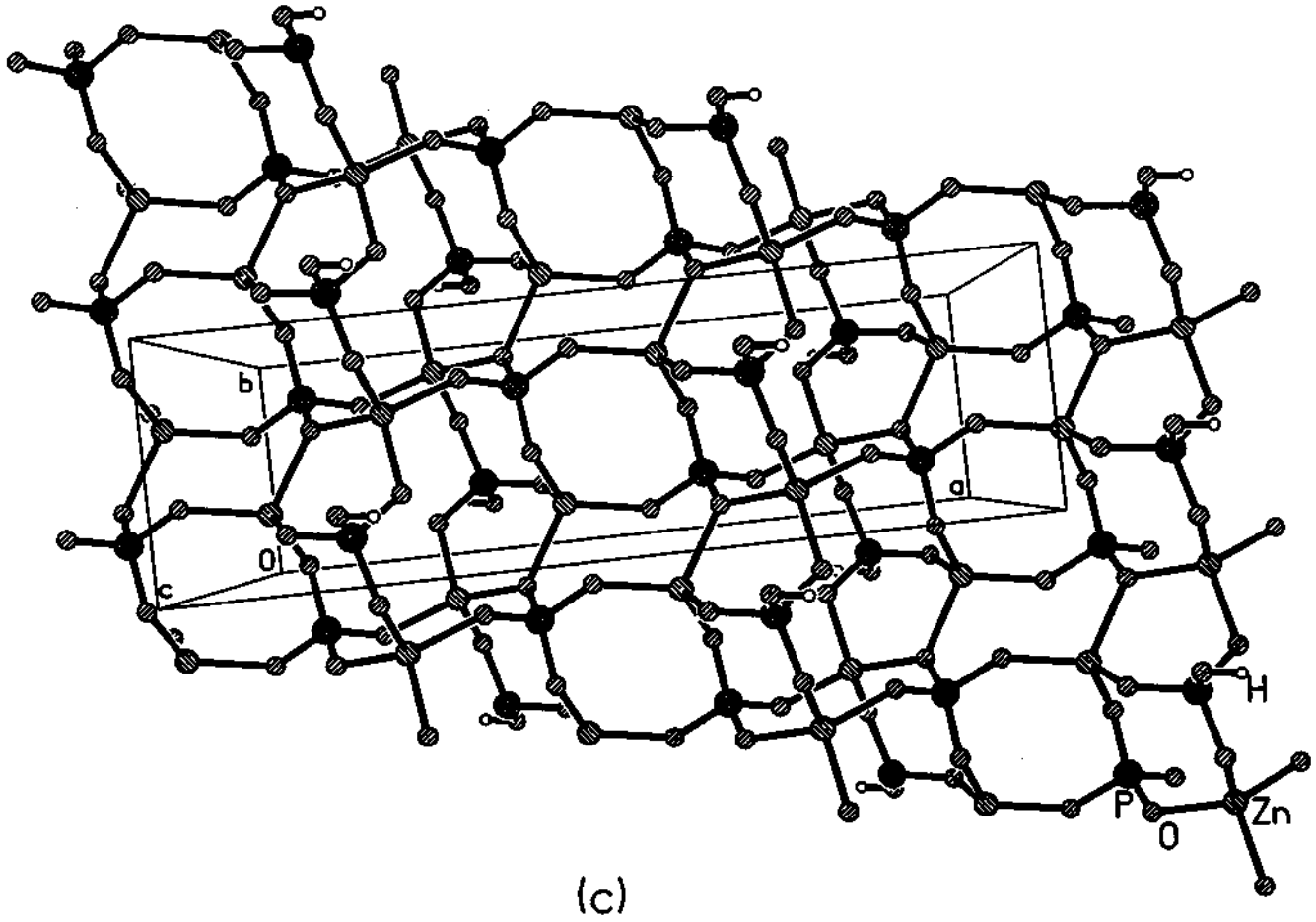

Fig. 1.24. (c) Structure showing a single layer in **IV**.

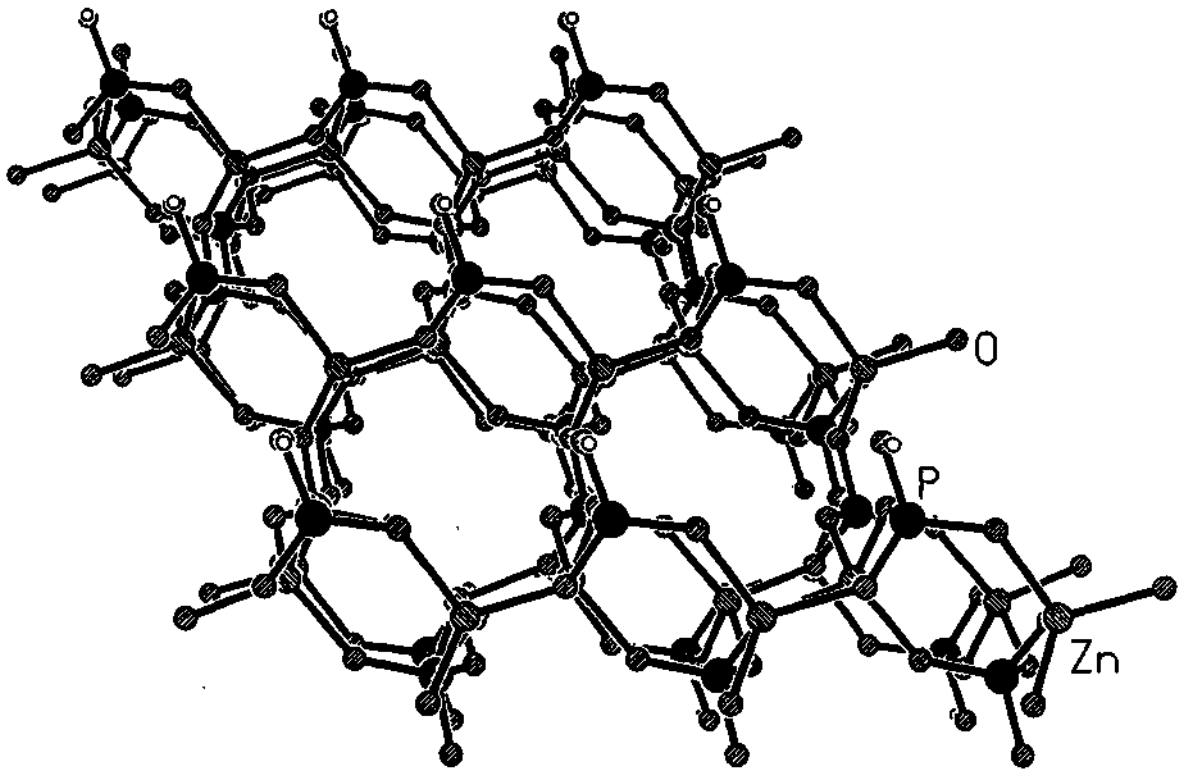

Fig. 1.25. Structure showing the channel type arrangement that is seen in **IV** within the layers.

and the remaining vertex being a terminal hydroxyl group. Thus, 75% of the T atoms in this material are four connected.

The layered structure of the framework is stabilized by hydrogen bonding between the P(1)-O(8)H with that of the next layer leading to the formation of pseudo 10-membered channels (Fig. 1.26). The formation of such pseudo channels by hydrogen bonding is known to occur in layered zinc phosphates.[232] The guest molecule diprotonated DAP occupies the interlamellar space formed by the framework species and sits in the middle of the pseudo 10-membered channels (Fig. 1.26). The DAP molecule also participates in strong hydrogen bonding with the framework species and offers additional structural stability. The selected hydrogen bond interactions are presented in Table 1.26.

The Zn – O bond distances [ave: 1.948Å for Zn(1) and 1.959Å for Zn(2)] and the O – Zn – O angles [ave: 109.2° for Zn(1) and 109.2° for Zn(2)] are in the range expected for this type of bonding. The P – O bond distances [ave: 1.539Å for P(1) 1.536Å for P(2)] and O – P – O angles [ave: 109.4° for P(1) and 109.4° for p(2)] are also as expected. The longest bond distances and the largest bond angles, however, are observed for oxygens involved in 3-coordination. The P(1) – O(8) distance of 1.586 Å is protonated leading to the formation of HPO_4 units (Table 1.25).

The synthesis of this material was carried out hydrothermally using a zinc amine complex as the starting source for Zn in the presence of phosphoric and oxalic acid. The use of zinc-amine complex, we believe helps in the release of amine molecules in a controlled manner during the hydrothermal reaction resulting in the formation of this new phase. Similar observations have been made earlier in the synthesis of open-framework materials.[231-233] The role of oxalic acid as mentioned before seems to be primarily in maintaining the delicate pH balance, but much detailed investigation can lead to a more consolidated reasoning.

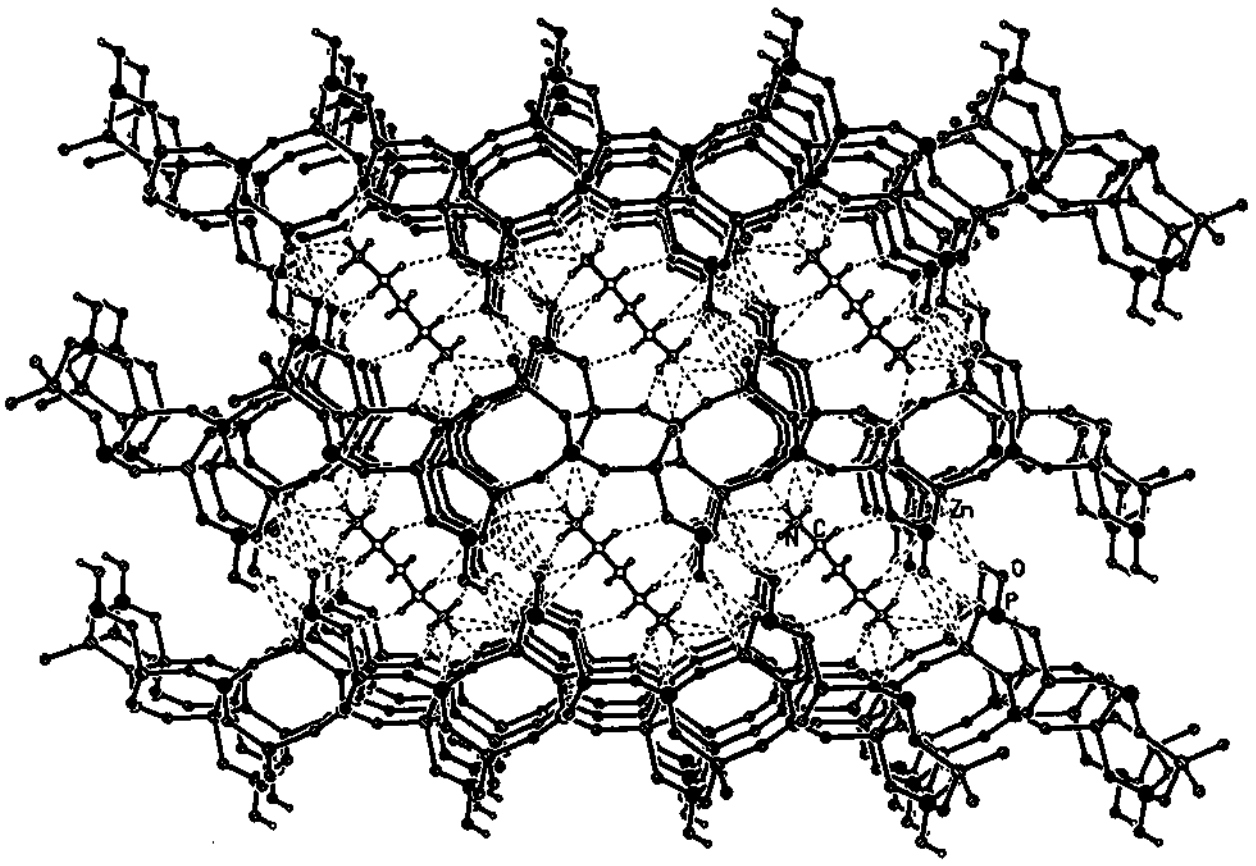

Fig. 1.26. Structure of **IV** viewed along the *[010]* direction showing the alternate inorganic and organic layers. Dotted lines represent hydrogen bond interactions observed in the material.

Table 1.26. Selected hydrogen bond interactions in **IV**, $[NH_3(CH_2)_3NH_3]^{2+}$ $2[Zn_2PO_4(HPO_4)]^-$.

Moiety	Distance (Å)	Moiety	Angle (°)
O(7) - H(1)	1.9456	O(7) – H(1) - N(1)	156.52
O(8) - H(2)	2.2048	O(8) – H(2) - N(1)	157.87
O(4) - H(10)$^{\#}$	1.8455	O(4) – H(10) - O(8)$^{\#}$	150.59
O(6) - H(4)	2.5436	O(6) – H(4) - C(1)	158.36
O(8) - H(5)	2.4221	O(8) – H(5) - C(1)	161.41

$^{\#}$ Intra-layer

$[NH_3(CH_2)_2NH(CH_2)_2NH_3]^{2+}$ $2[Zn_2PO_4(HPO_4)]^-$, V : The asymmetric unit of the zinc phosphate, $[NH_3(CH_2)_2NH(CH_2)_2NH_3]^{2+}$ $2[Zn_2PO_4(HPO_4)]^-$, contains 16 independent non-hydrogen atoms of which 12 belong to the 'framework' (2 Zn, 2 P and 8 O atoms) and 4 to the guest (2 N and 2 C atoms) (Fig.1.27 and atomic coordinates, Table 1.27). Of the eight oxygens in the asymmetric unit, two are three-coordinated linking two Zn atoms and one P atom (25%) and the remaining are normal Zn – O – P links. The linkages involving the three-coordinated oxygen atoms result in the formation of 3-membered rings in this material.

The framework structure is made from the tetrahedral linkage between ZnO_4 and PO_4 moieties sharing the vertices. The connectivity between these units form layers, which are anionic. The structure-directing agent, diethylenetriamine (DETA), is doubly protonated and occupies spaces between the layers. Thus, the entire structure can be considered to be made up of alternating anionic (inorganic) and cationic (organic) layers. The connectivity between the ZnO_4 and PO_4 units is such that it produces three distinct types of chains, labeled A, B and C in Fig. 1.28. The A type chain consists of alternate stacking of 3- and 4-membered rings (involving Zn(1) and Zn(2)) while the B type chain is made up of only 4-membered rings (involving only Zn(2) and P(2)). The C type chain is made up of only 3-membered rings (involving only Zn(1) and P(1)) (Fig. 1.28). The chains are connected to one another other forming the layer as shown in Fig. 1.29a. To our knowledge, this zinc phosphate is the first example of an open-framework material where different types of chain arrangements are connected to each other forming a layer with ladder-like steps. Isolated and short-chain 3-membered rings are common in many of the open-framework zinc phosphates,[92,247-249] but this is the first instance a continuous 3-member ladder (chain) is present in an open-framework material. The presence of the exclusive 3-membered chains of ladders creates some strain in the layer, which is otherwise nearly planar and causes the formation of a step and a ladder-like feature in the material. Furthermore, we find a ABAC repeating unit along the *bc* plane giving rise to the repeat ring sequence of 3343344433 along the *c*

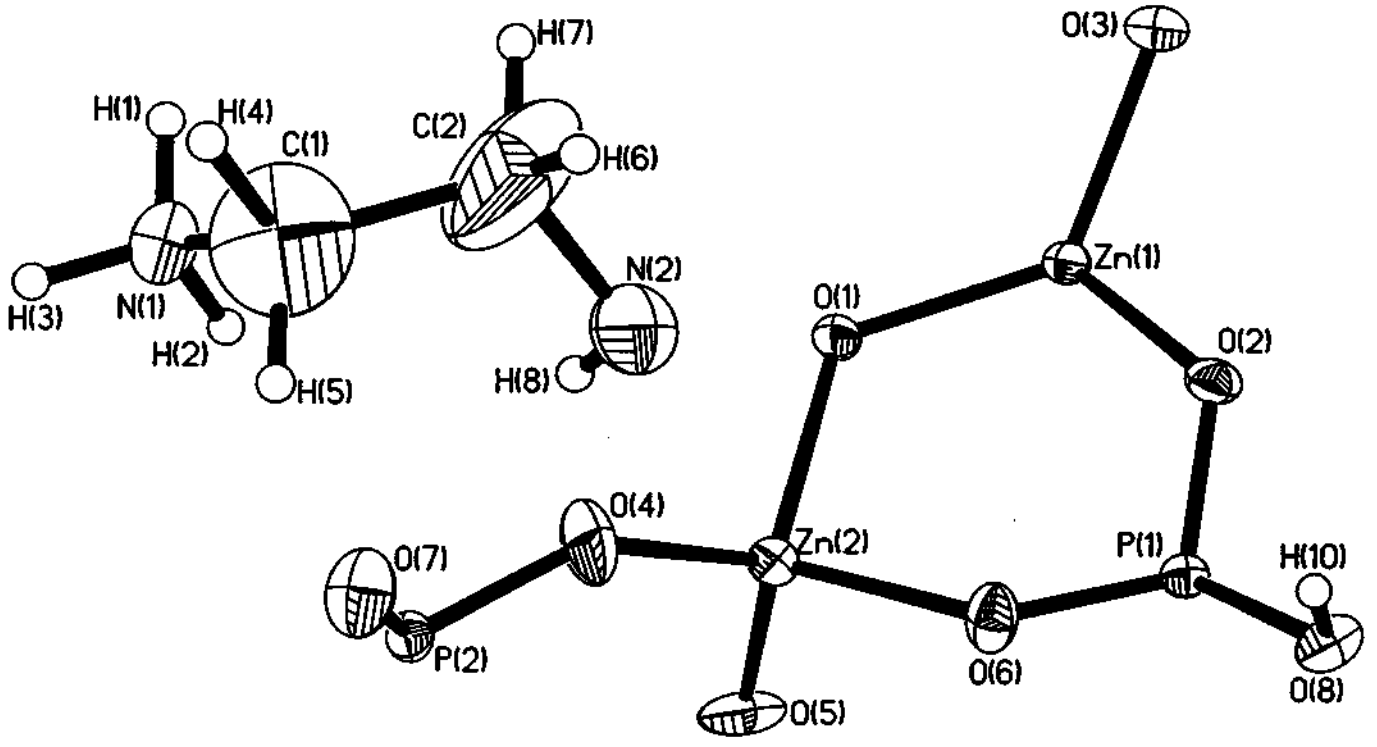

Fig. 1.27. ORTEP plot of **V**, $[NH_3(CH_2)_2NH(CH_2)_2(NH_3)]$ $2[Zn_2(PO_4)(HPO_4)]$ showing the labelling scheme. Thermal ellipsoids are shown at 50% probability.

Table 1.27. Atomic coordinates [x 10^4] and equivalent isotropic displacement parameters [$Å^2$ x 10^3] for V, $[NH_3(CH_2)_2NH(CH_2)_2NH_3]^{2+}2[Zn_2PO_4(HPO_4)]^-$

Atom	x	y	z	U(eq)
Zn(1)	0.2048(1)	0.2860(1)	0.1826(1)	0.013(1)
Zn(2)	0.0751(1)	0.7083(1)	0.0506(1)	0.016(1)
P(1)	0.2164(1)	0.7850(3)	0.0989(1)	0.012(1)
P(2)	-0.0671(1)	0.7724(3)	-0.1435(1)	0.014(1)
O(1)	0.1133(2)	0.3697(7)	0.1231(2)	0.018(1)
O(2)	0.2370(2)	0.5020(7)	0.1272(3)	0.018(1)
O(3)	0.2427(2)	-0.0563(7)	0.1902(2)	0.017(1)
O(4)	0.0007(2)	0.6616(9)	-0.0740(3)	0.032(1)
O(5)	0.0716(2)	0.9359(7)	0.1340(3)	0.030(1)
O(6)	0.1427(2)	0.8206(8)	0.0352(3)	0.022(1)
O(7)	-0.0884(2)	0.7102(8)	-0.2410(3)	0.027(1)
O(8)	0.2486(2)	0.8972(7)	0.0545(2)	0.018(1)
N(1)	-0.1449(2)	0.2412(10)	-0.3371(4)	0.031(1)
N(2)	0.0000	0.4082(15)	-0.2500	0.041(2)
C(1)	-0.1119(3)	0.2764(19)	-0.3848(5)	0.075(3)
C(2)	-0.0395(3)	0.2170(18)	-0.3273(6)	0.099(4)

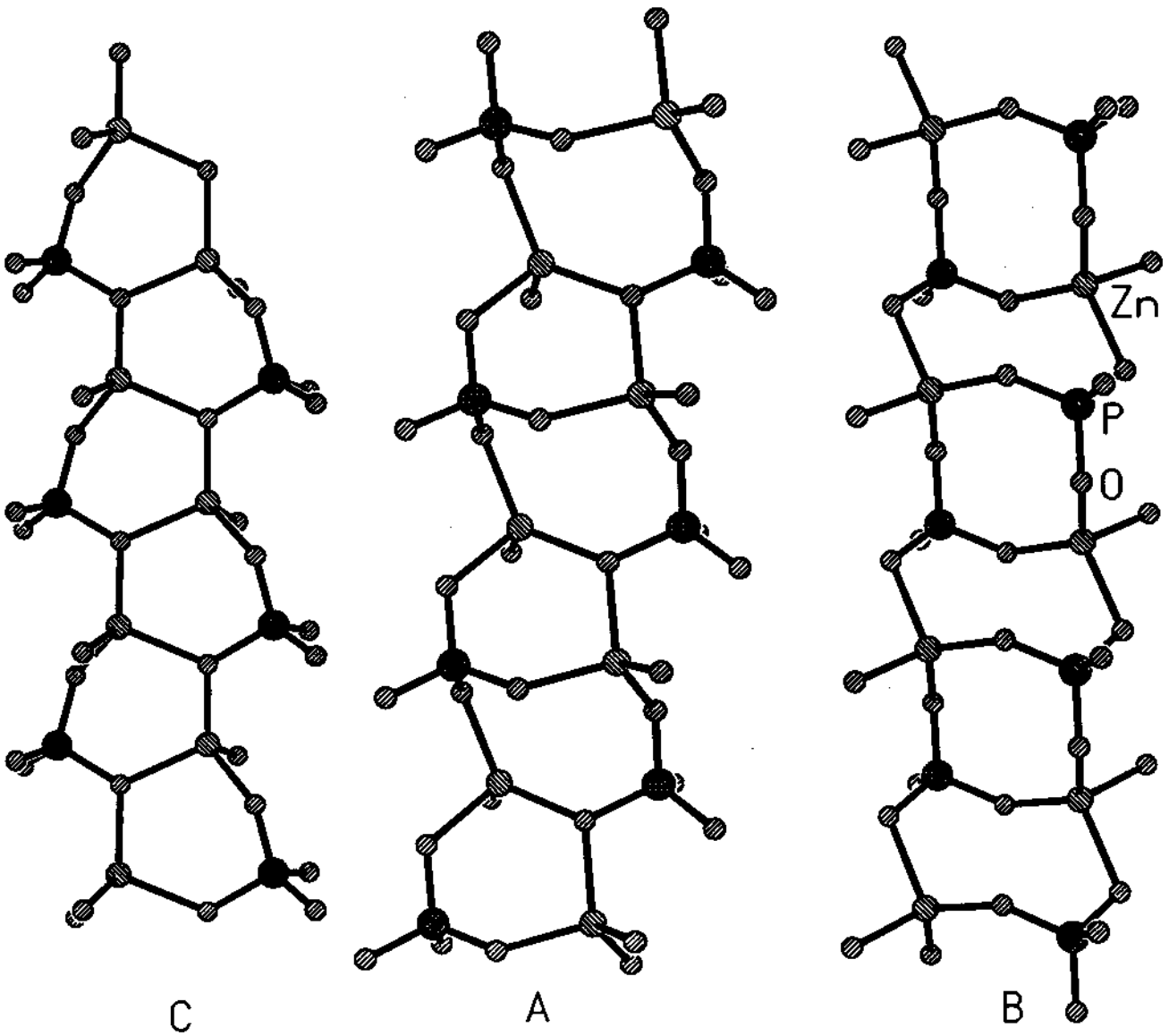

Fig. 1.28. Figure showing the different type of chain arrangement that are seen in V,

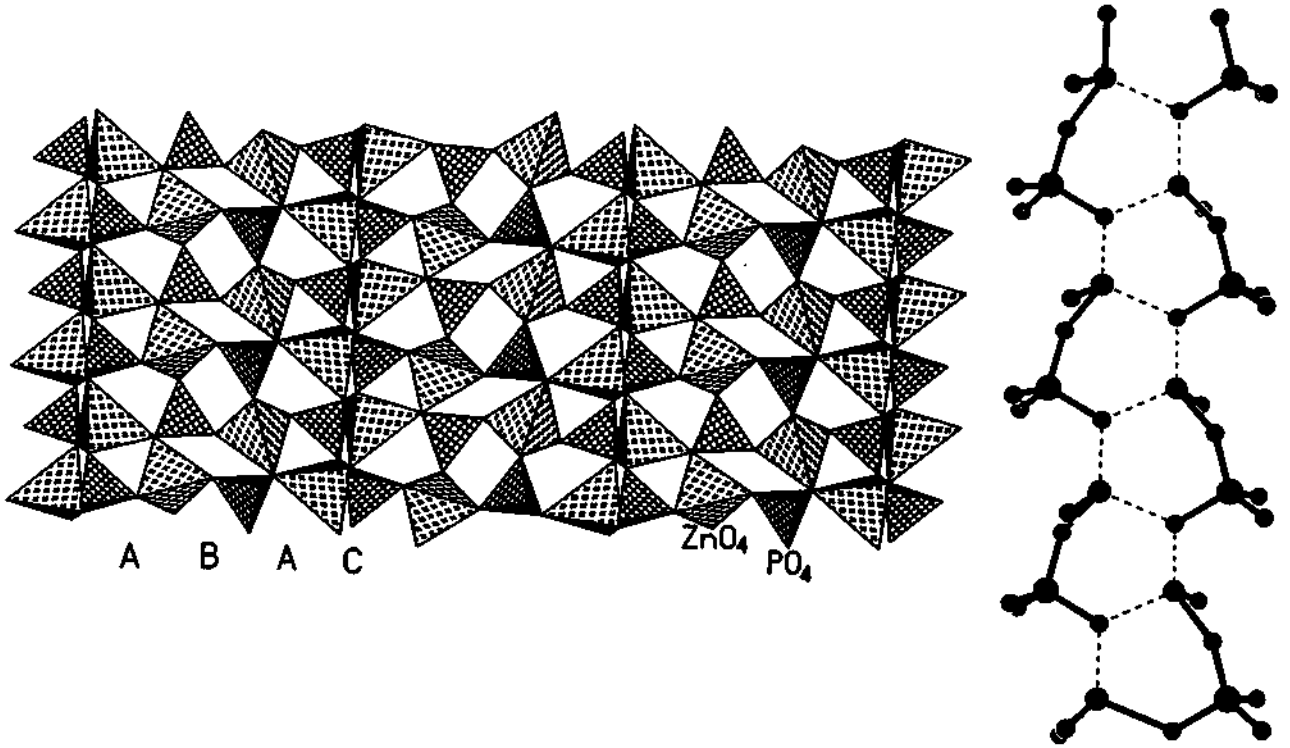

Fig. 1.29. Polyhedral view of **V** along the [010] direction showing the layers, the various chains and the connectivity between them. Note that the 3–membered ring (C type) forms the step in the layer. (b) Structure showing the infinite one–dimensional Zn – O – Zn chains (dashed lines), formed due to the presence of 3–membered ladders, observed in **V**.

axis (Fig. 1.29a). Recalling that the 3-membered ring is the smallest possible ring size and that two 3-membered rings can make a 4-member ring, the present structure can, in principle, evolve into a layer structure with only 4-membered rings, which are rarely seen in open-framework materials.

The framework of the Zn phosphate is also characterized by the presence of infinite Zn – O – Zn chains (Fig. 1.29b). The Zn – O – Zn linkage is accompanied by the trigonal coordination of the bridging oxygen atoms, the third coordination being always to a P atom. Such a trigonal coordination of the oxygen atom in the Zn – O – Zn bridge, is an electrostatic valence requirement of the bridging oxygen atoms. 25% of the oxygens in the asymmetric unit are 3-coordinated (two of the eight framework oxygen atoms). Thus, it can be concluded that the presence of 3-coordinated oxygen bridges tends to give rise to more dense frameworks. There are other examples of such electrostatic valence requirements of oxygens known in the literature.[92,247-249] The trigonal and tetrahedral coordination of the oxygen atoms observed in some of the structures reported in the literature, suggests that these bridges occur when divalent tetrahedral atoms are involved. It is therefore expected that the presence of such features in the zinc phosphate system would lead to novel open-framework topologies, which have no structural counterparts in aluminosilicates or aluminophosphates. The infinite one-dimensional Zn – O – Zn chain is formed only by the Zn(1) atoms (forming the 3-membered ladders) as shown in Fig.1.29b but isolated short chain Zn – O – Zn linkages involving both Zn(1) and Zn(2) atoms are also present in the present structure.

An interesting aspect of this layered zinc phosphate is the connectivity between the Zn atoms within each layer. From the Zn sub-network is presented in Fig. 1.30, it can be seen that the arrangement resembles the *fish backbone*. This feature has been seen for the first time in this study. The Zn(1) forms the vertebrae onto which Zn(2) atoms are grafted completing the *fish backbone* type arrangement. This type of connectivity may be attributed to the presence of the 3-membered chains and the 3-coordinated oxygen atoms.

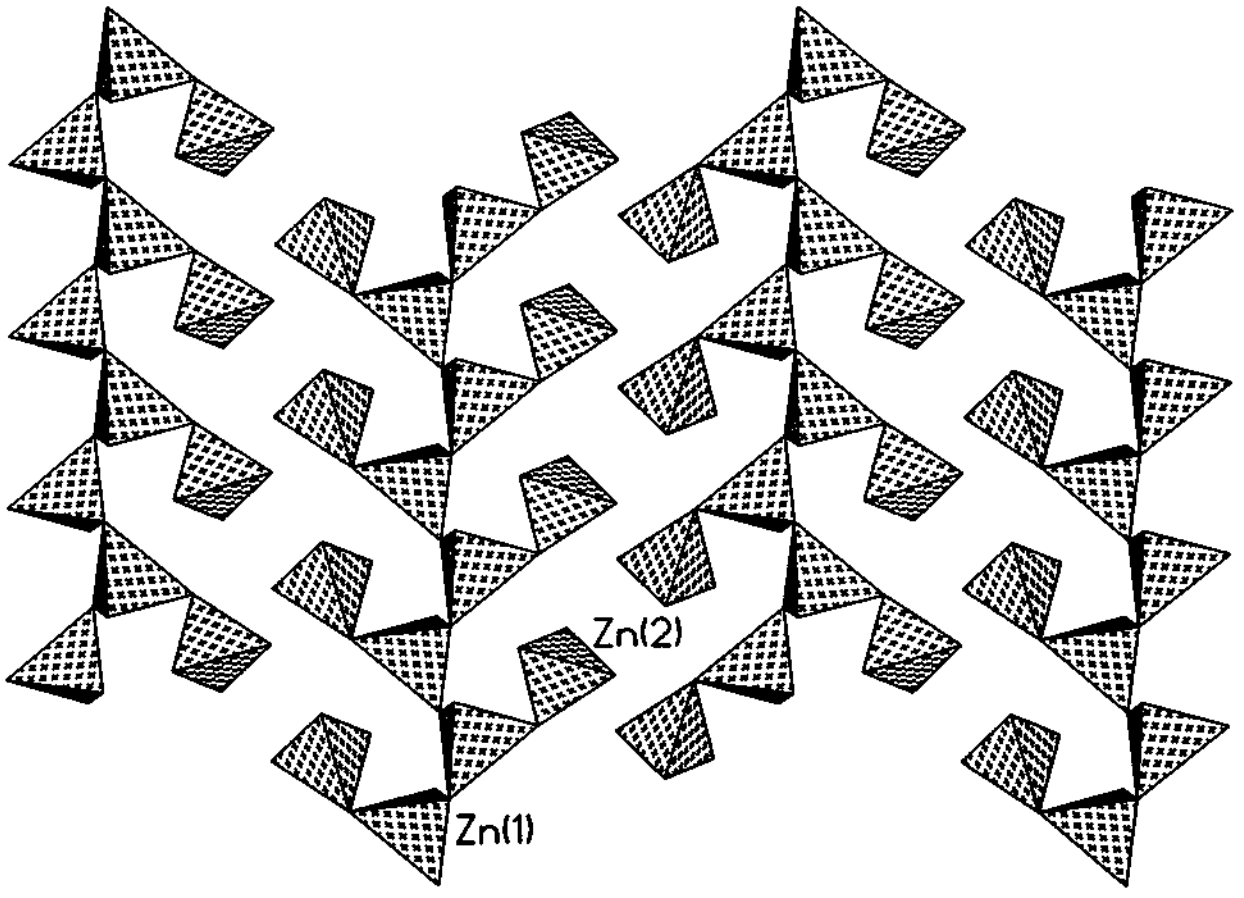

Fig. 1.30. The Zn tetrahedra sub–network showing the *fish backbone* arrangement.

The connectivity between the ZnO_4 and PO_4 units gives rise to another unique feature whereby each Zn atom is surrounded by 3- and 4-membered rings. The circuit symbol, which enumerates the six distinct, smallest T-atom loop pathways[218] (including the central atom itself), can be written as ($4^4 6^2$ or 4,4,4,4,6,6) for all tetrahedral atoms. This type of tetrahedral atom configuration is not known in aluminosilicates or aluminophosphates. In the present material, Zn(1) and Zn(2) are connected to P through all the four vertices of the tetrahedron, whereas P(1) and P(2) are connected to Zn atoms only through three vertices the remaining vertex being a terminal oxygen (Fig. 1.31). Thus, 50% of the T-atoms are four connected. . There is, however, one example of a zinc arsenate where all the T atoms are four-connected.[219]

The Zn(1) atom is surrounded by three 3-membered rings and one 4-membered ring and makes 4-membered and 5-membered loops, the Zn(2) atom is surrounded by a 3-membered ring and three 4-membered rings, makes 5-membered and 6-membered loops (Fig.1.31a-d). The T-atom connectivity observed in this material can be represented in the circuit symbol of Smith[218] as [3,3,3,4,4,5] and [3,4,4,4,5,6]. The loop configurations for Zn(1) and Zn(2) though are different, it is to be noted that both of them are bonded into an 8-ring of neighboring TO_4 groups. The loop configuration for P(1), though is identical to that of Zn(1), however, is bonded into a 6-ring of neighboring TO_4 groups (Fig.1.31a-b). P(2), on the other hand, is identical to Zn(2) bonded into a 8-ring of neighboring TO_4 groups. We believe, that, this is the first time such a loop network for a T atom has been observed in an open-framework material.

The coordination environment of the various sites in this material can also be represented using the Schläfli symbol, which specifies the connectivities of the various vertex-linked polygons. The description of the various types of plane nets, commonly observed in crystal chemistry, using the above symbolism has been reviewed by O'Keeffe and Hyde.[250] Acccording to the Schläfli notation, the coordination environment for P(1) can be represented as $\mathbf{3^3 4^1}$, meaning P(1) is surrounded by three triangles (3-membered rings) and one square (4-membered

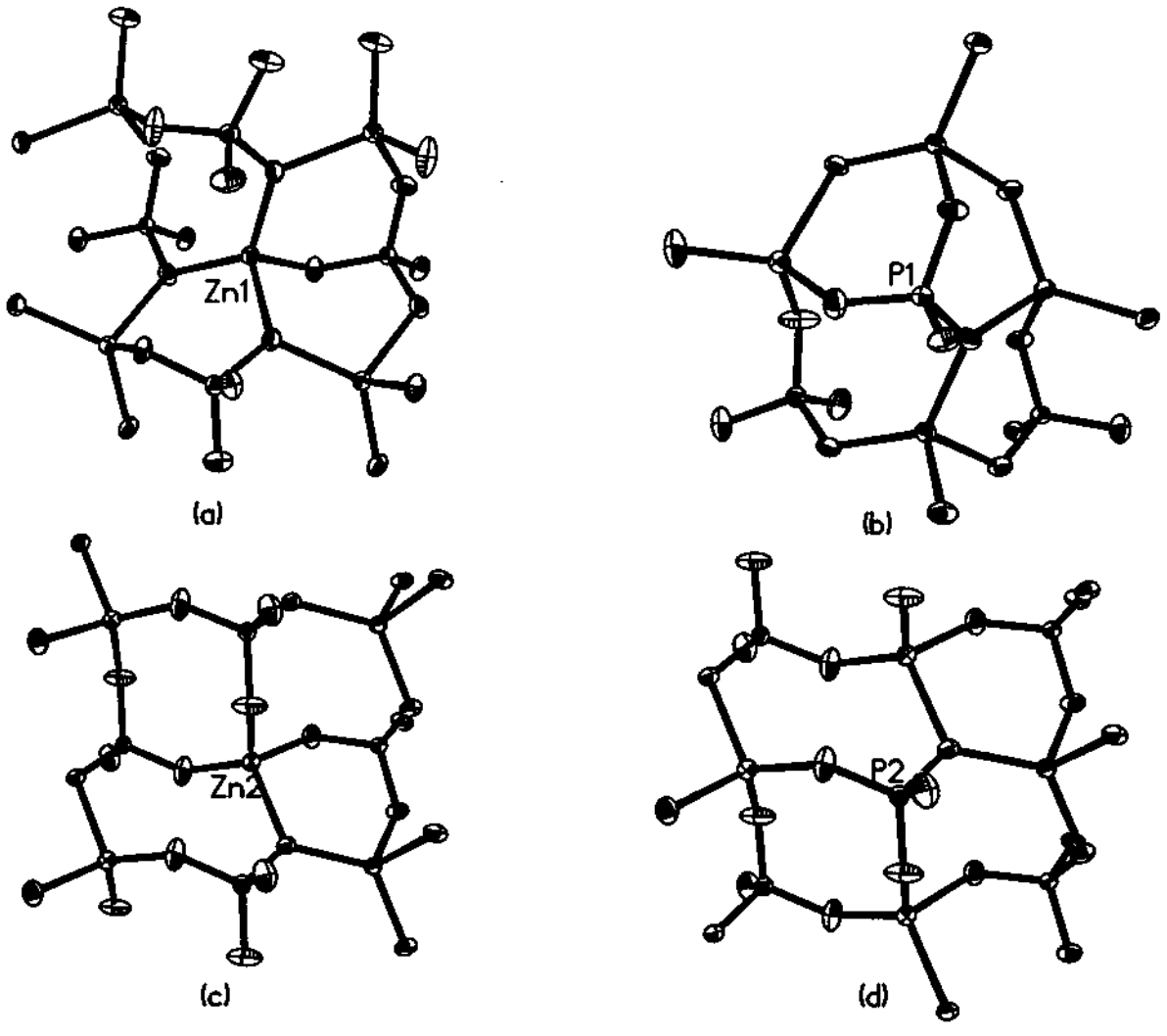

Fig. 1.31. Details of the environment around Zn(1), P(1), Zn(2) and P(2). Note that the $Zn(1)O_4$ unit is bonded to a 8–ring of neighbouring TO_4 groups and the $P(1)O_4$ unit is bonded to a 6–ring of neighbouring TO_4 groups. (see text).

rings). Likewise, the notation for the other species would be: P(2) – $3^1 4^3$; Zn(1) – $3^6 4^1$ and Zn(2) – $3^2 4^3$. This type of representation clearly shows the different situation for each site and its connectivity (Fig.1.31a-d).

The ZnO_4 tetrahedra have the Zn – O distances in the range 1.908 – 2.039Å [1.962Å for Zn(1) and 1.956Å for Zn(2)]. The O – Zn – O bond angles are in the range 98.4 – 127.5° [ave. 108.8° for Zn(1) and 109.2° for Zn(2)]. The tetrahedral P atoms have P – O bond distances in the range 1.516 – 1.580Å [ave: 1.537Å for P(1) and 1.532 Å for P(2)] and the O – P – O bond angles in the range 105.5 – 113.5° [ave. 109.5° for P(1) and 109.5° for P(2)]. The longest bond distances and the largest bond angles, however, are observed for oxygens involved in 3-coordination. One of the P – O distance [P(1) – O(8)] is protonated leading to the formation of HPO_4 units in the material. These values are typical of Zn and P in tetrahedral oxygen environment. From the above values, it is clear that the P atoms form more regular tetrahedron than the Zn atoms. The selected bond distances and angles are presented in Table 1.28.

The layered structure of the framework is stabilized by hydrogen bonding between the P(1) – O(8)H with that of the next layer leading to the formation of a pseudo 10-membered channels (Fig. 1.32). Unlike in aluminosilicates,[16] the 10-membered ring is rare in open-framework zinc phosphate materials, having been reported only in one material so far. The formation of such pseudo channels by hydrogen bonding between the terminal PO_4 and $PO_3(OH)$ of adjacent layers is known to occur in layered zinc phosphates.[232] The guest molecule, diethylenetriamine, is doubly protonated and occupies the interlamellar space formed by the framework species and sits in the middle of the pseudo 10-membered channels (Fig. 1.32). The DETA molecule also participates in strong hydrogen bonding with the framework which lends additional structural stability to this material. The selected hydrogen bond interactions that are observed is presented in Table 1.29.

Table 1.28. Selected bond lengths [Å] and angles [°] for $V,[NH_3(CH_2)_2NH(CH_2)_2NH_3]^{2+}$ $2[Zn_2PO_4(HPO_4)]^-$

Moiety	Distance, Å	Moiety	Distance, Å
Zn(1) – O(1)	1.938(4)	P(1) – O(2)	1.524(4)
Zn(1) – O(2)	1.939(4)	P(1) – O(6)	1.518(4)
Zn(1) – O(3)	1.962(4)	P(1) – O(8)	1.529(4)
Zn(1) – O(3)$^{\#1}$	2.008(3)	P(1) – O(3)$^{\#2}$	1.574(4)
Zn(2) – O(1)	2.039(4)	P(2) – O(4)	1.516(4)
Zn(2) – O(4)	1.908(4)	P(2) – O(7)	1.517(4)
Zn(2) – O(5)	1.925(4)	P(2) – O(5)$^{\#3}$	1.517(4)
Zn(2) – O(6)	1.953(4)	P(2) – O(1)$^{\#4}$	1.580(4)
Moiety	Angle (°)	Moiety	Angle (°)
O(1) – Zn(1) – O(2)	107.8(2)	O(6) – P(1) – O(2)	113.2(2)
O(1) – Zn(1) – O(3)	127.5(2)	O(6) – P(1) – O(8)	110.5(2)
O(2) – Zn(1) – O(3)	102.6(2)	O(2) – P(1) – O(8)	110.4(2)
O(1) – Zn(1) – O(3)$^{\#1}$	108.7(2)	O(6) – P(1) – O(3)$^{\#2}$	107.9(2)
O(2) – Zn(1) – O(3)$^{\#1}$	98.4(2)	O(2) – P(1) – O(3)$^{\#2}$	107.1(2)
O(3) – Zn(1) – O(3)$^{\#1}$	107.91(10)	O(8) – P(1) – O(3)$^{\#2}$	107.6(2)
O(4) – Zn(2) – O(5)	121.0(2)	O(4) – P(2) – O(7)	109.7(2)
O(4) – Zn(2) – O(6)	102.8(2)	O(4) – P(2) – O(5)$^{\#3}$	113.6(3)
O(5) – Zn(2) – O(6)	111.0(2)	O(7) – P(2) – O(5)$^{\#3}$	109.5(2)
O(4)– Zn(2) – O(1)	114.2(2)	(4) – P(2) – O(1)$^{\#4}$	105.5(2)
O(5) – Zn(2) – O(1)	104.3(2)	O(7) – P(2) – O(1)$^{\#4}$	110.0(2)
O(6) – Zn(2) – O(1)	102.1(2)	O(5)$^{\#3}$ – P(2) – O(1)$^{\#4}$	108.4(2)
P(2)$^{\#4}$ – O(1) – Zn(1)	124.6(2)	P(2)$^{\#4}$ – O(1) – Zn(2)	113..4(2)
P(1) – O(2) – Zn(1)	123.3(2)	Zn(1) – O(1) – Zn(2)	120.5(2)
P(1)$^{\#5}$ – O(3) – Zn(1)	119.6(2)	P(2) – O(4) – Zn(2)	141.0(3)
P(1)$^{\#5}$ – O(3) – Zn(1)$^{\#6}$	123.9(2)	P(2)$^{\#3}$ – O(5) – Zn(2)	136.3(3)
Zn(1) – O(3) – Zn(1)$^{\#6}$	114.4(2)	P(1) – O(6) – Zn(2)	129.9(2)
Organic Moiety			
Moiety	Distance, Å	Moiety	Angle (°)
N(1) – C(1)	1.4994(11)	C(2) – N(2) – C(2)$^{\#7}$	98.3(10)
N(2) – C(2)	1.4992(11)	N(1) – C(1) – C(2)	115.8(6)
N(2) – C(2)$^{\#7}$	1.4993(11)		
C(1) – C(2)	1.5090(12)		

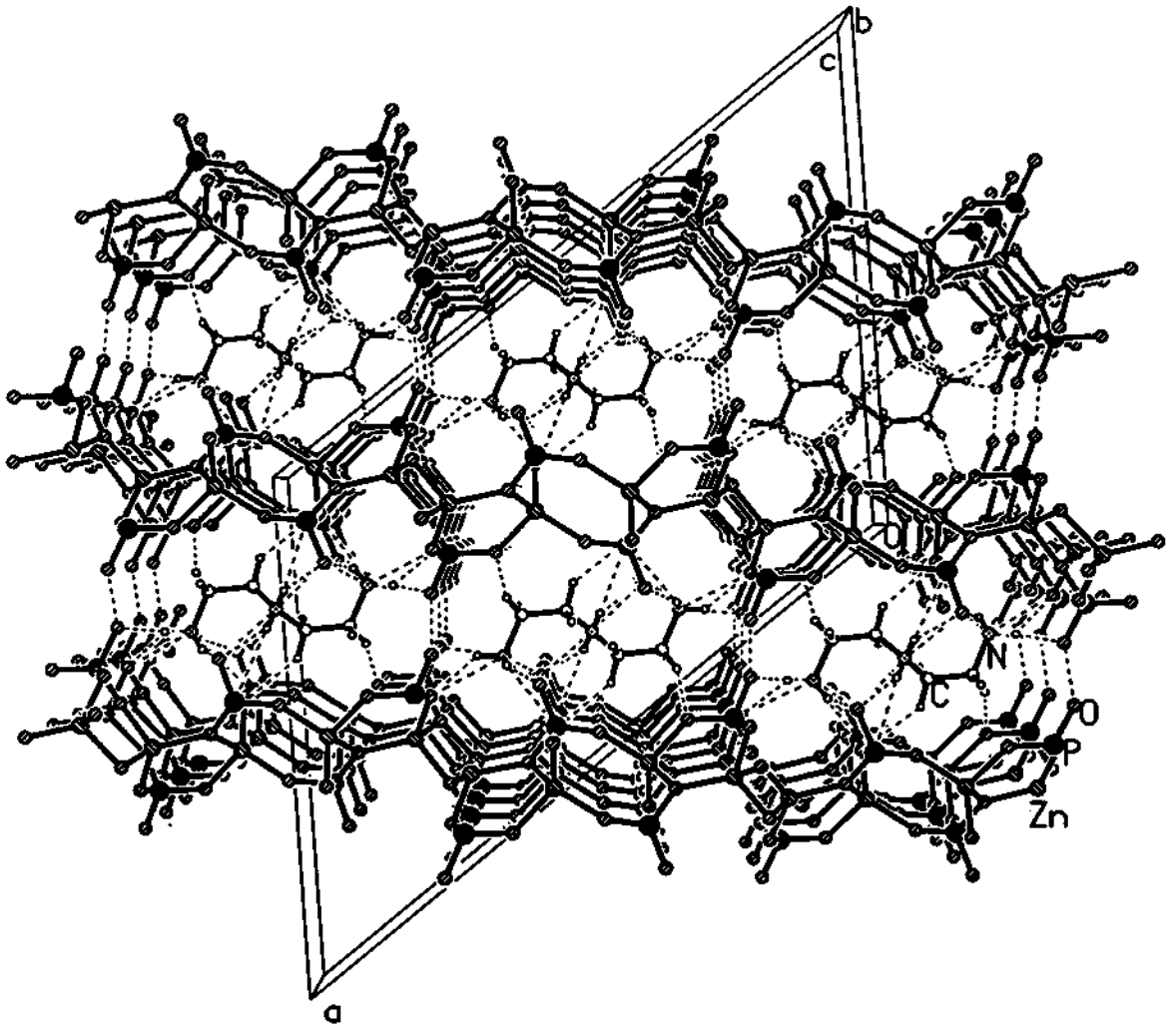

Fig. 1.32. (a) Structure of **V** along the [001] direction showing alternating anionic and cationic layers and pseudo 10–memberd channels.

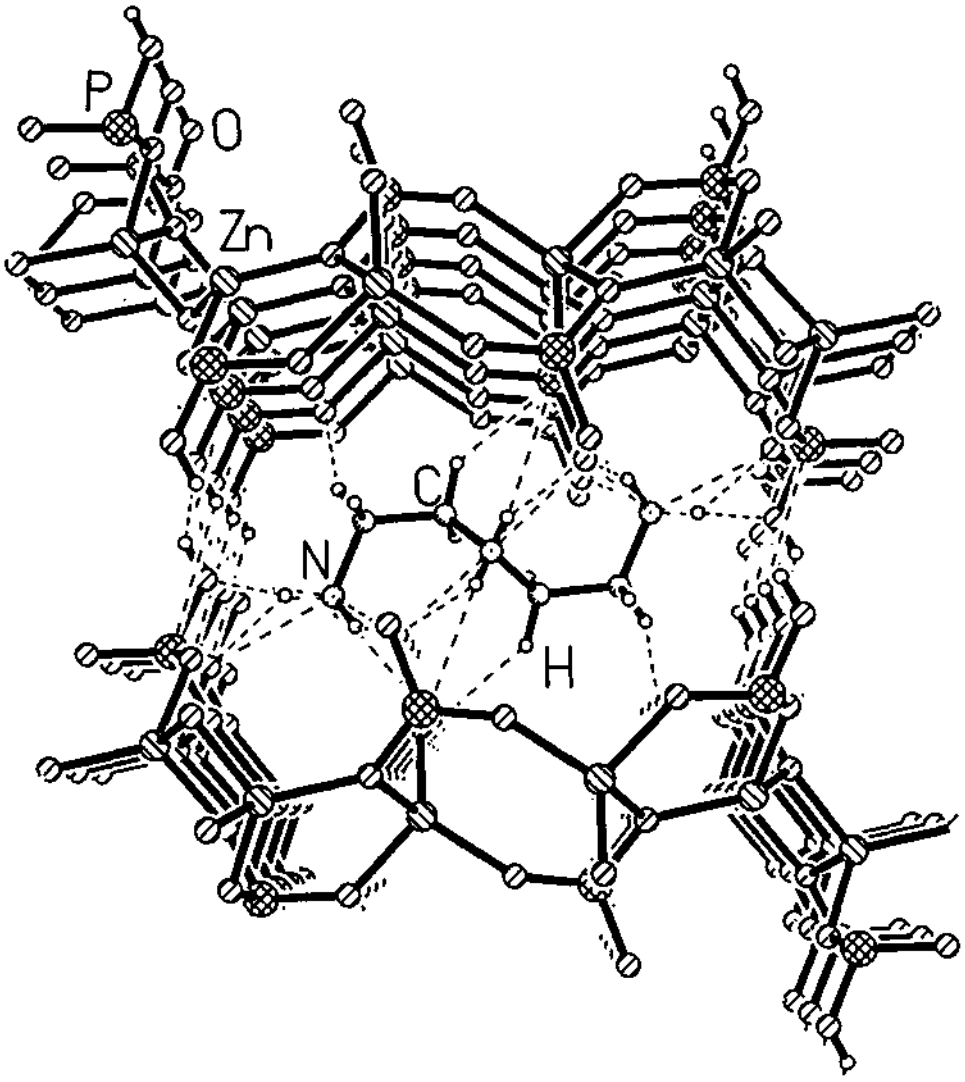

Fig. 1.32. (b) A single pseudo 10–membered channel in V. The amine molecules sit in the middle of the channel..

Table 1.29. Selected hydrogen bond interactions in **V**, $[NH_3(CH_2)_2NH(CH_2)_2NH_3]^{2+}$ $2[Zn_2PO_4(HPO_4)]^-$

Moiety	Distance, Å	Moiety	Angle (°)
O(7) – H(1)	2.246(1)	O(7) – H(1) – N(1)	157.03(9)
O(7) – H(2)	2.042(1)	O(7) – H(2) – N(1)	143.7(1)
O(8) – H(3)	2.131(1)	O(8) – H(3) – N(1)	141.7(1)
O(7) – H(8)	2.164(1)	O(7) – H(8) – N(2)	147.1(1)
O(8) – H(10)*	1.760(1)	O(8) – H(10) – O(8)*	146.2(1)
O(6) – H(4)	2.371(1)	O(6) – H(4) – C(1)	156.4(1)
O(5) – H(6)	2.530(1)	O(5) – H(6) – C(2)	139.4(1)

*interaction between two framework layers

Thermogravimetric analysis (TGA) carried out in static air indicates only one sharp mass loss in the region 240-260°C. The mass loss of 25% corresponds to the loss of amine from the structure (calc. 24.2%) and subsequent collapse of the framework. The decomposed sample was found to be poorly crystalline (powder XRD) and corresponds to a dense zinc phosphate indicating the loss of framework structure with the loss of the amine.

$[NH_3(CH_2)_2NH_2(CH_2)_2NH_3]^{3+}[Zn_4(PO_4)_3(HPO_4)]^{3-}$, VI : The asymmetric unit contains 32 non-hydrogen atoms and the atomic coordinates are given in Table 1.30. The structure is built from the networking of ZnO_4, PO_4 and HPO_4 tetrahedral units. The vertex linkage between these units creates an anionic framework of the formula $[Zn_4(PO_4)_3(HPO_4)]^{3-}$ and charge compensation is achieved by the protonated amine $[NH_3(CH_2)_2NH_2(CH_2)_2NH_3]^{3+}$. The structure has one water molecule in the channel formed by the networking of the various units.

The most interesting aspect of this zinc phosphate is that it crystallizes in a polar space group $P2_1$. The entire framework of **VI**, can be considered to be built from the networking of three-, four-, six- and eight-membered rings. The 3- and 4-membered rings are connected together, edge wise, forming one-dimensional helical columns along the *b* axis as shown in Fig. 1.33. The figure shows how these columns are interconnected via the HPO_4 group forming a 8-membered channel system along the *a* axis. This 8-membered channel along the *a*-axis is connected to another 8-membered channels along the *b* axis, forming a helical interconnected one-dimensional channel system. The amine and water molecules are situated in these channels. Fig. 1.34 shows the connectivity between the ZnO_4 and PO_4 moiety that creates the other 8-membered channel system along the *b* axis. Thus, **VI,** possesses an interpenetrating 8-membered channel system. There is strong hydrogen bonded interaction between the framework and the structure directing amine providing structural stability. The framework density for this material is 16.7, indicating a degree of openness

Table 1.30 Atomic coordinates [x 10^4] and equivalent isotropic displacement parameters [$Å^2$ x 10^3] for **VI**

Atom	x	y	z	U_{eq}
Zn(1)	16773(2)	5303(2)	14704(1)	13(1)
Zn(2)	13781(2)	5521(2)	15704(1)	13(1)
Zn(3)	9268(2)	3254(2)	11632(1)	12(1)
Zn(4)	13363(2)	4422(2)	12142(1)	14(1)
P(1)	6456(4)	3444(5)	12404(3)	12(1)
P(2)	15828(4)	2565(4)	16258(3)	11(1)
P(3)	10730(4)	5954(4)	10450(3)	12(1)
P(4)	11731(4)	3287(5)	13971(3)	12(1)
O(1)	17058(11)	4897(13)	13173(9)	22(2)
O(2)	18298(10)	6743(13)	15302(9)	19(2)
O(3)	16873(10)	3386(12)	15691(8)	15(2)
O(4)	15096(9)	1237(13)	15403(7)	15(2)
O(5)	6500(13)	1911(12)	13109(9)	29(3)
O(6)	14779(10)	3685(13)	16553(8)	21(2)
O(7)	12037(10)	4778(12)	14769(8)	17(2)
O(8)	7302(10)	3188(13)	11471(7)	16(2)
O(9)	10311(10)	3567(14)	13180(8)	22(2)
O(10)	10288(10)	6336(12)	9181(8)	16(2)
O(11)	9518(10)	5396(13)	10953(8)	17(2)
O(12)	12835(11)	3042(13)	13274(9)	23(2)
O(13)	5013(10)	3833(15)	11720(8)	27(3)
O(14)	16589(10)	1741(12)	17390(8)	16(2)
O(15)	11920(9)	4742(12)	10689(8)	15(2)
O(16)	11260(11)	7601(12)	11065(9)	19(2)
O(100)	17378(12)	5870(18)	18471(12)	48(4)
N(1)	-56(16)	2010(18)	6230(12)	36(4)
N(2)	2008(12)	3055(16)	8588(11)	19(3)
N(3)	5825(12)	3698(15)	9254(9)	17(3)
C(1)	196(16)	3588(22)	6788(13)	27(4)
C(2)	1699(15)	3800(21)	7395(12)	21(3)
C(3)	3491(15)	2651(19)	9024(13)	22(4)
C(4)	4342(16)	4169(19)	9057(12)	23(3)

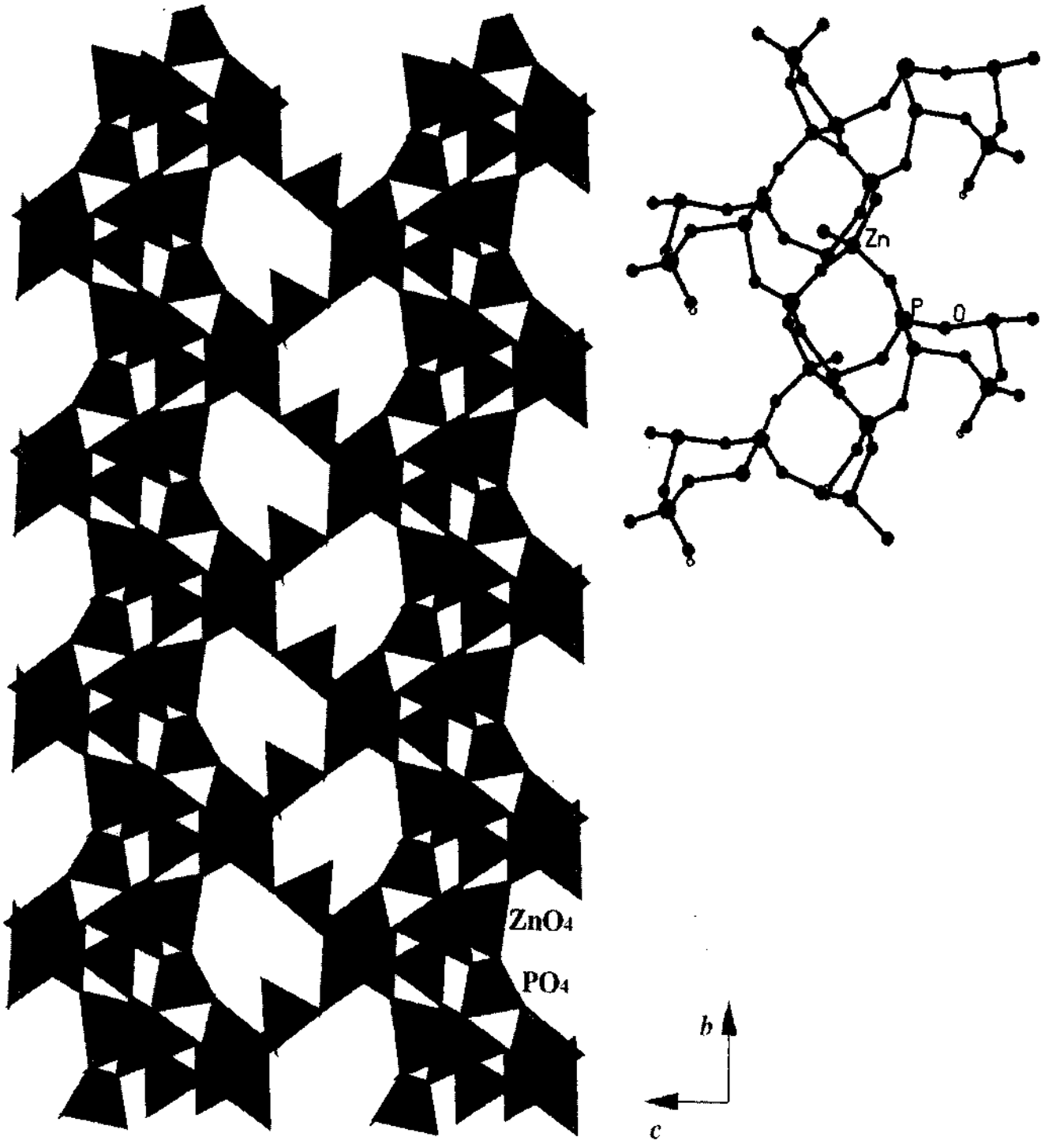

Fig. 1.33. Structure of **VI**, $[NH_3(CH_2)_2NH_2(CH_2)_2NH_3]^{3+}[Zn_4(PO_4)_3(HPO_4)]^{3-}H_2O$ showing the 8-membered cavities (channels) along *100* direction and the helical channels. Amine and water molecules are omitted for clarity. Inset shows the connectivity in the one-dimensional columns

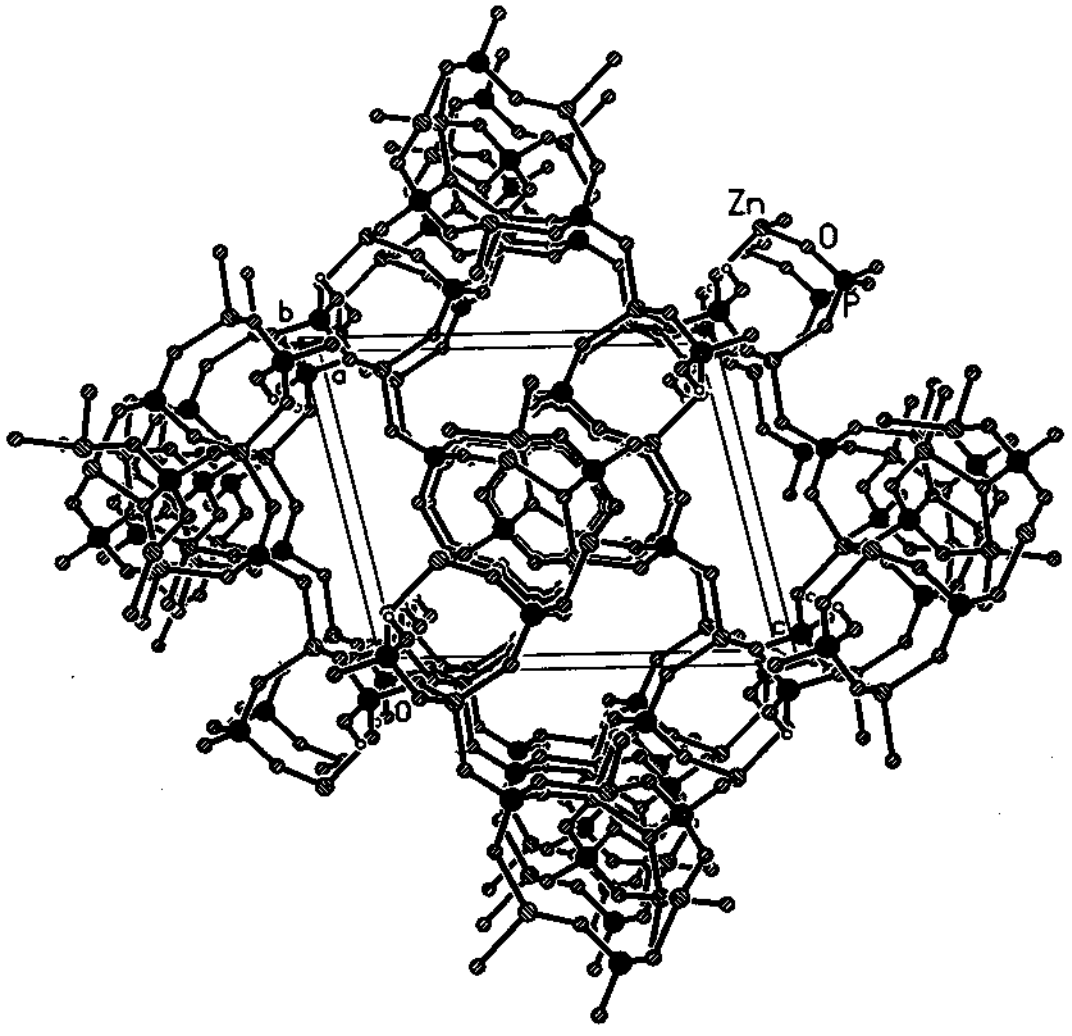

Fig. 1.34. (a) Structure of **VI** showing the 8–membered channel along the [010] direction. Amine and water molecules are not shown.

comparable to aluminophosphate molecular sieves such as AlPO-12[16] and AlPO-16.[16]

On the structural front, of the sixteen oxygens in the asymmetric unit, one makes a trigonal connection with two Zn atoms and one P atom forming a 3-membered ring and one is a terminal oxygen the rest of the oxygens form Zn – O – P linkage. The P – O bond distances are in the range 1.502 – 1.581Å (ave. 1.537Å) and the bond angles in the range 104.8 – 114.5° (ave. 109.5°), in agreement with those observed previously in such materials. The P – O distance of 1.581Å [P(3) – O(16)] is protonated leading to the formation of the HPO_4 unit. The Zn atoms are all connected with P through oxygens, with the Zn – O distances in the range 1.890 – 2.004Å (ave. 1.954Å). The O – Zn – O bond angles are in the range 94.5 – 120.6° (ave. 109.4°). The longest Zn – O distance, and the largest O – Zn – O angle, are found with oxygens involved in three-coordination (Table 1.31).

$[NH(CH_2)_2NH_2(CH_2)_2NH_3]^{2+}[Zn_5(PO_4)_4]^{2-}$, VII : The asymmetric unit contains 32 non-hydrogen atoms, of which 25 belong to the framework and 7 to the guest species (Fig. 1.35a). The atomic coordinates are presented in Table 1.32. The framework is built-up of a network of ZnO_4 and PO_4 tetrahedra resulting in a three-dimensional architecture. The framework has the formula, $[Zn_5(PO_4)_4]^{2-}$ and the charge neutrality is achieved by the presence of a diprotonated DETA molecule, $[N_3C_4H_{16}]^{2+}$. There is one amine molecule present per formula unit. The framework structure of **VII** has several unique features, the most important of which is the presence of the 4-membered Zn_4O_4 unit formed only by Zn tetrahedra [Zn(1) Zn(2), Zn(3) and Zn(4)] linked to each other (Fig. 1.35b). Each oxygen atom of the 4-membered Zn_4O_4 tetramer is 3-coordinated being connected to a PO_4 tetrahedron [P(1), P(2), P(3) and P(4)]. The phosphate units are further linked to $Zn(5)O_4$ tetrahedra forming the *basket-shaped* basic building unit as shown in Fig. 1.35c. The *basket-shaped* building units are connected to each other via oxygens, in an alternate up-down manner, to form the three-

Table 1.31 Selected bond distances (Å) and angles (°) for **VI**.

Moiety	Distance (Å)	Moiety	Angle (°)
Zn(1)-O(1)	1.930(10)	O(5)$^{\#2}$-Zn(2)-O(6)	103.6(4)
Zn(1)-O(2)	1.941(10)	O(7)-Zn(2)-O(6)	109.5(4)
Zn(1)-O(3)	1.961(10)	O(5)$^{\#2}$-Zn(2)-O(4)$^{\#1}$	120.6(5)
Zn(1)-O(4)$^{\#1}$	2.004(9)	O(7)-Zn(2)-O(4)$^{\#1}$	106.6(4)
Zn(2)-O(5)$^{\#2}$	1.890(10)	O(6)-Zn(2)-O(4)$^{\#1}$	105.6(4)
Zn(2)-O(7)	1.945(10)	O(9)-Zn(3)-O(8)	114.9(4)
Zn(2)-O(6)	1.968(10)	O(9)-Zn(3)-O(10)$^{\#3}$	116.5(4)
Zn(2)-O(4)$^{\#1}$	2.002(9)	O(8)-Zn(3)-O(10)$^{\#3}$	105.5(4)
Zn(3)-O(9)	1.911(9)	O(9)-Zn(3)-O(11)	100.1(4)
Zn(3)-O(8)	1.937(9)	O(8)-Zn(3)-O(11)	101.8(4)
Zn(3)-O(10)$^{\#3}$	1.961(10)	O(10)$^{\#3}$-Zn(3)-O(11)	117.5(4)
Zn(3)-O(11)	1.988(10)	O(13)$^{\#4}$-Zn(4)-O(12)	115.1(5)
Zn(4)-O(13)$^{\#4}$	1.897(10)	O(13)$^{\#4}$-Zn(4)-O(14)$^{\#1}$	110.7(5)
Zn(4)-O(12)	1.926(10)	O(12)-Zn(4)-O(14)$^{\#1}$	111.8(4)
Zn(4)-O(14)$^{\#1}$	1.997(10)	O(13)$^{\#4}$-Zn(4)-O(15)	108.1(4)
Zn(4)-O(15)	2.000(9)	O(12)-Zn(4)-O(15)	114.8(4)
P(1)-O(5)	1.515(11)	O(14)$^{\#1}$-Zn(4)-O(15)	94.5(4)
P(1)-O(13)	1.523(10)	O(5)-P(1)-O(13)	112.1(7)
P(1)-O(1)$^{\#5}$	1.548(11)	O(5)-P(1)-O(1)$^{\#5}$	111.6(6)
P(1)-O(8)	1.554(9)	O(13)-P(1)-O(1)$^{\#5}$	110.2(6)
P(2)-O(6)	1.502(11)	O(5)-P(1)-O(8)	109.0(6)
P(2)-O(3)	1.527(10)	O(13)-P(1)-O(8)	104.8(5)
P(2)-O(14)	1.545(10)	O(1)$^{\#5}$-P(1)-O(8)	108.8(6)
P(2)-O(4)	1.562(10)	O(6)-P(2)-O(3)	114.5(6)
P(3)-O(10)	1.503(10)	O(6)-P(2)-O(14)	107.7(6)
P(3)-O(15)	1.535(10)	O(3)-P(2)-O(14)	109.1(6)
P(3)-O(11)	1.541(10)	O(6)-P(2)-O(4)	109.6(6)
P(3)-O(16)	1.581(10)	O(3)-P(2)-O(4)	107.2(6)
P(4)-O(9)	1.534(10)	O(14)-P(2)-O(4)	108.6(6)
P(4)-O(12)	1.537(10)	O(10)-P(3)-O(15)	111.2(6)
P(4)-O(7)	1.543(10)	O(10)-P(3)-O(11)	111.8(6)
P(4)-O(2)$^{\#6}$	1.547(11)	O(15)-P(3)-O(11)	112.3(6)
		O(10)-P(3)-O(16)	105.8(6)
Moiety	Angle (°)	O(15)-P(3)-O(16)	108.3(5)
O(1)-Zn(1)-O(2)	100.2(4)	O(11)-P(3)-O(16)	107.0(6)
O(1)-Zn(1)-O(3)	114.9(4)	O(9)-P(4)-O(12)	111.9(6)
O(2)-Zn(1)-O(3)	110.5(4)	O(9)-P(4)-O(7)	106.3(6)
O(1)-Zn(1)-O(4)$^{\#1}$	110.1(4)	O(12)-P(4)-O(7)	111.6(6)
O(2)-Zn(1)-O(4)$^{\#1}$	115.7(4)	O(9)-P(4)-O(2)$^{\#6}$	109.5(6)
O(3)-Zn(1)-O(4)$^{\#1}$	105.7(4)	O(12)-P(4)-O(2)$^{\#6}$	107.3(6)
O(5)$^{\#2}$-Zn(2)-O(7)	110.5(5)	O(7)-P(4)-O(2)$^{\#6}$	110.3(5)

Organic

Moiety	Distance (Å)	Moiety	Angle (°)
N(1)-C(1)	1.46(2)	C(3)-N(2)-C(2)	113.0(11)
N(2)-C(3)	1.50(2)	N(1)-C(1)-C(2)	112(2)
N(2)-C(2)	1.51(2)	N(2)-C(2)-C(1)	111.4(12)
N(3)-C(4)	1.50(2)	N(2)-C(3)-C(4)	109.4(13)
C(1)-C(2)	1.53(2)	N(3)-C(4)-C(3)	108.6(12)
C(3)-C(4)	1.51(2)		

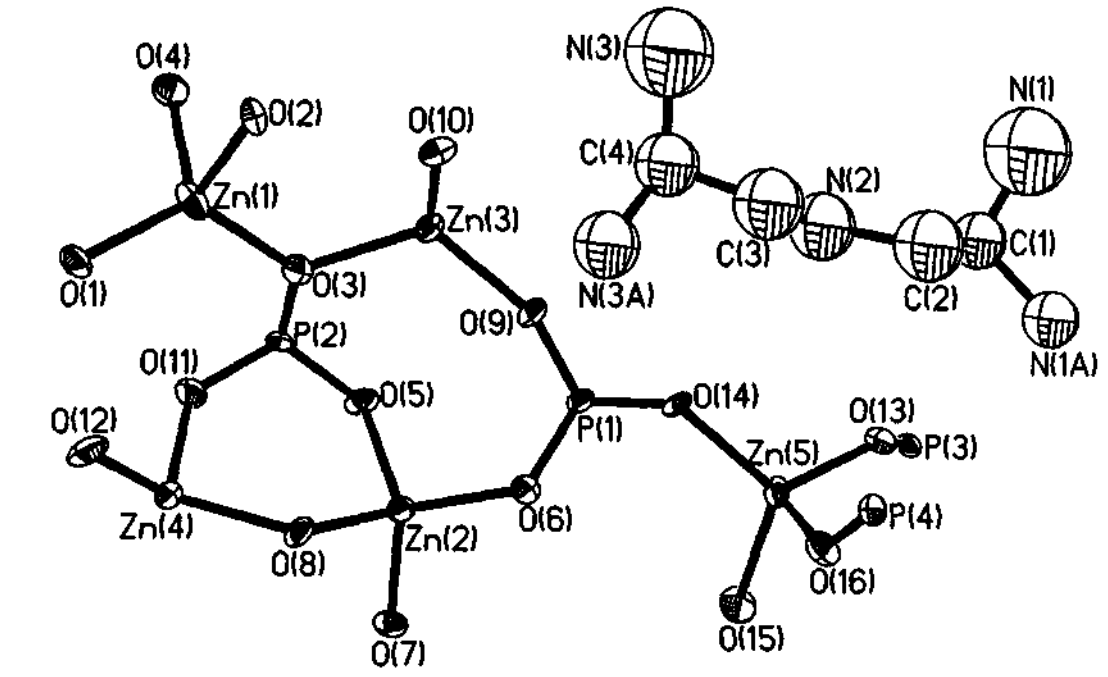

(a)

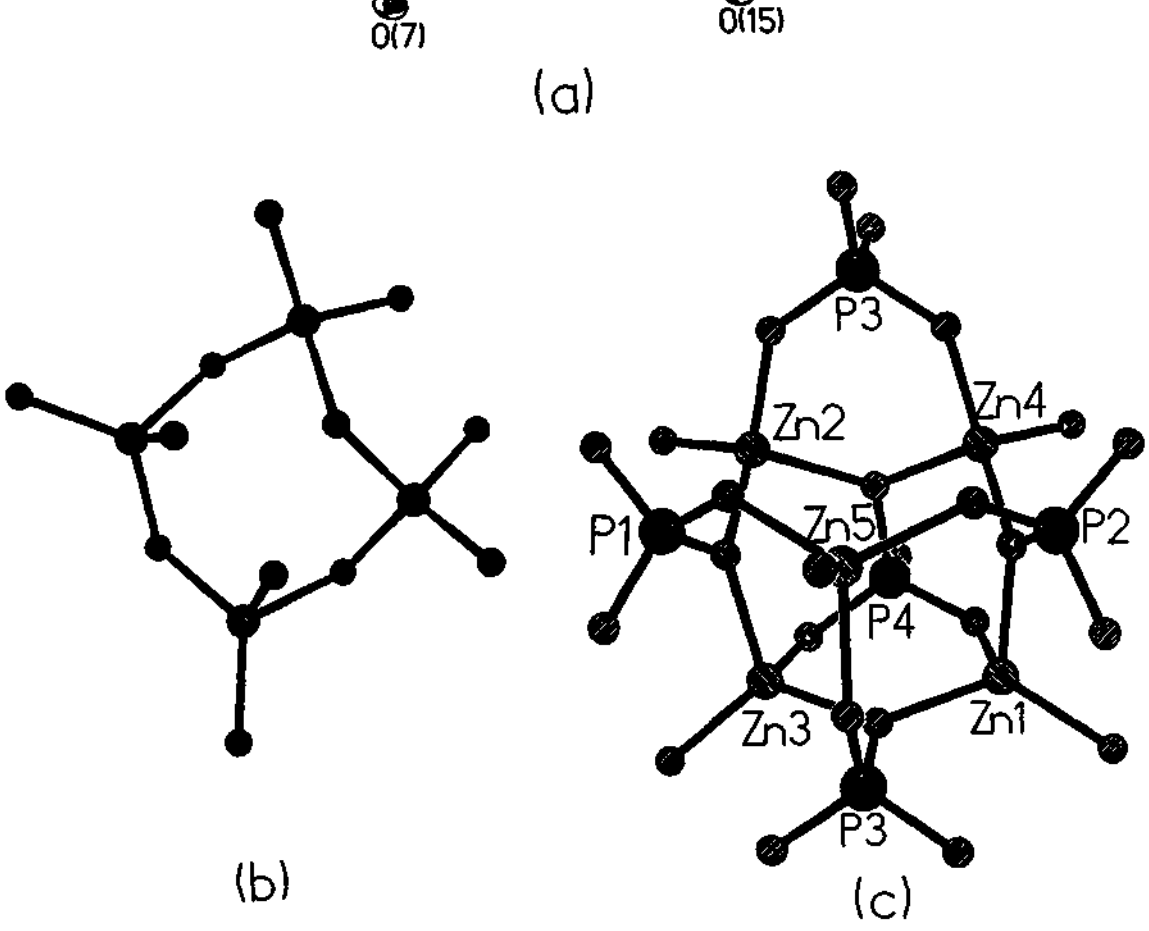

(b) (c)

Fig. 1.35. (a) ORTEP Plot of **VII**, $[N_3C_4H_{16}][Zn_5(PO_4)_4]$. Thermal ellipsoids are given at 50% probability. (b) The Zn_4O_4 tetramer. Note the 4-membered ring formation. (c) The basic building unit. Note that the connectivity between the Zn_4O_4 tetramer and the PO_4 units form a *basket-like* arrangement.

Table 1.32. Atomic coordinates [x 10^4] and equivalent isotropic displacement parameters [$Å^2$ x 10^3] for **VII**.

Atom	x	y	z	U_{eq}
Zn(1)	13824(1)	5695(2)	-5009(1)	23(1)
Zn(2)	12715(1)	233(2)	-3468(1)	17(1)
Zn(3)	12551(1)	5741(2)	-3728(1)	20(1)
Zn(4)	14019(1)	140(2)	-4683(1)	19(1)
Zn(5)	9592(1)	1474(2)	-2885(1)	17(1)
P(1)	11370(2)	2766(3)	-3100(2)	15(1)
P(2)	14166(2)	3187(3)	-3337(2)	18(1)
P(3)	9339(2)	2508(3)	-1107(2)	15(1)
P(4)	7811(2)	1677(3)	-4683(2)	14(1)
O(1)	14106(5)	4366(9)	-5877(4)	26(2)
O(2)	12811(4)	7281(9)	-5671(4)	18(2)
O(3)	13571(5)	4659(9)	-3989(5)	28(2)
O(4)	14637(4)	7778(9)	-4400(4)	24(2)
O(5)	13568(4)	2152(9)	-2964(4)	21(2)
O(6)	11560(4)	964(9)	-3463(4)	24(2)
O(7)	13082(4)	-2180(9)	-2919(4)	20(2)
O(8)	12778(4)	-190(9)	-4663(4)	19(2)
O(9)	11650(4)	4385(9)	-3511(4)	23(2)
O(10)	11805(4)	7102(9)	-4777(4)	21(2)
O(11)	14592(4)	1998(9)	-3837(5)	27(2)
O(12)	13834(5)	995(9)	-5856(4)	26(2)
O(13)	9110(4)	2636(8)	-2105(4)	18(2)
O(14)	10363(4)	2952(8)	-3282(4)	18(2)
O(15)	10087(5)	-898(9)	-2422(5)	31(2)
O(16)	8564(4)	736(9)	-3942(4)	21(2)
N(1)	8004(23)	8554(29)	-2257(24)	166(16)
N(1A)	7608(14)	5401(32)	-2327(18)	67(10)
C(1)	8236(9)	6728(20)	-2512(8)	63(4)
C(2)	8211(8)	6460(26)	-3445(9)	94(6)
N(2)	9148(8)	6600(20)	-3451(8)	87(4)
C(3)	9120(9)	6821(25)	-4382(8)	92(6)
C(4)	10044(9)	7354(20)	-4355(11)	78(5)
N(3)	9995(24)	9328(23)	-4576(23)	148(14)
N(3A)	10173(20)	5765(30)	-4870(19)	78(12)

dimensional architecture of **VII**, with channels along the *b* axis (7.7 X 6.4 Å; shortest atom-atom contact distances not including van der Waals radii) (Fig. 1.36). The amine molecules are present within these channels.

The Zn – O bond distances in the ZnO_4 tetrahedra in **VII** are in the range 1.889 – 2.019 Å (av. 1.955 Å) and the P – O distances in the range 1.512-1.573Å (av. 1.531Å) (Table 1.33). The O – Zn – O angles are in the range 93.3 – 126.2° (av. 109.11°) and the O – P – O angles are in the range 107.2 –113.6° (av. 109.46°) (Table 1.34). These geometric parameters are typical of that observed in open-framework zinc phosphates. The terminal nitrogen atoms of the amine molecule are disordered with a site occupancy of 0.5.

In Fig. 1.37 we compare the various structural motifs encountered in open-framework zinc phosphates with the Zn_4O_4 clusters found in the present study. Short, infinite Zn – O – Zn linear chains have been reported in a few Zn phosphates. Tetrahedral OZn_4 building units are found in framework phosphates and arsenates[85,251] and this feature has been observed recently in zinc-1,4-benzenedicarboxylate.[98] The Zn_4O_4 tetramer obtained in this study, however, is unique, manifesting itself in the form of a 4-membered ring structure. This ring structure is not unlike the 4-membered $M_2P_2O_4$ ring commonly observed in open-framework phosphates, and considered to be the basic building unit of these materials. The formation of the 4-membered Zn_4O_4 clusters in **I**, is a result of the presence of three-coordinated oxygens. The formation of such M – O clusters with transition elements might create a situation wherein it would be possible to synthesize materials possessing magnetic channel.

4.2 Three-dimensional open-framework zinc phosphates with organic amines acting as ligands

$[NH(CH_2)_2NH_2(CH_2)_2NH_3]^{2+}[Zn_5(PO_4)_4]^{2-}$, VIII : The asymmetric unit of **VIII** is shown in Fig. 1.38a and the atomic coordinates are listed in Table 1.35.

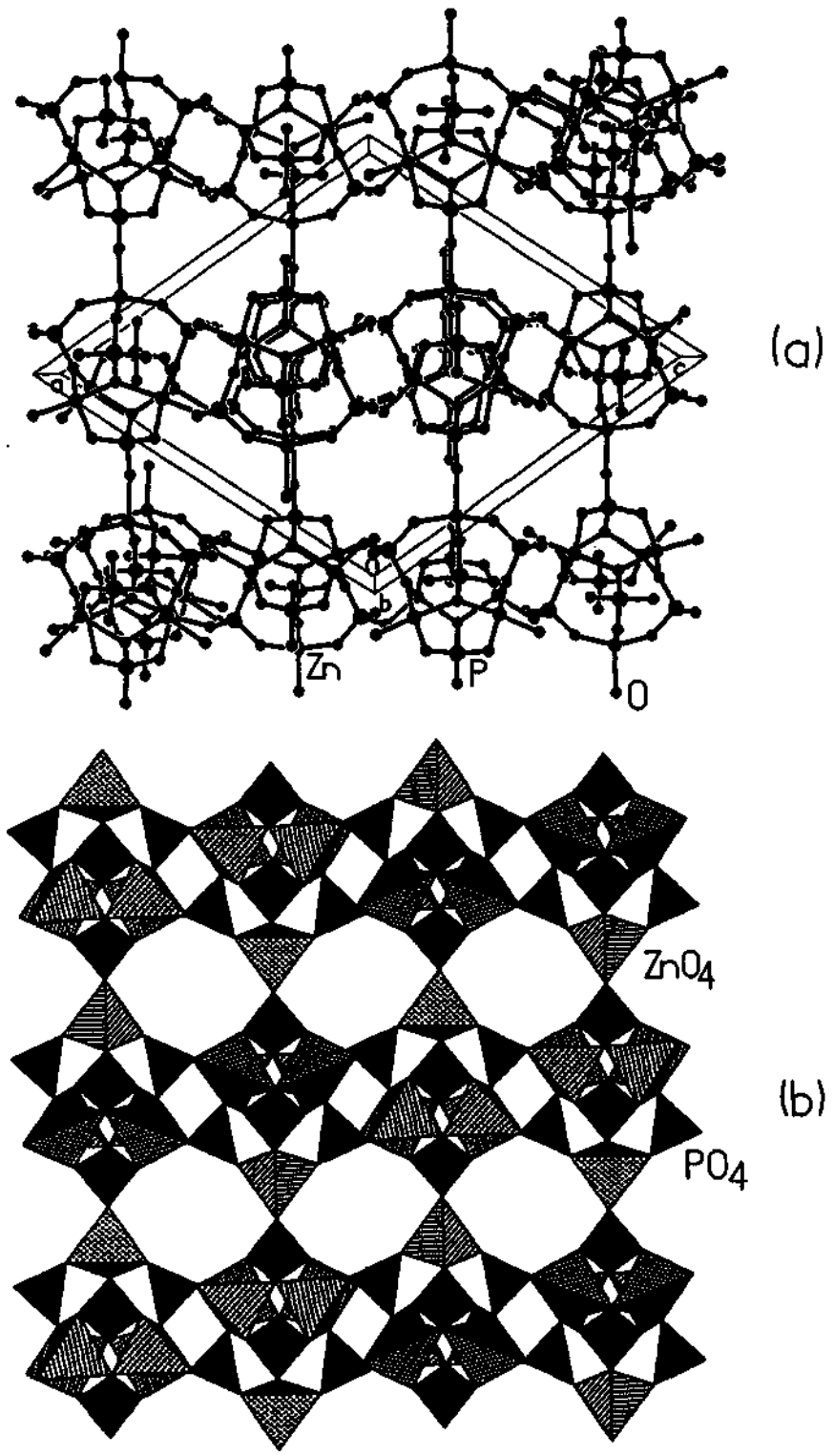

Fig. 1.36. Structure of **VII**, $[N_3C_4H_{16}][Zn_5(PO_4)_4]$, along the *ac* plane showing the channels (a) ball and stick view (b) polyhedral view. Amine molecules are not shown for clarity.

Table 1.33. Bond Lengths [Å] for **VII**.

Moiety	Distance (Å)	Moiety	Distance (Å)
Zn(1)-O(1)	1.902(6)	Zn(5)-O(15)	1.957(7)
Zn(1)-O(2)	1.960(6)	Zn(5)-O(16)	1.957(6)
Zn(1)-O(3)	1.995(7)	P(1)-O(9)	1.517(7)
Zn(1)-O(4)	2.019(7)	P(1)-O(14)	1.526(7)
Zn(2)-O(6)	1.921(7)	P(1)-O(6)	1.533(7)
Zn(2)-O(5)	1.925(6)	P(1)-O(7)#3	1.555(7)
Zn(2)-O(7)	1.985(7)	P(2)-O(5)	1.514(7)
Zn(2)-O(8)	2.001(6)	P(2)-O(15)#3	1.516(7)
Zn(3)-O(9)	1.889(6)	P(2)-O(11)	1.518(7)
Zn(3)-O(10)	1.953(6)	P(2)-O(3)	1.568(7)
Zn(3)-O(7)#1	1.994(6)	P(3)-O(12)#4	1.512(7)
Zn(3)-O(3)	1.995(7)	P(3)-O(1)#4	1.518(7)
Zn(4)-O(11)	1.916(7)	P(3)-O(13)	1.524(7)
Zn(4)-O(12)	1.920(7)	P(3)-O(4)#5	1.541(7)
Zn(4)-O(4)#2	1.975(7)	P(4)-O(16)	1.514(7)
Zn(4)-O(8)	2.005(7)	P(4)-O(2)#6	1.527(7)
Zn(5)-O(13)	1.912(6)	P(4)-O(10)#6	1.534(7)
Zn(5)-O(14)	1.926(6)	P(4)-O(8)#7	1.573(6)

Organic			
Moiety	Distance (Å)	Moiety	Distance (Å)
N(1)-C(1)	1.4998(11)	N(2)-C(3)	1.5002(11)
N(1)-N(1A)#9	1.67(3)	C(3)-C(4)	1.5100(11)
N(1A)-C(1)	1.5098(11)	C(4)-N(3)	1.4999(11)
N(1A)-N(1)#10	1.67(3)	C(4)-N(3A)	1.5002(11)
C(1)-C(2)	1.5101(11)	N(3)-N(3)#11	1.70(5)
C(2)-N(2)	1.5003(11)	N(3A)-N(3A)#6	1.26(4)

Symmetry transformations used to generate equivalent atoms:

#1 x, y+1, z #2 x, y-1, z #3 –x+5/2, y+1/2, -z-1/2 #4 x-1/2, -y+1/2, z+1/2
#5 –x+5/2, y-1/2, -z-1/2 #6 –x+2, -y+1, -z-1 #7 –x+2, -y, -z-1
#8 x+1/2, -y+1/2, z-1/2 #9 –x+3/2, y+1/2, -z-1/2 #10 –x+3/2, y-1/2, -z-1/2
#-x+2, -y+2, -z-1

Table 1.34. Selected bond angles [°] for **VII**.

Moiety	Angle (°)	Moiety	Angle (°)
O(1)-Zn(1)-O(2)	106.2(3)	O(13)-Zn(5)-O(16)	107.0(3)
O(1)-Zn(1)-O(3)	126.2(3)	O(14)-Zn(5)-O(16)	107.3(3)
O(2)-Zn(1)-O(3)	107.7(3)	O(15)-Zn(5)-O(16)	99.9(3)
O(1)-Zn(1)-O(4)	118.1(3)	O(9)-P(1)-O(14)	107.7(4)
O(2)-Zn(1)-O(4)	93.3(3)	O(9)-P(1)-O(6)	112.8(4)
O(3)-Zn(1)-O(4)	100.4(3)	O(14)-P(1)-O(6)	110.4(4)
O(6)-Zn(2)-O(5)	108.4(3)	O(9)-P(1)-O(7)#3	107.8(4)
O(6)-Zn(2)-O(7)	112.0(3)	O(14)-P(1)-O(7)#3	109.6(4)
O(5)-Zn(2)-O(7)	115.5(3)	O(6)-P(1)-O(7)#3	108.5(4)
O(6)-Zn(2)-O(8)	116.2(3)	O(5)-P(2)-O(15)#3	108.8(4)
O(5)-Zn(2)-O(8)	104.2(3)	O(5)-P(2)-O(11)	113.2(4)
O(7)-Zn(2)-O(8)	100.4(3)	O(15)#3-P(2)-O(11)	108.7(4)
O(9)-Zn(3)-O(10)	100.3(3)	O(5)-P(2)-O(3)	108.0(4)
O(9)-Zn(3)-O(7)#1	117.0(3)	O(15)#3-P(2)-O(3)	109.4(4)
O(10)-Zn(3)-O(7)#1	98.4(3)	O(11)-P(2)-O(3)	108.8(4)
O(9)-Zn(3)-O(3)	124.2(3)	O(12)#4-P(3)-O(1)#4	113.6(4)
O(10)-Zn(3)-O(3)	107.5(3)	O(12)#4-P(3)-O(13)	107.4(4)
O(7)#1-Zn(3)-O(3)	105.7(3)	O(1)#4-P(3)-O(13)	109.5(4)
O(11)-Zn(4)-O(12)	109.2(3)	O(12)#4-P(3)-O(4)#5	109.0(4)
O(11)-Zn(4)-O(4)#2	114.0(3)	O(1)#4-P(3)-O(4)#5	107.2(4)
O(12)-Zn(4)-O(4)#2	113.7(3)	O(13)-P(3)-O(4)#5	110.2(4)
O(11)-Zn(4)-O(8)	106.6(3)	O(16)-P(4)-O(2)#6	111.6(4)
O(12)-Zn(4)-O(8)	105.5(3)	O(16)-P(4)-O(10)#6	110.9(4)
O(4)#2-Zn(4)-O(8)	107.3(3)	O(2)#6-P(4)-O(10)#6	111.7(4)
O(13)-Zn(5)-O(14)	115.4(3)	O(16)-P(4)-O(8)#7	108.0(4)
O(13)-Zn(5)-O(15)	110.8(3)	O(2)#6-P(4)-O(8)#7	107.4(4)
O(14)-Zn(5)-O(15)	115.0(3)	O(10)#6-P(4)-O(8)#7	107.0(4)

Organic

Moiety	Angle (°)	Moiety	Angle (°)
C(1)-N(1)-N(1A)#9	143(3)	N(2)-C(3)-C(4)	109.6(11)
C(1)-N(1A)-N(1)#10	142(2)	N(3)-C(4)-N(3A)	130(2)
N(1)-C(1)-N(1A)	106(2)	N(3)-C(4)-C(3)	107(2)
N(1)-C(1)-C(2)	118(2)	N(3A)-C(4)-C(3)	96(2)
N(1A)-C(1)-C(2)	110(2)	C(4)-N(3)-N(3)#11	138(3)
N(2)-C(2)-C(1)	110.1(11)	N(3A)#6-N(3A)-C(4)	139(4)
C(3)-N(2)-C(2)	110.9(10)	N(1A)-C(1)-C(2)	110(2)

Symmetry transformations used to generate equivalent atoms:

#1 x, y+1, z #2 x, y-1, z #3 –x+5/2, y+1/2, -z-1/2 #4 x-1/2, -y+1/2, z+1/2
#5 –x+5/2, y-1/2, -z-1/2 #6 –x+2, -y+1, -z-1 #7 –x+2, -y, -z-1
#8 x+1/2, -y+1/2, z-1/2 #9 –x+3/2, y+1/2, -z-1/2 #10 –x+3/2, y-1/2, -z-1/2
#-x+2, -y+2, -z-1

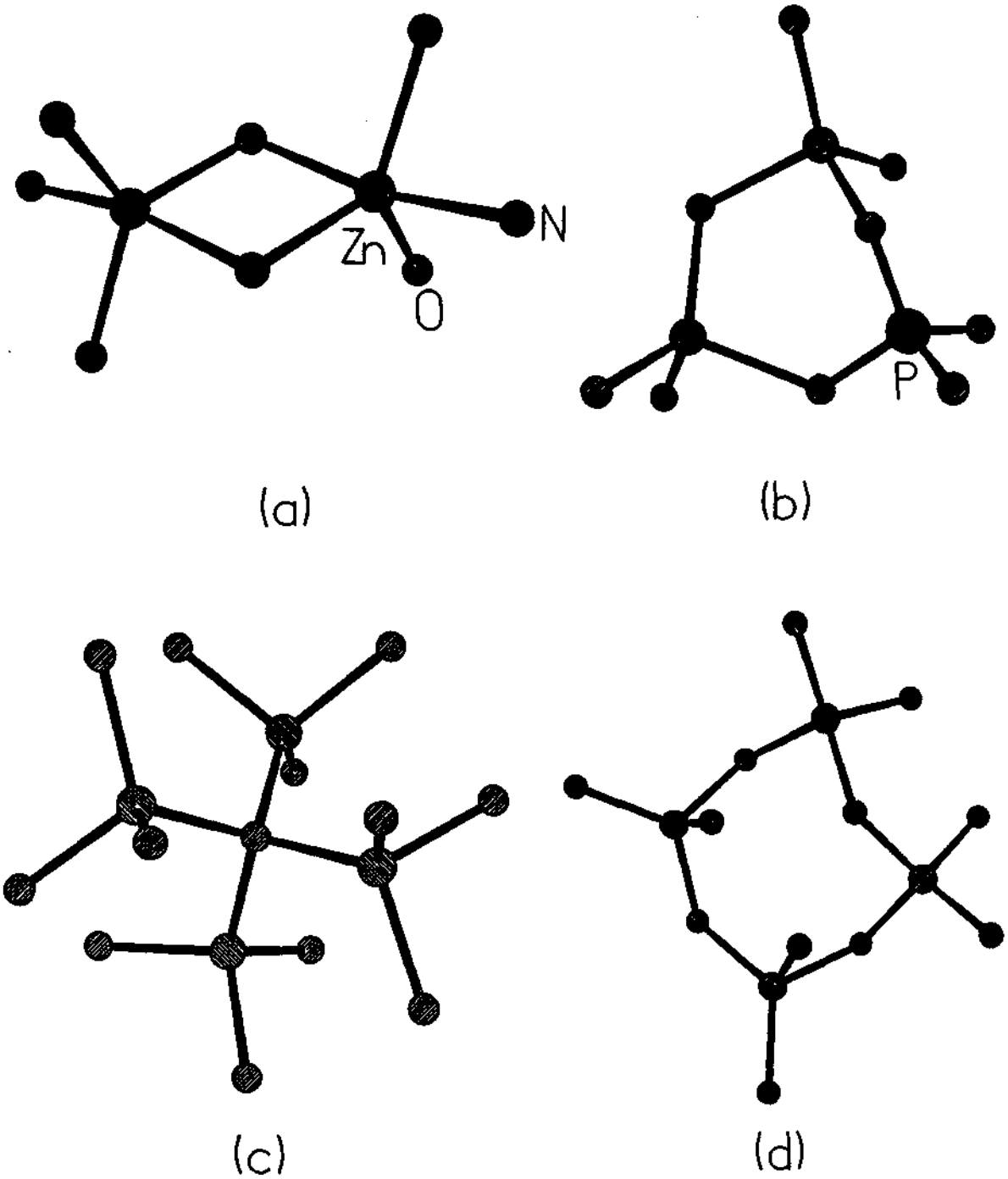

Fig. 1.37. Structural units observed in open-framework zinc phosphates: (a) The Zn_2O_2 dimer, (b) Zn_2PO_3 trimer, (c) OZn_4 tetrahedral clusters and (d) The 4-membered Zn_4O_4 tetramer cluster.

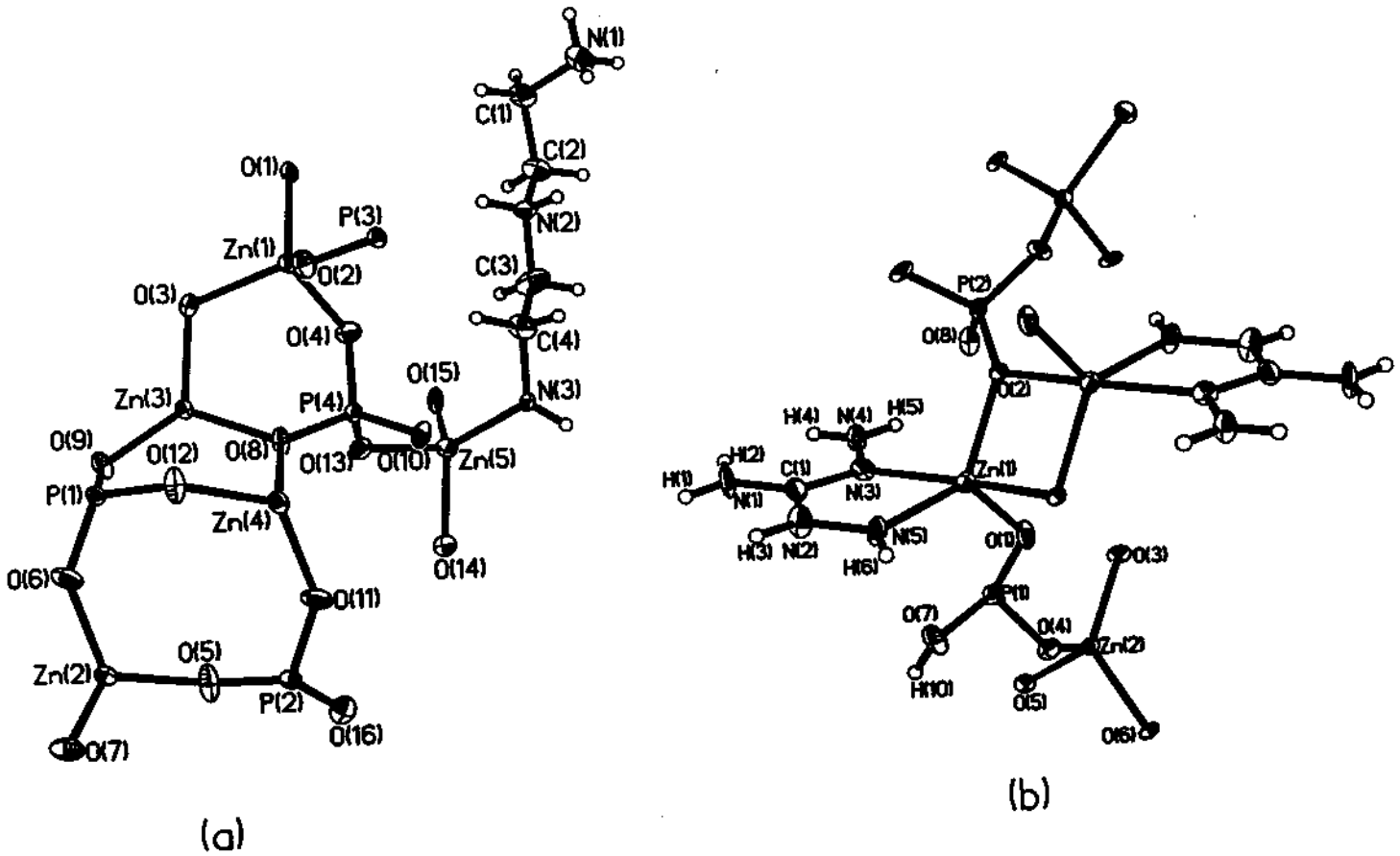

Fig. 1.38. (a) Asymmetric unit of **VIII**, $[NH(CH_2)_2NH_2(CH_2)_2NH_3]$ $[Zn_5(PO_4)_4]$. (b) Asymmetric unit of **IX**, $[CN_5H_6]$ $[Zn_2(PO_4)(HPO_4)]$. Thermal ellipsoids are shown at 50% probability.

Table 1.35. Atomic coordinates [x 10^4] and equivalent isotropic displacement parameters [$Å^2$ x 10^3] for **VIII**.

Atom	x	y	z	U_{eq}
Zn(1)	-4099(1)	-13149(3)	-8699(1)	12(1)
Zn(2)	-7827(1)	-17957(3)	-12742(1)	14(1)
Zn(3)	-5355(1)	-17189(2)	-9744(1)	12(1)
Zn(4)	-6324(1)	-12283(2)	-11069(1)	14(1)
Zn(5)	-5233(1)	-11260(3)	-7023(1)	14(1)
P(1)	-6397(2)	-17481(6)	-12055(3)	11(1)
P(2)	-7726(2)	-12772(6)	-11649(3)	12(1)
P(3)	-4239(2)	-8102(6)	-9751(3)	11(1)
P(4)	-5251(2)	-12159(6)	-8740(3)	11(1)
O(1)	-3178(4)	-13757(16)	-7645(6)	15(2)
O(2)	-4378(4)	-10947(16)	-9766(6)	19(2)
O(3)	-4482(4)	-16596(16)	-9275(7)	18(2)
O(4)	-4529(5)	-12316(17)	-8199(7)	20(2)
O(5)	-7780(5)	-15624(17)	-11857(7)	27(2)
O(6)	-7094(4)	-18388(20)	-12684(7)	25(2)
O(7)	-8519(4)	-17477(17)	-14131(8)	22(2)
O(8)	-5630(4)	-13743(16)	-9721(6)	15(2)
O(9)	-5997(4)	-18841(16)	-11041(6)	17(2)
O(10)	-5500(4)	-9351(15)	-9025(6)	17(2)
O(11)	-7054(4)	-11758(19)	-11142(8)	25(2)
O(12)	-6317(4)	-14596(17)	-11890(7)	24(2)
O(13)	-5416(4)	-13171(16)	-8131(7)	18(2)
O(14)	-6123(4)	-11644(17)	-7542(7)	16(2)
O(15)	-4601(5)	-12920(15)	-5784(7)	18(2)
O(16)	-7892(5)	-12227(16)	-10991(8)	22(2)
N(2)	-3078(6)	-7651(21)	-5521(9)	20(3)
N(1)	-1675(5)	-5528(23)	-4335(8)	26(3)
N(3)	-4874(5)	-7723(19)	-6878(9)	15(3)
C(2)	-2512(7)	-8033(26)	-4483(11)	22(3)
C(1)	-1892(6)	-8107(26)	-4327(11)	25(3)
C(3)	-3674(7)	-7845(31)	-5671(12)	31(4)
C(4)	-4250(8)	-7430(29)	-6711(12)	25(4)

The structure of **VIII** consists of a network of ZnO_4, PO_4 and ZnO_3N moieties, connected by Zn – O – P bonds. The framework has the formula $[Zn_5(PO_4)_4]^{2-}$ and charge neutrality is achieved by the incorporation of the doubly protonated amine molecule. The Zn atoms are all tetrahedrally coordinated and connected to P atoms via oxygen links and to each other via three-coordinated oxygen atoms (bonding two Zn atoms and one P atom). Four oxygens out of the 16 oxygen atoms in the asymmetric unit are three-coordinated. This is an unusually large percentage (25%) of such units in an open-framework material.

The Zn atoms in **VIII** make three Zn – O – P bonds with four P neighbours, with a spread of Zn – O – P angles of (ave. 127.3°) as given in Table 1.36 and Table 1.37. The fourth connection needed for a tetrahedral linkage in the case of Zn(1) to Zn(4) are obtained through Zn – O – Zn linkages (ave. 115.7°), and via the terminal N atom of the amine in the case of Zn(5). Thus, there are infinite one-dimensional Zn – O – Zn chains in this structure. The average values of Zn – O bond lengths d_{av}[Zn(1) – O = 1.947Å]; d_{av}[Zn(2) – O = 1.956Å]; d_{av}[Zn(3) – O = 1.957Å]; d_{av}[Zn(4) – O = 1.958Å]; d_{av}[Zn(5) – O = 1.968Å] and O – Zn – O bond angles [O – Zn(1) – O = 109.1°; O – Zn(2) – O = 109.1°; O – Zn(3) – O = 109.4°; O – Zn(4) – O = 108.1°; O – Zn(5) – O = 109.4°] indicate that the environment around the Zn atoms is tetrahedral and the values are in good agreement with those reported earlier.[79-95,252] The four distinct phosphorus atoms are linked to Zn atoms via the oxygens. The P – O bond lengths are in the range 1.517 – 1.582Å and the O – P – O bond angles are in the range 104.8 – 113.9°. The longest P – O distances, however, involve the three-coordinated oxygen atom. These values agree well with those reported in the literature.

The polyhedral connectivity between the ZnO_4 and PO_4 units leads to the formation of infinite Zn – O – Zn chains and 3-membered rings via the three-coordinated oxygen atoms. The structure also possesses 4-membered $Zn_2P_2O_4$ units. It should be noted that 4-membered rings appear to be the basic building blocks of many of the open-framework structures such as aluminophosphates and

Table 1.36. Selected bond lengths [Å] for **VIII**, $[NH(CH_2)_2NH_2(CH_2)_2NH_3]^{2+}[Zn_5(PO_4)_4]^{2-}$.

Moiety	Distance, Å	Moiety	Distance, Å
Zn(1) – O(1)	1.950(8)	Zn(5) – O(15)	1.922(9)
Zn(1) – O(2)	1.919(9)	Zn(5) – N(3)	2.022(10)
Zn(1) – O(3)	1.997(8)	P(1) – O(6)	1.518(9)
Zn(1) – O(4)	1.922(9)	P(1) – O(12)	1.522(9)
Zn(2) – O(1)$^{\#1}$	2.021(8)	P(1) – O(14)$^{\#4}$	1.536(9)
Zn(2) – O(5)	1.938(9)	P(1) – O(9)	1.561(9)
Zn(2) – O(6)	1.931(9)	P(2) – O(11)	1.510(10)
Zn(2) – O(7)	1.934(10)	P(2) – O(5)	1.518(9)
Zn(3) – O(3)	1.953(8)	P(2) – O(16)	1.535(10)
Zn(3) – O(8)	1.956(8)	P(2) – O(1)$^{\#5}$	1.580(9)
Zn(3) – O(9)	1.986(8)	P(3) – O(15)$^{\#6}$	1.525(10)
Zn(3) – O(10)$^{\#2}$	1.933(8)	P(3) – O(7)$^{\#7}$	1.526(10)
Zn(4) – O(8)	2.020(9)	P(3) – O(2)	1.527(8)
Zn(4) – O(9)$^{\#3}$	1.987(8)	P(3) – O(3)$^{\#3}$	1.582(9)
Zn(4) – O(11)	1.913(9)	P(4) – O(13)	1.517(10)
Zn(4) – O(12)	1.911(9)	P(4) – O(4)	1.521(10)
Zn(5) – O(13)	1.977(9)	P(4) – O(10)	1.554(8)
Zn(5) – O(14)	1.952(9)	P(4) – O(8)	1.580(9)

Table 1.37 Selected bond angles (°) for **VIII**, $[NH(CH_2)_2NH_2(CH_2)_2NH_3]^{2+}[Zn_5(PO_4)_4]^{2-}$

Moiety	Angle (°)	Moiety	Angle(°)
O(2) – Zn(1) – O(4)	111.3(4)	O(15) – Zn(5) – N(3)	105.5(4)
O(2) – Zn(1) – O(1)	119.7(3)	O(14) – Zn(5) – N(3)	119.8(4)
O(4) – Zn(1) – O(1)	111.5(4)	O(13) – Zn(5) – N(3)	112.1(4)
O(2) – Zn(1) – O(3)	106.6(4)	O(6) – P(1) – O(12)	113.9(5)
O(4) – Zn(1) – O(3)	100.1(4)	O(6) – P(1) – O(14)$^{\#4}$	108.1(5)
O(1) – Zn(1) – O(3)	105.4(3)	O(12) – P(1) – O(14)$^{\#4}$	110.2(5)
O(6) – Zn(2) – O(7)	101.0(4)	O(6) – P(1) – O(9)	108.5(5)
O(6) – Zn(2) – O(5)	120.5(4)	O(12) – P(1) – O(9)	108.6(5)
O(7) – Zn(2) – O(5)	118.0(4)	O(14) – P(1) – O(9)	107.5(5)
O(6) – Zn(2) – O(1)$^{\#1}$	114.9(4)	O(11) – P(2) – O(5)	112.2(5)
O(7) – Zn(2) – O(1)$^{\#1}$	95.9(3)	O(11) – P(2) – O(16)	108.1(6)
O(5) – Zn(2) – O(1)$^{\#1}$	104.3(4)	O(5) – P(2) – O(16)	109.9(5)
O(10)$^{\#2}$ – Zn(3) – O(3)	121.0(4)	O(11) – P(2) – O(1)$^{\#5}$	104.8(5)
O(10)$^{\#2}$ – Zn(3) – O(8)	106.1(3)	O(5) – P(2) – O(1)$^{\#5}$	109.6(5)
O(3) – Zn(3) – O(8)	102.5(4)	O(16) – P(2) – O(1)$^{\#5}$	112.2(5)
O(10)$^{\#2}$ – Zn(3) – O(9)	97.2(3)	O(15)$^{\#6}$ – P(3) – O(7)$^{\#7}$	109.3(6)
O(3) – Zn(3) – O(9)	118.2(4)	O(15)$^{\#6}$ – P(3) – O(2)	111.1(5)
O(8) – Zn(3) – O(9)	111.5(4)	O(7)$^{\#7}$ – P(3) – O(2)	112.9(5)
O(12) – Zn(4) – O(11)	124.1(4)	O(15)$^{\#6}$ – P(3) – O(3)$^{\#3}$	108.4(5)
O(12) – Zn(4) – O(9)$^{\#3}$	111.4(4)	O(7)$^{\#7}$ – P(3) – O(3)$^{\#3}$	106.9(5)
O(11) – Zn(4) – O(9)$^{\#3}$	107.2(4)	O(2) – P(3) – O(3)$^{\#3}$	108.0(5)
O(12) – Zn(4) – O(8)	102.6(4)	O(13) – P(4) – O(4)	112.2(6)
O(11) – Zn(4) – O(8)	104.9(4)	O(13) – P(4) – O(10)	107.3(5)
O(9)$^{\#3}$ – Zn(4) – O(8)	104.8(3)	O(4) – P(4) – O(10)	111.4(5)
O(15) – Zn(5) – O(14)	114.0(4)	O(13) – P(4) – O(8)	109.7(5)
O(15) – Zn(5) – O(13)	113.0(4)	O(4) – P(4) – O(8)	108.9(5)
O(14) – Zn(5) – O(13)	92.2(4)	O(10) – P(4) – O(8)	107.1(5)

Organic Moiety

Moiety	Distance, Å	Moiety	Angle (°)
N(2) – C(3)	1.46(2)	C(3) – N(2) – C(2)	110.3(12)
N(2) – C(2)	1.47(2)	C(4) – N(3) – Zn(5)	119.8(8)
N(1) – C(1)	1.47(2)	N(2) – C(2) – C(1)	111.2(12)
N(3) – C(4)	1.52(2)	N(1) – C(1) – C(2)	112.2(11)
C(2) – C(1)	1.51(2)	N(2) –C(3) – C(4)	111.2(13)
C(3) – C(4)	1.48(2)	C(3) – C(4) – N(3)	111.5(12)

Symmetry transformations used to generate equivalent atoms:

#1 x-1/2, -y-7/2, z-1/2	#2 x, y-1, z	#3 x, y+1, z	#4 x, -y-3, z-1/2
#5 x-1/2, -y-5/2, z-1/2	#6 x, -y-2, z-1/2	#7 x+1/2, -y-5/2, z+1/2	
#8 x+1/2, -y-7/2, z+1/2	#9 x, -y-3, z+1/2	#10 x, -y-2, z+1/2	

phosphates.[235] The 3- and 4-membered rings, in **VIII** share the edges forming a one-dimensional chain (Fig.1.39). The individual ribbons (columns of one-dimensional chains) are joined together by ZnO_3N tetrahedra giving rise to a 10-membered channel system along the *a*-axis. Such a linkage between one-dimensional chains by the ZnO_3N moiety requires the amine molecule to be in the middle of the 10-membered channel (10.36 x 4.62 Å; oxygen to oxygen contact distance excluding the van der Waals radii).

$[CN_5H_6]^+[Zn_2(PO_4)(HPO_4)]^-$, IX : Fig. 1.38b represents the asymmetric unit. The atomic coordinates are listed in Table 1.38. The structure is built-up from the vertex-linkage of PO_4, ZnO_4 and ZnO_3N_2 moieties. The framework is anionic and has the formula $[Zn_2(PO_4)(HPO_4]^-$. Charge neutrality is achieved by the incorporation of the protonated amine molecule, with one protonated 1,3-diaminoguanidine, $[CN_5H_6]^+$, per framework formula unit. From the eight oxygens in the asymmetric unit, one is three-coordinated.

There are two crystallographically distinct Zn as well as P atoms. Of the two Zn atoms in the asymmetric unit, [Zn(1)] is bound with two nitrogens and three oxygens forming a distorted trigonal bipyramidal ZnO_3N_2 unit, while [Zn(2)] is tetrahedrally coordinated to four oxygens. The observation of the distorted trigonal bipyramidal environment for the Zn atom is unusual and only few examples have been known for such coordination of the Zn atom, for example in $Zn(acac)_2$.[253] The average Zn – O bond distances d_{av}[Zn(1) – O/N = 2.062Å]; d_{av}[Zn(2) – O = 1.952Å] and O – Zn – O bond angles [O – Zn(1) – O/N = 106.8; O – Zn(2) – O = 109.0°] are consistent with the coordination environment of the Zn atoms (Table 1.39). Both P(1) and P(2) are connected by three oxygens to Zn atoms and the last neighbor is a terminal oxygen [(P(1) – O(7) and P(2) – O(8)]. The average bond distances involving P atoms [P(1) – O = 1.538Å; P(2) – O = 1.536Å] and bond angles [O – P – O = 109.5°] suggest a regular P tetrahedron, unlike in the case of Zn. Bond valence sum calculations[244] indicate that the oxygen O(7) is protonated and O(8) has a double - bond

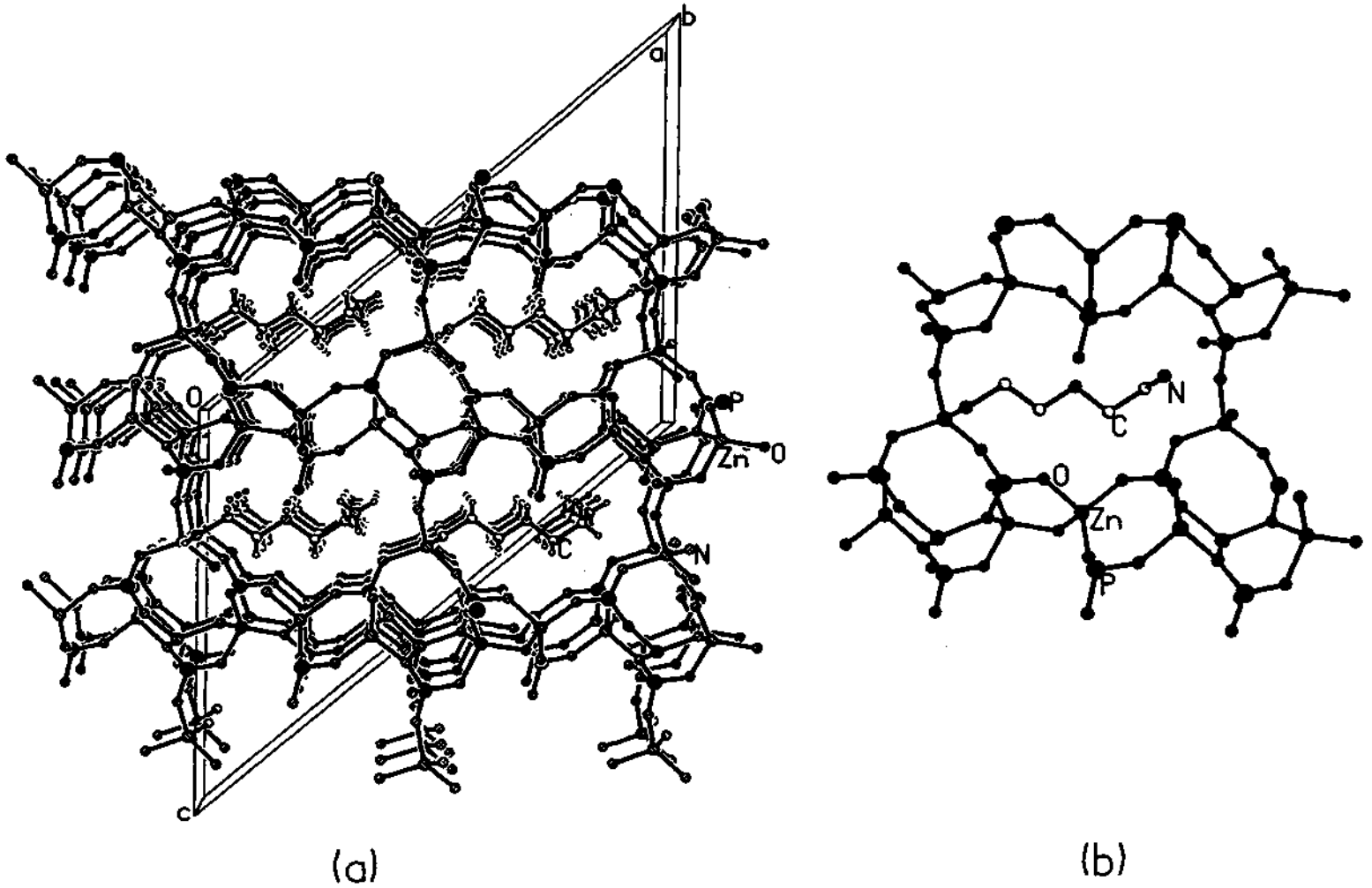

Fig. 1.39. (a) Structure off **VIII**, $[NH(CH_2)_2NH_2(CH_2)_2NH_3]$ $[Zn_5(PO_4)_4]$, showing the one–dimensional 10–membered channel system along the a–axis. (b) Figure showing the connectivity between the chain units and ZnO3N unit leading to the formation of the 10–membered ring.

Table 1.38 Atomic coordinates [x 10^4] and equivalent isotropic displacement parameters [$Å^2$ x 10^3] for **IX.**

Atom	x	y	z	U_{eq}
Zn(1)	1254(1)	5960(1)	238(1)	14(1)
Zn(2)	-2261(1)	9910(1)	455(1)	12(1)
P(1)	512(2)	8208(1)	749(2)	12(1)
P(2)	107(2)	5066(1)	-2828(2)	11(1)
O(1)	-254(6)	7147(4)	279(5)	19(1)
O(2)	183(6)	4967(3)	-1289(5)	12(1)
O(3)	-3542(6)	9461(4)	-1354(5)	17(1)
O(4)	-710(6)	8816(4)	1416(5)	16(1)
O(5)	-888(6)	11167(4)	423(5)	15(1)
O(6)	-3243(6)	10426(4)	1925(5)	15(1)
O(7)	2185(6)	8010(4)	1939(5)	21(1)
O(8)	-6(6)	6217(4)	-3247(5)	17(1)
N(1)	6108(8)	6837(5)	-315(7)	27(2)
N(2)	5021(8)	5947(5)	1254(6)	25(2)
N(3)	3125(7)	6670(4)	-582(6)	14(1)
N(4)	2846(7)	7260(5)	-1831(6)	18(1)
N(5)	3601(7)	5599(5)	1680(6)	21(2)
C(1)	4745(9)	6519(6)	78(7)	17(2)

Table 1.39. Select bond lengths (Å) and angles (^{0}) for **IX**, $[CN_5H_6]^+[Zn_2(PO_4)(HPO_4)]^-$

Moiety	Distance, (Å)	Moiety	Distance, (Å)
Zn(1) – O(1)	1.954(5)	P(1) – O(1)	1.514(5)
Zn(1) – O(2)	2.004(4)	P(1) – O(5)$^{\#2}$	1.521(5)
Zn(1) – N(3)	2.110(6)	P(1) – O(4)	1.543(5)
Zn(1) – N(5)	2.115(6)	P(1) – O(7)	1.573(5)
Zn(1) – O(2)$^{\#1}$	2.126(4)	P(2) – O(3)$^{\#3}$	1.526(5)
Zn(2) – O(3)	1.929(5)	P(2) – O(8)	1.526(5)
Zn(2) – O(4)	1.955(5)	P(2) – O(2)	1.539(5)
Zn(2) – O(5)	1.957(5)	P(2) – O(6)$^{\#4}$	1.553(5)
Zn(2) – O(6)	1.968(5)		
Moiety	**Angle (°)**	**Moiety**	**Angle (°)**
O(1) – Zn(1) – O(2)	111.2(2)	O(4) – Zn(2) – O(6)	101.6(2)
O(1) – Zn(1) – N(3)	101.0(2)	O(5) – Zn(2) – O(6)	94.6(2)
O(2) – Zn(1) – N(3)	100.5(2)	O(1) – P(1) – O(5)$^{\#2}$	112.1(3)
O(1) – Zn(1) – N(5)	127.4(2)	O(1) – P(1) – O(4)	109.3(3)
O(2) – Zn(1) – N(5)	121.1(2)	O(5)$^{\#2}$ – P(1) – O(4)	110.9(3)
N(3) – Zn(1) – N(5)	75.9(2)	O(1) – P(1) – O(7)	107.1(3)
O(1) – Zn(1) – O(2)$^{\#1}$	89.7(2)	O(5)$^{\#2}$ – P(1) – O(7)	111.6(3)
O(2) – Zn(1) – O(2)$^{\#1}$	81.2(2)	O(4) – P(1) – O(7)	105.7(3)
N(3) – Zn(1) – O(2)$^{\#1}$	167.6(2)	O(3)$^{\#3}$ – P(2) – O(8)	110.9(3)
N(5) – Zn(1) – O(2)$^{\#1}$	92.7(2)	O(3)$^{\#3}$ – P(2) – O(2)	108.0(3)
O(3) – Zn(2) – O(4)	111.7(2)	O(8) – P(2) – O(2)	109.9(3)
O(3) – Zn(2) – O(5)	113.2(2)	O(3)$^{\#3}$ – P(2) – O(6)	109.5(3)
O(4) – Zn(2) – O(5)	107.5(2)	O(8) – P(2) – O(6)$^{\#4}$	109.7(3)
O(3) – Zn(2) – O(6)	125.9(2)	O(2) – P(2) – O(6)$^{\#4}$	108.7(3)

Organic Moiety

Moiety	Distance, (Å)	Moiety	Angle, (^{0})
N(1) – C(1)	1.330(9)	C(1) – N(2) – N(5)	118.6(6)
N(2) – C(1)	1.359(9)	C(1) – N(3) – N(4)	115.1(6)
N(2) – N(5)	1.401(8)	C(1) – N(3) – Zn(1)	117.4(5)
N(3) – C(1)	1.318(9)	N(4) – N(3) – Zn(1)	127.3(4)
N(3) – N(4)	1.432(8)	N(2) – N(5) – Zn(1)	112.4(4)
		N(3) – C(1) – N(1)	126.7(7)
		N(3) – C(1) – N(2)	105.5(6)
		N(1) – C(1) – N(2)	117.7(6)

Symmetry transformations used to generate equivalent atoms :

#1 -x , -y +1, -z #2 -x, -y+2 , -z #3 -x-1/2, y-1/2, -z-1/2
#4 x+1/2, -y+3/2, z-1/2 #5 -x-1/2, y+1/2, -z-1/2 #6 x-1/2, -y+3/2, z+1/2

character. As usual, the longest P – O [P(1) – O(7) = 1.573Å] distance is the P – O ...H one.

The polyhedral connectivity between the ZnO_4, ZnO_3N_2 and PO_4 leads to the formation of the observed three-dimensional structure. Linking of two ZnO_3N_2 units results in the formation of a 2-membered Zn_2O_2 ring (Fig. 1.38b), N atoms being part of the amine molecule. The two membered ring is connected to P atoms via the Zn – O – P links. The formation of a 2-membered ring in an open-framework solid is not common and to our knowledge, there is only one such report in the literature.[254] The ZnO_4 and PO_4 units form two interconnected 4-membered rings (Fig. 1.40b) which are three-dimensionally connected through the ZnO_3N_2 units involving the 2-membered Zn – O – Zn linkage. The linkages between these building blocks lead to the formation of two 8-membered channels running along the [100] (7.67 x 5.64Å) and [101] (7.30 x 5.81Å) direction (Fig. 1.40). The amine molecule protrudes from the Zn centers into the channels along the *101* direction.

Two zinc phosphates, $[NH(CH_2)_2NH_2(CH_2)_2NH_3]^{2+}[Zn_5(PO_4)_4]^{2-}$ **VIII**, and $[CN_5H_6]^{+}[Zn_2(PO_4)(HPO_4)]^{-}$ **IX**, have been synthesized by hydrothermal methods in the presence of structure-directing agents. As with kinetically controlled processes, there is no relation between the starting stoichiometry and the final composition of the product. Compound **VIII** has been prepared in the presence of HCl and it appears that the role of Cl^- is similar to that of F^- ions in some of the phosphate-based open-framework materials reported in the literature.[28,234] The structures of **VIII** and **IX** are both built up from the regular ZnO_4, PO_4, the unusual ZnO_3N tetrahedra and the distorted trigonal bipyramidal ZnO_3N_2 leading to the three-dimensional connectivity. We may recall that most of the known zinc phosphates contain ZnO_4 and PO_4 tetrahedra only, although distinct differences exist between the structures.

The two structures, described here, are unusual in that they form Zn – O – Zn linkages although the Zn/P ratio is 1 in **IX** and 1.25 in **VIII**. The presence of

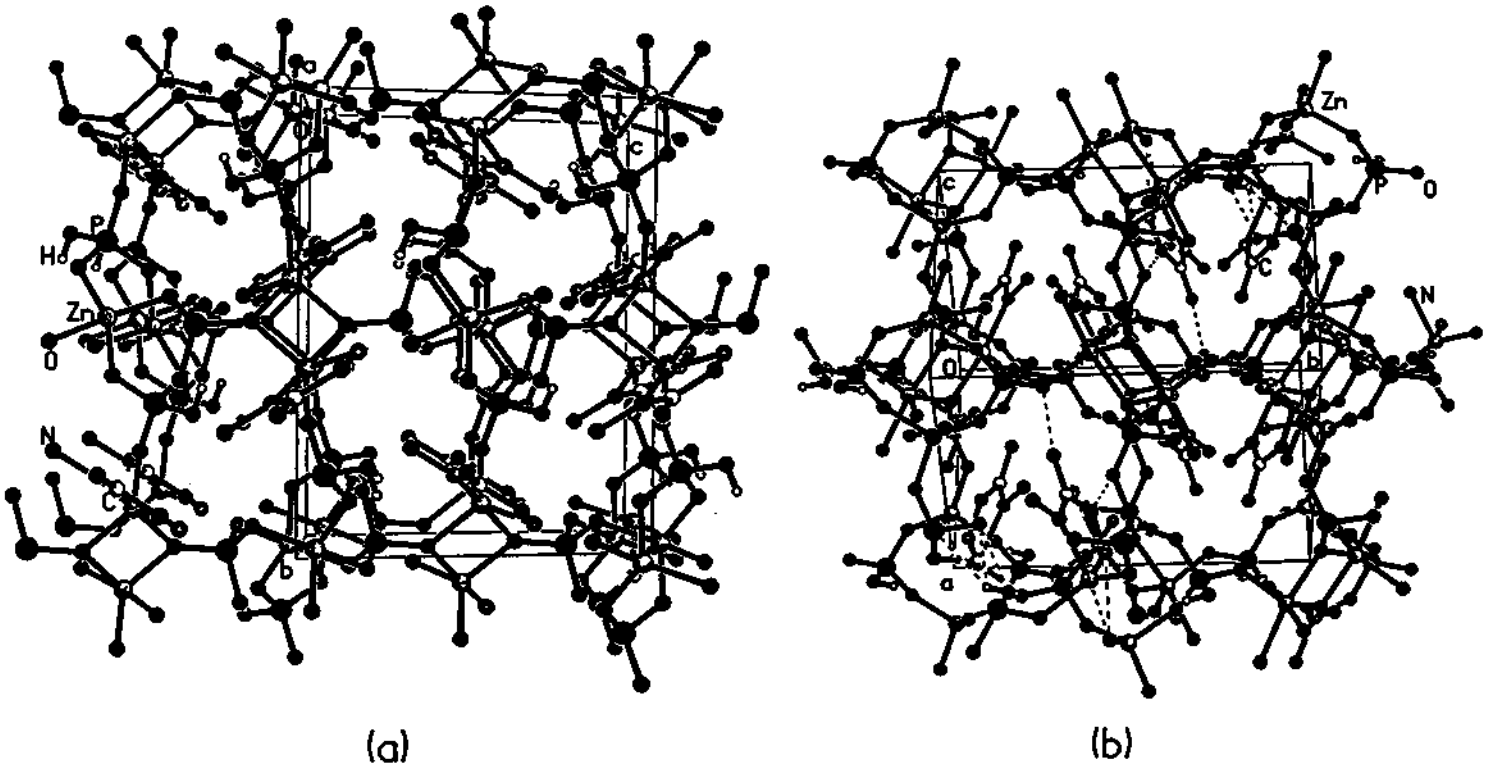

Fig. 1.40. Structure of **IX**, $[CN_5H_6]$ $[Zn_2(PO_4)(HPO_4)]$, showing the 8–membered channels (a) along [100] axis and (b) along [101] direction. Note that the amine molecules protrude into the channels along the [101] direction. Hydrogens of the amine molecules are not shwon for clarity.

more Zn than P in **VIII**, may be responsible for the infinite one-dimensional – Zn – O – Zn – linkages. In **IX**, these linkages may be attributed to the presence of the rare trigonal bipyramidal coordination of the Zn atom. No P – O – P type linkages are seen in both the materials. The – Zn – O – Zn – linkages is always accompanied by the three-coordinated bridging oxygen atoms and the third coordination is to a Phosphorus. The trigonal coordination of the oxygen in the – Zn – O – Zn – bridge is apparently an electrostatic valence requirement of bridging oxygen atoms as mentioned earlier. The trigonal and tetrahedral coordinations of oxygen bridges are generally common when divalent tetrahedral atoms are involved and we would therefore expect such a feature in the zinc phosphates to yield novel open-framework topologies, which have no analogues in aluminosilicates and aluminophosphates.

Another interesting aspect of the Zn phosphates examined here relates to the protonation of the framework oxygen atoms. In **IX**, only one oxygen atom is protonated in spite of the fact that the Zn:P = 1, and no oxygens is protonated in **VIII**. This may be due to the presence of Zn – N linkages present in these materials. In the zinc phosphates reported in the literature, some of the oxygen atoms are invariably protonated to compensate the charge imbalance. It is also hypothesized that the oxygens are protonated due to the difficulty in packing enough bulky organic cations into the extra framework pores to achieve charge balance.[94] In the case of the aluminosilicate materials, the Si : Al ratio is variable (for the same framework topology) and affects the charge-balancing requirement, the zinc phosphates appear to have a precisely defined Zn:P ratio for a particular topology. In compounds **VIII** and **IX**, the nitrogen atoms of the amine molecule covalently binding with Zn centers possibly create a situation where the bulky organic cation can be accommodated within the pores/channels and achieve charge balance. This type of observation is unique as in many of the channel structures the structure-directing organic amine molecules sits in channels and cavities and interact with the framework through hydrogen bonds only.

In the present materials, the framework densities are 18.6 for **VIII** and 16.0 for **IX**. These values are in the middle range FD values observed in aluminosilicate zeolites[16] where the presence of channels is common. Furthermore, the position of the amine is such that the linear chain diethylenetriamine (compound **VIII**) forms a well-defined 10-membered channel system. In **IX**, however, the presence of the distorted trigonal pyramidal ZnO_3N_2 unit links with another ZnO_3N_2 unit forming two – Zn – O – Zn – linkages (2-membered rings) which connect the double 4-membered rings creating distortion of the 8-membered channels.

Thermogravimetric analysis (TGA) of **VIII** and **IX** was carried out in air from room temperature to 600°C. The results show only one mass loss for **VIII** in the region 350-440°C. The mass loss of 16.5% corresponds to the loss of the amine molecule from the structure (calc. 13%) and some adsorbed water. In the case of **IX**, the mass loss of 22.6% occurring in the temperature range 350-450°C corresponds to the loss of the amine molecule (calc. 21.5%). In both the cases the loss of the amine molecule resulted in the collapse of the framework structure leading to the formation of largely amorphous weakly diffracting materials (XRD) that corresponds to dense zinc phosphate phases consistent with their structures.

In addition to the coordination of the amine with the metal atoms in the framework, both the structures show dominant hydrogen bond interaction between the amine and the framework (Table 1.40). In **VIII**, since the amine has a linear chain, hydrogen bonding is prominent. The strongest hydrogen bonding in **VIII** is between the hydrogens attached to the nitrogen N(1) and N(2) and the framework oxygens. The following hydrogen bond parameters reveal these: O(10)...H(3) = 1.986Å and O(10)...H(3) – N(1) = 175.8°; O(16)...H(9) = 1.930Å and O(16)...H(9) – N(2) = 172.9°. Here, O(16) is one of the terminal double bonded oxygen atoms attached to P. There is only one strong hydrogen bond in **IX** as given by, O(6)...H(3) = 1.991Å and O(6)...H(3) – N(2) = 170.6°.

Table 1.40. Important hydrogen bond interactions in **VIII** and **IX**.

Compound VIII			
Moiety	Distance (Å)	Moiety	Angle (°)
O(11) - H(1)	2.235(1)	O(11) - H(1) - N(1)	136.5(1)
O(16) - H(1)	2.185(1)	O(16) - H(1) - N(1)	154.9(1)
O(14) - H(2)	1.925(1)	O(14) - H(2) - N(1)	156.0(1)
O(10) - H(3)	1.968(1)	O(10) - H(3) - N(1)	175.8(1)
O(5) - H(8)	2.362(1)	O(5) - H(8) - N(2)	140.7(1)
O(16) - H(9)	1.930(1)	O(16) - H(9) - N(2)	172.9(1)
O(4) - H(12)	2.467(1)	O(4) - H(12) - C(4)	161.9(1)
Compound IX			
O(1) - H(1)	2.176(1)	O(1) - H(1) - N(1)	137.7(1)
O(7) - H(2)	2.447(1)	O(7) - H(2) - N(1)	133.5(1)
O(6) - H(3)	1.991(1)	O(6) - H(3) - N(2)	170.6(1)

Compared to other open-framework zinc phosphates, **VIII** and **IX** are novel also because of the three-dimensional connectivity arising from the linkage between the ZnO_4, ZnO_3N, PO_4 tetrahedra and distorted trigonal bipyramidal ZnO_3N_2. In the work of Halasyamani et al[252] where similar bonding of the amine with the Zn centers is reported, the linkages between the ZnO_3N and PO_3F tetrahedra lead to the formation of layers. Covalent bonding between the nitrogen of the amine and the Zn atoms and the position of the amine molecule in the organic-inorganic hybrid structure described by these workers are reminiscent of pillared materials.

4.3. An open-framework zinc chlorophosphate, $[C_6NH_{14}][ZnCl(HPO_4)]$, X :

The asymmetric unit of $[C_6NH_{14}][ZnCl(HPO_4)]$ consists of 14 non-hydrogen atoms (Fig 1.41). There is only one crystallographically independent zinc and phosphorus atom in the asymmetric unit (Table 1.41). Both the zinc and phosphorus atoms are tetrahedrally coordinated with respect to the nearest atom neighbors but there exit only three Zn – O – P bonds. The remaining connection needed for the tetrahedral linkage comes from a terminal bonding with the zinc having a chlorine (Zn(1) – Cl(1) = 2.220 Å) and phosphorus with an oxygen atom (P(1) – O(4) = 1.579 Å), which is formally a –OH group. Bond valence sum calculations[244] also agree with the above formalism. The Zn – O and P – O bond distances as well as the O – Zn – O and O – P – O angles are all as expected for this type of bonding (Table 1.42).

The framework structure of $[C_6NH_{14}][ZnCl(HPO_4)]$ consists of alternating inorganic and organic layers. The macroanionic inorganic layers are built up from a network of ZnO_3Cl and $PO_3(OH)$ tetrahedra sharing vertices. Each inorganic layer consists of strictly alternating Zn and P tetrahedra forming 4- and 8-membered apertures within the layer as shown in Fig. 1.42. The chlorine atoms are so arranged as to project in a direction perpendicular to the layer. This

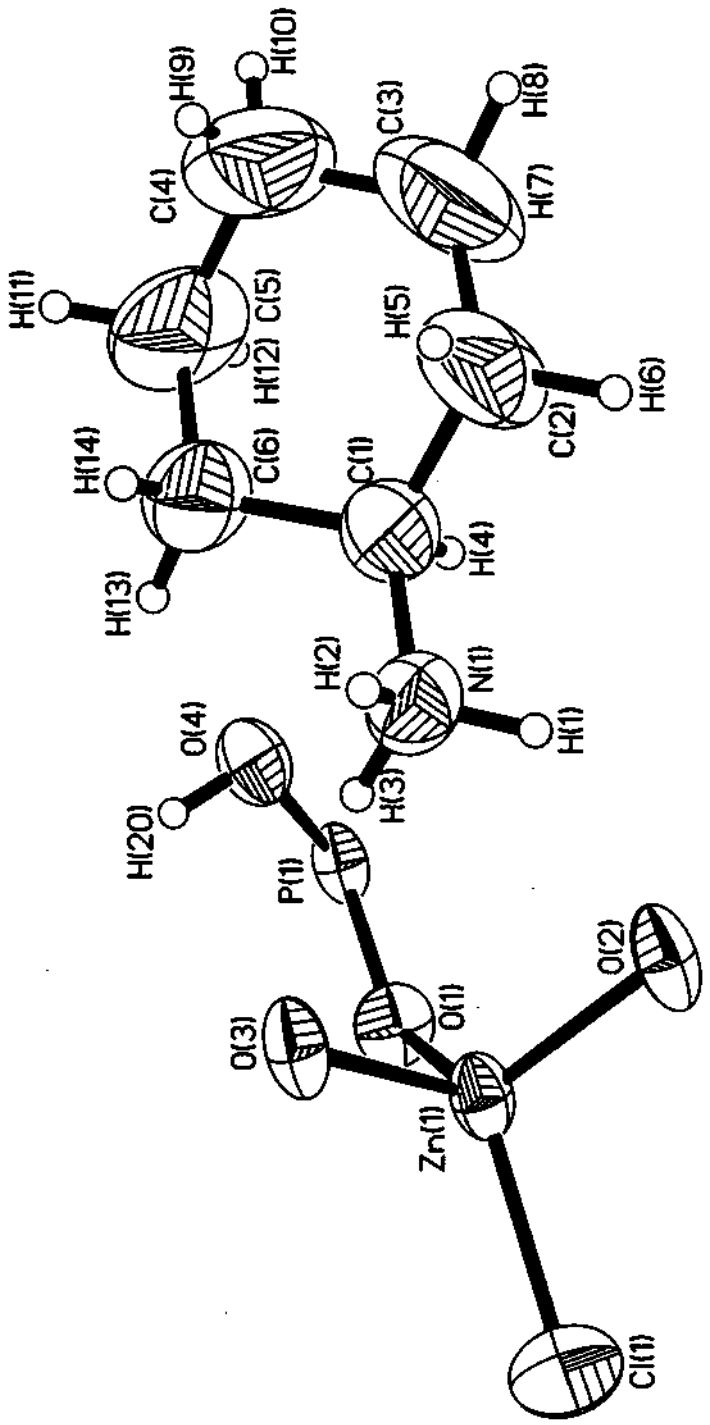

Fig. 1.41.(a) Asymmetric unit of **X**, $[C_6NH_{14}]$ $[ZnCl(HPO_4)]$. Thermal ellipsoids are shown at 50% probability).

Table 1.41. Atomic coordinates [x 10^4] and equivalent isotropic displacement parameters [$Å^2$ X 10^3] **X**, $[C_6NH_{14}][ZnCl(HPO_4)]$.

Atom	x	y	z	U_{eq} [a]
Zn(1)	4027(1)	524(1)	1873(1)	36(1)
P(1)	5004(1)	2270(1)	-640(1)	32(1)
O(1)	4120(2)	1796(3)	163(3)	43(1)
O(2)	4708(3)	-1252(3)	1864(4)	44(1)
O(3)	4836(2)	1311(3)	3648(3)	40(1)
O(4)	5921(2)	2365(3)	595(4)	43(1)
Cl(1)	2480(1)	146(2)	2356(2)	66(1)
N(1)	6688(3)	-396(5)	4021(6)	56(1)
C(1)	7467(5)	-134(7)	2970(7)	60(2)
C(2)	8242(6)	-1176(8)	3129(14)	128(4)
C(3)	9059(8)	-865(12)	2071(16)	166(6)
C(4)	9473(7)	526(10)	2279(15)	122(4)
C(5)	8659(6)	1563(9)	2103(12)	111(3)
C(6)	7853(5)	1295(7)	3164(9)	74(2)

[a] U_{eq} is defined as one third of the trace of the orthogonalized U_{ij} tensor.

Table 1.42. Selected bond distances and angles in **X**, $[C_6NH_{14}][ZnCl(HPO_4)]$

Moiety	Distance, Å	Moiety	Distance, Å
Zn(1)-O(1)	1.945(3)	P(1)-O(1)	1.518(3)
Zn(1)-O(2)	1.961(3)	P(1)-O(3)$^{\#1}$	1.521(3)
Zn(1)-O(3)	1.972(3)	P(1)-O(2)$^{\#2}$	1.529(3)
Zn(1)-Cl(1)	2.220(2)	P(1)-O(4)	1.579(3)
	Organic Moiety		
N(1)-C(1)	1.482(7)	C(1)-C(2)	1.463(10)
C(2)-C(3)	1.536(11)	C(3)-C(4)	1.470(13)
C(4)-C(5)	1.499(12)	C(5)-C(6)	1.518(9)
C(6)-C(1)	1.490(9)		
Moiety	Angle (°)	Moiety	Angle (°)
O(1)-Zn(1)-O(2)	119.62(13)	O(1)-P(1)-O(3)$^{\#1}$	111.3(2)
O(1)-Zn(1)-O(3)	106.40(13)	O(1)-P(1)-O(2)$^{\#2}$	112.7(2)
O(2)-Zn(1)-O(3)	96.38(14)	O(3)$^{\#1}$-P(1)-O(2)$^{\#2}$	110.0(2)
O(1)-Zn(1)-Cl(1)	112.06(11)	O(1)-P(1)-O(4)	108.7(2)
O(2)-Zn(1)-Cl(1)	108.31(12)	O(3)$^{\#1}$-P(1)-O(4)	107.8(2)
O(3)-Zn(1)-Cl(1)	113.17(10)	O(2)$^{\#2}$-P(1)-O(4)	105.9(2)
	Organic Moiety		
N(1) – C(1) - C(2)	112.0(6)	C(1)-C(2)-C(3)	111.3(8)
C(2)-C(3)-C(4)	113.5(8)	C(3)-C(4)-C(5)	109.4(8)
C(4)-C(5)-C(6)	113.1(7)	C(5)-C(6)-C(1)	111.1(6)
C(6)-C(1)-C(2)	112.9(6)	N(1)-C(1)-C(6)	110.9(5)

#1 x, -y+1/2, z-1/2; #2 –x+1, -y, -z

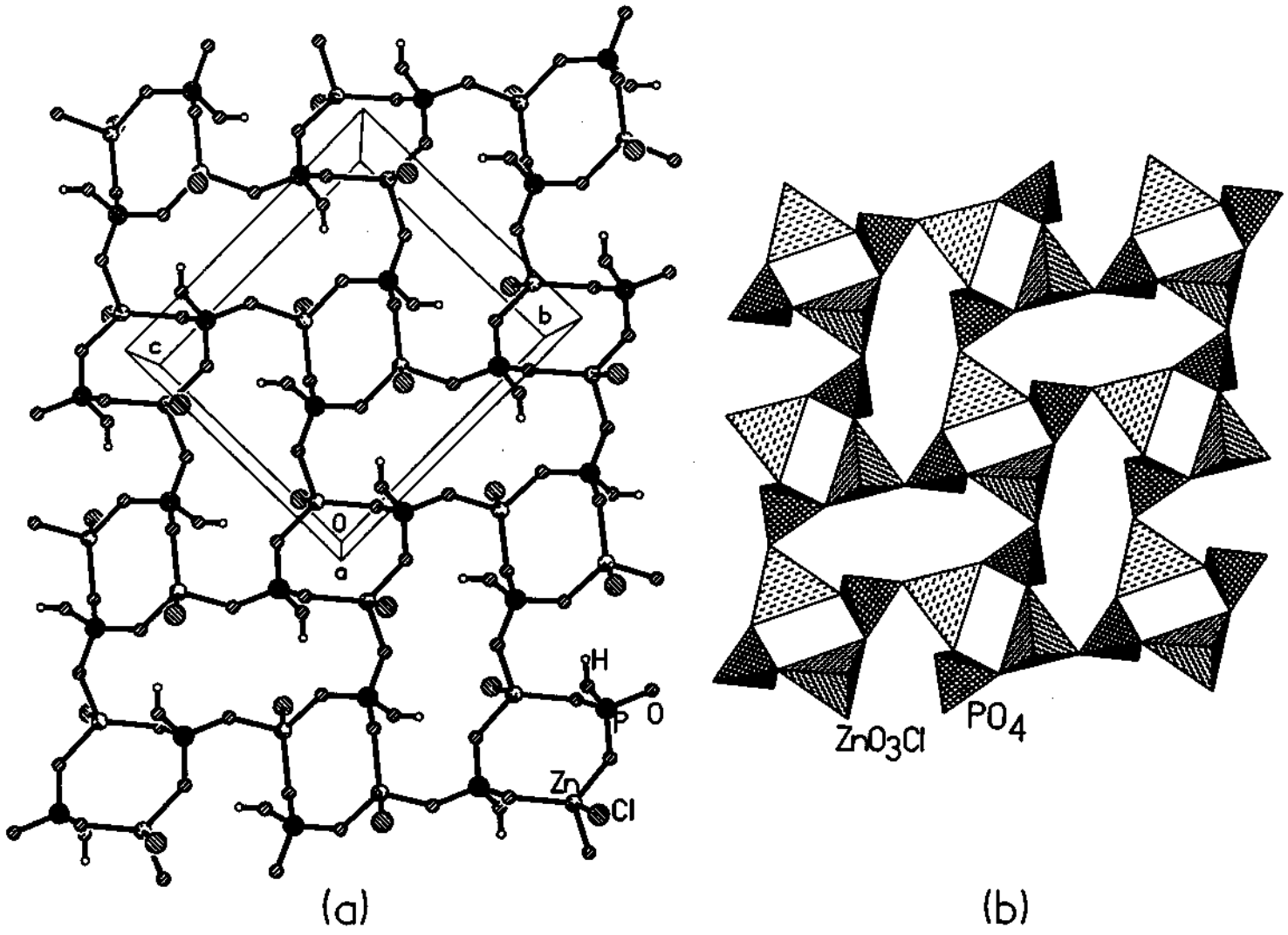

Fig. 1.42. Structure of **X**, along *a* axis showing a single layer. Note that the layers are made of 4– and 8– membered rings only. (a) Ball and stick view (b) Polyhedral view..

arrangement of the chlorine atoms facilitates closer interaction with the structure-directing amines via Cl....H-N/C type interaction. The compensating protonated amine molecule is situated between the inorganic layers that are separated by a distance of ~7 Å as shown in Figs. 1.43 and 1.44. As can be seen, there are two amine molecules that are present in between the layers, which is similar to the amine positioning observed in a layered aluminum phosphate,[134] though such occurrences are rare. Since the Cl^- ions project into the layers, a shorter inter-layer distance would experience repulsive interactions from the Cl^- ions of the adjacent layers and hence the layers are, probably, needed to be apart. The two-amine molecules, present in between the layers, may, therefore, be needed to impart stability to such a framework via hydrogen bonding.

It is instructive to compare the role of the chlorine atoms in these solids with that of the lone-pair of electrons of Sn(II) atoms in some of the tin(II) phosphates.[232,233] It is clear from Figs. 1.42-1.44, that the chlorine atoms are directed perpendicular to the plane of the layer. Similar positioning have been observed for the lone-pair of electrons in the tin phosphate as shown in Figs. 1.45 and 1.46. In the tin(II) phosphates, the Sn atoms are usually coordinated with three oxygen atoms and occupy the vertex of a trigonal pyramid. The oxygens are, in turn, connected to phosphorus completing the tin phosphate structure. The lone pair of electrons provides the fourth vertex needed for the tetrahedron, in the case of Sn(II). The stereo-active lone-pairs manifest themselves in the lattice by creating open-space between the two layers in these tin phosphates. In the present compounds, we have a similar situation with three oxygens bonded to the Zn are linked to the phosphorus forming the layer arrangement. Since Zn is tetrahedrally coordinated, the fourth connection comes from the chlorine atoms, which occupy identical position to that of the lone-pair of electrons of Sn(II).

Multipoint hydrogen bond interactions are important in the structural stability, and possibly, in the formation, of many of the low-dimensional open-framework solids. In $[C_6NH_{14}][ZnCl(HPO_4)]$, the hydrogens of the amine

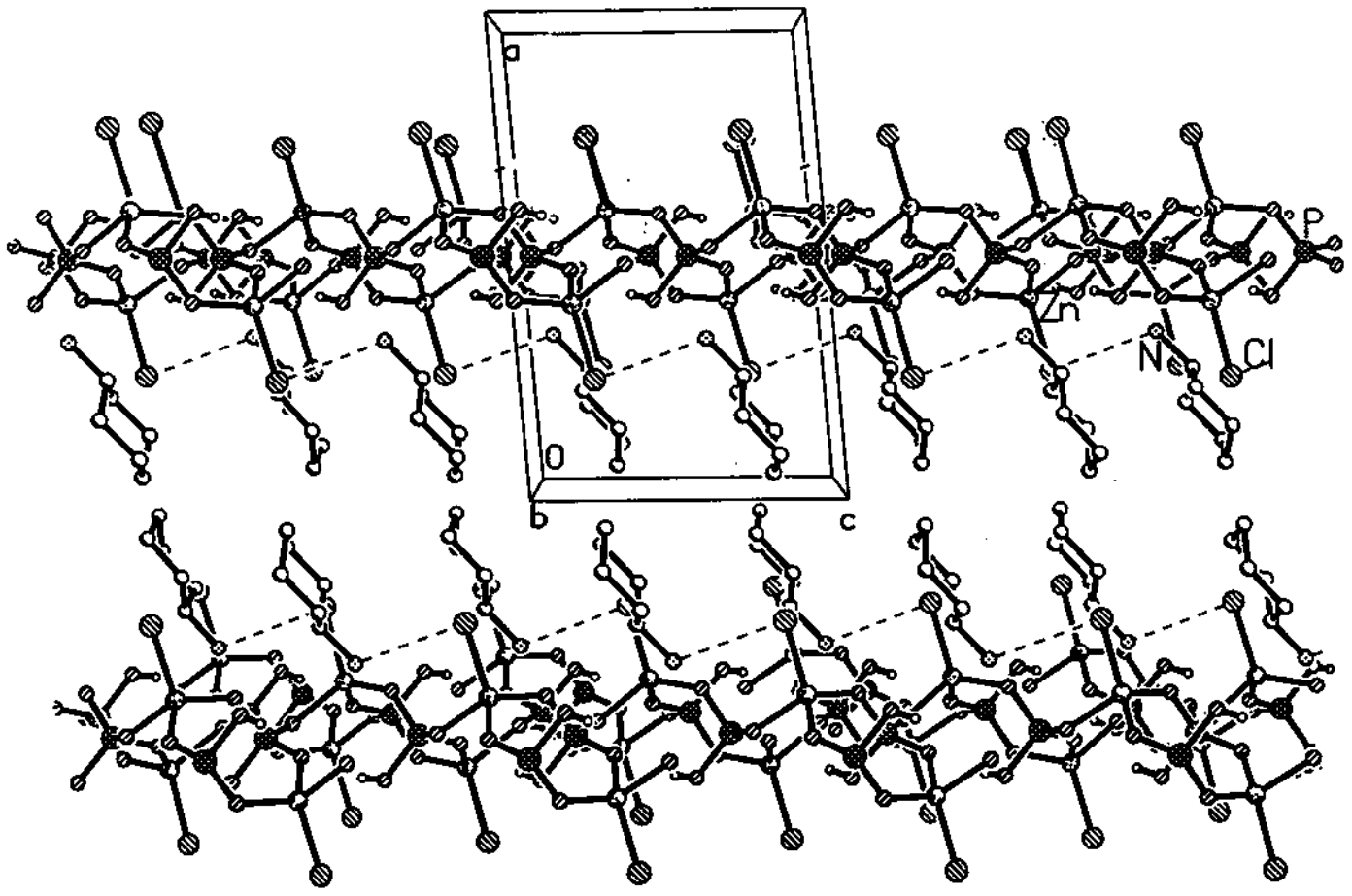

Fig. 1.43. Structure of **X**, along*b* axis showing the layer arrangement. Note that the chlorine atoms point into the inter–layer space and two cyclohexylamine molecules reside in the inter–lamellar space. .

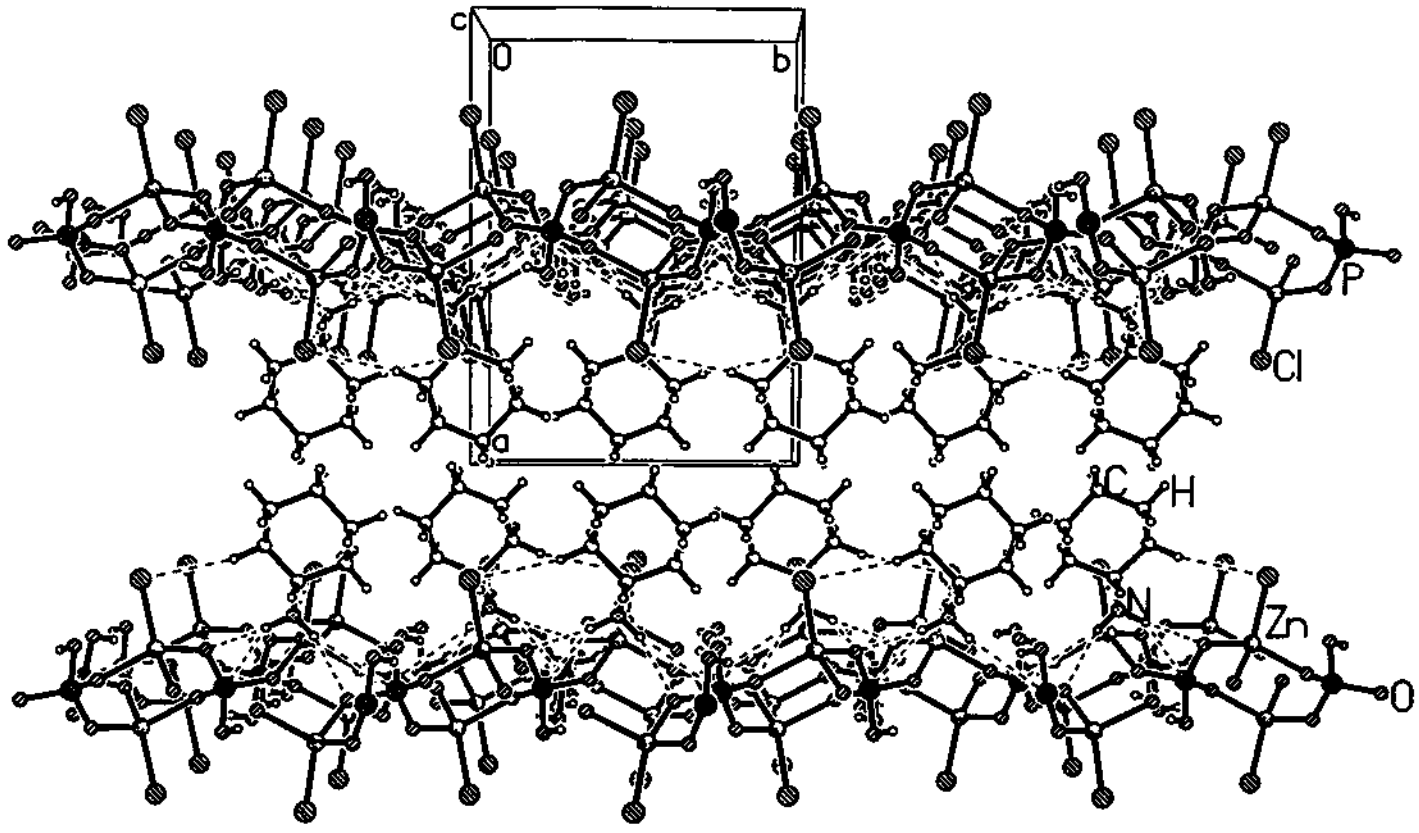

Fig. 1.44. Structure of **X**, along*c* axis showing the layer arrangement and the organic molecules. The dotted lines represent the various hydrogen bond interactions (Table 1.43). .

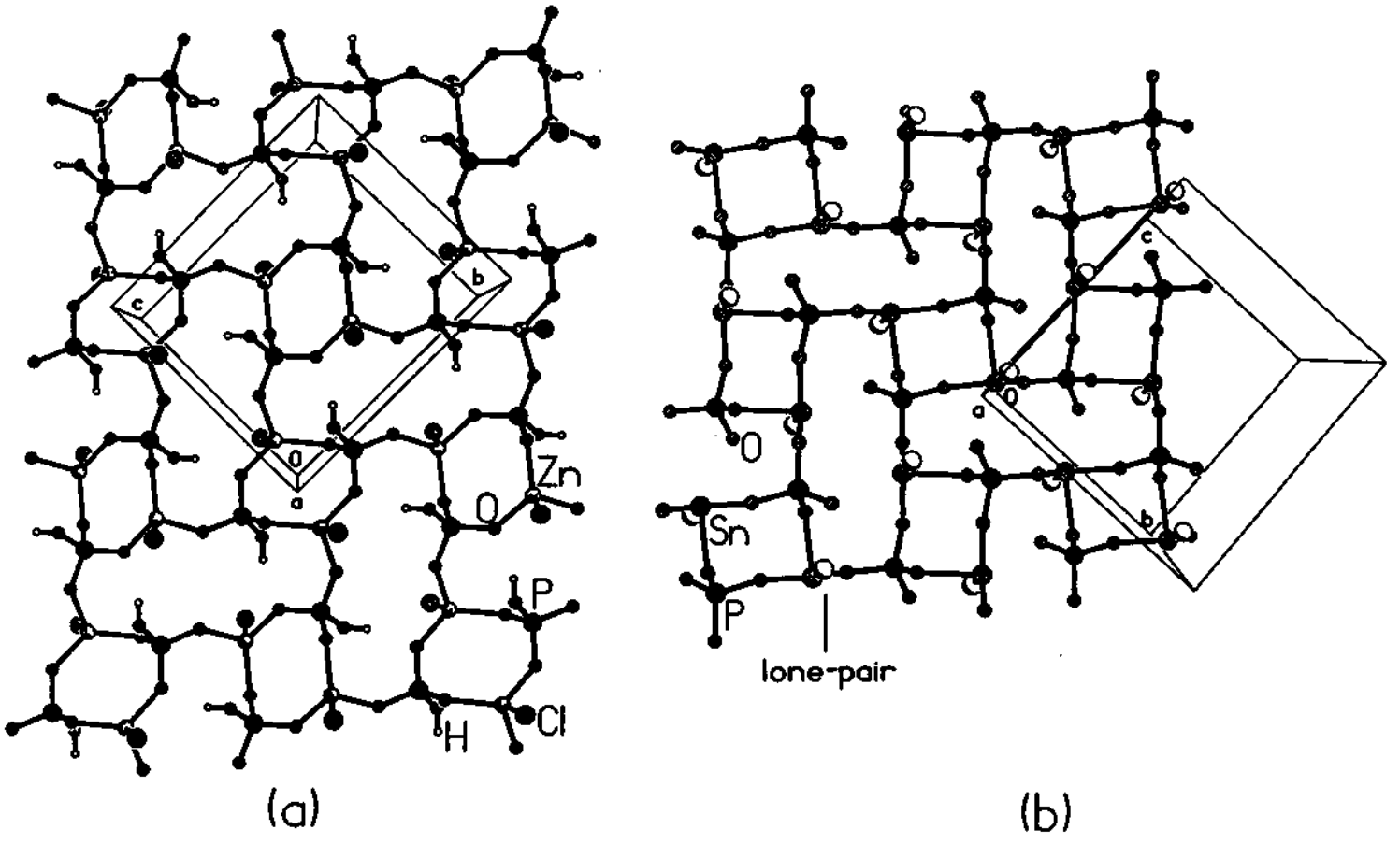

Fig. 1.45. (a) Structure showing the layer arrangement in **X**. (b) Structure showing a single layer of tin(II) phosphate, $[C_3N_2H_{12}]_{0.5}[SnPO_4]$. .Note the identical positions for chlorine atoms and the lone pair of Sn(II).

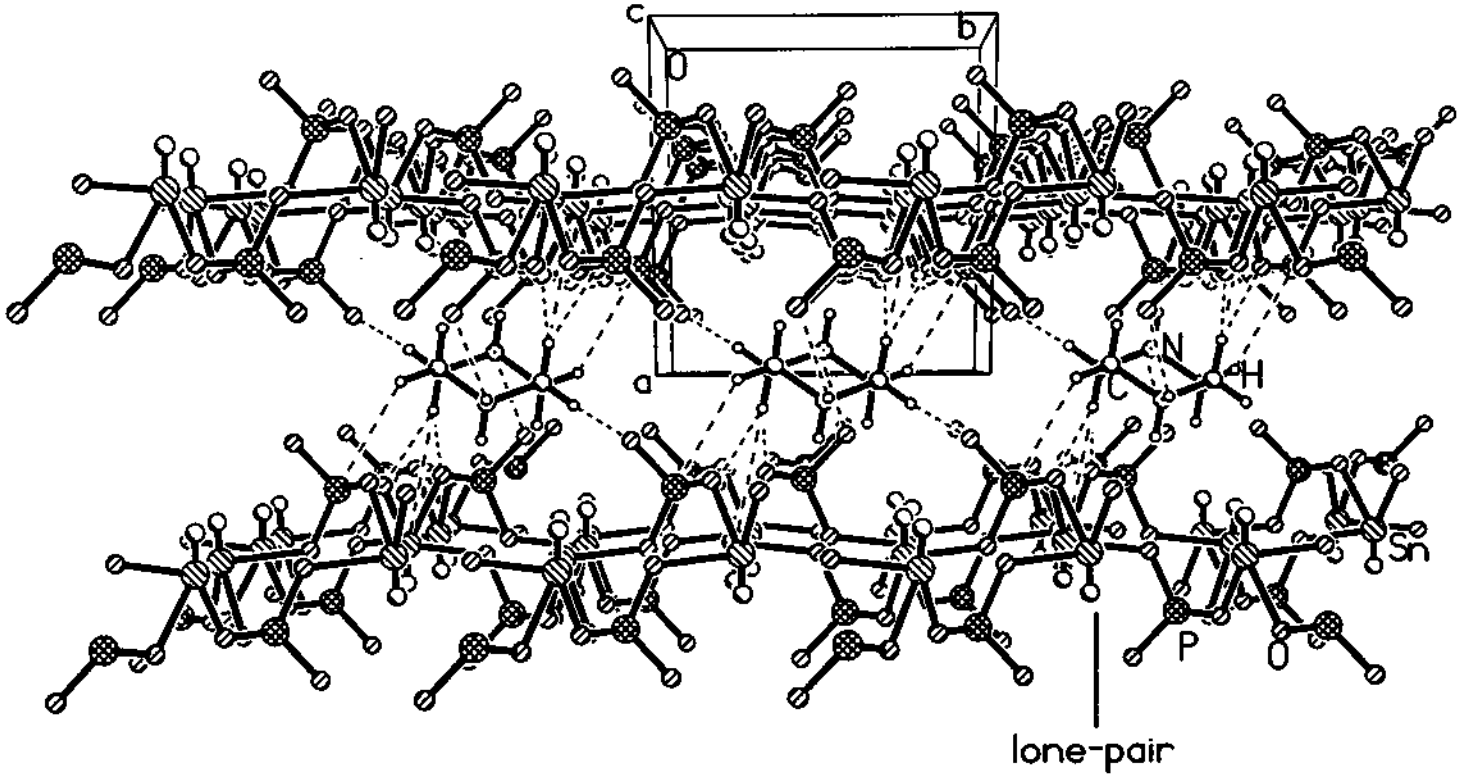

Fig. 1.46. Structure of the tin(II) phosphate $[C_4N_2H_{12}]_{0.5}[SnPO_4]$., Note that the lone pair of electrons associated with Sn(II) point into the layers similar to the chlorine atoms in **X**. .Note the identical positions for chlorine atoms and the lone pair of Sn(II).

molecule interact strongly with the framework oxygens, especially with the chlorine. The important hydrogen bond interactions are: O(3) – H(3) = 2.157 Å, O(3) – H(3) – N(1) = 162.7°; Cl(1) – H(2) = 2.377 Å, Cl(1) – H(2) – N(1) = 173.2°. Furthermore, the terminal –OH group of the $PO_3(OH)$ unit also participates in intra-layer hydrogen bonding (O(2) – H(20) = 1.994 Å, O(2) – H(20) – O(4) = 161.7°). The complete hydrogen bond interactions are presented in Table 1.43. **X**, thus, illustrate the importance of multipoint hydrogen bond interactions in the stability of two-dimensional solids.

The structure of **X** has common structural features with many of the previously known layered phosphate materials.[216,255-260] The layered phosphates are, in general, made from the vertex linkage between the MO_x polyhedra and PO_4 tetrahedra and have either terminal double bonded oxygen atoms and or hydroxyl groups originating from the phosphorus center. The organic amine molecules are usually situated in between these layers. The layers are held together by strong hydrogen bond interactions involving the framework and the organic moieties. In **X**, in addition to the above there are terminal chlorine atoms, which participate in hydrogen bonding.

Summary of Zinc phosphates: In the process of understanding the various issues linked to the formation of phosphate based open-framework architectures, we have successfully synthesized a large number open-framework zinc phosphates in the presence of organic amines such as 1,3-diamino-2-hydroxypropane (DAHP), 1,3-diaminopropane (DAP), diethylenetriamine (DETA), 1,3-diaminoguanidine hydrochloride (DAG) and cyclohexylamine (CHA) under hydrothermal conditions. The compounds **I, IV, V,** and **X** are two-dimensional layered solids, where as compounds **II, III,** and **VI - IX** possess three-dimensional architectures. The salient features observed in them involve the observation of intersecting helical channels in **VI,** the Zn_4O_4 clusters in **VII,** the amine molecules ligated to the zinc center in **VIII** and **IX** and synthesis of first open-framework zinc chlorophosphate, **X**.

Table 1.43. Important Hydrogen bond interactions in **X**, $[C_6NH_{14}][ZnCl(HPO_4)]$.

Moiety	Distance (Å)	Moiety	Angle (°)
O(1) – H(1)	2.279	O(1) – H(1) – N(1)	144.9
O(3) – H(3)	2.157	O(3) – H(3) – N(1)	162.7
O(2) – H(20)$^{\#1}$	1.994	O(2) – H(20) – O(4)	161.7
Cl(1) – H(2)	2.377	Cl(1) – H(2) – N(1)	173.2
Cl(2) – H(6)	2.773	Cl(2) – H(6) – C(2)	166.2

$^{\#1}$ Intra-layer

4.4. Amine Phosphates as Possible Intermediates in the formation of Open-framework structures

Amine phosphates are often found as by-products in the hydrothermal synthesis of open-framework phosphates,[237] They are normally not observed because of their high solubility in water. The fact that they are isolated from the synthesis mixtures suggested that they possibly could be the elusive reaction intermediate, which can lead to the open-framework phosphates. Initial experiments showed that the amine phosphates react with metal ions under hydrothermal conditions in absence of additional phosphoric acid to give open-framework metal phosphates. This suggested that amine phosphates could indeed act as intermediates in the formation of open-framework structures. We have carried out an extensive and systematic investigation to confirm and extend the initial results. Apart from the isolation from regular reaction mixtures, amine phosphates can be readily prepared by the reaction of amines with phosphoric acid, under normal conditions, in an appropriate solvent.[261]

Reaction of 1,3 diaminopropane phosphate (DAPP); (Fig. 1.47a) with Zn^{II} ions under hydrothermal conditions initially gives a zinc phosphate with a ladder structure involving edge-shared four-ring metal phosphate units (Fig 1.47b). It is noteworthy that this ladder structure is also produced in the conventional hydrothermal synthesis with 1,3- diaminopropane (DAP) as structure-directing agent.[216] More significantly, DAPP reacts with Zn^{II} to give this ladder structure at much lower temperatures (30°C for 96h).[210] In addition, we obtained a new layer structure (Fig. 1.47c) when DAPP was reacted with Zn^{II} for extended periods ($\geq$ 96h) at moderate temperatures ($\leq$ 85 °C). This observation suggests that the layer structure may be a transformation product of the ladder structure.

Reaction of piperazine phosphate (PIPP) with Zn^{II} ions under hydrothermal conditions gave a new linear-chain structure of corner-sharing

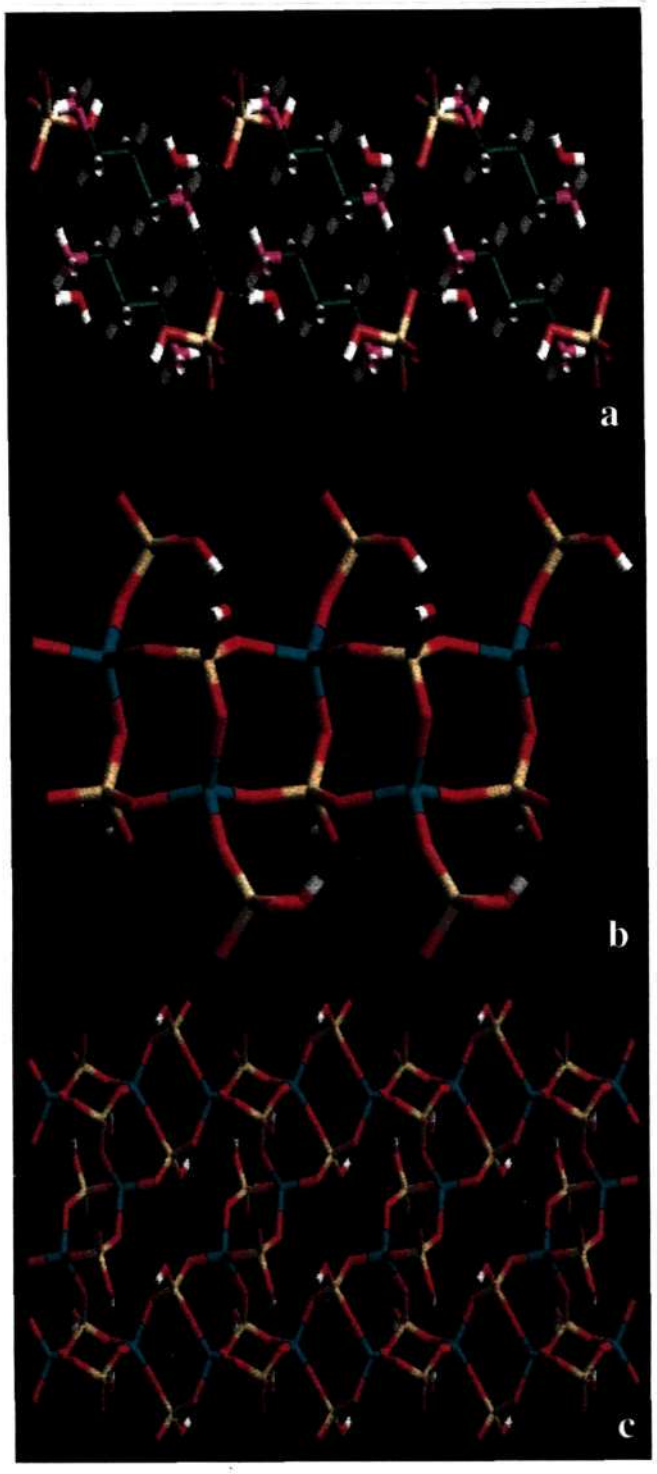

Fig. 1.47. (a) The diamino propane phosphate (DAPP); (b) The one-dimensional zinc phosphate chain structure. Note that the water molecules in (a) is replaced by Zn ions forming this structure; (c) The layered zinc phosphate.

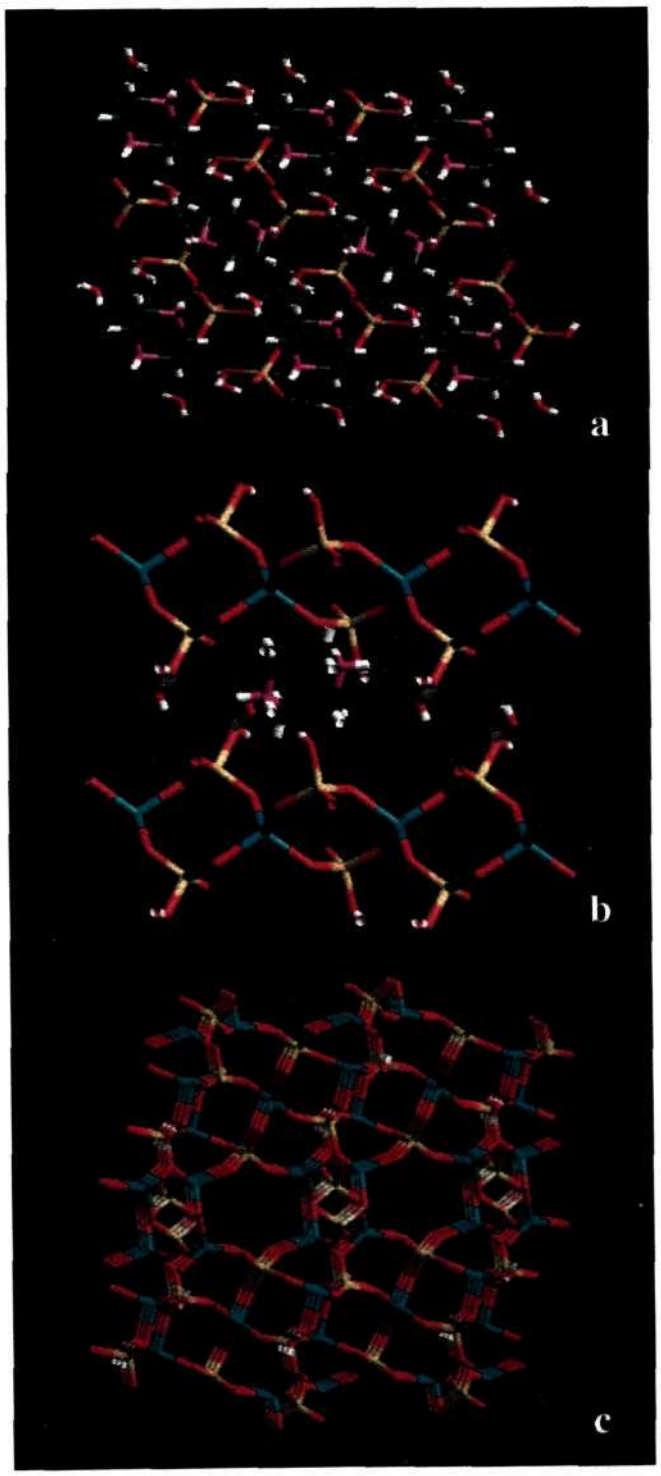

Fig. 1.48. (a) The hydrogen bonded piperazine phosphate assembly (PIPP). (b) The corner shared zinc phosphate chain structure. Note that this is the simplest chain structure; (c) The 3D zinc phosphate. This structure can be derived from the corner-shared chain structure.

metal phosphate units, along with a new three-dimensional structure (Fig 1.48); two known three-dimensional structures[239] were also obtained. Reaction of PIPP with Zn^{II} ions at 85 °C also yielded the three-dimensional structures. Similarly, the phosphate of 1,4-diazabicylco [2.2.2] octane (DABCO-P) was reacted with Zn^{II} ions at room temperature to give the three-dimensional structure, which was obtained at 150°C, or by direct hydrothermal synthesis.[87] Reaction of ethylenediamine phosphate (ENP) with Zn^{II} ions at 150 °C gave new ladder, layer and 3-dimensional structures. The last two were also obtained in a reaction carried out at 50 °C. Table 1.44 lists the various open-framework zinc phosphates obtained by the reactions of amine phosphates with Zn^{II} ions at different temperatures.

The above results suffice to indicate the key role of amine phosphates in the formation of open-framework phosphates. Furthermore there is a close similarity between the structures of DAPP (Fig 1.47a) and the zinc phosphate ladder structure (Fig 1.47b). The former consists of a hydrogen-bonded network with water molecules, resembling the loosely held hydrogen-bonded network with water molecules and resembles the loosely hydrogen-bonded structures involved in the synthesis of aluminosilicates.[4,262] The mechanism of formation of the initial ladder phosphate can be understood in terms of the displacement of the water molecules from the amine phosphate by Zn^{II} ions (Fig 1.49).

To further substantiate that the amine phosphates undergo facile reactions with metal ions, we monitored the reaction between the DAPP and Zn^{2+} ions at 85 °C in aqueous medium by *in-situ* ^{31}P NMR spectroscopy. The intensity of the signal of amine phosphate (δ = 0.056ppm) decreases, while that of a zinc phosphate precursor at (δ = 3.82ppm) increases (Fig. 1.50 and Fig 1.51). The intensity of the signal of the phosphate precursor decreases after some time, due to the formation of more complex open-framework phosphates. This suggests that the unidentified intermediate reported recently[263] in the *in-situ* EDXRD study of the formation of the gallophosphate ULM-5 may be an amine phosphate. Heating the intermediate with gallium salts is reported to yield the

Table 1.44. Open-framework zinc phosphates synthesized from amine phosphates.

Composition	Cell Parameters						Sp.grp	
	a, Å	b, Å	c, Å	α, °	β, °	γ, °		
Piperazine phosphate (PIPP)								
$[C_4N_2H_{12}][Zn(HPO_4)_2(H_2O)]$	8.931	14.025	9.311	90.0	95.4	90.0	$P2_1/n$	new
$[C_4N_2H_{12}][Zn_{3.5}(PO_4)_3(H_2O)]$	16.105	8.256	22.998	90.0	104.0	90.0	C2/c	new
$[C_4N_2H_{12}][Zn(H_2O)Zn(HPO_4)(PO_4)]_2$	12.076	14.889	11.836	90.0	97.7	90.0	C2/c	
$[C_4N_2H_{12}][Zn_2(PO_4)(H_2PO_4)_2]$	13.388	12.839	8.225	90.0	94.8	90.0	C2/c	
$[C_4N_2H_{12}][Zn_2(HPO_4)_2(H_2PO_4)_2]$	13.414	12.871	8.225	90.0	94.8	90.0	C2/c	new
1,3-diaminopropane phosphate (DAPP)								
$[C_3N_2H_{12}][Zn(HPO_4)_2]$	5.220	12.756	15.674	90.0	90.0	90.0	$P2_12_12_1$	
$[C_3N_2H_{12}][Zn_2(HPO_4)_3]$	8.615	9.619	17.038	90.0	93.6	90.0	$P2_1/c$	new
$[C_3N_2H_{12}][SnPO_4]_2$	18.097	7.889	9.151	90.0	111.8	90.0	C2/c	
Ethylenediamine phosphate (ENP)								
$[C_2N_2H_{10}][Zn(HPO_4)_2]$	5.161	15.842	12.027	90.0	92.4	90.0	$P2_1/c$	
$[C_2N_2H_{10}][Zn_2(HPO_4)_2(H_2PO_4)_2]$	16.420	7.826	14.640	90.0	116.5	90.0	$P2_1/c$	
$[C_2N_2H_{10}][Zn_6(PO_4)_4(HPO_4)]$	19.182	5.036	21.202	90.0	103.3	90.0	C2/c	
Diethylenetriamine phosphate (DETAP)								
$[C_4N_3H_{16}][Zn_4(PO_4)_3(HPO_4)]H_2O$	10.021	8.286	11.856	90.0	103.1	90.0	$P2_1$	
$[C_4N_3H_{15}][Zn_2PO_4(HPO_4)]_2$	20.075	5.127	17.726	90.0	125.4	90.0	C2/c	
$[C_4N_3H_{15}][Zn_5(PO_4)_4]$	27.071	5.215	17.920	90.0	130.3	90.0	Cc	
1,4diazabicyclo [2.2.2]octane phosphate (DABCO-P)								
$[C_6N_2H_{14}][Zn_2(HPO_4)_3]$	9.528	9.948	9.996	107.7	98.1	114.9	P(-1)	
$[C_6N_2H_{14}][Zn_4(PO_4)_2(HPO_4)_2]3H_2O$	9.475	9.525	12.312	93.7	91.0	98.7	P(-1)	

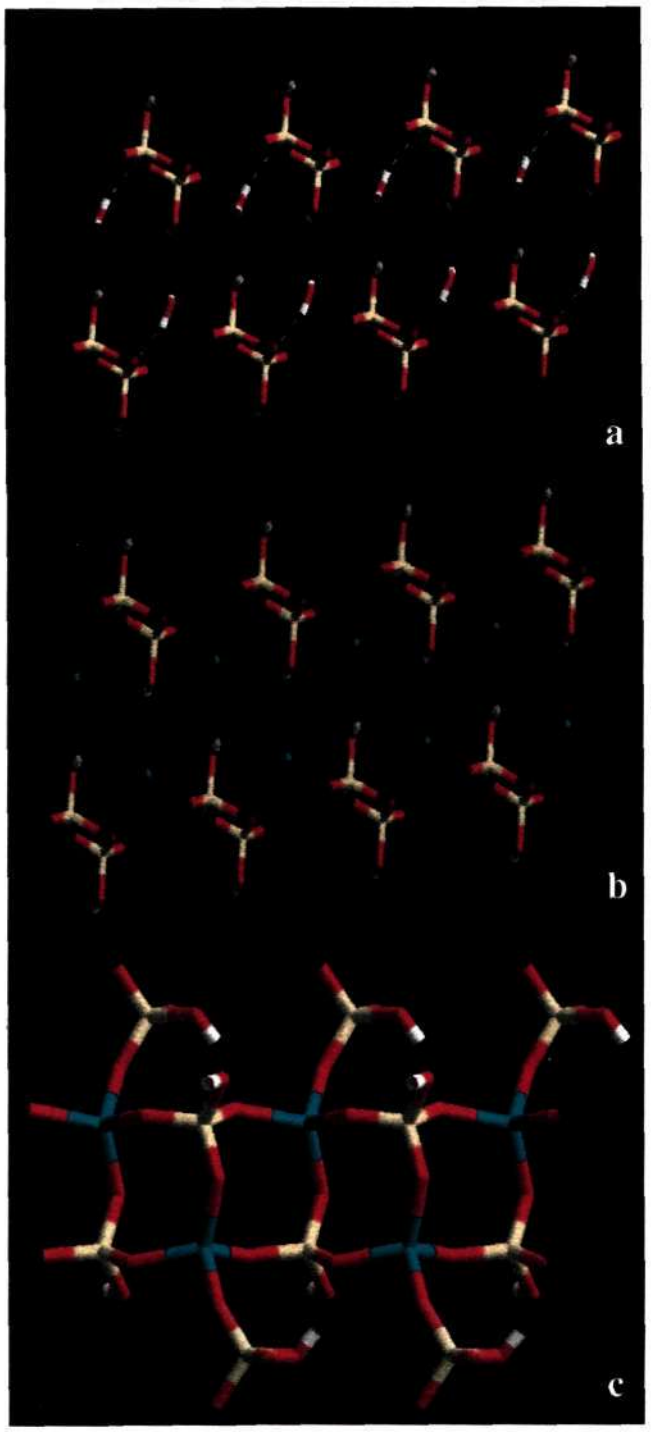

Fig. 1.49. (a) The hydrogen bonded DAPP phosphate without the amine molecule. (b) The water molecules are replaced by Zn ions for facile bond formation. (c) The edge-shared chain zinc phosphate.

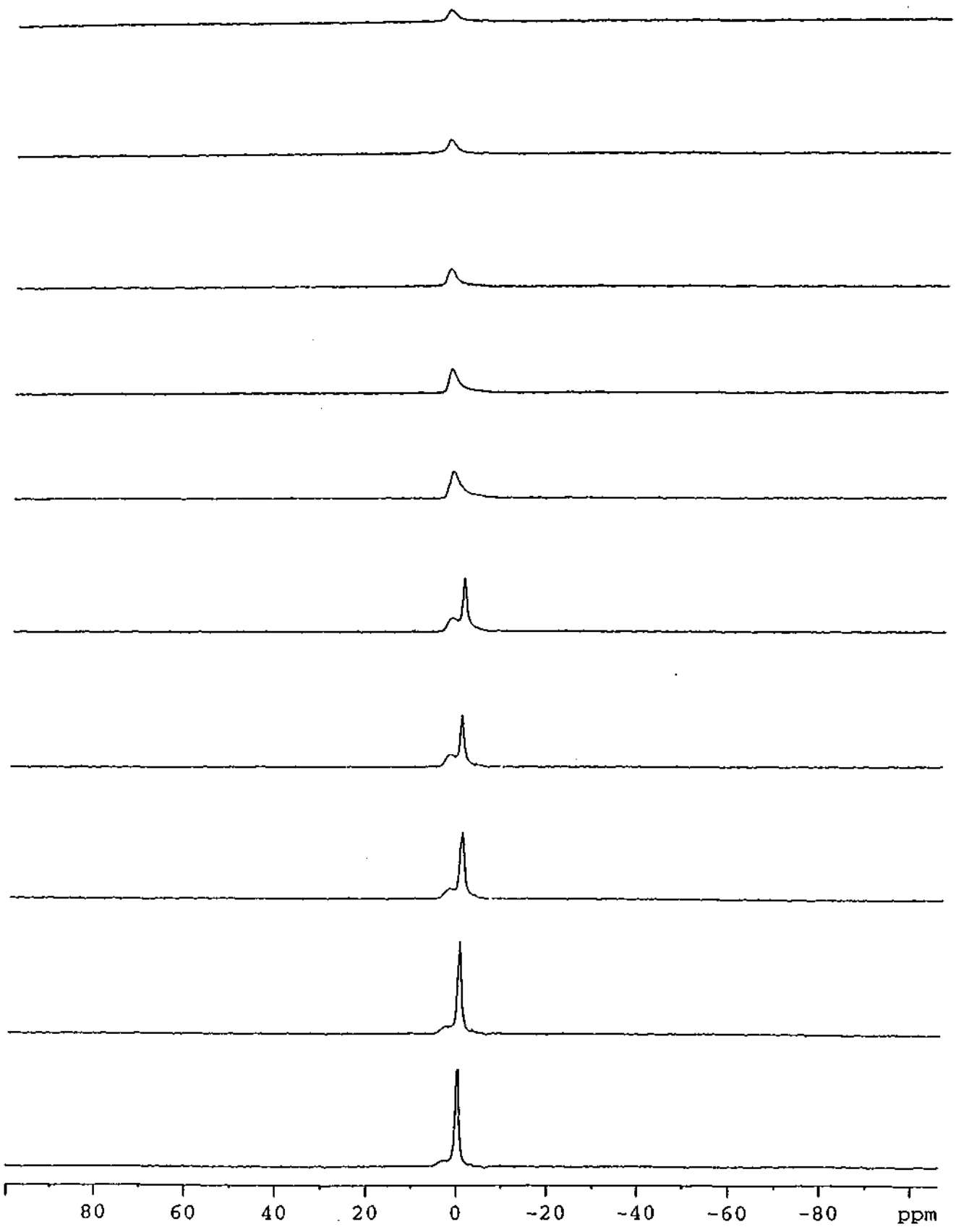

Fig. 1.50. In situ ^{31}P NMR spectra of the reaction of DAPP with Zn^{II} ions.

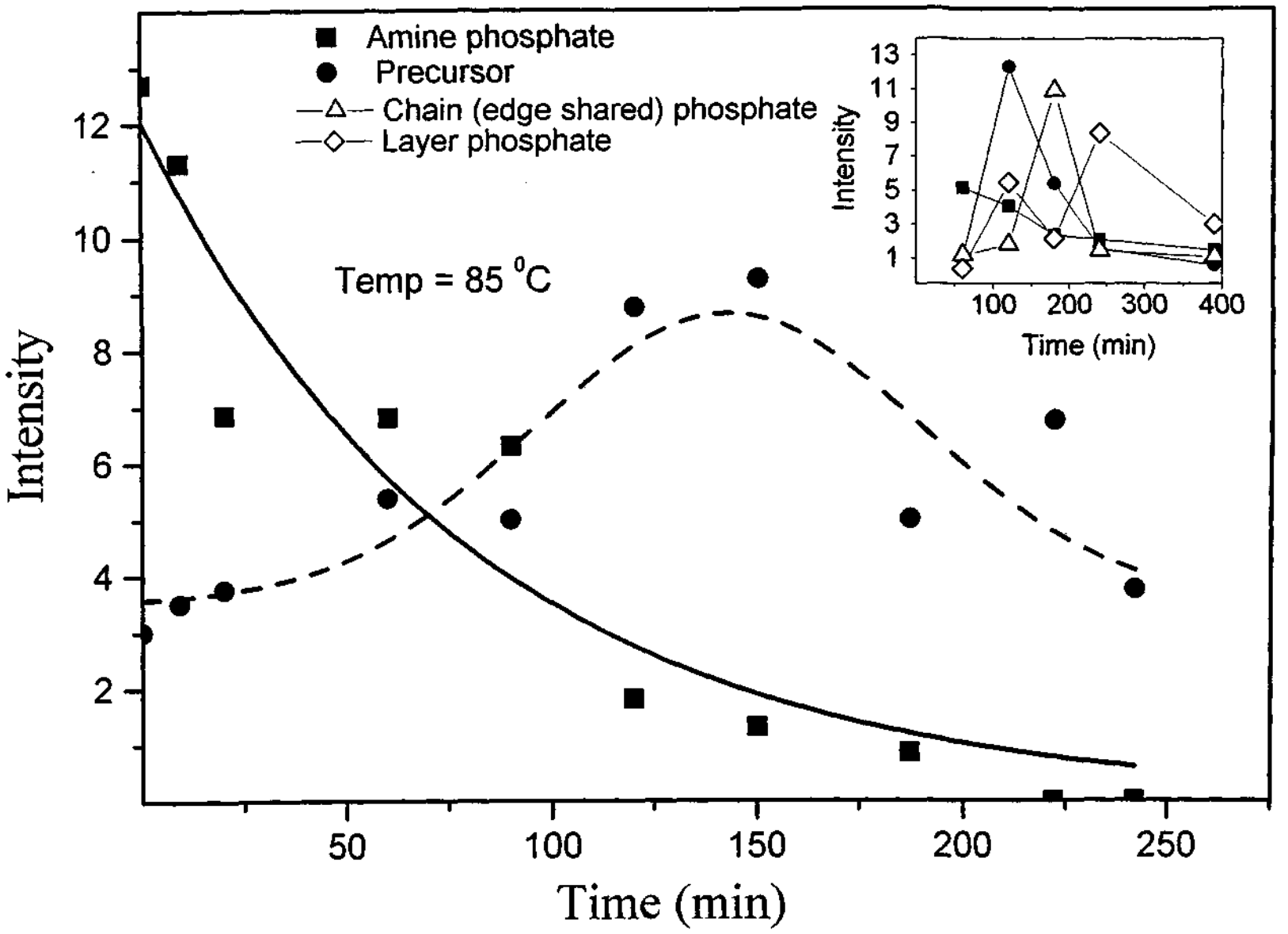

Fig. 1.51 Intensity *vs*. Time plot of the amine phosphate and the precursor phase by *in situ* ^{31}P NMR studies. Note that when the precursor is formed the amine phosphate is completely consumed. Inset shows the Intensity *vs* Time plots generated from the time–dependent powder XRD (*ex situ*) showing the drop in intensity of the amine phosphate, precursor, chain phases as the layered material starts forming.

gallophosphate.[263] Reaction of the amine phosphate with Zn^{II} at all temperatures first yields a fine particulate open-framework zinc phosphate with a low angle XRD line (d_{hkl} = 11.8Å). Time-dependent XRD studies show that the low-angle line due to the precursor decreases in intensity when the characteristic reflections of the ladder, layer, and three-dimensional structures start to appear. DAPP-Zn^{II} reaction thus lends credence to this suggestion (see inset of Fig. 1.51).

To demonstrate the universality of the amine phosphate route to open-framework structures, we carried out the reaction of DAPP with tin(II) oxalate and obtained the layer structure shown in Fig 1.52. This structure is obtained at temperatures as low as 50 °C (see Table 1.44). The reaction of DAPP with Co^{II} and Al^{III} ions, gave a new three-dimensional cobalt aluminum phosphate, that belongs to a recently described family of materials.[49,50,73]

4.5. Exploration of a Simple Universal Route to the Myriad of Open-framework metal phosphates

4.5.1. Zinc phosphates by the amine phosphate route

We first examine the products of the reaction of PIPP with zinc ions. The reaction of PIPP with zinc ions yielded five different framework structures. Particularly noteworthy is the fact that one of the products is a linear chain phosphate, **XI**, which has been suggested to be a building block of open-framework phosphates.[133] In addition to the linear chain, we have obtained 3-dimensional structures (**XII, XIII, XIV** and **XV**).

$[C_4N_2H_{12}][Zn(HPO_4)_2]H_2O$, XI : The linear chain compound **XI**, has the formula, and possesses a network of corner-shared ZnO_4 and HPO_4 tetrahedra. The atomic coordinates are listed in Table 1.45. The asymmetric unit of **XI** contains 18 independent non-hydrogen atoms (Fig. 1.53a) with two phosphate groups linked via oxygens to two zinc atoms to form the basic four membered ring of the linear chain. The P-O distances are in the range 1.510(4) - 1.576(4) Å

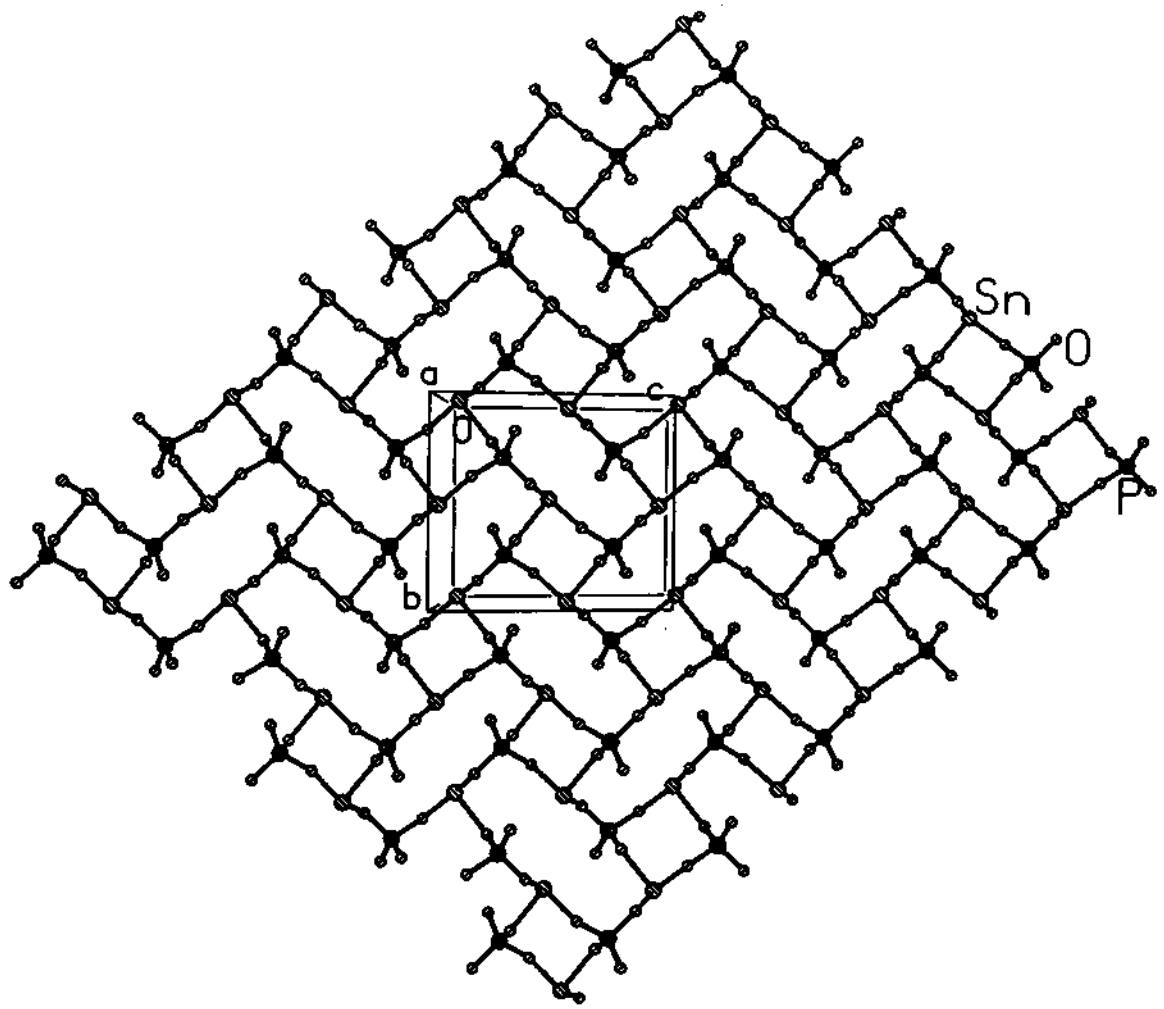

Fig. 1.52 Layered tin(II) phosphate structure formed between the reaction of DAPP with tin(II) oxalate at around room temperature .

Table 1.45. Atomic coordinates [x 10^4] and equivalent isotropic displacement parameters [$Å^2$ x 10^3] for **XI**.

Atom	x	y	z	U(eq)
Zn(1)	-2383(1)	4688(1)	10088(1)	17(1)
P(1)	-92(2)	4152(1)	7872(2)	17(1)
P(2)	-5108(2)	4144(1)	11730(2)	16(1)
O(1)	-1520(4)	3961(3)	8587(4)	25(1)
O(2)	-3434(4)	5805(3)	9285(4)	23(1)
O(3)	-3776(4)	3837(3)	10932(4)	26(1)
O(4)	-691(4)	4934(3)	11546(4)	23(1)
O(5)	-5426(5)	3324(3)	12818(4)	28(1)
O(6)	-4828(4)	5042(3)	12610(4)	25(1)
O(7)	952(4)	3296(3)	7993(4)	27(1)
O(8)	-518(5)	4297(3)	6227(4)	38(1)
O(100)	3135(6)	5100(5)	14689(7)	56(2)
N(2)	-3885(5)	6928(3)	12151(5)	22(1)
N(1)	-6131(5)	8298(3)	12677(5)	29(1)
C(1)	-5838(6)	8049(4)	11186(6)	25(1)
C(2)	-4229(7)	7742(4)	11159(6)	27(2)
C(3)	-4199(6)	7163(4)	13637(6)	26(2)
C(4)	-5815(7)	7479(5)	13668(7)	33(2)

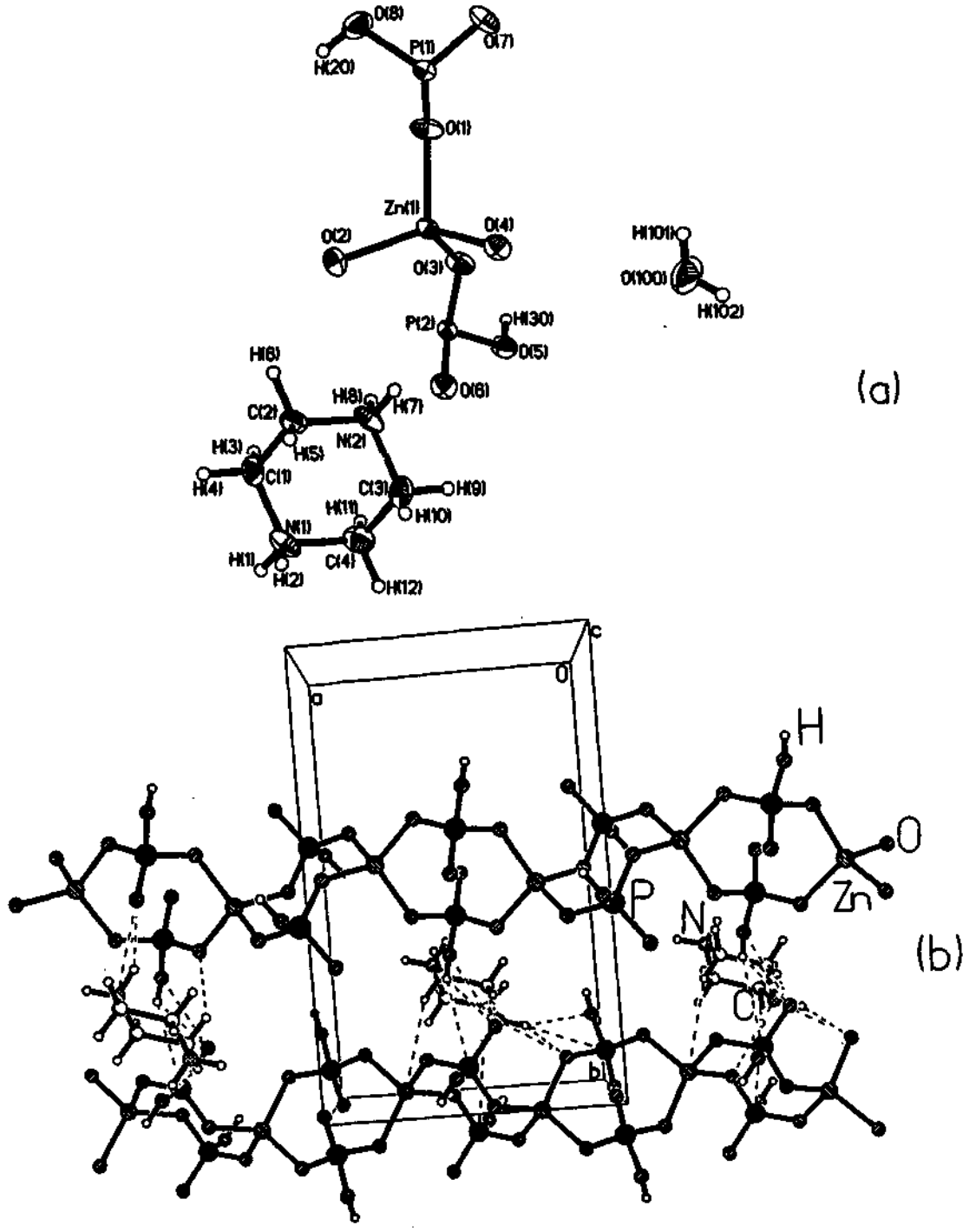

Fig. 1.53. (a) ORTEP plot of **XI**, $[C_4N_2H_{12}][Zn(HPO_4)_2(H_2O)]$. Thermal ellipsoids are given at 50% probability. (b)Structure of **XI**, $[C_4N_2H_{12}][Zn(HPO_4)_2(H_2O)]$, showing the linear chains of corner-shared 4-membered rings and the amine. Dotted lines represent possible hydrogen bond interactions.

(av. 1.534(4) Å) and the bond angles in the range 103.6(2) – 113.8(2)° (av. 109.4(2)°). All the zinc atoms are four-coordinated with respect to oxygen with Zn – O distances in the range 1.940(4) – 1.964(4) Å (av. 1.948(4) Å) and the O – Zn – O bond angles are in the range 104.9(2) – 115.9(2)° (av. 109.4(2)°). The important bond distances and angles are listed in Table 1.46. The framework structure consists of infinite chains along the *a*-axis, each chain consisting of corner-shared 4-membered rings. The anionic chains are held together by strong hydrogen bond interactions between the terminal –OH groups, water molecules *and the piperazinium cation that are located in between the two chains* (Fig.1.53b).

$[C_4N_2H_{12}][Zn_{3.5}(PO_4)_3(H_2O)]$, XII : The structure of **XII,** is based on a complex network of ZnO_4 and PO_4 tetrahedra giving rise to a 3-dimensional topology. The asymmetric unit of **XII** consists of 26 independent non-hydrogen atoms (Fig.1.54a and atomic coordinates Table 1.47). There is one molecule of diprotonated piperazine per asymmetric unit. There are four distinct Zn and three P atoms. One of the Zn atoms bears a terminal oxygen atom, which is a water molecule. All the Zn atoms are linked to P atoms via oxygens. There are both 3- and 4-membered rings present in the structure. All the P – O distances are in the range 1.513(2) – 1.578(2) Å (av. 1.538(2) Å) and the O – P – O bond angles are in the range 105.1(1) – 112.6(1)° (av. 109.4(1)°). The longer P – O distance and the larger O – P – O angle is associated with the 3-coordinated oxygen atom, *i.e.*, oxygen that bonds two Zn atoms and one P atom. The presence of trigonal coordinated oxygen results in Zn – O – Zn linkages. All the zinc atoms are 4-connected with respect to oxygen with the Zn – O distances lying in the range 1.915(2) - 2.045(2) Å (av. 1.963(2) Å) and the O – Zn - O bond angles in the range 89.9(1) – 127.4(1)° (av. 109.0(1)°). The important bond distances and angles are presented in Table 1.48. The Structure of **XII** is made up building units consist of 3- and 4-membered rings. The complex connectivity between these building units gives rise to 8-membered channels along the [001] and [011] direction (Fig.1.54b). The basic building unit comprises a ladder-like structure

Table 1.46 Bond distances (Å) and Angles (°) for **XI**

Moiety	Distance (Å)	Moiety	Angle (°)
Zn(1) - O(2)	1.940(4)	O(3) – Zn(1) – O(4)	108.0(2)
Zn(1) - O(3)	1.943(4)	O(1) – Zn(1) – O(4)	104.9(2)
Zn(1) - O(1)	1.946(4)	O(1) – P(1) – O(7)	111.3(2)
Zn(1) - O(4)	1.964(4)	O(1) – P(1) – O(4)$^{\#1}$	111.5(2)
P(1) – O(1)	1.517(4)	O(7) – P(1) – O(4)$^{\#1}$	112.2(2)
P(1) – O(7)	1.517(4)	O(1) – P(1) – O(8)	108.5(2)
P(1) – O(4)$^{\#1}$	1.534(4)	O(7) – P(1) – O(8)	105.5(2)
P(1) – O(8)	1.557(4)	O(4)$^{\#1}$ – P(1) – O(8)	107.4(2)
P(2) – O(6)	1.510(4)	O(6) – P(2) – O(3)	113.8(2)
P(2) – O(3)	1.523(4)	O(6) – P(2) – O(2)$^{\#2}$	112.4(2)
P(2) – O(2)$^{\#2}$	1.537(4)	O(3) – P(2) – O(2)$^{\#2}$	111.6(2)
P(2) – O(5)	1.576(4)	O(6) – P(2) – O(5)	106.9(2)
		O(3) – P(2) – O(5)	107.7(2)
Moiety	Angle (°)	O(2)$^{\#2}$ – P(2) – O(5)	103.6(2)
O(2) – Zn(1) – O(3)	110.3(2)	P(1) – O(1) – Zn(1)	128.9(2)
O(2) – Zn(1) – O(1)	110.9(2)	P(2)$^{\#2}$ – O(2) – Zn(1)	128.7(2)
O(3) – Zn(1) – O(1)	106.3(2)	P(2) – O(3) – Zn(1)	125.7(2)
O(2) – Zn(1) – O(4)	115.9(2)	P(1)$^{\#1}$ – O(4) – Zn(1)	133.3(2)

Organic Moiety

Moiety	Distance (Å)	Moiety	Angle (°)
N(2) – C(3)	1.475(7)	C(3) – N(2) – C(2)	111.4(4)
N(2) – C(2)	1.483(7)	C(1) – N(1) – C(4)	111.2(5)
N(1) – C(1)	1.479(7)	N(1) – C(1) – C(2)	109.7(5)
N(1) – C(4)	1.483(8)	N(2) – C(2) – C(1)	110.6(5)
C(1) – C(2)	1.503(8)	N(2) – C(3) – C(4)	110.5(5)
C(3) – C(4)	1.513(8)	N(1) – C(4) – C(3)	110.0(5)

Symmetry transformations used to generate equivalent atoms:

#1 -x, -y+1, -z+2 #2 -x-1, -y+1, -z+2

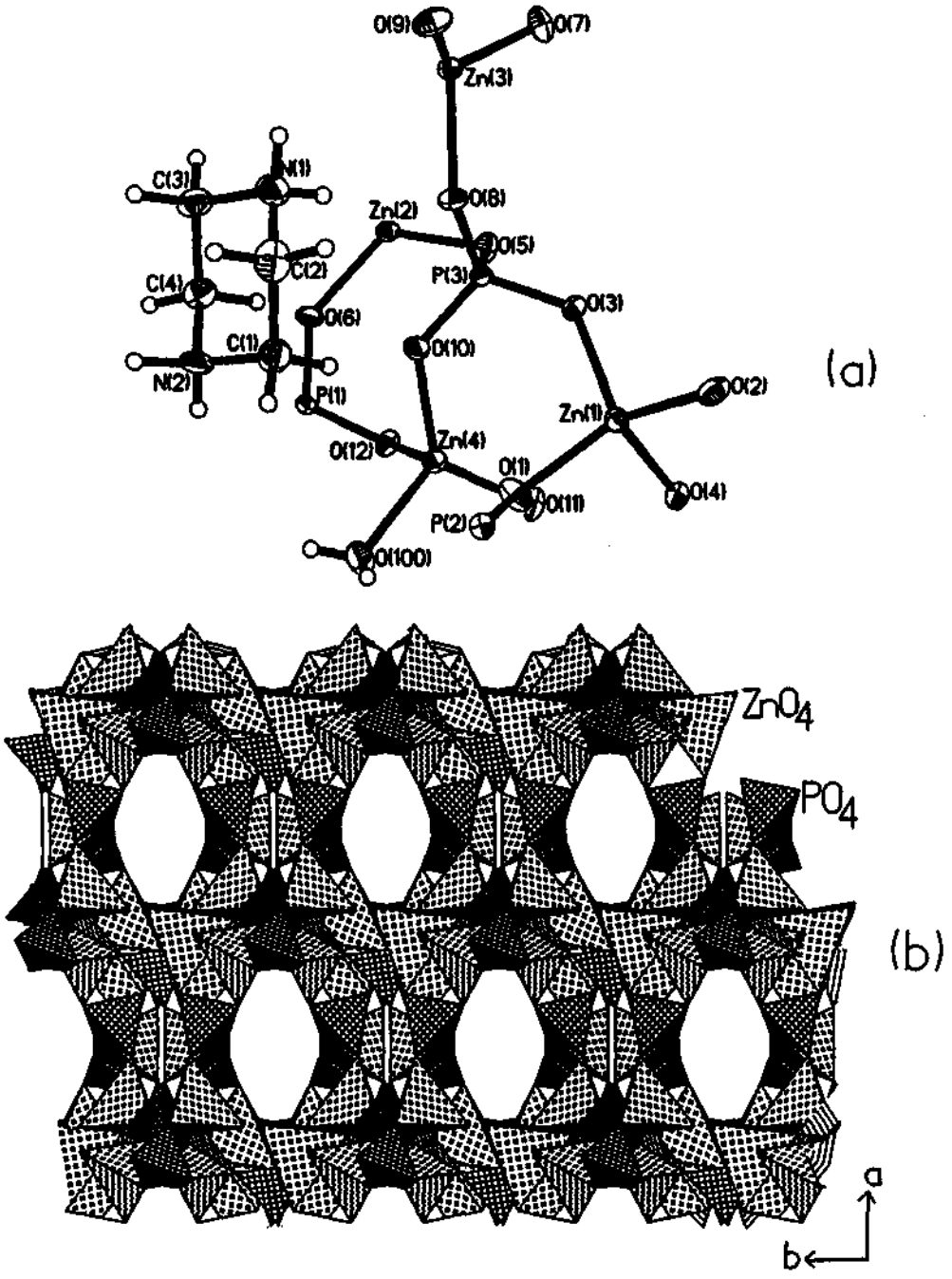

Fig. 1.54. (a) ORTEP plot of **XII**, $[C_4N_2H_{12}][Zn_{3.5}(PO_4)_3(H_2O)]$. Thermal ellipsoids are given at 50% probability. (b) Polyhedral view of **XII**, $[C_4N_2H_{12}][Zn_{3.5}(PO_4)_3(H_2O)]$ along the *[001]* direction showing the 8-membered channels.

Table 1.47 Atomic coordinates [x 10^4] and equivalent isotropic displacement parameters [$Å^2$ x 10^3] for **XII.**

Atom	x	y	z	U(eq)
Zn(1)	3015(1)	1552(1)	4262(1)	13(1)
Zn(2)	5000	3300(1)	2500	14(1)
Zn(3)	6489(1)	3498(1)	4273(1)	13(1)
Zn(4)	2640(1)	3824(1)	3045(1)	16(1)
P(1)	3191(1)	5107(1)	1893(1)	11(1)
P(2)	2320(1)	4904(1)	4559(1)	12(1)
P(3)	4483(1)	2891(1)	3670(1)	12(1)
O(1)	2439(2)	3612(3)	4103(1)	20(1)
O(2)	3289(1)	765(3)	5075(1)	23(1)
O(3)	4099(1)	1585(3)	4015(1)	16(1)
O(4)	2135(1)	-57(3)	3810(1)	15(1)
O(5)	4748(2)	2030(3)	3151(1)	19(1)
O(6)	4149(1)	4840(3)	2053(1)	20(1)
O(7)	6892(2)	1341(3)	4180(1)	21(1)
O(8)	5255(1)	3715(3)	4099(1)	17(1)
O(9)	6821(1)	4640(3)	5032(1)	22(1)
O(10)	3814(1)	4212(3)	3438(1)	17(1)
O(11)	2056(2)	1775(3)	2928(1)	20(1)
O(12)	2726(1)	3792(3)	2172(1)	17(1)
O(100)	1828(2)	5642(3)	3025(1)	23(1)
N(1)	5474(2)	7174(4)	4155(2)	29(1)
N(2)	3911(2)	8548(4)	3522(2)	22(1)
C(1)	3950(3)	7597(5)	4073(2)	25(1)
C(2)	4830(3)	7707(5)	4484(2)	30(1)
C(3)	5426(2)	8158(5)	3602(2)	25(1)
C(4)	4549(2)	8003(5)	3193(2)	24(1)

Table 1.48. Bond distances (Å) and angles (°) for **XII**.

Moiety	Distance (Å)	Moiety	Angle (°)
Zn(1) - O(2)	1.928(2)	$O(5)^{\#1}$ – Zn(2) – O(6)	101.21(9)
Zn(1) - O(1)	1.930(2)	O(5) – Zn(2) – O(6)	120.04(9)
Zn(1) - O(3)	1.962(2)	$O(5)^{\#1}$ – Zn(2) – $O(6)^{\#1}$	120.04(9)
Zn(1) - O(4)	2.036(2)	O(5) – Zn(2) – $O(6)^{\#1}$	101.21(9)
Zn(2) - $O(5)^{\#1}$	1.950(2)	O(6) – Zn(2) – $O(6)^{\#1}$	99.50(14)
Zn(2) - O(5)	1.950(2)	O(7) – Zn(3) – O(8)	114.77(10)
Zn(2) - O(6)	1.968(2)	O(7) – Zn(3) – O(9)	121.56(10)
Zn(2) - $O(6)^{\#1}$	1.968(2)	O(8) – Zn(3) – O(9)	100.71(10)
Zn(3) - O(7)	1.925(2)	O(7) – Zn(3) – $O(4)^{\#2}$	104.70(9)
Zn(3) - O(8)	1.939(2)	O(8) – Zn(3) – $O(4)^{\#2}$	117.65(9)
Zn(3) - O(9)	1.941(2)	O(9) – Zn(3) – $O(4)^{\#2}$	96.94(9)
Zn(3) - $O(4)^{\#2}$	2.045(2)	O(10) – Zn(4) – O(11)	127.40(10)
Zn(4) - O(10)	1.915(2)	O(10) – Zn(4) – O(100)	117.00(11)
Zn(4) - O(11)	1.923(2)	O(11) – Zn(4) – O(100)	111.38(12)
Zn(4) - O(100)	1.985(3)	O(10) – Zn(4) – O(12)	99.97(9)
Zn(4) - O(12)	2.045(2)	O(11) – Zn(4) – O(12)	89.90(9)
P(1) – O(6)	1.513(2)	O(100) – Zn(4) – O(12)	100.79(11)
P(1) – $O(11)^{\#3}$	1.518(2)	O(6) – P(1) – $O(11)^{\#3}$	112.56(14)
P(1) – O(12)	1.544(2)	O(6) – P(1) – O(12)	111.41(13)
P(1) – $O(4)^{\#3}$	1.578(2)	$O(11)^{\#3}$ – P(1) – O(12)	109.85(13)
P(2) – $O(9)^{\#4}$	1.521(2)	O(6) – P(1) – $O(4)^{\#3}$	107.70(12)
P(2) – $O(7)^{\#5}$	1.534(2)	$O(11)^{\#3}$ – P(1) – $O(4)^{\#3}$	108.20(13)
P(2) – $O(2)^{\#6}$	1.540(2)	O(12) – P(1) – $O(4)^{\#3}$	106.88(13)
P(2) – O(1)	1.540(2)	$O(9)^{\#4}$ – P(2) – $O(7)^{\#5}$	112.18(14)
P(3) – O(5)	1.534(2)	$O(9)^{\#4}$ – P(2) – $O(2)^{\#6}$	110.85(13)
P(3) – O(10)	1.535(2)	$O(7)^{\#5}$ – P(2) – $O(2)^{\#6}$	109.28(14)
P(3) – O(8)	1.546(2)	$O(9)^{\#4}$ – P(2) – O(1)	110.34(13)
P(3) – O(3)	1.554(2)	$O(7)^{\#5}$ – P(2) – O(1)	105.12(13)
Moiety	Angle (°)	$O(2)^{\#6}$ – P(2) – O(1)	108.87(14)
O(2) – Zn(1) – O(1)	117.88(10)	O(5) – P(3) – O(10)	111.33(13)
O(2) – Zn(1) – O(3)	105.93(9)	O(5) – P(3) – O(8)	111.66(13)
O(1) – Zn(1) – O(3)	110.72(10)	O(10) – P(3) – O(8)	107.25(13)
O(2) – Zn(1) – O(4)	104.12(9)	O(5) – P(3) – O(3)	107.21(13)
O(1) – Zn(1) – O(4)	103.58(9)	O(10) – P(3) – O(3)	109.75(12)
O(3) – Zn(1) – O(4)	114.78(9)	O(8) – P(3) – O(3)	109.64(13)
$O(5)^{\#1}$ – Zn(2) – O(5)	114.93(14)		

Organic

Moiety	Distance (Å)	Moiety	Angle (°)
N(1) – C(2)	1.492(5)	C(2) – N(1) – C(3)	111.8(3)
N(1) – C(3)	1.493(5)	C(1) – N(2) – C(4)	112.6(3)
N(2) – C(1)	1.480(5)	N(2) – C(1) – C(2)	110.2(3)
N(2) – C(4)	1.486(5)	N(1) – C(2) – C(1)	109.2(3)
C(1) – C(2)	1.504(6)	N(1) – C(3) – C(4)	109.6(3)
C(3) – C(4)	1.502(5)	N(2) – C(4) – C(3)	108.4(3)

Symmetry transformations used to generate equivalent atoms:

#1 -x+1, y, -z+1/2 #2 x+1/2, y+1/2, z #3 –x+1/2, -y+1/2, -z+1/2 #4 -x+1, -y+1, -z+1
#5 x-1/2, y+1/2, z #6 -x+1/2, -y+1/2, -z+1 #7 –x+1/2, y-1/2, -z+1/2 #8 x-1/2, y-1/2, z
#9 x+1/2, y-1/2, z

consisting of 3- and 4-memebred rings connected via the edges (Fig.1.55a). These building units are linked to each other by a 4-membered ring, which is formed by the connection between two 3-membered rings in an *out-of-plane* fashion as shown in Figure 1.55b. Two such units are fused together forming the 8-membered aperture as shown in Figure 1.55c. This type of connectivity gives rise to an 8-membered elliptical channel of dimensions 4.8 x 8.6 Å, along the [001] direction (Figure 1.55b). Along the [011] direction, the connectivity leads to another 8-membered channel. The piperazinium cations sit in the middle of these channels.

$[C_4N_2H_{12}]_{0.5}[Zn(HPO_4)(H_2PO_4)]$, XIII : The structure of **XIII**, is based on a three dimensional network involving ZnO_4, $PO_3(OH)$ and $PO_2(OH)_2$ tetrahedra. The asymmetric unit of **XIII** consists of 12 independent non-hydrogen atoms (Fig.1.56a, atomic coordinates Table 1.49). The Zn – O distances are in the range 1.915(2) - 1.973(2) Å (av. 1.938(2) Å) and the O – Zn – O bond angles are in the range 104.0(1) -113.5(1)° (av. 109.4(1)°) which are typical of zinc in tetrahedral environment. All the zinc atoms are connected to P atoms via oxygen atoms. The P – O distances are in the range 1.492(2) - 1.574(2) Å (av. 1.534(2) Å), and the O – P – O bond angles are in the range 104.7(1) – 114.1(1)° (av. 109.4(1)°) (Table 1.50). There are 0.5 $[C_4N_2H_{12}]^{2+}$ ions per framework formula unit. The connectivity between ZnO_4, $PO_3(OH)$ and $PO_2(OH)_2$ moieties gives rise to a 3-dimensional framework. The connectivity between the tetrahedra form 4-membered rings, which are connected by their corners. The complex three-dimensional framework of **XIII**, can be considered to be built-up from smaller fragments. Thus, the structure of **XIII** possesses infinite corner-shared linear chains, comprising of 4-memberd rings, running in two different directions (Fig.1.56b). At the junction where such building units meet, the connectivity is such that one goes in the downward direction of the plane, the other goes upward creating the three-dimensional connectivity (Fig.1.56c). Four such junctions make a 16-membered *clover* like aperture, with each point where such a junction occurs form a terminal of a *clover* (Fig.1.57). The –OH groups of the HPO_4 unit

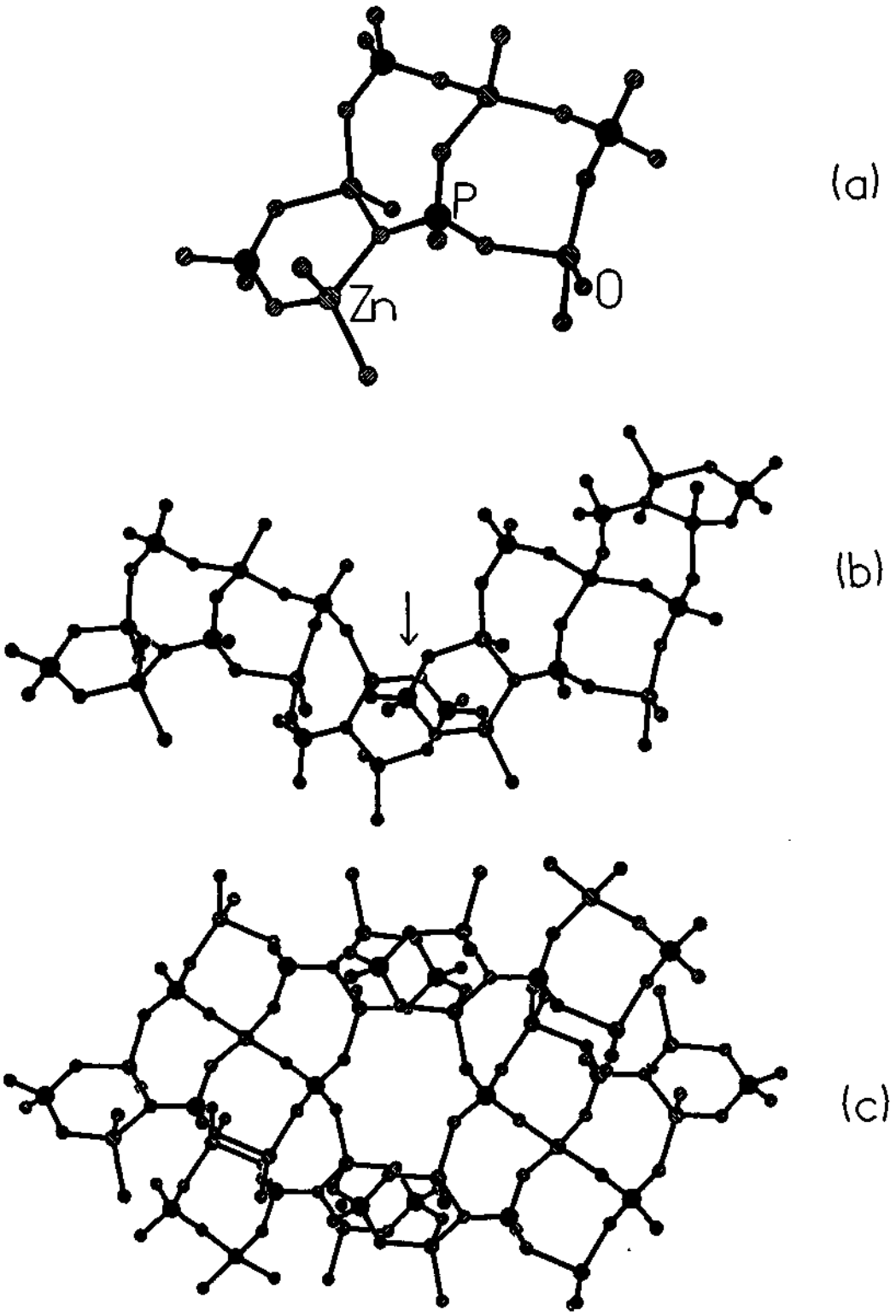

Fig. 1.55. (a) The basic building fragment in **XII**, showing the nearest environment for the phosphorus atom (see text). (b)Linkages between the basic building fragment in **XII**. The arrow indicates the *out-of-plane* 4-membered ring. (c) Evolution of the three-dimensional structure from the basic building fragment in **XII**.

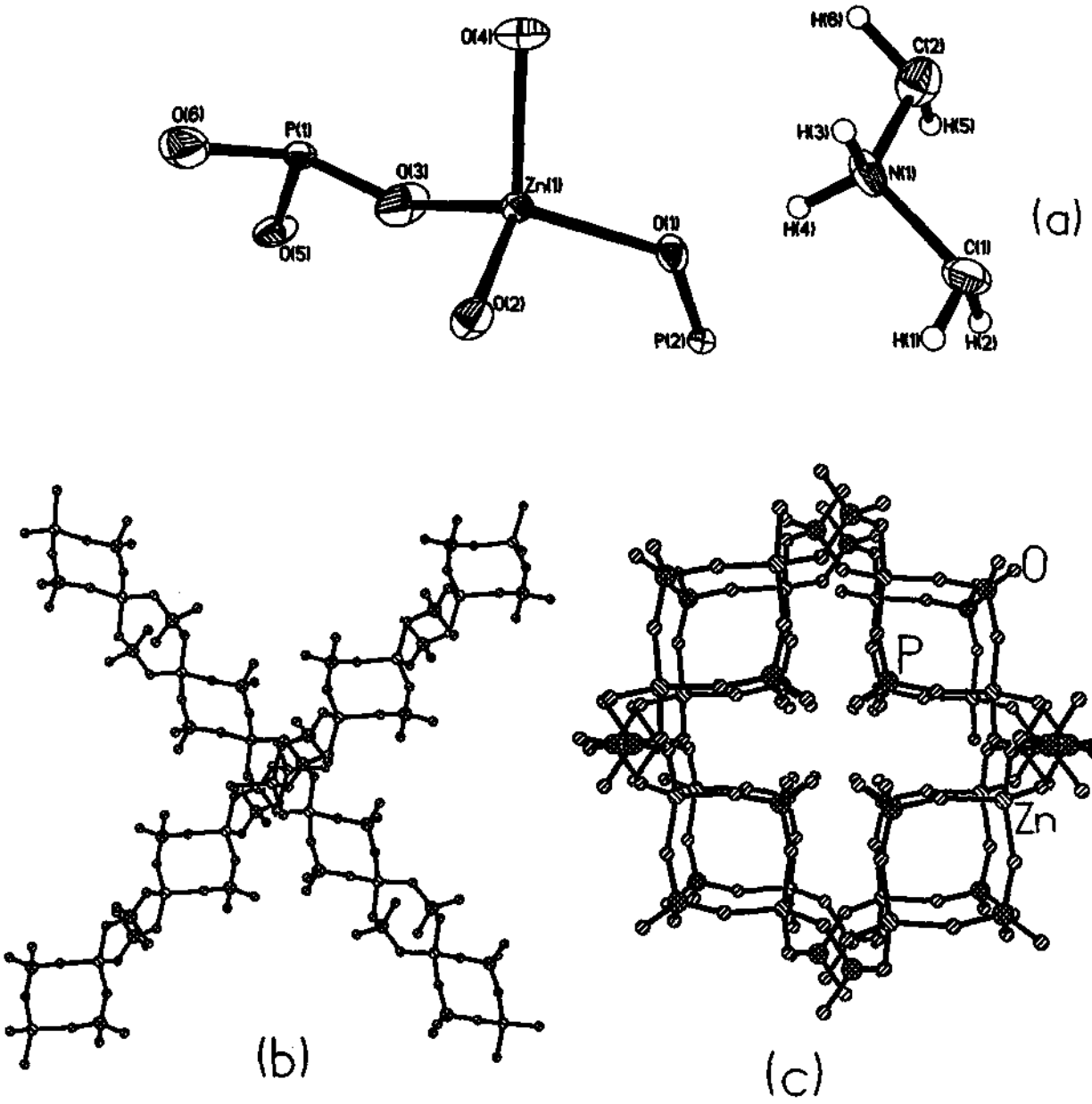

Fig. 1.56. (a) ORTEP plot of **XIII**, $[C_4N_2H_{12}]_{0.5}[Zn(HPO_4)(H_2PO_4)]$. Thermal ellipsoids are given at 50% probability. (b) Cross-linking of corner-shared 4-membered chains. (c) Structure of a single 16-membered clover-like channel in **XIII**, formed by the linkages between the corner shared chains.

Table 1.49. Atomic coordinates [x 10^4] and equivalent isotropic displacement parameters [$Å^2$ x 10^3] for **XIII**

Atom	x	y	z	U(eq)
Zn(1)	3794(1)	6217(1)	393(1)	13(1)
P(1)	1415(1)	6293(1)	-982(1)	14(1)
P(2)	5000	5409(1)	-2500	11(1)
O(1)	4868(2)	6119(2)	-1023(3)	17(1)
O(2)	4055(2)	5253(2)	2176(3)	20(1)
O(3)	2504(2)	6043(2)	-756(4)	34(1)
O(4)	3809(2)	7589(2)	1462(3)	22(1)
O(5)	918(2)	5557(2)	-2291(3)	24(1)
O(6)	889(2)	6131(2)	639(4)	36(1)
N(1)	6529(2)	7080(2)	280(3)	21(1)
C(1)	7444(2)	6410(3)	373(4)	24(1)
C(2)	6629(3)	7967(3)	-843(4)	26(1)

Table 1.50. Bond lengths (Å) and angles (°) for **XIII**.

Moiety	Distance (Å)	Moiety	Angle (°)
Zn(1) - O(3)	1.915(2)	O(2) – Zn(1) – O(4)	104.04(9)
Zn(1) - O(1)	1.931(2)	O(3) – P(1) – O(4)$^{\#1}$	114.05(14)
Zn(1) - O(2)	1.931(2)	O(3) – P(1) – O(5)	108.45(14)
Zn(1) - O(4)	1.973(2)	O(4)$^{\#1}$ – P(1) – O(5)	109.66(13)
P(1) – O(3)	1.492(2)	O(3) – P(1) – O(6)	111.6(2)
P(1) – O(4)$^{\#1}$	1.516(2)	O(4)$^{\#1}$ – P(1) – O(6)	104.66(13)
P(1) – O(5)	1.543(2)	O(5) – P(1) – O(6)	108.2(2)
P(1) – O(6)	1.574(3)	O(2)$^{\#2}$ – P(2) – O(2)$^{\#3}$	112.5(2)
P(2) – O(2)$^{\#2}$	1.532(2)	O(2)$^{\#2}$ – P(2) – O(1)	108.58(11)
P(2) – O(2)$^{\#3}$	1.532(2)	O(2)$^{\#3}$ – P(2) – O(1)	109.88(11)
P(2) – O(1)	1.542(2)	O(2)$^{\#2}$ – P(2) – O(1)$^{\#4}$	109.88(11)
P(2) – O(1)$^{\#4}$	1.542(2)	O(2)$^{\#3}$ – P(2) – O(1)$^{\#4}$	108.58(11)
Moiety	Angle (°)	O(1) – P(2) – O(1)$^{\#4}$	107.3(2)
O(3) – Zn(1) – O(1)	112.55(11)	P(2) – O(1) – Zn(1)	130.88(13)
O(3) – Zn(1) – O(2)	113.54(11)	P(2)$^{\#3}$ – O(2) – Zn(1)	125.74(13)
O(1) – Zn(1) – O(2)	108.63(9)	P(1) – O(3) – Zn(1)	150.7(2)
O(3) – Zn(1) – O(4)	107.41(10)	P(1)$^{\#1}$ – O(4) – Zn(1)	137.7(2)
O(1) – Zn(1) – O(4)	110.32(9)		

Organic Moiety

Moiety	Distance (Å)	Moiety	Angle (°)
N(1) – C(1)	1.486(6)	C(1) – N(1) – C(4)	111.0(3)
N(1) – C(4)	1.495(6)	C(3) – N(2) – C(2)	111.5(4)
N(2) – C(3)	1.492(6)	N(1) – C(1) – C(2)	110.8(4)
N(2) – C(2)	1.493(6)	N(2) – C(2) – C(1)	111.3(4)
C(1) – C(2)	1.525(7)	N(2) – C(3) – C(4)	110.7(4)
C(3) – C(4)	1.511(7)	N(1) – C(4) – C(3)	110.3(4)
N(3) – C(5)	1.486(6)	C(5) – N(3) – C(6)	110.8(4)
N(3) – C(6)	1.489(6)	N(3) – C(5) – C(6)$^{\#4}$	110.2(4)
C(5) – C(6)$^{\#4}$	1.507(7)	N(3) – C(6) – C(5)$^{\#4}$	109.1(4)

Symmetry transformations used to generate equivalent atoms:

#1 x, -y+3/2, z-1/2 #2 x, -y+3/2, z+1/2 #3 –x+1, -y+1, -z #4 -x, -y+1, -z+1

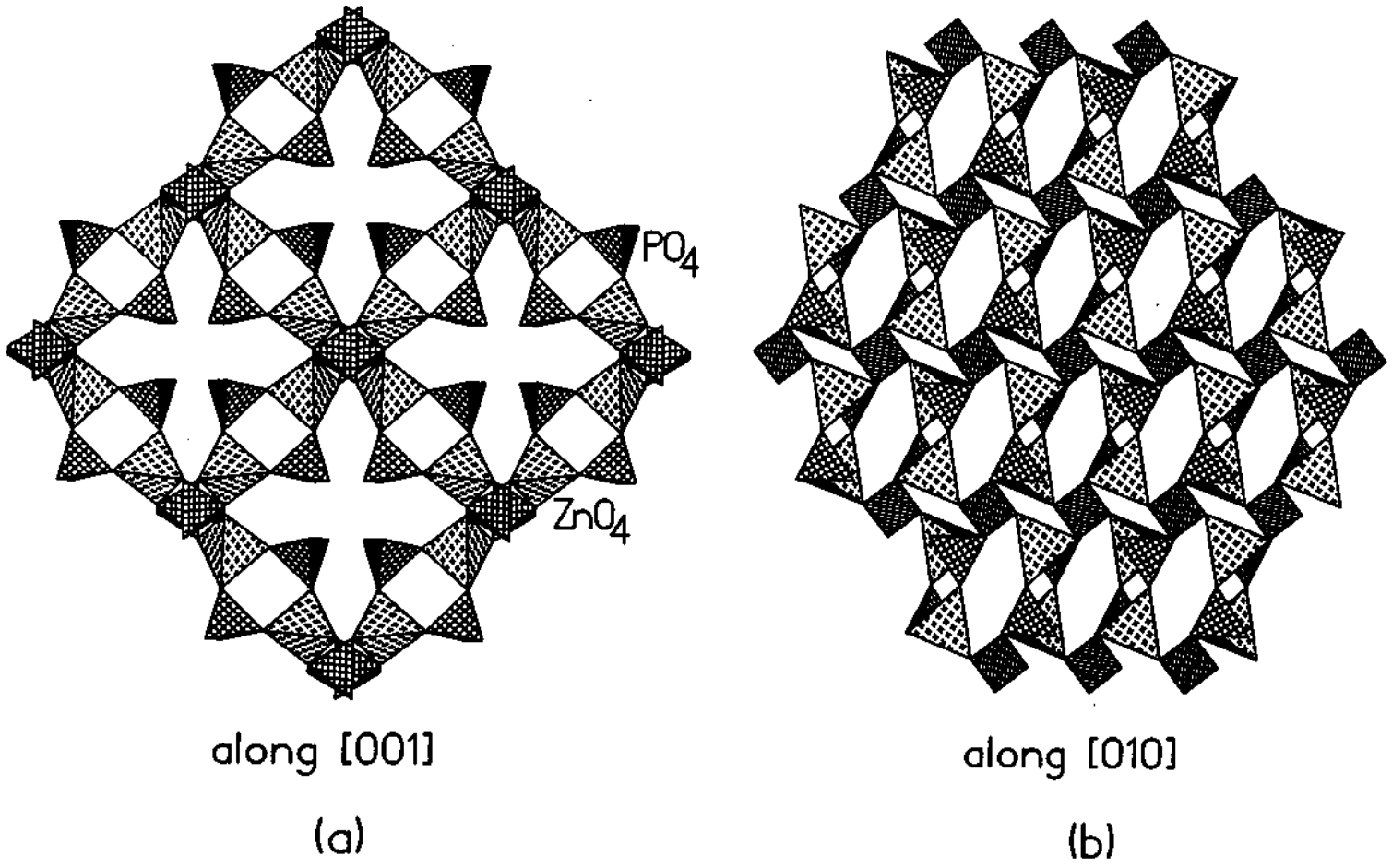

Fig. 1.57 (a) Polyhedral view of **XIII** al;ong the *c* axis showing the 'clover' like 16–membered channels. Amine molecules are omitted for clarity. (b) Polyhedral view of **XIII** al;ong the *b* axis showing the 8–membered channels.

protrude into this aperture. These apertures (channels) are reminiscent of the gallophosphate- 'cloverite', which has similar 20-membered channels wherein fluoride ions protrude into the channel.[11] The piperazinium cations occupy the four-membered rings.

The open-framework Zn phosphates **XIV** and **XV** had the compositions, $[C_4N_2H_{11}][Zn_2(PO_4)(H_2PO_4)_2]$ and $[C_4N_2H_{12}][Zn_2(H_2O)(PO_4)(H_2PO_4)_2]_2H_2O$ respectively, and, were identical to those reported by Feng et al.[239] We shall, therefore, not elaborate on the structures of these two compounds here. In addition to these the reaction of imidazole phosphate with Zn^{II} ions has yielded a three-dimensional zinc phosphate, **XVI.**

$[C_3N_2H_6][Zn_4(OH)(PO_4)_3]$, XVI : The framework structure of **XVI,** consists of a three-dimensionally extended network built up from ZnO_4 and PO_4 moieties, forming a unidimensional channel bound by 8-T atoms (T = Zn and P). In addition to the presence of the usually observed Zn – O – P bonds, **XVI** contains Zn – O – Zn linkages as well. These linkages form the channels, which are occupied by extra-framework diprotonated imidazolium cations. The asymmetric unit, presented in Fig.1.58a, consists of 20 framework atoms and 5 atoms of the guest species respectively. The atomic coordinates are listed in Table 1.51. There are four crystallographically independent zinc and three phosphorus atoms. Of the 13 oxygens of the asymmetric unit, three are three-coordinated [O(2), O(3) and O(4)] leading to Zn – O – Zn linkages.

The four zinc atoms in **XVI,** are all tetrahedrally coordinated by their O atom neighbors with average zinc – oxygen bond distances of 1.963 for Zn(1), 1.951 for Zn(2), 1.946 for Zn(3) and 1.942 Å for Zn(4) (Table 1.52). The Zn atoms, except Zn(4), make four Zn – O – P bonds to three distinct P atom neighbors and an average Zn – O – P bond angle of 129.3° resulting from a fairly wide spread of angles (Table 1.53). The Zn(4), on the other hand, has one terminal linkage with a Zn – O distance of 2.020 Å (Table 1.52). While, Zn(1) makes two Zn – O – Zn linkages, Zn(2) and Zn(3) make one such bonding.

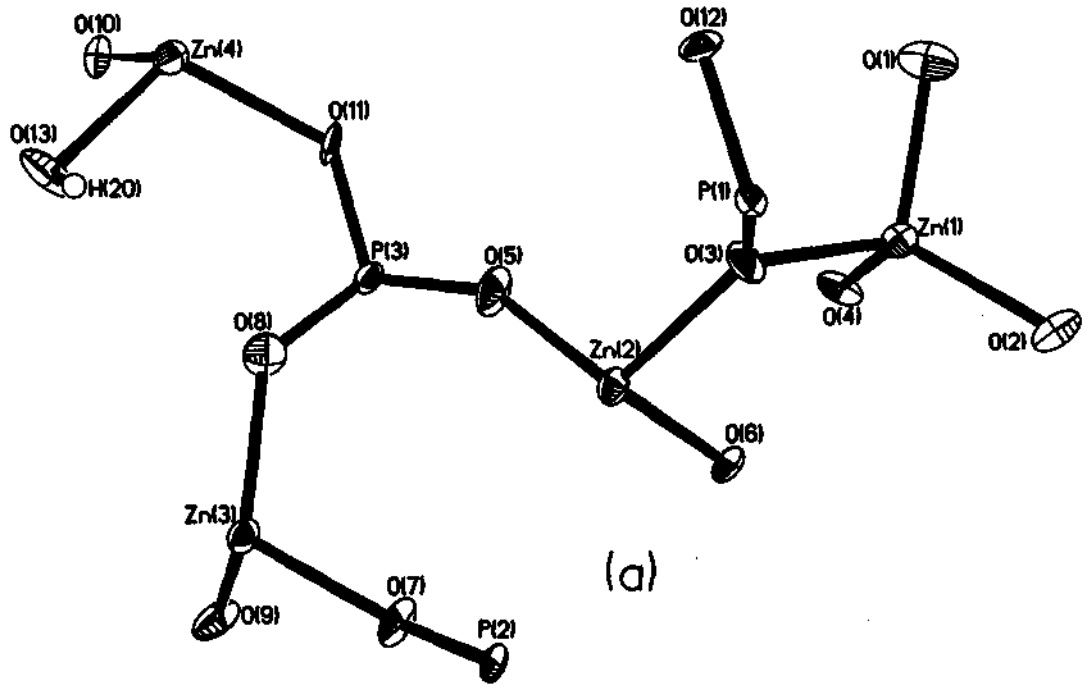

(a)

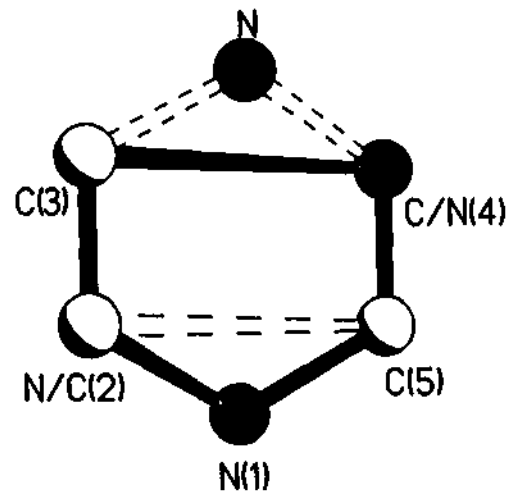

(b)

Fig. 1.58. (a) ORTEP plot of the framework of **XVI**, $[C_3N_2H_6][Zn_4(OH)(PO_4)_3]$. The thermal ellipsoids are given at 50% probability. (b) The structure showing the disorder in the amine molecule (dotted lines).

Table 1.51. Atomic Coordinates [x 10^4] and equivalent isotropic displacement parameters [$Å^2$ x 10^3] for **XVI**, $[C_3N_2H_6][Zn_4(OH)[PO_4)_3]$.

Atom	x	y	z	U(eq)[#]
Zn(1)	615(4)	7650(1)	6988(1)	13(1)
Zn(2)	5673(4)	8916(1)	7434(1)	13(1)
Zn(3)	10752(4)	10951(1)	8037(1)	14(1)
Zn(4)	6095(4)	12252(1)	5682(1)	15(1)
P(1)	5393(9)	7625(3)	6056(3)	12(1)
P(2)	*10733(9)*	*8857(3)*	*8385(3)*	*10(1)*
P(3)	5607(9)	10998(3)	7060(3)	13(1)
O(1)	-1752(22)	7781(9)	6167(7)	23(3)
O(2)	1025(21)	6439(8)	7327(6)	15(3)
O(3)	4012(23)	8087(8)	6711(7)	20(3)
O(4)	-829(22)	8515(8)	7680(7)	16(3)
O(5)	4962(27)	10039(8)	7090(7)	25(3)
O(6)	3522(23)	8628(8)	8270(7)	18(3)
O(7)	10280(24)	9827(7)	8451(7)	20(3)
O(8)	8409(23)	11193(8)	7216(7)	21(3)
O(9)	10322(26)	11686(8)	8922(7)	24(3)
O(10)	5159(22)	13417(7)	5918(6)	13(3)
O(11)	4760(24)	11358(8)	6301(7)	20(3)
O(12)	4511(23)	8058(8)	5338(6)	15(3)
O(13)	9882(23)	12254(8)	5933(8)	27(3)

[#] U(eq) is defined as one third of the trace of the orthogonalised U_{ij} tensor.

Table 1.52. Selected bond lengths in **XVI**, $[C_3N_2H_6][Zn_4(OH)[PO_4)_3]$.

Moiety	Distance (Å)	Moiety	Distance (Å)
Zn(1) – O(1)	1.907(12)	Zn(4) – O(11)	1.919(12)
Zn(1) – O(2)	1.976(12)	Zn(4) – O(13)	2.020(12)
Zn(1) – O(3)	1.980(12)	P(1) – O(9)$^{\#4}$	1.499(13)
Zn(1) – O(4)	1.990(11)	P(1) – O(12)	1.512(12)
Zn(2) – O(5)	1.874(12)	P(1) – O(1)$^{\#1}$	1.521(13)
Zn(2) – O(6)	1.957(12)	P(1) – O(3)	1.572(13)
Zn(2) – O(4)$^{\#1}$	1.970(12)	P(2) – O(10)$^{\#4}$	1.510(12)
Zn(2) – O(3)	2.002(12)	P(2) – O(7)	1.520(12)
Zn(3) – O(7)	1.907(12)	P(2) – O(6)$^{\#1}$	1.523(13)
Zn(3) – O(8)	1.925(13)	P(2) – O(4)$^{\#1}$	1.579(12)
Zn(3) – O(9)	1.972(13)	P(3) – O(8)	1.515(13)
Zn(3) – O(2)$^{\#2}$	1.978(11)	P(3) – O(5)	1.521(13)
Zn(4) – O(12)$^{\#3}$	1.912(12)	P(3) – O(11)	1.527(13)
Zn(4) – O(10)	1.916(11)	P(3) – O(2)$^{\#5}$	1.570(12)

#1 x+1, y, z; #2 –x+3/2, y+1/2, -z+3/2; #3 –x+1, -y+2, -z+1; #4 –x+3/2, y-1/2, -z+3/2;

#5 –x+1/2, y+1/2

Table 1.53. Selected bond angles in **XVI**, $[C_3N_2H_6][Zn_4(OH)[PO_4)_3]$.

Moiety	Angle (°)	Moiety	Angle (°)
O(1) – Zn(1) – O(2)	113.6(6)	O(11) – Zn(4) – O(13)	104.1(6)
O(1) – Zn(1) – O(3)	109.7(5)	$O(9)^{\#4}$ – P(1) – O(12)	112.4(7)
O(2) – Zn(1) – O(3)	108.0(5)	$O(9)^{\#4}$ – P(1) – $O(1)^{\#1}$	113.3(8)
O(1) – Zn(1) – O(4)	99.3(5)	O(12) – P(1) – $O(1)^{\#1}$	108.4(7)
O(2) – Zn(1) – O(4)	118.8(5)	$O(9)^{\#4}$ – P(1) – O(3)	107.3(7)
O(3) – Zn(1) – O(4)	106.9(5)	O(12)– P(1) – O(3)	107.7(7)
O(5) – Zn(2) – O(6)	110.5(5)	$O(1)^{\#1}$ – P(1) – O(3)	107.6(7)
O(5) – Zn(2) – $O(4)^{\#1}$	122.6(6)	$O(10)^{\#4}$ – P(2) – O(7)	109.0(7)
O(6) – Zn(2) – $O(4)^{\#1}$	108.0(5)	$O(10)^{\#4}$ – P(2) – $O(6)^{\#1}$	109.3(7)
O(5) – Zn(2) – O(3)	107.4(6)	O(7) – P(2) – $O(6)^{\#1}$	113.1(7)
O(6) – Zn(2) – O(3)	96.0(5)	$O(10)^{\#4}$ – P(2) – $O(4)^{\#1}$	110.4(7)
$O(4)^{\#1}$ – Zn(2) – O(3)	109.1(5)	O(7) – P(2) – $O(4)^{\#1}$	108.3(7)
O(7) – Zn(3) – O(8)	112.8(5)	$O(6)^{\#1}$ – P(2) – $O(4)^{\#1}$	106.7(7)
O(7) – Zn(3) – O(9)	100.9(5)	O(8) – P(3) – O(5)	113.7(8)
O(8) – Zn(3) – O(9)	114.9(5)	O(8) – P(3) – O(11)	110.2(7)
O(7) – Zn(3) – $O(2)^{\#2}$	126.7(5)	O(5)– P(3) – O(11)	109.0(7)
O(8) – Zn(3) – $O(2)^{\#2}$	101.7(5)	O(8) – P(3) – $O(2)^{\#5}$	109.2(7)
O(9) – Zn(3) – $O(2)^{\#2}$	99.7(5)	O(5) – P(3) – $O(2)^{\#5}$	105.8(7)
$O(12)^{\#3}$ – Zn(4) – O(10)	114.4(5)	O(11) – P(3) – $O(2)^{\#5}$	108.7(7)
$O(12)^{\#3}$ – Zn(4) – O(11)	108.9(5)	Zn(1) – O(2) – $Zn(3)^{\#4}$	110.1(5)
O(10) – Zn(4) – O(11)	116.5(5)	Zn(1) – O(3) – Zn(2)	115.5(6)
$O(12)^{\#3}$ – Zn(4) – O(13)	110.3(5)	$Zn(2)^{\#6}$ – O(4) – Zn(1)	116.0(6)
O(10)– Zn(4) – O(13)	101.8(5)		

#1 x+1, y, z; #2 –x+3/2, y+1/2, -z+3/2; #3 –x+1, -y+2, -z+1; #4 –x+3/2, y-1/2, -z+3/2;

#5 –x+1/2, y+1/2

These linkages result in infinite one-dimensional Zn – O – Zn units. To our knowledge, this is the first instance of such linkages in a three-dimensional open-framework zinc phosphate. The O – Zn – O bond angles are in the range 96.0 – 126.7° (ave. 109.3°). The structural parameters of **XVI**, are in agreement with the results of previous structure determinations on similar compounds.[79-95] All the P atoms, make four P – O – Zn bonds. The P – O bond distances are in the range 1.499 – 1.572 Å [$(P(1) - O)_{av.}$ = 1.526, $(P(2) - O)_{av.}$ = 1.533, $(P(3) - O)_{av.}$ = 1.533 Å] and the O – P – O angles are the range 105.8 – 118.1° [$(O - P(1) - O)_{av.}$ = 109.5, $(O - P(2) - O)_{av.}$ = 109.5, $(O - P(3) - O)_{av.}$ = 109.5°]. These values agree with the earlier literature reports on open-framework phosphates.[49,50,73,79-95] Clearly, both the ZnO_4 and PO_4 tetrahedra are more or less regular. However, the longest bond distances as well as the largest bond angles are observed for bonding involving the trigonally coordinated oxygen atoms. Assuming the valences of Zn, P and O to be +2, +5 and –2 respectively, the framework stoichiometry of $Zn_4(PO_4)_3$ creates a framework charge of -1. If both the nitrogen atoms of imidazole are protonated, we still require an additional negative charge consistent with the hydrogen positions observed in the difference Fourier maps, associated with the terminal Zn – O unit. Thus, the Zn(4) – O(13) distance of 2.02Å corresponds to the Zn – OH moiety. The attachment of a proton with the terminal oxygen of the Zn atom is also in agreement with bond-valence sum calculations.[244]

The framework structure of **XVI** is built up from ZnO_4 and PO_4 units sharing vertices forming 3- and 4-membered rings. Along the *a*-axis, the 3- and 4-membered rings are so arranged that they form 3443443 repeat unit chains as shown in Fig.1.59a. The chains are, of course, connected in a extended way forming a layer-like arrangement. The layers are formed by Zn(1), Zn(2), Zn(3) connected via oxygens with P(1), P(2) and P(3) as shown in Fig.1.59b. These layers are joined by $Zn(4)O_4$ units completing the 3-dimensional architecture. Along the *c* axis, the connectivity between the Zn(1) and Zn(2) form an infinite one-dimensional chain with Zn(3) coming off the chain like a branch as shown in

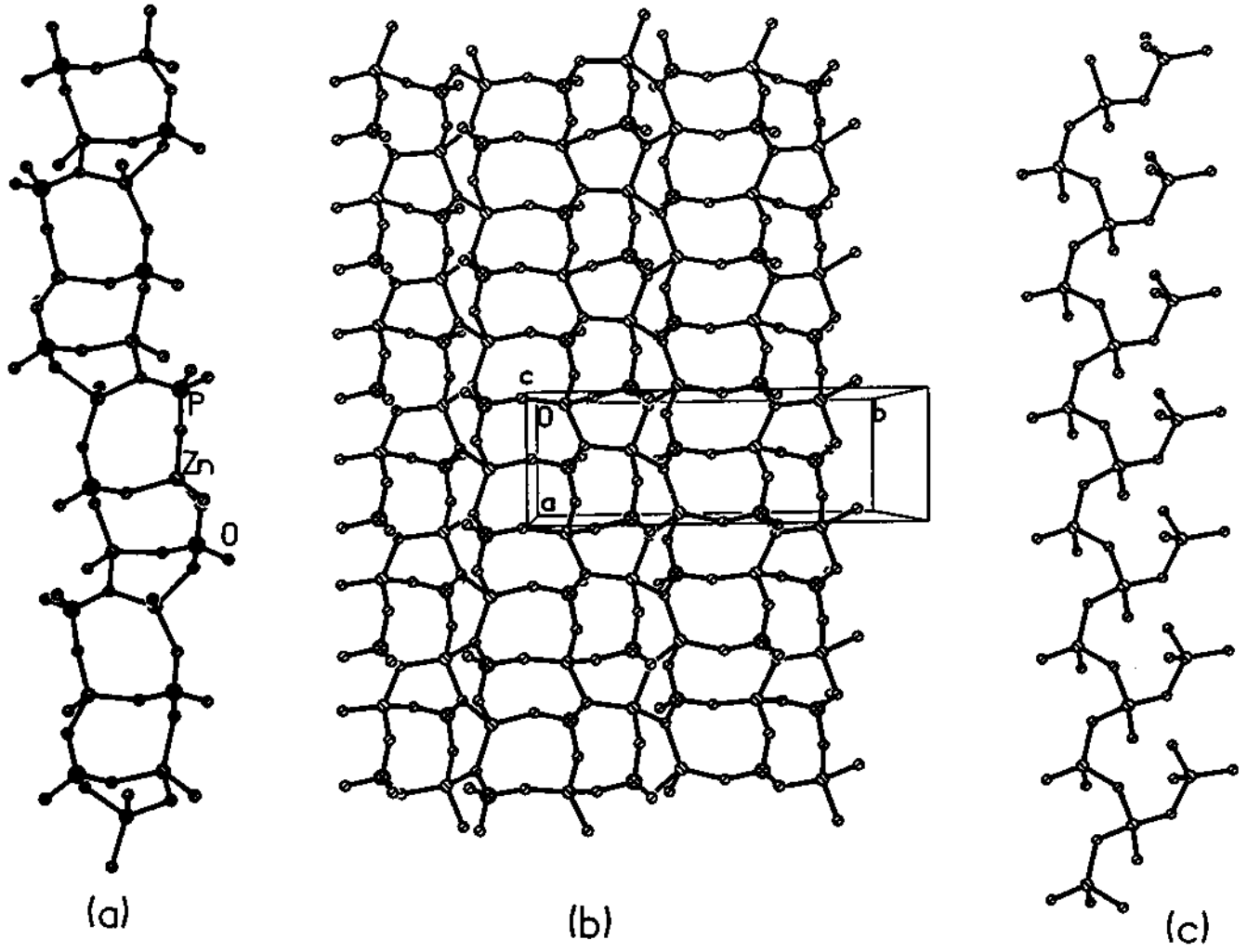

Fig. 1.59 (a) 3443443 ring arrangement in **XVI** . (b) layer–like arrangement formed by the linkages between Zn(1), Zn(2), Zn(3), P(1), P(2) and P(3) (see text). These layers are connected by $Zn(4)O_4$ tetrahedra. (c) one–dimensional infinite chain Zn – O – Zn– chains. Note that Zn(3) atoms are branching from the main chain.

Fig.1.59c. The connectivity between the chains via phosphates and $Zn(4)O_4$ tetrahedra form a one-dimensional channels bound by 8-T atoms (T = Zn and P) as shown in Fig.1.60. The structure directing amine, diprotonated imidazolium, sits in the middle of these channels. The amine in this structure is disordered and similar disorder involving imidazolium ions has been noticed earlier in an open-framework aluminum phosphate.[264]

The reaction of imidazole-phosphate with Zn(II) ions forms a new three-dimensional structure. The M:P ratio in **XVI** is 4:3, indicating the likely chance of finding M – O – M linkages. It is also clear that there are no P – O – P linkages The connectivity between the tetrahedra leads to one-dimensional channels. The structure-directing amine molecules in both the compounds occupy the channels and interact with the framework through hydrogen bond interactions. In **XVI**, the connectivity between the ZnO_4 and PO_4 units gives rise to Zn – O – Zn linkages involving trigonal coordination of oxygen atoms. The previous observation of Zn – O – Zn linkages are always accompanied by three-coordinated bridging oxygen atoms and the third coordination is to a phosphorus atom. Similar structural features have also been observed in **XVI**. The trigonal coordination of the oxygens in the Zn – O – Zn – bridge is apparently an electrostatic valence requirement of bridging oxygen atoms. The number of T atoms per 1000 $Å^3$ is 19.3 for **XVI** and indicates a less-open structure and this may result from large number of trigonal coordinated oxygen atoms (23%) which tend to form more condensed structure rather than an open one. It is likely that protonated imidazolium cations, which are planar, may occupy lesser space, and result in smaller cavity, hence higher framework density.

4.5.2. Cobalt phosphates by the amine phosphate route

Unlike in the reaction with Zn(II), the reaction of PIPP with Co(II) did not yield a linear chain structure. We, however, obtained two relatively simple architectures, **XVII** and **XVIII**, derived from the linear chain structure. Whilst, **XVII** can simply result from the fusion of two linear chains via a three-

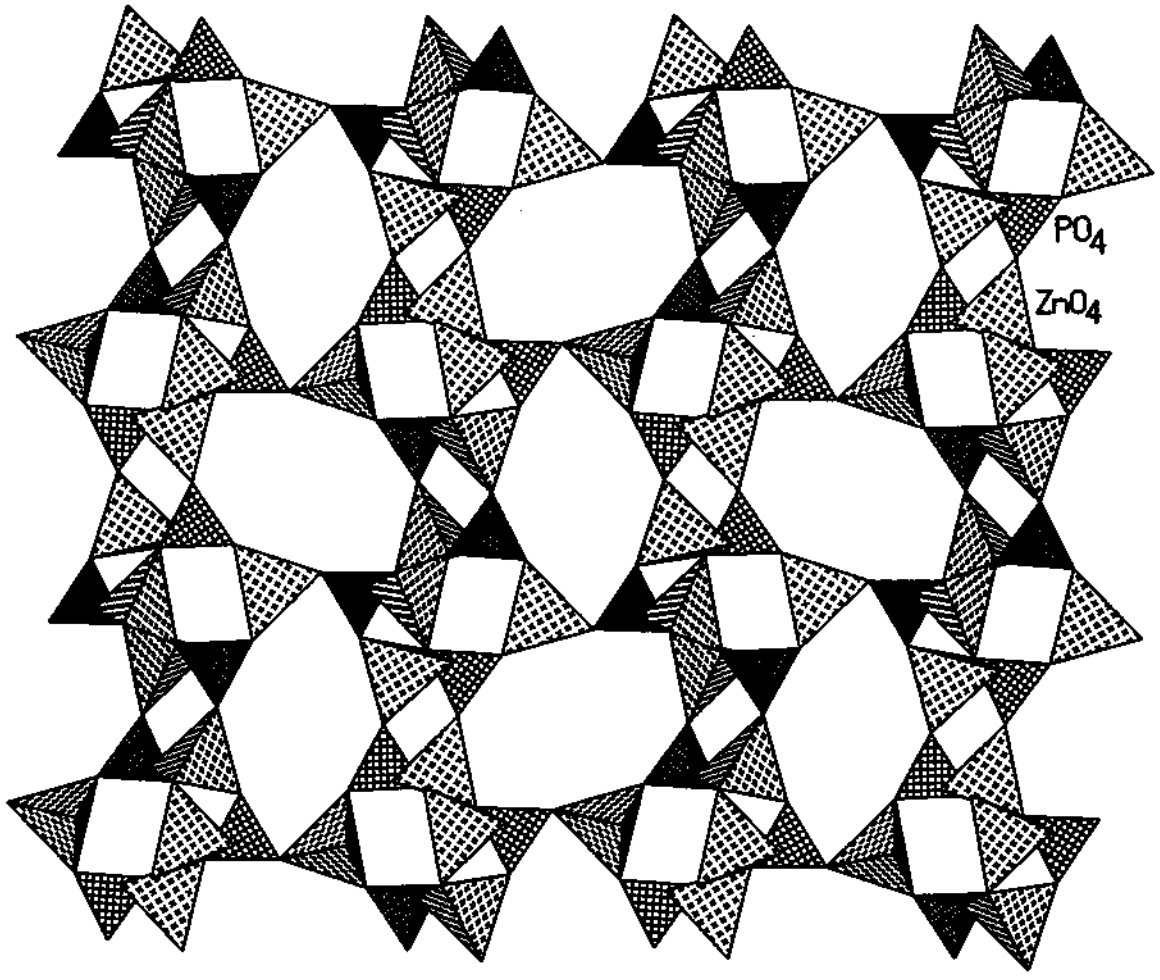

Fig. 1.60 Polyhedral view of the structure of **XVI** along *a* axis showing 8–membered channels.

coordinated oxygen, **XVIII** can be obtained from the fusion of two ladders. These new Co(II) phosphates are valuable addition to the handful of such structures known in cobalt phosphates family.[49,50,73]

$[C_4N_2H_{12}]_{1.5}[Co_2(HPO_4)_2(PO_4)(H_2O)]$, XVII : The structure of **XVII**, is based on a network of CoO_4, $PO_3(OH)$ and PO_4 tetrahedra forming a strip-like arrangement. The asymmetric unit contains 27 independent non-hydrogen atoms (Fig.1.61a and atomic coordinates Table 1.54): three phosphate groups are linked via oxygens to two cobalt atoms to form the building block of the framework. All the P-O distances are in the range 1.506(3)-1.597(3)Å (av. 1.537(3)Å) and the bond angles are in the range 105.3(2)–112.9(2)° (av. 109.4(2)°) (Table 1.55). Bond valence sum calculations[244] indicate the bond distances of 1.597Å [P(1) - O(9)] and [P(2) - O(12)] are formally OH groups. The bond distance of 1.578(3) Å [P(3) - O(4)] is associated with the 3-coordinated oxygen atom. The observation of 3-coordinated oxygen atoms are common in open-framework zinc phosphates, but this is the first instance where 3-coordinated oxygen atoms are formed in a pure open-framework cobalt phosphate synthesized in the presence of organic amines. All the cobalt atoms are four coordinated with respect to oxygen with Co-O distances in the range 1.922(3) – 2.003(3) Å (av. 1.965(3) Å) and the O – Co – O bond angles are in the range 98.3(2) –116.7(2)° (av. 109.2(2)°) (Table 1.55). These values are typical of tetrahedral cobalt. The deep blue color of the product is consistent with tetrahedral Co(II). The entire framework structure consists of infinite *strip-like* arrangement along the c-axis (Fig.1.61b). Each individual *strip* consists of a linkage between 3- and 4-membered rings. One way to describe the structure is to consider the *strip* as a one-dimensional 3-membered ring chain, along *c* axis, that is connected by 4-membered rings edgewise on either side. A better way would be to consider two corner-shared one-dimensional linear chains fused together via a 3-coordinated oxygen atom to form the strip-like arrangement. To our knowledge, this is the first instance where such architecture has been observed in an open-framework material. The strips are held in position by strong hydrogen bond interactions

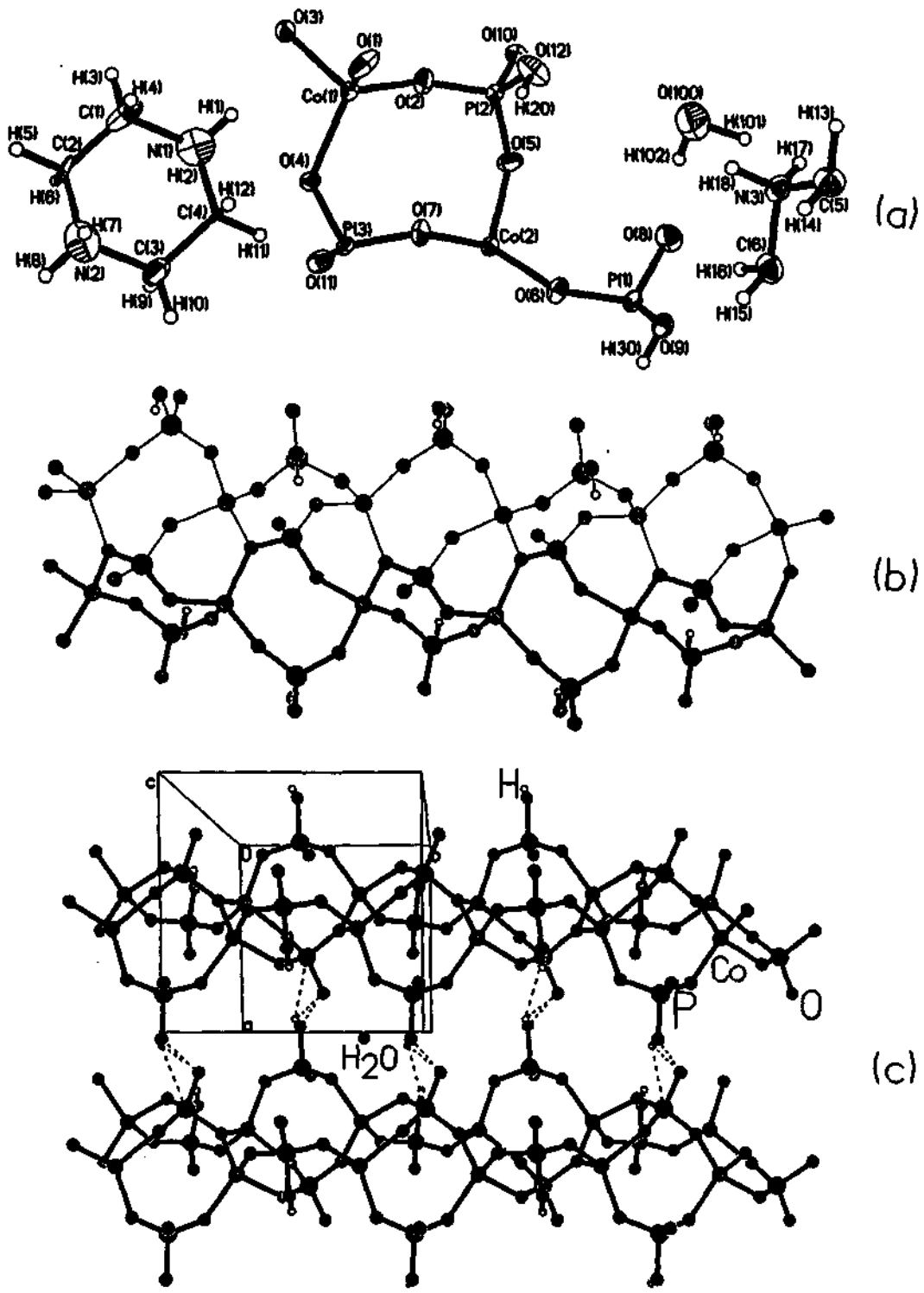

Fig. 1.61. (a) ORTEP plot of **XVII**, $[C_4N_2H_{12}]_{1.5}[Co_2(HPO_4)(PO_4)H_2O]$. Thermal ellipsoids are given at 50% probability. (b) The strip structure of **XVII**. Note that the two linear-chains are merged via a 3-coordinated oxygen atom (one of them is outlined by darker lines). (c) Structure of **XVII** along the *ab* plane showing the arrangement of the strips. Amine molecules are not shown for clarity.

Table 1.54. Atomic coordinates [x 10^4] and equivalent isotropic displacement parameters [$Å^2$ x 10^3] for **XVII.**

Atom	x	y	z	U(eq)
Co(1)	4336(1)	2743(1)	1783(1)	15(1)
Co(2)	3977(1)	7824(1)	1855(1)	14(1)
P(1)	1612(1)	10460(1)	1311(1)	15(1)
P(2)	5039(1)	5535(1)	884(1)	15(1)
P(3)	3288(1)	5010(1)	2722(1)	13(1)
O(1)	2219(4)	2020(4)	1549(2)	29(1)
O(2)	5348(4)	4125(4)	1264(1)	25(1)
O(3)	5805(4)	941(4)	1818(1)	22(1)
O(4)	4391(4)	3611(3)	2563(1)	17(1)
O(5)	4980(4)	7037(4)	1214(1)	27(1)
O(6)	2093(4)	9107(4)	1702(1)	21(1)
O(7)	2921(4)	5988(4)	2190(1)	20(1)
O(8)	2011(4)	10206(4)	713(1)	29(1)
O(9)	-292(4)	10566(4)	1289(1)	18(1)
O(10)	6354(4)	5324(4)	478(1)	19(1)
O(11)	1725(4)	4367(4)	2916(1)	21(1)
O(12)	3382(4)	5330(4)	544(1)	32(1)
O(100)	306(7)	7930(6)	-44(2)	60(1)
N(1)	1440(6)	482(6)	2952(2)	44(1)
N(2)	45(6)	-121(6)	4006(2)	47(1)
C(4)	293(5)	1583(4)	3184(2)	8(1)
C(3)	333(6)	1516(5)	3808(2)	26(1)
C(2)	1190(5)	-1226(5)	3770(2)	16(1)
C(1)	1109(6)	-1153(6)	3149(2)	35(1)
N(3)	-3994(5)	8650(4)	6(2)	22(1)
C(6)	-3774(6)	9861(6)	453(2)	26(1)
C(5)	-5696(6)	8574(6)	-223(2)	27(1)

Table 1.55. Bond distances (Å) and Angles (°) for **XVII**.

Moiety	Distance (Å)	Moiety	Angle (°)
Co(1) - O(1)	1.927(3)	O(5) – Co(2) – O(7)	105.87(13)
Co(1) - O(2)	1.951(3)	O(6) – Co(2) – O(7)	98.32(13)
Co(1) - O(3)	1.975(3)	$O(4)^{\#1}$ – Co(2) – O(7)	106.72(12)
Co(1) - O(4)	2.003(3)	O(8) – P(1) – O(6)	113.8(2)
Co(2) - O(5)	1.922(3)	O(8) – P(1) – $O(1)^{\#2}$	112.9(2)
Co(2) - O(6)	1.939(3)	O(6) – P(1) – $O(1)^{\#2}$	111.9(2)
Co(2) - $O(4)^{\#1}$	2.000(3)	O(8) – P(1) – O(9)	105.3(2)
Co(2) - O(7)	2.001(3)	O(6) – P(1) – O(9)	106.6(2)
P(1) – O(8)	1.506(3)	$O(1)^{\#2}$ – P(1) – O(9)	105.6(2)
P(1) – O(6)	1.525(3)	O(5) – P(2) – O(10)	110.0(2)
P(1) – $O(1)^{\#2}$	1.527(3)	O(5) – P(2) – O(2)	112.0(2)
P(1) – O(9)	1.597(3)	O(10) – P(2) – O(2)	108.6(2)
P(2) – O(5)	1.512(3)	O(5) – P(2) – O(12)	107.8(2)
P(2) – O(10)	1.520(3)	O(10) – P(2) – O(12)	109.3(2)
P(2) – O(2)	1.525(3)	O(2) – P(2) – O(12)	109.1(2)
P(2) – O(12)	1.570(3)	$O(3)^{\#1}$ – P(3) – O(11)	111.6(2)
P(3) – $O(3)^{\#1}$	1.519(3)	$O(3)^{\#1}$ – P(3) – O(7)	111.9(2)
P(3) – O(11)	1.524(3)	O(11) – P(3) – O(7)	108.8(2)
P(3) – O(7)	1.536(3)	$O(3)^{\#1}$ – P(3) – O(4)	107.5(2)
P(3) – O(4)	1.578(3)	O(11) – P(3) – O(4)	109.3(2)
Moiety	Angle (°)	O(7) – P(3) – O(4)	107.6(2)
O(1) – Co(1) – O(2)	116.3(2)	$P(1)^{\#3}$ – O(1) – Co(1)	131.8(2)
O(1) – Co(1) – O(3)	108.64(14)	P(2) – O(2) – Co(1)	142.9(2)
O(2) – Co(1) – O(3)	101.79(13)	$P(3)^{\#4}$ – O(3) – Co(1)	136.2(2)
O(1) – Co(1) – O(4)	110.55(14)	P(3) – O(4) – $Co(2)^{\#4}$	118.2(2)
O(2) – Co(1) – O(4)	112.50(13)	P(3) – O(4) – Co(1)	122.1(2)
O(3) – Co(1) – O(4)	106.14(12)	$Co(2)^{\#4}$ – O(4) – Co(1)	119.45(14)
O(5) – Co(2) – O(6)	116.37(14)	P(2) – O(5) – Co(2)	138.3(2)
O(5) – Co(2) – $O(4)^{\#1}$	110.91(14)	P(1) – O(6) – Co(2)	136.4(2)
O(6) – Co(2) – $O(4)^{\#1}$	116.72(13)	P(3) – O(7) – Co(2)	133.8(2)
	Organic		
Moiety	Distance (Å)	Moiety	Angle (°)
N(1) – C(4)	1.482(6)	C(4) – N(1) – C(1)	109.8(4)
N(1) – C(1)	1.510(7)	C(2) – N(2) – C(3)	110.6(4)
N(2) – C(2)	1.488(7)	N(1) – C(4) – C(3)	112.2(4)
N(2) – C(3)	1.506(7)	C(4) – C(3) – N(2)	111.0(4)
C(4) – C(3)	1.490(6)	C(1) – C(2) – N(2)	111.5(4)
C(2) – C(1)	1.483(7)	C(2) – C(1) – N(1)	110.7(4)
N(3) – C(6)	1.491(6)	C(6) – N(3) – C(5)	111.1(4)
N(3) – C(5)	1.495(6)	N(3) – C(6) – $C(5)^{\#5}$	110.0(4)
C(6) – $C(5)^{\#5}$	1.505(7)	N(3) – C(5) – $C(6)^{\#5}$	110.2(4)

Symmetry transformations used to generate equivalent atoms:

#1 -x+1, -y+1/2, -z+1/2 #2 x, y+1, z #3 x, y-1, z #4 -x+1, y-1/2, -z+1/2
#5 -x-1, -y+2, -z

involving the terminal –OH groups, water molecules and the piperazinium cation that are located in between the two strips.

$[C_4N_2H_2]_{1.5}[Co_2(H_2PO_4)_2(PO_4)H_2O]$, XVIII : The asymmetric unit of **XVIII**, contains 27 distinct non-hydrogen atoms (Fig.1.62a). The atomic coordinates are presented in Table 1.56. The structure is made from vertex sharing of CoO_4, $PO_3(OH)$ and PO_4 tetrahedra forming layers, which are held together by hydrogen bond interactions. The Co-O distances are in the range 1.931(3) – 1.989(3) Å (av. 1.965(3) Å) and the O – Co – O angles are in the range 95.8(2) – 122.9(2)° (av. 109.4(2)°). The three P atoms have P-O distances in the range 1.507(3) – 1.584(3) Å (av. 1.539(3) Å) and the O – P – O angles are in the range 105.2(2) – 113.1(2)° (av. 109.4(2)°). The important bond distances and angles are presented in Table 1.57. The connectivity between CoO_4, HPO_4 and PO_4 form 4-membered rings, which are joined to give rise to a layered topology based on a two-dimensional network of bifurcated 12-membered rings. The 12-membered ring consists of 12-T atoms (T = Co or P) formed by 6 cobalt and 6 phosphorus atoms which strictly alternate. These layers are arranged along the *bc* plane (Fig.1.62b). The 4-membered rings form a zigzag ladder which are connected by HPO_4 moieties forming the 12-membered aperture. The di-protonated piperazinium cation occupies the space between the layers and interacts with the layers through N-H...O hydrogen bonds.

It is interesting that both **XVII** and **XVIII** have an identical framework composition. The connectivity between the 4-membered rings, however, gives rise to the differences observed between them. While, **XVII** forms a strip-like architecture made of corner-shared 4-membered rings, **XVIII** forms a layer made from zigzag edge-shared 4-membered rings. We can rationalize the formation of **XVII** and **XVIII** by the mechanism proposed by Oliver et. al.[133] shown in Fig. 1.8. In addition to the structures reported above various other amine phosphates such as 1,4*bis*(3-aminopropyl)piperazine phosphate (AP), Diethylenetriamine phosphate (DETAP), 1,4diazabicyclo[2.2.2]octane phosphate (DABCO-P), have

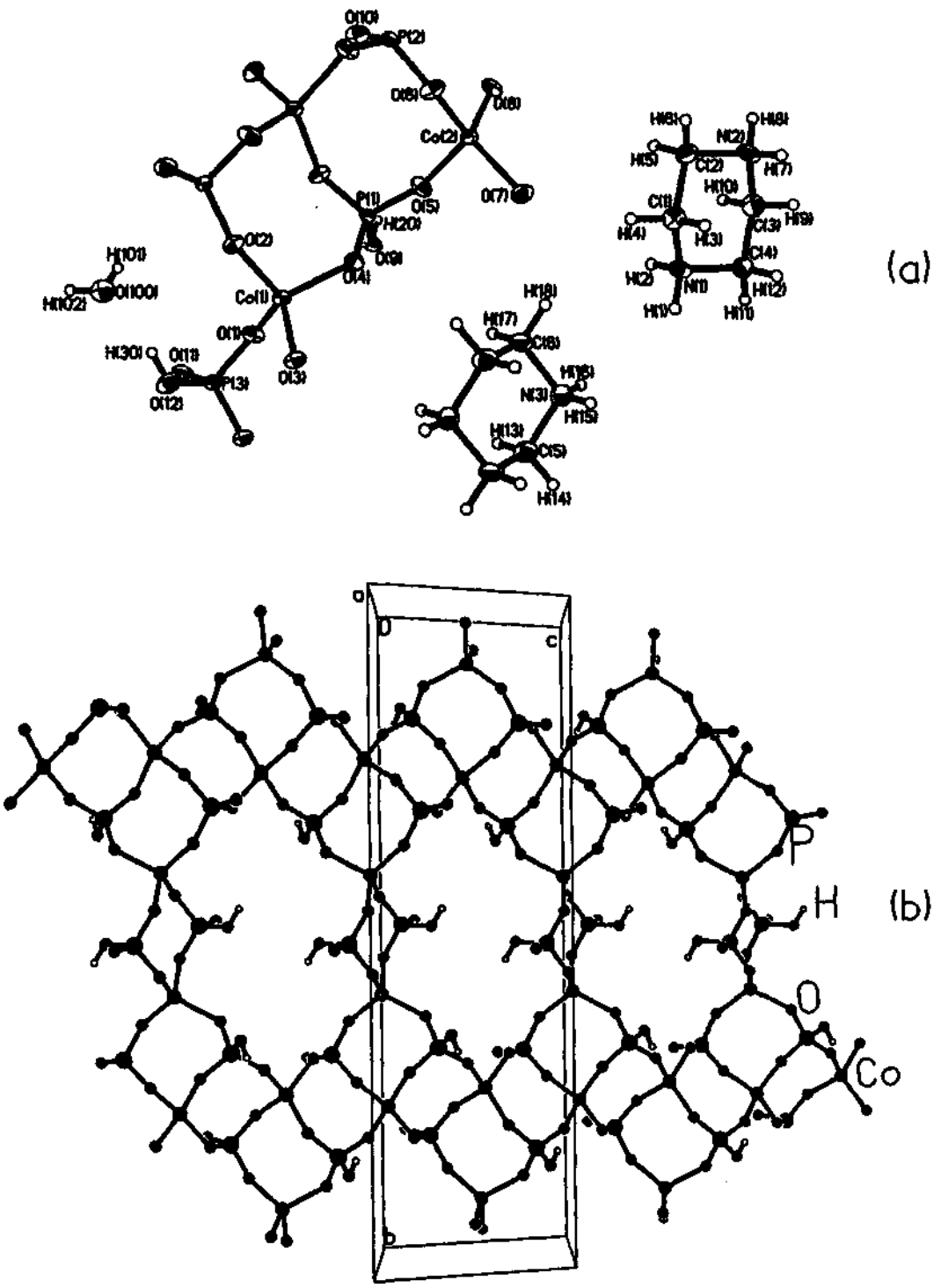

Fig. 1.62. (a) ORTEP plot of **XVIII**, $[C_4N_2H_{12}]_{1.5}[Co_2(HPO_4)(PO_4)H_2O]$. Thermal ellipsoids are given at 50% probability. (b) A single layer of **XVIII**, $[C_4N_2H_{12}]_{1.5}[Co_2(HPO_4)(PO_4)H_2O]$. Note that the zig-zag ladder-like chains are connected by phosphate groups.

Table 1.56. Atomic coordinates [x 10^4] and equivalent isotropic displacement parameters [$Å^2$ x 10^3] for **XVIII**.

Atom	x	y	z	U(eq)
Co(1)	4721(1)	5903(1)	250(1)	15(1)
Co(2)	5030(1)	7381(1)	5524(1)	15(1)
P(1)	6776(2)	6706(1)	3148(1)	14(1)
P(2)	2879(1)	8158(1)	2597(2)	13(1)
P(3)	6842(2)	5149(1)	-1231(2)	16(1)
O(1)	6747(4)	5596(1)	-95(4)	22(1)
O(2)	2968(4)	6322(1)	-1510(4)	20(1)
O(3)	3062(4)	5353(1)	279(4)	20(1)
O(4)	5558(4)	6248(1)	2490(4)	20(1)
O(5)	6475(4)	6968(1)	4617(4)	24(1)
O(6)	3072(4)	7724(1)	3858(4)	25(1)
O(7)	4326(4)	6858(1)	6816(4)	24(1)
O(8)	6675(4)	7928(1)	6692(4)	22(1)
O(9)	8701(4)	6495(1)	3806(4)	23(1)
O(10)	1049(4)	8093(1)	1232(4)	23(1)
O(11)	8370(4)	5225(1)	-1831(4)	25(1)
O(12)	5055(4)	5125(1)	-2810(4)	32(1)
O(100)	4367(6)	5916(2)	-4872(6)	36(1)
N(1)	7(5)	6134(1)	9428(5)	19(1)
N(2)	-69(5)	7089(1)	11092(5)	22(1)
C(1)	-1423(6)	6505(2)	8636(6)	21(1)
C(2)	-804(6)	7044(2)	9193(6)	22(1)
C(3)	1345(6)	6709(2)	11869(6)	24(1)
C(4)	684(6)	6177(2)	11331(6)	20(1)
N(3)	919(5)	5106(2)	6764(5)	24(1)
C(5)	1255(6)	4633(2)	5963(6)	25(1)
C(6)	373(7)	5525(2)	5492(6)	26(1)

Table 1.57. Bond Distances (Å) and angles (°) for **XVIII**.

Moiety	Distance (Å)	Moiety	Angle (°)
Co(1) - O(1)	1.953(3)	O(5) – Co(2) – O(7)	99.25(14)
Co(1) - O(2)	1.985(3)	O(6) – Co(2) – O(8)	105.03(14)
Co(1) - O(3)	1.989(3)	O(5) – Co(2) – O(8)	101.60(13)
Co(1) - O(4)	1.976(3)	O(7) – Co(2) – O(8)	121.38(14)
Co(2) - O(5)	1.949(3)	O(5) – P(1) – O(8)$^{\#1}$	112.7(2)
Co(2) - O(6)	1.931(3)	O(5) – P(1) – O(4)	112.3(2)
Co(2) - O(7)	1.962(3)	O(8)$^{\#1}$ – P(1) – O(4)	111.3(2)
Co(2) - O(8)	1.975(3)	O(5) – P(1) – O(9)	108.1(2)
P(1) – O(5)	1.507(3)	O(8)$^{\#1}$ – P(1) – O(9)	105.4(2)
P(1) – O(8)$^{\#1}$	1.534(3)	O(4) – P(1) – O(9)	106.6(2)
P(1) – O(4)	1.536(3)	O(6) – P(2) – O(10)	105.3(2)
P(1) – O(9)	1.571(3)	O(6) – P(2) – O(7)$^{\#1}$	111.6(2)
P(2) – O(6)	1.528(3)	O(10) – P(2) – O(7)$^{\#1}$	111.7(2)
P(2) – O(10)	1.534(3)	O(6) – P(2) – O(2)$^{\#2}$	110.6(2)
P(2) – O(7)$^{\#1}$	1.543(3)	O(10) – P(2) – O(2)$^{\#2}$	109.0(2)
P(2) – O(2)$^{\#2}$	1.549(3)	O(7)$^{\#1}$ – P(2) – O(2)$^{\#2}$	108.6(2)
P(3) – O(11)	1.517(3)	O(11) – P(3) – O(3)$^{\#3}$	113.1(2)
P(3) – O(3)$^{\#3}$	1.530(3)	O(11) – P(3) – O(1)	109.5(2)
P(3) – O(1)	1.535(3)	O(3)$^{\#3}$ – P(3) – O(1)	110.1(2)
P(3) – O(12)	1.584(3)	O(11) – P(3) – O(12)	110.5(2)
		O(3)$^{\#3}$ – P(3) – O(12)	105.2(2)
Moiety	Angle (°)	O(1) – P(3) – O(12)	108.2(2)
O(1) – Co(1) – O(4)	107.87(13)	P(3) – O(1) – Co(1)	130.0(2)
O(1) – Co(1) – O(2)	122.95(13)	P(2)$^{\#1}$ – O(2) – Co(1)	138.4(2)
O(4) – Co(1) – O(2)	111.31(13)	P(3)$^{\#3}$ – O(3) – Co(1)	136.6(2)
O(1) – Co(1) – O(3)	108.54(13)	P(1) – O(4) – Co(1)	131.5(2)
O(4) – Co(1) – O(3)	109.26(13)	P(1) – O(5) – Co(2)	150.8(2)
O(2) – Co(1) – O(3)	95.78(12)	P(2) – O(6) – Co(2)	134.8(2)
O(6) – Co(2) – O(5)	116.05(14)	P(2)$^{\#2}$ – O(7) – Co(2)	132.3(2)
O(6) – Co(2) – O(7)	113.42(14)	P(1)$^{\#2}$ – O(8) – Co(2)	133.4(2)

Organic Moiety

Moiety	Distance (Å)	Moiety	Angle (°)
N(1) – C(1)	1.486(6)	C(1) – N(1) – C(4)	111.0(3)
N(1) – C(4)	1.495(6)	C(3) – N(2) – C(2)	111.5(4)
N(2) – C(3)	1.492(6)	N(1) – C(1) – C(2)	110.8(4)
N(2) – C(2)	1.493(6)	N(2) – C(2) – C(1)	111.3(4)
C(1) – C(2)	1.525(7)	N(2) – C(3) – C(4)	110.7(4)
C(3) – C(4)	1.511(7)	N(1) – C(4) – C(3)	110.3(4)
N(3) – C(5)	1.486(6)	C(5) – N(3) – C(6)	110.8(4)
N(3) – C(6)	1.489(6)	N(3) – C(5) – C(6)$^{\#4}$	110.2(4)
C(5) – C(6)$^{\#4}$	1.507(7)	N(3) – C(6) – C(5)$^{\#4}$	109.1(4)

Symmetry transformations used to generate equivalent atoms:

#1 x, -y+3/2, z-1/2 #2 x, -y+3/2, z+1/2 #3 –x+1, -y+1, -z #4 -x, -y+1, -z+1

also yielded open-framework cobalt phosphates. The cobalt phosphate obtained with APPIP-P bears chloride anion as a part of the framework and they project into the interlayer space. DETAP and DABCO-P both yield the three-dimensional cobalt phosphates and Imidazole phosphate yielded three-dimensional zinc phosphate.

The asymmetric unit of APPIP-P shown in Fig. 1.63a, consists of one HPO_4 molecule and half a molecule of the diprotonated amine. The sheet-like architecture of APPIP-P contains two phosphate units on either side of the amine molecule as shown in Fig.1.63b. The water molecules are situated between the amine molecule.

$[C_{10}N_4H_{28}]_{0.5}[Co(PO_4)Cl]$, XIX : The atomic coordinates of the cobalt chlorophosphate, **XIX**, are listed in Table1.58. The asymmetric unit of **XIX**, is shown in Fig. 1.64, consists of 14 non-hydrogen atoms. There is only one crystallographically independent cobalt and phosphorus atom in the asymmetric unit. Phosphorus is coordinated by four oxygen atoms, whereas, cobalt is coordinated by three oxygens and one chlorine atom. Though, cobalt and phosphorus are tetrahedrally coordinated with respect to the nearest atom neighbors, they are only three Co – O – P bonds. The remaining connection needed for the tetrahedral linkage comes from a terminal bonding of a chlorine with cobalt (Co(1) – Cl(1) = 2.291 Å) and for phosphorus from a double bonded oxygen atom (P(1) – O(4) = 1.538 Å). Bond valence sum calculations[244] on the framework also agree with the above formulations. The Co – O and P – O bond distances as well as the O – Co – O and O – P – O angles are in the expected range for this type of bonding (Table 1.59).

The layered framework structure of **XIX**, is built up from a network of CoO_3Cl and PO_4 tetrahedra sharing vertices. The vertex-shared linkages between these tetrahedra give rise to a two-dimensional macroanionic layer with 4- and 8-membered apertures within each layer as shown in Fig.1.65. The chlorine atoms, bonded to cobalt atoms, point in a direction perpendicular to the plane of the

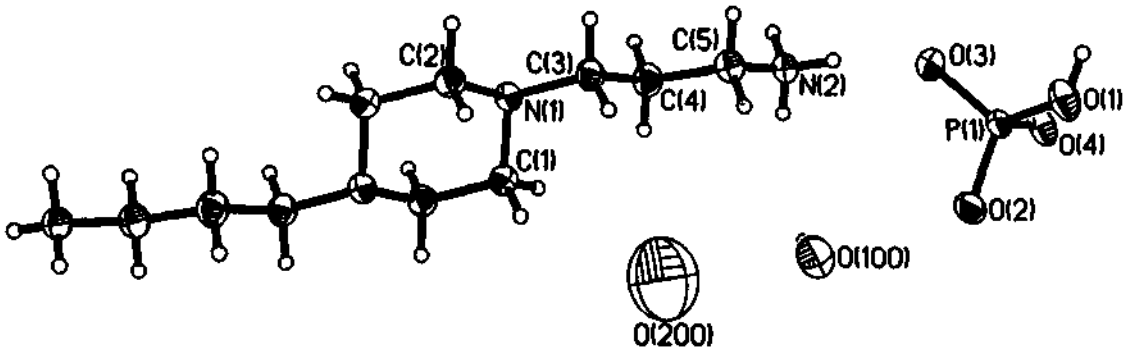

(a)

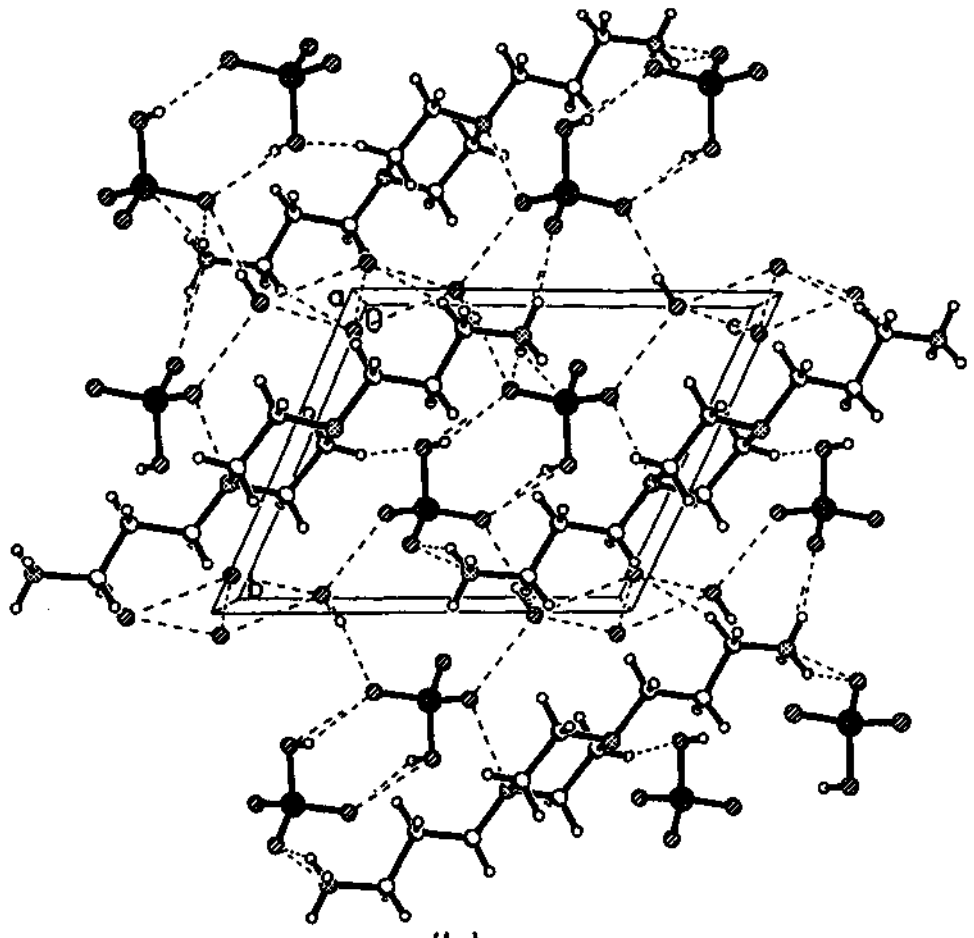

(b)

Fig. 1.63. (a) ORTEP plot of the structure of APIP-P. Thermal ellipsoids are given at 50% probability. (b) Structure showing the hydrogen bond assembly between the HPO_4, diprotanated amine molecules and water molecules. Dotted lines represent hydrogen bonding.

Table 1.58. Atomic coordinates [x 10^4] and equivalent isotropic displacement parameters [$Å^2$ x 10^3] for, **XIX**, $[C_{10}N_4H_{28}]_{0.5}[Co(PO_4)Cl]$

Atom	x	y	z	U_{eq}[1]
Co(1)	1441(1)	977(1)	6924(1)	13(1)
P(1)	-1041(1)	-1243(1)	6050(1)	12(1)
Cl(1)	3427(1)	-2(1)	7771(1)	22(1)
O(1)	1448(2)	2583(2)	8162(2)	23(1)
O(2)	285(2)	-685(2)	6892(2)	24(1)
O(3)	1003(2)	1983(2)	5210(2)	20(1)
O(4)	-1966(2)	107(2)	5679(2)	19(1)
N(1)	1136(2)	6930(3)	4407(2)	19(1)
C(1)	2026(3)	5729(3)	5158(3)	24(1)
C(2)	2472(3)	5991(3)	6610(3)	23(1)
C(3)	3452(3)	4778(3)	7279(3)	18(1)
N(2)	3966(2)	4919(2)	8733(2)	15(1)
C(4)	4757(3)	3558(3)	9339(3)	18(1)
C(5)	4728(3)	6338(3)	9194(3)	18(1)

[1] U_{eq} is defined as one third of the trace of the orthogonalized U_{ij} tensor.

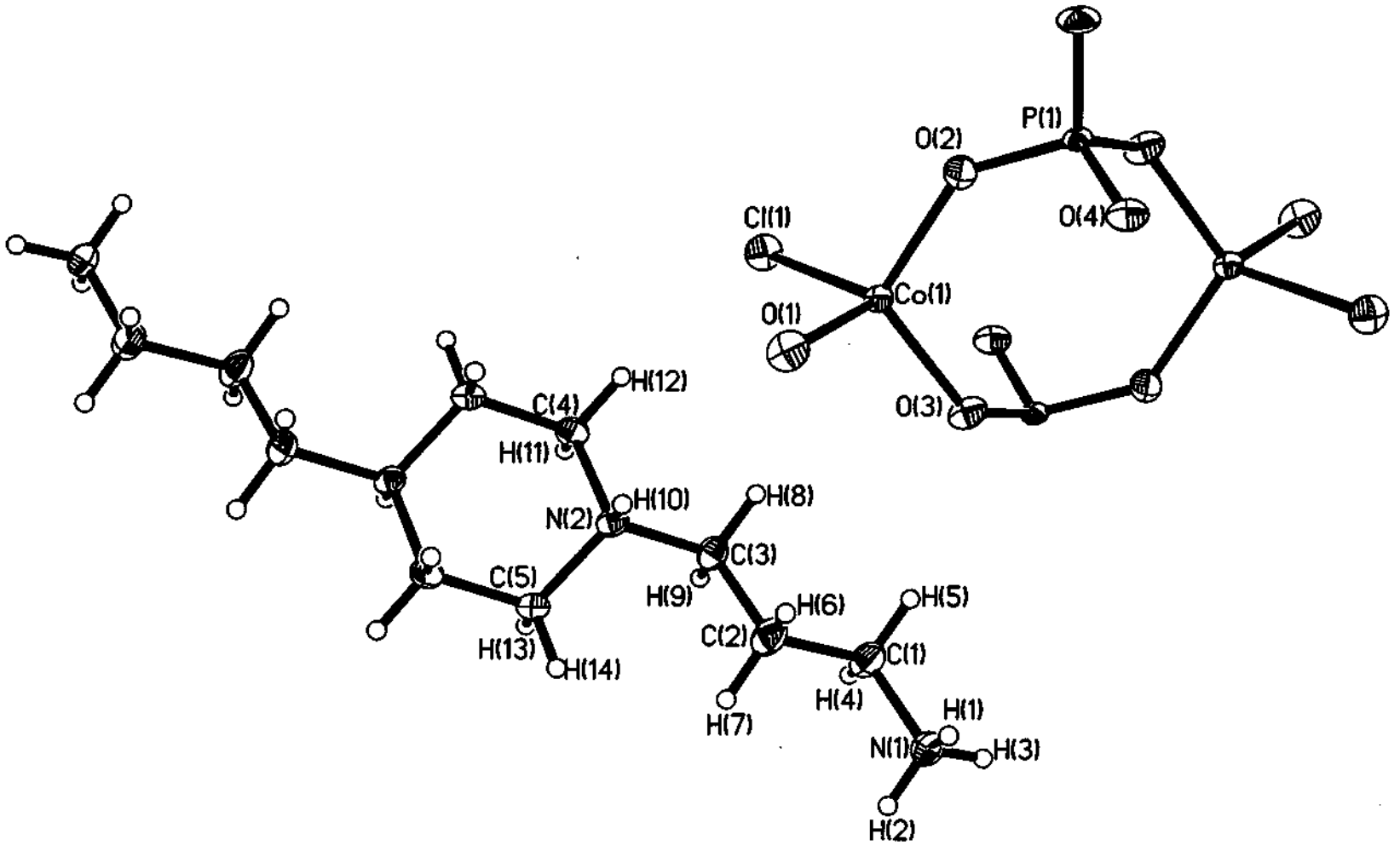

Fig. 1.64 ORTEP plot of **XIX** $[C_{10}N_4H_{28}]_{0.5}$ $[Co(PO_4)Cl]$. Thermal ellipsoids are given at 50% probability.

Table 1.59. Selected bond distances and angles in **XIX**, $[C_{10}N_4H_{28}]_{0.5}[Co(PO_4)Cl]$

Moiety	Distance, Å	Moiety	Distance, Å
Co(1) – O(1)	1.952(2)	P(1) – O(1)$^{\#1}$	1.522(2)
Co(1) – O(2)	1.957(2)	P(1) – O(2)	1.544(2)
Co(1) – O(3)	1.973(2)	P(1) – O(3)$^{\#2}$	1.546(2)
Co(1) – Cl(1)	2.291(1)	P(1) – O(4)	1.538(2)
	Organic Moiety		
N(1) – C(1)	1.487(4)	C(1) – C(2)	1.507(5)
C(2) – C(3)	1.525(4)	C(3) – N(2)	1.496(4)
N(2) – C(4)	1.497(4)	N(2) – C(5)	1.494(4)
Moiety	Angle (°)	Moiety	Angle (°)
O(1) – Co(1) – O(2)	112.0(1)	O(1)$^{\#1}$ – P(1) – O(2)	108.1(1)
O(1) – Co(1) – O(3)	106.5(1)	O(1)$^{\#1}$ – P(1) – O(3)$^{\#2}$	110.2(1)
O(2) – Co(1) – O(3)	112.2(1)	O(2) – P(1) – O(3)$^{\#2}$	109.1(1)
O(1) – Co(1) – Cl(1)	103.5(1)	O(1)$^{\#1}$ – P(1) – O(4)	109.9(1)
O(2) – Co(1) – Cl(1)	107.4(1)	O(2) – P(1) – O(4)	110.7(1)
O(3) – Co(1) – Cl(1)	115.1(1)	O(3)$^{\#2}$ – P(1) – O(4)	108.9(1)
	Organic Moiety		
N(1) – C(1) – C(2)	112.5(2)	C(1) – C(2) – C(3)	108.2(2)
C(2) – C(3) – N(2)	113.2(2)	C(3) – N(2) – C(4)	110.5(2)
C(3) – N(2) – C(5)	112.7(2)	C(4) – N(2) – C(5)	108.7(2)
N(2) – C(4) – C(5)$^{\#3}$	111.6(2)	N(2) – C(5) – C(4)$^{\#3}$	111.5(2)

#1 -x, y-1/2, -z+3/2; #2 -x, -y, -z+1; #3 -x+1, -y+1, -z+2

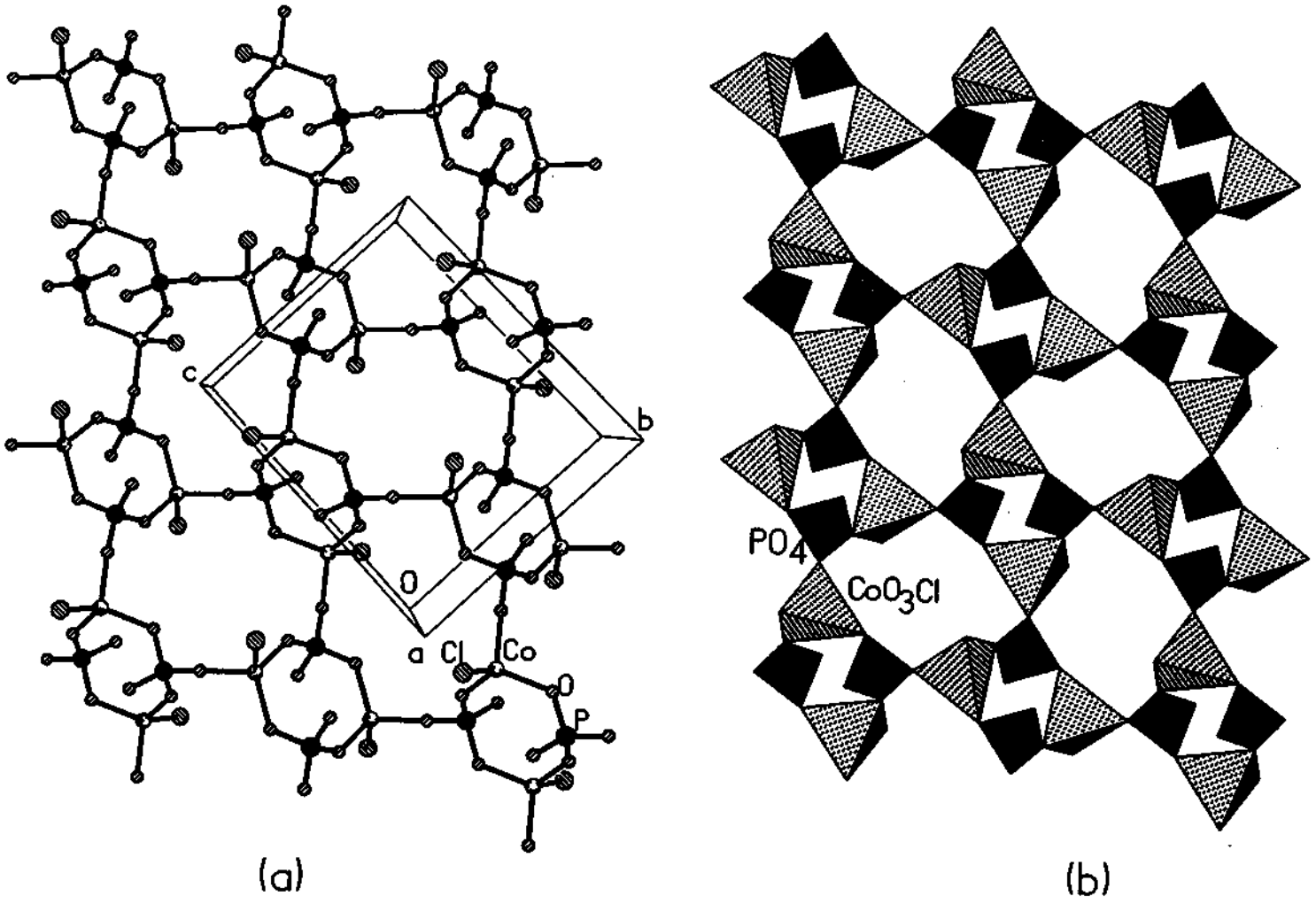

Fig. 1.65 Structure of **XIX,** along a axis showing a single layer. Note that the layers are made of 4– and 8–membered rings only. (a) Ball and stick view (b) polyhedral view.

layer. This arrangement of the chlorine atoms facilitates closer interaction with the structure-directing amines via Cl....H – N / C type interaction. The compensating cationic structure-directing amine molecule, 1,4-*bis*(3-aminopropyl)piperazine, is situated in between these inorganic layers as shown in Figs. 1.66 and 1.67. Thus, $[C_{10}N_4H_{28}]_{0.5}[Co(PO_4)Cl]$, is a typical example of a two-dimensional structure possessing alternating inorganic and organic layers.

Apart from the strip and the layered cobalt phosphates amine phosphate route has also yielded three-dimensional cobalt phosphate structures with novel architectures.

$[C_4N_3H_{16}]_3[Co_6(PO_4)_5(HPO_4)_3]H_2O$, XX : The structure of **XX,** contains 67 non-hydrogen atoms in the asymmetric unit (Fig.1.68). The atomic coordinates are listed in Table 1.60. The structure comprises a network of CoO_4 and PO_4 tetrahedra that strictly alternate and consist entirely of Co – O – P linkages. The amine molecule, diethylenetriamine (DETA), sits in the middle of the channels formed by these linkages. The six distinct cobalt atoms are all tetrahedrally coordinated to oxygens with an average bond distance of 1.966 Å [Co(1) – O =1.963; Co(2) – O = 1.972; Co(3) – O = 1.951; Co(4) – O = 1.985; Co(5) – O = 1.963; Co(6) – O = 1.959 Å]. The cobalt atoms make four Co – O – P bonds to eight distinct P atom neighbors, with angles spread over the range 109.1 – 162.2°, with an average value of 135.5°. There are eight crystallographically independent phosphate tetrahedra in **XX**. The P atoms, on the other hand, makes only three connections with the adjacent Co atoms via P – O – Co bonds and the remaining being terminal. The P – O distances are in the range 1.515 – 1.575 Å (ave. 1.538 Å) and the O – P – O bond angles are in the range 105.4 – 113.5° (ave. 109.5°). From the bond distances and bond angles it is clear that the PO_4 tetrahedra is more regular than the CoO_4 tetrahedra (Tables 1.61 and 1.62). The resulting $Co_6(PO_4)_8$ framework stoichiometry has a total charge of –12. There are three extra-framework guest species, in the form of diethylenetriamine (DETA), cations. Assuming all the nitrogen atoms of the DETA are protonated,

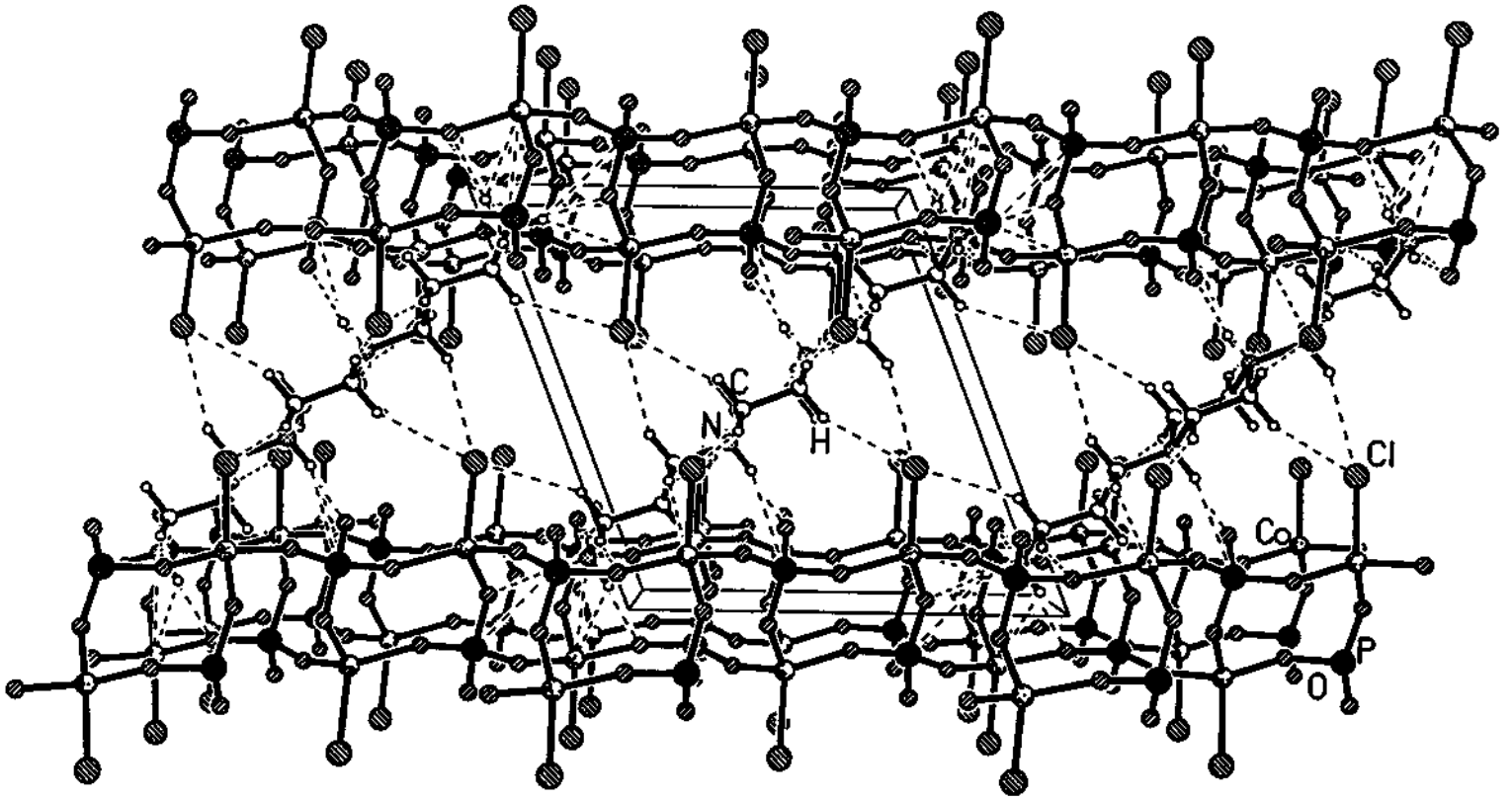

Fig. 1.66 Structure of **XIX,** along *b* axis showing the inorganic layers and the amine in between. Note that the chlorine atoms point in the inter–lamellar space.

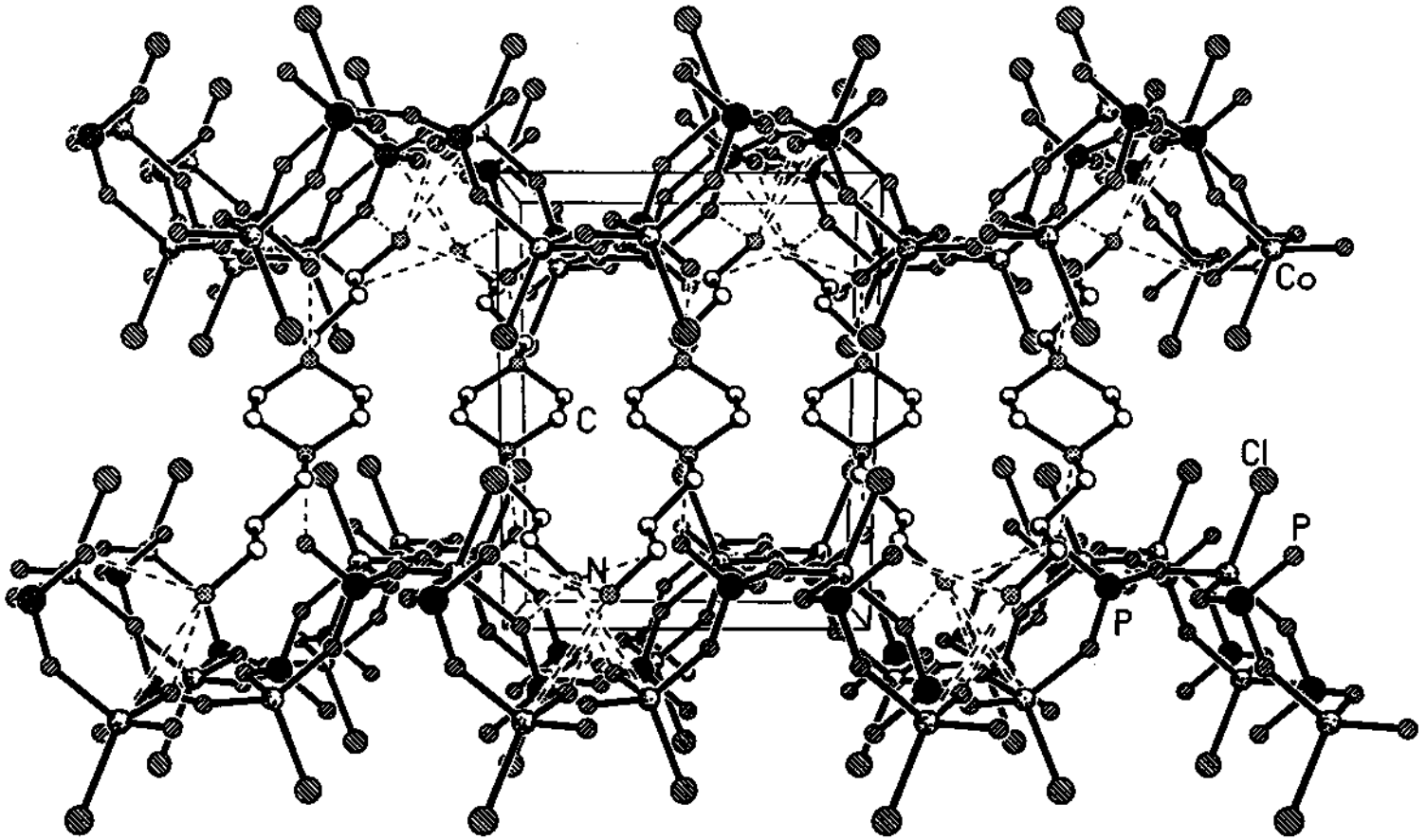

Fig. 1.67 Structure of **XIX,** along *b* axis showing the layers and the amine molecules. Dotted lines represent the various hydrogen bond interactions in **XIX.**

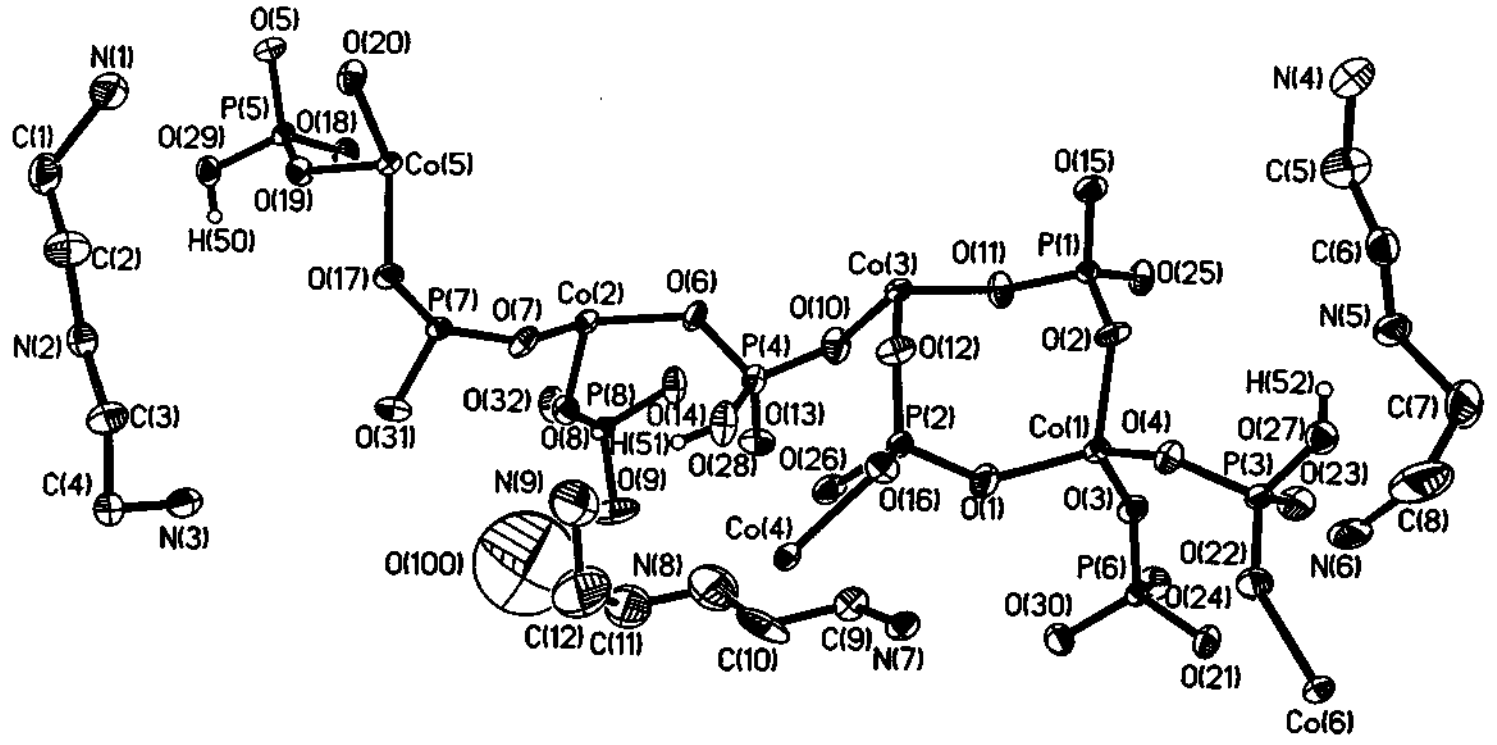

Fig. 1.68 ORTEP plot of **XX**, $[C_4N_3H_{16}]_3\ [Co_6(PO_4)_5(HPO_4)_3].H_2O$. The hydrogen atoms of the amine molecules are not shown. Thermal ellipsoids are given at 50% probability.

Table 1.60. Atomic coordinates [x 10^4] and equivalent isotropic displacement parameters [$Å^2$ x 10^3] for XX, $[C_4N_3H_{16}]_3[Co_6(PO_4)_5(HPO_4)_3]H_2O$.

Atom	x	y	z	$U_{(eq)}$
Co(1)	1282(1)	-2809(1)	595(1)	16(1)
Co(2)	3716(1)	-7919(1)	-896(1)	17(1)
Co(3)	2495(1)	-4950(1)	1088(1)	16(1)
Co(4)	2465(1)	137(1)	-1333(1)	17(1)
Co(5)	5077(1)	-7381(1)	-115(1)	15(1)
Co(6)	64(1)	2412(1)	-136(1)	18(1)
P(1)	1693(1)	-5320(2)	2054(1)	14(1)
P(2)	2190(1)	-2071(2)	-97(1)	17(1)
P(3)	638(1)	-173(2)	1098(1)	18(1)
P(4)	2817(1)	-6551(2)	-584(1)	19(1)
P(5)	5648(1)	-10371(2)	-600(1)	16(1)
P(6)	564(1)	-4452(2)	-807(1)	16(1)
P(7)	4428(1)	-5190(2)	-1289(1)	14(1)
P(8)	3255(1)	-10299(2)	-2232(1)	17(1)
O(1)	1714(2)	-2309(7)	-119(3)	34(1)
O(2)	1489(2)	-3757(6)	1686(3)	24(1)
O(3)	854(2)	-4228(6)	25(3)	23(1)
O(4)	1092(1)	-710(6)	1040(3)	21(1)
O(5)	5948(2)	-10473(6)	207(3)	24(1)
O(6)	3245(2)	-7299(7)	-279(3)	26(1)
O(7)	4000(2)	-5886(6)	-1147(3)	24(1)
O(8)	3533(2)	-8824(6)	-2019(3)	25(1)
O(9)	2952(2)	-9914(8)	-3011(4)	47(2)
O(10)	2548(2)	-6373(6)	133(3)	28(1)
O(11)	1990(2)	-6015(6)	1440(3)	24(1)
O(12)	2436(2)	-2743(6)	708(3)	24(1)
O(13)	2580(2)	-7515(6)	-1317(3)	24(1)
O(14)	3020(2)	-10786(6)	-1487(3)	30(1)
O(15)	1945(2)	-4893(7)	2894(3)	27(1)
O(16)	2290(2)	-275(6)	-181(3)	21(1)
O(17)	4781(2)	-6451(6)	-1141(3)	26(1)
O(18)	5296(2)	-11640(7)	-638(3)	28(1)

O(19)	5462(2)	-8686(6)	-723(3)	23(1)
O(20)	5483(2)	-6247(6)	690(3)	26(1)
O(21)	190(2)	-3268(7)	-829(3)	27(1)
O(22)	511(2)	1074(7)	420(3)	37(2)
O(23)	344(2)	-1627(7)	1052(3)	32(1)
O(24)	387(2)	-6184(6)	-830(3)	25(1)
O(25)	1357(2)	-6576(6)	2145(3)	26(1)
O(26)	2325(2)	-2865(6)	-904(3)	27(1)
O(27)	615(2)	692(6)	1967(3)	26(1)
O(28)	2893(2)	-4849(6)	-963(4)	29(1)
O(29)	5905(2)	-10700(6)	-1366(3)	26(1)
O(30)	795(2)	-4226(7)	-1579(3)	27(1)
O(31)	4420(2)	-4591(6)	-2205(3)	25(1)
O(32)	3540(2)	-11748(6)	-2398(4)	32(1)
O(100)	3317(6)	-6722(27)	-3551(13)	106(7)
N(3)	5146(2)	3217(7)	-2743(4)	24(2)
N(2)	5920(2)	3863(7)	-1580(3)	21(1)
N(1)	6387(2)	2796(9)	507(4)	32(2)
C(4)	5426(2)	4651(8)	-2830(4)	24(2)
C(3)	5641(2)	5186(8)	-1963(4)	24(2)
C(2)	6173(2)	4413(9)	-782(4)	31(2)
C(1)	6445(2)	3013(10)	-407(4)	34(2)
N(6)	563(2)	4636(9)	1583(4)	38(2)
N(5)	846(2)	3443(8)	3377(4)	29(2)
N(4)	1651(2)	3380(8)	5315(4)	30(2)
C(8)	520(4)	5589(13)	2364(5)	73(4)
C(7)	472(3)	4513(14)	3091(6)	65(4)
C(6)	1156(2)	4137(9)	4074(4)	28(2)
C(5)	1402(3)	2757(9)	4521(5)	38(2)
N(9)	3338(3)	-5049(14)	-2430(6)	81(3)
N(8)	2412(3)	-6151(11)	-2831(5)	61(2)
N(7)	1576(2)	-3527(7)	-2026(4)	26(2)
C(12)	3067(4)	-4830(16)	-3262(7)	83(4)
C(11)	2748(3)	-6121(14)	-3420(7)	66(3)
C(10)	2142(3)	-4685(10)	-2788(5)	49(3)
C(9)	1786(2)	-5066(8)	-2239(5)	28(2)

[1] Ueq is defined as one third of the trace of the orthogonalized U_{ij} tensor.

Table 1.61. Selected bond distances in **XX**, $[C_4N_3H_{16}]_3[Co_6(PO_4)_5(HPO_4)_3]H_2O$.

Moiety	Distance (Å)	Moiety	Distance (Å)
Co(1) – O(1)	1.931(5)	P(2) – O(12)	1.530(5)
Co(1) – O(2)	1.954(5)	P(2) – O(1)	1.532(5)
Co(1) – O(3)	1.953(5)	P(2) – O(16)	1.544(5)
Co(1) – O(4)	2.013(5)	P(2) – O(26)	1.551(5)
Co(2) – O(5)#1	1.971(5)	P(3) – O(22)	1.521(6)
Co(2) – O(6)	1.960(5)	P(3) – O(4)	1.531(5)
Co(2) – O(7)	1.988(5)	P(3) – O(23)	1.532(6)
Co(2) – O(8)	1.967(5)	P(3) – O(27)	1.571(5)
Co(3) – O(9)#2	1.928(5)	P(4) – O(10)	1.515(5)
Co(3) – O(10)	1.953(5)	P(4) – O(6)	1.531(5)
Co(3) – O(11)	1.979(5)	P(4) – O(13)	1.542(5)
Co(3) – O(12)	1.944(5)	P(4) – O(28)	1.575(5)
Co(4) – O(13)#4	1.996(5)	P(5) – O(5)	1.514(5)
Co(4) – O(14)#4	1.975(5)	P(5) – O(19)	1.533(5)
Co(4) – O(15)#13	1.960(5)	P(5) – O(18)	1.541(5)
Co(4) – O(16)	2.008(5)	P(5) – O(29)	1.571(5)
Co(5) – O(17)	1.952(5)	P(6) – O(21)	1.547(5)
Co(5) – O(18)#1	1.965(5)	P(6) – O(3)	1.537(5)
Co(5) – O(19)	1.978(5)	P(6) – O(24)	1.553(5)
Co(5) – O(20)	1.957(5)	P(6) – O(30)	1.518(5)
Co(6) – O(21)#5	1.954(5)	P(7) – O(7)	1.526(5)
Co(6) – O(22)	1.945(5)	P(7) – O(20)#6	1.540(5)
Co(6) – O(23)#5	1.953(5)	P(7) – O(17)	1.543(5)
Co(6) – O(24)#4	1.982(5)	P(7) – O(31)	1.540(5)
P(1) – O(15)	1.521(5)	P(8) – O(9)	1.518(6)
P(1) – O(25)	1.521(5)	P(8) – O(14)	1.530(5)
P(1) – O(2)	1.545(5)	P(8) – O(8)	1.535(5)
P(1) – O(11)	1.553(5)	P(8) – O(32)	1.556(5)
	Organic moiety		
N(3) – C(4)	1.512(7)	N(5) – C(6)	1.513(7)
C(4) – C(3)	1.535(7)	C(6) – C(5)	1.526(8)
C(3) – N(2)	1.505(7)	C(5) – N(4)	1.506(7)
N(2) – C(2)	1.497(7)	N(9) – C(12)	1.508(9)
C(2) – C(1)	1.536(8)	C(12) – C(11)	1.486(9)
C(1) – N(1)	1.499(7)	C(11) – N(8)	1.505(8)
N(6) – C(8)	1.496(8)	N(8) – C(10)	1.503(8)
C(8) – C(7)	1.488(9)	C(10) – C(9)	1.548(8)
C(7) – N(5)	1.520(8)	C(9) – N(7)	1,507(7)

#1 -x+1, -y-2, -z; #2 x, -y-3/2, z+1/2; #3 x, -y-1/2, z-1/2; #4 x, y+1, z; #5 -x, -y, -z;

#6 -x+1, -y-1, -z.

Table 1.62. Selected bond angles in **XX**, $[C_4N_3H_{16}]_3[Co_6(PO_4)_5(HPO_4)_3]H_2O$.

Moiety	Angle (°)	Moiety	Angle (°)
O(1) – Co(1) – O(3)	111.6(2)	O(12) – P(2) – O(1)	112.5(3)
O(1) – Co(1) – O(2)	114.8(2)	O(12) – P(2) – O(16)	109.8(3)
O(3) – Co(1) – O(2)	108.3(2)	O(1) – P(2) – O(16)	109.7(3)
O(1) – Co(1) – O(4)	106.5(2)	O(12) – P(2) – O(26)	111.8(3)
O(3) – Co(1) – O(4)	118.0(2)	O(1) – P(2) – O(26)	109.7(3)
O(2) – Co(1) – O(4)	97.2(2)	O(16) – P(2) – O(26)	105.4(3)
O(6) – Co(2) – O(8)	113.1(2)	O(22) – P(3) – O(4)	109.6(3)
O(6) – Co(2) – O(5)$^{\#1}$	107.6(2)	O(22) – P(3) – O(23)	113.5(3)
O(8) – Co(2) – O(5)$^{\#1}$	109.2(2)	O(4) – P(3) – O(23)	110.1(3)
O(6) – Co(2) – O(7)	105.6(2)	O(22) – P(3) – O(27)	105.9(3)
O(8) – Co(2) – O(7)	103.9(2)	O(4) – P(3) – O(27)	109.2(3)
O(5)$^{\#1}$ – Co(2) – O(7)	117.7(2)	O(23) – P(3) – O(27)	108.4(3)
O(9)$^{\#2}$ – Co(3) – O(12)	109.0(2)	O(10) – P(4) – O(6)	111.4(3)
O(9)$^{\#2}$ – Co(3) – O(10)	114.6(3)	O(10) – P(4) – O(13)	110.4(3)
O(12) – Co(3) – O(10)	110.5(2)	O(6) – P(4) – O(13)	111.6(3)
O(9)$^{\#2}$ – Co(3) – O(11)	109.5(3)	O(10) – P(4) – O(28)	109.1(3)
O(12) – Co(3) – O(11)	117.6(2)	O(6) – P(4) – O(28)	108.6(3)
O(10) – Co(3) – O(11)	95.3(2)	O(13) – P(4) – O(28)	105.4(3)
O(15)$^{\#3}$ – Co(4) – O(14)$^{\#4}$	126.1(2)	O(5) – P(5) – O(19)	111.0(3)
O(15)$^{\#3}$ – Co(4) – O(13)$^{\#4}$	104.6(2)	O(5) – P(5) – O(18)	112.5(3)
O(14)$^{\#4}$ – CO(4) – O(13)$^{\#4}$	102.6(2)	O(19) – P(5) – O(18)	110.9(3)
O(15)$^{\#3}$ – Co(4) – O(16)	104.5(2)	O(5) – P(5) – O(29)	108.2(3)
O(14)$^{\#4}$ – CO(4) – O(16)	113.3(2)	O(19) – P(5) – O(29)	106.9(3)
O(13)$^{\#4}$ – Co(4) – O(16)	103.1(2)	O(18) – P(5) – O(29)	107.0(3)
O(17) – Co(5) – O(20)	125.1(2)	O(30) – P(6) – O(3)	112.4(3)
O(17) – Co(5) – O(18)$^{\#1}$	113.9(2)	O(30) – P(6) – O(21)	110.4(3)
O(20) – Co(5) – O(18)$^{\#1}$	101.8(2)	O(3) – P(6) – O(21)	109.2(3)
O(17) – Co(5) – O(19)	121.6(2)	O(30) – P(6) – O(24)	107.8(3)
O(20) – Co(5) – O(19)	100.7(2)	O(3) – P(6) – O(24)	108.4(3)
O(18)$^{\#1}$ – Co(5) – O(19)	121.6(2)	O(21) – P(6) – O(24)	108.6(3)
O(22) – Co(6) – O(23)$^{\#5}$	122.6(3)	O(7) – P(7) – O(20)$^{\#6}$	108.2(3)
O(22) – Co(6) – O(21)$^{\#5}$	101.7(2)	O(7) – P(7) – O(31)	110.3(3)
O(23)$^{\#5}$ – Co(6) – O(21)$^{\#5}$	114.1(2)	O(20)$^{\#6}$ – P(7) – O(31)	108.3(3)
O(22) – Co(6) – O(24)$^{\#4}$	101.0(2)	O(7) – P(7) – O(17)	111.7(3)

$O(23)^{\#5}$ – Co(6) – $O(24)^{\#4}$	97.4(2)	$O(20)^{\#6}$ – P(7) – O(17)	111.0(3)
$O(21)^{\#5}$ – Co(6) – $O(24)^{\#4}$	120.8(2)	O(31) – P(7) – O(17)	107.4(3)
O(15) – P(1) – O(25)	112.7(3)	O(9) – P(8) – O(14)	111.4(3)
O(15) – P(1) – O(2)	107.0(3)	O(9) – P(8) – O(8)	108.0(3)
O(25) – P(1) – O(2)	110.4(3)	O(14) – P(8) – O(8)	111.5(3)
O(15) – P(1) – O(11)	110.0(3)	O(9) – P(8) – O(32)	110.9(4)
O(25) – P(1) – O(11)	107.0(3)	O(14) – P(8) – O(32)	105.9(3)
O(2) – P(1) – O(11)	109.8(3)	O(8) – P(8) – O(32)	109.1(3)
		Organic Moiety	
N(3) – C(4) – C(3)	110.9(6)	N(5) – C(6) – C(5)	108.1(6)
C(4) – C(3) – N(2)	109.4(6)	C(6) – C(5) – N(4)	108.9(6)
C(3) – N(2) – C(2)	110.8(5)	N(9) – C(12) – C(11)	111.9(10)
N(2) – C(2) – C(1)	108.7(6)	C(12) – C(11) – N(8)	115.6(10)
C(2) – C(1) – N(1)	109.9(6)	C(11) – N(8) – C(10)	117.9(8)
N(6) – C(8) – C(7)	110.6(8)	N(8) – C(10) – C(9)	108.7(6)
C(8) – C(7) – N(5)	116.1(7)	C(10) – C(9) – N(7)	109.1(6)
C(7) – N(5) – C(6)	114.7(7)		

#1 -x+1, -y-2, -z; #2 x, -y-3/2, z+1/2; #3 x, -y-1/2, z-1/2; #4 x, y+1, z; #5 -x, -y, -z; #6 -x+1, -y-1, -z.

the framework must have three protons, for charge-balancing purposes. Of the eight terminal P – O bonds, three are likely to have protons, which were located in difference Fourier maps, and also matches with the uncoordinated P-O bond lengths. Bond valence sum calculations[244] on the framework also agrees with the above formalism. Thus, O(27), O(28) and O(29) with P–O distances of 1.571, 1.575 and 1.571 Å are formally –OH groups consistent with the known range of values (~1.56 – 1.60Å).[265] The geometrical data are in agreement with the available structures of similar compounds.[49,50,71-73,268]

The polyhedral connectivity in **XX** leads to the open-framework network shown in Fig.1.69. The CoO_4, PO_4 and HPO_4 groups are connected, in a manner to form 4-membered rings, which may be the fundamental building in open-framework metal phosphates. Thus, there are no Co – O – Co or P – O – P linkages seen in this material. The 4-membered rings are joined together edge- and corner-wise forming 16-membered elliptical one-dimensional channels, of width 17.1 x 4.0 Å, along the *b* axis as shown in Fig.1.70. This is the first time, to our knowledge, such large channels are formed in an open-framework cobalt phosphate material. The structure-directing amine, triply protonated DETA species occupies the channels along with water molecules and interact with the framework via hydrogen bonding.

$C_4N_3H_{16}]_3[Co_6(PO_4)_5(HPO_4)_3]H_2O$, has been synthesized by the reaction of an amine phosphate with Co^{2+} ions under hydrothermal conditions at 150°C, with the triply protonated DETA molecules present within the channels. The framework is built from strictly alternating tetrahedra of Co and P, thereby leading to absence of Co–O–Co or P–O–P linkages and the entire structure is constituted of only Co–O–P connections, despite a Co:P ratio of 1:1.33. The structure possesses one terminal P–O linkage for each of the phosphorus atom. **XX** forms one-dimensional channels bound by 16-T (T = Co, P) atoms. Although large apertures are known to occur within many framework solids, including layered materials,[267] 16-membered channels are rarely observed. Examples of such apertures and channels are very few,[30,119] the apertures being generally

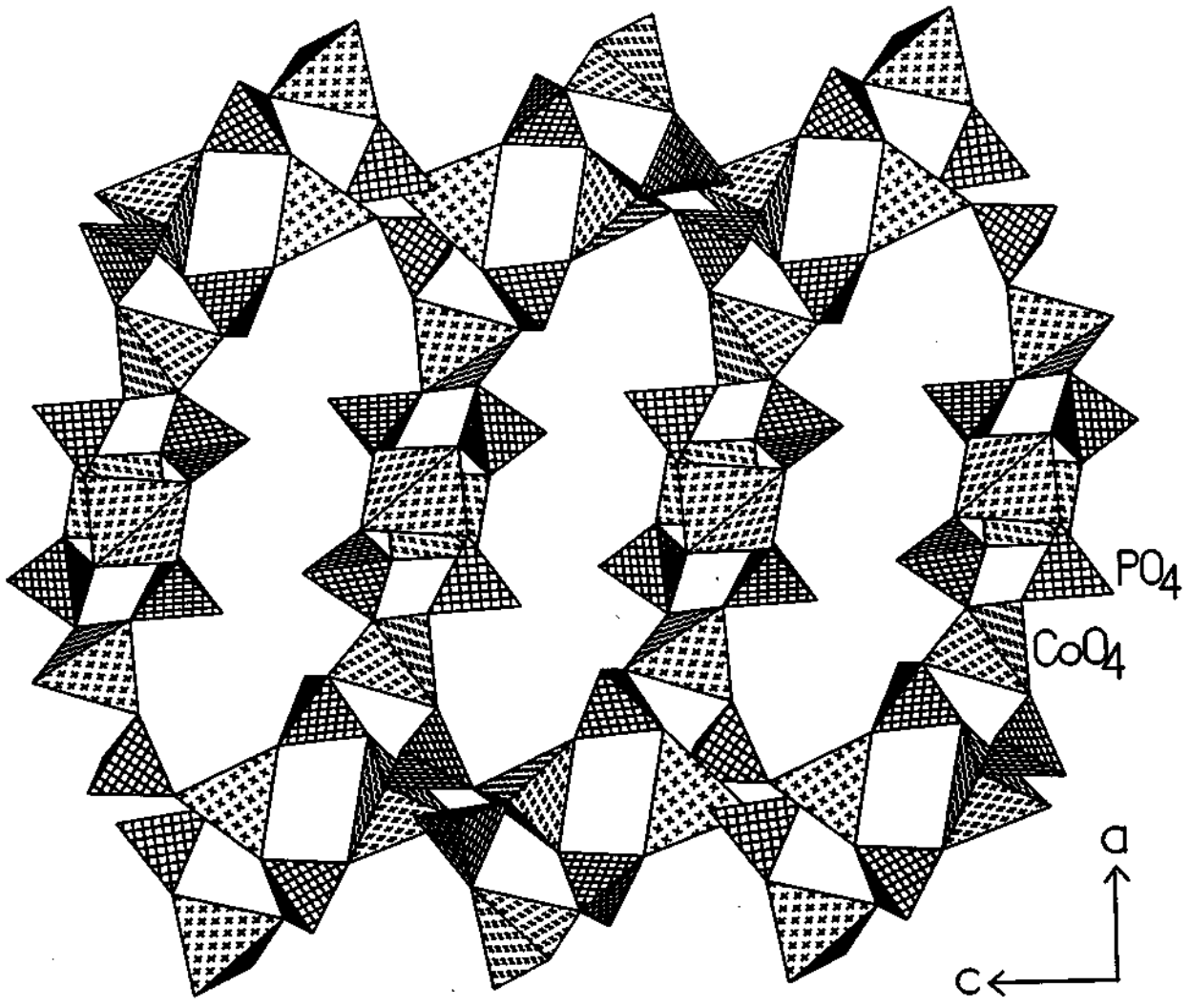

Fig. 1.69 Polyhedral view of **XX**, along the [010] direction showing the 16–membered channels. Amine and water molecules are not shown for clarity.

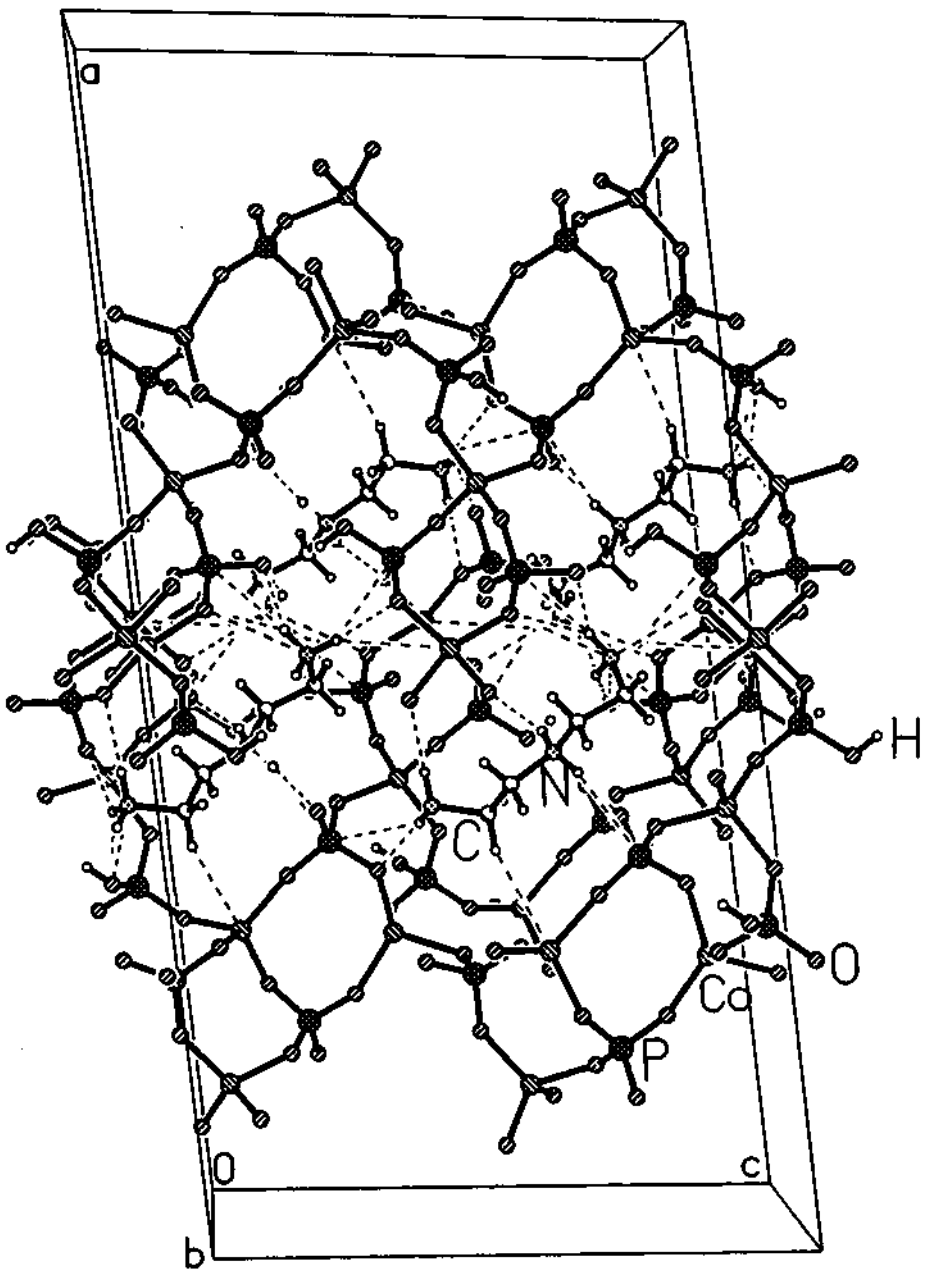

Fig. 1.70 Structure of **XX**, along the [010] direction showing the position of the amine within the channels. Dotted lines represent hydrogen– bond interactions.

restricted to a maximum of 12-membered rings.[95] In cobalt phosphates, **XX** appears to be the first example with such a large channel.

In case of **XX**, the FD values are found to be as low as, 13.3, indicating a more open architecture. This is the lowest FD value observed for open-framework cobalt phosphates and the value is close to that of MAPSO-46, which has only 8- and 12-membered channels.[16]

Dominant hydrogen bonding involving the amine and the framework is observed in **XX** (Table 1.63). The strongest hydrogen bond interactions are observed for the hydrogen atoms attached to the nitrogen and the framework oxygens. The donor-acceptor (O ...H) distances around 2.0 Å and the majority of the angles above 150° (O...H-N) indicate that the hydrogen bond interactions are strong. On the basis of the structure of **XX** and the hydrogen bond interactions present therein, a tentative mechanism for the formation of such large voids can be proposed. The triply protonated DETA molecules are positioned in such a manner that they interact strongly with the framework oxygens forming N-H...O bonds (Fig.1.70). DETA is known to direct the formation of 8- and 10-membered channels in open-framework zinc phosphates. In **XX**, however, two DETA cations along with one molecule of water present in 16-membered channels interact with the framework through hydrogen bonds. These interactions, along with the positions of the amine and water molecules could impose constraints on the framework and give rise to the large channels.

Although a few amine phosphates have been described in the literature, the synthesis of DABCO-phosphate has been effected for the first time during this investigation. The structure comprises a hydrogen bonded assembly of layers wherein the hydrogen phosphate groups form one set of layer and the doubly protonated DABCO along a molecule of water form the adjacent layer (Fig. 1.71). This is somewhat typical of a layered framework material where the alternating inorganic and organic layers are usually present. This hydrogen-bonded assembly is stable even under hydrothermal conditions and can be stored

Table 1.63. Selected hydrogen bond interaction observed in **XX**, $[C_4N_3H_{16}]_3$ $[Co_6(PO_4)_5(HPO_4)_3]H_2O$.

Moiety	*Distance (Å)*	*Moiety*	*Angle (°)*
O(20) – H(2)	2.282(2)	O(20) – H(2) – N(1)	143.6(1)
O(14) – H(3)	2.008(1)	O(14) – H(3) – N(1)	159.2(1)
O(32) – H(8)	1.665(1)	O(32) – H(8) – N(2)	170.3(2)
O(19) – H(9)	2.147(2)	O(19) – H(9) – N(2)	158.2(1)
O(31) – H(14)	1.975(1)	O(31) – H(14) – N(3)	142.2(1)
O(17) – H(15)	2.159(2)	O917) – H(15) – N(3)	145.8(4)
O(31) – H(15)	2.393(1)	O(31) – H(15) – N(3)	143.5(1)
O(18) – H(16)	1.972(1)	O(18) – H(16) – N(3)	153.1(1)
O(16) – H(17)	1.900(1)	O(16) – H(17) – N(4)	165.0(1)
O(4) – H(18)	2.151(1)	O(4) – H(18) – N(4)	151.8(1)
O(11) – H(19)	1.944(2)	O(11) – H(19) – N(4)	160.9(1)
O(27) – H(25)	2.505(1)	O(27) – H(25) – N(5)	143.8(1)
O(25) – H(30)	1.945(1)	O(25) – H(30) – N(6)	155.8(2)
O(21) – H(31)	1.959(1)	O(21) – H(31) – N(6)	158.6(3)
O(3) – H(32)	2.108(2)	O(3) – H(32) – N(6)	148.9(3)
O(26) – H(33)	2.103(3)	O(26) – H(33) – N(7)	143.8(2)
O(2) – H(34)	1.991(2)	O(2) – H(34) – N(7)	149.0(1)
O(30) – H(35)	1.919(3)	O(30) – H(35) – N(7)	152.1(1)
O(13) – H(40)	1.844(2)	O(13) – H(40) – N(8)	150.7(2)
O(11) – H(41)	2.030(2)	O(11) – H(41) – N(8)	162.1(3)
O(28) – H(46)	1.994(2)	O(28) – H(46) – N(9)	170.8(2)
O(8) – H(47)	2.468(3)	O(8) – H(47) – N(9)	149.8(3)
O(32) – H(48)	2.100(1)	O(32) – H(48) – N(9)	139.2(1)
O(31) – H(50)[1]	1.826(1)	O(31) – H(50) – O(29)[1]	148.5(2)
O(9) – H(51)[1]	2.061(2)	O(9) – H(51) – O(28)[1]	172.5(2)
O(30) – H(52)[1]	1.833(1)	O(30) – H(52) – O(27)[1]	161.4(3)
O(7) – H(7)	2.597(1)	O(7) – H(7) – C(2)	141.3(2)
O(15) – H(22)	2.571(2)	O(15) – H(22) – C(6)	145.0(4)
O(25) – H(37)	2.365(1)	O(25) – H(37) – C(9)	147.6(1)
O(10) – H(43)	2.229(1)	O(10) – H(43) – C(11)	161.2(3)

[1] Intra-framework

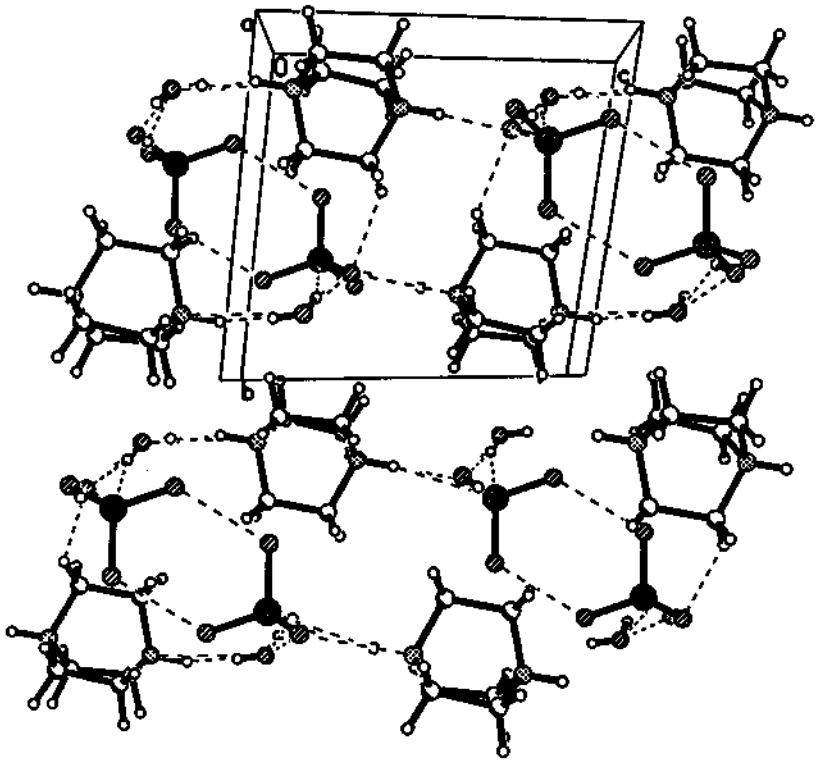

Fig. 1.71. Structure of the DABCO-phosphate along (a) *bc* plane and (b) *ac* plane showing layer-like arrangement.

and used for reactions with metal ions. The reaction of Co(II) ions with DABCO-P, however, gave a three-dimensional cobalt phosphate $[C_6N_2H_{14}][Co_2(HPO_4)_2]$, **XXI**, along with many condensed cobalt phosphate phases.

$[C_6N_2H_{14}][Co_2(HPO_4)_2]$, XXI : XXI, possesses a new three-dimensional open-framework structure containing one-dimensional channels bound by 8-T atoms (T = Co and P). The structure is built up from CoO_4 and PO_4 building units and are connected via Co – O – P bonds, surrounding channels occupied by extra-framework diprotonated 1,4-diazabicyclo[2,2,2]octane (DABCO) cations. The 25 non-hydrogen atoms of the asymmetric unit consist of 17 framework and 8 atoms of the guest species respectively (Fig. 1.72, atomic coordinates Table 1.64). The asymmetric unit contains two crystallographically independent cobalt and three phosphorus atoms. The two cobalt atoms in **XXI**, are both tetrahedrally coordinated by their O atom neighbors with average cobalt – oxygen bond distances of 1.951 Å for Co(1) and 1.950 Å for Co(2)(Table 1.65). Both cobalt atoms make four Co – O – P bonds to three distinct P atom neighbors and an average Co–O–P bond angle of 135.1° resulting from a fairly wide spread of angles (Table1.66). These structural parameters are in good agreement with the results of previous structure determinations on similar compounds.[49,50,71-73,266,268] The P atoms, make three P – O – Co bonds and the remaining is a terminal P – O bond. The P – O bond distances are in the range 1.504 – 1.592 Å [$(P(1) - O)_{av.}$ = 1.537, $(P(2) - O)_{av.}$ = 1.538, $(P(3) - O)_{av.}$ = 1.536Å] and the O – P – O angles are the range 104.8 – 115.2° [$(O - P(1) - O)_{av.}$ = 109.5, $(O - P(2) - O)_{av.}$ = 109.4, $(O - P(3) - O)_{av.}$ = 109.4°]. These values are in good agreement with those observed in other open-framework phosphates.[49,50,71-73] Assuming the valences of Co, P and O to be +2, +5 and –2 respectively, the framework stoichiometry of $Co_2(PO_4)_3$ creates a framework charge of -5. If both the nitrogen atoms of the DABCO are protonated, we would still require three 'framework' protons for charge balance in agreement with the hydrogen positions associated with the terminal P – O units observed in the difference Fourier maps. Accordingly, the P(1) – O(10) , P(2) – O(11) and P(3) – O(12) distances of 1.590, 1.592 and

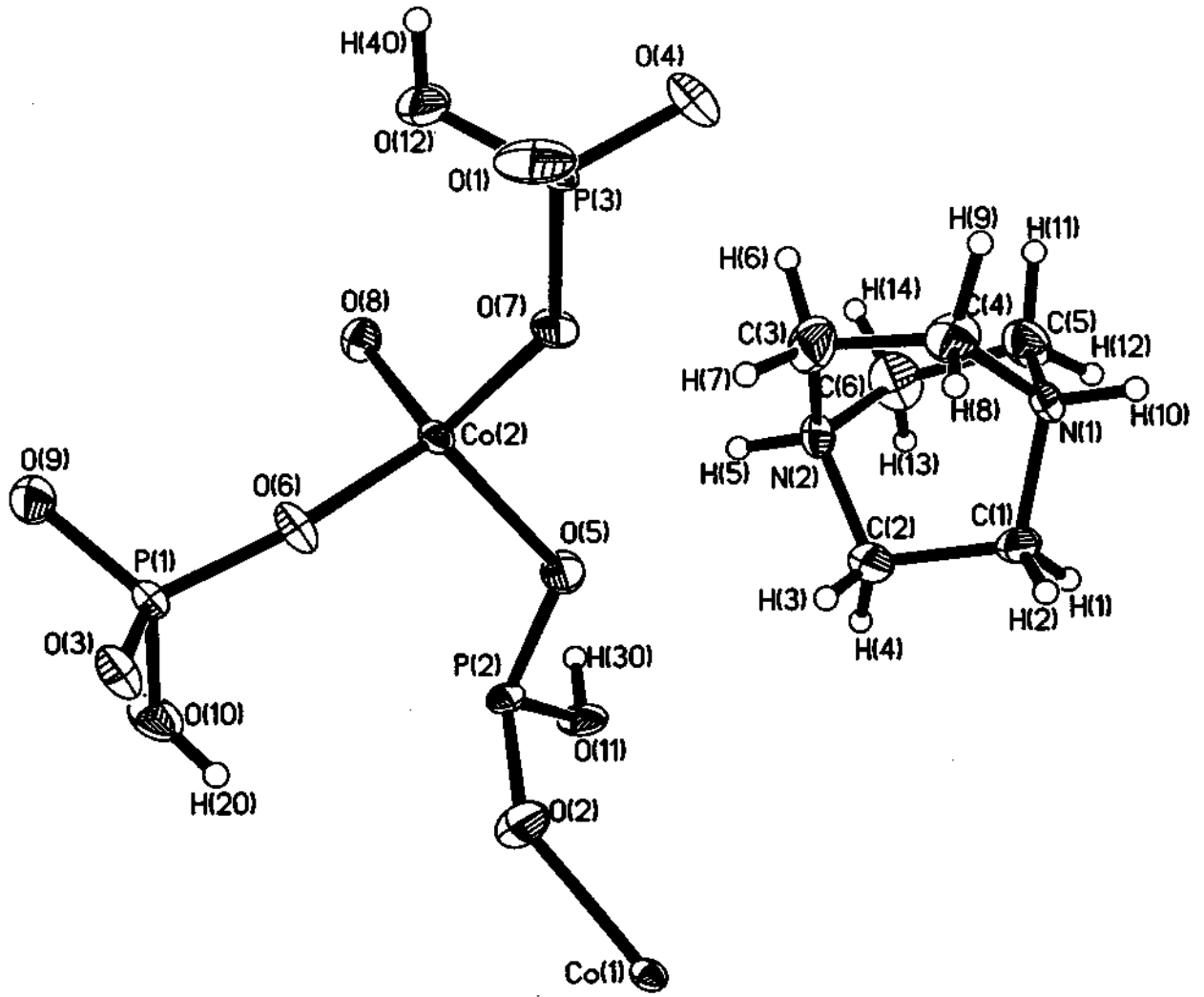

Fig. 1.72. ORTEP plot of **XXI**, $[C_6N_2H_{14}]$ $[Co_2(HPO_4)_3]$. Thermal ellipsoids are given at 50% probability.

Table 1.64. Atomic coordinates [x 10^4] and equivalent isotropic displacement parameters [$Å^2$ x 10^3] for **XXI**, $[C_6N_2H_{14}][Co_2(HPO_4)_3]$.

Atom	x	y	z	U(eq)[#1]
Co(1)	-3144(1)	12066(1)	1567(1)	12(1)
Co(2)	-1362(1)	10330(1)	6126(1)	12(1)
P(1)	1749(1)	14007(1)	7300(1)	13(1)
P(2)	-1558(1)	10292(1)	3063(1)	14(1)
P(3)	-3369(1)	9695(1)	8385(1)	13(1)
O(1)	-3412(4)	11094(3)	9492(3)	28(1)
O(2)	-1770(4)	11592(3)	2757(3)	26(1)
O(3)	1710(3)	15587(3)	7892(3)	20(1)
O(4)	-4908(3)	8108(3)	7966(3)	24(1)
O(5)	-2495(3)	9646(3)	4038(3)	24(1)
O(6)	65(3)	12640(3)	6982(3)	20(1)
O(7)	-3062(3)	9996(3)	7032(3)	19(1)
O(8)	-262(3)	9069(3)	6258(3)	18(1)
O(9)	3043(3)	13956(3)	8320(3)	22(1)
O(10)	2190(4)	13844(3)	5803(3)	27(1)
O(11)	-2191(3)	8822(3)	1513(3)	21(1)
O(12)	-1869(3)	9546(4)	9083(3)	25(1)
		Organic moiety		
N(1)	-8487(4)	5199(4)	2469(3)	19(1)
N(2)	-5594(4)	5996(4)	2703(4)	21(1)
C(6)	-6599(6)	4208(5)	1955(6)	33(1)
C(5)	-8316(6)	3717(5)	2005(5)	27(1)
C(4)	-7474(5)	6289(5)	4042(5)	27(1)
C(3)	-5746(6)	6559(6)	4197(5)	33(1)
C(2)	-6126(5)	6753(5)	1813(5)	28(1)
C(1)	-7954(5)	6056(5)	1488(4)	22(1)

[#1] U(eq) is defined as one-third of the trace of the orthogonalized $U_{i,j}$ tensor.

Table 1.65. Selected bond distances in **XXI**, $[C_6N_2H_{14}][Co_2(HPO_4)_3]$.

Moiety	Distance (Å)	Moiety	Distance (Å)
Co(1) – O(1)$^{\#2}$	1.932(3)	P(1) – O(3)	1.525(3)
Co(1) – O(2)	1.949(3)	P(1) – O(10)	1.590(3)
Co(1) – O(3)$^{\#3}$	1.994(3)	P(2) – O(2)	1.504(3)
Co(1) – O(4)$^{\#1}$	1.930(3)	P(2) – O(5)	1.518(3)
Co(2) – O(5)	1.971(3)	P(2) – O(8)$^{\#4}$	1.538(3)
Co(2) – O(6)	1.933(3)	P(2) – O(11)	1.592(3)
Co(2) – O(7)	1.924(3)	P(3) – O(7)	1.513(3)
Co(2) – O(8)	1.970(3)	P(3) – O(1)	1.516(3)
P(1) – O(6)	1.515(3)	P(3) – O(4)	1.520(3)
P(1) – O(9)	1.519(3)	P(3) – O(12)	1.590(3)
		Organic Moiety	
N(1) – C(1)	1.495(5)	N(2) – C(2)	1.493(5)
N(1) – C(4)	1.500(5)	N(2) – C(3)	1.479(6)
N(1) – C(5)	1.496(5)	N(2) – C(6)	1.488(6)
C(1) – C(2)	1.523(6)	C(3) – C(4)	1.533(6)
C(5) – C(6)	1.514(7)		

Symmetry transformations used to generate equivalent atoms:

#1 -x-1, -y+2, -z+1 #2 x, y, z-1 #3 –x, -y+3, -z+1

Table 1.66. Selected bond angles in **XXI**, $[C_6N_2H_{14}][Co_2(HPO_4)_3]$.

Moiety	Angle (°)	Moiety	Angle (°)
$O(4)^{\#1}$ – Co(1) – $O(2)^{\#2}$	115.27(13)	O(6) – P(1) – O(10)	109.3(2)
$O(4)^{\#1}$ – Co(1) – O(2)	117.32(13)	O(9) – P(1) – O(10)	106.4(2)
$O(1)^{\#2}$ – Co(1) – O(2)	111.68(13)	O(3) – P(1) – O(10)	107.7(2)
$O(4)^{\#1}$ – Co(1) – $O(3)^{\#3}$	105.35(11)	O(2) – P(2) – O(5)	115.2(2)
$O(1)^{\#2}$ – Co(1) – $O(3)^{\#3}$	103.33(13)	O(2) – P(2) – $O(8)^{\#4}$	108.8(2)
O(2) – Co(1) – $O(3)^{\#3}$	101.57(12)	O(5) – P(2) – $O(8)^{\#4}$	110.0(2)
O(7) – Co(2) – O(6)	105.00(11)	O(2) – P(2) – O(11)	106.9(2)
O(7) – Co(2) – O(8)	115.31(12)	O(5) – P(2) – O(11)	107.3(2)
O(6) – Co(2) – O(8)	114.32(11)	$O(8)^{\#4}$ – P(2) – O(11)	108.4(2)
O(7) – Co(2) – O(5)	103.43(11)	O(7) – P(3) – O(1)	111.4(2)
O(6) – Co(2) – O(5)	108.90(12)	O(7) – P(3) – O(4)	111.1(2)
O(8) – Co(2) – O(5)	109.17(11)	O(1) – P(3) – O(4)	111.5(2)
O(6) – P(1) – O(9)	112.2(2)	O(7) – P(3) – O(12)	104.8(2)
O(6) – P(1) – O(3)	107.8(2)	O(1) – P(3) – O(12)	109.4(2)
O(9) – P(1) – O(3)	113.4(2)	O(4) – P(3) – O(12)	108.3(2)
P(3) – O(1) – $Co(1)^{\#5}$	140.9(2)	P(2) – O(5) – Co(2)	120.0(2)
P(2) – O(2) – Co(1)	145.8(2)	P(1) – O(6) – Co(2)	146.3(2)
P(1) – O(3) – $Co(1)^{\#3}$	139.2(2)	P(3) – O(7) – Co(2)	136.6(2)
P(3) – O(4) – $Co(1)^{\#1}$	124.3(2)	$P(2)^{\#4}$ – O(8) – Co(2)	127.8(2)
	Organic Moiety		
C(1) – N(1) – C(5)	109.2(3)	N(2) – C(6) – C(5)	109.0(3)
C(1) – N(1) – C(4)	110.0(3)	N(1) – C(5) – C(6)	108.2(3)
C(5) – N(1) – C(4)	110.0(3)	N(1) – C(4) – C(3)	107.9(3)
C(3) – N(2) – C(6)	109.7(4)	N(2) – C(3) – C(4)	108.5(3)
C(3) – N(2) – C(2)	110.4(3)	N(2) – C(2) – C(1)	108.2(3)
C(6) – N(2) – C(2)	109.8(3)	N(1) – C(1) – C(2)	108.5(3)

Symmetry transformations used to generate equivalent atoms:

#1 -x-1, -y+2, -z+1; #2 x, y, z-1; #3 -x, -y+3, -z+1; #4 -x, -y+2, -z+1; #5 x, y, z+1

1.590Å, respectively, are P – OH moieties. Thus, all the phosphorus units in **XXI**, are actually HPO_4 units. The long P – O(H) distances in **XXI**, agrees with the similar distances observed in such bonding situations, for example in $H_3PO_4.0.5H_2O$ and α-zirconium phosphates.[270] The attachment of a proton with the terminal oxygens of the P atoms is consistent with the bond-valence sum calculations.[244] It is to be noted that there are no Co – O – Co or P – O – P bonds present in the structure of **XXI**.

The framework structure of **XXI**, is built up from CoO_4 and $PO_3(OH)$ tetrahedra sharing vertices forming four-membered rings. The three-dimensional structure can be derived made from two-dimensional sheets made by Co(1), Co(2), P(2) and P(3) and are connected by the third phosphate [P(1)] units. Within each sheet, there are two different types of four membered rings; one made by Co(1) – P(3) – Co(1) and the other by Co(2) – P(2) – Co(2). These four-membered rings are linked *via* oxygen atoms forming 8-membered pore openings within the layer, which is distorted. These sheets are connected by P(1) units forming one-dimensional channels bound by 8-T atoms (T = Co and P) as shown in Fig.1.73. The channels are formed along the *bc* plane and the width is ~3.6 x 4.8Å. Along the *ac* direction there is another 8-membered channels formed by the linkages between the tetrahedra. The –OH groups of the $PO_3(OH)$ tetrahedra protrude into this channels. The doubly protonated DABCO molecules are located in the 8-ring channels as shown in Fig.1.74.

Multi-point hydrogen bonding, involving the guest species and framework atom is present in the structure of **XXI** and the important hydrogen bond interactions are presented in Table 1.67. In addition to the normally observed amine-framework interactions, strong hydrogen bond interactions also arise from the participation of the hanging –OH group of the phosphates (intra-framework). The intra-framework hydrogen bond interactions with O – H – O angles in the range of ~170° indicates that near linear hydrogen bonding has been established in **XXI**. Near planar hydrogen bond interactions are commonly observed in

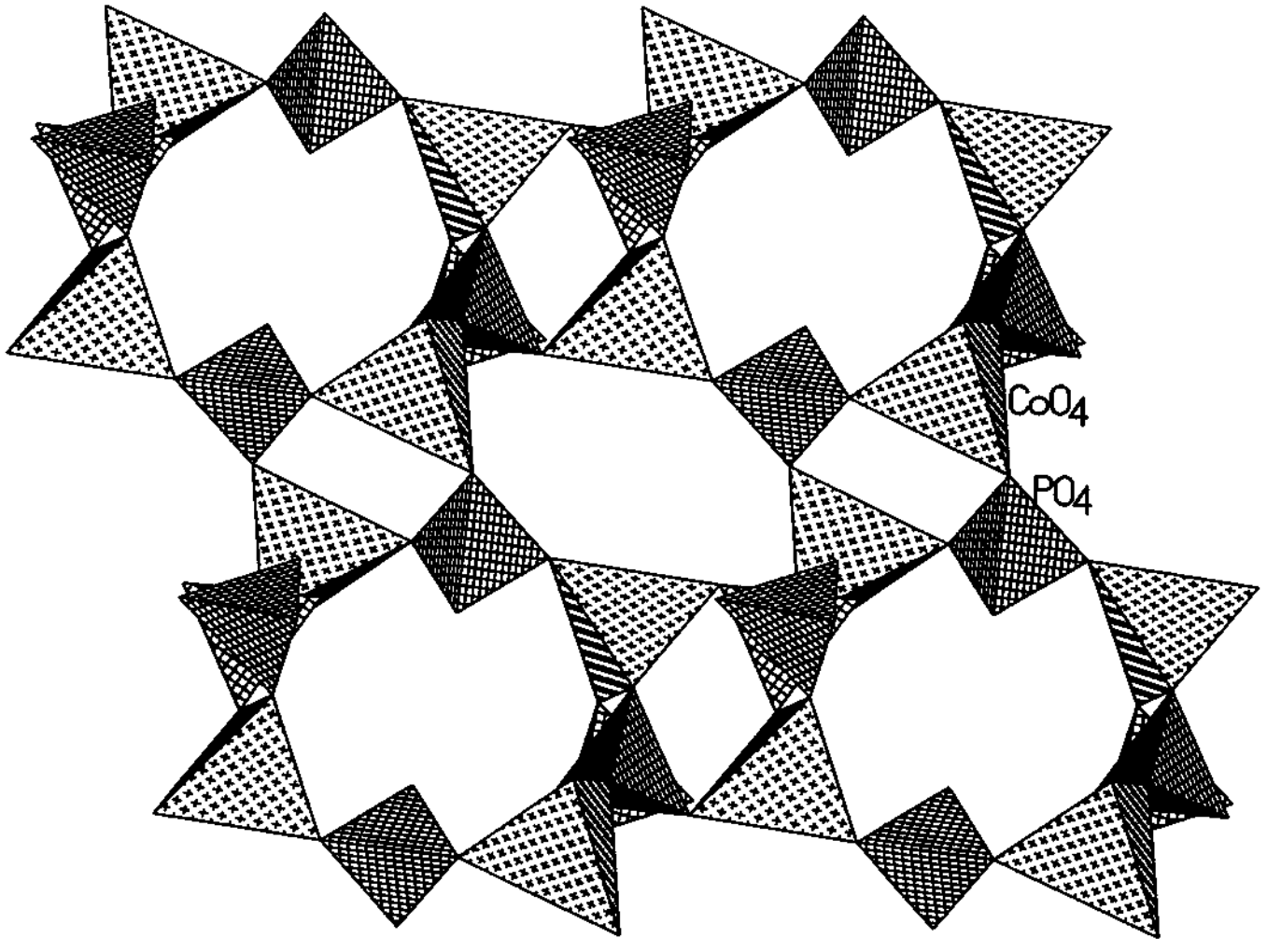

Fig. 1.73. Polyhedral view of the structure of **XXI**, along the *ab* direction showing the 8–membered channel.

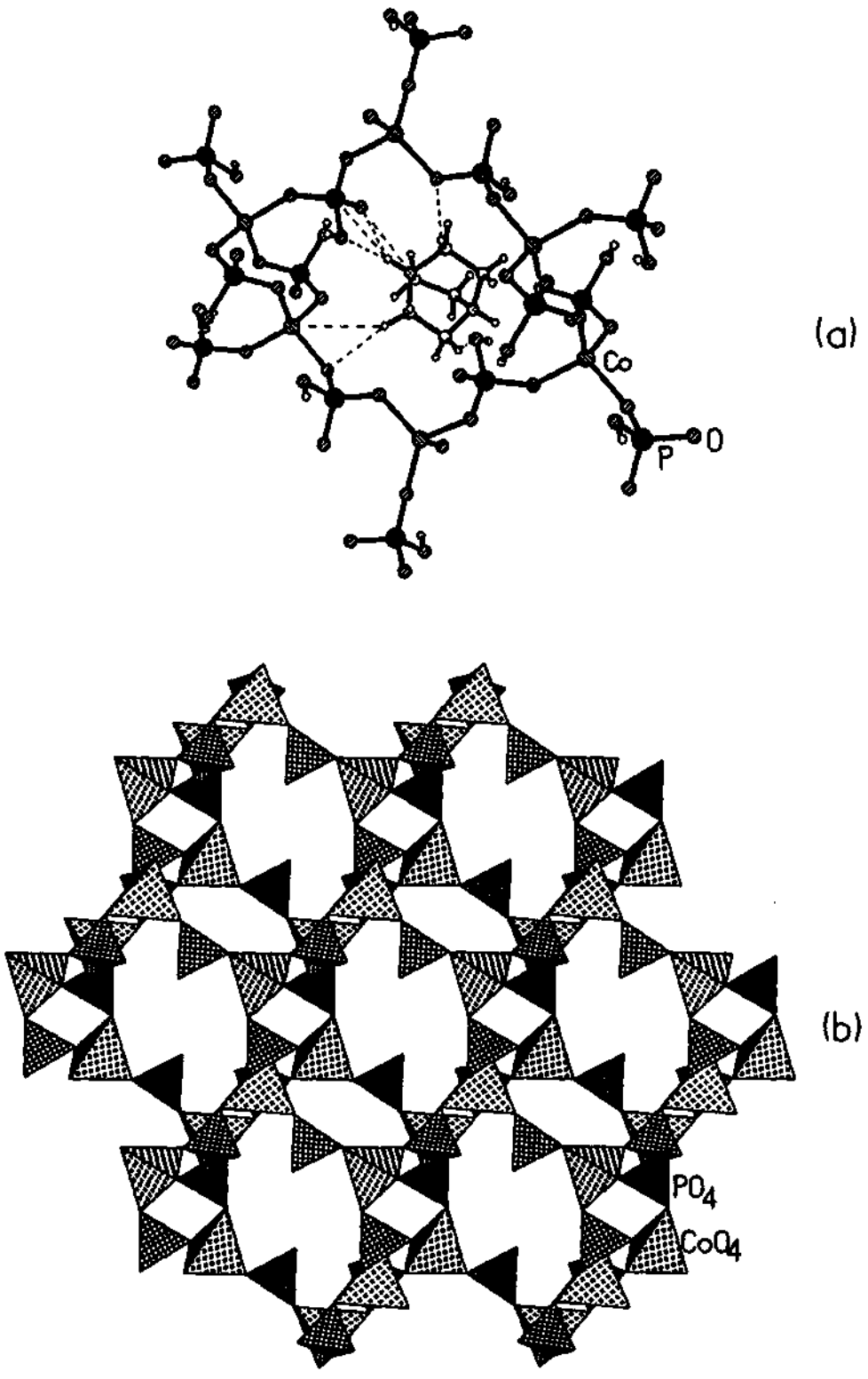

Fig. 1.74. (a) Structure of **XXI** along the *ac* direction showing a single 8-membered channel with the amine. Dotted lines represent the hydrogen bond interactions. (b) Polyhedral view of the structure of **XXI** along the *bc* direction showing the 8-membered channels.

Table 1.67. Selected hydrogen bond interactions in **XXI**, $[C_6N_2H_{14}][Co_2(HPO_4)_3]$.

Moiety	Distance (Å)	Moiety	Angle (°)
O(9) – H(5)	1.967(4)	O(9) – H(5) – N(2)	144.3(1)
O(10) – H(5)	2.552(1)	O(10) – H(5) – N(2)	140.2(2)
O(3) – H(10)	1.870(1)	O(3) – H(10) – N(1)	175.1(1)
O(11) – H(30)[1]	1.868(2)	O(11) – H(30) – O(9)[1]	149.2(1)
O(12) – H(40)[1]	1.941(1)	O(12) – H(40) – O(11)[1]	175.2(1)
O(7) – H(2)	2.576(1)	O(7) – H(2) – C(1)	141.7(3)
O(7) – H(7)	2.440(1)	O(7) – H(7) – C(3)	151.6(1)
O(10) – H(9)	2.549(1)	O(10) – H(9) – C(4)	140.8(3)
O(4) – H(14)	2.387(1)	O(4) – H(14) – C(6)	142.4(1)

[1] Intra-framework

coordination complexes and the presence of such interactions in **XXI** enhances the inherent structural stability.

There is a remarkable similarity between the structures of DABCO-phosphate and the cobalt phosphate as revealed by Figs. 1.75a and 1.75b. It appears that **XXI** can be derived from the structure of DABCO-phosphate. The cobalt ions could replace the water molecules in DABCO-phosphate and make bonds with the phosphates to yield **XXI** (Fig.1.74a). This situation allows the doubly protonated DABCO molecules to sit in the channels. This mechanism proves that the ammonium phosphate intermediate route is an important step in the formation of framework solids.

The synthesis of these cobalt phosphates **XX** and **XXI** is significant as these represent only the second report of three-dimensional pure cobalt phosphate materials, synthesized hydrothermally in the presence of organic amines. We attribute this to the novel synthetic route employed in this study. Our study establishes the possible role of amine phosphates as intermediates in the formation of open-framework phosphate materials.

4.5.3. Tin phosphate by the amine phosphate route

In order to establish the universality of the reaction of amine phosphates with metal ions to yield open-framework architectures, we carried out the reaction of PIPP with Sn(II) ions. The reaction of PIPP with Sn^{II} ions gave a open-framework structure, **XXII**, $[C_4N_2H_{11}]_{0.5}[Sn(PO_4)]$, with a layered architecture.

$[C_4N_2H_{11}]_{0.5}[Sn(PO_4)]$, XXII : The structure of **XXII**, is based on a network of strictly alternating SnO_3 and PO_4 units that form infinite layers. The asymmetric unit contains 9 independent non-hydrogen atoms (Fig. 1.76a, atomic coordinates Table 1.68) and the layers with the amine molecules are shown in Fig. 1.76b. The Sn atom is coordinated to three oxygens and occupies the vertex of a trigonal pyramid ; the lone pair presumably occupies the fourth vertex of the

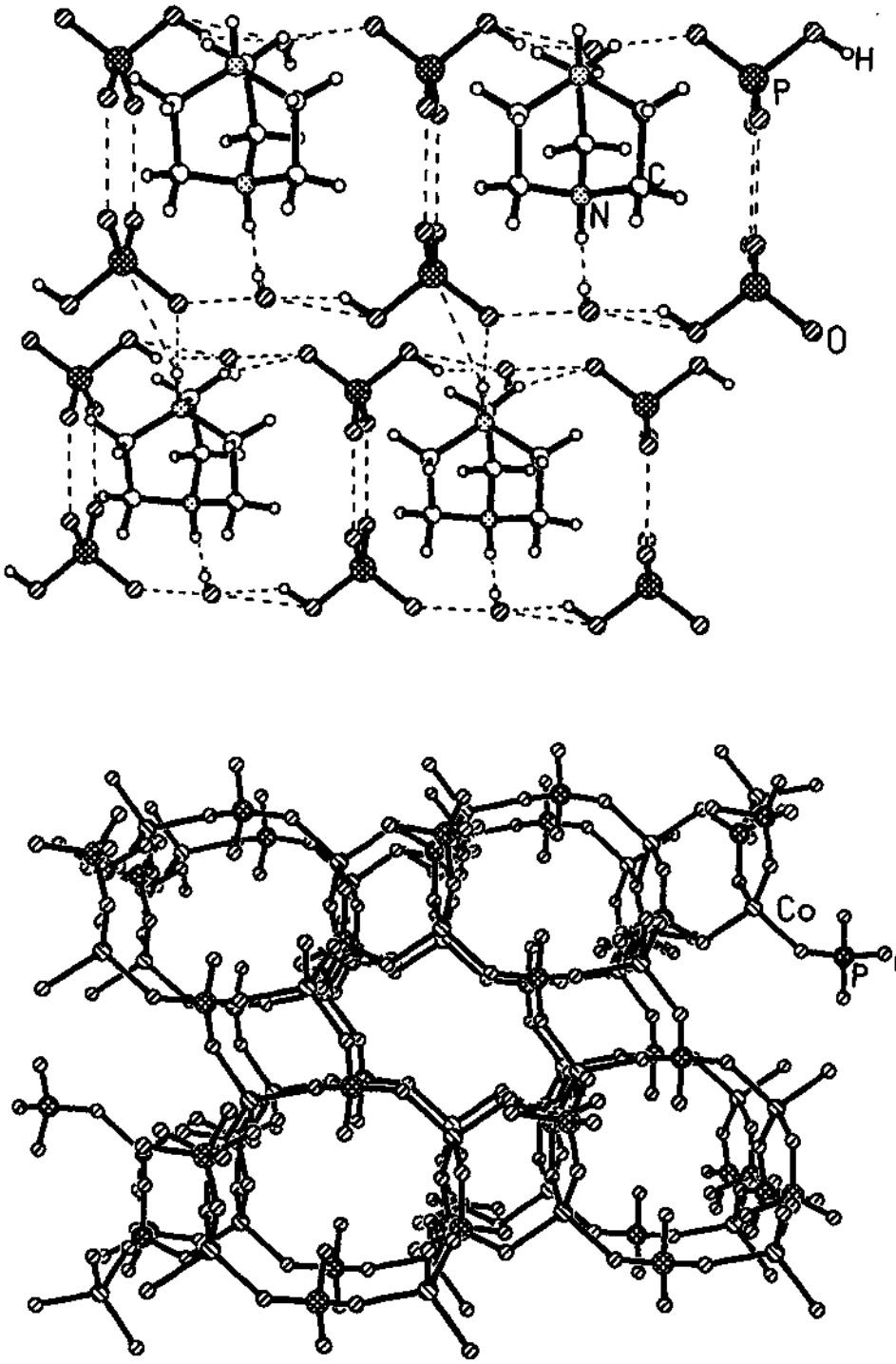

Fig. 1.75. (a) Structure of the DABCO-phosphate. (b) Structure of **XXI**, $[C_6N_2H_{14}][Co_2(HPO_4)_3$. Note that the Co atoms replace the water molecules in the structure of (a).

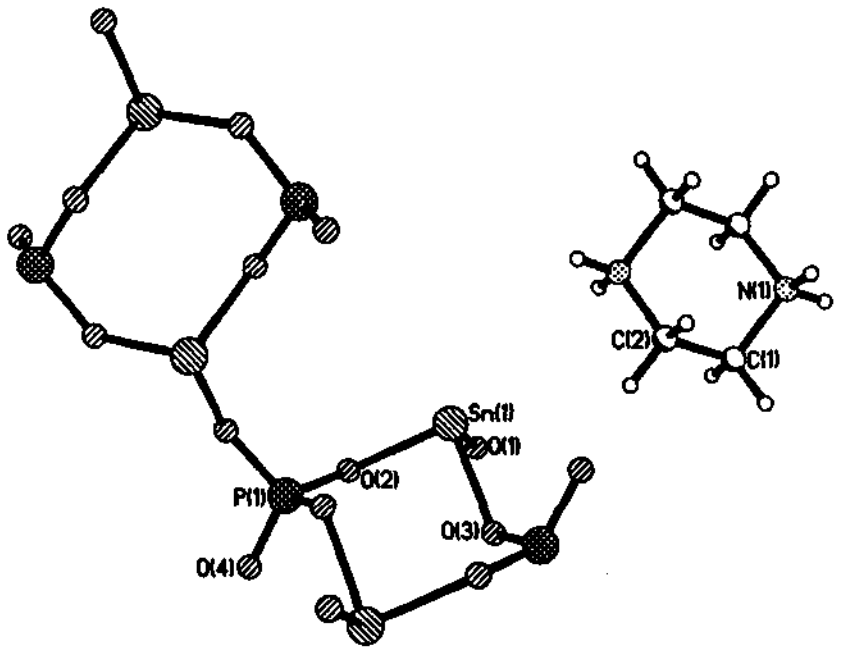

(a)

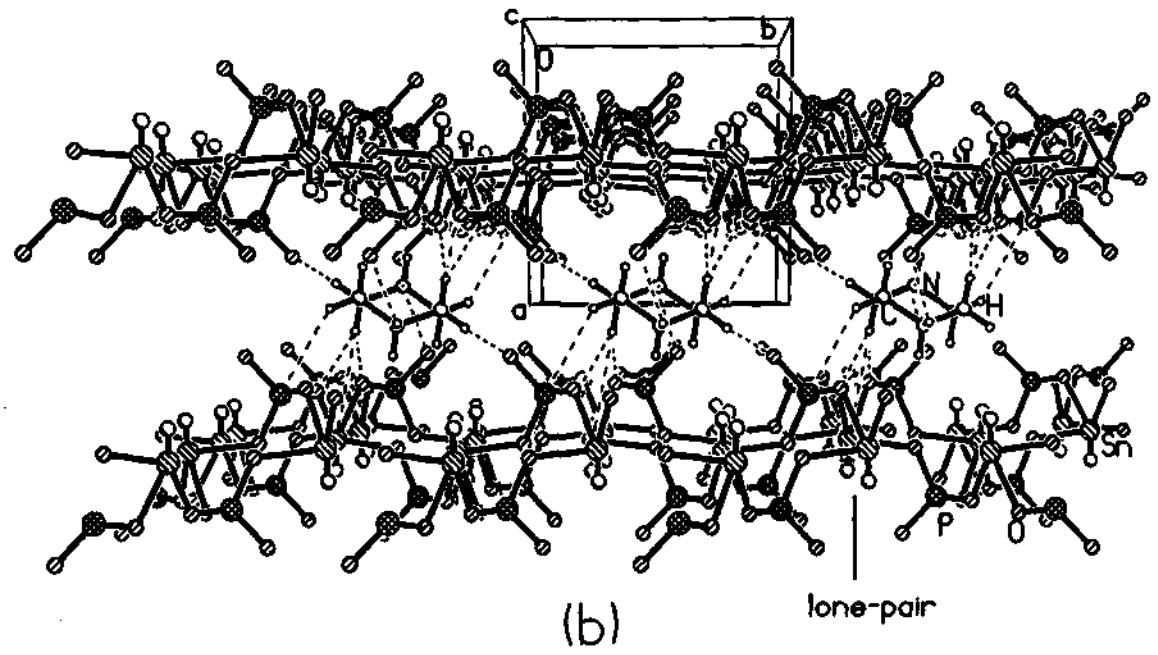

(b)

Fig. 1.76. (a) ORTEP plot of **XXII**, $[C_4N_2H_{12}]_{0.5}[Sn(PO_4)]$. Thermal ellipsoids are given at 50% probability. (b) Structure of **XXII** along the *ab* plane showing the layer arrangement. Note that the lone pairs associated with Sn^{II} ions point into the inter-layer spacing. The dotted lines represent hydrogen bond interactions.

Table 1.68. Atomic coordinates [x 10^4] and equivalent isotropic displacement parameters [$Å^2$ x 10^3] for **XXII**.

Atom	x	y	z	U(eq)
Sn(1)	4899(1)	2357(1)	668(1)	21(1)
P(1)	3140(2)	4375(2)	-2391(2)	20(1)
O(1)	3094(5)	1815(6)	1362(5)	30(1)
O(2)	2898(5)	3238(6)	-1220(4)	28(1)
O(3)	5134(5)	4822(6)	1645(4)	28(1)
O(4)	1813(6)	5685(6)	-2952(5)	35(1)
C(1)	9714(9)	1466(9)	5709(7)	31(1)
C(2)	9843(7)	1610(7)	4280(6)	14(1)
N(1)	10719(8)	-17(8)	6587(6)	46(2)

tetrahedron. The Sn–O bond distances lie in the range 2.079(4)–2.131(4)Å (av. 2.105(4) Å) and the O – Sn – O angles are in the range 82.6(2) – 90.0(2)° (av. 86.9(2)°). The P – O distances are in the range 1.548(4) – 1.564(4)Å (av.1.554 Å), and the O – P – O angles are in the range 107.6(3)– 112.9(3)° (av. 109.1(3)°) (Table 1.69). The structure is constructed by networking of SnO_3 and PO_4 units forming infinite anionic layers. The connectivity between these moieties creates 4- and 8-membered rings along the a axis formed by the T atoms (T = Sn , P). Each 4-memberd ring is attached to four 8-membered rings in and each 8-membered ring is connected to four 4-membered rings (Fig 1.77). The structure of **XXII** is comparable to the layered Sn(II) phosphate structures obtained by conventional hydrothermal methods.[235] The universality of the amine phosphate route is also corroborated by the synthesis of a well-known open-framework gallium phosphate ULM-5,[263] by the reaction of 1,6-diaminohexane phosphate with Ga^{3+} ions at 180°C. The isolation of a variety of open-framework architectures obtained by the reaction between an amine phosphate (PIPP) with different metal ions, demonstrates the efficacy of the amine phosphate route to the synthesis of the open architectures and underscores the role of amine phosphates in the formation of these compounds.

Summary of open-framework metal phosphates obtained by amine phosphate route

The present study demonstrates the seminal role of amine phosphates in the formation and synthesis of open-framework metal phosphates. We have successfully isolated open-framework zinc (**XI-XVI**), cobalt (**XVII-XXI**) and tin phosphates (**XXII**) by the reaction of amine phosphates with respective metal ions. In addition to this we have also synthesized new amine phosphates and characterized them using single crystal x-ray diffraction. These metal phosphates range from one-dimensional linear-chain (**XI**), strip-like (**XVII**) structures, two-dimensional layers (**XVIII, XIX, XXII**) and three-dimensional architectures with channels (**XII-XVI, XX, XXI**). The compound **XIX** is a cobalt chlorophosphate

Table 1.69. Bond distances (Å) and angles (°) for **XXII**.

Moiety	Distance (Å)	Moiety	Angle (°)
Sn(1) – O(1)	2.079(4)	O(2) – Sn(1) – O(3)	90.0(2)
Sn(1) – O(2)	2.106(4)	O(4) – P(1) – O(1)$^{\#1}$	111.5(3)
Sn(1) – O(3)	2.131(4)	O(4) – P(1) – O(3)$^{\#2}$	112.9(3)
P(1) – O(4)	1.494(5)	O(1)$^{\#1}$ – P(1) – O(3)$^{\#2}$	107.9(2)
P(1) – O(1)$^{\#1}$	1.548(4)	O(4) – P(1) – O(2)	108.9(3)
P(1) – O(3)$^{\#2}$	1.550(5)	O(1)$^{\#1}$ – P(1) – O(2)	107.9(3)
P(1) – O(2)	1.564(4)	O(3)$^{\#2}$ – P(1) – O(2)	107.6(2)
Moiety	Angle (°)	P(1)$^{\#3}$ – O(1) – Sn(1)	130.0(3)
O(1) – Sn(1) – O(2)	82.6(2)	P(1) – O(2) – Sn(1)	121.5(2)
O(1) – Sn(1) – O(3)	88.1(2)	P(1)$^{\#2}$ – O(3) – Sn(1)	118.1(2)
Organic Moiety			
Moiety	Distance (Å)	Moiety	Angle (°)
C(1) – C(2)	1.497(8)	C(2) – C(1) – N(1)	110.3(5)
C(1) – N(1)	1.505(9)	N(1)$^{\#4}$ – C(2) – C(1)	110.8(5)
C(2) – N(1)$^{\#4}$	1.480(9)	C(2)$^{\#4}$ – N(1) – C(1)	109.3(5)

Symmetry transformations used to generate equivalent atoms:

#1 x, -y+1/2, z-1/2 #2 -x+1, -y+1, -z#3 x, -y+1/2, z+1/2 #4 -x+2, -y, -z+1

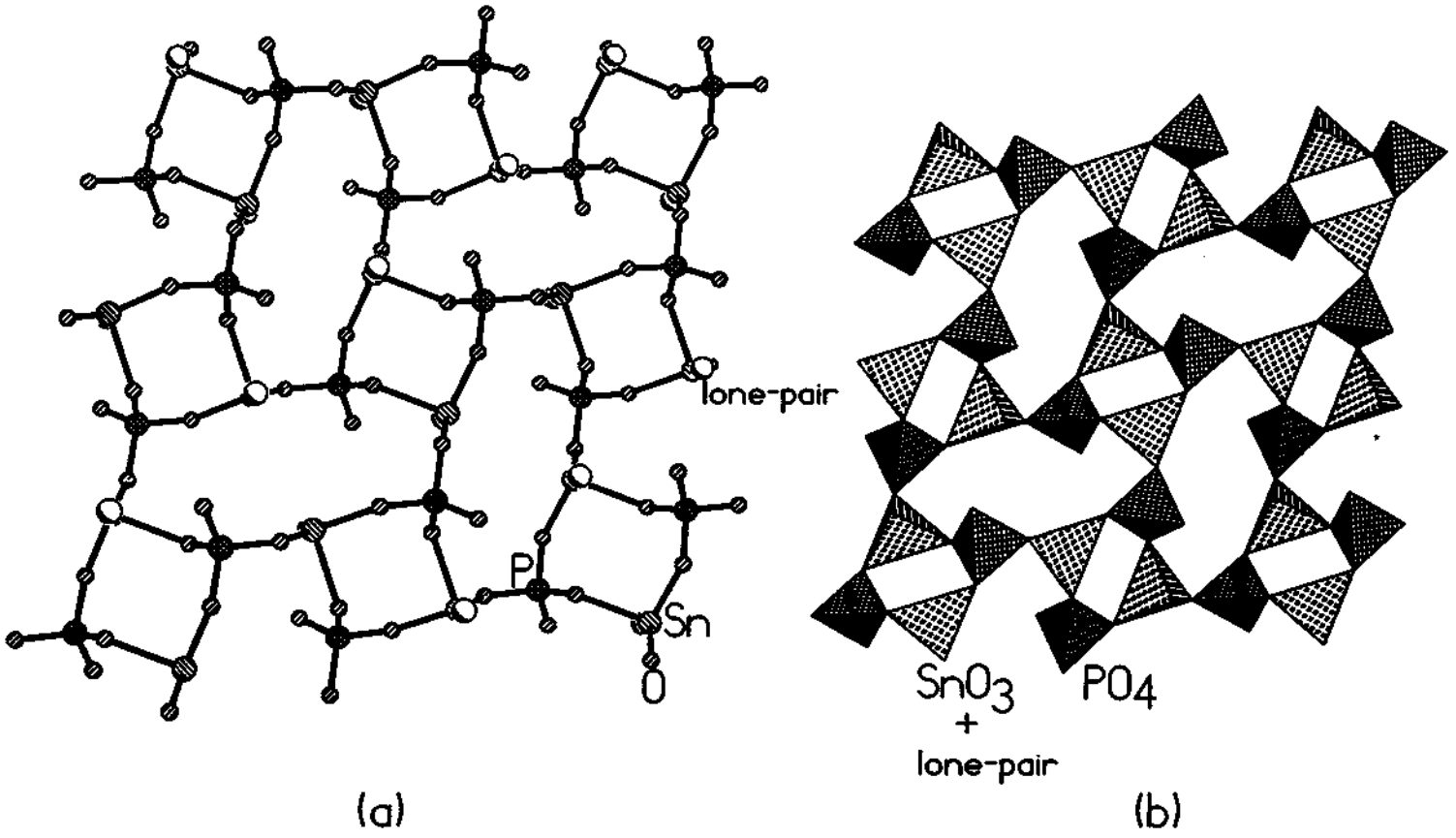

Fig. 1.77. Structure of a single tin phosphate layer of **XXII**, showing the elliptical 8–membered rings attached to 4–membered rings. (a) Ball and stick view (b) polyhedral view.

and has been reported for first time in the literature. That a large number and variety of metal phosphates could be made starting from the amine phosphates clearly demonstrates that the amine phosphates are likely to be the reaction intermediates in the hydrothermal synthesis of these open-framework phosphates.

4.6. Isolation of a Zinc phosphate primary building unit, and its transformation to an open-framework Phosphate

$[C_6N_2H_{18}]^{2+}[Zn(H_2PO_4)_2(HPO_4)]^{2-}$, XXIII : The asymmetric unit of monomeric zinc phosphate, **XXIII,** consists of 23 non-hydrogen atoms, and is presented in Fig. 1.78a and the final atomic coordinates are listed in Table 1.70. There are three crystallographically independent phosphorus and a single zinc atom in the asymmetric unit. The Zn atoms are tetrahedrally coordinated with respect to oxygens with the average Zn – O bond distances of 1.950Å and O – Zn – O angles of 100.4°. The zinc atoms are connected to three distinct P atoms via Zn – O – P links with the average bond angles of 133.6°. Of the three independent P atoms, P(1) and P(3) are connected to Zn atoms via one P – O – Zn linkage and have three terminal P – O bonds and P(2) is connected to Zn via two P – O – Zn linkages with two terminal P – O bonds. The average P – O distances of 1.536, 1.539, 1.542 Å result for P(1), P(2) and P(3), respectively. The P – O distances in the region of ~1.561 – 1.588 Å are formally P – O(H) groups (Table 1.71). The P – O distances with values in the range 1.506 – 1.531 Å are typically P = O bonds. This assignment is also consistent with the bond valence sum calculations.[244] The structure of **XXIII** consists of 4-membered rings formed by ZnO_4 and $PO_2(OH)_2$ tetrahedra. The $PO_3(OH)$ and $PO_2(OH)_2$ moieties hang from the Zn center as shown in Fig.1.78a and are stabilized by extensive intra-molecular multi-point hydrogen bonding involving the phosphate units as well as the doubly protonated amine molecule, forming a sheet-like structure (Fig.1.78b). To our knowledge, this is the first time such a structure has been isolated for a zinc phosphate material.

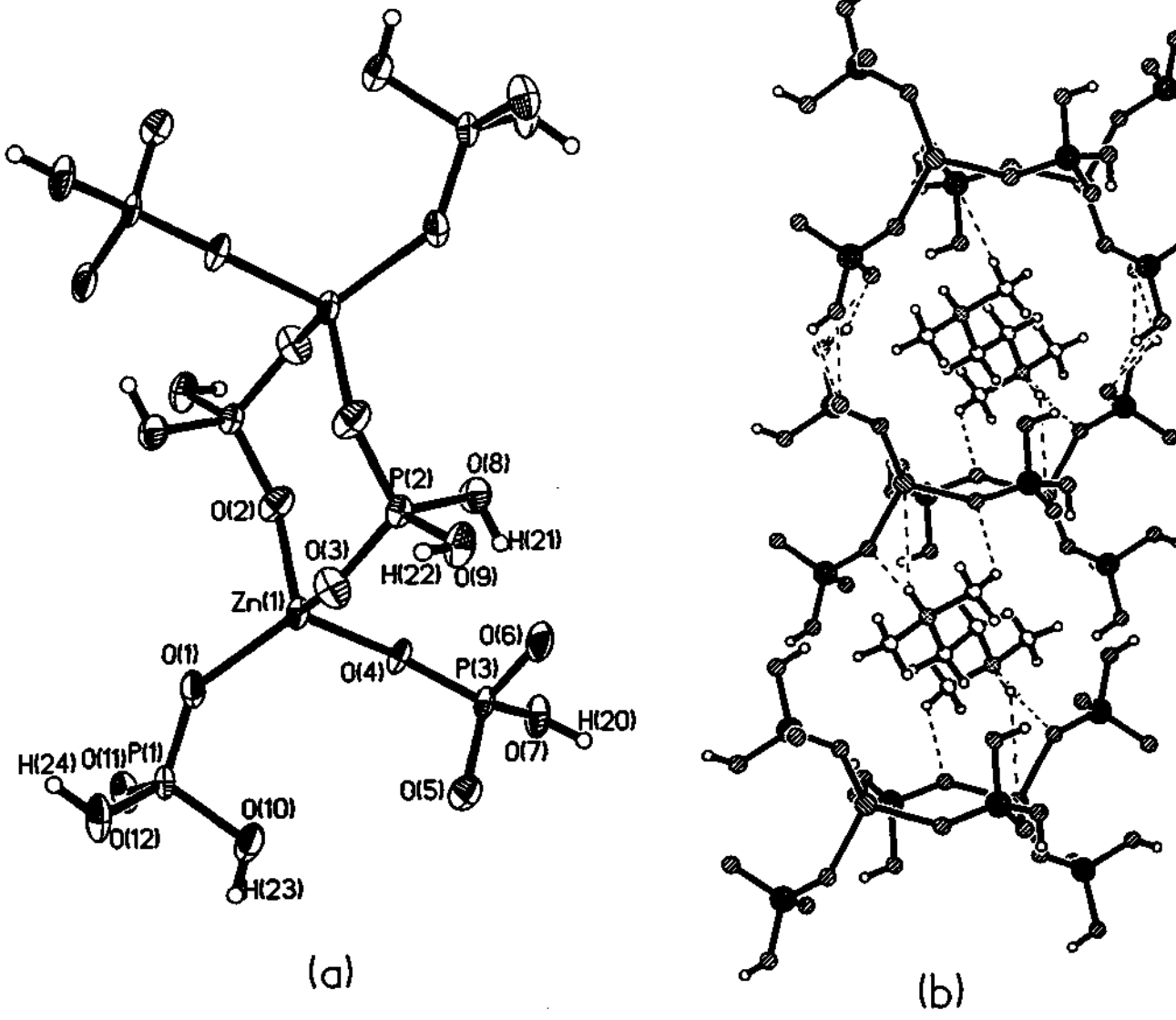

Fig. 1.78. (a) ORTEP plot of the structure of the 4–membered zinc phosphate monomer **XXIII**, Notice the HPO_4 and H_2PO_4 units hanging from the Zn Center. Thermal ellipsoids are given at 50% probability. The asymmetric unit is labeled. (b) Hydrogen bonded assembly of the monomer and the amine. The shee–like architecture has cavities where the amine molecules reside. Dotted lines represent hydrogen–bond interactions.

Table 1.70. Atomic coordinates [x 10^4] and equivalent isotropic displacement parameters [$Å^2$ x 10^3] for **XXIII**, $[C_6N_2H_{18}][Zn(H_2PO_4)(HPO_4)]$.

Atom	x	y	z	U(eq)[1]
Zn(1)	2567(1)	5192(1)	1537(1)	19(1)
P(1)	-1415(1)	7714(1)	3123(1)	19(1)
P(2)	6452(2)	4817(1)	1094(1)	17(1)
P(3)	3867(2)	2229(1)	3013(1)	18(1)
O(1)	198(4)	7054(4)	2141(3)	32(1)
O(2)	2999(5)	4569(4)	-14(3)	29(1)
O(3)	4455(4)	5760(4)	1685(3)	28(1)
O(4)	2871(4)	3046(4)	2141(3)	22(1)
O(5)	2969(4)	3315(4)	4105(3)	26(1)
O(6)	5871(4)	1784(4)	2590(3)	28(1)
O(7)	3750(4)	500(4)	3134(3)	28(1)
O(8)	7076(4)	2869(4)	880(3)	24(1)
O(9)	7568(4)	4910(4)	1869(3)	28(1)
O(10)	-800(5)	6667(4)	4073(3)	32(1)
O(11)	-3060(4)	7686(4)	2924(3)	27(1)
O(12)	-1919(5)	9582(4)	3525(3)	30(1)
N(1)	2549(5)	6377(5)	4968(3)	28(1)
C(1)	4122(8)	5456(8)	5461(5)	42(1)
C(2)	2623(9)	7677(8)	4236(5)	43(1)
C(3)	911(8)	7174(7)	5938(5)	40(1)
N(2)	12485(5)	896(5)	736(3)	24(1)
C(4)	14418(6)	-394(6)	315(4)	25(1)
C(5)	11428(7)	101(7)	1433(4)	34(1)
C(6)	11631(7)	1698(7)	-162(5)	35(1)

[1] U(eq) is defined as one third of the trace of the orthogonalized U_{ij} tensor.

Table 1.71 Bond distances (Å) and angles (°) for **XXIII**.

Moiety	Distance (Å)	Moiety	Angle (°)
Zn(1)-O(1)	1.920(3)	O(1)-P(1)-O(11)	114.0(2)
Zn(1)-O(2)	1.947(3)	O(1)-P(1)-O(10)	106.8(2)
Zn(1)-O(3)	1.961(3)	O(11)-P(1)-O(10)	112.6(2)
Zn(1)-O(4)	1.973(3)	O(1)-P(1)-O(12)	109.3(2)
P(1)-O(1)	1.494(4)	O(11)-P(1)-O(12)	109.1(2)
P(1)-O(11)	1.515(3)	O(10)-P(1)-O(12)	104.6(2)
P(1)-O(10)	1.561(3)	$O(2)^{\#1}$-P(2)-O(3)	114.6(2)
P(1)-O(12)	1.573(3)	$O(2)^{\#1}$-P(2)-O(9)	109.7(2)
$P(2)-O(2)^{\#1}$	1.507(3)	O(3)-P(2)-O(9)	109.3(2)
P(2)-O(3)	1.512(3)	$O(2)^{\#1}$-P(2)-O(8)	108.2(2)
P(2)-O(9)	1.568(3)	O(3)-P(2)-O(8)	110.5(2)
P(2)-O(8)	1.570(3)	O(9)-P(2)-O(8)	103.9(2)
P(3)-O(5)	1.506(3)	O(5)-P(3)-O(6)	112.2(2)
P(3)-O(6)	1.531(3)	O(5)-P(3)-O(4)	112.2(2)
P(3)-O(4)	1.542(3)	O(6)-P(3)-O(4)	110.5(2)
P(3)-O(7)	1.588(3)	O(5)-P(3)-O(7)	109.6(2)
Moiety	Angle (°)	O(6)-P(3)-O(7)	107.6(2)
O(1)-Zn(1)-O(2)	111.3(2)	O(4)-P(3)-O(7)	104.4(2)
O(1)-Zn(1)-O(3)	111.17(14)	P(1)-O(1)-Zn(1)	143.4(2)
O(2)-Zn(1)-O(3)	108.13(14)	$P(2)^{\#1}$-O(2)-Zn(1)	137.5(2)
O(1)-Zn(1)-O(4)	113.35(13)	P(2)-O(3)-Zn(1)	126.8(2)
O(2)-Zn(1)-O(4)	101.04(13)	P(3)-O(4)-Zn(1)	126.8(2)
O(3)-Zn(1)-O(4)	111.35(13)		

Organic

Moiety	Distance (Å)	Moiety	Angle (°)
N(1)-C(2)	1.483(7)	C(2)-N(1)-C(3)	110.0(4)
N(1)-C(3)	1.498(7)	C(2)-N(1)-C(1)	117.4(4)
N(1)-C(1)	1.519(7)	C(3)-N(1)-C(1)	104.8(4)
$C(1)-C(1)^{\#2}$	1.527(12)	$N(1)-C(1)-C(1)^{\#2}$	109.5(6)
N(2)-C(4)	1.489(6)	C(4)-N(2)-C(5)	109.6(4)
N(2)-C(5)	1.504(6)	C(4)-N(2)-C(6)	113.3(4)
N(2)-C(6)	1.507(6)	C(5)-N(2)-C(6)	109.9(4)
$C(4)-C(4)^{\#3}$	1.531(9)	$N(2)-C(4)-C(4)^{\#3}$	111.5(5)

Symmetry transformations used to generate equivalent atoms :
#1 -x+1,-y+1,-z #2 -x+1,-y+1,-z+1 #3-x+3,-y,-z

$[C_6N_2H_{18}][Zn_3(H_2O)_4(HPO_4)_4]$, XXIV : Compound **XXIV** was obtained by heating the zinc phosphate monomer, **XXIII** in water at 50 °C for 2 days. The final atomic coordinates for **XXIV** are presented in Table 1.72. The asymmetric unit consists of 35 non-hydrogen atoms, out of which 27 belong to the framework and 8 belong to the guest species. There are two crystallographically independent phosphorus and zinc atoms present in the asymmetric unit. Of the two crystallographically distinct Zn atoms, one is in tetrahedral environment (Zn(1)) and the other is octahedral (Zn(2)) with respect to oxygen atoms with an average bond distance of 2.028 Å. Zn(2), which is in octahedral coordination, occupies a special position with a site occupancy of 0.5. Zn(1) makes four Zn – O – P linkages with nearest P neighbors and Zn(2) makes only two Zn – O – P linkages resulting in an average Zn – O – P bond angle of 128.1°. The remaining Zn – O linkages in the case of Zn(2) are terminal Zn – O linkages and are found to be water molecules. Such terminal water coordinated to Zn centers is known to occur in zinc phosphates. It is to be noted, however, that an octahedral environment for Zn in framework phosphates is rather rare. Of the two phosphorus atoms, P(1) makes three P – O – Zn linkages with one terminal P – O bond and P(2) make two P – O – Zn linkages with two P – O terminal bonds. Average P – O bond distances of 1.535 Å result for both P(1) and P(2). The terminal P – O distances of 1.583 Å [P(1) – O(8)] and 1.569 Å [P(2) – O(10)] are formally –OH linkages. The O – P – O bond angles are in the expected range (av. 109.4°) (Table 1.73). Bond valence sum calculations also agree with the above assignment.[244] The structure of **XXIV** comprises a network of $Zn(1)O_4$, $Zn(2)O_2(H_2O)_4$ and $PO_3(OH)$ moieties, in which the vertices are shared. The connectivity between these units gives rise to a macroanionic layers with bifurcated 8-membered apertures within each layer as shown in Fig.1.79a. Zn(2) links only with P(1) and the remaining Zn(2) – O linkages are terminal water molecules which point into the 8-membered aperture within the layers. As typical of layered structures, the charge compensating cationic amine molecules are situated in between the anionic inorganic layers as shown in Fig.1.79b. The doubly protonated amine molecule interacts with the framework via multi-point

Table 1.72. Atomic coordinates [x 10^4] and equivalent isotropic displacement parameters [$Å^2$ x 10^3] for **XXIV**, $[C_6N_2H_{18}][Zn_3(H_2O)_4(HPO_4)_4]$.

Atom	x	y	z	U(eq)[1]
Zn(1)	400(1)	956(1)	6262(1)	22(1)
Zn(2)	0	5000	5000	22(1)
P(1)	525(1)	3724(1)	7276(1)	22(1)
P(2)	-2674(1)	204(1)	5053(1)	20(1)
O(1)	330(4)	-842(3)	6863(3)	31(1)
O(2)	858(4)	2187(3)	7388(2)	31(1)
O(3)	-1420(3)	1224(3)	5356(2)	24(1)
O(4)	2102(4)	1055(3)	5472(2)	28(1)
O(5)	-282(4)	4043(3)	6267(2)	32(1)
O(6)	1846(5)	6225(4)	5595(4)	34(1)
O(7)	-1552(4)	6519(4)	5556(3)	30(1)
O(8)	2053(4)	4554(4)	7330(2)	33(1)
O(9)	-3495(3)	-253(3)	5927(2)	27(1)
O(10)	-3776(4)	1049(3)	4306(2)	29(1)
N(1)	-3850(5)	4560(5)	6235(3)	35(1)
C(2)	-4229(7)	5724(6)	6883(4)	46(2)
C(3)	-3727(7)	3256(6)	6821(5)	52(2)
C(1)	-4981(6)	4386(6)	5346(4)	38(1)

[1] U(eq) is defined as one third of the trace of the orthogonalized U_{ij} tensor.

Table 1.73. Bond distances (Å) and angles (°) for **XXIV**.

Moiety	Distance (Å)	Moiety	Angle (°)
Zn(1)-O(1)	1.930(3)	O(5)-Zn(2)-O(6)	95.6(2)
Zn(1)-O(2)	1.947(3)	O(5)$^{\#1}$-Zn(2)-O(6)	84.4(2)
Zn(1)-O(3)	1.952(3)	O(6)$^{\#1}$-Zn(2)-O(6)	180
Zn(1)-O(4)	1.953(3)	O(5)-Zn(2)-O(7)$^{\#1}$	97.0(2)
Zn(2)-O(5)	1.989(3)	O(5)$^{\#1}$-Zn(2)-O(7)$^{\#1}$	83.0(2)
Zn(2)-O(5)$^{\#1}$	1.989(3)	O(6)$^{\#1}$-Zn(2)-O(7)$^{\#1}$	89.4(2)
Zn(2)-O(6)$^{\#1}$	2.126(4)	O(6)-Zn(2)-O(7)$^{\#1}$	90.6(2)
Zn(2)-O(6)	2.126(4)	O(5)-Zn(2)-O(7)	83.0(2)
Zn(2)-O(7)$^{\#1}$	2.212(4)	O(5)$^{\#1}$-Zn(2)-O(7)	97.0(2)
Zn(2)-O(7)	2.212(4)	O(6)$^{\#1}$-Zn(2)-O(7)	90.6(2)
P(1)-O(5)	1.509(3)	O(6)-Zn(2)-O(7)	89.4(2)
P(1)-O(1)$^{\#2}$	1.519(4)	O(7)$^{\#1}$-Zn(2)-O(7)	180
P(1)-O(2)	1.527(3)	O(5)-P(1)-O(1)$^{\#2}$	113.9(2)
P(1)-O(8)	1.583(4)	O(5)-P(1)-O(2)	111.2(2)
P(2)-O(3)	1.521(3)	O(1)$^{\#2}$-P(1)-O(2)	107.7(2)
P(2)-O(9)	1.522(3)	O(5)-P(1)-O(8)	105.5(2)
P(2)-O(4)$^{\#3}$	1.529(3)	O(1)$^{\#2}$-P(1)-O(8)	109.0(2)
P(2)-O(10)	1.569(3)	O(2)-P(1)-O(8)	109.5(2)
Moiety	Angle (°)	O(3)-P(2)-O(9)	112.5(2)
O(1)-Zn(1)-O(2)	103.85(14)	O(3)-P(2)-O(4)$^{\#3}$	111.9(2)
O(1)-Zn(1)-O(3)	108.9(2)	O(9)-P(2)-O(4)$^{\#3}$	109.9(2)
O(2)-Zn(1)-O(3)	120.25(14)	O(3)-P(2)-O(10)	103.3(2)
O(1)-Zn(1)-O(4)	109.67(14)	O(9)-P(2)-O(10)	109.3(2)
O(2)-Zn(1)-O(4)	106.6(2)	O(4)$^{\#3}$-P(2)-O(10)	109.7(2)
O(3)-Zn(1)-O(4)	107.31(14)	P(1)$^{\#4}$-O(1)-Zn(1)	128.0(2)
O(5)-Zn(2)-O(5)$^{\#1}$	180	P(1)-O(2)-Zn(1)	120.0(2)
O(5)-Zn(2)-O(6)$^{\#1}$	84.4(2)	P(2)-O(3)-Zn(1)	128.8(2)
O(5)$^{\#1}$-Zn(2)-O(6)$^{\#1}$	95.6(2)	P(2)$^{\#3}$-O(4)-Zn(1)	122.2(2)
		P(1)-O(5)-Zn(2)	141.7(2)

Organic

Moiety	Distance (Å)	Moiety	Angle (°)
N(1)-C(2)	1.491(7)	C(2)-N(1)-C(3)	109.8(4)
N(1)-C(3)	1.493(7)	C(2)-N(1)-C(1)	112.5(4)
N(1)-C(1)	1.499(7)	C(3)-N(1)-C(1)	109.7(4)
C(1)-C(1)$^{\#5}$	1.514(11)	N(1)-C(1)-C(1)$^{\#5}$	112.1(5)

Symmetry transformations used to generate equivalent atoms :

#1 -x,-y+1,-z+1 #2 -x,y+1/2,-z+3/2 #3 -x,-y,-z+1
#4 -x,y-1/2,-z+3/2 #5 -x-1,-y+1,-z+1

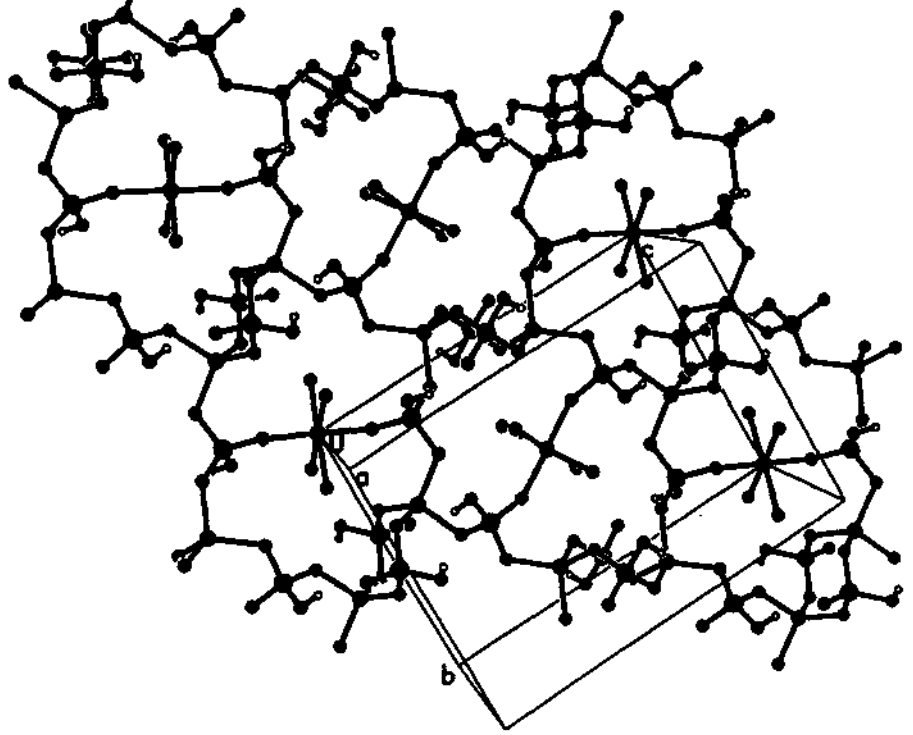

(a)

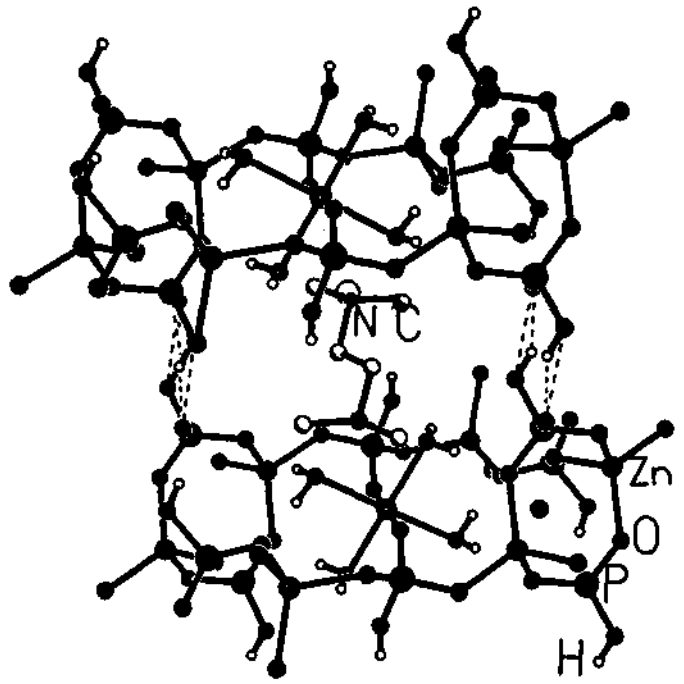

(b)

Fig. 1.79. A single layer of **XXIV**. Note that the octahedral Zn connects two phosphate units forming the bi-furcated 8-membered aperture. (b) Structure of the layered open-framework zinc phosphate, **XXIV**, showing two layers with the amine in between. Hydrogens on the amine are omitted for clarity. The dotted lines represent inter-layer hydrogen bond interactions.

hydrogen bonding and is partly responsible for the observation of such an architecture.

The structures of **XXIII** and **XXIV**, reveal that they are somewhat related. It is conceivable that a building unit of the type **XXIII** can give rise to many framework architectures, although presently we have observed one in the present study. In Fig.1.80, we schematically show a plausible pathway of the transformations of **XXIII** to open-framework structures. Thus, **XXIII** (shown as **1** in Fig.1.80) can assemble and transform into a corner-shared linear chain, **3**, via encapsulation of a metal ion between the hanging phosphate groups of two monomeric units followed by condensation. The corner-shared chain can easily get converted into an edge-shared ladder, **5**, by acid hydrolysis of the Zn – O – P bond followed by a bond rotation, which can subsequently form the layer, **8**. The formation of **XXIV** can be visualized from **XXIII** by the loss of a phosphate from **1** to form **9** which after losing another phosphate can condense to form a layer structure, **11** (*via* **10**). The layer further react with Zn^{2+} ions and add on a $ZnO_2(H_2O)_4$ unit to give **XXIV**. This mechanism can be written as follows:

$$2[Zn(HPO_4)(H_2PO_4)_2] \xrightarrow{-H_2PO_4} [Zn_2(HPO_4)_2(H_2PO_4)_3] \xrightarrow[+Zn]{-H_2PO_4} [Zn_3(HPO_4)_4]$$

From the above, it is clear that the monomer containing the 4-membered ring is likely to be the primary building block of open-framework metal phosphates. The formation of **XXIV** may require free Zn^{2+} ions in solution, it is possible that they are produced during the reaction by the dissociation of **XXIII** (**1**). It would be both of great interest and importance to investigate the transformation of **XXIII** to various types of open-framework structures by carrying out reactions under different conditions and the preliminary results obtained indeed bear a lot of promise.

The synthesis of a zinc phosphate monomer comprising only a four-membered ring and its subsequent condensation into a layered open-framework structure is vital for our understanding of the possible pathways involved in the

formation of open-framework architectures. It would be of extreme significance to isolate such intermediate species and study their transformations under varying reaction conditions, which may throw light on the intricate details of the formation of these extended solids.

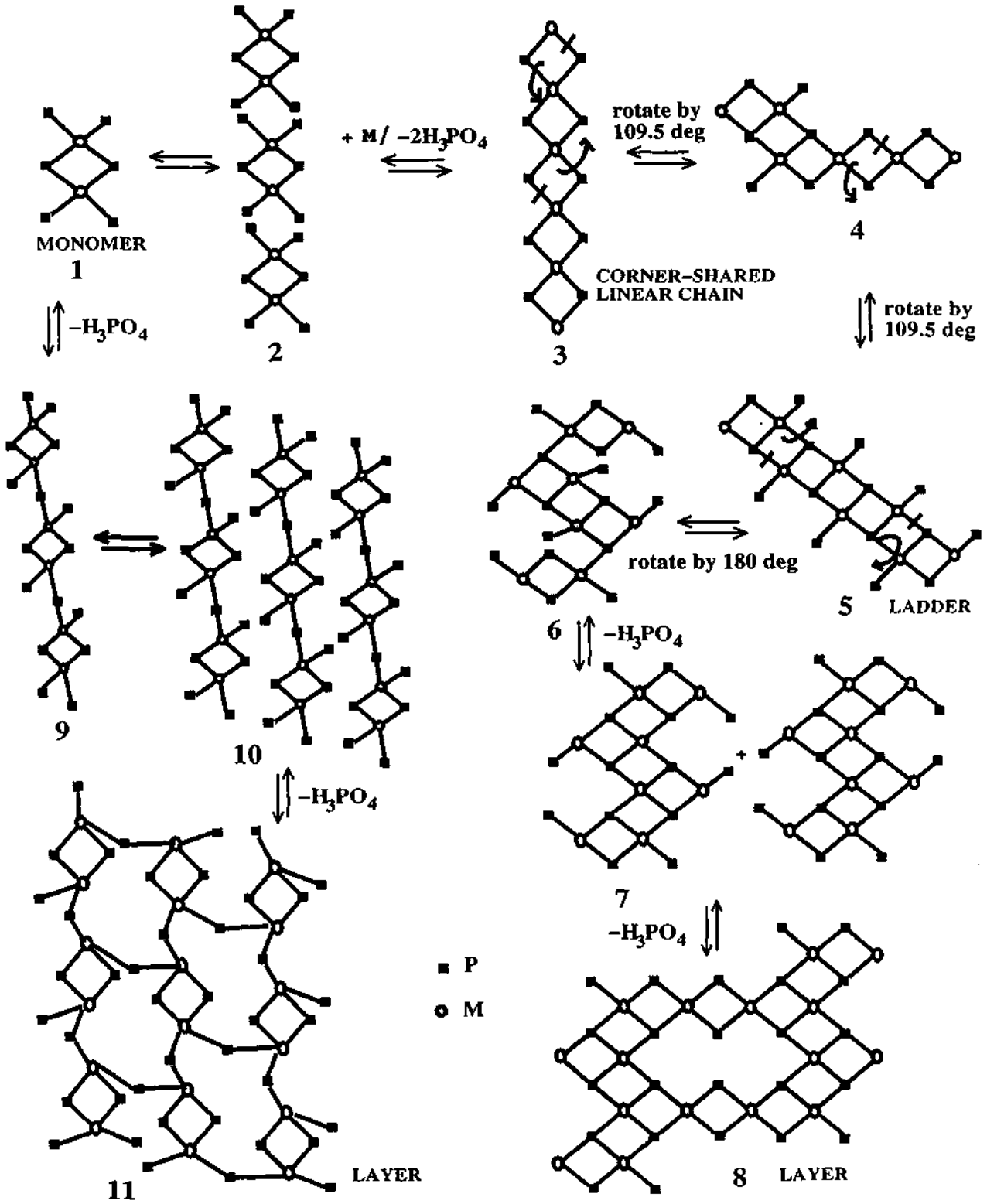

Fig. 1.80. A schematic reaction pathway showing the primary building unit XXIII consisting of the 4-membered ring zinc phosphate monomer, 1 can transform into chain, 3, ladder, 5, and layer (8 and 11) structures. Note that XXIV can be obtained by the reaction between 11 and Zn^{2+} ions.

References

1. A.F. Cronsted. *Svenska Vetenskaps Akademiens Handlingar Stockholm*, **17**, 120 (1756).
2. R. Szostak '*Molecular sieves Principles of Synthesis and Identification*' Van Nostrand Reinhold, New York (1989); "*Handbook of Molecular Sieves*", Academic Press (London), (1994).
3. A. Dyer, *An Introduction to Zeolite Molecular Sieves*, Wiley, Chichester (1988).
4. M. E. Davis, R. F. Lobo, *Chem. Mater.* **4**, 756 (1992).
5. J. M. Thomas, *Angew. Chem. Int. Ed. Engl.*, **38**, 3588 (1999).
6. R.M.Barrer, J. Chem. Soc. 127 (1948); R.M.Barrer, "*Hydrothermal Chemistry of Zeolites*", Academic Press (London), (1982).
7. W. Lowenstein, *Amer. Mineral.*, **39**, 92 (1954).
8. P. E. Halstead, A. E. Moore, *J. Appl. Chem.*, **12**, 413 (1962).
9. A. K. Gupta, N. O. Chatterjee, *Amer. Mineral.* **63**, 58 (1978).
10. W. M. Meier *Molecular sieves. Society of Chemical Industry* (1968).
11. M. Estermann, L. B. McCusker, C. Baerlocher, A. Merrouche, H. Kessler, *Nature*, **352**, 320 (1991).
12. E. de Vos Burchart, V. A. Verheij, H. Van Bekkum, B. van de Graaf, *Zeolites*, **12**, 183 (1992).
13. G. J. Kramer, A. J. M. de Man, R. A. van Santen, *J. Am. Chem. Soc.*, **113**, 6435 (1991).
14. N. J. Henson, A. K. Cheetham, J. D. Gale, *Chem. Mater.*, **6**, 1647 (1994).
15. S. T. Wilson, B. M. Lok, C. A. Messina, T. R. Cannan, E. M. Flanigen, *J. Am. Chem. Soc.*, **104**, 1146 (1982).
16. W. M. Meier, D. H. Olsen, C. Baerlocher, *Atlas of Zeolite Structure Types*, Elsevier London, (1996).
17. M. E. Davis, C. Saldarriaga, C. Montes, J. M. Garces, C. Crowder, *Nature*, **331**, 698 (1988).
18. R. M. Dessau, J. L. Schlinker, J. B. Higgins, *Zeolites*, **10**, 522 (1990).

19. R. Kniep, *Angew. Chem. Int. Ed. Engl.*, **25**, 525 (1986).
20. J. J. Pluth, J. V. Smith, *Acta Crystallogr. Sect. C.*, **43**, 866, (1987).
21. J. M. Bennett, J. M. Cohen, G. Artioli, J. J. Pluth, J. W. Richardson, Jr., J. V. Smith, Inorg. Chem., **24**, 188 (1985).
22. J. B. Parise, *Inorg Chem.*, **24**, 4312 (1985).
23. J. B. Parise, *J. Chem. Soc. Chem. Commun.*, 606 (1985).
24. J. B. Parise *Acta Crystallogr. Sect. C.*, **42**, 144 (1986).
25. H. Kessler, *Stud. Surf. Sci. Catal.*, **52**, 17 (1989).
26. H. Kessler, *Mater. Res. Soc. Symp. Ser.* **233**, 47 (1991).
27. T. Loiseau, G. Férey, *J. Chem. Soc. Chem. Commun.*, 1197 (1992).
28. G. Férey *J. Fluorine Chem.*, **72**, 187 (1995); *C. R. Acad. Sci. Ser.* C., **1**, 1 (1998).
29. F. C. Hawthorne, *Z. Kristallogr,*. **192**, 1 (1990).
30. T. Loiseau, G. Férey, *J. Solid State Chem.*, **111**, 403 (1994).
31. S. J. Weigel, S. C. Weston, A. K. Cheetham, G. D. Stucky, *Chem. Mater.*, **9**, 1293 (1997).
32. S. S. Dhingra, R. C. Haushalter, *J. Chem. Soc. Chem. Commun.*, 1665 (1993).
33. A. M. Chippindale, S. J. Brech, A. R. Cowley, W. M. Simpson, *Chem. Mater.*, **8**, 2259 (1996).
34. A. M. Chippindale, S. J. Brech, *Chem. Commun.*, 2781 (1996).
35. H. Du, J. Chen, W. Pang, *Stud. Surf. Sci. Catal.*, **105,** 397 (1997).
36. Y. Xu, L. L. Koh, L. An, R. Xu, S. Qui, *J. Solid State Chem.*, **117**, 373 (1995).
37. L. L. Koh, Y. Xu, H. B. Du, W. Q. Pang, *Stud. Surf. Sci. Catal.*, **105**, 373 (1997).
38. I. D. Williams, J. Yu, H. Du, J. Chen, W. Pang, *Chem. Mater.*, **10**, 773 (1998).
39. B. M. Lok, C. A. Messina, R. L. Patton, R. T. Gajek, T. R. Cannan, E. M. Flanigen, *J. Am. Chem. Soc.*, **106**, 6092 (1984).
40. P. A. Wright, R. H. Jones, S. Natarajan, R. G. Bell, J. Chen, M. B. Hursthouse, J.M. Thomas, *J. Chem. Soc. Chem. Commun.*, 633 (1993).

41. G. W. Noble, P. A. Wright, P. Lightfoot, R. E. Morris, K. J. Hudson, Å. Kvick, H. Graafsma, *Angew. Chem. Int. Ed. Engl.*, **36**, 81 (1997).
42. M. H. Zahedi-Niaki, P. N. Joshi, S. Kaliaguine, *Chem. Commun.*, 47 (1996).
43. E. M. Flanigen, B. M. Lok, R. L. Patton, S. T. Wilson, *Pure Appl. Chem.*, **58**, 1351 (1986).
44. E. M. Flanigen, Report at 1987 *Int. Symp. on Innovations in Zeolite Material Science*, Nieuwpoort, Belgium (Sept. 1987).
45. A. M. Chippindale, R. I. Walton, *J. Chem. Soc. Chem. Commun.*, 2453 (1994).
46. A. R. Cowley, A. M. Chippindale, *Chem. Commun.*, 673 (1996).
47. A. D. Bond, A. M. Chippindale, A. R. Cowley, A. V. Powell, *Zeolites*, **19**, 326 (1997).
48. A. M. Chippindale, A. R. Cowley, *Zeolites*, **18**, 176 (1997).
49. P. Feng, X. Bu, G. D. Stucky, *Nature*, **388**, 735 (1997).
50. P. Feng, X. Bu, G. D. Stucky, *Science*, **278**, 2080 (1997).
51. A. M. Chippindale, A. R. Cowley, R. I. Walton, *J. Mater. Chem.*, **6**, 611 (1996).
52. N. Zabukovec, L. Golié, P. Fajdiga, V. Kauéié, *Zeolites*, **15**, 104 (1995).
53. A. M. Chippindale, A. D. Bond, A. R. Cowley, A. V. Powell, *Chem. Mater.*, **9**, 2830 (1997).
54. G. Constentin, A. Leclaire, M. M. Borel, A. Grandin, B. Raveau, *Rev. Inorg. Chem.*, **13**, 77 (1993).
55. R. C. Haushalter, L. A. Mundi, *Chem. Mater.*, **4**, 31 (1992).
56. R. C. Haushalter, K. G. Strohmaier, F. W. Lai, *Science*, **246**, 1289 (1989).
57. D. Riou, M. Cavellec, G. Férey, *Acta Crystallogr. Sect.* C. **50**, 1379 (1994).
58. L. A. Mundi, L. Yacullo, R. C. Haushalter, *J. Solid State Chem.*, **95**, 283 (1991).
59. G. Bonavia, R. C. Haushalter, J. Zubieta, *J. Solid State Chem.*, **126**, 292 (1996).
60. V. Soghomanian, Q. Chen, R. C. Haushalter, J. Zubieta, J. O' Connor, *Science*, **259** 1596 (1993).

61. T. Loiseau, G. Férey, *J. Solid State Chem.*, **111**, 416 (1994).
62. M. I. Khan, L. M. Meyer, R. C. Haushalter, A. L. Schweitzer, J. Zubieta, J. L. Dye, *Chem. Mater.*, **8**, 43 (1996).
63. V. Soghomanian, Q. Chen, R. C. Haushalter, J. Zubieta, J. O' Connor, *Angew. Chem. Int. Ed. Engl.*, **32**, 610 (1993).
64. D. Riou, G. Férey, *J. Solid State Chem.*, **111**, 422 (1994).
65. P. B. Moore, J. Shen, *Nature*, **306**, 356 (1983).
66. M. Cavellec, D. Riou, C. Ninclaus, J. Greneéche G. Férey, *Zeolites*, **17**, 260 (1996).
67. K. -H. Lii, Y. -F. Huang, V. Zima, C.-Y. Huang, H. -M. Lin, Y. -C. Jiang, F. -L. Liao, S. -L. Wang, *Chem. Mater.*, **10**, 2599 (1998) and references therein.
68. P. Caullet, J. L. Guth, J. Hazm, J. M. Lamblin, H. Gies, *Eur. J. Solid State Inorg Chem.*, **28**, 345 (1991).
69. T. Loiseau, D. Riou, F. Taulelle, G. Férey, *Stud. Surf. Sci. Catal.*, **84**, 395 (1994).
70. N. Rajic, N. Logar, V. Kaucic, *Zeolites*, **15**, 672 (1995), and references therein.
71. J. Chen, R. H. Jones, S. Natarajan, M. B. Hursthouse, J. M. Thomas, *Angew. Chem. Int. Ed. Engl.*, **33**, 639 (1994).
72. J. R. D. DeBord, R. C. Haushalter, J. Zubieta, *J. Solid State Chem.*, **125**, 270 (1996).
73. P. Feng, X. Bu, S. H. Tolbert, G. D. Stucky, *J. Am. Chem. Soc.*, **119**, 2497 (1997), and references therein.
74. S. Fernández, J. L. Mesa, J. L. Pizarro, L. Lezama, M. I. Arriortua, R. Olazcuaga, T. Rojo *Chem. Mater.*, **12**, 376 (2000) .
75. N. Guillou, Q. Gao, M. Nogues, R.E. Morris, M. Hervieu, G. Férey, A. K. Cheetham, *C. R. Acad. Sci. Ser. IIC*, **2**, 387 (1999).
76. E. Kemnitz, M. Wloka, S. I. Trojanov, A. Stiewe, *Angew. Chem. Int. Ed. Engl.*, **35**, 2677 (1996).
77. M. Wloka, S. I. Trojanov, E. Kemnitz, *J. Solid State Chem.*, **135**, 293 (1998).
78. C. Serre, G. Férey, *C. R. Acad. Sci. Ser. IIC*, **2**, 85 (1999).

79. T. E. Gier, G. D. Stucky, *Nature*, **349**, 508 (1991).
80. T. E. Gier, W. T. A. Harrison, *Angew. Chem. Int. Ed. Engl.*, **30**, 1169 (1991).
81. T. M. Nenoff, W. T. A. Harrison, T. E. Gier, G. D. Stucky, *J. Am. Chem. Soc.*, **113**, 378 (1991).
82. W. T. A. Harrison, T. E. Gier, K. L. Moran, J. M. Eckert, G. D. Stucky, , *Chem. Mater.*, **3**, 27 (1991).
83. W. T. A. Harrison, T. E. Gier, J. M. Nicol, G. D. Stucky, *J. Solid State Chem.*, **114**, 249 (1995).
84. W. T. A. Harrison, T. E. Gier, G. D. Stucky, R. W. Broach, R. A. Bedard, *Chem. Mater.*, **8**, 145 (1996).
85. W. T. A. Harrison, R. W. Broach, R. A. Bedard, T. E. Gier, G. D. Stucky, *Chem. Mater.*, **8**, 691 (1996).
86. W. T. A. Harrison, T. E. Gier, G. D. Stucky, *J. Mater. Chem.*, **1**, 153 (1991).
87. W. T. A. Harrison, T. E. Martin, T. E. Gier, G. D. Stucky, *J. Mater. Chem.*, **2**, 175 (1992).
88. W. T. A. Harrison, T. M. Nenoff, M. M. Eddy, T. E. Martin, G. D. Stucky, *J. Mater. Chem.*, **2**, 1127 (1992).
89. R. H. Jones, J. Chen, G. Sankar, J. M. Thomas, *Stud. Surf. Sci. Catal.*, **84**, 2229 (1994).
90. T. Song, J. Xu, Y. Zhao, Y. Yue, Y. Xu, R. Xu, N. Hu, G. Wei, H. Jia, *J. Chem. Soc. Chem. Commun.*, 1171 (1994).
91. K. Ahmadi, A. Hardy, J. Patarin, L. Huve, *Eur. J. Solid State Inorg. Chem.*, **32**, 209 (1995).
92. X. Bu, P. Feng, G. D. Stucky, *J. Solid State Chem.*, **125**, 243 (1996).
93. W. T. A. Harrison, M. L. F. Phillips, *Chem. Commun.*, 2771 (1996).
94. W. T. A. Harrison, M. L. F. Phillips, *Chem. Mater.*, **9**, 1837 (1997).
95. W. T. A. Harrison, L. Hannooman, *Angew. Chem. Int. Ed. Engl.*, **36**, 640 (1997).
96. S. L. Suib, L. E. Iton, *Chem. Mater.*, **6**, 429 (1994).

97. K. Maeda, J. Akimoto, Y. Kiyozumi, F. Mizukami, *J. Chem. Soc. Chem. Commun.*, 1033 (1995); K. Maeda et.al., *Angew. Chem. Int. Ed. Engl.*, **34**, 1199 (1995).

98. H. Li, M. Eddaoudi, M. O'Keefe, O. M. Yaghi, *Nature*, **402**, 276 (1999); M. Reineke, M. Eddaoudi, M. Fehr, D. Kelly, O. M. Yaghi, *J. Am. Chem. Soc.*, **121**, 1651 (1999) and references therein.

99. S. S. -Y. Chui, S. M. - F. Lo, J. P. H. Charmant, A. G. Orpen, I. D. Williams, *Science*, **283**, 1148 (1999).

100. S. Ayyappan, A. K. Cheetham, S. Natarajan, C. N. R. Rao, *Chem. Mater.*, **10**, 3746 (1998); S. Natarajan, R. Vaidyanathan, C. N. R. Rao, S. Ayyappan, A. K. Cheetham, *Chem. Mater.*, **11**, 3636 (1999).

101. F. Serpaggi, G. Férey, *J. Mater. Chem.*, **8**, 2737 (1998); C. Livage, C. Egger, M. Nogues, G. Férey, *J. Mater. Chem.*, **8**, 2743 (1998); C. Livage, C. Egger, G. Férey, *Chem. Mater.*, **11**, 1546 (1999).

102. Y. F. Huang, K. H. Lii, *J. Chem. Soc. Dalton Trans.*, 4085 (1998)

103. P. Lightfoot, Z.A. D. Lethbridge, R. E. Morris, D. S. Wragg, P. A. Wright, *J. Solid State Chem.*, **143**, 74 (1999).

104. A. Choudhury, S. Natarajan, C. N. R. Rao, *Chem. Mater.*, **11**, 2316 (1999); A. Choudhury, S. Natarajan, C. N. R. Rao, *Chem. Eur. J.*, **6**, 1168 (1999).

105. C. Y. Chen, P. P. Chu, K. H. Lii, *Chem. Commun.*, 1473 (1999)

106. R. L. Bedard, S. T. Wilson, L. D. Vail, J. M. Bennett, E. M. Flanigen, *Stud. Surf. Sci. Catal.*, **49**, 375 (1989); J. B. Parise, *J. Chem. Soc. Chem. Commun.*, 1553 (1990); C. L. Cahill, Y. Ko, K. Tan, S. Koch, J. B. Parise, *Chem. Mater.*, **10**, 19 (1998).

107. O. M. Yaghi, Z. Sun, D. A. Richardson, T. A. Groy, *J. Am. Chem. Soc.*, **116**, 807 (1994); H. Li, A. Laine, M. O'Keefe, O. M. Yaghi, *Science*, **283**, 1145 (1999) and references therein.

108. J. D. Martin, K. B. Greenwood, *Angew. Chem. Int. Ed. Engl.*, **36**, 2072 (1997).

109. W. Schnick, J. Lücke, *Angew. Chem. Int. Ed. Engl.*, **31**, 213 (1992); N. Stock, E. Irran, W. Schnick, *Chem. Eur. J.*, **4**, 1822 (1998); S. Horstmann, E. Irran, W. Schnick, *Angew. Chem. Int. Ed. Engl.*, **36**, 1992 (1997).

110. S. T. Wilson, B. M. Lok, C. A. Messina, T. R. Cannan, E. M. Flanigen, *ACS Symp. Ser.*, **218**, 79 (1983).

111. E. M. Flanigen, R. L. Patton, S. T. Wilson, *Stud. Surf. Catal.*, **37**, 13 (1983).

112. B. Duncan, R. Szostak, K. Sorby, J. G. Ulan, *Catal. Lett.*, **7**, 367 (1990).

113. E. M. Flanigen, J. M. Bennett, R. W. Grose, J. P. Cohen, R. L. Patton, R. M. Kirchner, J. V. Smith, *Nature (London)*, **271**, 512 (1978).

114. B. M. Lok, T. R. Cannan, C. A. Messina, *Zeolites*, **3**, 282 (1983).

115. L. D. Rollmann, *Adv. Chem. Ser.*, **173**, 387 (1978).

116. F. Y. Dai, M. Suzuki, H. Takahashi, Y. Saito, *Stud. Surf. Sci. Catal.*, **28**, 223 (1986).

117. R. H. Jones, J. M. Thomas, J. Chen, R. Xu, Q. Huo, S. Li, Z. Ma, A. M. Chippindale, *J. Solid State Chem.*, **102**, 204 (1993).

118. R. M. Dessau, J. L. Schlinker, and J. B. Higgins, *Zeolites*, **10**, 522 (1990).

119. T. Loiseau, G. Férey, *J. Mater. Chem.*, **6**, 1073 (1996).

120. H. Gies, B. Marler, *Zeolites*, **12**, 42 (1992).

121. S. L. Burkett and M. E. Davis, *J. Phys. Chem.*, **98**, 4647 (1994).

122. J. Ciric, *U.S. Pat.*, **39**, 504496 (1976).

123. S. L. Burkett and M. E. Davis, *Chem. Mater.*, **7**, 920 (1995).

124. S. L. Burkett and M. E. Davis, *Chem. Mater.*, **7**, 1453 (1995).

125. M. E. Davis, *Stud. Surf. Sci. Catal.*, **97**, 35 (1995).

126. H. S. Frank, M.W. Evans, *J. Chem. Phys.*, **13**, 50 (1945).

127. N. Muller, *Acc. Chem. Res.*, **23**, 23 (1990).

128. G. R. Millward, S. Ramdas, J. M. Thomas, M. T. Barlow. *J. Chem. Soc. Faraday. Trans.*, **1**, 1075 (1983).

129. R. F. Lobo, M. E. Davis, *J. Am. Chem. Soc.*, **117**, 3766 (1995).

130. R. F. Lobo, M. Pan, I. Chan, H. –X. Li, R. C. Medrud, S. I. Zones, P. A. Crozier, M.E. Davis, *Science*, **262**, 1543 (1993).

131. H. Y. He, J. Klinowski, *J. Phys. Chem.*, **98**, 1192 (1994).

132. M. E. Davis, D. Young, *Stud. Surf. Sci. Catal.*, **60**, 53 (1991).

133. S. Oliver, A. Kuperman, G. A. Ozin, *Angew. Chem. Int. Ed. Engl.*, **37**, 46 (1998).

134. S. Oliver, A. Kuperman, A. Lough, G. A. Ozin, *Chem. Mater.*, **8**, 2391 (1996).

135. D. W. Lewis, C. R. A. Catlow, J. M. Thomas, *Faraday Discuss. R. Soc. Chem.*, **106**, 451 (1997).

136. A. P. Stevens, A. M. Gorman, C. M. Freeman, P. A. Cox, *J. Chem. Soc. Faraday Trans.*, 2065 (1996).

137. R. E. Boyett, A. P. Stevens, M. G. Ford, P. A. Cox, *Zeolites*, **17**, 508 (1996).

138. R. E. Boyett, A. P. Stevens, M. G. Ford, P. A. Cox, *Stud. Surf. Sci. Catal.*, **105**, 117 (1997).

139. C. M. Freeman, D. W. Lewis, T. V. Harris, A. K. Cheetham, N. J. Henson, P. A. Cox, A. M. Gorman, S. M. Levine, J. M. Newsam, E. Hernandez, C. R. A. Catlow. *ACS Symp. Ser.*, **589**, 326 (1995).

140. T. V. Harris, S. I. Zones, *Stud. Surf. Sci. Catal.*, **84**, 29 (1994).

141. D. W. Lewis, C. M. Freeman, C. R. A. Catlow, *J. Phys. Chem.*, **99**, 11194 (1995).

142. D. W. Lewis, D. J. Willock, C. R. A. Catlow, J. M. Thomas, G. J. Hutchings, *Nature(London)*, **382**, 604 (1996).

143. D. J. Willock, D. W. Lewis, C. R. A. Catlow, G. J. Hutchings, J. M. Thomas, *J. Mol. Catal. A*, **119**, 415 (1997).

144. D. W. Lewis, G. Sankar, J. K. Wyles, J. M. Thomas, C. R. A. Catlow, D. J. Willock, *Angew. Chem. Int. Ed. Engl.*, **36**, 2675 (1997).

145. A. K. Cheetham, C. F. Mellot, *Chem. Mater.*, **9**, 2269 (1997).

146. Ch. Baerlocher, A. Hepp, W. M. Meier *DLS-76 A Fortran program for the Simulation of Crystal Structures by Geometric Refinement. Institut fuer Kristallographie*, ETH, Zurich, Switzerland (1977).

147. L . B. McCusker, *Acta Crystallogr. Sect. A.*, **47**, 297 (1991).

148. H. M. Reitveld, *J. Appl. Cryst.*, **2**, 65(1969).

149. G. Engelhardt, D. Michel, *High-Resolution Solid-State NMR of Silicates and Zeolites* John Wiley & Sons Norwich (1987); A. T. Bell and A. Pines, *NMR Techniques in Catalysis* Marcel Dekker, Inc. New York 1994.

150. A Llor, J. Virlet, *Chem. Phys. Lett.*, **152**, 248 (1988), A. Samoson, E. Lippmaa, A. Pines, *Mol. Phys.*, **65**, 1013 (1988).

151. B. F. Chmelka, K. T. Mueller, A. Pines, J. Stebbins, Y. Wu, J. W. Zwanziger, *Nature (London)*, **339**, 42 (1989).

152. K. T. Mueller, B. Q. Sun, G. C. Chingas, J. W. Zwanziger, T. Terao, A. Pines, *J. Magn. Reson.*, **86**, 470 (1990).

153. N. Kutz, *Heterogeneous Catalysis-II,* B. L. Shapiro, ed. Texas A& M University Press, College Station, 121, (1984). D. W. Lewis, G. Sastre, *Chem. Commun.*, 349, (1999).

154. S. Brunauer, *The Adsorption of Gases and Vapors*, Princeton University, Princeton, N.J. 68 (1945). L. Gurvitsch, *J. Phys. Chem. Soc., Russ.*, **47**, 805 (1915).

155. D. Domine, J. Quobex, *Molecular Sieves, Soc. Chem. Ind.*, 78 (1968).

156. S. T. Wilson, B. M. Lok, C. A. Messina, E. M. Flanigen, *Proc. 6th Int. Conf. On Zeolites,* D. Olson, A. Bisio, *eds.*, Butterworth 97 (1984).

157. J. M. Thomas, D. E. W. Vaughan, *J. Phys. Chem. Solids*, **50**, 449 (1989); J. M. Thomas, *Chem. Eur. J.*, **3**, 1557 (1997).

158. J. M. Newsam, D. E. W. Vaughan, *Zeolites: Synthesis, Structure, Technology and Applications* (Ed. B. Drzaj, S. Hočevar, S. Pejovnik), Elsevier, Amsterdam, 239 (1985).

159. L. B. McCusker, *J. Appl. Crystallogr.*, **21**, 305 (1988); J. P. Attfield, A. W. Sleight, A. K. Cheetham, *Nature*, **322**, 620 (1986).

160. Ch. Baerlocher, P. Schicker, *Abstr. 14th Intl. Congr. Crystallogr.*, **12**, 5 (1987); B. H. Toby, M. M. Eddy, C. A. Fyfe, G. T. Koktailo, H. Strohl, D. E. Cox, *J. Mater. Res.*, **3**, 563 (1988).

161. A. K. Cheetham, A. P. Wilkinson, *Angew. Chem. Int. Ed. Engl.*, **31**, 1557 (1992); G. E. Bacon, *Neutron Diffraction,* 3rd *ed.*, Oxford, (1975).

162. J. V. Smith, *Adv. Chem. Ser.*, **101**, 171 (1971).

163. J. A. Rabo, R. D. Bezman, M. L. Poutsma, *Symposium on Zeolites, Acta. Phys. Chem.*, **24**, 39 (1978).

164. J. J. Verdnok, P. A. Jacobs, J. B. Uytterhoeven, *J. Chem. Soc. Chem. Commun.*, 181 (1979).

165. J. N. Miale, N. Y. Chen, P. B. Weisz, *J. Catal.*, **6**, 278 (1966).

166. C. D. Anderson, et. al. *I beroamerican Symp. Cat.*, Lisbon, Portugal, (Jul., 1984).

167. N. Y. Chen, J. Mazijuk, A. B. Schwartz, P. B. Weisz, *Oil Gas J.*, **66**, 154 (168).

168. H. R. Ireland et.al. *Hydrocarbon Processes.*, **58**, 119 (1979).

169. C. D. Chang, A. J. Silverestri, *J. Catal.*, **47**, 249 (1977).

170. S. E. Voltz, J. J. Wise (eds) *Development Studies on Conversion of Methanol and Related Oxygenates to Gasoline, Ornl/FE-1*, Springfield: NTIS, (1977).

171. M. Deeba, M. E. Ford, *J. Org. Chem.*, **53**, 4594 (1988).

172. R. W. Weber, J. C. Q. Fletcher, K. P. Möller, C. I. O'Conner, *Microporous Mater.*, 7, 151 (1996).

173. L. Abrams, D. R. Corbin, M. Keane, *J. Catal.*, **126**, 610 (1990).

174. S. B. Ogunwumni, T. Bein, *Chem. Commun.*, 901 (1997); A. Corma et.al., *J. Organomet. Chem.*, **44**, 147 (1997).

175. I. W. C. E. Arends, R. A. Sheldon, M. Wallau, U. Schuchardt, *Angew. Chem. Int. Ed. Engl.*, **36**, 1144 (1997).

176. J. C. Van der Waal, H. Van Bekkum, *J. Porous Mater.*, **5**, 289 (1998).

177. A. Corma, H. García, *J. Chem. Soc. Dalton Trans.*, 1381 (2000).

178. T. Bein, *Chem. Mater.*, **8**, 1636, (1996).

179. M. Sykora, J. R. Kincaid, *Nature*, **387**, 162 (1997).

180. R. Raja, J. M. Thomas, *Chem. Commun.*, 1841 (1998); G. Sankar, R. Raja, J. M. Thomas, *Catal. Lett.*, **55**, 15 (1998).

181. J. M. Thomas, R. Raja, G. Sankar, R. G. Bell, *Nature*, **398**, 227 (1999); R. Raja, G. Sankar, J. M. Thomas, *Chem. Commun.*, 525 (1999).

182. S. Ayyappan, A. K. Cheetham, C. N. R. Rao, *Int. J. Inorg. Mater.*, **2**, 21 (2000).

183. C. Bhardwaj, H. Hu, A. Clearfield, *Inorg. Chem.*, **32**, 4299 (1993).

184. E. Jaimez, et.al. *J. Chem. Soc. Dalton. Trans.*, **11**, 2285 (1996).

185. G. Alberti, et.al., *Solid State Ionics*, **46**, 61 (1992).

186. L. Vermuelen, M. Thompson, *Nature*, **358**, 656 (1992).

187. D. E. W. Vaughan, *Chem. Eng. Prog.*, 25 (1988).

188. F. Rey, G. Sankar, J. M. Thomas, P. A. Barrett, D. W. Lewis, C. R. A. Catlow, *Chem. Mater.*, **7**, 1435 (1995).

189. G. Sankar, J. M. Thomas, F. Rey, G. N. Greaves, *J. Chem. Soc. Chem. Commun.*, 2549 (1995).

190. O. M. Yaghi, H. Li, C. Davis, D. Richardson, T. L. Groy, *Acc. Chem. Res.*, **31**, 474 (1998).

191. A. Muller, H. Reuter, S. Dillinger, *Angew. Chem. Int. Ed. Engl.*, **34**, 2328 (1995).

192. S. R. Batten, R. Robson, Angew. Chem. Int. Ed. Engl. 37, 1460 (1998).

193. L. R. MacGillivray, J. L. Atwood, *Angew. Chem. Int. Ed. Engl.*, **38**, 1018 (1999).

194. T. Bein, *Angew. Chem. Int. Ed. Engl.*, **38**, 323 (1999) and references therein.

195. S. M. Senkan, *Nature*, **394**, 350 (1998).

196. X. -D. Xiang *Science*, **270**, 1738 (1995).

197. G. Briceno, H. Chang, X. Sun, P. G. Schultz, X. -D. Xiang *Science*, **270**, 273 (1995).

198. X. -D. Sun, *Adv. Mater.*, **9**, 1046 (1997).

199. E. Danielson et.al., *Nature*, **389**, 944 (1997).

200. R. B. van Dover, L. F. Schneemeyer, R. M. Fleming, *Nature*, **392**, 164 (1998).

201. K. Choi, D. Gardner, N. Hilbrandt, T. Bein, *Angew. Chem Int. Ed. Engl.*, **38**, 2891 (1999)

202. C. T. Kresge, M. E. Leonowicz, W. J. Roth, J. C. Vartuli, J. S. Beck, *Nature*, **359**, 712 (1992).

203. J. S. Beck, J. C. Vartuli, W. J. Roth, M. E. Leonowicz, C. T. Kresge, K. D. Schmitt, C. T. W. Chu, D. H. Olson, E. W. Sheppard, S. B. McCullen, J. B. Higgins, J. L. Schlenker, *J. Am. Chem. Soc.*, **114**, 10834 (1992).

204. J. S. Beck, J. C. Vartuli, *Curr. Opinion Solid State Mater. Sci.*, **1**, 76 (1996).

205. J. M. Lehn, *Supramolecular Chemistry*, VCH, Weinheim, (1995); F. Vogtle, *Supramolecular Chemistry: An Introduction*, Wiley, Chichester (1991).

206. G. R. Desiraju, *Crystal Engineering: The design of Organic Solids*, Elsevier, Amsterdam, (1989).

207. G. R. Desiraju, *Angew. Chem. Int. Ed. Engl.*, **34**, 2311 (1995).

208. V.R. Pedireddi, S. Chaterjee, A. Ranganathan, C.N.R. Rao, *J.Am.Chem.Soc.*, **119**, 10867 (1997).

209. A. Ranganathan, V.R. Pedireddi, C.N.R. Rao, *J.Am.Chem.Soc.*, **121**, 1752 (1999).

210. V.R. Pedireddi, S. Chaterjee, A. Ranganathan , C.N.R. Rao, *Tetrahedron*, **54**, 9457 (1998).

211. M. J. Mio, J. S. Moore, *MRS Bull.*, **36**, (Apr. 2000).

212. J. S. Moore, *Curr. Opinion Solid State Mater. Sci.*, **4**, 108 (1999).

213. G. Ertl, H. Knözinger, J. Weitkamp, *Handbook of Heterogeneous Catalysis* Eds., VCH, Weinheim, (1997).

214. A. K. Cheetham, T. Loiseau, G. Férey, *Angew. Chem. Int. Ed. Engl.*, **38**, 3268 (1999).

215. G. Férey, C. R. Acad. Sci. Paris, **2**, 1 (1998).

216. W. T. A. Harrison, Z. Bircsak, L. Hannooman, Z. Zhang, J. Solid State Chem., **136**, 93 (1998).

217. X. Bu, P. Feng, T.E. Gier, G.D. Stucky, *Zeolites*, **19**, 200 (1997).

218. J.V. Smith, *Am. Mineral.*, **62**, 703, (1977); *Chem. Rev.*, **88**, 149 (1988).

219. X. Bu, T.E. Gier, G.D. Stucky, *Chem. Commun.*, 2271 (1997).

220. A. Baiker, *Curr.-Opin. Solid State Mater. Sci.*, **3**, 86,(1998).

221. A. Corma, M. Iglesias, C. del Pina, F. Sanchez, *J. Chem. Soc., Chem. Commun.*, 1235 (1991); *Organomet. Chem.*, **431**, 233 (1992).

222. J.M. Newsam, M.M.J. Treacy, W.T. Koetsier, C.B. de Gruyter, *Proc. R. Soc. London,A*, , **420**, 375 (1998).

223. K. Morgan, G. Gainsford, N. Milestone, *J. Chem. Soc., Chem. Commun.*, 425 (1995); D.A. Bruce, A.P. Wilkinson, M.G. White, J.A. Bertrand, *J. Solid State Chem.*, **125**, 228 (1996).

224. H.-M. Lin, K.-H. Lii, *Inorg. Chem.*, **37**, 4220 (1998).

225. S. Ayyappan, X. Bu, A.K. Cheetham, C.N.R. Rao, *Chem. Mater.*, **10**, 3308 (1998).

226. R. Kniep, H.G. Will, I. Boy, C. Röhr, *Angew. Chem. Int. Ed. Engl.*, **36**, 1013 (1997).

227. T.E. Gier, X. Bu, P. Feng, G.D. Stucky, *Nature*, **395**, 154 (1998).

228. C.C. Freyhardt, M. Tsapatsis, R.F. Lobo, K.J. Balkus, and M.E. Davis, *Nature*, **381**, 295 (1996).

229. D. A. Bruce, A. P. Wilkinson, M.G. White, J. A. Bertrand,, *J. Chem. Soc. Chem.Commun.*, 2059 (1995).

230. M. J. Gray, J. D. Jasper, A. P. Wilkinson, J. C. Hanson, *Chem. Mater.*, **9**, 976 (1997).

231. S. Natarajan, , J. -C. P. Gabriel, and A. K. Cheetham, , *J. Chem. Soc. Chem. Commun.*, 1415 (1996).

232. S. Natarajan, M. P. Attfield, A. K. Cheetham, *J. Solid State Chem.*, **133**, 229 (1997).

233. D. Chidambaram, S. Natarajan, *Mater. Res. Bull.*, **33**, 1275 (1998).

234. A.M. Chippindale, S. Natarajan, J.M. Thomas and R.H. Jones, *J. Solid State Chem.*, **111**, 18 (1994).

235. S. Ayyappan, X. Bu, A.K. Cheetham, S. Natarajan, C.N.R. Rao, Chem. Commun., 2181 (1998).

236. R. Vaidhyanathan and S. Natarajan, *J. Mater. Chem.*, **9**, 1807 (1999).

237. S. Oliver, A. J. Lough, G. A. Ozin, *Inorg. Chem.*, **37**, 5021 (1998) and references therein.

238. D. Riou, T. Loiseau, G. Férey, *Acta Crystallogr. Sect. C.*, **49,** 1237 (1993).

239. P. Feng, X. Bu, G.D. Stucky, *Angew. Chem. Int. Ed. Engl.*, **34**, 1745 (1995).

240. S. Kamoun, A. Jouini, A. Dasud, *Acta Crystallogr. Sect.C.*, **36**, 1481 (1980).

241. G.M. Sheldrick, *SHELX-86, Program for Crystal Structure Determination*, University of Göttingen, Germany, (1986).

242. G.M. Sheldrick, *SADABS User Guide*, University of Göttingen, Germany, (1995).

243. G.M. Sheldrick, *SHELXL-93, A Program for Crystal Structure Solution and Refinement*, University of Göttingen, Germany, (1993).

244. I.D. Brown, D. Aldermatt, *Acta Crystallogr., Sect. B*, **41**, 244 (1984).

245. W.T.A. Harrison, M.L.F. Phillips, W. Clegg, S.J. Reat, *J. Solid State* Chem., **148**, 433 (1999) and references therein.

246. R. Vaidhyanathan, S. Natarajan, C.N.R. Rao, *J. Mater. Chem.*, **9**, 2789 (1999).

247. W.T.A. Harrison, T. E. Gier, G. D. Stucky, *Angew. Chem. Int. Ed. Engl.*, **32**, 1745 (1993).

248. Song, T., Hursthouse, M.B., Chen, J., Xu, J., Abdul Malik, K.M. Jones, R.H., Xu, R., and Thomas, J.M. *Adv. Mater.*, **6**, 679 (1994).

249. P. Smith-Verdier, S. Garcia-Blanco, Z. Kristallogr., **151**, 175 (1980).

250. M. O'Keeffe, B.G. Hyde, *Phil. Trans. Roy. Soc. (London)*, **A295**, 553 (1980).

251. W.T.A. Harrison, M.L.F. Phillips, A.V. Chavez and T.M. Nenoff, *J. Mater. Chem.*, **9**, 3087 (1999).

252. P.S. Halasyamani, M.J. Drewitt and D. O'Hare, *Chem. Commun.*, 867 (1997).

253. A.F. Wells, *Structural Inorganic Chemistry*, 5th Ed., Oxford Science Publications, 1986.

254. D. Whang, N. H. Hur and K. Kim, *Inorg. Chem.*, **34**, 3363 (1995).

255. A.M. Chippindale and C. Turner, *J. Solid State Chem.*, **128**, 318 (1997).

256. A.M. Chippindale, A.V. Powell, L.M. Bull, R.H. Jones, A.K. Cheetham, J.M. Thomas and R. Xu, *J. Solid State Chem.*, **96**, 199 (1992).

257. Y. Piffard, S. Oyetola, S. Courant and A. Lachgar, *J. Solid State Chem.*, **60**, 209 (1985).

258. Y. Piffard, A. Lachgar and M. Tournoux, *Rev. de. Chim. Miner.*, **22**, 101 (1985).

259. Y. Piffard, V. Verbeare, S. Oyetola, S. Courant and M. Tournoux, *Eur. J. Solid State Inorg. Chem.*, **26**, 113 (1989).

260. U. Costantino, R. Vivani, V. Zima and E. Cernoskova, *J. Solid State Chem.*, **132**, 17 (1997) and references therein.

261. S. M. Golubev, Y. D. Kondrashev, Zh. Strukt. Khim. 25, 471 (1984); M. T. Averbuch-Pouchot, A. Durif, *Acta. Crystallogr.* **C43,** 1894 (1987); S. Kamoun, A. Jouini, A. Daoud, *Acta. Crystallogr.* **C47**, 117 (1991); S. Kamoun, A. Jouini, A. Daoud, A. Durif, J. C. Guitel, *Acta. Crystallogr.* **C48,** 133 (1992).

262. R. E. Morris, S. J. Weigel, *Chem. Soc. Rev.* **26**, 309 (1997); R. J. Francis, D. O'Hare, *J. Chem. Soc., Dalton Trans.* 3133 (1998).

263. R.J. Francis, S.O'Brien, A.M. Fogg, P.S. Halasyamani, D. O'Hare, T. Loiseau and G. Ferey, *J. Am. Chem. Soc.*, **121**, 1002 (1999).

264. J. Yu, I.D. Williams, *J. Solid State Chem.*, **136**, 141 (1998).

265. P. Lightfoot, D. Masson, *Acta Crystallogr., Sect. C.*, **52**, 1077 (1996).

266. A.M. Chippindale; A.R. Cowley, *J. Chem. Soc., Dalton Trans.*, 2147 (1999).

267. J.M. Thomas, R.H. Jones, J. Chen, R. Xu, A.M. Chippindale, S. Natarajan, A.K. Cheetham, *J. Chem. Soc., Chem. Commun.*, 929 (1992).

268. P. Feng, Bu X., G.D. Stucky, *J. Solid State Chem.*, **129** 328 (1997); P. Feng, Bu X., G.D. Stucky, *J. Solid State Chem.*, **131**, 160 (1997); P. Feng, Bu X., G.D. Stucky, *J. Solid State* Chem., **131**, 387 (1997).

269. Bu X., Feng P., Gier T.E., Stucky G.D., *J. Solid State Chem.*, 136, 210 (1998); W.T.A. Harrison, J.T. Vaughey, L.L. Dussack, A.J. Jacobson, T.E. Martin, G.D. Stucky, *J. Solid State Chem.*, **114**, 151 (1995); Z. Bircsak, W.T.A. Harrison, *Acta Crystallogr. Sec. C.*, **54**, 1554 (1998); N. Zabukovec, L. Golic, P. Fajdiga, P. Kaucic, *Zeolites*, **15**, 104 (1995)

270. J. M. Troup, A. Clearfield, *Inorg. Chem.*, **16**, 3311 (1977).

PART 2

INVESTIGATIONS OF MESOPOROUS SOLIDS*

SUMMARY

Synthesis of Mesoporous materials with pore sizes ranging from 20-100Å by Mobil chemists in 1992, broke the long-standing barrier on channel size imposed by the traditional microporous materials. The first mesoporous solid synthesized were lamellar, hexagonal and cubic forms of silica. These materials are synthesized using liquid crystalline surfactant aggregates as templates. Since then various other mesoporous materials have been synthesized and characterized. The template material can be removed by calcination, by solvent extraction or by acid leaching. The main impetus to study these materials comes from their potential use in catalysis, selective adsorption of large organic molecules from waste water, chromatographic separation, electronic, optical and other applications. The synthesis of these micro-skeletal and cellular inorganic materials in the laboratory via chemical procedures have also led us to a step closer towards biomimicking.

In this part of the thesis, the results of investigations of various mesoporous solids are presented. A variety of mesoporous oxides have been synthesized by employing self-organized assemblies of ionic as well as neutral surfactants. The following are the important mesoporous materials synthesized in the present study: ZrO_2, Al_2O_3, silicophosphates, RuO_2 and metal chalcogenides.

Mesoporous ZrO_2 has been prepared by employing a neutral amine template. Mesoporous alumina has also been prepared using neutral amine template with a surface area of $405 m^2 g^{-1}$. Mesoporous silicophosphates containing up to 22% phosphorus, have been prepared for the first time by employing cationic surfactants, where a silicophosphate of composition $Si_{19}P_4O_{48}$ has a surface area of $770 m^2 g^{-1}$, after removal of the template. We have found marginal success in preparing conducting mesoporous ruthenium dioxide by using anionic and neutral amine templates. Further work needs to be done in this study.

There is little information on the phase transitions of mesoporous materials in the literature. We have therefore examined the kinetics and mechanism of lamellar-hexagonal-cubic (L-H-C) phase transformation in solution and lamellar-hexagonal (L-H) in solid state of mesoporous zirconia. The transformation seems to occur by a loss of template molecules in both the solution and the solid states. The activation energy of the transformation is comparable to the hydrogen bond energy between the amine and oxo-zirconium species.

Hexagonal and lamellar nanostructured organic-metal chalcogenides; CdS, SnS_2, Sb_2S_3 and CdSe have been prepared by the reaction of metal salt aliphatic amine nanostructured adducts with Na_2S, Na_2Se or thiourea solution. Although it has not been possible to remove the amine template from these adducts, they are expected to show some interesting electronic and optical properties.

There has been much interest in mimicking enzymatic activity. Cu acetate dimer and $[Mn(bipy)_2]^+$ encapsulated in the pores of cubic mesoporous silica have shown extraordinarily high oxygen activation for oxidation of phenol to catechol and for oxidation of styrene to styrene oxide via singlet oxygen.

Hexagonal microporous phases of SiO_2 and $AlPO_4$ with pore sizes in the range intermediate between traditional microporous and mesoporous materials have been prepared, by making use of supramolecular organization of short-chain amine (hexylamine) template molecules. The pore diameters are around 1.4nm in both cases. The hexagonal microporous phase of $AlPO_4$ is formed only in presence of fluoride ions. The surface area of Silica after template removal is $800m^2g^{-1}$. In the case of $AlPO_4$, the surface area is $190m^2g^{-1}$ after removal of 60% of the template.

---

* Papers based on these studies have appeared in Chem. Commun., (1996); J. Mater. Chem., (1998), J. Mater Chem. (1998), Mater. Res. Bull. (1998), Chem. Commun. (1998); Proc. Indian Acad. Sci.(Chem Sci.) (1998), Microporous and Mesoporous Materials (1999)

1. MESOPOROUS SOLIDS: AN OVERVIEW

1.1 Introduction

Rational materials design is a challenging area of research and the past few years have witnessed a growing interest in mesoscopic systems with interesting properties and applications. In this direction, there has been some effort towards the synthesis of complex inorganic materials with novel pore structures. While physicists have attempted to fabricate such materials by slicing up the bulk material to go down the size scale, chemists have attempted to assemble the small atomic or molecular units to obtain the desired structures. One chemical approach has been to carefully manipulate atoms at the micro- or the meso-phase level to generate cluster arrays and control their growth by employing capping agents. Another approach involves solution growth of inorganic species over self-assembled two-dimensional structure directing assemblies and three-dimensional porous media, to design such mesoscopic porous materials.

Porous inorganic materials, due to their complex, ordered pore networks in zeolites and other such crystalline microporous materials have conventionally been restricted to the nanometer scale (less than 1.5nm). In these materials, the design of the pore architecture is controlled through the spatially confined assembly of inorganic building blocks, facilitated by cationic or neutral organic molecules. Microporous materials with three-dimensional frameworks are synthesized using molecular units or hydrated alkali or alkaline earth cations as templates. The pore structure and size (3 to 13Å) in these materials are well defined. The development of these materials has evolved from zeolites,[2,5] that possess crystalline aluminosilicate frameworks to pure silicate phases, and more recently compounds that exhibit similar framework structures have been synthesized but have compositions in which Al and/or Si are substituted by other elements such as Be, B, Ga, Ge, Zn, and P. The aluminosilicate and silicate microporous solids have found extensive application in the field of ion-exchange (use of zeolite A as water softener in detergents), desiccation, sorption (e.g. gas separation and

purification), and catalysis. For the latter two applications, the geometric restrictions imposed by the porous framework are of importance in size exclusion during intraporous sorption; and in the selectivity of the starting materials, transition states, and products of catalytic processes ("shape-selective catalysis").[6] In Fig.1.1 we show the evolution of the pore size in microporous materials.

The limitation of the pore size had always bothered the scientists and they have constantly explored synthetic methods, which would help them to break the size barrier restriction and crossover to materials with mesoscopic dimensions with the crystallinity same as that of microporous materials. A giant step in this direction was the successful synthesis of first ever ordered mesoporous silica MCM-41 (MCM stands for Mobil's Composition of Matter) by Mobil chemists in 1992 with a hexagonal arrangement of parallel channels,[7-8] which was seen directly in transmission electron microscope images. The arrangement of pores was very regular, and the pore size distribution measured by adsorption was quite sharp as in zeolites. This synthesis was achieved by the use of self-assembled surfactant aggregates as templates, which can be removed after the formation of the silica framework by calcination. Three forms of mesoporous silica, lamellar, hexagonal and cubic have been identified. The different forms of silica reported by mobil are listed below. These include MCM-41 (hexagonal), MCM-50 (lamellar) and MCM-48 (cubic) silica mesophases.

Since the syntheses of mesoporous silica, various other mesoporous materials have been synthesized and characterized. There are several recent reviews on the subject.[9-16] The various mesoporous materials known to date include mesoporous silicas,[7-8] mesoporous/ mesostructured metal oxides such as alumina,[17-19] titania,[20] zirconia,[21] niobia,[22] chromia,[23] tantalum oxide,[24] tungsten oxide,[25,26] iron oxide,[26] lead oxide,[26] molybdenum oxide,[26] oxides of cobalt, zinc, nickeland magnesium,[26] antimony oxide,[26] gallium oxide,[26] vanadium oxide,[27,28] tin oxide,[29] and manganese oxide.[30] Other mesoporous materials include vanadium phosphate,[31] aluminophosphate,[32] silicoaluminophosphates,[33] aluminoborates.[34] Removal of the template molecules from the composite structure is essential

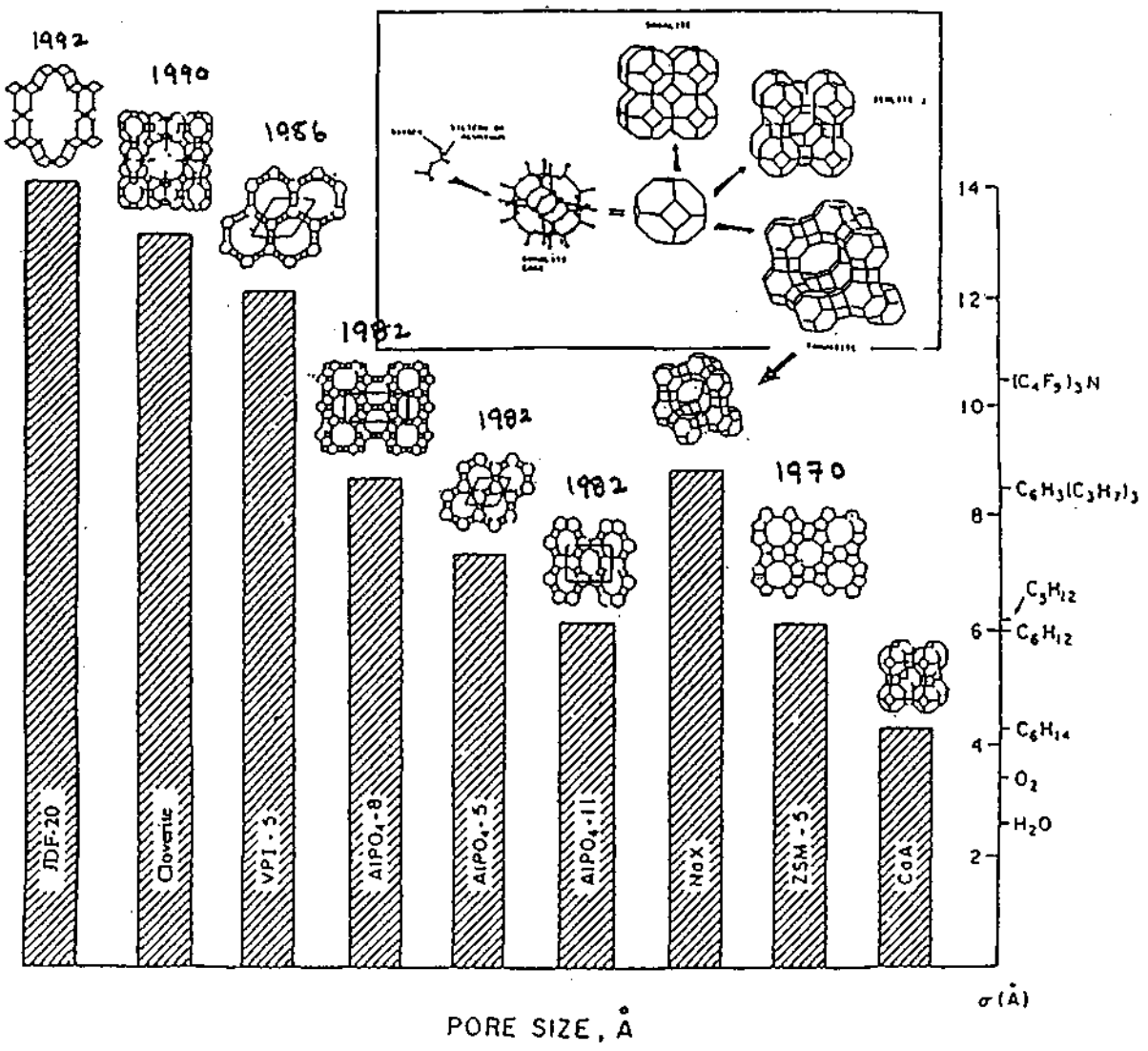

Fig. 1.1 Evolution of pore size in microporous materials.

before the materials can be considered mesoporous. This has been accomplished in many of these materials. Many metals have also been substituted into the framework of mesoporous silicates such as titanium,[35-38] zirconium,[39] boron,[40] aluminum,[7,8] gallium,[41] vanadium,[42-45] tin,[46,47] cobalt,[48] chromium,[49] manganese[50], iron[51] etc. There has been some recent interest in mesoporous chalcogenides and a few of them have been synthesized based on procedures similar to the synthesis of mesoporous oxides,[52-56] although the template molecules have not always been removed.

There are whole gamut of potential applications of mesoporous materials, such as in protein separation, selective adsorption of large organic molecules from waste water, chromatographic separation, catalysis (e.g. in processing of tar and of the high distillates of crude oil to valuable low-boiling products) as well as in electronic (quantum-confinement of guest molecules in these cavities, electron-transfer reactions), optical (nonlinear optics) and other applications. Also the synthesis of these micro-skeletal and cellular inorganic materials in laboratories via chemical procedures has led us a step closer towards mimicking Nature's sculptures.[57-60]

1.2 Formation of Mesoporous Solids

In case of zeolites, the crystallization of the silicate material occurs around a single molecule, which then directs the zeolitic framework. In the formation of mesoporous materials, the role of the structure-directing agent is played by the supramolecular ordered surfactant aggregates (micelles) which are formed in aqueous solution and the inorganic species interacts with these preformed aggregates and grows over it. Here too, the organic assemblies are encompassed within the inorganic framework.

Synthesis of MCM-41 form of silica involves liquid crystal templating (LCT) which involves pathways of the kind described below. The first pathway proposed by Chen et.al.,[61] involves the independent organization of surfactant

molecules in the form of randomly ordered rod like micelles prior to the interaction with inorganic species. Because of the charge interaction between the cationic headgroup and anionic inorganic species or anionic headgroup and cationic inorganic species, or via hydrogen bonding of the neutral head groups with hydrophilic inorganic silicates as shown by Tanev et.al.,[17] the inorganic species, which may be monomeric or oligomeric get attracted to the surface of the micellar rods. In the second pathway proposed by Huo et.al.,[26] there is no apriori formation of ordered surfactant aggregates. It is believed that the silicate anions in solution, by virtue of their charge balance with the cationic surfactants, force the surfactant molecules to form supramolecular arrays. This mechanism follows a charge matching criteria and operates under conditions where the surfactant mesophases precipitate out well below the critical micelle concentration of the surfactant. Both of these mechanisms indicate liquid crystal template formation.

Mesoporous silicates prepared via hydrothermal treatment of layered silicates such as kaenmite in the presence of alkyltrimethylammonium surfactants,[62-64] raises the question as to whether the silicate layer of the kaenmite structure is wholly or partially retained during the synthesis, or the role of kaenmite is restricted to being just the silica source. X-ray powder diffraction of the resulting material lacked any indication of kaenmite structure. In comparative synthetic studies on MCM-41 and the kaenmite derived material it was shown that different formation mechanisms operate in these materials.[61-66]

In Fig. 1.2,[66] the mechanisms responsible for the formation of mesoporous materials are shown. The liquid-crystal templating mechanism derives support from the surfactant solution chemistry in which such ordered surfactant mesophases are known. By progressively increasing the surfactant:silica molar ratio the formation of the three forms of mesoporous silica hexagonal, cubic and lamellar has been achieved (Fig. 1.2). Such mesophases are widely known in surfactant phase diagrams. These results support the liquid crystal template mechanism, wherein the silicate anions initiate the liquid crystal state formation and also serve as counter-ions and stabilizers for the liquid crystal arrays. Organic

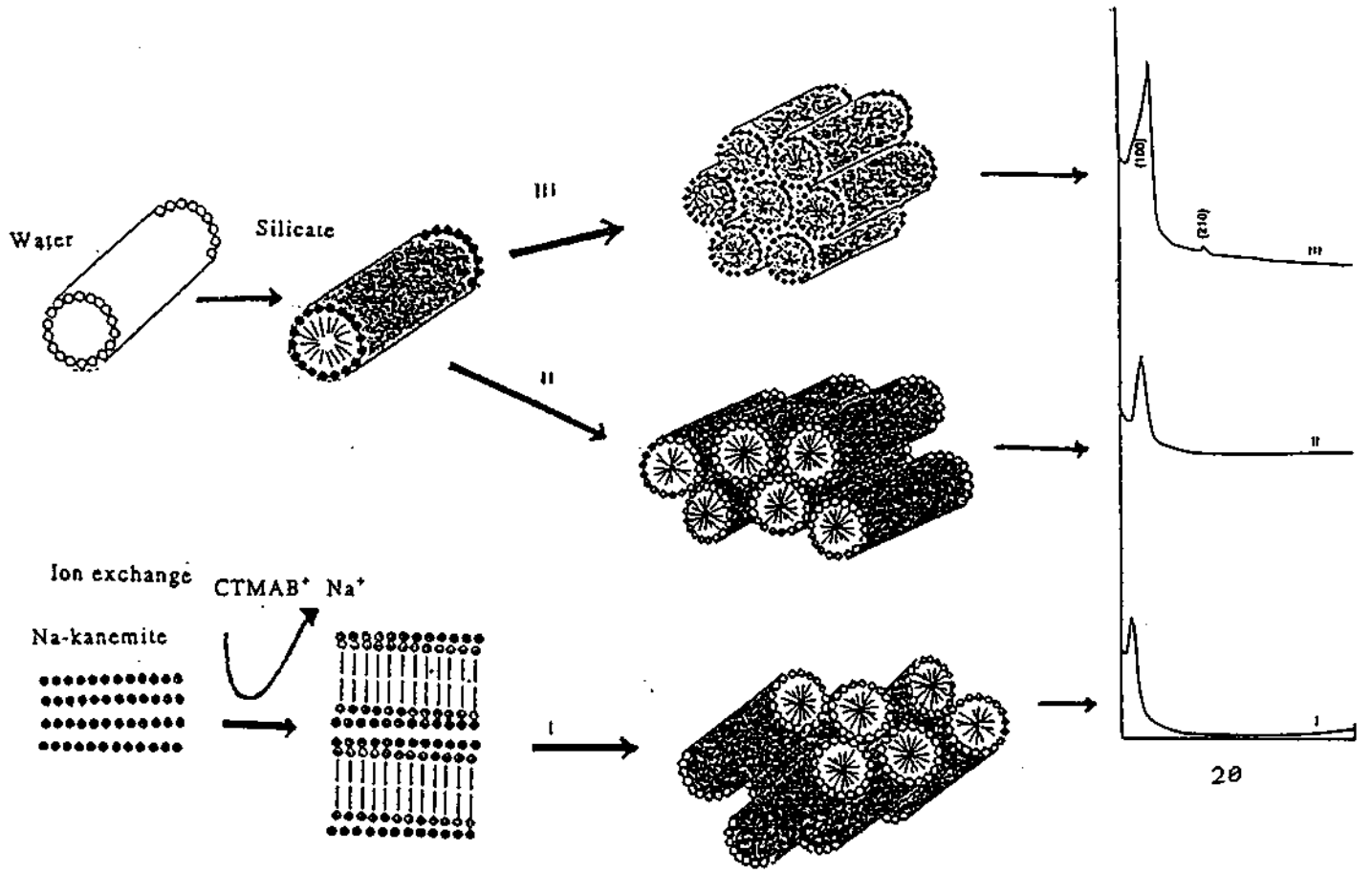

Fig. 1.2. Formation of mesoporous materials (I) derived from layered silicate kanemite (II), with disordered mesopores and (III) with well ordered hexagonal channels with typical X–ray diffraction patterns

solubilizates increase the pore sizes in these materials just as in surfactant chemistry.

Surfactants in solution assemble in various ways to yield micellar aggregates of various shapes and size. The surfactant mesophases essentially belong to three kinds, bilayer (lamellar), ordered cylindrical micelles (hexagonal) and cubic. The lamellar phase has one-dimensionally confined material where the inorganic species grow over a self-assembled surfactant bilayer analogous to the lipid bilayers known in biology. In the hexagonal phase, infinite surfactant cylinders are packed in a hexagonal manner over which the inorganic species are draped. The three-dimensional cubic phases have been described in the literature using the concept of periodic minimal surfaces, with the inorganic species occupying the gyroidal minimal surface and are bicontinuous in nature.[67-69] The employment of various surfactant assemblies with aggregated solution phases, have enabled scientists in the design of novel molecular sieve materials with the desired structure and pore size.

1.3 Synthetic strategies

For the synthesis of mesoporous structures, it is important to adapt the headgroup chemistry of the surfactants to that of inorganic component. In aqueous solution, the surfactants form oligomeric cations and anions depending on the pH and form aggregates with various morphologies depending on factors such as temperature, concentration etc. Cooperative organization of ion pairs formed between inorganic species in solution and surfactant molecules is determined at low temperatures by electrostatic interactions, hydrophobic van-der waals forces and hydrogen bonding.[26] By adjusting the charge density matching, surfactant geometry and relative reactant concentrations, various mesostructure geometries can be generated.

Silicate mesophases were originally synthesized by the condensation of anionic silanol species I^- over self-assembled cationic surfactants S^+, such mesostructures are designated as S^+I^-, (Fig. 1.3).[26] In S^-I^+ mesostructures

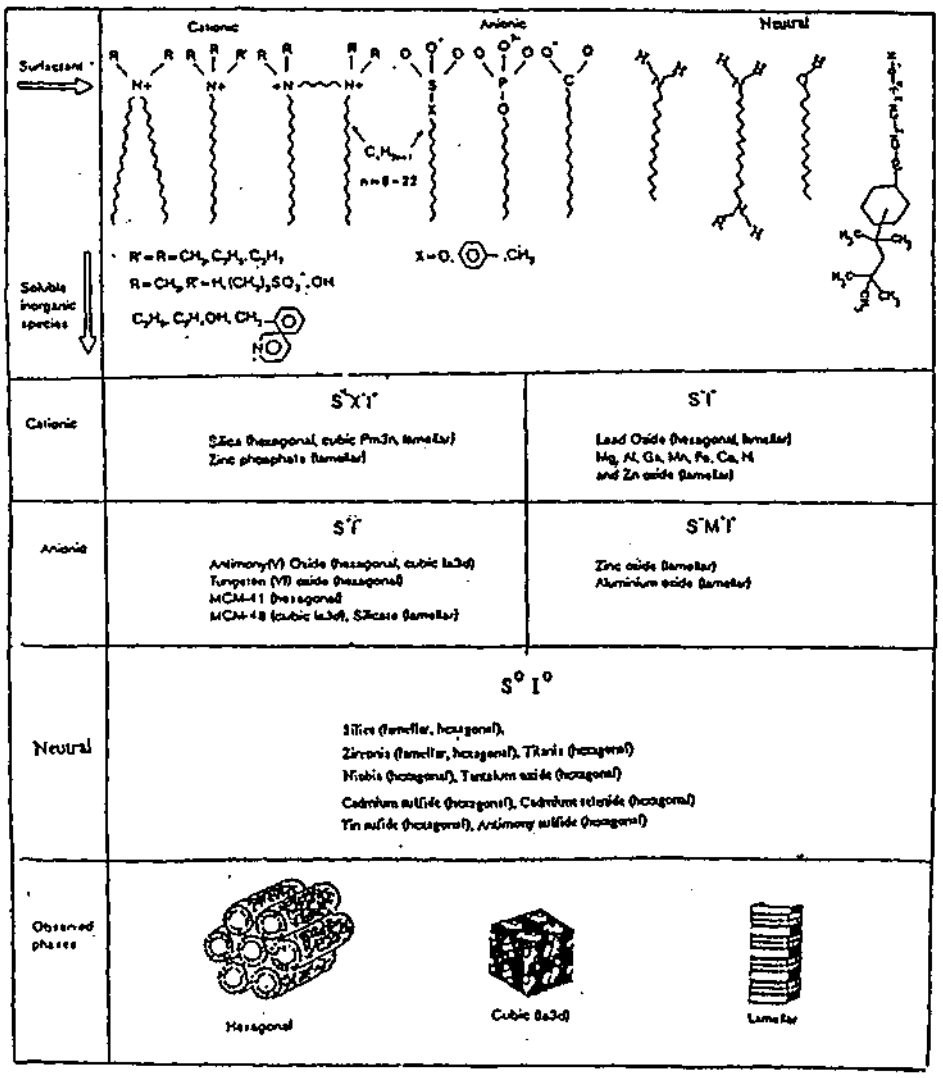

Fig. 1.3. Schematic diagram depicting the synthetic pathways by combinations of different surfactant and soluble inorganic species

(Fig.1.3) cationic $\mathbf{I^+}$ species are assembled over anionic (alkyl sulfonate) surfactant species $\mathbf{S^-}$. This strategy extends further, where identically charged partners can also form mesostructures via mediation of counter-charged ions which must be present in stoichiometric amounts (Fig. 3): $\mathbf{S^+X^-I^+}$ mesostructures, (for example with $\mathbf{S^+}$= tetraalkyl ammonium ion, $\mathbf{X^-}$=sulfate ion and $\mathbf{I^+}$= cationic zirconyl species, which form in strongly acidic solutions)[21] or $\mathbf{S^-X^+I^-}$ mesostructures, (for example with $\mathbf{S^-}$=alkylcarboxylate, $\mathbf{X^+}$=Na^+, and $\mathbf{I^-}$=zincate ions).[26] All these strategies involve electrostatic charge balancing and have failed by and large in the case of most oxides, which yield only the lamellar mesophase when the synthesis was based on ionic charge compensation at the **S/I** interface. These mesostructures collapse upon removal of the organic component and yield dense (in most cases amorphous) metal oxides. Iron, tungsten, lead, tin, lead and antimony oxides form hexagonal phases; antimony oxide in addition gives the cubic phase. However, these phases do not exhibit porosity after calcination; instead, the ordered mesopores collapse.[25-27,50,51,70] This could be due to the lower degree of condensation of the oligomeric ions compared to that of silicates, which form the walls of the mesopores. The redox instability of the metal cations may also play a crucial role. In the case of silicate mesophases softer routes such as ethanol extraction, and exchange treatment can remove the template. Such milder routes for template removal from mesoporous oxides have also been employed by Pinnavaia and coworkers.[17,18]

Mesophase formation is not restricted by charge-balancing criteria but it extends over nonionic domains as well, where such electrostatic interactions are absent. $\mathbf{S^0I^0}$ combinations are possible, where $\mathbf{S^0}$ is a nonionic surfactant assembly, which could be polyethylene oxide, or neutral long-chain amine surfactant, whereas $\mathbf{I^0}$ is the neutral inorganic precursor, which could be organometallic or metalorganic compounds (generally alkoxides). The interaction at **S/I** interface in such assemblies is probably mediated via hydrogen bonds, which are quite weak when compared to electrostatic interactions. This allows the possibility of removal of template via extraction with organic solvents. Mesoporous silica molecular

sieves have been prepared using neutral alkylamine[17] and polyethylene oxide[18] surfactants other than the cationic templates.[7,8] Various oxides have been prepared via nonionic surfactant routes such as niobia,[22] alumina,[17-19] zirconia,[21] titania.[20]

Metal alkoxides are the precursors of choice but the hydrolysis of the precursor needs to be carried out in a controlled manner. The hydrolysis can be controlled by carefully manipulating the coordinating agents around metal ion. Antonelli and Ying[20] employed titanium (acetylacetonate)tri(*iso*propoxide) instead of titanium *iso*propoxide which slowed down the rate of hydrolysis, and mesoporous titania was obtained, which could not be obtained earlier with titanium alkoxide. This was followed with synthesis of stable mesoporous niobium[22] and tantalum oxide[24] using neutral amine surfactants. They first observed covalent interactions between long-chain alkylamine and the inorganic component. On allowing for sufficient time, ordered hexagonal structures were formed. Addition of water, resulted in hydrolysis of the M-O-C bonds and the gel formed was treated hydrothermally to enhance the condensation. Template removal was achieved by washing the sample with a HNO_3/EtOH solution. To circumvent the problem of faster rates of hydrolysis nonaqueous solvents were employed in few cases. Investigations are on for employing surfactants in which head group of it acts as building entity for the inorganic material whereas the alkyl chain attached serves as the hydrocarbon tail, for example trialkoxyalkylsilanes where the Si-O-C bonds are hydrolyzed during the synthesis, thereby generating an anionic surfactant.

1.4 Characterization techniques

The as-synthesized mesoporous materials are characterized using a variety of experimental techniques, of which the foremost is powder X-ray diffraction which gives a clear indication about the formation and nature of the mesophase depending upon the bragg reflections corresponding to various d-spacings. In

Fig.1.4 we show typical x-ray diffraction patterns of three types of the mesoporous phases. The lamellar mesophases give bragg peaks corresponding to spacing ratio (1:2:3:4:5:6...). The hexagonal mesophases give reflections corresponding to ratios (1:√3:√4:√7:√9:√12...), whereas three-dimensional cubic mesophases, which are optically isotropic, fall in space group symmetries such as *Ia3d* (√6:√8:√14:√16:√20:√22...), *Im3m* (√2:√4:√6:√8: √10:√12...), *Pn3m* (√2:√3:√4:√6:√8:√9...), *Fd3m* (√3:√8:√11:√12:√16: √19...), *Fm3m* (√3:√4:√8:√11:√12:√16...), and Pm3n (√2: √4: √5: √6: √8: √10...) and give bragg peaks corresponding to these spacing ratios.[71]

High-resolution transmission electron microscopy gives a visual description of the nature of mesophase, the wall thickness, pore diameter or interlamellar spacing. Scanning electron microscopy gives the surface morphology of the mesophase. Thermogravimetric analysis gives idea about the thermal stability, the composition of the mesophase and the template decomposition temperature. The surface area measurement and pore size distribution can be estimated by adsorption measurements. The methods generally employed to calculate pore size distribution are BJH (Barrett Joyner Halender)[72] and HK (Horvath- Kawazoe)[73] method. The nature of the inorganic and organic species involved in the formation of mesophases and the nature of species present, degree of polymerization, coordination and how they transform on calcination can be studied using solid-state MASNMR[74] (Magic angle spinning nuclear magnetic resonance) and EXAFS[75] (Extended X-ray absorption fine structure) studies. EXAFS is also useful to examine the environment of probe atoms/molecules in mesoporous solids. Neutron have low absorption cross sections compared to x-rays and are better suited for diffraction studies involving weak scatterers like hydrogen which can be substituted by deuterium.

1.5 Relation between zeolite and mesoporous materials synthesis

It is instructive to examine the pathways for the formation of mesoporous materials in relation to those of microporous materials. The study shows that

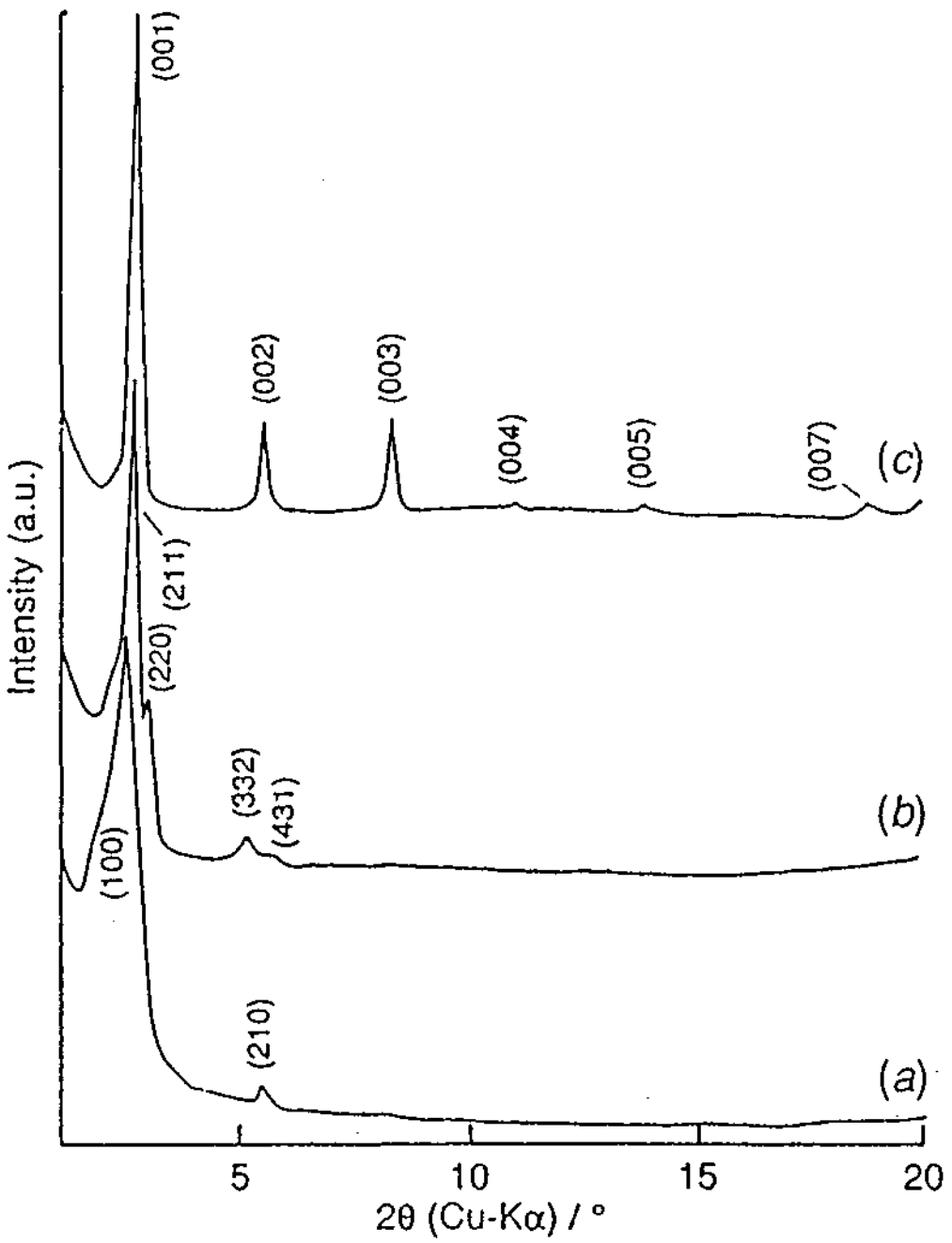

Fig. 1.4. X–ray diffraction patterns of the aluminoborate mesophases:

(a) hexagonal (b) cubic (c)lamellar.

alkyltrimethyl ammonium surfactants can act as templates for both the microporous and the mesoporous materials. Surfactant chain length and reaction conditions are the parameters that can be carefully manipulated to get either microporous or mesoporous materials. When short chain alkyltrimethylammonium surfactants (e.g.,n=6,8 $C_6H_{13}[CH_3]_3N^+$) are utilized, the formation of micellar/liquid crystal phase is generally an energetically unfavorable event.[76,77] The solubilities of these short chain quaternaries is quite high (> 50 wt % in water is easily achieved), and assemblies of these are not necessary to minimize hydrophobic interactions and with such short chain surfactants microporous materials such as ZSM-5 are isolated. With longer surfactant chain lengths, hydrophobic forces are dominant and the formation of self-assembled structures is favoured. In such cases, mesoporous materials are isolated. At high reaction temperatures (150°C), even the long chain length surfactants (C-10 and C-12) do not form aggregates, and yield amorphous material. Only C-14 and C-16 surfactants form well defined-hexagonal mesophases at this temperature and give mesoporous materials.[78] At still high temperatures, amorphous materials are obtained, most probably due to disruption of surfactant aggregates.

1.6 Phase transitions in mesoporous materials

Various kinds of phase transitions have been reported in mesoporous materials in the solution phase.[34,79-84] This involves a transition from lamellar to hexagonal and then to the cubic mesophase. Factors such as the ageing period, surfactant to silica concentration, temperature, pH of the medium,[34] addition of counterions and alcohols, can induce mesostructural phase transitions by modifying the rigidity and curvature of the interfaces. All this follows from surfactant literature where such phase transitions between various surfactant mesophases are widely known,[67,68,85,86] where increasing surfactant concentration usually gives rise to the following transformation: micellar solution L1→hexagonal H1→intermediate I→lamellar Lα.[85,86] In general, the principal factor driving the lamellar to non lamellar transitions in surfactant systems is the tendency of one or both monolayer halves of the bilayer to curl away from a planar configuration

which arises from an imbalance of lateral stresses from the headgroup region, the polar/nonpolar interface, and the hydrocarbon chain regions of the bilayer.[87]

In a bilayer or lamellar mesophase a deformation on one side inevitably influences the other side, resulting in an opposing response. Both halves of the bilayer can curve in opposite directions one curving towards the hydrocarbon chain with a positive curvature and another towards the aqueous exterior with a negative curvature or in the same fashion i.e. with the same curvature depending on the conditions around each monolayer. In the former case, the energy can be minimized by curling up into a cylindrical geometry whereas is in latter case it leads to frustration.[87]

Size, charge and shape of the surfactants are important structure determining parameters. The classical description of how the amphiphiles assemble in liquid-crystal phase is described in terms of the local effective surfactant packing parameter,[88,89] $g = V_{par}/(A.R_{par})$, where V_{par} is the total volume of the surfactant chains plus any cosolvent, organic molecules between the chains, A is the effective head group area at the micellar surface, and R_{par} is the surfactant tail length or the curvature elastic energy. The interface surface bending energy is expressed in terms of values of g. The g value governs the structure and form of mesophases.

g	Mesophase
1/3	Spheres
½	Hexagonal (P6m)
1	Lamellar
> 1	Inverse

These transitions reflect a decrease in surface curvature as we move from cubic phases to lamellar. For surfactants to assemble in spherical phases, the head group area should be large. If the head groups are packed tightly, higher aggregation numbers leads to lamellar or rod mesophases. So it's presumed that

the phase transitions in mesoporous materials essentially involve the phase transitions of the surfactant mesophase and not just the inorganic framework which is much more difficult to rearrange. The above approach does give some idea about the transitions from one mesophase from the another based on concentration of the surfactant, electrolyte added etc. but it neglects the insight to predict the existence of bicontinuous cubic mesophases. Not just that this theory also neglects the geometry dependence of the chain contribution to free energy.

A transformation from the lamellar to hexagonal mesophase has been observed in silicate mesophases on ageing the as-synthesized samples for increasing times.[79] This has been explained on the basis of extensive polymerization of silica network and charge balancing. In the early stages, highly charged silica species favour a small head group area and hence lamellar configuration is preferred, whereas with the progress of ageing process the density of charged anionic silanol species diminishes, so that the head group area increases, while the number of compensating cations decreases. The silicate wall on condensation leads to optimum head group area for the hexagonal phase according to the charge-density matching criteria. It has been concluded that the lamellar phase is favored at a high pH and a low degree of polymerization and that the hexagonal phase at a low pH, with highly condensed silica. In the case of aluminoborates, the three mesophases have been obtained on varying the pH of the synthesis medium.[34] At a pH of 2, the hexagonal phase was obtained, where as pH of 3.5 and 5.5 resulted in the cubic and the lamellar mesophases. It has been reported by Yanagisawa et.al.,[62] that inclusion of cetyltrimethyl ammonium cations inside sheet silicate kaenmite leads to formation of a mesostructure. The mechanism proposed is based on the Israelachvili model.[88,89] Monnier et.al.[79] give a probable description of the cubic mesophases formed but there has been no schematic mechanism proposed to throw light on the transformation process. They maintain that cubic phase can be described on the basis of the Q_{230} model proposed by Mariani et.al.,[67] for water surfactant systems, where silicate layer sits on the gyroid periodic minimal surface. Such a cubic surface is bicontinuous in nature and contains surfactant species into two equal and disconnected volumes.

Periodic minimal surface (PMS) cubic phases are presumed to be kinetically difficult to form, and are governed by competition between curvature and packing. It is impossible to transform between these structures without tearing the surfactant water-interface, without compensating for expensive hydrocarbon-water interaction.[90] The kinetic barrier for obtaining these PMS cubic phases can be overcome if the energy needed to cause the interfacial tears can be compensated. This may be possible, only by the gain in energy from the interaction of inorganic species with the surfactant mesophases.

1.7 Applications

There has been a whole range of potential applications envisaged for the mesoporous molecular sieves based on their high surface areas (between 700 and 1200m^2g^{-1}) and uniform pore diameter (20 to 100Å). Such applications include the use of these materials as improved adsorbent materials to remove toxic metal ions from aqueous media,[91] volatile organic compounds in the industries.[92] Various studies have been performed on these materials to determine the adsorption of various gases on these materials (MCM-41).[93] The adsorption isotherm for these materials depends on the material composition, pore size, and nature of adsorbent. Adsorption studies using argon,[8,93] nitrogen,[93,94-98] oxygen,[95] water[99,100] and hydrocarbons such as cyclopentane[98,101] and benzene[8] have confirmed the narrow pore size distribution and large pore volumes of MCM-41. The above mentioned characteristic features make mesoporous metal oxide mesostructures promising catalysts, catalysts supports, for the reactions which need large pore volumes.

Acid sites in MCM-41 silicates can be created by isomorphous substitution of Si by trivalent metal ions such as Al or B. The Al-MCM-41 has been reported in both literature[7-8,102-109] and in patents.[110] The aluminum is found to be tetrahedral in all these materials and various compositions with Si/Al ratio of 62-2.5 have been synthesized. Acidity of Al-MCM-41 was studied using TPD of ammonia Bronsted acidity of which is comparable to that of amorphous silica

alumina. As for catalytic applications are concerned Ni/Mo impregnated Al-MCM-41 has been used for hydrocracking of vacuum gas oil.[111] It was found that the catalyst had higher hydrodesulfurization and hydrodenitrogenation activity than Ni/Mo loaded either on USY or amorphous silica, alumina. The higher activity has been attributed to high surface area on which the catalytic species are dispersed and also to its large pore volume accessible to large molecules.

The acid form of mesoporous Al-MCM-41 has been used by Armengol et.al.,[112] to carry out alkylation reactions of bulky aromatic compounds such as di-tert-butyl-phenol with bulky cinnamyl alcohol. Kloestra et.al.,[113]used basic properties of Na^+- and Cs^+- exchanged Al-MCM-41 to carry out the Knoevenegel condensation of benzaldehyde. Boron has also been introduced into the MCM-41 framework.[40,114] The boron incorporated into the framework is tetrahedrally coordinated and the B/Si ratio on calcination remains 8%. Yuan et.al.,[51] have reported Fe-modified MCM-41. No catalytic applications for these materials have been reported.

Acid sites can be prepared by supported heteropolyacids (HPA). Kozhevnikov et.al.,[115] prepared phosphotungstic acid loaded MCM-41 samples. Various alkylation and isomerization reactions have been carried out using these heteropolyacid-loaded catalysts. Ti-MCM-41,[35,38] and hexagonal mesoporous silica (HMS) have been found to be better catalytic agents than Ti-silicalite for catalytic peroxide based oxidations of wide range of substituted aromatics. Tanev et.al.,[38] attributed this enhanced catalytic activity to the increased ease of diffusion of substrate through the mesoporous channels of MCM-41 and HMS as compared to that of microporous Ti-silicalite.

It has been speculated that MCM-41 materials may find great utility in a variety of optical, electronic and other applications. 2,4,6 triphenylpyrylium ion incorporated in MCM-41 has been shown to be a highly efficient electron transfer material,[116] it functions as a sensitizer in isomerization of *cis*-stilbene to *trans*-stilbene. Mesoporous materials can serve as hosts for anchoring organometallic

complexes which can be subsequently coneverted to metal clusters.[117] Aniline has been polymerized inside Fe- or Cu-MCM-41 and the resulting polyaniline has been found to show electrical conductivity thus realizing our goal of conducting wires,[118,119] which may have sharp implications on our future information technology. Mesoporous silicate channels have also help in controlled polymerization of styrene, methylmethacrylate and vinyl acetate.[120] Mesoporous manganese oxide can be used as a redox catalyst,[30] also there is a big scope for these materials like mesoporous silica films in optical devices.[121]

1.8 Concluding Remarks

The past few years have witnessed a tremendous surge of interest in mesoporous materials. Many novel synthetic strategies have come up. Amphiphilic block copolymers,[122,123] stablized emulsions,[124,125] polystyrene and latex spheres[126-128] have been employed as templates to create highly ordered mesoporous materials. Patterned surfaces have been generated over large length length scales.[129] Mann and coworkers have coated the bacterial threads with silica-surfactant mesophases.[130] A whole range of functional groups have been grafted onto MCM-41 surfaces including amino groups,[131] thiol groups,[132,133] epoxides,[134] ferrocenyl[135] and organometallic lanthanide silylamides,[136] vinyl,[137] phenyl, aminopropyl and methaacrylate.[138] Hybrid products have been synthesized with tailored inorganic precursors, which incorporate low molecular weight organics, in them and are known as ceramers or ormocers (organiccally modified ceramics). These materials have also found applications in coating and electrochemistry. There has been a lot of studies on cubic mesophase MCM-48, focussed specially on improving the synthesis procedure, structural characterization of the pores, surface and their properties, improvement of thermal and mechanical stability, surface modification via bonding of organosilanes, grafting or immobilization of metal complexes and preparation of polymer-silica composities.[139] There are also reports on using the silica surface for nanoscale assemblies of metal clusters.[140] Thin films and porous membranes are

other fields where these materials have been put to use. The advent of these novel applications in past few years shows a tremendous scope for these materials in future. A lot of effort has been directed towards understanding the mechanistic pathways that lead to the formation of various mesostructures in these materials. Despite all the progress made the field still continues to expand, creating lot of avenues for further research, which may include both fundamental aspects and applications.

2. SCOPE OF THE PRESENT INVESTIGATIONS

2.1 Mesoporous zirconia

Mesoporous solids are generally prepared by making use of self-assembled ordered aggregates of surfactants as templates, thus rendering the structures exhibited by the mesoporous solids to be similar to those of the self-assembled[67-69] surfactants. It is possible to obtain hexagonal or lamellar forms of mesoporous silica by varying the pH or surfactant: tetraethylorthosilicate (TEOS) ratio.[69,79] The hexagonal form of silica has also been prepared by Tanev and Pinnavaia by a neutral templating route based on hydrogen-bonding interactions and self-assembly between primary aliphatic amine micelles and TEOS[15b]. These workers employed a neutral diamine to obtain lamellar silica of vesicular morphology[141]. We have investigated the formation of lamellar phase of mesoporous zirconia prepared by the neutral amine route and find that chain length of the amine and the composition of the solvent, in particular the water content, play a crucial role. More interestingly, the lamellar form of zirconia transforms into the hexagonal form in solid state, upon the removal of amine by calcination.

Phase transitions among lamellar, hexagonal and cubic forms, occur in mesoporous materials in the solution phase. For example, changing the pH of the medium or ageing, leads to transformation of the lamellar phase of silica to the hexagonal phase.[79] Lamellar, hexagonal and cubic forms of aluminoborates have

been prepared by changing the pH.[34] Other factors such as temperature, presence of counter ions and concentration of the surfactant also affect the phase transitions.[79,84] The phase transitions in mesoporous solids also bear some similarity to those in surfactant assemblies.

In surfactant systems, decreasing the concentration of the surfactant instantaneously transforms the lamellar phase to hexagonal phase.[11,12] The transitions in the surfactant self-assemblies are commonly understood in terms of the surface/interface energies of the ordered aggregates.[87] The effect of ageing on the lamellar to hexagonal phase transformation in mesoporous silica has been related to the extent of polymerization of the silica framework and the balancing of charges.[79] High pH and a low degree of polymerization favour the lamellar phase whereas low pH and highly condensed silica favour the hexagonal phase of silica.[79] The transformation from the hexagonal to the cubic phase in silica has been explained in terms of the formation of a periodic minimal surface governed by a competition between the curvature and packing and the transformation is associated with kinetic barriers.[90] Since there is limited quantitative information on the nature of the phase transitions in mesoporous solids in the literature, we considered it important to investigate the transitions in some detail. For this purpose, we have chosen to investigate mesoporous zirconia, which exhibits interesting phase transitions both in solution and in the solid state. We have also investigated the kinetics of the lamellar→ hexagonal→cubic transitions of mesoporous zirconia in the presence of phosphoric acid and of the thermal lamellar→hexagonal transition of zirconia in the solid state.

2.2 Mesoporous alumina

High surface area alumina is of vital interest in catalysis. Although there are several reports in the literature on the synthesis of porous alumina, most of the preparations seem to possess purely textural porosity or to be amorphous.[142-144] There have been some recent efforts to prepare mesoporous alumina, but they have not been entirely successful in obtaining ordered structures. Yada et.al.[17]

prepared alumina by the homogeneous precipitation method using urea, and obtained a product with a somewhat disordered structure (d_{100} = 3.4nm). Vaudry et.al.[18] have prepared alumina mesophases starting with a mixture of aluminum sec-butoxide and aliphatic carboxylic acids. They obtained high surface area alumina with a mesoporous structure, which is not well defined. Bagshaw and Pinnavaia[19] have examined alumina prepared by the hydrolysis of aluminum sec-butoxide in the presence of polyethylene oxide surfactants, and found the presence of worm-like structures with no long-range order. It therefore seems that alumina with a reasonably ordered hexagonal mesoporous structure has not been prepared hitherto. We have investigated the synthesis of mesoporous alumina by the neutral amine route[15]. A specific advantage of the method is that the long chain amine template, is weakly hydrogen bonded to the metal alkoxide, is readily removed. We have also employed Polyoxyethylene sorbitanmonooleate (Tween 80) as the template to prepare mesoporous alumina.

2.3 Mesoporous silicophosphates

Since the synthesis of mesoporous silica,[7] several mesoporous oxides have been prepared by using ionic as well as neutral templates[11]. Some of the examples include ZrO_2,[21] TiO_2,[20] SnO_2,[29] Al_2O_3[17] and Nb_2O_5[22]. Mesoporous aluminophosphate[32] and aluminoborate,[34] which are analogous to silica have also been prepared and characterized. We were interested to investigate the synthesis of mesoporous silicophosphates by employing suitable templates. Crystalline and glassy silicophosphates are known and in some of them, silicon occurs with octahedral coordination[145-147]. Silicophosphates find applications as hosts for fast ionic conductors and optical fibres[146] and as catalysts[148]. We have successfully attempted the synthesis of mesoporous silicophosphates of varying phosphorus content, by employing cationic surfactants.

2.4 Mesoporous ruthenium dioxide

RuO_2 has wide application as conductors, catalysts for oxidation reactions and in electrocatalysis. In particular, RuO_2 coatings on titanium anodes find commercial applications where chlorine and oxygen evolutions occur from chloric and other acidic media.[149,150] We have attempted the synthesis of mesoporous ruthenium dioxide in the search of metallic mesoporous oxides.

2.5 Mesoporous chalcogenides

Braun et.al.[52] have recently described semiconductor-organic nanostructured composites of hexagonal symmetry based on cadmium sulfide obtained by using non-ionic amphiphiles such as polyethylene oxide. Such nanocomposites have been prepared by starting with different cadmium salts.[54] By employing hydrated polyol amphiphiles, Osenar et.al.[53] have obtained lamellar, nanostructured cadmium sulfide. In all these preparations, the nanostructured adduct of a cadmium salt with the amphiphiles was treated with H_2S gas. Since the preparation of the chalcogenide nanocomposites using amphiphiles involves methods akin to those employed in the synthesis of mesoporous metal oxides,[12,14,34] we considered it important to evolve a general method for the synthesis of mesostructured semiconductor chalcogenide-organic nanostructures and characterize the materials suitably. By employing long-chain amines as the amphiphiles[17], we have investigated the preparation of hexagonal and lamellar nanostructures of CdS, SnS_2, Sb_2S_3 and CdSe.

2.6 Catalytic activity of transition metal complexes encapsulated in a cubic mesoporous phase

Transition metal complexes encapsulated in the cavities of zeolites are known to exhibit high catalytic activity in certain oxidation reactions, suggesting that these catalytic systems are good enzyme mimics.[151] Oxidation of phenols with O_2 by copper acetate dimer incorporated in MCM-22 or VPI-5 is a case in

instance wherein the Cu(II) complex mimics the phenolase activity of tyrosinase.[152,153] Besides the activation of O_2, there have been studies of the oxidation of organic compounds with singlet oxygen sources such as H_2O_2, by metal complexes encapsulated in molecular sieves. Selective oxidation of alkenes by Mn(II) bis-2,2'-bipyridyl encapsulated in zeolites X and Y is one such example.[154] The Manganese (II) 2,2'-bipyridyl complex immobilized in mesoporous Al-MCM-41 has been recently shown to exhibit high catalytic activity for styrene oxidation.[155] Based on the geometry of the pore structures of mesoporous solids, it was our view that the cubic phase should be an excellent host for enhancing the catalytic activity of metal complexes.

We have therefore investigated the catalytic activity of two transition metal complexes incorporated in mesoporous Al-MCM-48, in oxidation reactions. The metal complexes examined are Cu(II) acetate dimer which has the structural features of Cu-containing monooxygenase enzymes[152,153] and Mn(II) bis-2,2'-bipyridyl. While Cu(II) acetate incorporated in Al-MCM-48 was primarily meant to examine the catalytic activity for oxygen at ambient conditions, the Mn(II) complex system was intended to study the oxidation of styrene by singlet oxygen.

2.7 Hexagonal microporous silica and aluminophosphate with intermediate pore sizes by supramoleular templating of a short-chain amine

A variety of crystalline microporous oxides with pore diameters in the 0.4-1nm range have been prepared over the last few years, by using organic template molecules.[156-158] By making use of self-assembled aggregates of long-chain surfactant molecules, mesoporous oxides (pore dia. 2-10nm) have been prepared, the very first instance being that of silica by Mobil chemists.[7,34] There is however a lacunae in the spectrum of hexagonal porous solids corresponding to those with pore diameters in the range of 1-2nm, i.e., in the intermediate range of pore sizes between those of the traditional microporous and mesoporous solids. Mesoporous MCM-41 silicates prepared with C_8-C_{10} surfactants are known to have pore sizes in the range 1.6-2.0nm.[159] Silica with a bimodal pore size distribution containing

both micro and mesopores with diameters of 1nm and 3nm respectively has been obtained using a cationic surfactant, on postsynthesis hydrothermal treatment.[160] Hexagonal, mesoporous aluminophosphate with a pore diameter of 3.5nm has been prepared using a cationic surfactant by Zhao et.al.[161] The use of neutral amine surfactants however, does not yield the hexagonal mesoporous aluminophosphate. Recently, Sun et.al.[162] have reported that hexagonal microporous niobia with pore diameter of less than 2nm can be prepared by supramolecular templating using short chain C_4-C_7 n-alkylamines. We have investigated the synthesis of hexagonal microporous silica and aluminophosphate using a short chain amine as the template molecule and have succeeded in obtaining these materials with well-defined pore distributions between 1 and 2nm.

3. EXPERIMENTAL

3.1 Preparation and transformations of mesoporous zirconia

In a typical synthesis, $Zr(OPr^i)_4$ (0.01mol) was added to a solution of the amine (0.01mol) in propan-1-ol (0.01mol) to which $(NH_4)_2SO_4$ (0.12mol) and water (x mol) were added under stirring. The pH of the gel was adjusted to 1.5-2.0 by using dilute HCl. The gel was subjected to hydrothermal treatment at 373K for 20h, filtered and washed with water and acetone. The dried sample was characterized using X-ray diffraction (XRD) and transmission electron microscopy (TEM).

The lamellar form of mesoporous zirconium oxide was prepared using dodecylamine (DA) as the surfactant. In a typical synthesis zirconium isopropoxide (0.01mol) was added to a solution of the dodecylamine (DA) (0.03mol) in *n*-propanol (0.1mol) to which ammonium sulphate (0.12mol) was added under stirring. The pH of the gel was adjusted to 1.5-2.0 by using dilute hydrochloric acid (HCl). The gel was subjected to hydrothermal treatment at 373K for 20h, filtered washed with acetone and dried at 373K for 2h. The lamellar nature of the product was verified using X-ray diffraction (XRD) and transmission

electron microscopy (TEM). To study the transformation of lamellar ZrO_2 in solution phase, ~100mg of the as-synthesized sample was taken in 50ml of 0.87M phosphoric acid and stirred for different times, filtered, washed with water, acetone and dried at ambient. The XRD patterns and TEM images of the samples were recorded each time.

The kinetics of the lamellar→hexagonal→cubic transition of zirconia in phosphoric acid solution was studied as follows. The (*100*) reflections of the lamellar and hexagonal phases differ both in intensity and position. Thus, as the lamellar phase (d_{100} = 3.34nm) transforms to hexagonal phase the intensity of (*100*) reflection decreases until it attains a much smaller value, characteristic to that of a disordered hexagonal mesophase (Fig. 1.5). In addition, the *d*-spacing of (*100*) reflection decreases until it reaches a minimum value after the transformation to hexagonal phase is complete. The intensities of the (*200*) and (*300*) reflections of the lamellar phase also decrease continuously with time, as the lamellar→hexagonal transformation proceeds. We have employed both the intensity and position of the (*100*) reflection to follow the kinetics of the lamellar-hexagonal transformation. These two measurements give slightly different estimates of the phase compositions and we have taken the average value in the kinetic study. The hexagonal to cubic transformation of zirconia was followed by the increase in the intensity of the (*220*) reflection of the cubic phase with time (Fig. 1.5).

The lamellar→hexagonal thermal transformation of zirconia in the solid state was studied by heating the lamellar form at a fixed temperature for different periods of times. The phase composition of the sample subjected to heat treatment was estimated on the basis of the intensity of (*100*) reflection, the *d*-spacing showing only small change in the thermal transformation (Fig. 1.6). The kinetics of the transformation was studied as a function of time at 373, 403 and 413K. The transformation was also studied by heating the lamellar sample for a fixed period of 2h at different temperatures ranging between 360-430K.

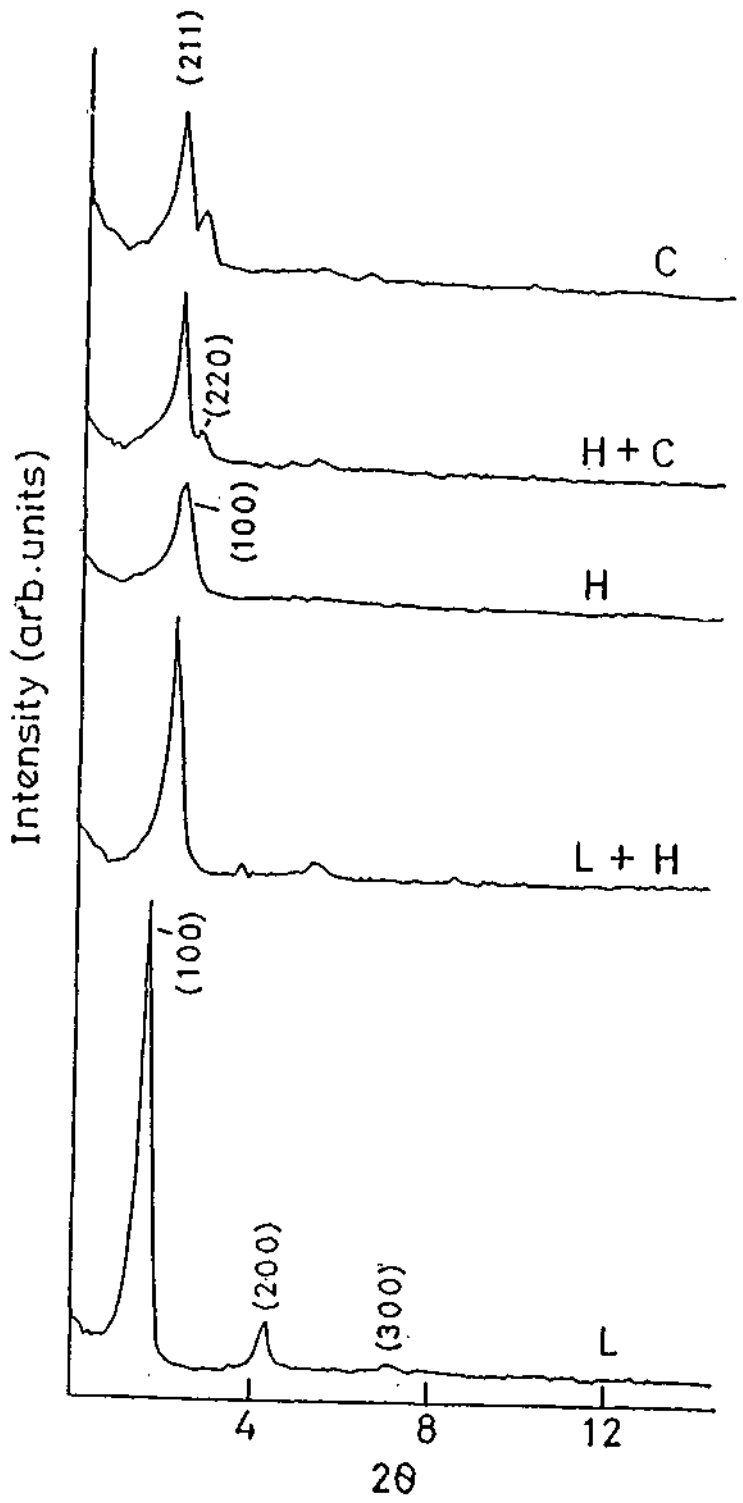

Fig. 1.5. XRD patterns showing the transformation of lamellar(L) zirconia to hexagonal (H) and then cubic (C) phases in phosphoric acid solution. Intermediate stages during the L–H and H–C transformations are shown

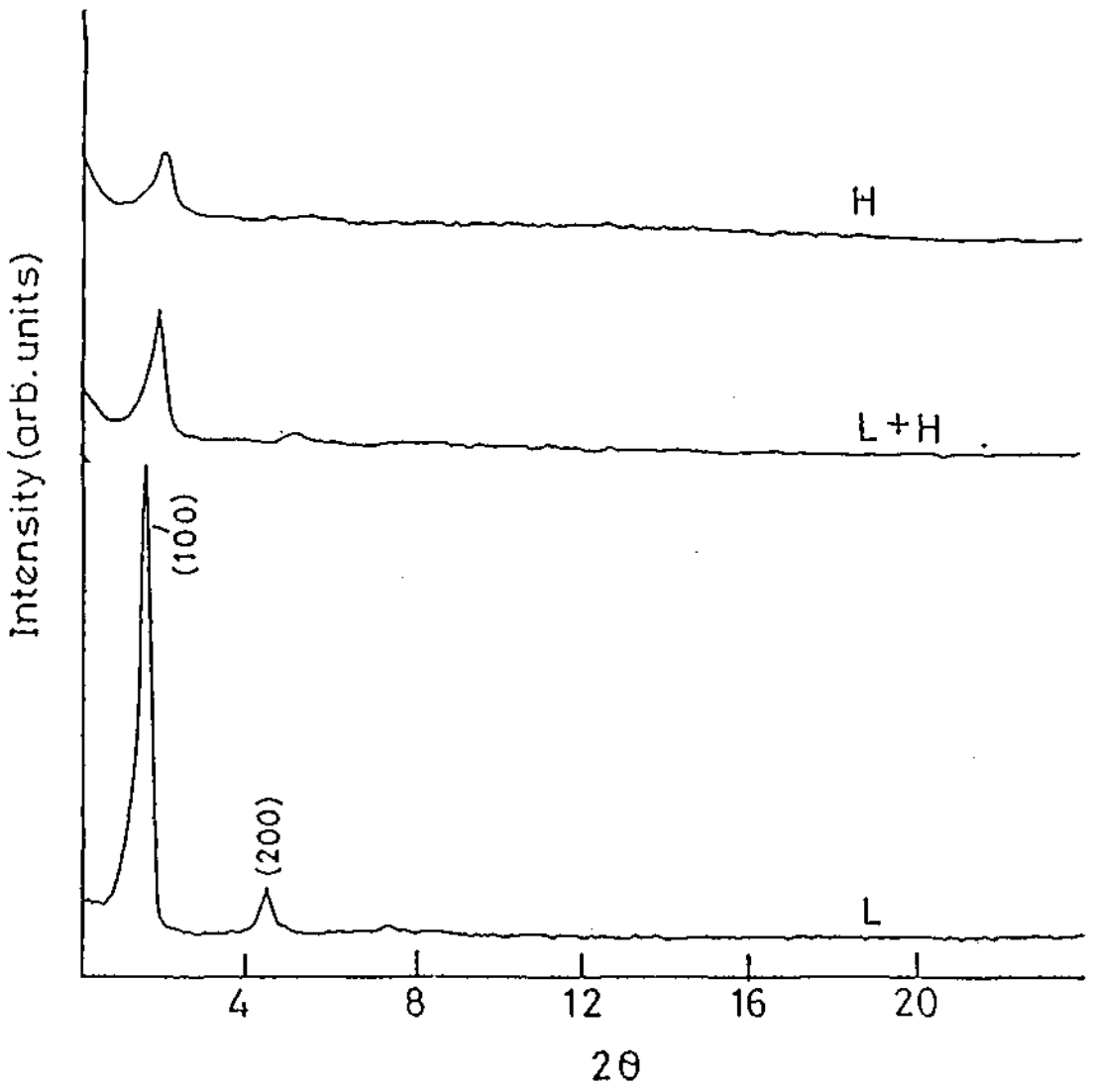

Fig. 1.6. XRD patterns showing the thermal transformation of lamellar (L) zirconia to the hexagonal (H) form. An intermediate stage during the transformatioin is shown

3.2 Mesoporous alumina

In a typical synthesis, aluminum sec-butoxide (0.01mol) was added to an ethanolic solution (10ml) of dodecylamine or hexadecylamine (0.0082mol). Water (5ml) was added to the mixture in a dropwise manner, under stirring. The gel thus obtained was aged at 323K for 22h, filtered and washed with water, acetone and dried at 363K.

Similar procedure was employed for synthesis with polyoxyethylene sorbitanmonooleate (Tween80) Here aluminum *sec*-butoxide (10mmol) was added to an ethanolic solution (10ml) of the surfactant (0.3ml). We also tried to prepare mesoporous alumina by using partially hydrolyzed aluminum iso-propoxide. In this experiment, hexylamine/octylamine (3.8mmol) was taken in isopropanol (10ml) and stirred for 10min. To this, aluminum iso-propoxide (5mmol) partially hydrolyzed with water (83mmol) was added. The mixture was stirred for 30 min and the resulting gel was aged at 298K for 20h, filtered, washed with water and dried at 363K. X-ray diffraction patterns were recoreded for the dried gels to check the nature of the mesophase and thermogravimetric analysis curves were obtained to check the composition and template removal. Transmission electron microscope images were recorded to confirm the nature of the mesophase. N_2 Adsorption measurements were carried out to determine the surface area and pore size distribution of the mesoporous samples after calcination.

3.3 Mesoporous silicophosphates

For the preparation of mesoporous silicophosphates, we have used tetraethylorthosilicate (TEOS) and phosphoric or phosphinic acid as the starting materials with cetyltrimethylammonium bromide (CTAB) and cetylpyridinium bromide (CPB) as the surfactants (SA). The preparation was carried out in acidic media, unlike that of silica which is carried out in basic medium. In a typical synthesis, the SA 7-8mmol was taken in water stirred for 20min and 2.8ml of HCl (5.6M) added to the solution. TEOS (16mmol) was added to this SA solution,

stirred for 15min, followed by addition of H_3PO_4/H_3PO_2 (~20mmol). The pH of the resulting mixture was adjusted to 3.5 using 5M NaOH solution and the stirring continued to obtain a gel. The gel was aged at ambient temperature for 20h. The final product was filtered and dried at 373K for 4h.Thermogravimetric analysis (TGA) of the dried product was carried out in O_2 atmosphere to 1273K. Energy dispersive analysis of X-rays (EDAX) was performed to analyze the composition of the mesophase. TEM images were obtained to confirm the nature of the mesophase.

3.4 Mesoporous ruthenium dioxide

For the synthesis of mesoporous ruthenium dioxide ruthenium trichloride hydrate ($RuCl_3.xH_2O$) (0.72mmol) dissolved in water (6ml) and acetylacetone (1.0mmol) was added dropwise to a solution of sodium dodecyl sulphate (SDS) (0.3mmol) under stirring over a period of 30min. 6ml of H_2O_2 solution (30%) was added to the resulting mixture slowly with the stirring continued. The final pH was adjusted to 8.5-9.0 with 25% ammonia solution. The mixture was aged for 3 days at ambient temperature, filtered, washed, dried at 353K, and XRD recorded. TGA was done to check the template loss and composition. TEM images were obtained to confirm the nature of the mesophase. The electrical resistivity studies as a function of temperature was carried out on the as-prepared mesoporous sample.

3.5 Mesoporous chalcogenides

The general procedure for the synthesis employed by us is as follows. To an aqueous solution of cadmium acetate (5mmol) an alcoholic solution of the amphiphilic amine (5mmol) was added and stirred to obtain a gel. The gel was aged at ambient temperature for 18h and dried. X-ray diffraction (XRD) patterns of the gel indicated that nanostructured mesophases of the amine and $Cd(CH_3COO)_2$ had indeed formed. To the gel, a concentrated aqueous solution of sodium sulfide was slowly added and the pH adjusted to 9.0-9.5. The resulting

product was aged at 333K for 18h. The product thus obtained was washed first with water, followed by ethanol-ether (50:50) mixture and dried at 333K. The X-ray diffraction pattern of the product was then recorded. EDX analysis of these products was performed to find Cd:S ratio. Thermogravimetric analysis (TGA) was done to check the amine loss and composition. The nature of the CdS-amine adduct mesophase was also confirmed by recording transmission electron microscope (TEM) images.

We also employed a $Cd(CH_3COO)_2$:amine ratio of 1:2 instead of 1:1 to check the nature of mesophase obtained. We have also used long chain thiols with Cd-acetate to check the formation of mesophases. We have attempted synthesis of metal sulfide-organic amphiphile nanostructures of tin and antimony by starting with $SnCl_4.2H_2O$ and $SbCl_3.5H_2O$ respectively and keeping the metal salt:amine ratio at 1:1. In order to prepare CdSe-amine nanostructures, we employed a procedure similar to that with CdS, except that an aqueous solution of Na_2Se was reacted with the Cd-acetate-amine gel.

3.6 Catalysis in cubic mesophase of silica

Al-MCM-48 was prepared by employing a modified procedure. To a solution of 2.9g of cetyltrimethylammonium bromide in 40ml of deionised water, 2.8ml of 5MNaOH was added and the solution stirred for 30min. To this mixture, a solution containing 0.09g of aluminum sulfate dissolved in 10ml of water was added followed by the dropwise addition of 6.2ml of tetraethylorthosilicate. The mixture was stirred for 1h, transferred to a stainless steel autoclave and kept at 383K for 5 days. The final product was filtered, washed several times with deionised water, dried at 353K for 3h and calcined at 773K for 10h in air to remove the template.

Cu-acetate-Al-MCM-48 was prepared by stirring 0.4g of Al-MCM-48 with 0.2g of copper acetate monohydrate in distilled, deionised water for 12h. The product was filtered, washed with water and dried at 383K for 24h in vacuum.

Al-MCM-48-$[Mn(2,2'\text{-bipy})_2]^{2+}$ was prepared by the treatment of Al-MCM-48 (0.3g) with a solution of 0.3g of $[Mn(bipy)_2](NO_3)_2$ in 20ml of 1:9 (by volume) DMF/acetonitrile mixture at room temperature for 48h. The sample was filtered, washed with acetonitrile and dried at 353K under vacuum for 1h. Both the catalysts were studied by Electron paramagnetic resonance (EPR), Electronic absorption spectroscopy and elemental analyses.

Oxidation of phenol by the Cu-Al-MCM-48 was studied by stirring 100mg of the catalyst in a phosphate buffer solution with 0.57mmol of phenol in an oxygen atmosphere at 303K. Oxidation of styrene was studied by taking 100mg of the catalyst in a solution 0.87mmol of styrene in 5ml of acetonitrile, to which 3.5mmol of H_2O_2 was added. Gas chromatography using a flame ionization detector (FID) was done to analyze the products.

3.7 Microporous silica and aluminophosphate with intermediate pore sizes

In a typical preparation of hexagonal microporous silica, to a solution of 0.019mol of hexylamine in 50ml of H_2O, 0.01mol of TEOS was added and stirred for 30min. The mixture was aged at ambient temperature for 5 days. The product was filtered, washed with water and dried at 343 K for 24h.The as-synthesized sample was calcined at different temperatures in a N_2 atmosphere.

In order to prepare hexagonal microporous aluminophosphate, 1g of $Al(OH)_3.xH_2O$ was added to a solution containing 40ml of H_2O and 10ml of methanol and stirred for 10min. To this slurry, 0.5ml of 85% H_3PO_4 was added followed by 1.5ml of 48% hydrofluoric acid, to obtain a clear solution. The final pH was adjusted to 7-8 using ~ 4ml of hexylamine. The gel formed was allowed to stir for 3h, and aged at ambient temperature for 24h. The product was filtered, washed with water and dried at 343K for 24h. The presence of F^- medium was essential, in the absence of which only a lamellar phase was obtained.

The materials were characterized using XRD and TGA. Energy dispersive X-ray (EDX) analysis was carried out to get the Al/P rations in case of aluminophosphates. TEM images were obtained to confirm the pore sizes and nature of the pores. Surface areas were determined by the Brunnauer-Emmett-Teller (BET) method. Pore size distribution was calculated using the Barrett-Joyner-Halenda[14] or the Horvath-Kawazoe method.[74]

3.8 Characterization techniques

The X-ray diffraction (XRD) patterns were recorded for the as-synthesized and calcined mesophases on a Rich Seifert-3000TT X-ray powder diffractometer. The Thermogravimetric analysis (TGA) of the samples was carried out using a Mettler-Toledo TG850 instrument. Surface areas and adsorption isotherm of the samples were measured using (Brunauer-Emmett- by adding Teller) BET method with the help of adsorption setup fitted with a Cahn-2000 microbalance. Energy dispersive analysis of X-rays (EDAX) and scanning electron microscope (SEM) images were obtained on a Leica S440i scanning electron microscope fitted with a link spectrometer. Transmission electron microscope (TEM) images were obtained with a Jeol-JEM3010 instrument operated at 300 kV. Magic angle spinning nuclear magnetic resonance (MASNMR) spectra were recorded on a Bruker DX-300 spectrometer. Fourier transform infrared (FT-IR) spectra were recorded on a Bruker spectrometer. Electron spin resonance (ESR) spectra were recorded on a Varian X band E-line spectrometer fitted with a magnetic field of 100 kHz modulation. Diffuse reflectance spectra (DRS) were recorded using a Unicam (Model SP8-100) spectrometer.

4. RESULTS AND DISCUSSION

4.1 Preparation and characterization of mesoporous zirconia

With hexadecylamine as template, we obtained the lamellar phase of ZrO_2 independent of the water content (x=1-2mol). We show a typical XRD pattern in Fig. 1.7a with *d* values 3.44, 1.71 and 1.13nm due to the *001*, *002* and *003* reflections. A lamellar phase was obtained with dodecylamine as well as (Fig. 1.7b) with *d* values of 3.3 and 1.66nm due to the *001* and *002* reflections. When octylamine was used as the surfactant with x=1.5mol, we obtained a lamellar phase (probably in mixture with a small proportion of the hexagonal phase), as can be seen from the XRD pattern (Fig. 1.7c) with *d* values of 2.55 and 1.28nm for the *001* and *002* reflections. The TEM image shows essentially the lamellar phase with a layer separation of 2.6nm (Fig. 1.8a). By reducing the water content in the reaction mixture (x=0.6mol), we obtained the hexagonal phase of ZrO_2 with d_{100}=2.65nm in the XRD pattern (Fig. 1.7d). The TEM image also bears evidence for the hexagonal structure (Fig. 1.8b).

This preparation of the hexagonal mesophase of ZrO_2 is an alternative to the methods recently reported in the literature.[21,163] More importantly, we have found that the lamellar phase obtained with octylamine transforms into the hexagonal phase on removal of the amine.

The lamellar form of mesoporous zirconia obtained with hexadecylamine, on keeping in 0.87M phosphoric acid, first transforms to the hexagonal form. This transformation is complete in 7h. We have followed the lamellar →hexagonal transformation as a function of time. In Fig. 1.9 we show the progress of the lamellar→hexagonal transformation by plotting the percentages of the lamellar and hexagonal phases against time. We see that the proportion of the lamellar form decreases while that of hexagonal form increases. It is noteworthy that the transformation of the hexagonal form to the cubic from starts only after the lamellar phase has completely transformed to hexagonal phase. The hexagonal to cubic transformation occurs in a short time (<3 h).

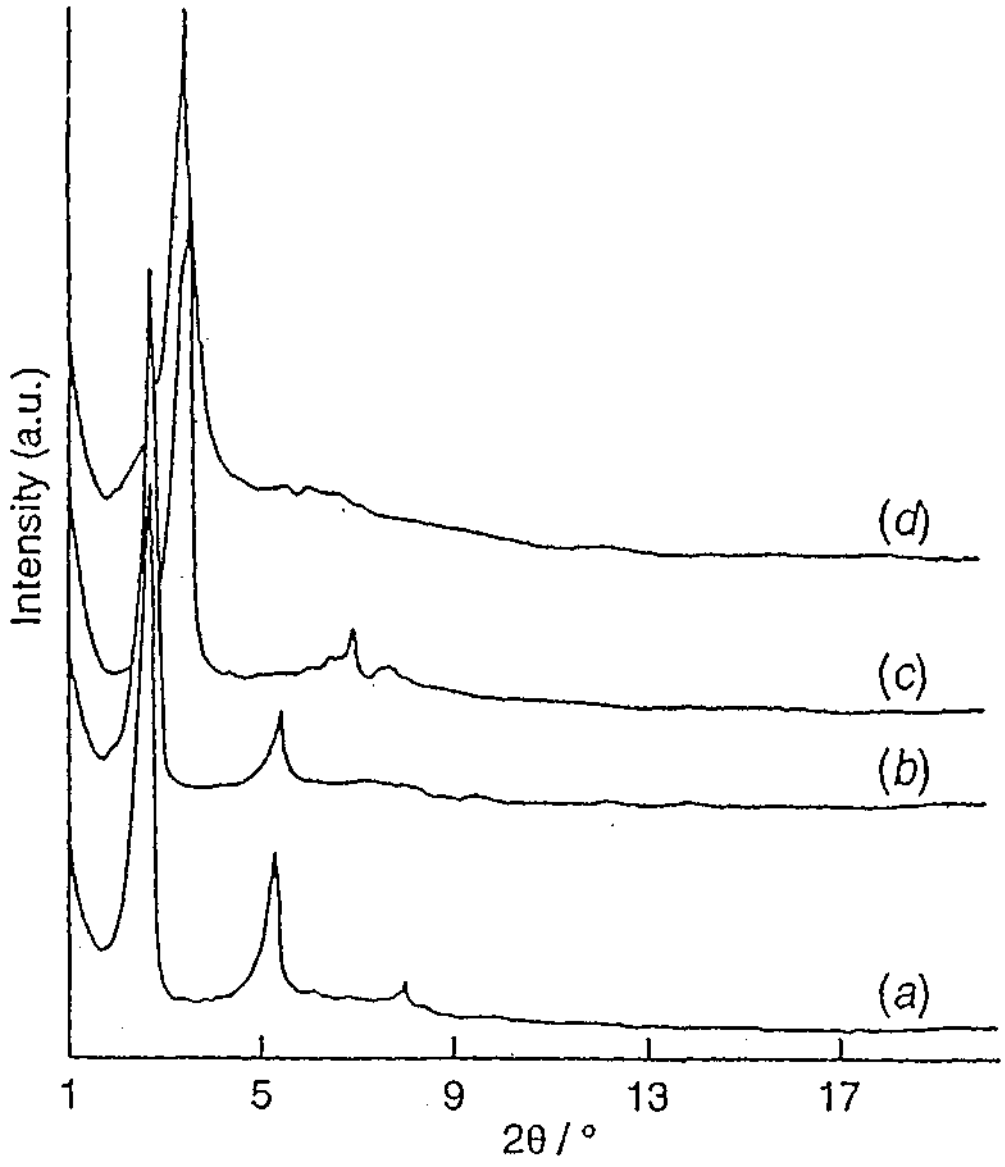

Fig. 1.7. XRD patterns of the mesophases of zirconia: (a) lamellar phase obtained with hexadecylamine; (b) lamellar phase obtained with dodecylamine; (c) lamellar phase obtained with octylamine (x = 1.5 mol) and (d) hexagonal phase obtained with octylamine (x = 0.6mol).

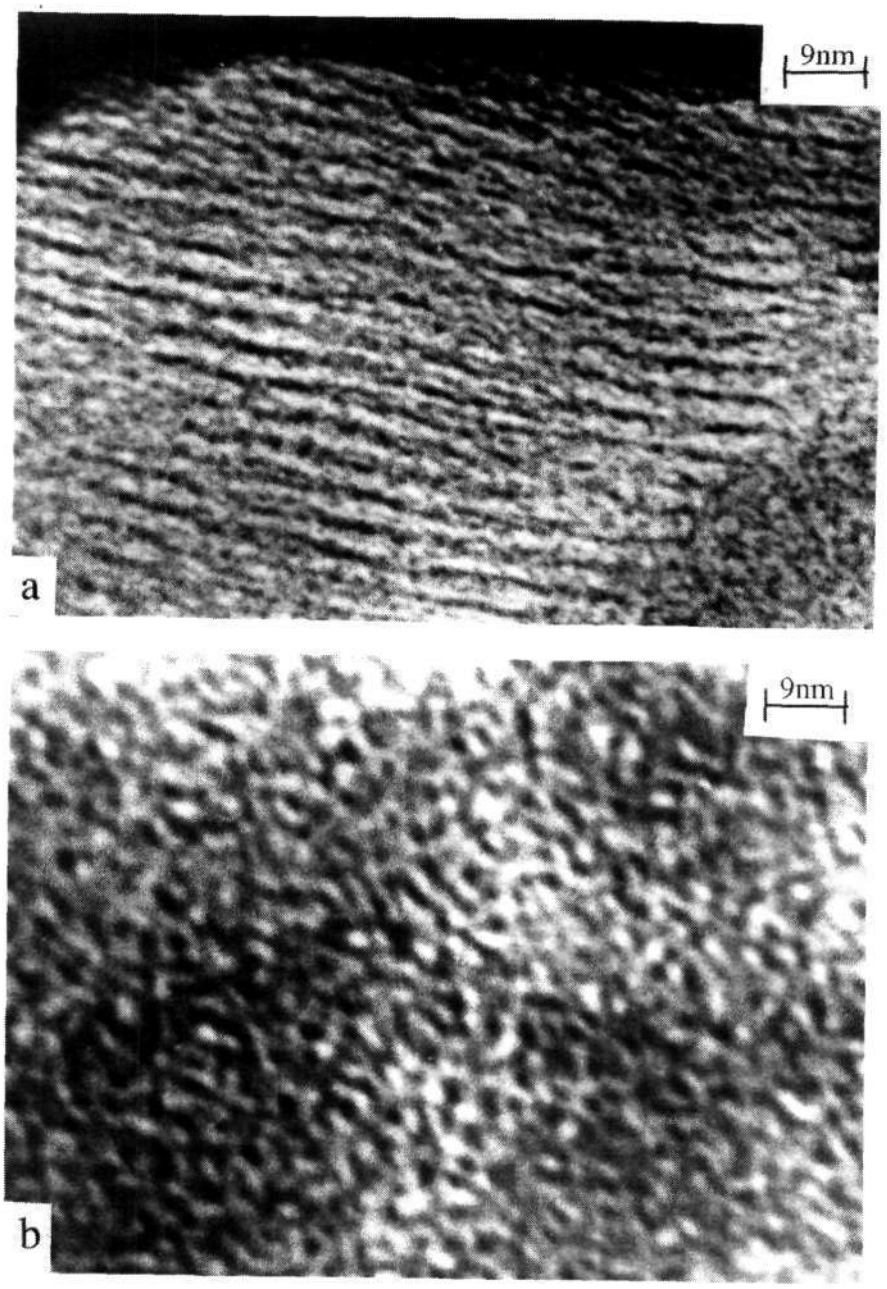

Fig 1.8. TEM images of the mesophases of Zirconia: (a) lamellar mesophase obtained with octylamine (x = 1.5) and (b) disordered hexagonal mesophase obtained with octylamine (x = 0.6 mol)

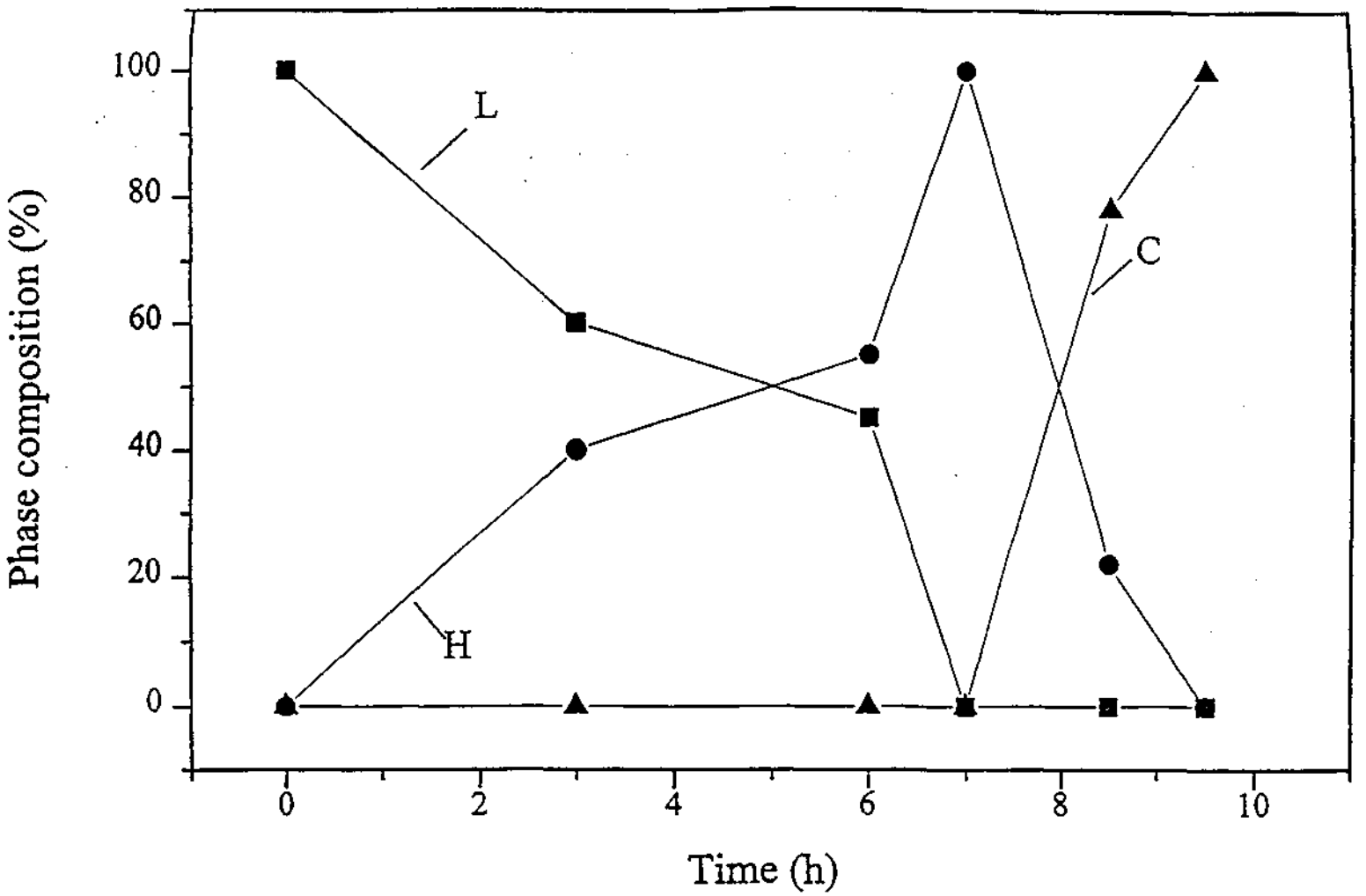

Fig. 1.9. Time variation in the phase composition of zirconia in phosphoric acid solution; L, lamellar; H, hexagonal; C, cubic

The lamellar→hexagonal transformation of ZrO_2 is likely to be initiated first by the removal of some of the surfactant species, followed by the curling of surfactant bilayer in order to minimize the surface/interface energy as shown in Fig. 1.10(a & b).[87,164] The curled bilayers transform to the cylindrical rods to further minimize the surface energy as shown in Fig. 1.10c and the cylindrical rods assemble to give the ordered hexagonal structure shown in Fig. 1.10d. In order to examine whether the loss of the surfactant species precedes the lamellar→hexagonal transformation, we have carried out TGA studies. We find that there is a significant loss of the surfactant in the lamellar→hexagonal→cubic transformation in phosphoric acid solution as well (Fig. 1.11). Thus, the TGA of the lamellar ZrO_2 sample treated for 3h in phosphoric acid showed 8 % loss of the surfactant, where as the sample treated for 7h showed a loss of 23% of the surfactant. On phosphoric acid treatment for 9.5h, ~30% of the template had been removed. These studies show that the loss of the surfactant to be a necessary initial step in the lamellar→hexagonal transformation. The transformation from the hexagonal to the cubic phase is driven by the tendency of the cylindrical rods of the hexagonal phase to minimize their energy by forming 3D network of rods, forming bicontinuous cubic phases as shown in Fig.1.10(e & f). The cubic phase can be described using the concept of periodic minimal surface,[71,164] with the space groups *Pn3m*, *Pm3n*, $P4_332$, *Im3m*, *Ia3d* or *Fd3m*.[71] The cubic phase obtained after the complete transformation of the hexagonal ZrO_2 phase in phosphoric acid, appears to be consitent with the *Ia3d* space group.

The thermal transformation of the lamellar form of ZrO_2 to the hexagonal form occurs in the solid state. Thus, on heating at 428K for 2h, the lamellar phase completely transforms to the hexagonal phase. We have followed the kinetics of the lamellar→hexagonal transformation at three fixed temperatures. In Fig. 1.12 we show the kinetics of the lamellar→hexagonal transformation at different temperatures. We have also examined the kinetics of this transformation by heating lamellar zirconia at different temperatures for a fixed period of 2 h. In the

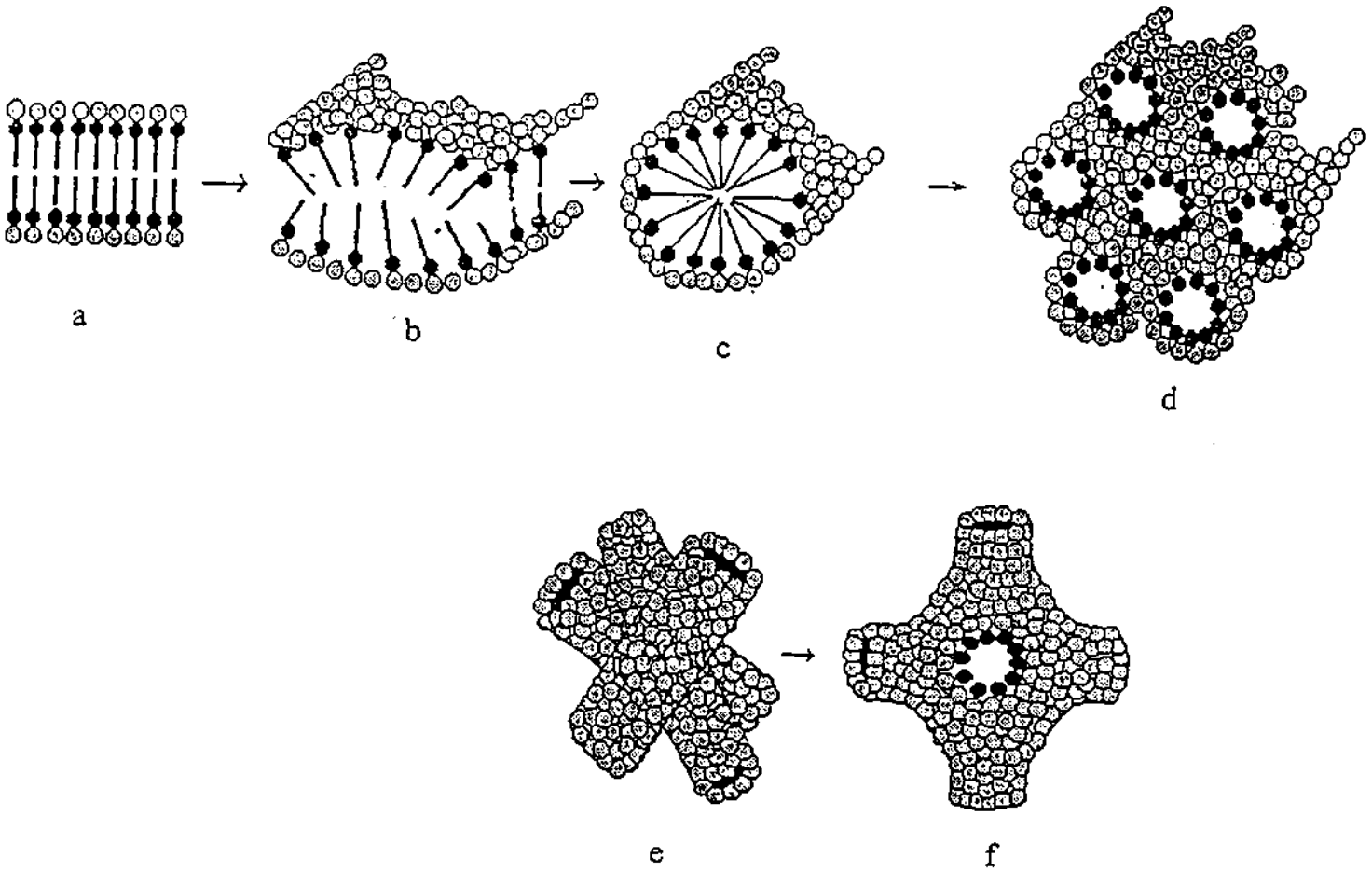

Fig. 1.10. Schematic representation of lamellar –>hexagonal phase transformation (a through d) and the hexagonal –>cubic transformation(e and f). The shaded circles around the surfactant aggregates represent the inorganic species (generally metal alkoxides or other metal–oxo species)

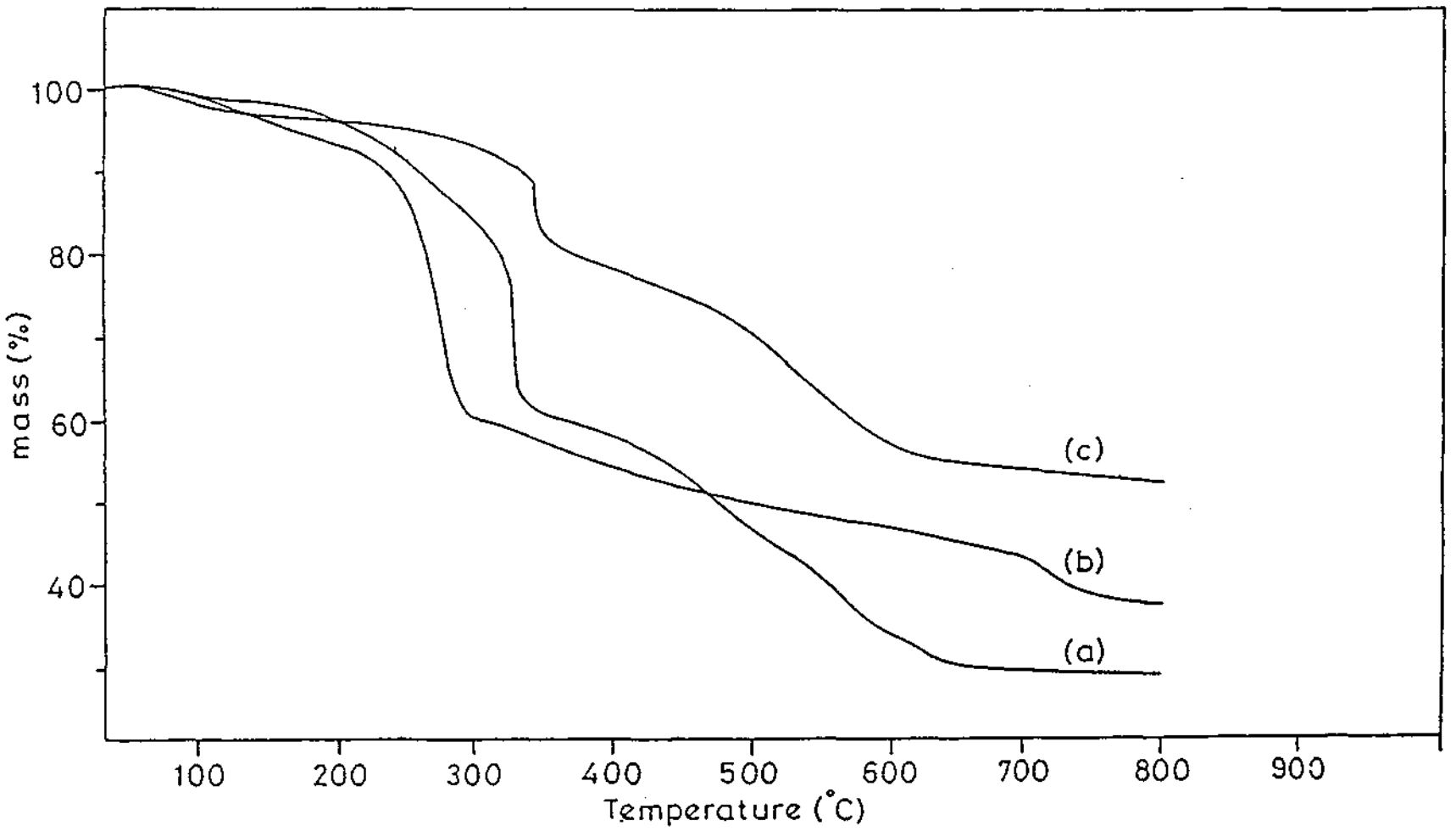

Fig. 1.11. Thermogravimetric curves of lamellar zirconia maintained for different periods in phosphoric acid solution:

(a) as– prepared lamellar zirconia, (b) after 3 h and (c) after 7 h

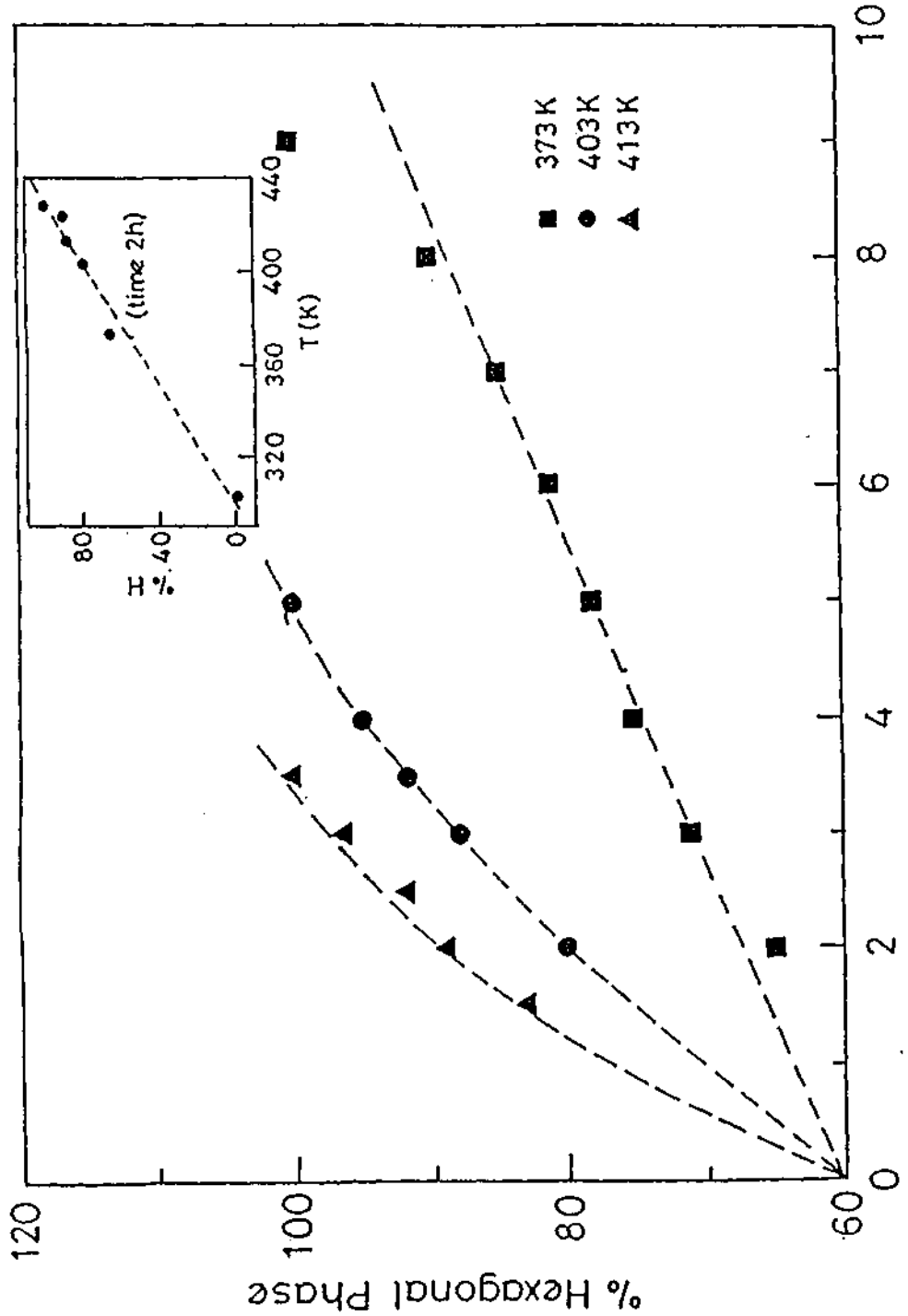

Fig 1.12. Kinetics of the lamellar to hexagonal transformation of zirconia at different temperatures. Inset shows the temperature variation of the percentage of the hexagonal (H) phase in a fixed period of 2 h.

inset of Fig. 1.12 we have shown how the proportion of the hexagonal form increases with temperature, as we keep the time constant. We were able to fit these kinetic data to a first order rate equation. The rate data follow the Arrhenius equation as shown in Fig. 1.13 The data give an activation energy ~22kJmol^{-1} for the lamellar→hexagonal transformation in the solid state. This value of the activation energy is comparable to the energy of a medium strength hydrogen bond. This is understandable since the removal of surfactant molecules from the lamellar phase is necessary for the transformation to occur. The surfactants interact with the oxo-zirconium species primarily through hydrogen bonding.

TGA studies show that on heating the lamellar phase to 403K for 2h, around 6% of the surfactant is lost (Fig. 1.14). On heating to 428K, the sample loses 11% of the surfactant. These data demonstrate that during the thermal transformation of the lamellar phase to the hexagonal phase, the amine template is removed partially, leading to the reorganization of the self-assembled surfactant aggregate. The magnitude of the loss of the surfactant in the thermal transformation is somewhat smaller than that accompanying in transformation in phosphoric acid solution.

In conclusion, the present study of the kinetics of the lamellar to hexagonal transformation of mesoporous zirconia shows that a loss of surfactant molecules accompanies the transformation. Transformation to the cubic form seems to require all the starting material in the hexagonal form. The thermal induced lamellar→hexagonal transformation is associated with activation energy comparable to the hydrogen bond energy.

4.2 Preparation and characterization of mesoporous alumina

The XRD patterns of the dried products showed reflections at d-values of 5.8nm and 6.3nm respectively with dodecylamine and hexadecylamine templates as shown in Fig. 1.15(a) and (b). TGA showed loss of the elements of water at 423K and complete loss of the template around 823K, just as in the hexagonal

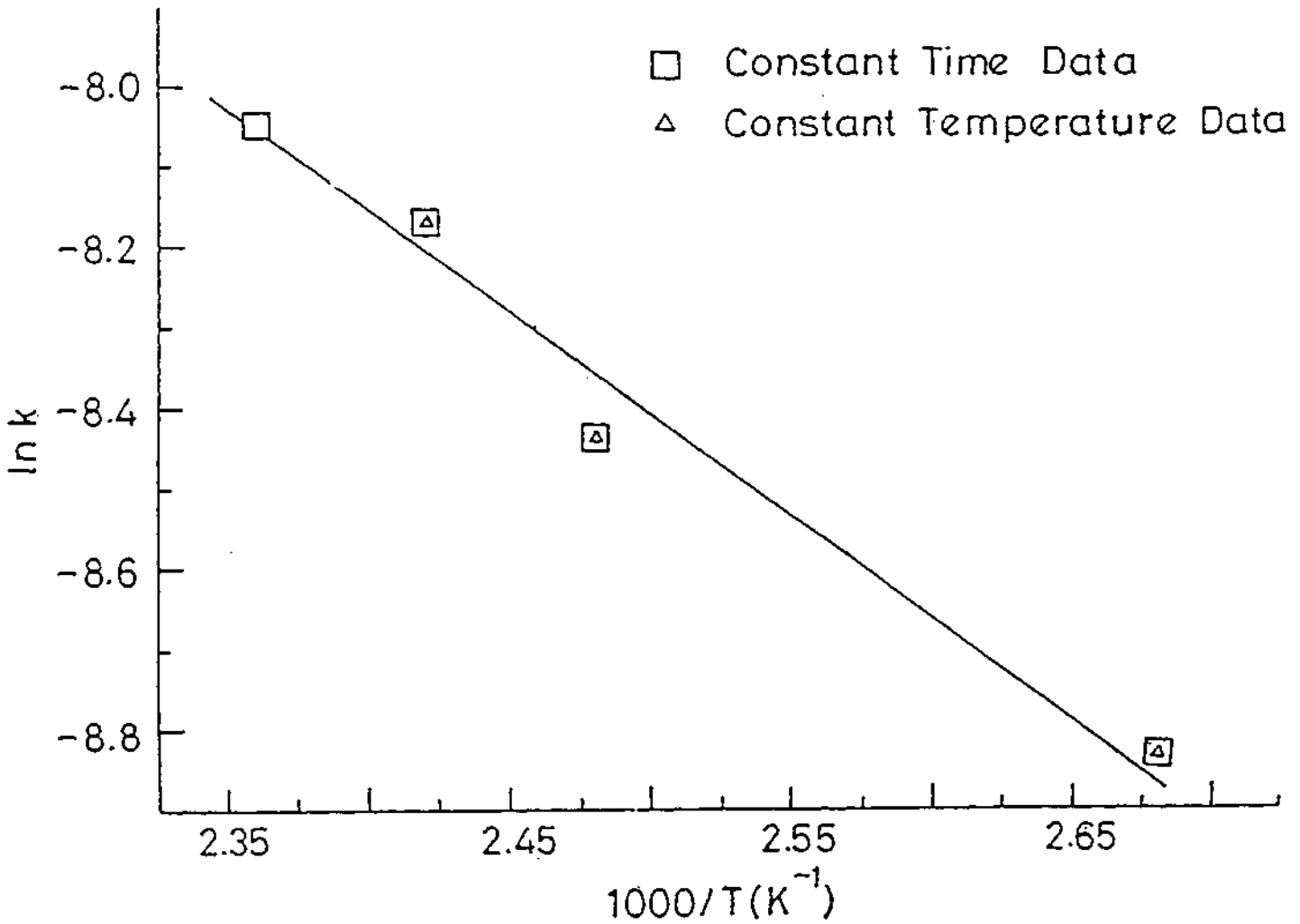

Fig 1.13. Arrhenius plots of the kinetic data of the lamellar---->hexagonal transformation of zirconia in the solid state.

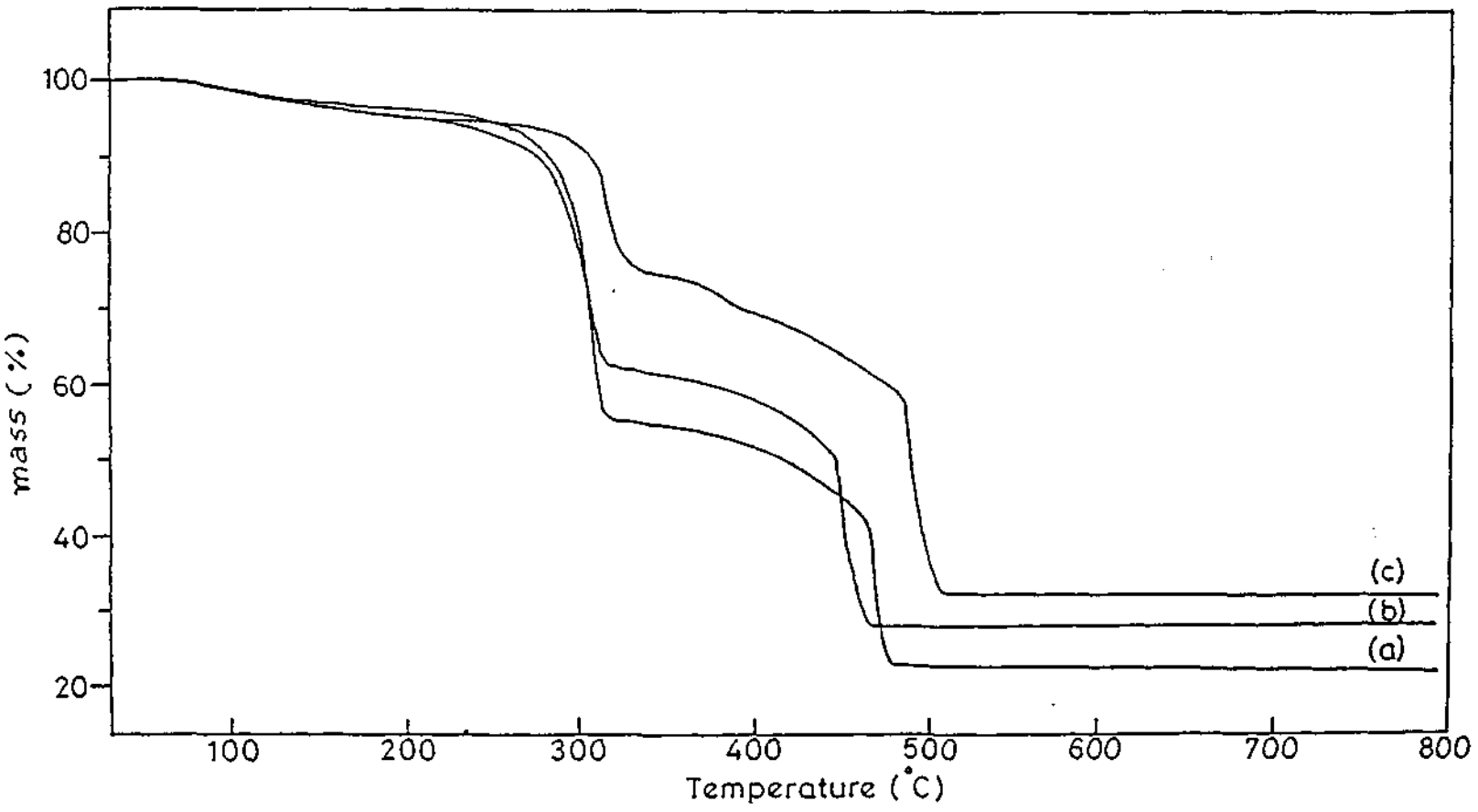

Fig 1.14. Thermogravimetric curves of lamellar form heated at different temperatures: (a) as –prepared lamellar zirconia, (b) 403K, 2h, and (c) 428K, 2h

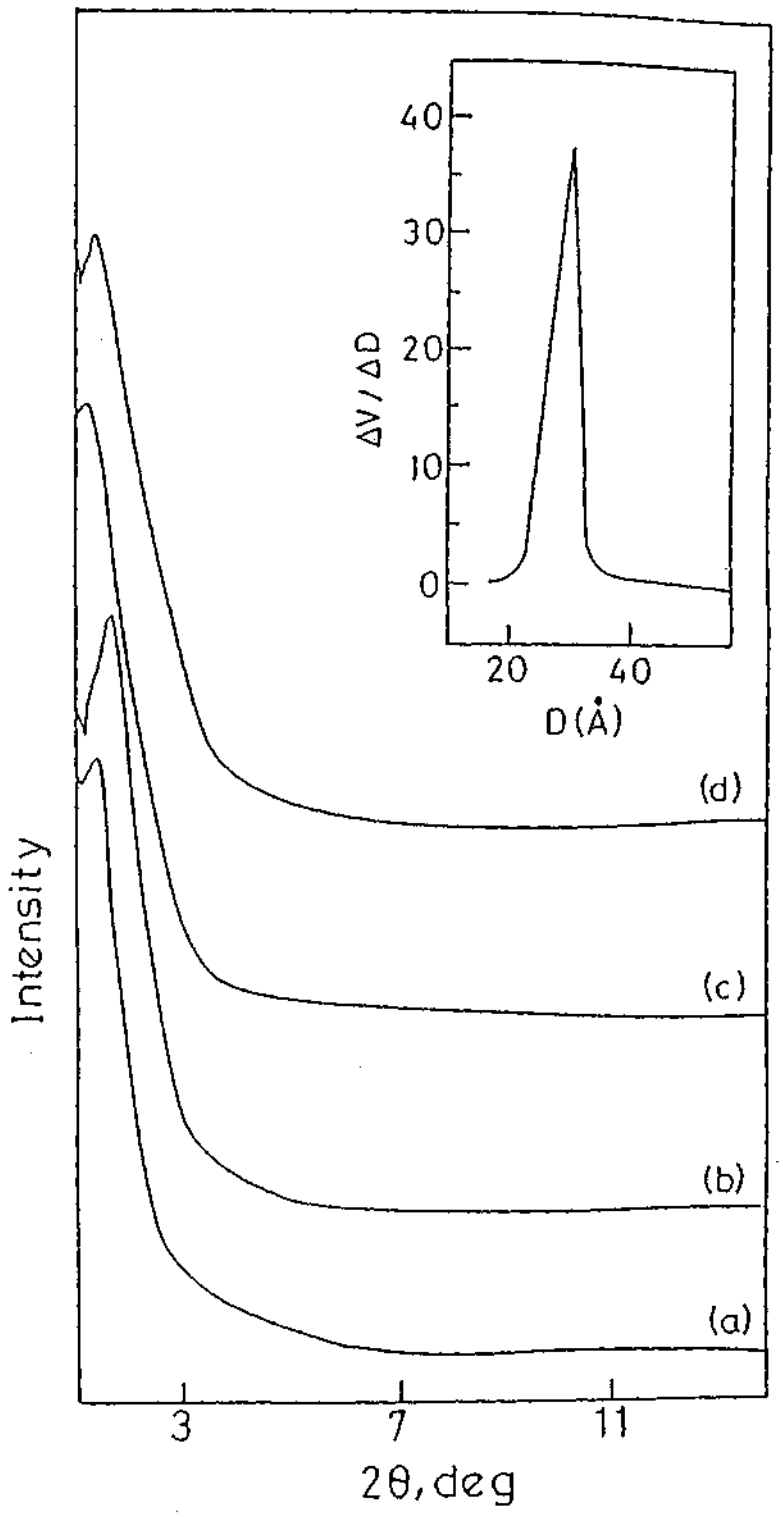

Fig 1.15. X– ray diffraction patterns of alumina prepared with dodecylamine and (b) hexadecylamine as templates. The diffraction patterns of the corresponding calcined samples are shown in (c) and (d) respectively. The inset shows the pore size distribution in a calcined sample (prepared with dodecylamine)

mesoporous structure prepared by electrostatic interactions.[25-27] From TGA data, the compositions of the hexagonal amine adduct of alumina work out to be $Al_2O_3.2H_2O$.amine and $Al_2O_3.H_2O$.amine with dodecylamine and hexadecylamine respectively. The entire amine is lost at 773K for 6h, the resulting products showed reasonably sharp XRD reflections at *d*-values of 9.4nm and 8.0nm for dodecylamine and hexadecylamine respectively (Fig. 1.15(c) and (d)). FT-IR spectra of the as-prepared and dehydrated samples show the presence of C-H stretching band around 2700-3000cm^{-1}, CH_2 scissor vibrations around 1250-1500cm^{-1} and NH_2 scissor vibration around 1590-1660cm^{-1} which are either absent or have very low intensity in calcined samples (Fig. 1.16). Calcined samples show a decrease in the intensity of the band due to OH/H_2O in the 3000-3600cm^{-1} region (Fig. 1.16). It is not entirely clear why the d_{100} spacing in XRD pattern increases from ~ 6nm to 8.0-9.0nm on calcination. Such large *d*-spacings are known in disordered silicas,[15b,15c,26,61] but we believe that the structure gets reorganized and textured after calcination. The XRD patterns in Fig. 1.15 and the TEM images suggest the presence of some disordered hexagonal structures.

The as-prepared samples possess a disordered lamellar structure as shown in the TEM image in Fig. 1.17a. This structure probably corresponds to the so-called worm-like features reported by Bagshaw and Pinnavaia.[19] The calcined samples show the presence of disordered hexagonal mesopores as seen in Fig. 1.17b. The average pore diameter from the image is ~3nm. The images in Fig. 1.17(a and b) represent the lamellar to hexagonal transformation of mesoporous alumina brought about thermally, on the removal of the amine template. The lamellar like structure in Fig. 1.17a corresponds to a layer separation of 2.8nm which is exactly what we would expect for a lamellar phase prepared with the dodecylamine with a chain length of 1.4nm. The *d*-spacing of 5.8nm of the as-prepared sample is however, roughly twice the interlamellar spacing. The d_{100} value of ~9.0nm of the calcined sample roughly corresponds to three times the interlamellar spacing.

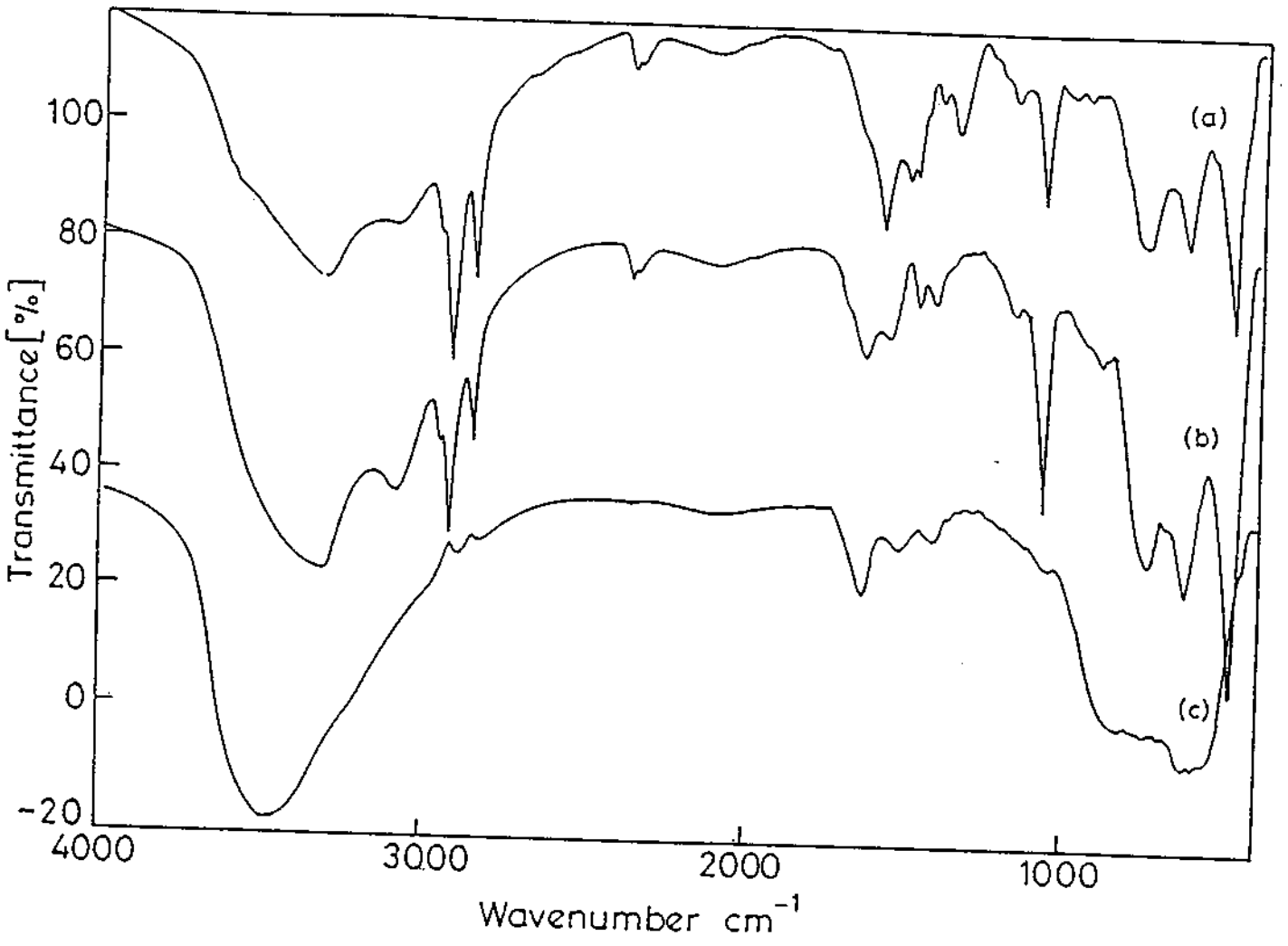

Fig. 1.16. FT – IR spectra of the alumina: (a) as – prepared , (b) dehydrated (c) calcined at 773 K.

Fig. 1.17. TEM images (a) of the as – prepared alumina (with dodecylamine) and (b) of the calcined sample.

^{27}Al MAS NMR spectra of the alumina samples subjected to different treatments are shown in Fig. 1.18. The as prepared sample shows a signal close to 0ppm due to octahedral aluminum.[165] On dehydration at 423K, the spectrum does not show any significant change. On calcination, however, a new feature around 69ppm due to tetrahedrally coordinated aluminum emerges. The ratio of the octahedral to the tetrahedral Al is approximately 75:25. The proportion of the penta-coordinated aluminum, if any, seems to be negligible, since we see no measurable intensity in the 35ppm region.[18]

We have measured the N_2 adsorption isotherms of the mesoporous alumina sample prepared by us. Fig. 1.19 shows the N_2 adsorption desorption isotherm for a hexagonal alumina adduct obtained with dodecylamine calcined at 773K. It shows small steps in adsorption isotherm between p/p_0~0.4-0.9 characteristic of disordered hexagonal pores, and a broad hysterisis in desorption isotherm over the same relative partial pressures. The hysterisis loop till p/p_0~0.9 suggests textural mesoporosity[19]. The BET surface areas for the samples obtained with dodecylamine and hexadecylamine were 405m^2g^{-1} and 377m^2g^{-1} respectively, the surface areas not high enough as expected of hexagonal mesoporous phase. By employing the Barrett-Joyner-Halender method[14] of analysis of the adsorption and desorption isotherms, we have obtained the pore size distribution in a calcined sample of alumina prepared with dodecylamine as the template. The distribution is narrow and is centered at 3nm, consistent with the average pore size revealed in some of the TEM images. With Tween 80 we obtained the hexagonal alumina adduct (Fig. 1.20a), but the mesostructure collapsed on calcination at 773K for 6h. The BET surface area of the calcined sample was 300 m^2g^{-1}. Our attempts to synthesize mesoporous alumina using partially hydrolysed aluminum iso-propoxide resulted in amorphous alumina (see Fig. 1.20b for the XRD pattern). However, the BET surface area of the samples calcined at 773K for 10h was ~340m^2g^{-1} which is comparable to that obtained earlier with the amine.

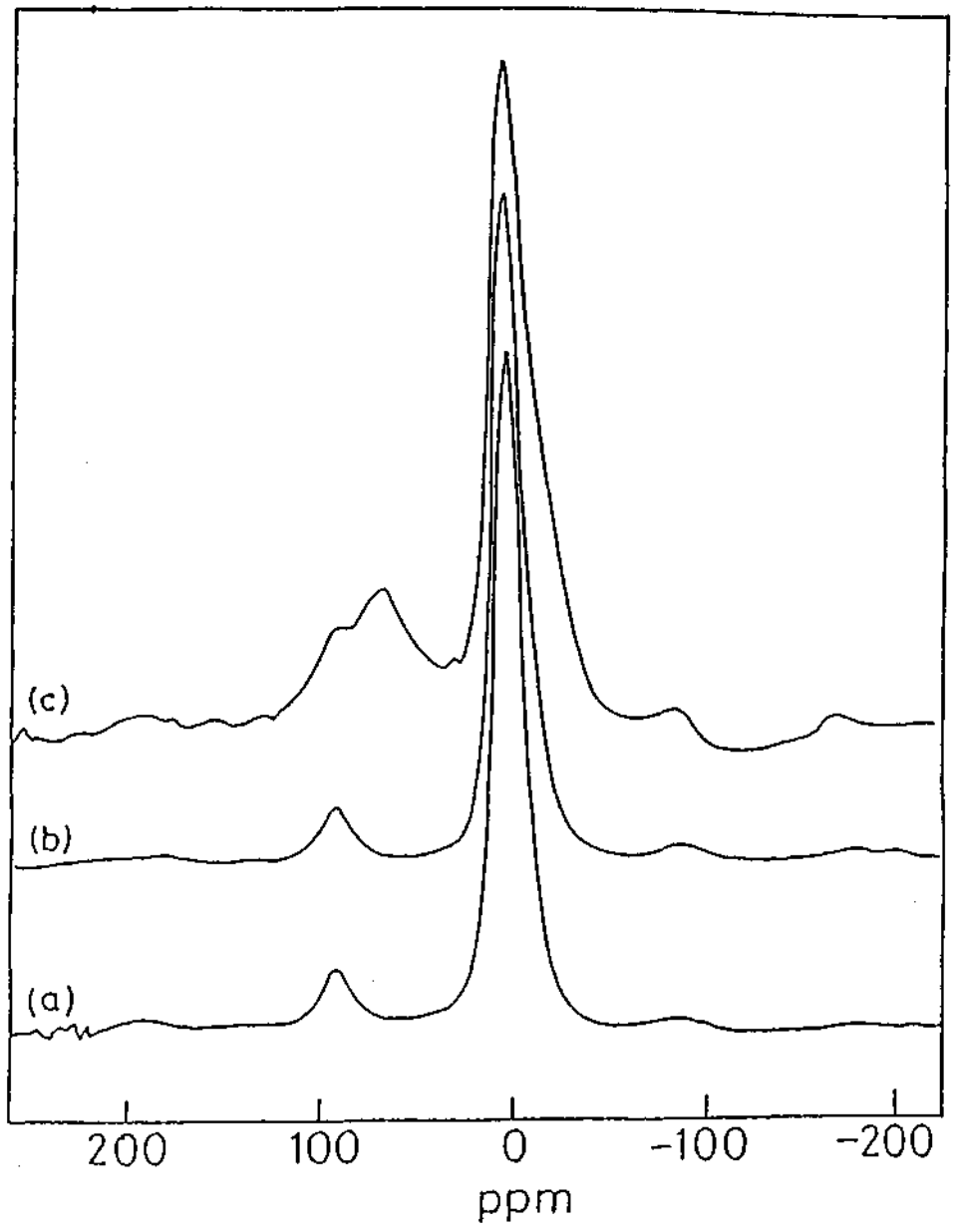

Fig. 1.18. ^{27}Al MASNMR spectra of the alumina samples (a) prepared with dodecylamine) and (c) of the calcined sample

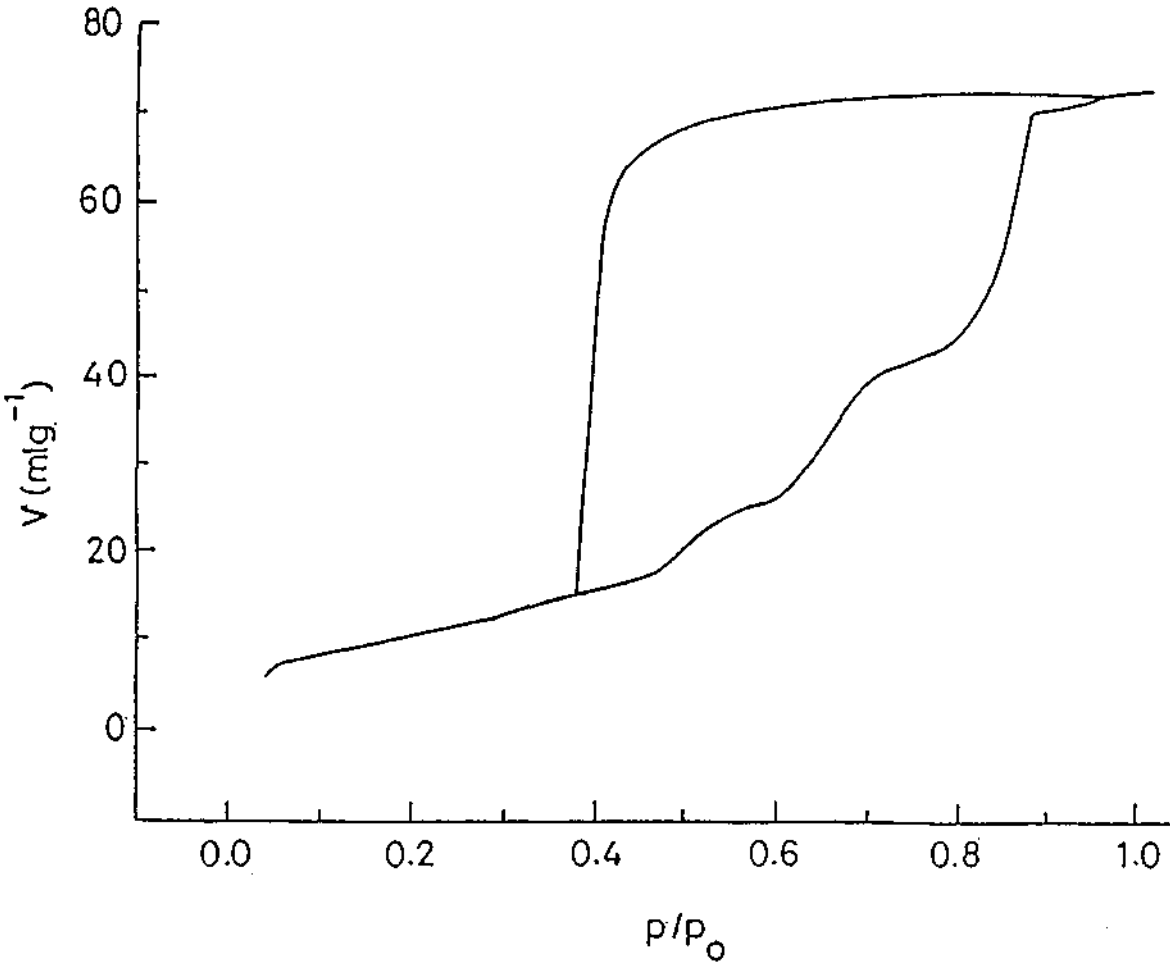

Fig. 1.19. N_2 adsorptiion – desorption isotherm of the calcined alumina (with dodecylamine)

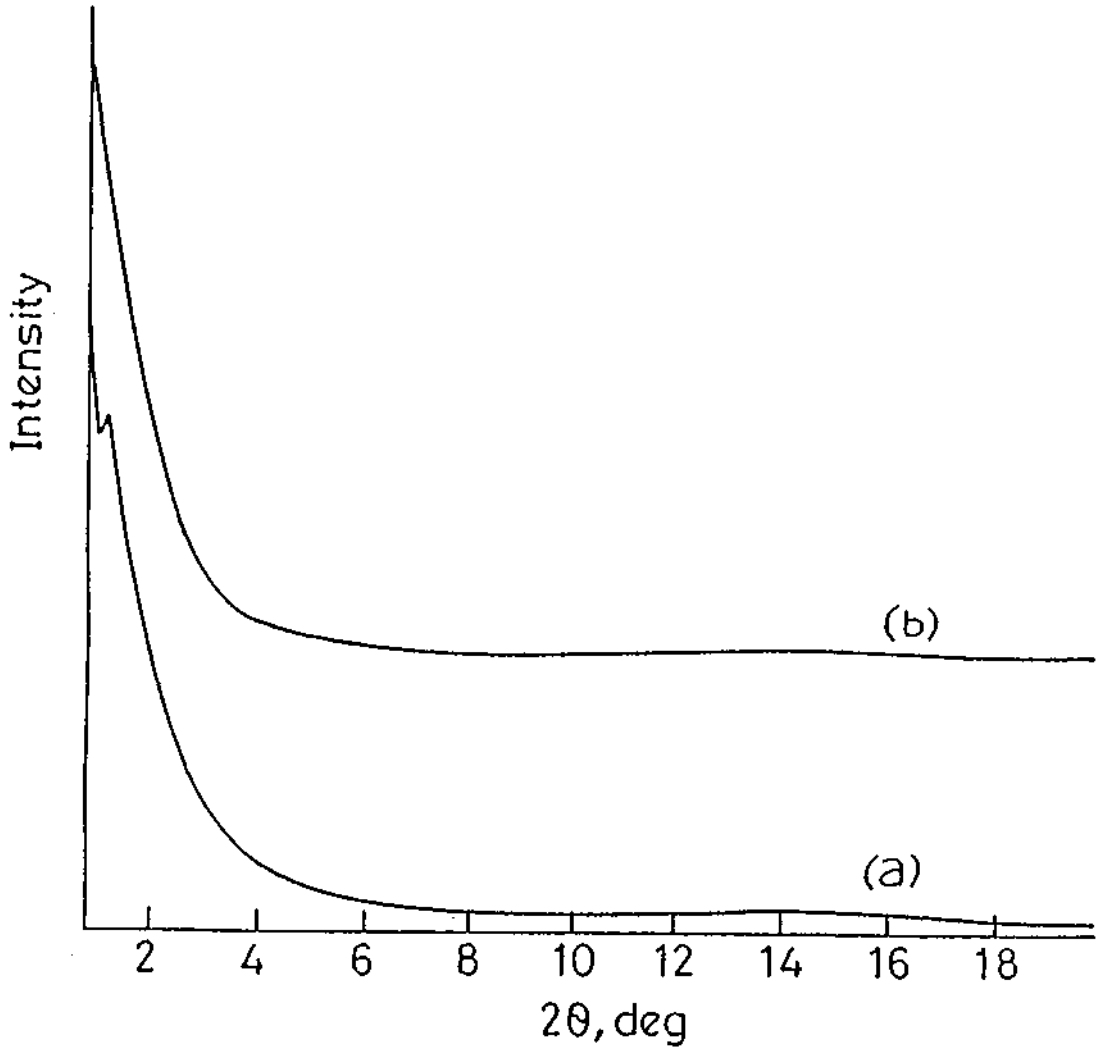

Fig 1.20. X– ray diffraction patterns of alumina prepared with (a) Tween 80 (b) with hexylamine.

4.3 Preparation and characterization of mesoporous silicophosphates

The various compositions prepared by us along with some preparative details are listed in Table 1.1 We see that phosphorus is incorporated in all the preparations carried out at a pH of 3.5. Higher pH led to the formation of pure mesoporous silica, independent of the presence of an excess of H_3PO_4/H_3PO_2. The extent of incorporation of phosphorus depends on the phosphorus source and the SA; H_3PO_4-CTAB and H_3PO_2-CPB combinations seem to favour the incorporation. We also find that the bromide of the SA is exchanged by chloride from HCl during the precipitation. Without the addition of HCl, however we failed to obtain the silicophosphates. In Fig. 1.21, we show the XRD patterns of the as-synthesized samples of the mesoporous silicophosphates **3** and **4** along with the XRD pattern of the mesoporous hexagonal phase of silica (1) with a d_{100} of 3.87nm. The diffraction patterns of **3** and **4** are quite similar to that of silica, giving the (*100*) reflection at *d* values between 3.8 and 3.9nm. The XRD pattern of the sample **3** has some features of the lamellar phase and TEM images showed the presence of hexagonal phase admixed with a small proportion of the lamellar phase. Calcination of the samples at 673K for 4h removed most of the surfactants as determined by TGA and elemental analysis. Infrared spectra showed the absence of the bands of the template. The mesoporous structure was fully retained in samples **1**,**2** and **3** after calcination at 673K as seen from the XRD patterns (see Fig. 1.21). The mesoporous structure of the sample **4** with ~40% P was however destroyed on calcination at 673K. The phosphorus content of the silicophosphates after calcination was close to the values in Table 1.1, giving a composition of $Si_{19}P_4O_{48}$ for sample **3**. It appears that silicon can be substituted upto a maximum of 25% by phosphorus in the hexagonal mesoporous phase. The BET surface areas of the samples **1**,**2** and **3** calcined at 673K were 1150, 965 and 770m^2g^{-1} respectively.

It was mentioned earlier that the as-synthesized sample of 3 contained a mixture of lamellar and hexagonal forms. On heating at 673K, the lamellar phase transforms to the hexagonal phase. In Fig. 1.22, we show the TEM images of

Table 1.1 Syntheses composition and conditions for mesoporous silicophosphates

Sample	Preparative conditions			Composition[a]	Surface area[b]
	Acid (mmol)	SA (mmol)	pH		(m^2g^{-1})
1.	H_3PO_2(18)	CTAB(8)	11	SiO_2. 0.1SA	1100
2.	H_3PO_4(22)	CPB(7)	3.5	$23SiO_2.P_2O_5.3.8SA.3\ H_2O$	965
3.	H_3PO_2(18)[c]	CPB(7)	3.5	9.4 $SiO_2.P_2O_5.3.0SA.1H_2O$	770
4.	H_3PO_4(22)	CTAB(8)	3.5	$3SiO_2.P_2O_5.0.9SA.0.7H_2O$	130[d]

(a) of the as-synthesized material.
(b) of the samples calcined at 673 K. In sample 3, over 80 % of the template had been removed on calcination .
(c) H_3PO_2 with CTAB under similar conditions give a product with 7 % P.
(d) not mesoporous.

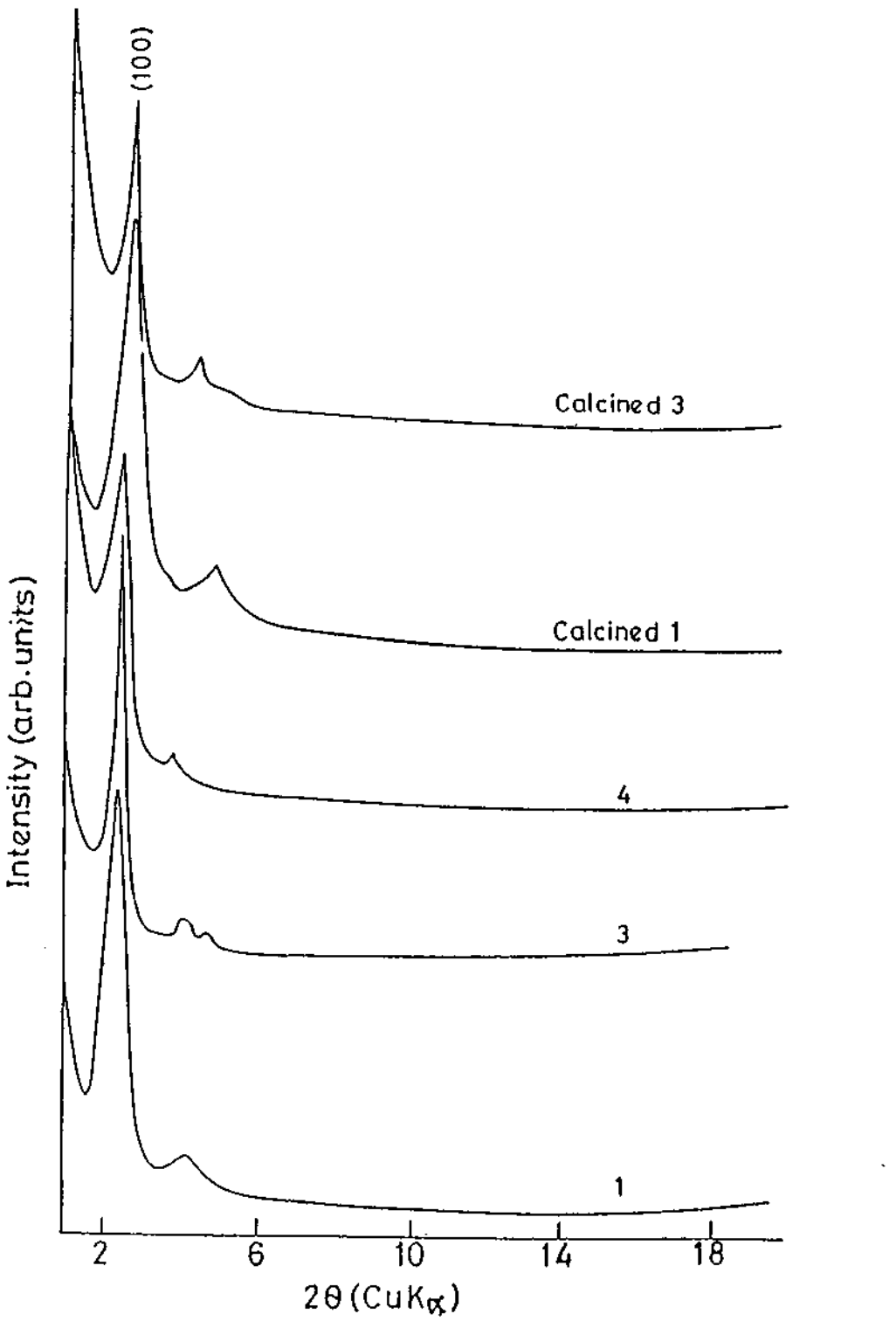

Fig. 1.21. XRD patterns of the as–synthesized samples of the mesoporous silicophosphates (1,3 and 4) and the calcined samples of 1 and 3. For a description of the compositions see Table 1.1

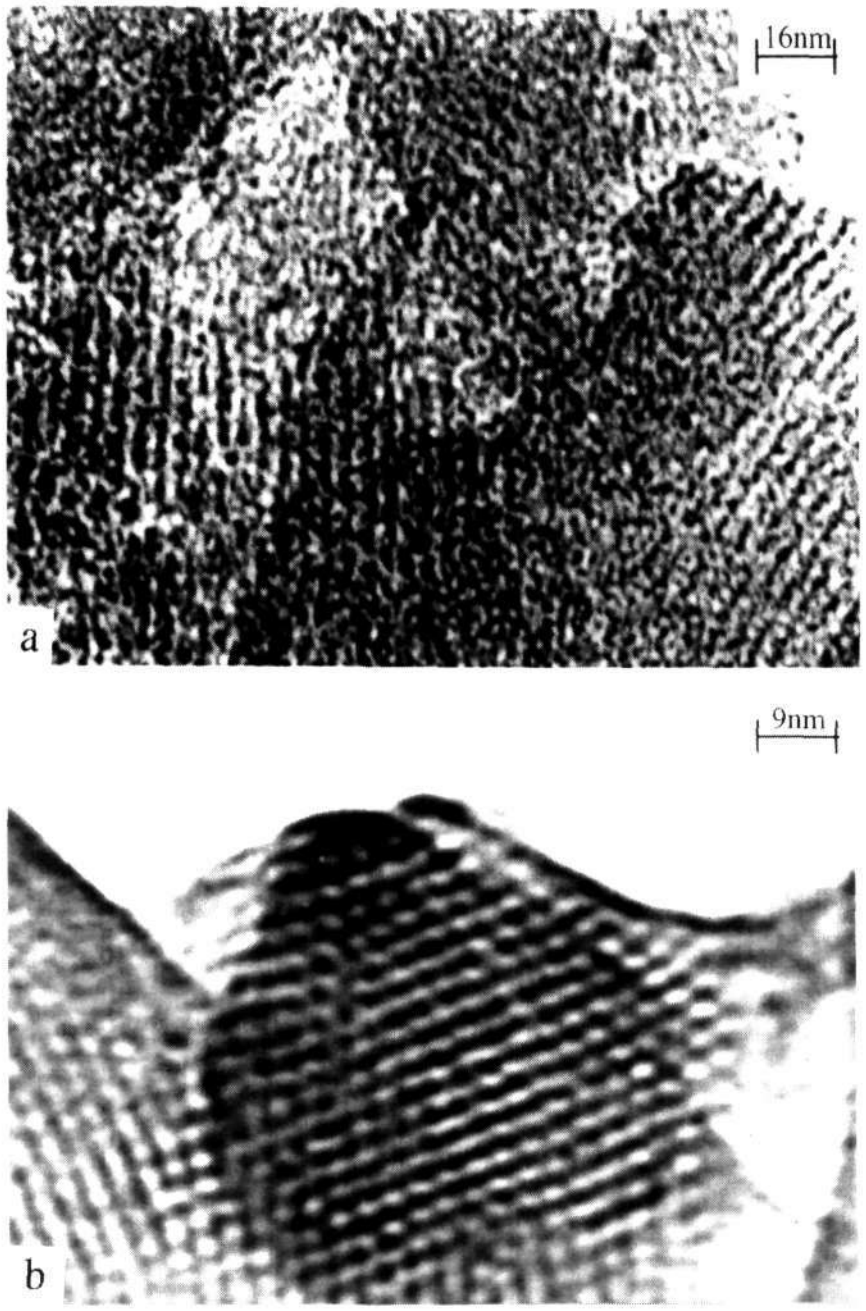

Fig 1.22 TEM image of the silicophosphate 3 (a) during calcination and (b) after calcination at 673 K

silicophosphate **3** with 22 % P to demonstrate the presence of both the lamellar and hexagonal phases during the course of transformation as well as the crystalline nature of the fully transformed hexagonal phase. Such a lamellar to hexagonal transformation in the solid state is interesting. It appears that the transformation is favoured by partial elimination of the template on heating the lamellar phase which enables the structure to curl up to produce the cylindrical structure.

The TGA curves, chemical, analysis and the compositional dependence of the thermal stabilities of the mesoporous structures indicated that the phosphorus was incorporated in the silica framework. Further evidence for the incorporation of phosphorus was obtained by NMR and infrared spectroscopy. We have examined the ^{31}P and ^{29}Si MASNMR spectra of the mesoporous silicophosphates. Both the spectra change on calcination as shown in Fig. 1.23 in case of sample **3**. The ^{31}P signals of the calcined sample **3** (relative to H_3PO_4) are at -13.0, -23.1 and -34.4ppm due to $OP(OSi \text{ or } P)(OH)_2$, $OP(OSi \text{ or } P)_2(OH)$ and $OP(OP)_{3-x}(OSi)_x$ respectively.[147] The ^{29}Si signals of the silicophosphates are at -91(Q_1, Q_2), -104(Q_3) and -111ppm (Q_4),[146,166,167] the slight shift to negative values arising from the presence of phosphorus. It appears that the silicon is present only as four-coordinated species in these silicophosphates. The infrared spectrum of the calcined sample of **3** showed a strong band at 1080cm^{-1} due to a coupled Si-O and P-O stretching vibration. Bands due to the bending vibrations of Si-O-P/Si-O-Si/P-O-P units are found at 815 and 455cm^{-1} (Fig. 1.24),[168] Thus, the present study establishes the mesoporous phase of silicophosphates where phosphorus in an integral part of the silica framework can be prepared. The use of these materials as hosts in catalysis is being explored.

4.4 Preparation and characterization of mesoporous ruthenium dioxide

We have obtained disordered hexagonal mesophase of ruthenium dioxide with sodium dodecylsulphate (SDS) as the template with a d_{100} value of 3.7nm as shown in the XRD pattern (Fig. 1.25a). The mesophase obtained shows the

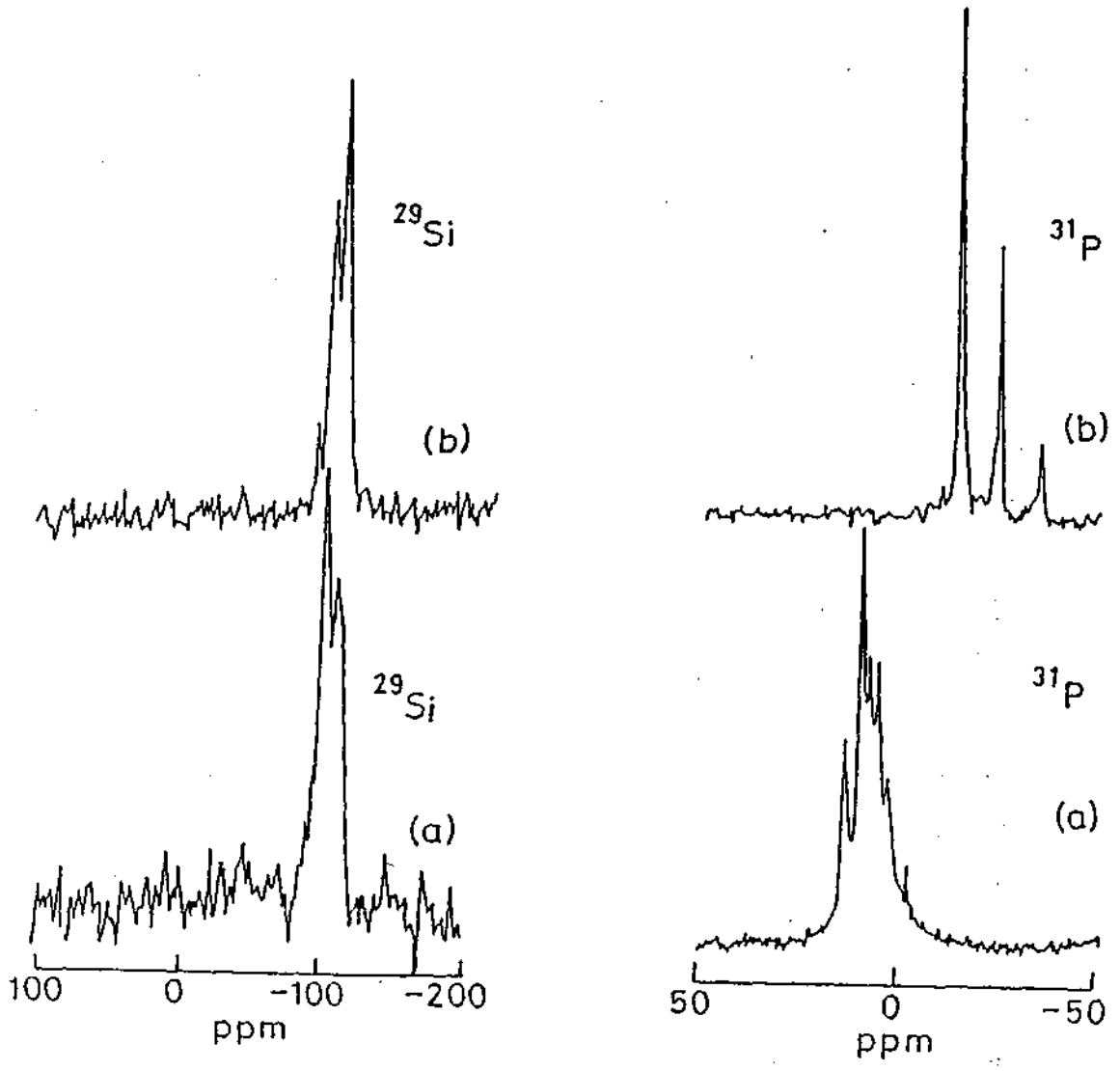

Fig. 1.23. ^{29} Si and ^{31}P MASNMR spectra of sample 3 (a) before and (b) after calcination

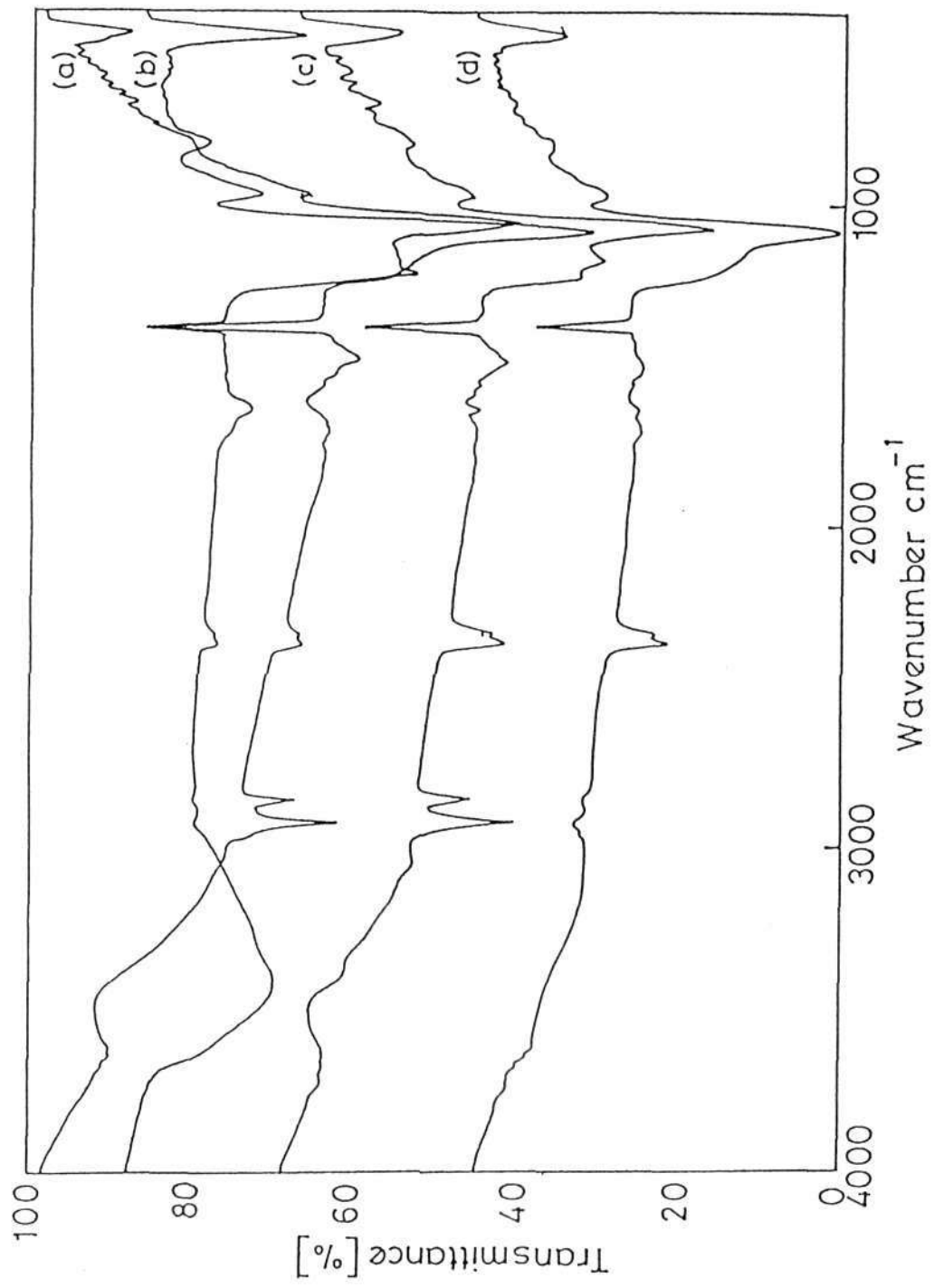

Fig. 1.24. FT – IR spectra of the silicophosphates (a) as – prepared sample 1, (b) calcined sample 1, (c) as – prepared sample 3 and (d) calcined sample 3.

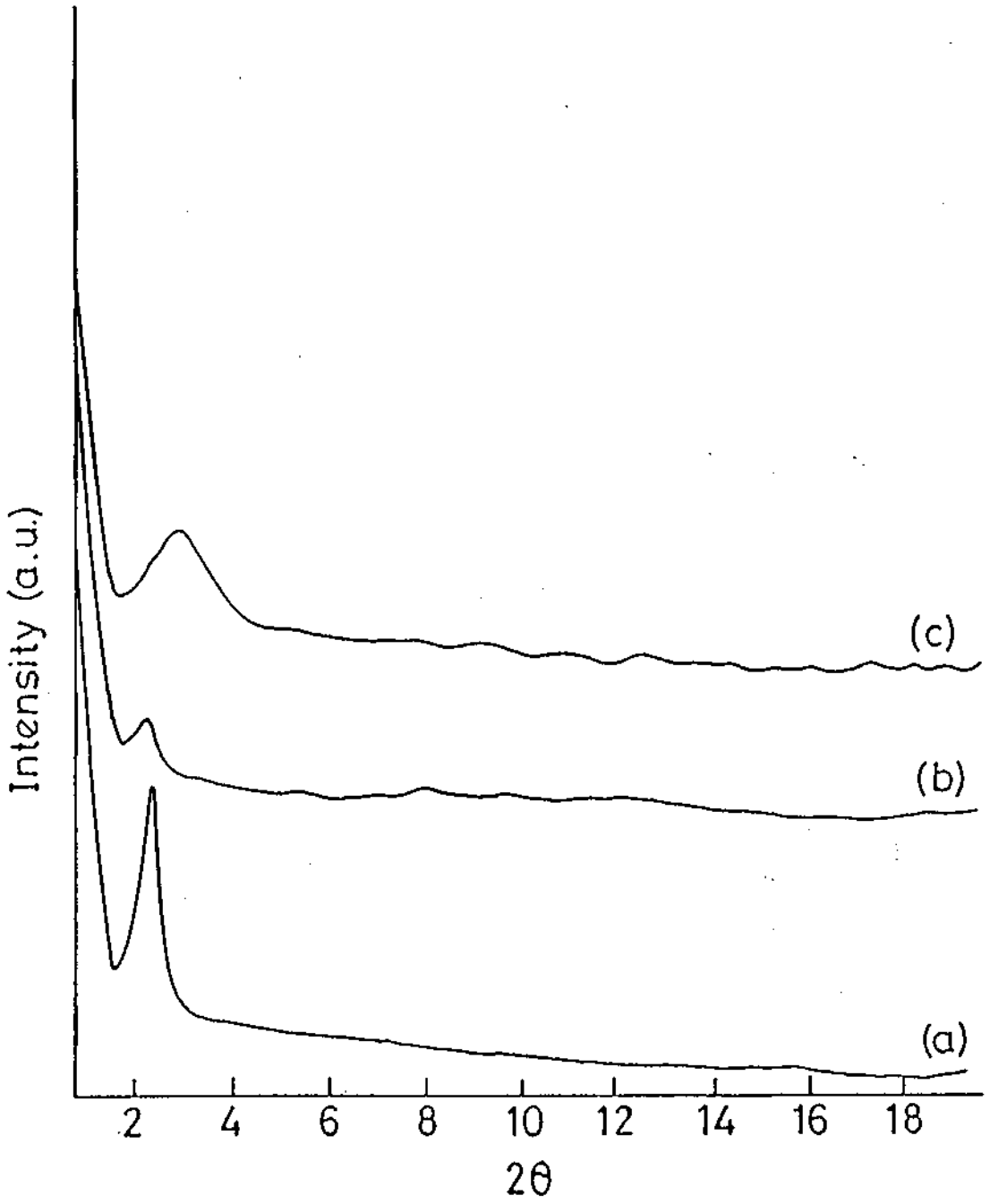

Fig. 1.25. XRD patterns of ruthenium dioxide (a) with sodium dodecylsulphate (b) calcined at 473 K (c) with dodecylamine.

complete loss of template around 573K in N_2 atmosphere. On heating the sample at 473K for 20min only a weak feature is retained in the XRD pattern (Fig. 1.25b) and ~45 % of the template is removed (Fig. 1.26). All Attempts to remove the template via solvent extraction lead to the collapse of mesophase. The disordered nature of the mesopores was confirmed by recording a transmission electron microscope (TEM) image shown in Fig. 1.27.

We have also obtained disordered hexagonal mesophase using dodecylamine as the template with a *d*-spacing of 2.9nm due to (*001*) reflection (Fig. 1.25c). The mesophase however, is unstable and collapses on either calcination or the template removal via solvent extraction in acidified alcohol. The electrical resistivity of the as-prepared mesophase and as well as the calcined mesophase show very high resistance and are insulating.

4.5 Preparation and characterization of mesoporous chalcogenides

In Fig. 1.28(a and b) we show the XRD patterns of the mesophases obtained with dodecylamine (DA) and stearylamine (SA) respectively. The diffraction patterns are characteristic of a hexagonal mesophase with d_{100} values of 4.1nm and 5.5nm respectively for DA and SA. EDX analysis of these products gave a Cd:S ratio of 1:1 (see inset of Fig. 1.28) showing that the sulfide had expected composition. Thermogravimetric analysis (TGA) showed that the amine template was completely removed below 573K while the water of hydration, if any, was removed at 393K. The analysis gave the compositions of the Chalcogenide amine adducts as 3CdS.DA and 7CdS.6SA.$9H_2O$ with DA and SA respectively. The hexagonal nature of the CdS-amine adducts was also confirmed by recording transmission electron microscope (TEM) images. The TEM image of the adduct of CdS with DA shown in Fig. 1.29a suggests that the mesophase has a hexagonal structure consistent with the XRD pattern in Fig. 1.28a. The image shows the wall thickness to be ~2.0nm, but there is considerable disorder.

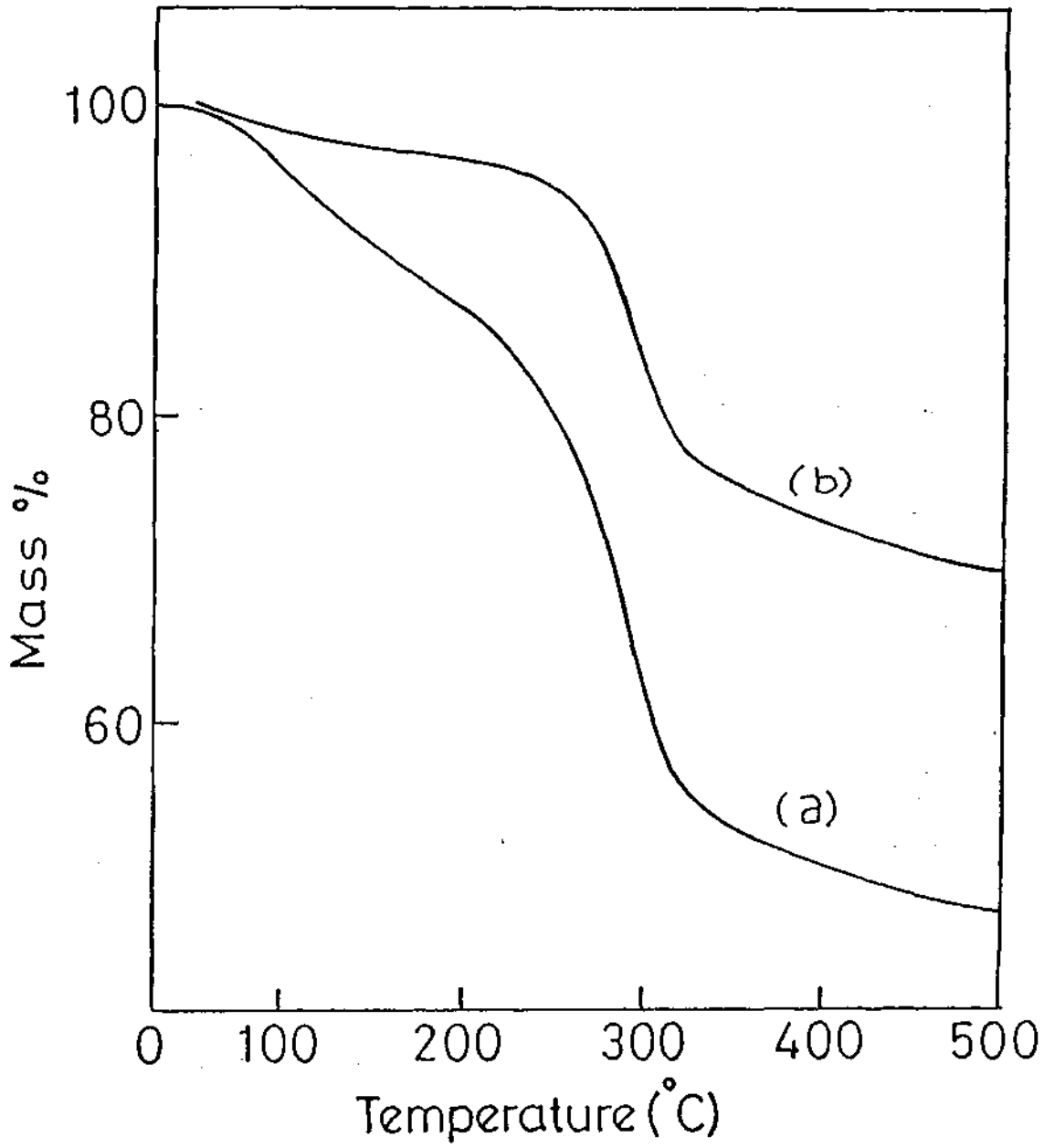

Fig. 1.26. TGA curves of ruthenium dioxide in N_2 atmosphere (a) as – prepared (b) calcined at 473 K.

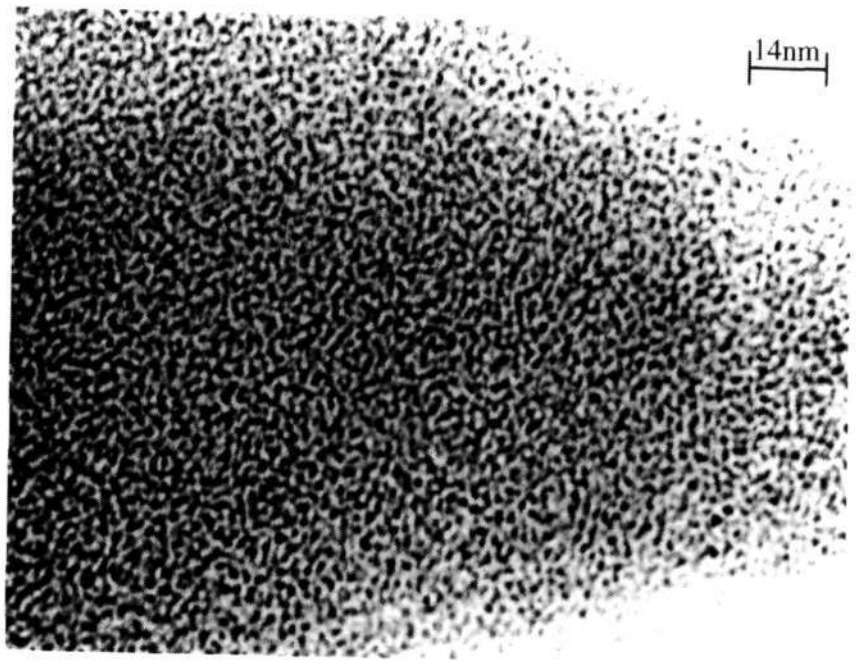

Fig. 1.27. TEM image of disordered hexagonal mesoporous ruthenium dioxide

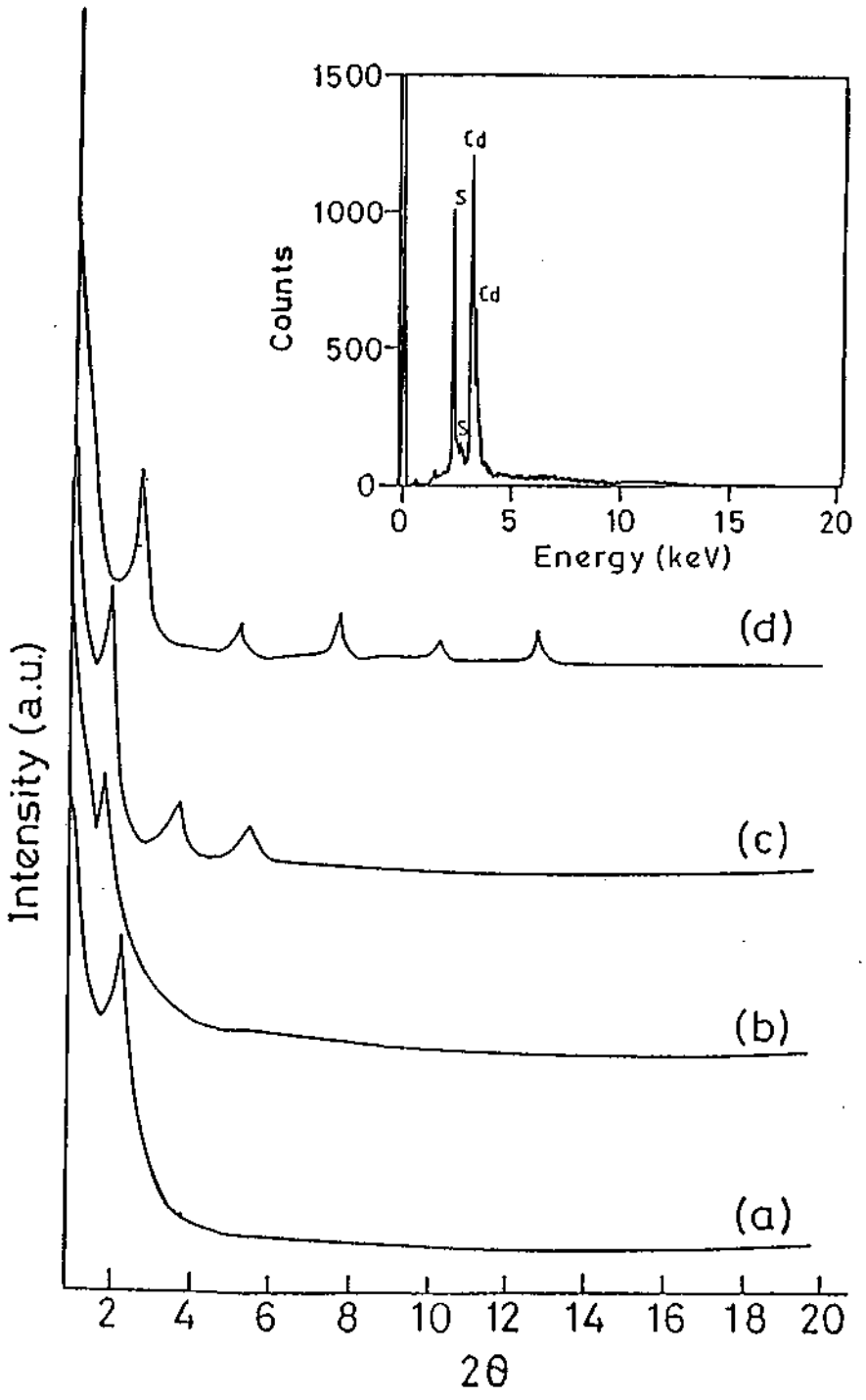

Fig. 1.28. X–ray diffraction patterns of (CuKα radiation) CdS – amine nanostructures : Hexagonal phases obtained with (c) dodecylamine and (b) stearylamine. Lamellar phases obtained with (c) stearylamine and (d) using thiourea as the sulfiding agent. Inset shows EDX of an adduct with dodecylamine.

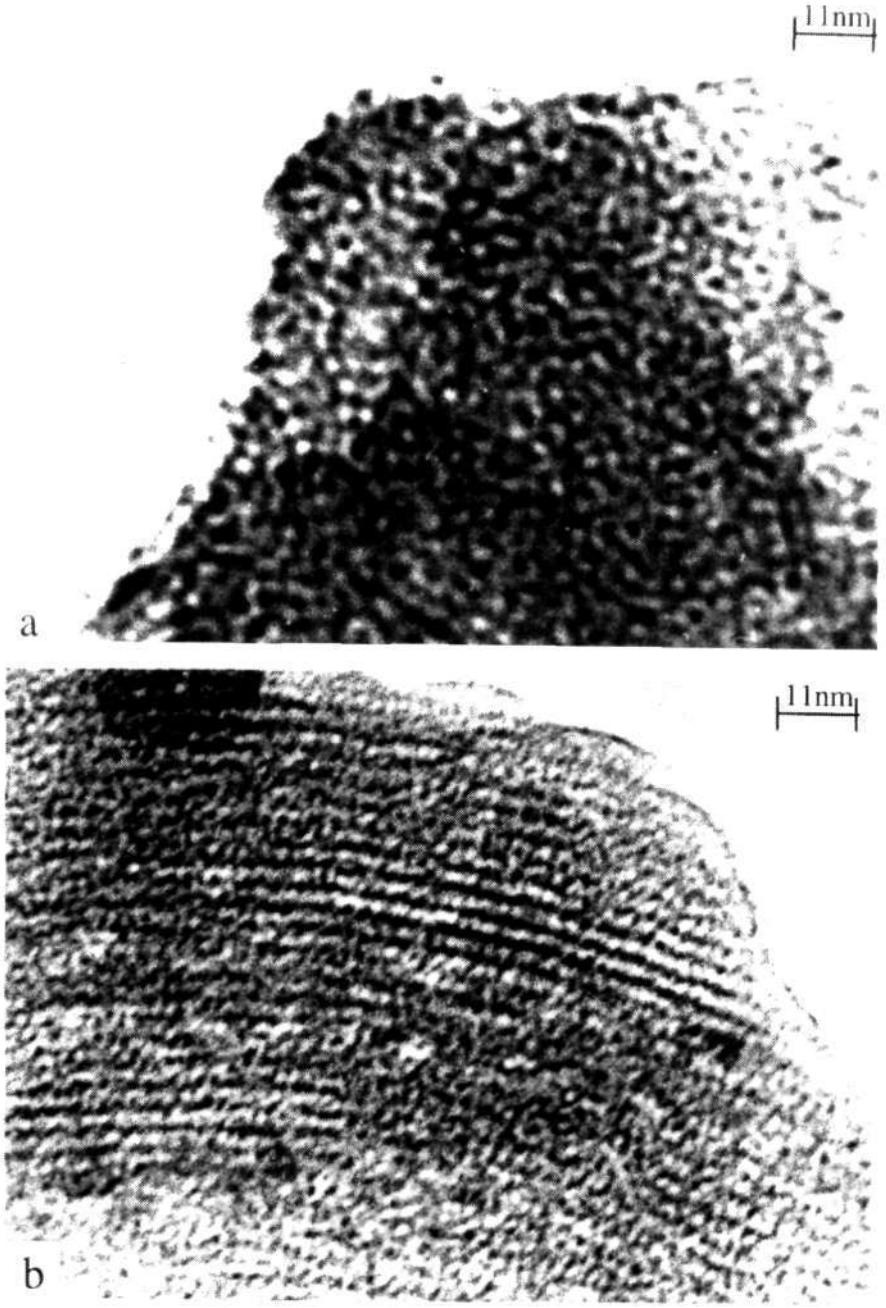

Fig. 1.29. TEM images of CdS– amine nanostructures : (a) hexagonal phase with dodecylamine, (b) lamellar phase with stearylamine.

When we employed a $Cd(CH_3COO)_2$:amine ratio 1:2 instead of the 1:1 as earlier, we obtained a lamellar structure as evident from the XRD pattern of an adduct with SA shown in Fig. 1.28c with *d*-values of 5.0, 2.5 and 1.64nm corresponding to the (*001*), (*002*) and (*003*) reflections. TGA showed that the amine was completely removed at 623K and the water removed at 393K. The composition of the chalcogenide-SA adduct from TGA gave the composition as $9CdS.8SA.3.5H_2O$. We show a typical TEM image of the lamellar mesophase in Fig. 1.29b, which shows the well defined striped pattern with a periodicity of ~5nm. No change was observed on tilting the particle perpendicular to the stripes, confirming the lamellar morphology. When we employed thiourea instead of Na_2S as the sulfiding agent, we obtained a lamellar nanostructure of CdS with DA of the composition 4CdS.3DA. The XRD pattern of this adduct is shown in Fig. 1.28d, with *d*-values of 3.53, 1.74, 1.17, 0.88 and 0.7nm respectively due to (*001*), (*002*), (*003*), (*004*) and (*005*) reflections. We also obtained excellent lamellar mesophases by using long chain thiols with Cd-acetate. For example, the adduct with dodecanethiol (DT) had the composition $3Cd(CH_3COO)_2$. 4DT. However, on heating this adduct we could not obtain pure CdS.

On heating the hexagonal CdS adduct with DA at 473K for 2h, the mesostructure collapsed, but the resulting sulfide exhibited high surface area ($90m^2g^{-1}$). We have been able to remove amine partly from the hexagonal phase of the CdS adduct with SA by heating it slowly at 448K for 2h. The XRD pattern of the product showed a feature corresponding to a d_{100} value of ~5.5nm, although somewhat weaker in intensity compared to the adduct.

We have been able to synthesize metal sulfide-organic amphiphile nanostructures of tin and antimony by starting with $SnCl_4.2H_2O$ and $SbCl_3.5H_2O$ respectively and keeping the metal salt : amine ratio at 1:1. We show the XRD patterns of the hexagonal mesophases of the adducts of SnS_2 and Sb_2S_3 with DA in Fig. 1.30(a and b) with d_{100} values of 3.12 and 3.57nm. We also see the d_{110} and d_{200} reflections at larger angles. The composition of the sulfides was confirmed by

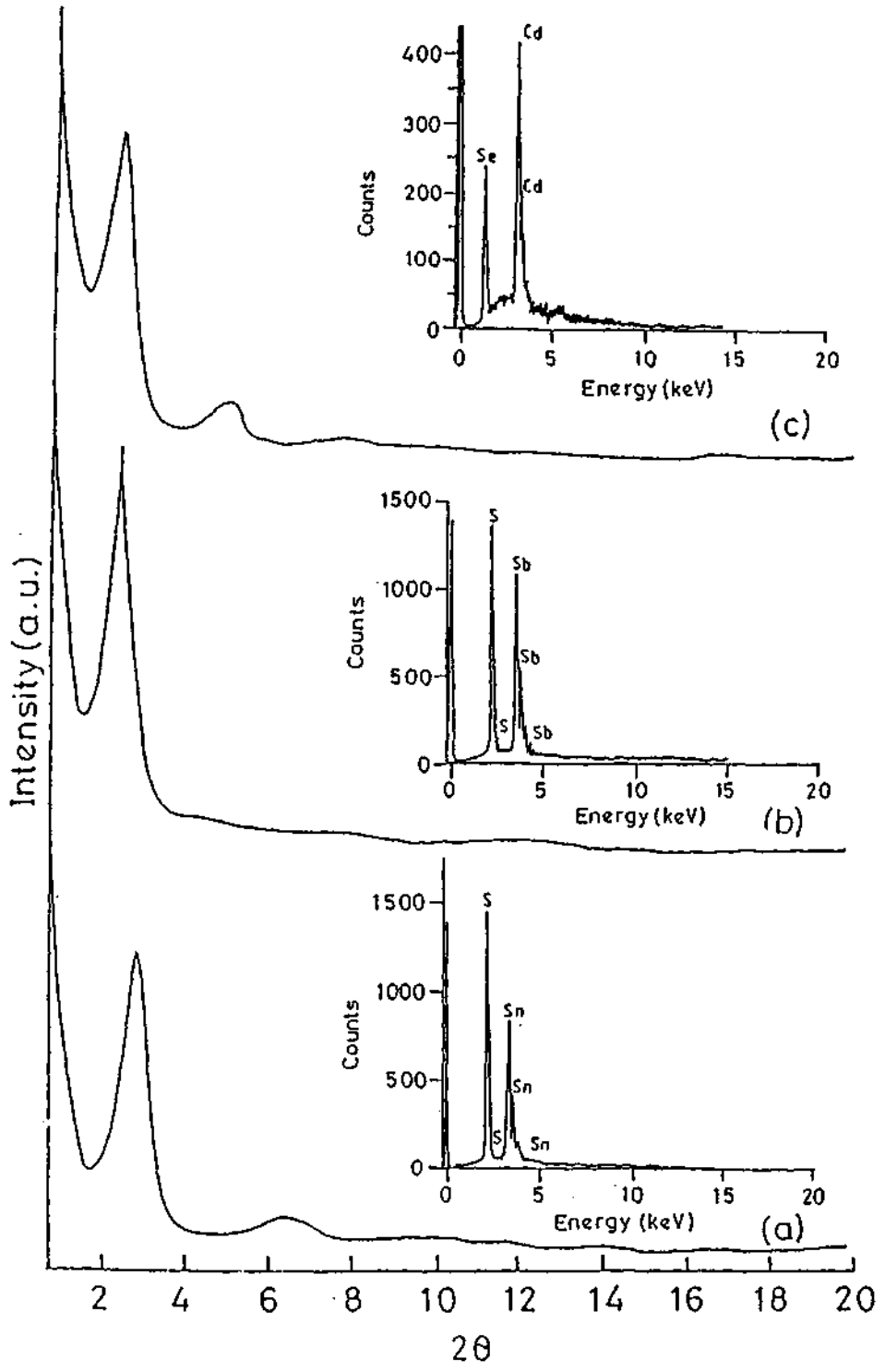

Fig. 1.30. X–ray diffraction patterns of metal chalcogenide–amine nanostructures : (a) SnS_2 – dodecylamine, (b) Sb_2S_3 – dodecylamine, (c) CdSe–dodecylamine. The EDX results are shown alongside the XRD pattern.

EDX analysis (see insets of Fig. 1.30). TGA gave the adduct compositions to be $2SnS_2.3DA.H_2O$ and $5Sb_2S_3.7DA.H_2O$. TEM images showed that the adducts possessed disordered hexagonal structures. In order to prepare CdSe-amine nanostructures, we employed a procedure similar to that with CdS, except that an aqueous solution of Na_2Se was reacted with the Cd-acetate-amine gel. In Fig. 1.30c we show the XRD pattern of the hexagonal mesophase of the CdSe-DA adduct with *d*-values of 3.66, 1.9 and 1.75nm for the (*100*), (*110*) and (*200*) reflections respectively. The adduct had the composition 9CdSe.4DA and the amine could be removed completely at 573K. We have also been able to obtain CdSe-amine nanostructures by employing sodium selenosulfate as a seleniding agent instead of Na_2Se; Na_2Se however appears to be a better seleniding agent.

4.6 High catalytic efficiency of transition metal complexes encapsulated in a cubic mesoporous phase

The cubic nature of the mesophase was confirmed by X-ray diffraction (Fig.1.31). Distinct *211*, *220*, *321*, *400* and *332* reflections were seen in the pattern. The XRD pattern given in Fig. 1.31 confirms the cubic mesoporous nature of the Cu-Al-MCM-48 catalyst. The Cu/Al ratio in the final product was 0.15.The surface area of the catalyst was $600m^2g^{-1}$.The XRD pattern (Fig. 1.31) confirmed that the cubic mesoporous structure was retained in case of Al-MCM-48-$[Mn(bipy)_2](NO_3)_2$. The surface area of the catalyst was $770m^2g^{-1}$. Chemical analysis of the showed that Mn/Al ratio in the product was 0.14.

The second derivative ESR spectrum of Cu-acetate-Al-MCM-48 ($g_\perp$ = 2.06, $g_{||}$ = 2.18) exhibited the hyperfine structure (Fig. 1.32a), establishing the presence of the Cu(II) acetate dimer.[153] The infrared spectrum showed the carboxylate absorption at $1629cm^{-1}$. The diffuse reflectance spectrum (Fig 1.33b) gave a band around 740nm, just in case of the Cu acetate encapsulated zeolites. Gas chromatographic analysis of the product obtained on oxidation of phenol by the Cu-Al-MCM-48 catalyst in presence of oxygen indicated 36% conversion, with catechol as the primary product. The turnover number was 37 (see Table

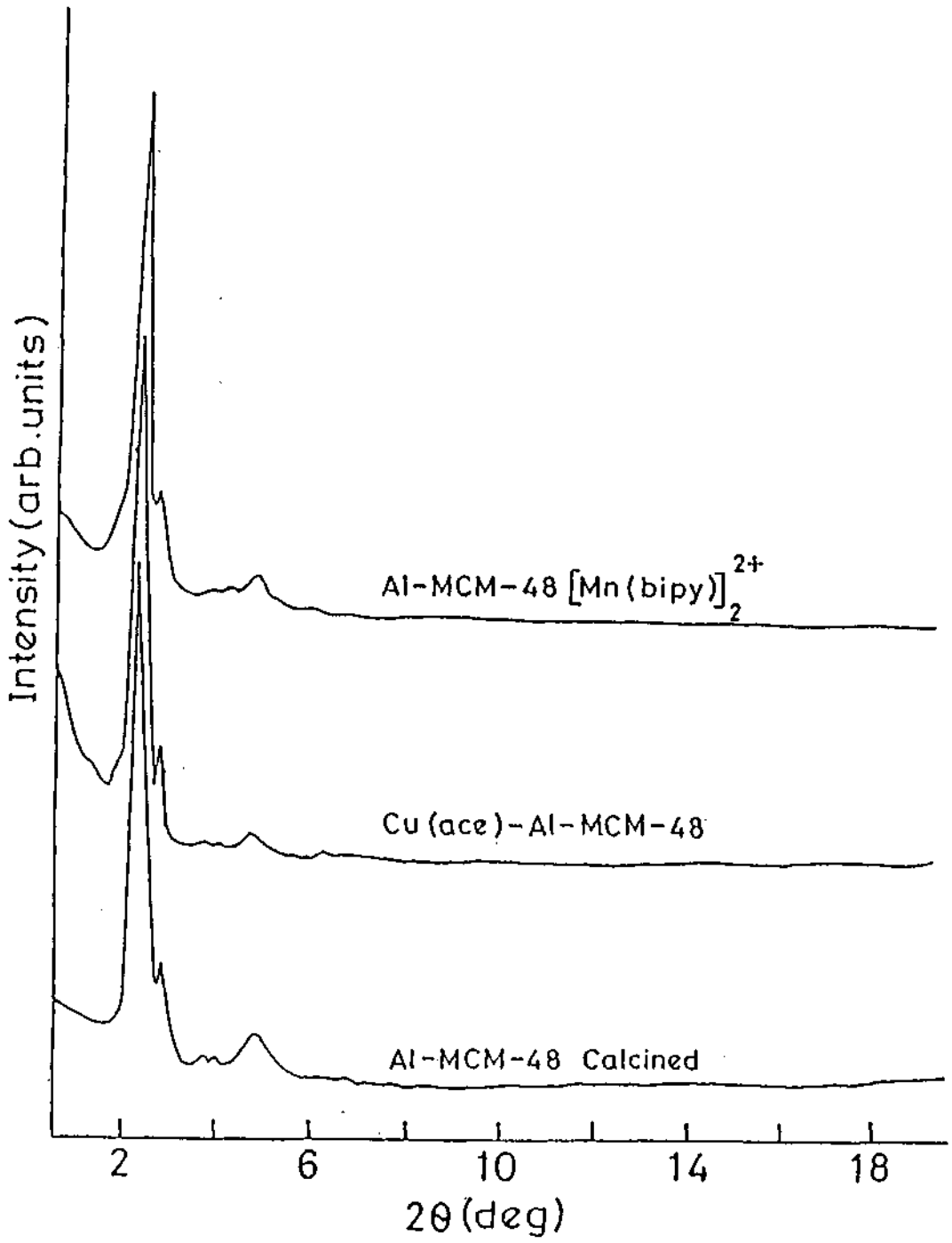

Fig. 1.31. X–ray diffraction patterns of (a) calcined Al–MCM–48. (b) Cu acetate dimer encapsulated Al–MCM–48 and $[Mn(2,2'–bipyridyl)_2]^{2+}$ encapsulated Al–MCM–48.

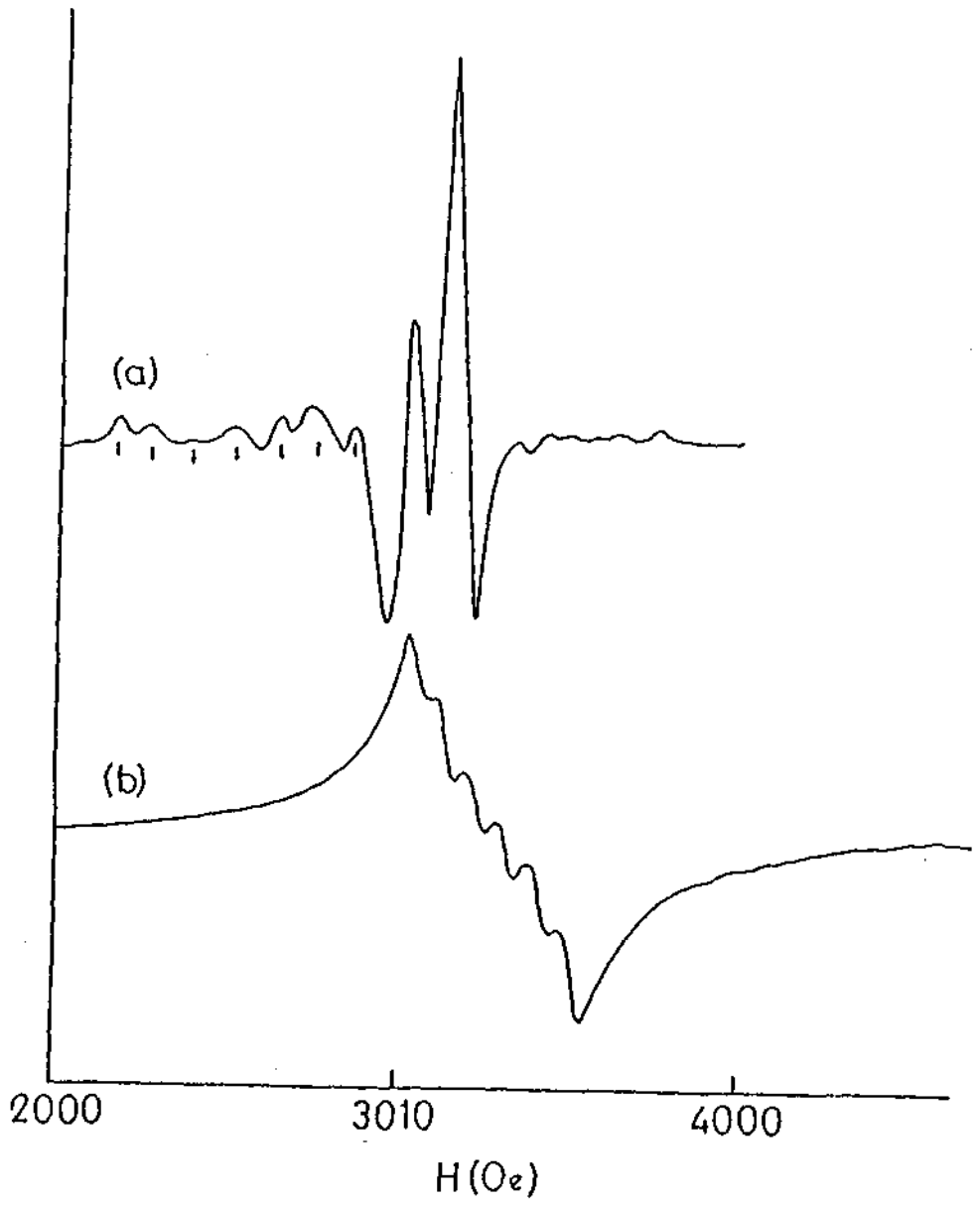

Fig. 1.32. EPR spectra of (a) Cu acetate dimer (b) $[Mn(2,2'-bipyridyl)_2]^{2+}$ encapsulated in Al–MCM–48

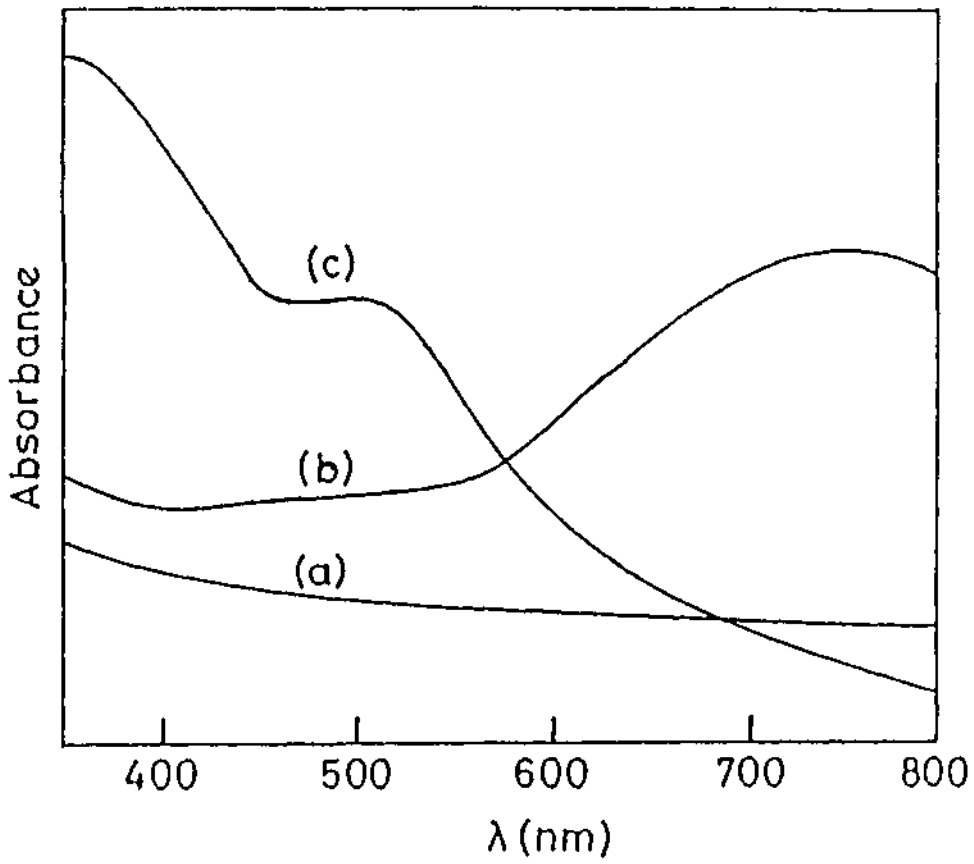

Fig. 1.33. Electronic absorption spectra of (a) Al–MCM–48 (b) Cu acetate dimer encapsulated Al–MCM–48 and (c) $[Mn(2,2'-bipyridyl)_2]^{2+}$ encapsulated Al–MCM–48.

1.2), a value considerably higher than that found (~4) with Cu(II) acetate alone. This result demonstrates the high catalytic activity of Cu-Al-MCM-48 in the ortho hydroxylation of phenol by oxygen activation.

The Al-MCM-48$[Mn(bipy)_2]^{2+}$ gave an EPR spectrum with the expected hyperfine structure due to Mn^{2+} (Fig. 1.32b). It was pink in colour with a broad band around 490nm in the DRS, due to the metal-ligand charge transfer transition (Fig. 1.33c). The infrared spectrum showed broad bands at 760 and 773cm^{-1} due to the out-of-plane C-H deformation of the 2,2' bipyridyl. Gas chromatographic analysis of the oxidation product of styrene by Al-MCM-48-$[Mn(bipy)_2]^{2+}$ with H_2O_2 showed the conversion to be ~40% with styrene oxide as the primary product. The turn-over number was 82 compared to that (~7) with the $[Mn(bipy)_2]^{2+}$ complex alone (see Table 1.3). In the hexagonal mesoporous host, Al-MCM-41, the maximum turnover number was 58.[155] This result establishes Al-MCM-48-$[Mn(bipy)_2]^{2+}$ to be an excellent catalyst for such oxidation reactions. It is to be noted that the turnover number for styrene oxidation with Cu-acetate-Al-MCM-48 catalyst was 46, but there was hardly 5% conversion to benzaldehyde. Similarly, the turnover number of the Mn catalyst for the oxidation of phenol through molecular oxygen was 14 and the product contained almost no catechol. These results reveal the specificity of the metal complexes encapsulated in the cubic mesoporous phase.

The present study demonstrates the high catalytic potential of transition metal complexes encapsulated in cubic mesoporous phases in oxidation reactions.

4.7 Hexagonal microporous silica and aluminophosphate by supramolecular templating of a short-chain amine

Thermogravimetric analysis of the as-synthesized silica sample showed complete removal of water around 393K and the complete loss of the amine around 573K. Dehydroxylation of the silanol groups occurs from 573 K upto 900K. Based on the TG analysis, the composition of the as-synthesized sample

Table 1.2 Hydroxylation of Phenol

Catalyst	Conversion wt %	Catechol wt %	Quinol wt %	Others wt %	TON
Cu-Acetate					3.7
Cu-Ac-Al-MCM-48	36	29	3	4	37
Mn-$(bipy)_2$Al-MCM-48	10	-	-	10	14

Table 1.3 Oxidation of Styrene

Catalyst	Conversion (wt %)	Products (wt %)			TON
		Benzaldehyde	Styrene -oxide	Others	
$Mn(bipy)_2(NO_3)_2$	4	-	-	4	7
Al-MCM-48	6	-	-	5	-
Al-MCM-48-$[Mn(bipy)_2]^{2+}$	40	6	22	10	82
Cu-Ac-Al-MCM-48	27	15	5	8	46

was SiO_2:0.12$C_6H_{13}NH_2$:0.33H_2O. The XRD pattern of the as-synthesized silica is characteristic of a hexagonal phase with a d_{100} value of 2.51nm (Fig. 1.34a). After calcination at 523K for 3h in N_2 atmosphere, the diffraction pattern showed little change (Fig. 1.34b), although ~80% of the amine template as well as water were removed. Calcination at 673K for 3h in N_2 atmosphere also, did not cause any significant change in the d_{100} spacing in the XRD pattern (Fig. 1.34c), eventhough entire template had been eliminated. Such an absence of any appreciable change in the d_{100} value on calcination, has to be contrasted with that of the mesoporous silica, where a considerable change in the *d*-value during calcination. Calcination at 723K for 3h in N_2 atmosphere, however gives rise to a small additional peak at a smaller angle (Fig. 1.34d).

In Fig. 1.35a, we show the N_2 adsorption isotherm of the porous silica sample calcined at 523K (corresponding to 80% loss of template). The isotherm is of Type I, similar to that found in zeolites[169] and microporous niobia.[162] The BET surface area of the sample was 700m^2g^1. The pore size distribution calculated by the Horvath-Kawazoe method shows two distinct pore diameters of 1.3 and 1.5nm (Fig. 1.35b). It is noteworthy that the pore diameters are well below the mesoporous range. The wall thickness for the calcined sample is around 1.5nm. The TEM image of the sample calcined at 523K (Fig. 1.36) shows the presence of disordered hexagonal channels with a pore diameter of ~1.42nm.

The N_2 adsorption isotherm of the porous silica calcined at 673K for 3h in a N_2 atmosphere was also examined. The isotherm is of Type I as can be seen from Fig. 1.37a, indicating the microporous nature of the sample. The BET surface area of this sample was 800m^2g^{-1}. The increase in surface area is not surprising since entire template is removed at this temperature. When the sample calcined at 673K for 3h in N_2 atmosphere was exposed to the atmosphere for 2 days, it lost part of the crystallinity and showed a Type IV adsorption isotherm (Fig. 1.37b). Accordingly, the pore size distribution obtained by the Barrett-Joyner-Halenda method showed the existence of both micropores (pore dia. ~1.5nm) and mesopores (pore dia. ~3.5nm) as shown in the inset of Fig. 1.37.

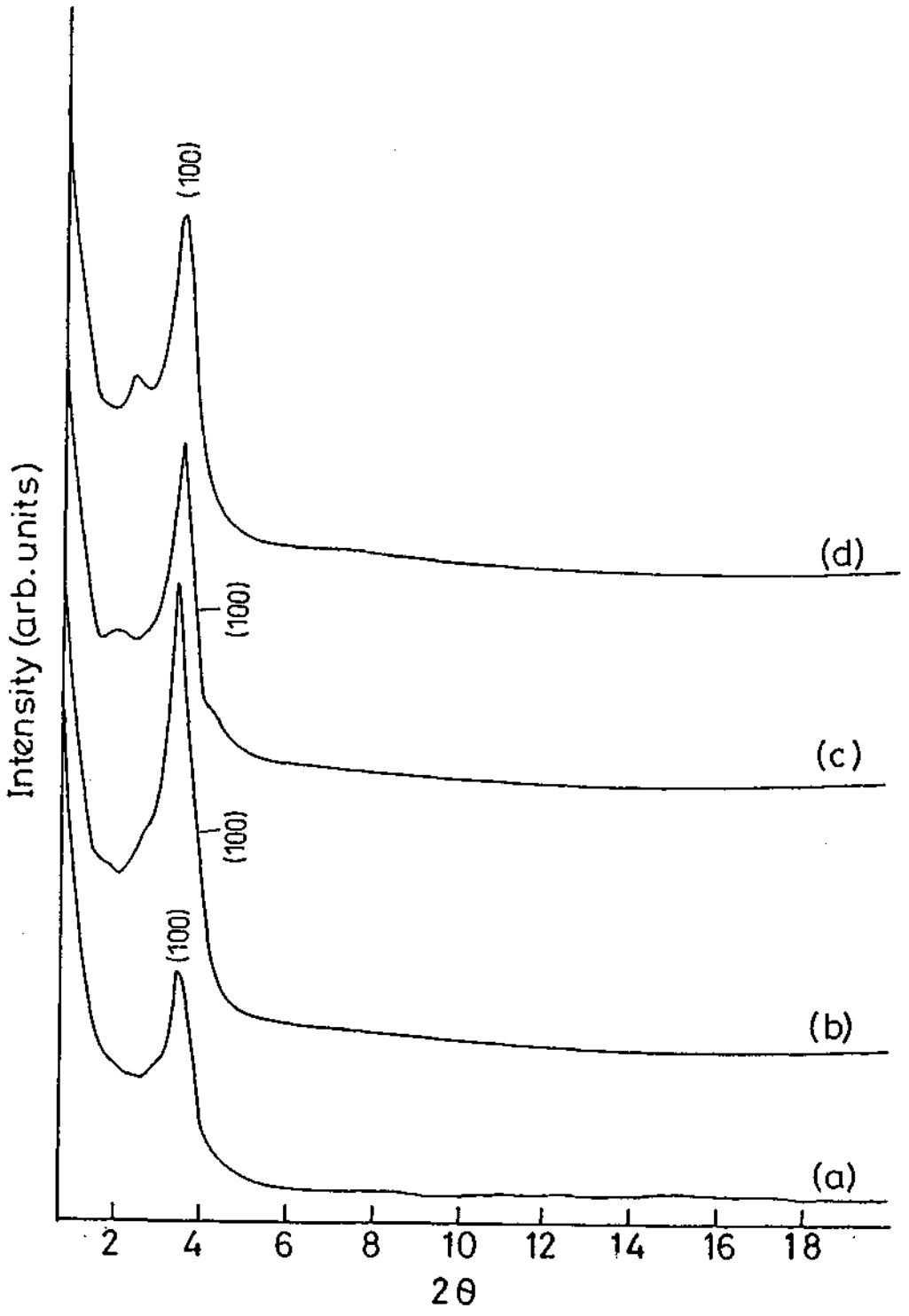

Fig. 1.34. X–ray diffraction patterns of microporous silica prepared with n–hexylamine as the templating agent: (a) as – synthesized; (b) calcined at 523K for 3h in N2; (c) calcined at 673K for 3h in N2. The small feature at low angles before the (100) reflection may be due to the impurity of a mesoporous phase

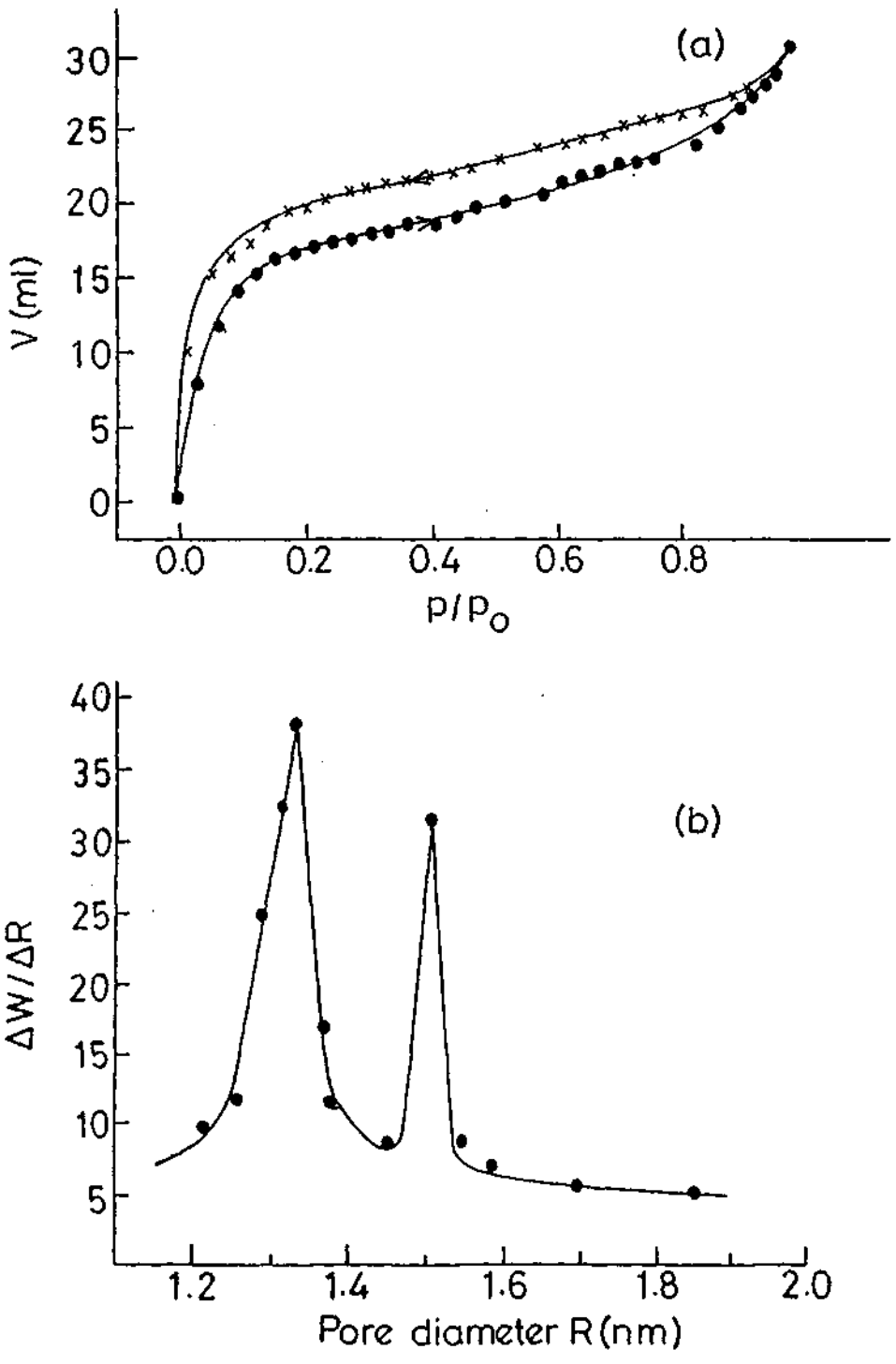

Fig. 1.35. (a) N_2 adsorption–desorption isotherm (at 77K) of microporous silica calcined at 523K for 3h. (b) Pore–size distribution of the same sample obtained by the Horvath–Kawazoe method

Fig. 1.36. TEM image of microporous silica calcined at 523 K for 3h

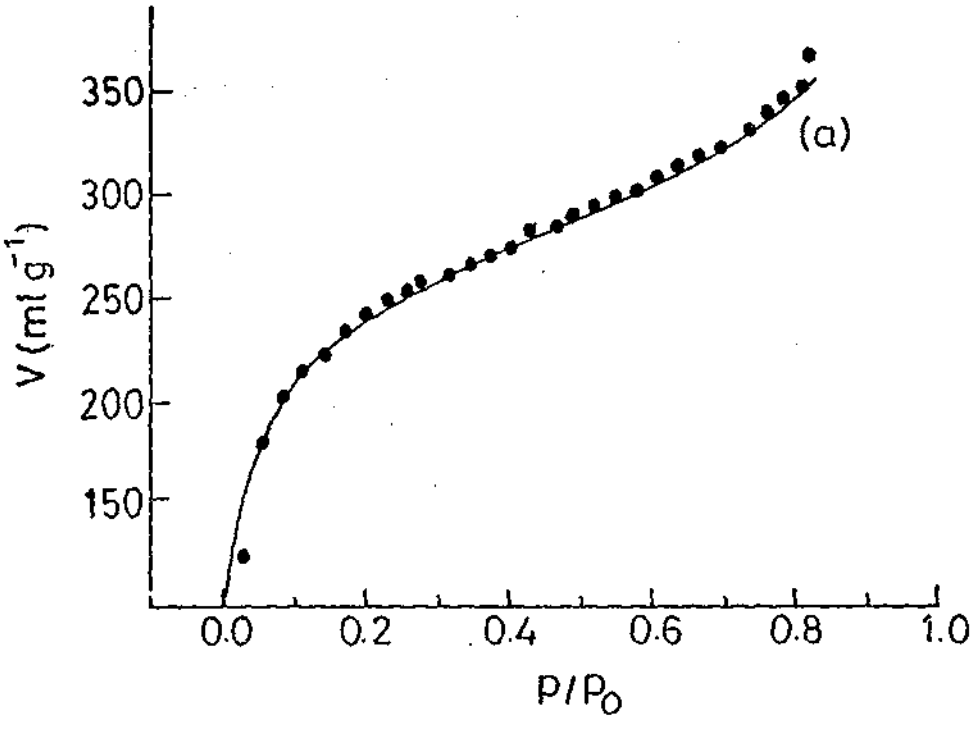

Fig. 1.37. (a) N_2 adsorption isotherm (at 77K) of microporous silica calcined at 673 K for 3h. (b) exposed to the atmosphere for 2 days. Inlet shows the pore size distribution of the samplein (b)

Thermogravimetric analysis of the as-synthesized sample of aluminophosphate (in presence of F^- ions) showed weight losses at three different temperatures: ~423K due to water, ~423-623K due to the loss of template and above ~623K due to dehydroxylation of the surface. The approximate composition of the as-synthesized material calculated from TG analysis (assuming absence of fluoride) was Al_2O_3:P_2O_5:2.6$C_6H_{13}NH_2$:H_2O. The Al/P ratio of unity was also verified by energy dispersive X-ray analysis. The presence of fluoride ions in the reaction mixture was found to be necessary to obtain the Al/P ratio of unity. In the absence of fluoride ions, the Al/P ratio was around 0.5. Furthermore, the $AlPO_4$ so obtained had a lamellar structure.

The XRD pattern of the as-synthesized aluminophosphate sample (prepared in the presence of fluoride ions) is shown in Fig. 1.38a. The presence of a low angle peak in the pattern with d_{100} value of 2.1nm is attributed to the hexagonal microporous material, rather than to a mesoporous material of the M41S family. Calcination of the as-synthesized $AlPO_4$ sample at 503K for 2h in N_2 atmosphere does not affect the crystallinity, as can be seen from Fig. 1.38b. On calcination at 573K for 2h in a N_2 atmosphere, we observe a significant decrease in the intensity of d_{100} reflection (Fig. 1.38c). This is likely to be due to the formation of disordered pores resulting from removal of the template. It is to be noted that calcination around 573K removes ~60% of the template. The BET surface area of this sample from N_2 adsorption was $190 m^2 g^{-1}$. The adsorption isotherm was of Type I as shown in Fig. 1.39a and the pore size distribution calculated by the Horvath-Kawazoe (HK) method, shows pores of two sizes, with diameters of 1.3 and 1.38nm as illustrated in Fig. 1.39b. The wall thickness of the sample obtained by subtracting the HK pore size from the a_0 value was ~1.0nm. The TEM image of the sample calcined at 503K (Fig. 1.40) reveals disordered hexagonal micropores, with a pore size comparable to that obtained from the N_2 adsorption-desorption data.

The XRD pattern of the aluminophosphate prepared, in the absence of fluoride ions using *n*-hexylamine as the template, is characteristic of a lamellar

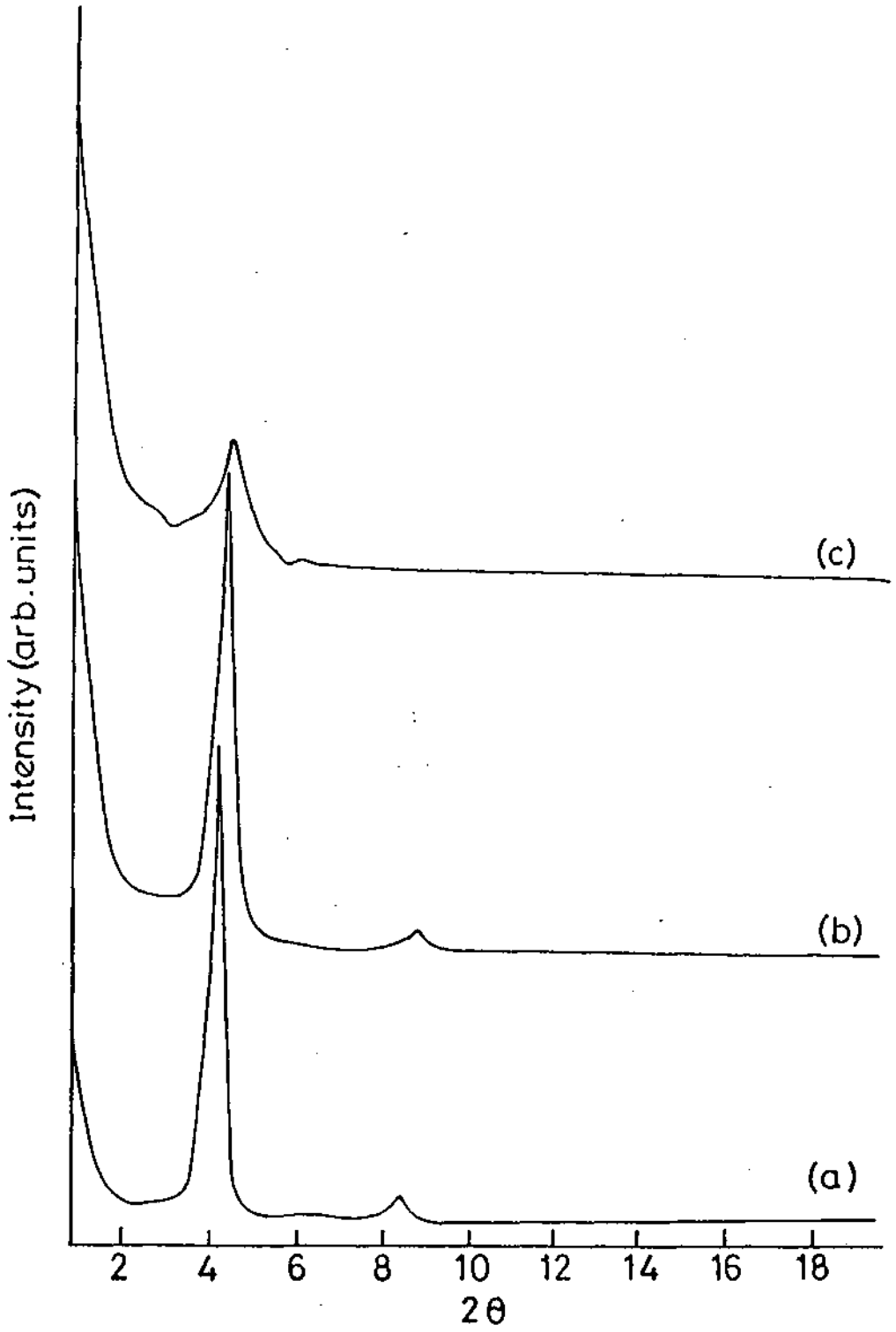

Fig. 1.38. X–ray diffraction patterns of microporous aluminophosphate prepared with n–hexylamine as template (in the presence of F– ions): (a) as –synthesized; (b) calcined at 503 K for 2h in N2 and (c) calcined at 573K for 2h in N_2

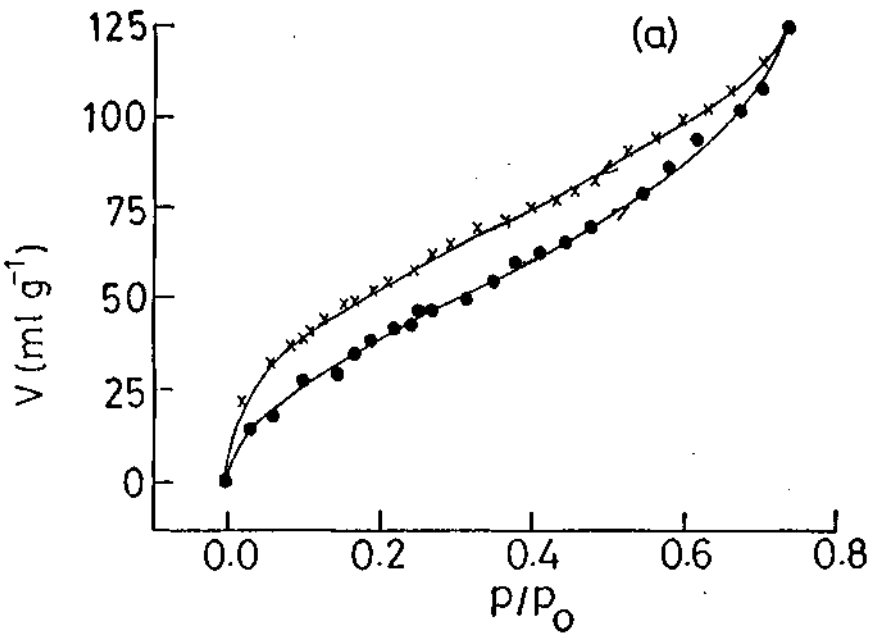

Fig. 1.39. N_2 adsorption–desorption (at 77K) of microporous aluminophosphate calcined at 573K for 2 h in N_2 ; (b) pore–size distribution of the sample in (a) calculated by the Horvath–Kawazoe method

Fig. 1.40. TEM image of microporous aluminophosphate calcined at 573 K for 3h

phase (Fig. 1.41c), with a d_{100} spacing of 2.05nm. It was possible to exchange the hexylamine with other amines, by soaking the lamellar aluminophosphate sample in the corresponding amine in methanol solution. The XRD patterns of the lamellar phases with different amines thus obtained are shown in Fig. 1.41. The *d*-spacing of the lamellar material varies in proportion to the chain length of the amine, as expected.

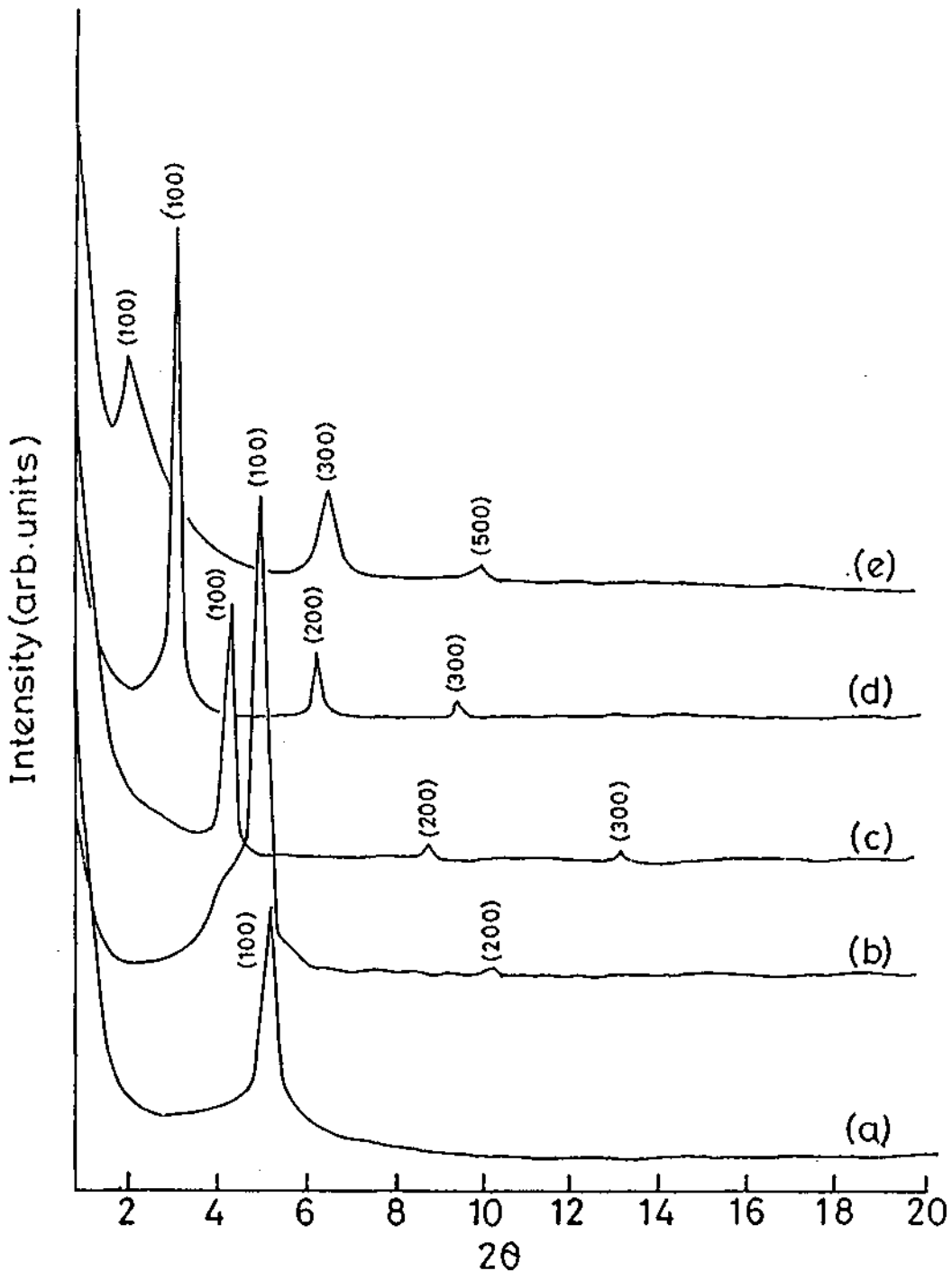

Fig. 1.41. X–ray diffraction patterns of lamellar aluminophosphate samples prepared with different amines in the absence of F^- ions; (a) 1,3–diaminopropane; (b) butylamine; (c) hexylamine (d) octylamine; and (e) dodecylamine.

References

1. IUPAC Manual of Symbols and Terminology *Pure appl. Chem.*, **31**, 578 (1972).
2. Introduction to Zeolite Science and Practice; Eds. H. van Bekkum, E.M. Flanigen, J.C. Jansen, Elsevier: Amsterdam, (1988).
3. Advanced Zeolite Science and Applications; Eds. J.C. Jansen, M. Stocker, H.G. Karge, J. Weitkamp, Elsevier: Amsterdam, (1994).
4. Atlas of Zeolite Structure types 2nd Edn. Butterworths, London, (1988).
5. M.E. Davis, R.F.Lobo, *Chem. Mater.* **4**, 756 (1992).
6. These aspects of properties and applications of microporous materials have been discussed: Introduction to Zeolites Science and Practice (*Stud. Surf. Sci. Catal.* 58 (1991).).
7. C.T.Kresge, M.E. Leonowicz, W.J. Roth, J.C. Vartuli, J.S. Beck, *Nature* **359**, 710 (1992).
8. J.S.Beck, J.C. Vartuli, W.J. Roth, M.E. Leonowicz, C.T. Kresge, K.D. Schmitt, C.T.-W. Chu, D.H. Olson, E.W. Sheppard, S.B. Mccullen, J.B. Higgins, J.L. Schlenker, *J. Am. Chem. Soc.*, **114**, 10834 (1992).
9. P. Behrens, *Adv. Mater.* **5**, 127 (1993).
10. I. Soten, G. A. Ozin, *Curr.Opinion Colloid & Interface Sci.*, **4**, 325 (1999).
11. P.Behrens, G.D.Stucky, *Angew. Chem. Int. Ed. Engl.* **32**, 696 (1993).
12. J.S. Beck, J.C. Vartuli, *Curr. Opinion Solid State Mater. Sci.*, **1**, 76 (1996).
13. D.M. Antonelli, J.Y. Ying, *Curr. Opinion Colloid Interface Sci.*, **1**, 523 (1996).
14. P.Behrens, *Angew. Chem. Int. Ed. Engl.*, **35**, 515 (1996).
15. (a) C.G. Göltner M. Antonietti, *Adv. Mater.* **9**, 431 (1997), (b) P.T. Tanev, T.J. Pinnavaia, *Science*, **267**, 365 (1995), (c) S. A. Bagshaw, E. Prouzet, T.J. Pinnavaia, *Science*, **269**, 1242 (1995), (d) S.A. Bagshaw, T.J. Pinnavaia, *Angew. Chem. Int. Ed. Engl.* **35**, 1102 (1996).

16. A. Sayari In recent advances and New Horizons in Zeolite Science and Technology; Eds. H. Chon, S.I. Woo, S.-E. Park, Elsevier; Amsterdam, (1996); chapter 1.
17. M. Yada, M. Machida, T. Kijima, *Chem. Commun.*, 769 (1996).
18. F. Vaudry, S. Khodabandeh, M.E. Davis, *Chem. Matter.*, **8**, 1451 (1996).
19. S.A. Bagshaw, T.J. Pinnavaia, Angew. *Chem. Int. Ed. Engl.*, **35**, 1102 (1996).
20. D.M. Antonelli, J.Y. Ying, *Angew. Chem. Int. Ed. Engl.*, **34**, 2014 (1995).
21. U. Ciesla, S. Schacht, G.D. Stucky, K.K. Unger, F. Schuth, *Angew. Chem. Int. Ed. Engl.*, **35**, 541 (1996).
22. D.M. Antonelli, J.Y. Ying, *Angew. Chem. Int. Ed. Engl.*, **35**, 426 (1996).
23. S. Ayyappan, N. Ulagappan, C.N.R. Rao, *J. Mater. Chem.*, **6**, 1737 (1996).
24. D.M. Antonelli, J.Y. Ying, *Chem. Mater.*, **8**, 874 (1996).
25. Q. Huo, D.I. Margolese, U. Ciesla, P. Feng, T.E. Gier, P. Sieger, R. Leon, P. M. Petroff, F. Schuth, G.D. Stucky, *Nature*, **368**, 317 (1994).
26. Q. Huo, D.I. Margolese, U. Ciesla, D.G. Demuth, P. Feng, T.E. Gier, P. Sieger, A. Firouzi, B.F. Chmelka, F. Schuth, G.D. Stucky, *Chem. Mater.*, **6**, 1176 (1994).
27. U. Ciesla, D. Demuth, R. Leon, P. Pierre, G.D. Stucky, K.K. Unger, F. Schuth, *Chem. Commun.*, 1387 (1994).
28. T. Abe, A. Taguchi, M. Iwamoto, *Chem. Mater.*, **7**, 1429 (1995).
29. N. Ulagappan, C.N.R. Rao, *Chem. Commun.*, 1685 (1996).
30. Z.R. Tian, W. Tong, J.Y. Wang, N.G. Duan, V.V. Krishnan, S.L. Suib, *Science*, **276**, 926 (1997).
31. T. Doi, T. Miyake, *Chem. Commun.*, 1635 (1996).
32. P. Feng, Y. Xia, J. Feng, X. Bu, G.D. Stucky, *Chem. Commun.*, 949 (1997).
33. B. Chakraborty, A.C. Pullikottil, S. Das, B. Viswanathan, *Chem. Commun.*, 911 (1997).
34. S. Ayyappan, C.N.R. Rao, *Chem. Commun.*, 575 (1997).
35. S.A. Bagshaw, F.D. Renzo, F. Fajula, *Chem. Commun.*, 2209 (1996).
36. W. Zhang, M. Fröba, J. Wang, P.T. Tanev, J. Wong, T.J. Pinnavaia, *J. Am. Chem. Soc.*, 118, 9164 (1996).

37 S. Gontier, A. Tuel, *Stud. Surf. Sci. Catal.*, **97**, 157 (1995).

38. P.T. Tanev, M. Chibwe, T.J. Pinnavaia, *Nature***368**, 321, (1994).

39. A. Tuel, S. Gontier R. J. Teissier, *Chem. Commun.*, 651 (1996).

40. U. Oberhagemann, I. Kinski, I. Diedorf, B. Marler, H. Gies, *J. Noncryst. Solids*, **197**, 145 (1996).

41. Y. X. Zhi, A. Tuel, Y. Ben-Taârit, C. Naccache, *Zeolites*, **12**, 138 (1992).

42. K.M. Reddy, I.L. Moudrakovski, A. *Sayari Chem. Commun.*, , 1059 (1994).

43. S. Gontier, A. Tuel, *Microporous Mater.*, **5**, 161 (1995).

44. A. Sayari, V.R. Karra and J.S. Reddy, I.L. Moudrakovski, *Mat. Res. Soc. Symp. Proc.*, **371**, 81 (1995).

45. K. J. Chao, C. N. Wu, H. Chang, L. J. Lee, S. F. Hu, *J. Phys. Chem. B.*, **101**, 6341 (1997).

46. T. K. Das, K. Chaudhari, A. J. Chandwadkar, S. Sivasanker, *Chem. Commun.*, 2495 (1995).

47. T.M. Abdel-Fattah, T.J. Pinnavaia, *Chem. Commun.*, 665 (1996).

48. A. Jentys, N.H. Pham, H. Vinek, M. Englisch, J.A. Lercher, *Microporous Mater.*, **6**, 13 (1996).

49. N. Ulagappan, C.N.R. Rao, *Chem. Commun.*, 1047 (1996).

50. D. Zhao, D. Goldfarb, *Chem. Commun.*, 875 (1995).

51. Z.Y. Yuan, S.Q. Liu, T.H. Chen, J. Z. Wang, H.X. Li *Chem. Commun.*, 973 (1995).

52. P.V. Braun, P. Osenar, S.I. Stupp, *Nature*, **380**, 325 (1996).

53. P. Osenar, P.V. Braun, S.I. Stupp, *Adv. Mater.*, **8**, 1022 (1996).

54. V. Tohver, P.V. Braun, M.U. Pralle, S.I. Stupp, *Chem. Mater.*, **9**, 1495 (1997).

55. J. Li, H. Kessler, L. Delmotte, *J. Chem. Soc. Faraday Trans.*, **93**, 665 (1997).

56. M. Fröba, N. Oberender, *Chem. Commun.*, 1997, 1729.

57. C.T. Kresge, *Adv. Mater.*, **8**, 181 (1996).

58. S. Mann, D. Walsh, *Chem. Br.* Nov., 31 (1996).

59. S. Mann, *Chemistry & Industry*, 6 Feb., 93 (1995).

60. S. Mann, G.A. Ozin, *Nature*, **382**, 313 (1996).

61. C.Y. Chen, S. L. Burkett, H.X. Li, and M. E. Davis, *Microporous Mater.*, **2**, 27 (1993).

62. T. Yanagisawa, T. Schimizu, K. Kuroda and C. Kato, *Bull. Chem. Soc. Jpn.* **63**, 988 (1990).

63. S. Inagaki, Y. Fukushima, K. Kuroda *J. Chem. Soc. Chem. Commun.*, 680 (1993).

64. S. Inagaki, Y. Fukushima, K. Kuroda, in Studies in Surface Science and Catalysis 92, Science and Technology in Catalysis (1994). Ed. Y. Izumi, H. Arai, M. Iwamoto Amsterdam : Elsevier Science; 125 (1994).

65. J.C. Vartuli, C.T.Kresge, M.E. Leonowicz, A. S. Chu, S. B. McCullen, I. D. Johnson, E.W. Sheppard *Chem. Mater.*, **6**, 2070 (1994).

66. C.Y. Chen, S. Q. Xiao, M. E. Davis, *Microporous Mater.*, **4**, 1 (1995).

67. P. Mariani, V. Luzatti, H. Delacroix, *J. Mol. Biol.*, **204**, 165 (1988).

68. P.O. Eriksson, G. Lindblom, G. Arvidson, *J. Phys. Chem.*, **89**, 1050 (1985).

69. J.C. Vartuli, K.D. Schmitt, C.T. Kresge, W.J. Roth, M.E. Leonowicz, S.B. Mccullen, S.D. Hellring, J.S. Beck, J.L. Schlenker, D.H. Olson, E.W. Sheppard, *Chem. Mater.* **6**, 2317 (1994).

70. A. Corma, M.L. Navarro, J. Pérez-Pariente, *Chem. Commun.*, 147 (1994).

71. S.T. Hyde, *Curr. Opinion in Solid State Mater. Sci.*, **1**, 653 (1996).

72. E.P. Barrett, L.G. Joyner, P.P. Halender, *J. Am. Chem. Soc.*, **73**, 373 (1951).

73. G. Horvath, J. Kawazoe, *J. Chem. Eng. Jpn.*, **16**, 470 (1983).

74. A. Steel, S.W. Carr, M.W. Anderson, *Chem. Mater.*, **7**, 1829 (1995).

75. B. Echchahed, A. Moen, D. Nicholson, L. Bonneviot, *Chem. Mater.*, **6**, 1716 (1997).

76. G.J.T. Tiddy, *Phys. Rev.*, **57**, 1 (1980).

77. P.A. Winsor, *Chem. Rev.*, **68**, 1 (1968).

78. J.S. Beck, J.C. Vartuli, G .D. Kennedy, C.T.Kresge, W.J. Roth, S.E. Schramm, *Chem. Mater.*, **6**, 1816 (1994).

79. A. Monnier, F. Schuth, Q. Huo, D. Kumar, D. Margolese, R.S. Maxwell, G.D. Stucky, M. Krishnamurthy, P. Petroff, A. Firouzi, M. Janicke, B.F. Chmelka, *Science*, **261**, 1299 (1993).

80. J. Luo, S.L. Suib, *Chem. Commun.*, 1031 (1997).

81. M. Ogawa, *J. Am. Chem. Soc.*, **116**, 7941 (1994).

82. S. Oliver, A. Kuperman, N. Coombs, A. Laugh, G.A. Ozin, *Nature*, **378**, 47 (1995).

83. C.A. Fyfe, G. Fu, *J. Am. Chem. Soc.*, **117**, 9709 (1995).

84. H.P. Lin, C.Y. Mou, *Science*, **273**, 765 (1996).

85. E.S. Blackmore, G.J.T. Tiddy, *J. Chem. Soc. Faraday Trans.* II, **84**, 1115 (1988).

86. A. Sein, J.B.F.N. Engberts, *Langmuir*, **11**, 455 (1995).

87. J.M. Seddon, *Biochim. Biophys. Acta.*, **1031**, 1 (1990).

88. J.N. Israelachvili, D.J. Mitchell, B.W. Ninham, *J. Chem. Soc. Faraday Trans.* II, **72**, 1525 (1976).

89. J.N. Israelachvili, D.J. Mitchell, B.W. Ninham, *Biochim. Biophys. Acta.*, **470**, 185 (1977).

90. S.M. Gruner, *J. Phys. Chem.*, **93**, 7562 (1989).

91. L. Mercier, T.J. Pinnavaia, *Adv. Mater.*, **9**, 500 (1997).

92. X. Feng, G.E. Fryxell, L.Q. Wang, A.Y. Kim, J. Liu, K.M. Kemner, *Science*, **276**, 923 (1997).

93. P.J. Branton, P.G. Hall, K.S.W. Sing, H. Reichert, F. Schuth, K.K. Unger, *J. Chem. Soc. Faraday Trans.*, **90**, 2965 (1994).

94. J. Rathousky, A. Zukal, O. Franke, G.S. Ekloff, *J. Chem. Soc. Faraday Trans.*, **90**, 2821 (1994).

95. P.J. Branton, P.G. Hall, K.S.W. Sing, *J. Chem. Soc. Chem. Commun.*, 1257 (1993).

96. P.L. Llewellyn, Y. Grillet, F. Schüth, H. Reichert, K.K. Unger, *Microporous Mater.*, **3**, 345 (1994).

97. R. Schmidt, M. Stöcker, E. Hansen, D. Akporiaye, O.H. Ellestad, *Microporous Mater.*, **3**, 443 (1995).

98. O. Franke, G.S. Ekloff, J. Rathousky, J. Starek, A. Zukal, *J. Chem. Soc. Chem. Commun.*, 724 (1993).

99. D. Akporiaye, E.W. Hansen, R. Schmidt and M. Stöcker, *J. Phys. Chem.*, **98**, 1926 (1994).

100. P.L. Llewellyn, F. Schüth, Y. Grillet, F. Rouquerol, K.K. Unger, *Langmuir*, **11**, 574 (1995).

101. J. Rathousky, A. Zukal, O. Franke, G.S. Ekloff, *J. Chem. Soc. Faraday Trans.*, **91**, 937 (1995).

102. A. Corma, V. Fornes, M.T. Navarro, J.P. Pariente, *J. Catal.*, **148**, 569 (1994).

103. K.R. Kloetstra, H.W. Zandbergen, H.J. Van Bekkum, *Catal. Lett.*, **33**, 157 (1995).

104. V. Alfredsson, M. Keung, A. Monnier, G.D. Stucky, K.K. Unger and F. Schuth, *Chem. Commun.*, 921 (1994).

105. Z. Luan, C.F. Cheng, W. Zhou, J. Klinowski, *J. Phys. Chem.*, **99**, 1018 (1995).

106. R. Schmidt, D. Akporiaye, M. Stöcker, O.H. Ellestad, *Chem. Commun.*, 1493 (1994).

107. R. Schmidt, D. Akporiaye, M. Stöcker, O.H. Ellestad, *Stud. Surf. Sci. Catl.*, **84**, 61 (1994).

108. R.B. Borade, A. Clearfield, *Catal. Lett.*, 31, 267 (1995).

109. M. Coustel, F.D. Renzo, F. Fajula, *Chem. Commun.*, 967 (1994).

110. J.S. Beck (Mobil Oil Company), USA 5057296, (1991); C.T. Kresge, M.E. Leonowicz, W.J. Roth, J.C. Vartuli (Mobil Oil Company), USA 5098684, (1992); M.E. Leonowicz, W.J. Roth, J.C. Vartuli (Mobil Oil Company), US-A 5108725.

111. A. Corma, A. Martinez, V.M. Soria, J.B. Monton, *J. Catal.*, **153** 25 (1995).

112. A. Armengol, M.L. Cano, A. Corma, H. Garcia, M. L. Navarro, *Chem. Commun.*, 519 (1995).

113. K.R. Kloetstra, H.J. Van Bekkum, *Chem. Commun.*, 1005 (1995).

114. A. Sayari, C. Danumah, I.L. Moudrakovski, *Chem. Mater.*, 7, 813 (1995).

115. I.V. Kozhevnikov, A. Sinnema, R.J.J. Jansen, K. Parmin, H. Van Bekkum, *Catal. Lett.*, **36**, 241 (1995).

116. A. Corma, V. Fornès, H. Garcia, M.A. Miranda, M.J. Sabater, *J. Am. Chem. Soc.*, **116**, 9767 (1994).

117. C. Huber, K. Moller, T. Bein, *Chem. Commun.*, 2619 (1994).

118. C.G. Wu, T. Bein, *Chem. Commun.*, 925 (1996).

119. C.G. Wu, T. Bein, *Science*, **266**, 1013 (1994).

120. P. Llewellyn, U. Ciesla, H. Decher, R. Stadler, F. Schuth, K. Unger, In Zeolites and Related Microporous Materials: State of the Art (1994), Stud. Surf. Sci and Catal. (1994). Proceeding of the 10th International Zeolite conference Garmisch- Partenkirchen, Germany (1994), Ed., J. Weitkamp, H.G. Karge, H. Pfeifer, W. Hölderich, Amsterdam, Elsevier Science **84**: 2013 (1994).

121. H. Yang, A. Kuperman, N. Coombs, S. Mamicht, A. Fara, G.A. Ozin, *Nature*, **379**, 703 (1996).

122. D. Zhao, J. Feng, Q. Huo, B. F. Chmelka, G. D. Stucky, *Science*, **279**, 548 (1998).

123. D. Zhao, J. Feng, Q. Huo, B. F. Chmelka, G. D. Stucky, *J. Am. Chem. Soc.*, **120**, 6024 (1998)

124. A. Imhof, D. J. Pine, *Nature*, **389**, 948 (1997).

125. A. Imhof, D. J. Pine, *Adv. Mater.*, **10**, 697 (1998).

126. B. T. Holland, C. F. Blanford, A. Stein, *Science*, **281**, 538 (1998).

127. J. E. G. J. Wijnhoven, W. L. Vos, *Science*, **281**, 802 (1998).

128. S. H. Park, D. Qin, Y. Xia, *Adv. Mater.*, **10**, 1028 (1998). S. H. Park, Y. Xia, *Adv. Mater.*, **10**, 1045 (1998).

129. M. Trau, N. Yao, E. Kim, Y. Xia, G. M. Whitesides, I. A. Aksay, *Nature*, **390**, 674 (1997).

130. S. A. Davis, S. L. Burkett, N. H. Mendelson, S. Mann, *Nature*, **385**, 420 (1997).

131. A. Cauvel, G. Renard, D. Brunel, *J. Org. Chem.*, **62**, 749 (1997).

132. M. H. Lim, C. F. Blanford, A. Stein, *Chem. Mater.*, **10**, 467 (1998).

133. W. M. VanRhijn, D. E. DeVos, B. F. Sels, W. D. Bossaert, P. A. Jacobs, *Chem. Commun.*, 317 (1998).

134. Y. V. S. Rao, D. E. DeVos, T. Bein, P.A Jacobs, *Angew. Chem. Int. Ed. Engl.*, **36**, 2661 (1997).

135. S. O'Brien, J. Tudor, S. Barlow, M. J. Drewitt, S. J. Heyes, D O'Hare, *Chem. Commun.*, 641 (1997).

136. R. Anwander, R. Roesky, *J. Chem. Soc. Dalton. Trans.*, 137 (1997).

137. M. H. Lim, C. F. Blanford, A. Stein, *J. Am. Chem. Soc.*, **119**, 4090 (1997).

138. K. Moller, T. Bein, R. X. Fischer, *Chem. Mater.*, **11**, 665 (1999).

139. M. Kruk, M. Jaroniec, R. Ryoo, J. M. Kim, *Chem. Mater.*, **11**, 2568 (1999) and references there in.

140. L-Z. Wang, J-L. Shi, W-H. Zhang, M-L. Ruan, J. Yu, D-S. Yan, *Chem. Mater.*, **11**, 3015 (1999).

141. P.T. Tanev, T.J. Pinnavaia, *Science*, **271**, 1267 (1996).

142. H. Adkins, S. H. Watkins, *J. Am. Chem. Soc.*, **73**, 2184 (1951).

143. D. Basmadjian, G. Fulford, B. I. Parsons, D. S. Montgomery, *J. Catal.* **1**, 547 (1962).

144. C. M. Chen, S. Y. Chen, S. Y. Peng, *Stud Surf. Sci. Catal.*, **91**, 427 (1995).

145. S. Prabhakar, K. J. Rao, C. N. R. Rao, *J. Mater. Res.*, **6**, 592 (1991).

146. R. Dupree, D. Holland, M.G. Morutza, *Nature*, **416**, 328 (1987).

147. S. -P. Szu, L. C. Klein, M. Greenblatt, *J. Non-Cryst. Solids.*, **143**, 21 (1992).

148. W. Oganowski, Polish patent PL 159643, (1992).

149. S. Trasatti, *Electrochim. Acta.*, **36**, 225 (1991),.

150. CH. Comninellis, G.P. Vercesi, *J. Appl. Electrochem.* **21**, 136 (1991).

151. D.R. Corbin, N. Herron, *J. Mol. Catal.*, **86**, 343 (1994).

152. L.M. Sayre, D.V. Nadkarni, *J. Amer. Chem. Soc.*, **116**, 3157 (1994).

153. R. Robert, P. Ratnasamy, *J. Mol. Catal.*, **100**, 93 (1995).

154. P.P. Knops-Gerrits, D.D Vos, F. Thibault-Starzyk, P.A. Jacobs, *Nature*, **369**, 543 (1994).

155. S.S. Kim, W. Zhang, T. J. Pinnavaia, *Catal. Lett.*, **43**, 149 (1997).

156. M.E. Davis, *Chem. Eur. J.* **3**, 1745 (1997).

157. J.M. Thomas, *Angew. Chem. Int. Ed. Engl.* **33**, 913 (1994).

158. C.J. Brinker, *Curr. Opinion Solid State Mater.* Sci. **1**, 795 (1996).

159. P.T. Tanev, T.J. Pinnavaia, *Chem. Mater.* **8**, 2068 (1996).

160. A. Sayari, M. Kruk, M. Jaroniec, *Catal. Lett.* **49**, 147 (1997).

161. D. Zhao, Z. Luan, L. Kevan, *Chem. Commun.* 1009 (1997).

162. T. Sun, J.Y. Ying, *Nature* **389**, 704 (1998).

163. J. A. Knowles, M.J. Hudson, *J. Chem. Soc. Chem. Commun.*, 2083 (1995).

164. G. Porte in *Micelles, Membranes, Microemulsions and Monolayers* Ed. W.M. Gelbart, A. Ben-Shaul, D. Roux, Springer Verlag, NewYork, 105 (1994).

165. J.W. Akitt, *Prog. Nucl. Magn. Resn. Spectrosc.*, **21**, 127 (1989).

166. J. Klinowski, *Prog. NMR Spectroc.*, **16**, 237 (1984).

167. S. Prabhakar, K. J. Rao, C. N. R. Rao, *Chem. Phys. Lett.*, **183**, 170 (1991).

168. I.N. Chakraborty, R.A. Condrate Sr, *Phys. Chem. Glasses.*, **183**, 170 (1991).

169. R. Szostak, *Molecular sieves; Principles of synthesis and identification*, Van Nostrand, NewYork, (1989).